

DEFORMATION OF CHALK THROUGH COMPACTION AND FLOW.

**A thesis submitted to the
University of London
(University College London)
for the degree of Doctor in Philosophy
in the
Department of Geological Sciences.**

by

Michael John Leddra.

December 1989

To Philippa and Ann

ABSTRACT

Hydrocarbon bearing chalks are of significant economic importance within the Central Graben of the North Sea. The reservoirs have formed within predominantly allochthonous deposits which exhibit a range of sedimentary and diagenetic features not necessarily found in their onshore equivalents. Reservoir quality is closely related to the preservation of high porosity and is associated with high pore pressures. Today, during hydrocarbon production, change in pore fluid pressure has led to both compactional deformation of the reservoir and localised flow of chalk through perforations into production wells.

This project has been undertaken to investigate, in the laboratory, the compaction and flow characteristics of chalks of medium and high porosity. The data obtained are used to evaluate the present day compaction and flow characteristics of chalk from the standpoint of reservoir engineering, and also to interpret the mechanical conditions that prevailed during allochthonous chalk deposition. This experimental investigation has shown that the mechanical behaviour of all porous chalks is similar. Quantitatively, this behaviour is dependent on a number of parameters, the most important of which is the pre-deformational porosity.

The experimental study, utilised high pressure triaxial equipment to determine the mechanical characteristics of a number of different chalks with pre-deformational porosities in the range 19-49%. Behaviour during loading under undrained triaxial and uniaxial strain conditions has been investigated. The former experiments provide data of importance to evaluating flow, both today, due to pore pressure drawdown in hydrocarbon production wells, and in the past during mobilisation and redeposition of the Central Graben chalks in Cretaceous and Palaeocene times. The experiments using the uniaxial strain path were conducted, primarily, to determine the compactional characteristics of the chalk for computer modelling of reservoir compaction and associated sea-floor subsidence using the finite element method. Compaction associated

factors such as permeability change, and possible instability of chalk during sea water injection have also been investigated. A number of experiments were conducted at slow strain rates in an attempt to determine the influence of strain rate on the magnitude of the deformation.

ACKNOWLEDGEMENTS.

The writing of this thesis has provided me with an excellent opportunity to thank a great many people who would otherwise remain anonymous, but who have all contributed more than they would imagine to my present position. Although it would be impossible to list them all, a number deserve to be mentioned by name.

The full blame for my introduction to geology and geomorphology must rest with "Uncle" Tom Lancaster and Clive Howlett. I doubt whether they realised then what seeds they were sowing. At the same time, two other people of this era also deserve an acknowledgement, namely Dave Bradley and the late John Bradnock. All four managed to achieve the impossible, they inspired to work!

Although my interest remained with geology, my career took a sideways step towards one of my other loves, maps, and I began work at the Department of Energy, where I was employed as a cartographic draughtsman. Very few people are lucky enough to have a forward thinking boss. But I am one of the lucky ones. Mine, Sid Gibbons, was often heard to say "Mike, you've got to keep studying, because sooner or later you'll need a degree to become a dustman!" I would also like to thank John Brooks for all his help.

After seven years, my career took another sideways step, back to geology and geography. Whilst study at King's College, London, I came into contact with a number of people who without knowing it, would have, and still have a profound influence on me, namely Mervyn Jones, Najwa Yassir and Tony Addis.

Without the help of a number of people both in the academic environment and through Mervyn Jones, with members of the Norwegian Petroleum Directorate, Norsk Hydro and Corrigan Associates this thesis could not have been written. Much of the work it contains was conducted on behalf of the Norwegian Petroleum Directorate. I would

like to thank Oystein Dretvik, Eric Mathiesen and Per Erik Overli and in particular Kjetil Tonstad and Ole Preben Berget for their help and assistance over the past three years. For the work undertaken with Norsk Hydro, one person in particular deserves a special mention, Knut Pederstad. Core analysis, in particular that involving North Sea chalk, is a time consuming and often confusing business. I was very fortunate to have a great deal of guidance from Tony Corrigan, who never failed to help me when ever I needed it to unravel the complex story locked in the chalk cores. I was also fortunate to be able to observe Dr Jim Kennedy from Oxford at work on the same core material. His comments and observations proved to be extremely useful.

A substantial part of the work reported in this thesis represents laboratory experiments conducted in the Soil Mechanics Laboratory, Department of Civil Engineering, Imperial College, London. Although this is not my parent department, the technical support provided has been unstinting. Without the unending help of Louis Spall, Steve Ackerley, Graham Keefe and Alan Bolser, this study could not have been completed. They have always been willing to rescue me when the machinery I was using broke down (a frequent occurrence) and help with any modifications that were needed with the minimum of delay. The members of staff within the Soil Mechanics section, in particular Dr's Angus Skinner, Dave Potts, Professors's Peter Vaughan and John Burland have also been incredibly patient in answering questions, explaining principles and turning a blind eye to the innumerable oil spillages with which I have been closely associated.

The technical staff at University College have shown the same level of patience as that exhibited by those at Imperial College. Three people deserve a special mention, Sean Houlding, Mike Gray and Ron Dudman. Ron in particular, has never ceased to amaze me with his immense enthusiasm and encouragement, even though my requests for the impossible frequently ended with a his owning more oil stained clothes.

I have been extremely privileged to work in a research group in which help and co-operation has never been in short supply. I would like to thank to past members of our research group, Tony Addis for his initial help and encouragement, Najwa Yassir for her assistance in a number of experiments, the many useful discussions and her friendship. A special thank you should also go to Tony Goldsmith. He has helped me with a large number of experiments, equipment development and has always been willing to rewrite sections of the database program he has been developing when I needed specific information. The biggest thank you of all goes to Meryvn Jones. Without his (and that of his wife Jane's) help, assistance, insistence and support this project would never have materialised. I would also like to thank Sediment Deformation Research for funding this project and for allowing me the privilege of working within such a dynamic and successful research group.

As such occasions are rare, I should take this opportunity to thank a number of people who, through their inspiration, have been the key to the maintenance of my sanity. They are too numerous to mention, but include such names as Camm, Bishop, Chadwick and most important of all Mitchell.

Finally, I would like thank my family for all of their encouragement during my studies and in particular my wife Ann. Without her never ending support none of this would have been possible. This thesis can only be a small reward for all that she has willingly given up to help me during my time at University.

CONTENTS

Page No.

CHAPTER 1

INTRODUCTION	1
1.1. Research objectives	1
1.2. Organisation of thesis	4
1.3. Scientific rationale	6

PART 1 ON THE NATURE OF CHALK.

CHAPTER 2

STRATIGRAPHY AND STRUCTURAL SETTING OF THE CHALKS OF NORTH WEST EUROPE.

2.1. Introduction	12
2.2. Structural control	13
2.3. The initial accumulation and diagenesis of the chalk	16
2.4. Danish onshore chalks (Stevn's Klint)	23
2.5. Onshore chalks from South East England (Buster Hill)	25

CHAPTER 3

NORWEGIAN HYDROCARBON RESERVOIR CHALKS.

3.1. Introduction	29
3.2. Sedimentology	29
3.2.1. Autochthonous chalks	31
3.2.2. Allochthonous chalks	34
3.3. Structural development and overpressuring	42

3.4. The lithostratigraphic characteristics of the Norwegian chalk formation s	58
3.4.1. Hidra Formation (Cenomanian)	60
3.4.2. Plenus Marl Formation (Cenomanian)	60
3.4.3. Hod Formation (Turonian to Upper Campanian)	60
3.4.4. Tor Formation (Upper Campanian to Maastrichtian)	61
3.4.5. Ekofisk Formation (Danian, Tertiary)	62
3.5. Fracture studies	62
3.5.1. Lithological and fracture study of well 2/7-B11	65

PART 2 EXPERIMENTAL STUDIES.

CHAPTER 4

UNIAXIAL EXPERIMENTS.

4.1. Introduction	104
4.2. Resume of uniaxial strain: theory and practice	106
4.3. Experimental equipment and sample preparation methodology	117
4.3.1. The triaxial cell	117
4.3.2. Measurement of horizontal and vertical displacements	119
4.3.3. The load frame	122
4.3.4. The drainage system	122
4.3.5. Data logging	122
4.3.6. Sample preparation and installation procedures	123
4.4. Slow strain-rate experiments	124
4.4.1. Introduction	124
4.4.2. Experimental methodology and results	127
4.4.2.1. Elongc1	131
4.4.2.2. E longc 2	132
4.4.2.3. Elongc3	137
4.4.2.4. Elongc4	137
4.4.3. Discussion	137

4.5. Stress relaxation experiments	144
4.5.1. Introduction	144
4.5.2. Experimental results	145
4.5.2.1. Vertical effective stress/axial strain	145
4.5.2.2. Horizontal and vertical effective stress	149
4.5.2.3. Deviatoric/mean effective stress	149
4.5.2.4. Void ratio/mean effective stress	157
4.6. Water injection experiments	157
4.6.1 Introduction	157
4.6.2 Experimental results	161
4.7 Discussion	173

CHAPTER 5

DETERMINATION OF RESERVOIR ROCK PERMEABILITY.

5.1. Introduction	186
5.2. Routine permeability analysis	189
5.3. High pressure falling-head methodology	192
5.4. High pressure constant-head equipment	192
5.5. High pressure constant-head methodology	193
5.6. Sample morphology	195
5.7. Experimental results	197
5.8. Microfacies analysis	230
5.9. Discussion and conclusions	232

CHAPTER 6

UNDRAINED SHEAR EXPERIMENTS

6.1. Introduction	241
6.2. Resume of the theoretical background of undrained shear behaviour	247
6.3. Previous studies on the undrained shear behaviour of calcareous sediments	254

6.4 . Methodology	266
6. 5. Experimental results	268
6.5.1. Isotropically consolidated samples	269
6.5.2. Anisotropically consolidated samples	277
6.5.3. Strain rate data	289
6.6. Discussion	294
6.6.1. The critical state for an elastic material	298
6.6.2. Influence of consolidation pressure on failure	300
6.6.2.1. Butser Hill	302
6.6.2.2.. Stevn's Klint	307
6.6.3. Influence of method of consolidation on the stress path	309
6.6.4. Influence of consolidation pressure on pore pressure generation	312
6.6.5. The influence of strain rate	315
6.6.6. Failure surface and consolidation path	317
6.7. Conclusions	327

CHAPTER 7

GENERAL DISCUSSION AND CONCLUSIONS

7.1. Introduction	331
7.2. Burial compaction and shear deformation during redeposition	332
7.3. Reservoir compaction and sea floor subsidence	337
7.3.1. Introduction	337
7.3.2. Surface subsidence over chalk oil fields	338
7.3.2.1. History of the Ekofisk subsidence	338
7.3.2.2. Subsidence history of West Ekofisk	340
7.3.2.3. Subsidence history of Valhall	340
7.3.2.4. Causes of the sea floor subsidence	340
7.3.3. Analysis and prediction of subsidence	342

7.3.3.1. The finite element models	342
7.3.3.1.1. The geology and model geometries	342
7.3.3.1.2. Mechanical behaviour of the reservoir rock	343
7.3.3.1.3. Mechanical behaviour of the overburden rock	345
7.3.3.1.4. Pore fluid pressures	347
7.3.3.2. Running the analysis	347
7.3.4. Results	347
7.3.4.1. Ekofisk subsidence	348
7.3.4.2. West Ekofisk subsidence	252
7.3.4.3. Eldfisk subsidence	352
7.3.4.4. Valhall subsidence	354
7.3.5. Discussion of chalk oil field compaction and subsidence	354
7.4. Flow of chalk in the near well bore region	357

BIBLIOGRAPHY	359
--------------------	-----

APPENDIX 1. Geological characterisation of outcrop chalks	369
---	-----

FIGURES.

Figure. 1.1. Location map of the Greater Ekofisk area.

Figure. 2.1. Structural map for the Late Cretaceous. (After Hancock, 1987.)

Figure. 3.1. Location map of the Greater Ekofisk Area.

Figure. 3.2. Schematic map indicating the predominant direction of sediment transportation and re-deposition during the deposition of the Tor Formation Chalks. (After Kennedy, 1987 a/b.)

Figure. 3.3. Four maps indicating the increasing intensity of allochthonous deposition, particularly around the Lindesnes Ridge, during the deposition of the Tor Formation Chalks. (After Hatton, 1986.)

Figure. 3.4. Schematic map indicating the predominant direction of sediment transportation and re-deposition during the deposition of the Lower Ekofisk Formation Chalks. (After Kennedy, 1987 a/b.)

Figure. 3.5. Schematic map based on isopach thicknesses indicating re-deposition during the deposition of the Upper Ekofisk Formation Chalks. (After Hatton, 1986.)

Figure. 3.6. Burial/effective stress curves assuming that overpressuring is related to burial rate, migration of hydrocarbons and increasing maturation pressure. (After Watts, 1983.)

Figure. 3.7. A generalised stratigraphic correlation between the chalks of the North Sea and those found in South East England.

Figure. 3.8. A log of well 2/7-B11 constructed to indicate facies control on fracture development.

Figure. 4.1. Graph of horizontal effective stress/vertical effective stress for a 38% porosity chalk.

Figure. 4.2. Graph of horizontal effective stress/vertical effective stress for three sample with different initial porosities (28, 38 and 48%).

Figure. 4.3. Graph of deviatoric stress/mean effective stress for a 38% porosity chalk.

Figure. 4.4. Graph of deviatoric stress/mean effective stress for a 48% porosity chalk.

Figure. 4.5. Graph of deviatoric stress/mean effective stress for a 28% porosity chalk.

Figure. 4.6. Graph of deviatoric stress/mean effective stress for three samples with different initial porosities (28, 38% and 48%).

Figure. 4.7. Graph of void ratio/mean effective stress for a 38% porosity chalk.

Figure. 4.8. Graph of void ratio/mean effective stress for a 28% porosity chalk.

Figure. 4.9. Graph of void ratio/mean effective stress for a 48% porosity chalk.

Figure. 4.10. Graph of void ratio/mean effective stress for three samples with different initial porosities (28, 38 and 48%).

Figure. 4.11. Cam Clay model (After Atkinson and Bransby, 1978).

Figure. 4.12. Schematic representation of the high triaxial cell used during this study.

Figure. 4.13. Sectioned drawing of a balanced ram.

Figure. 4.14. Schematic representation of a radial strain belt.

Figure. 4.15. Sectioned drawing of an Imperial College volume gauge.

Figure. 4.16. Schematic drawing of a sample assembled in the triaxial cell.

Figure. 4.17. Graph of vertical effective stress/axial strain for slow strain-rate experiment ELONGC1.

Figure. 4.18. Graph of horizontal effective stress/vertical effective stress for slow strain-rate experiment ELONGC1.

Figure. 4.19. Graph of deviatoric stress/mean effective stress for slow strain-rate experiment ELONGC1.

Figure. 4.20. Graph of void ratio/mean effective stress for slow strain-rate experiment ELONGC1.

Figure. 4.21. Graph of vertical effective stress/axial strain for slow strain-rate experiment ELONGC2.

Figure. 4.22. Graph of horizontal effective stress/vertical effective stress for slow strain-rate experiment ELONGC2.

Figure. 4.23. Graph of deviatoric stress/mean effective stress for slow strain-rate experiment ELONGC2.

Figure. 4.24. Graph of void ratio/mean effective stress for slow strain-rate experiment ELONGC2.

Figure. 4.25. Graph of vertical effective stress/axial strain for slow strain-rate experiment ELONGC3.

Figure. 4.26. Graph of horizontal effective stress/vertical slow strain-rate effective stress for experiment ELONGC3.

Figure. 4.27. Graph of deviatoric stress/mean effective stress for slow strain-rate experiment ELONGC3.

Figure. 4.28. Graph of void ratio/mean effective stress for slow strain-rate experiment ELONGC3.

Figure. 4.29. Graph of vertical effective stress/axial strain for slow strain-rate experiment ELONGC4.

Figure. 4.30. Graph of horizontal effective stress/vertical effective stress for slow strain-rate experiment ELONGC4.

Figure. 4.31. Graph of deviatoric stress/mean effective stress for slow strain-rate experiment ELONGC4.

Figure. 4.32. Graph of void ratio/mean effective stress for slow strain-rate experiment ELONGC4.

Figure. 4.33. Graph of vertical effective stress/axial strain which compares the result of slow strain-rate experiment ELONGC1 with samples of equivalent initial porosities.

Figure. 4.34. Graph of vertical effective stress/axial strain which compares the result of slow strain-rate experiment ELONGC2 with samples of equivalent initial porosities.

Figure. 4.35. Graph of vertical effective stress/axial strain which compares the result of slow strain-rate experiment ELONGC3 with samples of equivalent initial porosities.

Figure. 4.36. Graph of vertical effective stress/axial strain which compares the result of slow strain-rate experiment ELONGC4 with samples of equivalent initial porosities.

Figure. 4.37. Graph of vertical effective stress/axial strain for stress relaxation experiment VOBC5.

Figure. 4.38. Graph of vertical effective stress/axial strain for stress relaxation experiment VOBC7.

Figure. 4.39. Graph of vertical effective stress/axial strain for stress relaxation experiment VOHC2.

Figure. 4.40. Graph of vertical effective stress/axial strain for stress relaxation experiment VOHC3.

Figure. 4.41. Graph of vertical effective stress/axial strain for stress relaxation experiment VOTC1.

Figure. 4.42. Graph of horizontal effective stress/vertical effective stress for stress relaxation experiment VOBC5.

Figure. 4.43. Graph of horizontal effective stress/vertical effective stress for stress relaxation experiment VOBC7.

Figure. 4.44. Graph of horizontal effective stress/vertical effective stress for stress relaxation experiment VOHC2.

Figure. 4.45. Graph of horizontal effective stress/vertical effective stress for stress relaxation experiment VOHC3.

Figure. 4.46. Graph of horizontal effective stress/vertical effective stress for stress relaxation experiment VOTC1.

Figure. 4.47. Graph of deviatoric stress/mean effective stress for stress relaxation experiment VOBC5.

Figure. 4.48. Graph of deviatoric stress/mean effective stress for stress relaxation experiment VOBC7.

Figure. 4.49. Graph of deviatoric stress/mean effective stress for stress relaxation experiment VOHC2.

Figure. 4.50. Graph of deviatoric stress/mean effective stress for stress relaxation experiment VOHC3.

Figure. 4.51. Graph of deviatoric stress/mean effective stress for stress relaxation experiment VOTC1.

Figure. 4.52. Graph of void ratio/mean effective stress for stress relaxation experiment VOBC5.

Figure. 4.53. Graph of void ratio/mean effective stress for stress relaxation experiment VOBC7.

Figure. 4.54. Graph of void ratio/mean effective stress for stress relaxation experiment VOHC2.

Figure. 4.55. Graph of void ratio/mean effective stress for stress relaxation experiment VOHC3.

Figure. 4.56. Graph of void ratio/mean effective stress for stress relaxation experiment VOTC1.

Figure. 4.57. Graph of vertical effective stress/axial strain for water injection experiment EC18/26A.

Figure. 4.58. Graph of vertical effective stress/axial strain for water injection experiment EC18/26B.

Figure. 4.59. Graph of vertical effective stress/axial strain for water injection experiment EC25/29.

Figure. 4.60. Graph of horizontal effective stress/vertical effective stress for water injection experiment EC18/26A.

Figure. 4.61. Graph of horizontal effective stress/vertical effective stress for water injection experiment EC18/26B.

Figure. 4.62. Graph of horizontal effective stress/vertical effective stress for water injection experiment EC25/29.

Figure. 4.63. Graph of deviatoric stress/mean effective stress for water injection experiment EC18/26A.

Figure. 4.64. Graph of deviatoric stress/mean effective stress for water injection experiment EC18/26B.

Figure. 4.65. Graph of deviatoric stress/mean effective stress for water injection experiment EC25/29.

Figure. 4.66. Graph of radial strain/axial strain for water injection experiment EC18/26A.

Figure. 4.67. Graph of radial strain/axial strain for water injection experiment EC18/26B.

Figure. 4.68. Graph of radial strain/axial strain for water injection experiment EC25/29.

Figure. 4.69. Graph of void ratio/mean effective stress for water injection experiment EC18/26A.

Figure. 4.70. Graph of void ratio/mean effective stress for water injection experiment EC18/26B.

Figure. 4.71. Graph of void ratio/mean effective stress for water injection experiment EC25/29.

Figure. 4.72. Schematic effective stress/void ratio diagram indicating the compactional behaviour of two chinks (After Addis and Jones, 1989).

Figure. 4.73. Schematic effective stress/void ratio diagram indicating the compactional behaviour of three chinks proposed from the results of the current study.

Figure. 4.74. Effective stress/void ratio plot of a group of uniaxial strain experiments.

Figure. 4.75. The same data as shown in figure 4.74 but with the data projected on to the effective stress/void ratio planes.

Figure. 4.76. A set of 'standard' vertical effective stress/axial strain curves compiled from data determined during the present study.

Figure. 4.77. Plot of the yield behaviour of an artificially bonded material deformed under uniaxial strain conditions compared to that of a similar unbonded sample. (After Vaughan, et al.,1988.)

Figure. 4.78. Uniaxial and isotropically consolidated Butser Hill chalks presented in void ratio/mean effective stress space.

Figure. 4.79. Schematic porosity cross-section.

Figure. 5.1. Data sheet for permeability experiment NHEC1.

Figure. 5.2. Data sheet for permeability experiment NHEC2B.

Figure. 5.3. Data sheet for permeability experiment NHEC3B.

Figure. 5.4. Data sheet for permeability experiment NHEC5.

Figure. 5.5. Data sheet for permeability experiment NHEC6.

Figure. 5.6. Data sheet for permeability experiment NHEC10

Figure. 5.7. Data sheet for permeability experiment NHEC21B.

Figure. 5.8. Data sheet for permeability experiment NHEC24.

Figure. 5.9. Data sheet for permeability experiment NEOC1.

Figure. 5.10. Data sheet for permeability experiment NEOC3.

Figure. 5.11. Data sheet for permeability experiment NEOC6.

Figure. 5.12. Data sheet for permeability experiment NEOC7.

Figure. 5.13. Data sheet for permeability experiment NEOC8.

Figure. 5.14. Data sheet for permeability experiment NEOC9.

Figure. 5.15. Data sheet for permeability experiment NEOC11.

Figure. 5.16. Data sheet for permeability experiment NEOC12.

Figure. 5.17. Data sheet for permeability experiment NEOC14.

Figure. 5.18. Data sheet for permeability experiment NEOC15.

Figure. 5.19. Data sheet for permeability experiment NEOC16.

Figure. 5.20. Data sheet for permeability experiment NEOC17.

Figure. 5.21. Data sheet for permeability experiment NEOC18.

Figure. 5.22. Data sheet for permeability experiment NEOC19.

Figure. 5.23. Data sheet for permeability experiment NEOC21.

Figure. 5.24. Data sheet for permeability experiment NEOC22.

Figure. 5.25. Sedimentology versus FDC/CNL logs, porosity and permeability data in wells a) 2/4-A8, and b) 2/4-C8.

Figure. 5.26. A graph of porosity/permeability for each of the samples tested during the present experimental programme. The points represent the porosity and permeability recorded at a vertical effective stress of 14MPa. This graph also includes the porosity/permeability decreases observed by Addis (1987) during uniaxial experiments conducted on North Sea chalk samples and the trendline established by Scholle (1977) for pure chalk. (Based on Addis, 1987.)

Figure. 6.1. Annotated, schematic cross-section of the chalk-flow at Abbotts Cliff.

Figure. 6.2. A schematic representation of the fluid and stress changes around a well perforation during a "shut-in".

Figure. 6.3. An isometric diagram of the Hvorslev Surface as defined by undrained shear box experiments (After Roscoe et al., 1958.)

Figure. 6.4. Deviatoric stress/mean effective stress plots for undrained shear experiments on, a) Leighton Buzzard Sand, b) Dogs Bay carbonate sand, c) Ballyconneely Sand, d) Bombay Mix. (After Golightly and Hyde, 1988.)

Figure. 6.5. Deviatoric stress/mean effective stress plots of calcarenites from the North Rankin 'A' site, Australia. a) Three isotropically consolidated undrained shear experiments, b) anisotropically consolidated undrained shear experiments, c) an isotropically consolidated sample that was allowed to swell back to a lower pressure before being subject to undrained shear. (After Fahey, 1988.)

Figure. 6.6. Deviatoric stress/mean effective stress plots of calcarenites from the North Rankin 'A' site, Australia. a) An isotropically consolidated undrained shear experiment in which unload/reload cycles of the deviatoric stress were performed, b) an anisotropically consolidated undrained shear experiment. (After Carter et al., 1988.)

Figure. 6.7. Static undrained shear tests a) before and b) after cyclic loading. (After Dobry et al., 1988.)

Figure. 6.8. Yield surface proposed by Dunbaven (1988).

Figure. 6.9. Deviatoric stress/axial strain plot showing the effects of different grain size distributions during undrained shear. a) Uniform grain size distribution from clay size

to gravel, b) grain size concentrated between fine sand and silt. (After Tsuchida et al., 1988.)

Figure. 6.10. Graph of deviatoric stress/axial strain for isotropically consolidated undrained shear experiments on Butser Hill outcrop samples.

Figure. 6.11. Graph of deviatoric stress/axial strain for isotropically consolidated undrained shear experiments on Stevn's Klint outcrop samples.

Figure. 6.12. Graph of pore pressure/mean effective stress for isotropically consolidated undrained shear experiments on Butser Hill samples.

Figure. 6.13. Graph of pore pressure/mean effective stress for isotropically consolidated undrained shear experiments on Stevn's Klint samples.

Figure. 6.14. Graph of pore pressure/axial strain for isotropically consolidated undrained shear experiments on Butser Hill samples.

Figure. 6.15. Graph of pore pressure/axial strain for isotropically consolidated undrained shear experiments on Stevn's Klint samples.

Figure. 6.16. Graph of deviatoric stress/pore pressure for isotropically consolidated undrained shear experiments on Butser Hill samples.

Figure. 6.17. Graph of deviatoric stress/pore pressure for isotropically consolidated undrained shear experiments on Stevn's Klint samples.

Figure. 6.18. Deviatoric stress/mean effective stress graph for isotropically consolidated undrained shear experiments on Butser Hill samples.

Figure. 6.19. Deviatoric stress/mean effective stress graph for isotropically consolidated undrained shear experiments on Stevn's Klint samples.

Figure. 6.20. Graph of void ratio/mean effective stress for isotropically consolidated undrained shear experiments on Butser Hill samples.

Figure. 6.21. Graph of void ratio/mean effective stress for isotropically consolidated undrained shear experiments on Stevn's Klint samples.

Figure. 6.22. Graph of deviatoric stress/axial strain for anisotropically (K_o) consolidated undrained shear experiments on Butser Hill samples. (After Addis, 1987.)

Figure. 6.23. Graph of deviatoric stress/axial strain for anisotropically (K_o) consolidated undrained shear experiments on Stevn's Klint samples.

Figure. 6.24. Graph of pore pressure/mean effective stress for anisotropically (K_0) consolidated undrained shear experiments on Butser Hill samples. (After Addis, 1987.)

Figure. 6.25. Graph of pore pressure/mean effective stress for anisotropically (K_0) consolidated undrained shear experiments on Stevn's Klint samples.

Figure. 6.26. Graph of pore pressure/axial strain for anisotropically (K_0) consolidated undrained shear experiments on Butser Hill samples. (After Addis, 1987.)

Figure. 6.27. Graph of pore pressure/axial strain for anisotropically (K_0) consolidated undrained shear experiments on Stevn's Klint samples.

Figure. 6.28. Graph of deviatoric stress/pore pressure for anisotropically (K_0) consolidated undrained shear experiments on Butser Hill sample. (After Addis, 1987.)

Figure. 6.29. Graph of deviatoric stress/pore pressure for anisotropically (K_0) consolidated undrained shear experiments on Stevn's Klint samples.

Figure. 6.30. Deviatoric stress/mean effective stress graph for anisotropically (K_0) consolidated undrained shear experiments on Butser Hill samples. (After Addis, 1987.)

Figure. 6.31. Deviatoric stress/mean effective stress graph for anisotropically (K_0) consolidated undrained shear experiments on Stevn's Klint samples.

Figure. 6.32. Graph of void ratio/mean effective stress for anisotropically (K_0) consolidated undrained shear experiments on Butser Hill samples. (After Addis, 1987.)

Figure. 6.33. Graph of void ratio/mean effective stress for anisotropically (K_0) consolidated undrained shear experiments on Stevn's Klint samples.

Figure. 6.34. Graph of radial strain/axial strain for anisotropically (K_0) consolidated undrained shear experiments on Butser Hill samples. (After Addis, 1987.)

Figure. 6.35. Graph of radial strain/axial strain for anisotropically (K_0) consolidated undrained shear experiments on Stevn's Klint samples.

Figure. 6.36. Graph of deviatoric stress/axial strain for undrained shear experiments conducted at three different strain rates on samples of Butser Hill outcrop chalk.

Figure. 6.37. Graph of pore pressure/mean effective stress for undrained shear experiments conducted at three different strain rates on Butser Hill outcrop chalk.

Figure. 6.38. Deviatoric stress/mean effective stress graph for undrained shear experiments conducted at three different strain rates on Butser Hill outcrop chalk.

Figure. 6.39. Graph of void ratio/mean effective stress for undrained shear experiments conducted at three different strain rates on Butser Hill outcrop chalk.

Figure. 6.40. Combined stress path diagram for both the Butser Hill and Stevn's Klint isotropically consolidated samples.

Figure. 6.41. Stress path diagram indicating the proposed position of the elastic yield envelope for the Butser Hill samples.

Figure. 6.42. Stress path diagram indicating the proposed position of the elastic yield envelope for the Stevn's Klint samples.

Figure. 6.43. Combined stress path diagram for isotropically and anisotropically consolidated Butser Hill samples. (Anisotropically consolidated samples, after Addis, 1987.)

Figure. 6.44. Combined stress path diagram for isotropically and anisotropically consolidated Stevn's Klint samples.

Figure. 6.45. a) A Butser Hill sample consolidated using the step-wise method. b) The same curve in relation to the other Butser Hill samples isotropically consolidated using the ramp method.

Figure. 6.46. Top and bottom pore pressures generated during undrained shear for isotropically consolidated Stevn's Klint sample SKWC10.

Figure. 6.47. Top and bottom pore pressures generated during undrained shear of anisotropically (K_0) consolidated Stevn's Klint sample SKWC9.

Figure. 6.48. Values of Skempton's pore pressure parameter 'A' plotted against the maximum consolidation pressure for each of the Butser Hill isotropically consolidated samples.

Figure. 6.49. Values of Skempton's pore pressure parameter 'A' plotted against the maximum consolidation pressure for each of the Stevn's Klint isotropically consolidated samples.

Figure. 6.50. The isotropically consolidated Butser Hill experiments plotted against axes of void ratio/mean effective and deviatoric stress.

Figure. 6.51. The isotropically consolidated Stevn's Klint experiments plotted against axes of void ratio/mean effective and deviatoric stress.

Figure. 6.52. The isotropically and anisotropically (K_o) consolidated Butser Hill experiments plotted against axes of void ratio/mean effective and deviatoric stress.

Figure. 6.53. The isotropically and anisotropically consolidated Stevn's Klint experiments plotted against axes of void ratio/mean effective and deviatoric stress.

Figure. 6.54. The isotropically consolidated Butser Hill experiments plotted against axes of void ratio/mean effective and deviatoric stress, in which volume changes have been allowed during data processing, so that the stress paths follow the Critical State Line.

Figure. 6.55. The isotropically consolidated Stevn's Klint experiments plotted against axes of void ratio/mean effective and deviatoric stress, in which volume changes have been allowed during data processing, so that the stress paths follow the Critical State Line.

Figure. 6.56. Both sets of isotropically consolidated experiments plotted together in void ratio/mean effective and deviatoric stress space.

Figure. 7.1. Idealised compaction path for the North Sea Chalk.

Figure. 7.2 Ekofisk subsidence history.

Figure. 7.3. The Ekofisk reservoir model showing the layered porosity structure that was determined from the well-logs.

Figure. 7.4. The Ekofisk finite element mesh, with an expanded scale diagram for the reservoir section.

Figure. 7.5. Schematic representation of the variation of pore fluid pressure with depth over the Ekofisk Area chalk reservoirs, before (curve B), and after (curve A) a period of production. The geometry of the dotted part of the profile is unknown, but is widely held to be confined to narrow depth interval.

Figure. 7.6. Predicted reservoir compaction for the no gas injection (a) and gas injection (b) analyses for Ekofisk.

Figure. 7.7. Predicted sea floor subsidence for the no gas injection (a) and gas injection (b) cases for Ekofisk.

Figure. 7.8. Pattern of displacements that develops over the Ekofisk Oil field as a result of reservoir compaction.

Figure. 7.9. The changes in total vertical stress that occurs over the Ekofisk Oil Field as a consequence of reservoir compaction.

Figure. 7.10. Reservoir compaction and sea-floor subsidence predicted by a plane strain analysis of a short axis cross-section of the Ekofisk Oil Field.

Figure. 7.11. Displacements that develop over the West Ekofisk Oil Field as a consequence of reservoir compaction.

Figure. 7.12. Pattern of changes in total vertical stress that occur over the smaller West Ekofisk Oil Field as a consequence of reservoir compaction.

Figure. 7.13. The pattern of displacements that were modelled to develop over the Eldfisk Oil Field as a consequence of reservoir compaction.

Figure. 7.14. The pattern of changes in the total vertical stress that were predicted to occur over the Eldfisk Field as a consequence of compaction.

Figure. 7.15. The stress arch that develops due to compaction of the reservoir units in the Valhall model.

PLATES.

Plate 3.1. A periodite destroyed by bioturbation.

Plate 3.2. An example of the alternating depositional fabric of a periodite.

Plate 3.3. The Ekofisk Formation basal conglomerate.

Plate 3.4. A periodite in which pressure solution is observed to emphasise the primary laminations.

Plate 3.5. Inclined strata indicating the presence of a slide.

Plate 3.6. A small-scale slump further deformed by dewatering.

Plate 3.7. An example of post-depositional brecciation.

Plate 3.8. Small-scale shearing of a slump resulting in a shredded appearance.

Plate 3.9. Faulting in a chalk which sustained a high fluid content at the time.

Plate 3.10. Faulting in a competent chalk.

Plate 3.11. An example of a matrix supported debris flow.

Plate 3.12. An example of a coarse debris flow in which the matrix content is small.

Plate 3.13. An example of a water escape structure in a homogeneous chalk.

Plate 3.14. An example of a thin turbidite.

Plate 3.15. An alternating sequence of high porosity soft chalks (dark) and low porosity (light), bioturbated pelagic sediments.

Plate 3.16. A water escape structure close to the Ekofisk/Maureen Formation boundary.

Plate 3.17. An example of slickensides of a fracture face.

Plate 4.1. Scanning electron micrograph for a sample of Stevn's Klint chalk subject to approximately 28% axial strain.

Plate 4.2. Scanning electron micrograph for a sample of Stevn's Klint chalk subject to approximately 28% axial strain.

Plate 4.3. Scanning electron micrograph for a sample of Stevn's Klint chalk subject to approximately 28% axial strain.

Plate 5.1. a) Scanning electron micrographs of sample NEOC19 (figure 5.23) before uniaxial deformation, b) Scanning electron micrograph of sample NEOC19 following uniaxial deformation to an effective stress of 75MPa. Note the irregularity in the distribution of the deformation.

Plate 5.2. a) Scanning electron micrograph of sample NEOC6 (figure 5.11) before uniaxial deformation, b) Scanning electron micrograph of sample NEOC6 following uniaxial deformation to a vertical effective stress of 36MPa.

Plate 6.1. The chalk-flow at Abbotts Cliff which exhibits a form similar to a typical mudflow.

Plate 6.2. Sample BHW8 isotropically consolidated to 3MPa before being subject to undrained shear. Note the formation of large discrete shear planes.

Plate 6.3. Sample BHW3 isotropically consolidated to 10MPa before being subject to undrained shear. Note the formation of small discrete blocks that appear to have 'flowed' in a ductile manner.

Plate 6.4. A Butser Hill sample isotropically consolidated to 20MPa (BHW2). The sample contains no visible shears but has distorted around the tops of the inner membranes.

Plate 6.5. Sample BHWC4, isotropically consolidated to 40MPa. Undrained shear has resulted in a barrel shaped sample.

Plate 6.6. All of the isotropically consolidated Butser Hill samples showing a progressive change in the style of deformation with increasing consolidation pressure (left to right).

Plate 6.7. Three Stevn's Klint samples subject to undrained shear following isotropic consolidation to a) 1MPa (SKWC6), b) 2.8MPa (SKWC8), and c) 5.3MPa (SKWC7). Note all three sample have developed conjugate shears.

Plate 6.8. Two Stevn's Klint samples subject to undrained shear following isotropic consolidation to a) 9.5MPa (SKWC10) and b) 19.4MPa (SKWC5). These samples were observed to be extremely soft and had clearly distorted around the edges of the inner membranes.

Plate 6.9. Sample SKWC1, isotropically consolidated to 40MPa before shearing.

Plate 6.10. Enlargement showing the distortion around the top of the inner membranes on a Stevn's Klint sample.

TABLES.

Table 4.1. Uniaxial strain experimental data.

Table 4.2. Data for the slow strain-rate experiments.

Table 4.3. Water injection experimental data.

Table 5.1. Published permeability data for the chalks of the North Sea.

Table 5.2. Values taken for the viscosity and density of the hydrocarbons used as a permeant.

Table 5.3. Permeability experimental data.

Table 6.1. Undrained shear experimental data.

Table 6.2. Undrained shear, strain\rate experimental data.

Table 6.3a. Effects of increasing consolidation pressure (σ_3').

Table 6.3b. Effects of increasing consolidation pressure (σ_3').

Table 6.4. Typical values of Skempton's pore pressure parameter 'A' in a fully saturated soil. (After Lambe and Whitman, 1979).

Table 6.5. Pore pressure parameter 'A' data calculated for chalk samples at failure.

CHAPTER 1

INTRODUCTION.

1. INTRODUCTION

1.1. RESEARCH OBJECTIVES.

This thesis originated from a need to determine, through experimental studies, the mechanical behaviour of hydrocarbon bearing chalks. The mechanical behaviour of these chalks had already been identified as the cause of problems associated with the production of hydrocarbons from the chalk reservoirs in the Norwegian Sector of the North Sea. These reservoir chalks are located in the Greater Ekofisk Area (figure 1.1).

The research reported in the following chapters has extended the dataset of Addis (1987) through the use of both onshore and offshore chalks with a large spatial and temporal range; a wider distribution of sedimentological and diagenetic features; and a wide range of initial chalk porosities. Previous studies (Addis, 1987; Johnson and Rhett, 1986; Johnson et al., 1988; Jones et al., 1985a, 1985b, 1986, 1987b, 1989; Ruddy et al., 1988; Leddra, 1987, 1988; Leddra et al., 1989a) which have investigated the deformation of the chalk have concentrated on defining their behaviour using either the uniaxial strain (where the material is compacted under conditions of no lateral strain) or isotropic (equal vertical and horizontal stresses) stress paths. Other stress paths, particularly undrained triaxial shear, appear to have been regarded as of only secondary importance. This present study was designed to expand the available uniaxial strain data and investigate the response of these naturally cemented sedimentary rocks to the application of large triaxial shear stresses under undrained conditions. These latter experiments were conducted on two different high porosity outcrop chalks in which samples from the same chalk were considered to be essentially identical. They enabled a pattern of behaviour in response to shearing at different consolidation pressures to be established. Consolidation was achieved under conditions of either uniaxial strain or isotropic stress. This helped to provide a link between data following each of the three stress paths used.

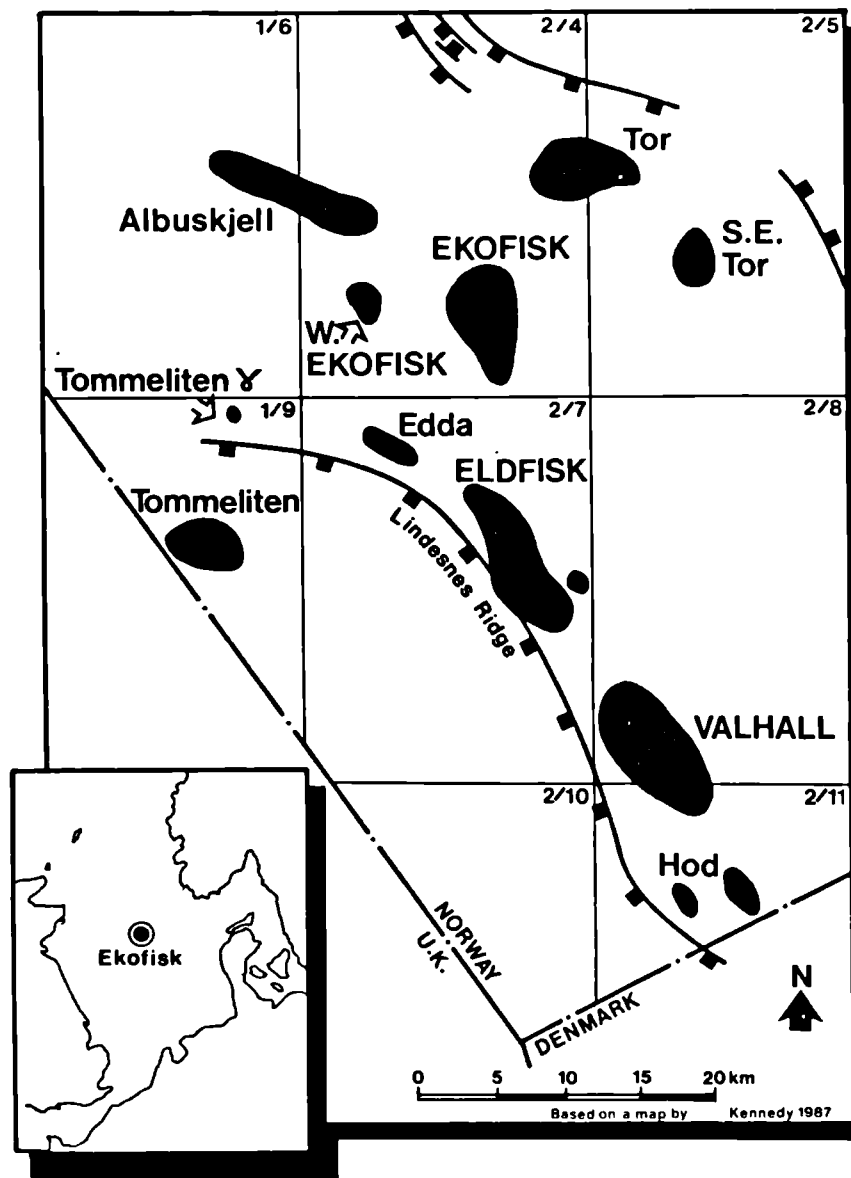


Figure. 1.1. Location map of the Greater Ekofisk area.

There is a need for a well defined set of mechanical data for porous cemented sedimentary rocks. Fulfilling this need is a fundamentally important part of the experimental programme reported below.

1.2. ORGANISATION OF THESIS.

This thesis has been divided into two parts. The first part, which comprises of two chapters, introduces and discusses the modes of deposition and diagenesis pertaining to both onshore and offshore chalks. It is therefore primarily a literature review.

The first of these chapters (chapter two) reviews the mechanisms, which are considered to be common to all chalks, by which porosity decreases following the initial deposition. This includes a discussion of the processes of mechanical and biological compaction as well as the effects of shallow burial diagenesis.

Chapter three is concerned with the formation of the chalks that are found in the Central Graben of the North Sea. These chalks reveal a number of significant sedimentological and diagenetic differences compared to onshore chalks. These differences are reviewed, and where the literature presents more than one opinion these are discussed. Fractures are observed to be an important factor in hydrocarbon emplacement and subsequent production from this low permeability rock. Chapter three also contains a section discussing the nature and distribution of fractures in relation to sedimentological and diagenetic fabrics. A log, constructed for one of the longest and most complete cores recovered from the chalk fields, forms the basis for this discussion. Where necessary observations from other cores are included.

The second part of this thesis, comprises four chapters, which report and discuss the results of the experimental programme.

Chapter four concentrates on uniaxial strain experiments conducted using chalk samples recovered from all three of the reservoir formations (Hod and Tor Formations

(Cretaceous) and Ekofisk (Tertiary)) from four of the nine fields that comprise the Greater Ekofisk Area (figure 1.1). These data include an investigation of strain rate, stress relaxation and the effects of replacing the hydrocarbon pore fluid with unconditioned sea water.

Chapter five extends this uniaxial test procedure into a study concerned with the determination of vertical permeability using the constant head method. These experiments were specifically designed to study permeability changes, that are a consequence of the increases in vertical effective stress, that develop in these oil fields due to pore pressure reduction during hydrocarbon production. For this part of the study samples were chosen that contained many of the sedimentological and diagenetic features reviewed in chapter three.

Chapter six presents the undrained shear experiments. Although a limited number of similar experiments have been previously conducted (Addis, 1987; (two of which are used here for comparative purposes) Clayton, 1978 (using remoulded chalk) these experiments constitute the largest (to date) systematic study of the undrained shear behaviour of chalk.

The final chapter (chapter seven) discusses the experimental data presented in chapters four, five and six with particular reference to processes of shear and compaction operative during burial of the chalk and those presently occurring as a consequence of hydrocarbon extraction.

The data presented in this thesis are applicable to the understanding and solution of a number of engineering problems. These include compaction of hydrocarbon reservoir forming chinks; well invasion and solids production in hydrocarbon reservoirs; collapse and flow of chalk during cliff falls; mechanisms of compaction and shear operative during deposition and burial of the chalk; stability problems during the construction of

chalk embankments and fills. Application of these data to engineering problems are described briefly in the following section.

1.3. SCIENTIFIC RATIONALE.

In the study reported below, laboratory experiments are used to evaluate the deformation characteristics of porous chalks. The experiments have been designed to explore both the compaction and shear behaviour of this material. This laboratory study was undertaken to quantify the important engineering and geological processes listed in the previous paragraph.

The hydrocarbon reservoirs of the Greater Ekofisk Area are predominantly composed of Upper Cretaceous and Tertiary chalks. These exhibit a wide range of sedimentological fabrics indicating shear and large-scale movement of sediments. This is thought to have occurred shortly after initial deposition on a gently dipping slope. Mass movement is thought to have been triggered by either earthquake activity (Hatton, 1986) or changes in the inclination of the continental shelf due to fault movements (Kennedy, 1983; Brewster and Dangerfield, 1984). A number of mass movement fabrics have been identified. These include slides, slumps, debris flows and turbidites (Kennedy, 1980, 1985, 1986, 1987a, 1987b), indicating progressive disaggregation of the sediments away from the original site of deposition. Many of these sediments (particularly the clasts in the debris flows) are observed to retain elements of an early cemented structure (Taylor and Lapre, 1987; Kennedy, 1987a; Pederstad et al., 1988). The existence of an original cement structure indicates that mass movement involved the chalk after it had been buried but when it still retained a high porosity. As the chalk is observed to exhibit low permeabilities (see chapter five), these sediments, which exhibit a wide spectrum of deformation fabrics (including convoluted bedding, folding and shearing), would have moved, beneath an overburden, under undrained or partially drained conditions. It is envisaged that the stability of the overburden was also compromised by this movement.

Undrained shear is thought to be an important process in the engineering environment. The talus resulting from cliff-falls to the east of Folkestone, Kent, exhibit many of the depositional fabrics observed in debris flows. Hutchinson (1980, 1983, 1988, 1989) has proposed that this debris formed under conditions of undrained shear as the chalk impacted on the wave-cut platform at the base of the cliff. Larger run-outs have resulted from these falls than those associated with other types of cliff-falls in the chalk.

Serious stability problems are also encountered during the construction of chalk embankments and fills. The cement structure of the chalk may be broken down by artificial compaction, vibration, excessive handling or the weight of the construction plant (Parsons and Broad, 1970; Ingoldby, 1978; Perry, 1978; Thomson and Buthee, 1989; Clayton, 1989; Rat and Schaeffner, 1989; Guy, 1989; Stroud and Mitchell, 1989; Privett, 1989). This break down frequently leads to a collapse and the transference of the load, temporarily, from the chalk structure to the pore fluid. The resulting excess pore pressure will persist until the permeability of the chalk allows it to dissipate. Once this has been achieved the 'putty chalk' reverts to a stable condition.

Undrained shear has been proposed as the method by which high porosity reservoir chalks fail and flow into the well-bore when the fluid pressure is drawn-down following the 'shut-in' of a well (Ruddy et al., 1988; Leddra and Jones, 1989). As the fluid pressure in the well is reduced the horizontal stress decreases. The resulting excess pore pressure cannot be dissipated immediately, therefore a pore pressure gradient develops in the chalks adjacent to the well and chalk flows into the well bore. Once the excess pore pressure has dissipated, the chalk behaves in a similar manner to that described above.

Compaction occurred naturally following the initial deposition of the 'chalk ooze' (Neugerbauer, 1973, 1974; Hardman, 1982; Hancock, 1983; Scholle et al., 1983; Clayton, 1989) through various processes. These include mechanical compaction (consolidation) (Hancock, 1983; Scholle et al., 1983) which leads to the onset of early pres-

sure solution (Neugebauer, 1973, 1974; Mapstone, 1975; Taylor and Lapre, 1987) which is believed to lead to the formation of the cement structure, and bioturbation (biological compaction) (Hancock, 1983; Scholle et al., 1983).

Compaction has also been observed to be an important consequence of pore pressure reduction due to fluid extraction (Jones et al., 1987; Jones and Leddra, 1987; Addis, 1987; Johnson and Rhett, 1986; Thomas et al., 1987). This includes the removal of water from aquifers (Wilson and Grace, 1942; Zeevaert, 1953; Belfiore et al., 1989; Barends and Spierenburg, 1989) and hydrocarbons from reservoirs (Jones et al., 1987, 1989a, 1989b; Sulak and Danielsen, 1988; Potts et al., 1988; Berget et al., 1989; D'Heur, 1989). Compaction of an aquifer or reservoir may have both beneficial and detrimental effects on the continuity of production. As the chalk compacts, the decrease in porosity is predicted to lead to a decrease in permeability (Jones, 1989) and the closure of fractures. In a number of reservoirs, production has been enhanced by the addition of compaction drive (Ruddy et al., 1988; Berget et al., 1989). A serious consequence of compaction of both chalk aquifers and reservoirs is subsidence of the land surface. Subsidence is a serious problem in the Netherlands (Van Den Bosch, 1983; Schoonbeck, 1976; Van Kersternen, 1973a, 1973b, De Loos, 1973) where extraction of water and hydrocarbons has led to an increased risk of flooding in areas already below sea level. Subsidence due to hydrocarbon extraction has been recorded for a number of reservoirs throughout the world (see the reviews in Jones et al., 1987; Addis, 1987). In the North Sea, surface subsidence resulting from compaction of chalk reservoirs has been identified as a serious problem. Many studies have been undertaken (Boade and Chin, 1986; Boade et al., 1988; Johnson et al., 1988; Potts et al., 1988; Jones et al., 1985a, 1985b, 1986, 1987b, 1989; Ruddy et al., 1988; Leddra, 1987, 1988; Leddra et al., 1989a; Barton, 1985, 1986) to determine the nature and magnitude of this phenomenon for a number of the oil fields in the Greater Ekofisk Area (figure 1.1). Subsidence has been recorded over Ekofisk (Rentsch and Mes, 1988; Jewhurst and Wiborg, 1988; Aam, 1988), Valhall (Ruddy et al., 1988) and West Ekofisk fields (Rentsch and Mes, 1988; Jewhurst and Wiborg, 1988). At Ekofisk vertical displacement of the sea floor could

reach 6m if reservoir pressures are allowed to continue to decline. Remedial action has been taken to minimise damage to the production complex. This has included cutting and extending the legs of the platforms by 6m (Aam, 1988), the injection of water (Brewster et al., 1986; Berget and Tonstad, 1986; Berget et al., 1989), the reinjection of gas (Berget et al., 1989) and the construction of a protective jacket around the central oil storage tank (D'Heur, 1989).

It may be observed from this brief resume of natural and man- induced examples of compaction and shear that these two types of behaviour are particularly important with regard to the chalk. This thesis reports the results of a programme of laboratory experiments which evaluate and quantify this deformation.

PART 1

ON THE NATURE OF CHALK

CHAPTER 2

STRATIGRAPHY AND STRUCTURAL SETTING OF THE CHALKS OF NORTH WEST EUROPE.

2. STRATIGRAPHY AND STRUCTURAL SETTING OF THE CHALKS OF NORTH WEST EUROPE.

2.1. INTRODUCTION.

Variations in the depositional and diagenetic history of a rock, can have a profound influence on its mechanical behaviour (Moshannski and Parabouchev, 1981). It is therefore important in a study of the type reported here to both review and discuss a number of aspects of the geological and geographical environments in which the chalk was deposited. This discussion should consider the components of the rock (both biological and mineralogical), its initial lithification and subsequent diagenesis. The three chalks used in this study followed different diagenetic paths shortly after the period of early lithification. This chapter will include a review which covers those aspects of deposition that are common to all chalks and a brief outline of the sedimentological and diagenetic features of the two outcrop chalks used in this study.

The following chapter will review the diagenetic and sedimentological history of the chalks found in the North Sea. It will be seen that these differ in a profound way to the chalks found onshore.

Chalk has been used as both a stratigraphic and petrographic term.

Hancock (1987) provides the following definition for the chalk in a petrographic sense. 'Chalk is a sediment dominantly composed of skeletal calcite from algae of the phylum Prymnesiophyta, subphylum Haptophyta, popularly known as the golden-brown algae.' He also points out that some authors include an element of hardness into the definition, 'readily deformed under the fingernail or the edge of a spatula blade,' and that if the sediment is harder than this it should be called a 'limestone'. This would mean however, that chalk does not occur in the North Sea. Kennedy (1987b) further defines

the chalk as 'friable to well cemented biomicrites built up mainly of the debris of planktonic haptophycean algae known as coccolithophoids'. With both definitions it can be seen that the chalk is primarily biogenic in origin. This means that many of the sediments described as chalks such as the shallow-water, predominantly 'chalky white' dolosilts and dolomitised limestones in the Middle East (Hancock and Hubbard, 1980) which are primarily formed by chemical precipitation cannot strictly be regarded as such, although some chalks exist in Israel (Hancock pers. comm., 1989) and Syria (Moshanski and Parabouchev, 1981). A further classification is provided by Buskinsky (1954) who classified true chalk as consisting of over 95% CaCO_3 , chalks with less than 95% CaCO_3 should be regarded as clay chalk and if they contain more than 10% clay they should be termed a marl. Chalk when used as a stratigraphic name is generally regarded as the equivalent of the Upper Cretaceous particularly in Western Europe (Whitten and Brooks, 1972).

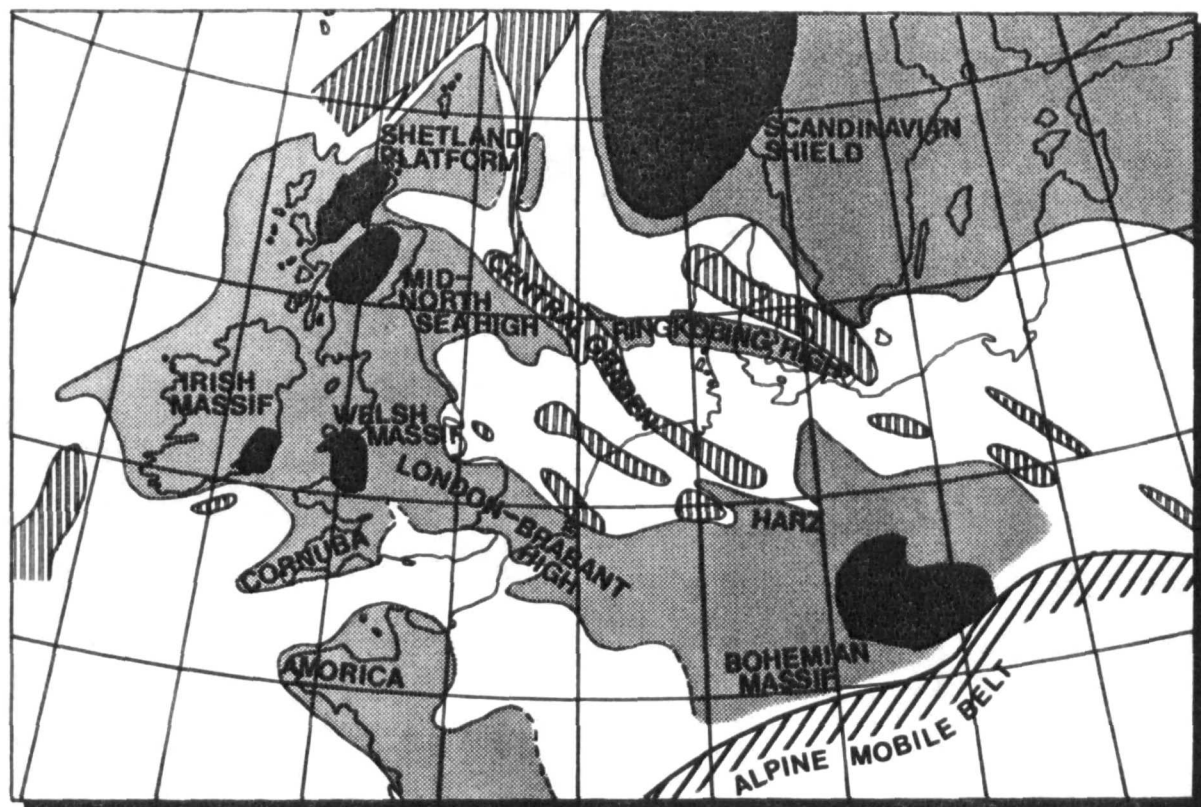
2.2. STRUCTURAL CONTROL

The high sea levels during the Upper Cretaceous period meant that water covered large areas of North America including the Gulf of Mexico and the American Western Interior as well as approximately 30% of Europe (Scholle, 1977). Chalk deposition within Northern Europe began in the Cenomanian stage of the Upper Cretaceous period and continued until the end of the Danian stage of the Tertiary period. It was deposited over an area from Northern Ireland to Northern Germany, and from Southern Sweden and the central North Sea to the Southern margins of the Paris Basin over a period of approximately 35 million (Sorensen et al., 1986) to 40 million (Skovbro, 1983) years. This, however, should not be taken as meaning that chalks representative of the whole of this time span can be found throughout the area.

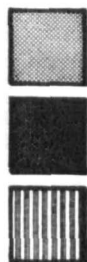
The following review will concentrate on the tectonic development of the North Sea in which the chalks investigated during this study were deposited. Exceptionally high eustatic sea levels existed around the North Sea during the Late Cretaceous (Scholle, 1977; Hancock and Kauffman, 1979). These represent the highest sea levels in geological his-

tory (Scholle, 1974). Various estimates have been made of the depth of water in which the chalk was deposited. These vary considerably, such as 30m-50m (Barr, 1962), 100m-150m (Schlanger et al., 1981), 200-300m (Scholle, 1974) and 650m (Hancock and Kaufman, 1979). Scholle (1977) notes that modern chalks are accumulating in seas with depths that may vary from 100-4000m. During the period in which the chalk was deposited, the areas of land exposed above these high sea levels were limited to Norway, central and northern Sweden, the Highlands of Scotland, the East Shetlands Platform, the Central Netherlands Inversion and a small part of the Utsira High (Hancock, 1987) (figure 2.1). Terrestrial material available for deposition in the chalk sea was therefore significantly reduced. The generally pure nature of the chalk throughout the region is a result of this restricted terrestrial input. Hardman (1982) notes that the North Sea chalks usually contain less than 5% detrital clay and quartz which increases to more than 15% in only a few well defined stratigraphic horizons (such as the Lower Chalk, the Plenus Marls and the Middle Hod). Hancock (1983) points out that even with a clay content as low as 5% in the North Sea chalks, this is generally higher than that found in the outcrop chalks of Southern England. The lack of clastic materials available also implies that a non-seasonal climate existed during the deposition of the chalk, probably that of an arid desert (Hancock, 1975).

Crustal movements during the Jurassic and Cretaceous periods which included rifting in North West Europe, the continental rupturing of the Central Atlantic and movements of Africa were controlled by a tectonic framework established during the Triassic period (Hancock, 1987). In the North Sea, the Central Trough (the name used by Ofstad, 1983 for the Central Graben) may be a somewhat older structure initiated prior to the Permian Period as a result of renewed movements of a Caledonide fault zone (Ofstad, 1983). However, Sorensen et al. (1986) state that the basin, in which the North Sea chalks were deposited, formed by Kimmeridgian movements (Jurassic). Hatton, (1986) says that the configuration of the Central Trough is a combination of two interacting structural trends, Permian and older (NNW-SSE) and Late Jurassic (WNW-ESE). Strike-slip fault movements resulted in the development of a series of en-echelon



100 km



MASSIFS AND STRUCTURAL HIGHS

PROBABLE LAND DURING LATE CAMPANIAN

TROUPHS WITHIN CHALK BASINS

Figure. 2.1. Structural map for the Late Cretaceous. (After Hancock, 1987.)

grabens within the North Sea. Generally, these movements were followed in the Late Cretaceous, by a period of tectonic stability and gradual basin subsidence (except for the very Late Cretaceous inversions). Chalk deposition occurred in these extensive basins between the exposed land masses. The Southern North Sea Basin for instance (containing the North Sea chalk oil fields) covers an area of approximately 180,000 km² and is almost twice as large as the Paris Basin (Hancock, 1983). It therefore represents the largest, continental shelf chalk basin in the world. During the latter part of the Cretaceous Period, the regional subsidence was dominated by structural inversions within the areas subject to the greatest subsidence during late Jurassic and early Cretaceous times. Details of the structural developments within the Central Graben will be outlined in the next section.

The opening of the Norwegian-Greenland Sea (60-65 million years ago) is thought to have changed the current circulation patterns in the North Sea region which led to cessation of chalk deposition (Talwani and Eldholm, 1977).

2.3. THE INITIAL ACCUMULATION AND DIAGENESIS OF THE CHALK.

The chalk is dominated by whole or disaggregated coccoliths (the skeletal remains of Haptophycean algae) the individual laths of which are of the order of 0.5-3 microns diameter (Hardman, 1982) with an average diameter of 2 microns (Neugebauer, 1974). These were deposited on the sea bed as faecal pellets which may have been as large as 120 microns (Hattin, 1975). It is inappropriate to describe the transport of the coccoliths to the sea floor here, see Hancock (1983) for details. However, it is important to note, that many of the coccoliths have been found to have a thin smectite coating 40 to 50 Å thick. This helps to protect them against diagenetic changes caused by reactions with their interstitial fluids (Hancock, 1983).

When the coccoliths settled on the sea floor they form a fluid/carbonate mixture, which is similar to a suspension of faecal pellets. This mixture is estimated by Hancock (1983)

to have an initial porosity of between 80% and 90%. Hardman (1982) gives a lower initial porosity of 60%-70%. This layer, which is estimated to be only a few centimetres thick (Hancock, 1983) was loose enough to have been easily resuspended by the movements of bottom currents. Neugebauer (1974) notes that the marine pore fluids trapped in this mixture are important in retarding the effects of pressure solution as they are already saturated with respect to low magnesium calcite (the primary constituent of the chalk). The pore fluids are thought to have been retained in the pore spaces from an early stage of burial. Scholle (1977) however, suggests that the chalks in the geological record do not necessarily imply fully marine conditions, as low salinity water could have been tolerated. He also points out that there are many of the Cretaceous chalks that may have been subject to saturation by fresh water for as long as 75 million years and which do not show signs of increased cementation or dissolution. This is probably because they have not been deeply buried.

By the time the chalk ooze was buried to a depth of approximately eight centimetres its structure was sufficient to support the majority of the animals now found as fossils. The porosity had been reduced to 75%-80% (Hancock, 1983), primarily due to the effects of bioturbation. The dewatering necessary to achieve this porosity reduction was so extensive that there are no longer any traces of the initial sedimentary structures. This is the zone termed the 'mixed layer' by Scholle et al. (1983).

The porosity of the chalk gradually decreases as it continues to be buried. At a depth of burial of 35cm Hancock (1983) estimates that the porosity may vary from between 70% and 80% depending on its initial value. This layer (8-35cm) is the 'transition zone' of Scholle et al. (1983) where the trace fossils which now dominate the chalk, were formed.

Further burial produced a slower decline in porosity, so that by the time the chalk was buried under an overburden of approximately one metre, the porosity had decreased to between 60% and 75%. This was approaching the depth below which the biological

contribution (bioturbation) to the processes of mechanical compaction (ie. the physical movement of grains by reorientation and repacking) as a result of burrowing, digestion and excretion, which may be termed biological compaction, declines in importance as the cause of porosity reduction.

With continued burial from 1m to a depth of 200m-300m the porosity of the chalk decreased to a value of between 40% and 65%. The increasing weight of the overburden led to the onset of a different form of mechanical compaction, namely stress induced reorientation, repacking and possible grain crushing, in which this weight is held partly by the calcite grains and partly by pore fluid. This form of mechanical compaction is termed consolidation. As the area of contact between the calcite grains may be as low as 1% at a depth of burial of 70m (Neugebauer, 1974) the effective stress on the grains (the difference between the total overburden pressure and that part of it supported by the pore fluid is termed the effective stress) allows a small amount of the calcite to pass into solution (pressure solution) to be redeposited on either side of the contact as a grain overgrowth. This early cementation has been given the name 'spot welding', the results of which can only be seen under a high magnification (X 30000) (Hancock, 1983). The small sizes of the grains enhance the development of this early rigid framework even though the extent of cementation is limited (0.003-0.07% of the volume (Neugebauer, 1974)). It is this early cement framework that gives the chalk its initial strength. The spot welds will grow until their surface areas have increased enough to bring the effective stress below the threshold pressure for solution (Neugebauer (1973) quotes this pressure as being 25-100MPa). Mapstone (1975) notes that spot welding has the appearance of a thin meniscus that is only a few molecules thick. These calcite overgrowths have also been seen in D.S.D.P. materials from both the South Atlantic and the Central Pacific where the chalks are under less than 15m of overburden (Wise and Hsu, 1971). Carbon/oxygen data (Lloyd and Hsu, 1972) has also indicated that these overgrowths were formed when the chalks were close to the sediment/water interface. The clay content of the chalk is important with respect to the formation of an initial rigid framework. Most chalks are remarkably pure. However, in chalks with

a high clay content (5%) (Hardman, 1982) the diagenetic processes described above are significantly modified. The presence of clays in chalk prevents the formation of an initial rigid framework (Hardman, 1982; Taylor and Lapré, 1987) as they are able to rotate under increasing load which leads to significantly greater compaction and grain crushing than would be found in a pure chalk in which a framework developed. However, the clay minerals also absorb magnesium ions which inhibit cementation. This means that, although a cement framework cannot be formed, dissolution resulting in increased compaction of the crushed, grains is significantly increased (Hardman, 1982).

The processes described above are referred to by Hancock (1983) as intrinsic diagenesis in that they are 'inevitable changes associated with the normal conditions of accumulation of chalk ooze'. Below a depth of burial of 300m there is little change in porosity until the chalk has accumulated an overburden of something like 1000m. This indicates that mechanical compaction (in the form of reorientation, repacking and grain crushing) is not the dominant process by which the porosity of the chalk is lost once the initial rigid 'spot welded' framework has formed. Scholle (1977) informs us that isotopic studies have shown that there is little change in the oxygen isotope value of the chalk until the porosity has been reduced to around 50% (Taylor and Lapré, 1987, suggest a value of 40%) ie. during the time that mechanical compaction is the dominant process of porosity decrease. Isotopic studies by Taylor and Lapré (1987) also indicate that most of the cementation found (presumably the 'spot welding') in the North Sea chalks was formed during early diagenetic processes. Carbon isotope signatures indicate that the carbonate for this cement originated from sea water which was partly introduced into the sediments by bioturbation. After this early stage mechanical compaction (as described above) ceases to be an important mechanism with regards to further loss in porosity. It is also from this point onwards that the diagenetic paths of the various chalks studied diverge.

At this stage in the burial process, a second type of diagenesis takes over, referred to as burial diagenesis. Under normal circumstances, continued burial below 1000m would

lead to a continued reduction in porosity. The stresses above a depth of 1000m are not sufficient to either break the 'spot welds' by further consolidation or lead to the onset of large-scale pressure solution. Below 1000m the chalks show a further decline in porosity so that another process must have been activated. For instance, Hancock (1983) quotes a porosity of 15%-30% at a depth from 1500m-2000m with the matrix permeability decreasing to 0.1- 1.0mD. Further burial will reduce the porosity to 2%-25% and the permeability to 0-0.5mD at depths between 2700m and 3000m. Scholle (1974) has concluded that cementation is a function of the depth of burial but that this differs considerably from area to area (ie. Northern Ireland, South East England and the North Sea). But Jones et al. (1985) demonstrated that it is a function of effective stress and that burial depth is a second order control. In his 1977 paper Scholle concluded that solution transfer (pressure solution) was the dominant process for porosity loss after the initial dewatering.

There is a clear difference between the styles of pressure solution for different lithologies (Buxton and Silbey, 1981) depending on the size and shapes of the grains. Halley and Schmoker (1983) studied samples taken at 25m intervals from carbonates in Southern Florida to a depth of 830m which indicated that early mineralogical stabilisation of shallow water carbonates does not greatly affect their average porosity. The values of the porosity loss/depth curves for these carbonates were similar to those for the Gulf Coast chalks, less than Southern England and greater than the North Sea. They also conclude, from a study of thin sections, that mechanical compaction (in the form of consolidation) was not the primary cause for the loss in porosity and that pressure solution is only important as a mechanism for porosity reduction when the porosity has fallen to around 20%. Experiments by Shinn and Robbin (1983) in which carbonates from modern environments were sampled and compacted indicate that mechanical compaction (consolidation) is of importance only in the early stages of porosity loss. Once the thickness of the sediments had been reduced by approximately 50% a further increase in vertical load resulted in almost no change in thickness. Chemical compaction (pressure solution) was noted only in the samples subjected to pressures equivalent

to a depth of burial of more than 3400m. They accepted however, that due to the fast strain-rates used in their experiments, chemical compaction (pressure solution) could begin, in nature, at shallower depths. They conclude that chemical compaction (pressure solution) can begin after mechanical compaction (consolidation) and before complete lithification (for which it provides the cement). Taylor and Lapre (1987) estimate that the chalks contain a minimum 25-40% of burial cement and a maximum of 60%. Stylolites are the most obvious features indicating the presence of pressure solution. Dunnington (1967) estimates that stylolites will not begin to form above a depth of burial of between 600-900m.

It seems, therefore that there is a consensus of opinion, in which, after the initial dewatering (including bioturbation) and mechanical compaction (consolidation), further loss of porosity is directly related to burial diagenesis and the onset of large scale pressure solution. As pressure solution and cementation continued with further burial the pore fluids gradually become depleted in magnesium and therefore the solution of the calcite grains will increase (Neugebauer, 1973). Neugebauer (1974) reports that cementation has often exhausted the magnesium in the pore fluids at a depth of burial of 1000m-1600m, but goes on to say that complete lithification will be achieved by a depth of burial of between 2000-4000m. Within the area of the North Sea, this missing magnesium may have come from the underlying evaporites. Pore fluids from the underlying Zechstein evaporites are also indicated by the strontium content of the later derived cements (Taylor and Lapre, 1987). This continuing cementation would have led to the development of a sparry calcite filling in both the pore spaces and around stylolites (Mapstone, 1975). Interestingly, Buxton and Silbey (1981) also say that stylolites may form in zones that have been previously cemented, but give no details of how this may occur.

Once the chalk has been buried below a depth of around 1000m pressure solution is the dominant process and mechanical compaction (consolidation) is of only secondary importance. This can be seen in the chalks of onshore U.K. The chalks in South East

England that had been subjected to only shallow burial contain few broken fossils (Scholle, 1977) indicating that mechanical compaction (consolidation) was limited. Wolfe (1986) reported that fossils in the chalks of Northern Ireland indicated that early mechanical compaction (consolidation) had been an important process. Many fossils showed signs of 15-30% shortening although fossil chambers filled with sparry calcite before compaction occurred had not been fractured. This is equally true for the chalks in Dorset. In both cases the increase in mechanical compaction can be shown to be the result of intense tectonic activity.

It is fair to say that the chalk goes through a three stage loss of porosity. Firstly, the sediments are dewatered primarily by bioturbation close to the sediment/water interface (termed biological compaction here). As the weight of the overburden increases with burial, mechanical compaction (consolidation) will lead to early (limited) pressure solution that produces a rigid framework by 'spot welding'. Cementation forming these 'spot welds' increases the contact area of the grains and the load per area decreases to a point beyond which these initial pressure solution processes cease (Neugebauer, 1974). It is then proposed that this framework was strong enough to resist further large scale mechanical compaction (consolidation). As the weight of the overburden continued to increase the stresses on the 'spot welded' grain contacts also increased until they were high enough to initiate pressure solution once again leading to further reductions in porosity. It might be envisaged that as the overburden increased 'spot welds' fractured and were then re-cemented by the re-activation of pressure solution processes. It can be seen, therefore, that pressure solution is a response to, and not separate from mechanical loading, and that mechanical compaction may take two different forms, namely bioturbation (termed biological compaction above) and consolidation (which is a purely mechanical restructuring of the sediments). The relative importance of mechanical compaction with or without limited pressure solution and large scale pressure solution with only limited mechanical compaction, would depend on the structural history of the area in which the chalk was accumulating. Any further discussions on variations in the loss of porosity will be held over until the next section.

Chalk deposition was not a continuous process. A hiatus or a period of winnowing by bottom currents (no longer considered to be shallow water or subareal features (Scholle, 1974)) may have allowed the formation of hardgrounds. Hardgrounds may also form during periods of slow sedimentation (Hardman, 1983). As the rate of burial decreases the pore fluids have a longer period over which they can escape. Exposure of the surface also allows establishment of burrowing organisms whose activities enhance the dewatering process. Because of the low permeability of most chinks it follows that, during periods of rapid subsidence or rapid sedimentation, pore fluids are more likely to be trapped (Hardman, 1983; D'Heur, 1984; Pederstad et al., 1988). It is unnecessary to detail the formation of hardgrounds (see Kennedy and Garrison, 1975). They are relatively unimportant in both onshore chinks of Denmark and the U.K. as well as the North Sea in that they represent horizons of low porosity and permeability and higher cementation (Mapstone, 1975; Hancock, 1975; Hardman, 1983; Kennedy and Garrison, 1975). Another important feature found in autochthonous (in situ) horizons of the chinks of all areas is a rhythmic fluctuation in the terrigenous clay content. These alternations of clay-rich and clay-poor sediments are termed periodites. They are particularly significant in the Lower Chalk of South East England, and the Plenus Marls and Middle Hod of the North Sea (Kennedy, 1983). It is generally accepted that these fluctuations in clay content represent increases and decreases in the amount of terrestrial runoff. It has also been proposed that they may represent alternations in coccolith production as a response to climatic changes, the timings of which may be linked to the Milankovitch cycles (Kennedy, 1983).

2.4. DANISH ONSHORE CHALKS (STEVN'S KLINT).

Stevn's Klint lies 40km south of Copenhagen on the eastern side of the island of Zealand (Zealand) on the Stevn's peninsula (Surlyk, 1979; Ekdale and Bromley, 1984) 200km away from the centre of the Norwegian-Danish Basin. It represents a marginal facies (Hardman, 1982) with pelagic deposition on a quiet shelf sea (Hakansson et al., 1974) with little or no downslope movements. The outcrop consists of a 70m high, 12km

long sea cliff in which Maastrichtian and Danian chalks are well-exposed (Ekdale and Bromley, 1984). The samples were collected from one of the quarries along this coastline. It contains the type section for the Lower Danian of Europe, in which the boundary between the two formations can be observed.

The Maastrichtian sequence begins with 5-10m of white Bryozoan chalk mounds (revealed by the undulating flints) (Ekdale and Bromley, 1984; Surlyk, 1979), in which some of the mounds are seen to overlap. This stratum is overlain by approximately 20m of horizontally bedded chalks which contain scattered flints. Samples taken from this layer, which exhibit porosities up to 48-50% (see appendix 1) were used in the undrained shear experiments (chapter 6) and as an analogue material for the North Sea Tor Formation chalks (chapter 4). (Parts of the Tor Formation are known to have porosities in excess of 45%, but sample preparation (coring) of these soft chalks proved extremely difficult.) This onshore Danish chalk has a high density of Zoophycos burrows (Surlyk, 1979) and a low fossil content. There is a prominent nodular flint layer 3-4m below the boundary between the formation containing the Bryozoan mounds and the overlying horizontal chalks. This flint layer lies below two hard grounds, the upper one of which shows signs of small overthrusts (Surlyk, 1979). The top 2.5-3.5m of the Maastrichtian chalk is grey in colour and again has a high Bryozoan content.

The famous Fish Clay, which is up to 35cm thick, represents the base of the Danian sequence. This was deposited in the low basins between the eroded tops of the Maastrichtian bioherms. It is followed by a hard *Cerithium* limestone hardground (Surlyk, 1979) which formed after the boundary event. The remaining Danian chalk is a creamy coloured limestone representing a lower sea level than existed during the Maastrichtian.

2.5. ONSHORE CHALKS FROM SOUTH EAST ENGLAND (BUTSER HILL).

Butser Hill Lime Quarry lies to the south of Petersfield, Hampshire on the eastern side of the main A3 road to Portsmouth. The quarry is situated at the western extent of the South Downs in the upper parts of the Lower Chalk (up to 30m thick). Samples were collected from the upper section of *Schloenbachia varians* zone, a division of the Grey Marl, where they pass into yellow- white chalks referred to as the *Holaster subglobosus* zone. These are described as a soft, slightly marly chalk, with a clay content of approximately 15% (see appendix 1). The chalks in this quarry are highly fractured resulting in a paucity of blocks suitable to provide samples for triaxial testing in the laboratory. They show evidence of extensive bioturbation and have a porosity of 34-36%. The Grey Marl is followed at the top of the Lower Chalk by the Plenus Marls.

It has been estimated that the chalk of South East England was buried beneath an overburden of approximately 1250 feet (Carter and Mallard, 1974) and had a fairly uniform geological history. This has resulted in the development of a fairly uniform diagenetic fabric, in which the strength and density increase towards the base of the succession. However, subsequent tectonic activity has modified this fabric in certain areas such as the Purbeck monocline in Dorset (Mimran, 1975; Jones et al., 1984).

BLANK PAGE

BLANK PAGE

CHAPTER 3

NORWEGIAN HYDROCARBON RESERVOIR CHALKS.

3. NORWEGIAN HYDROCARBON RESERVOIR CHALKS.

3.1. INTRODUCTION.

Hydrocarbon exploration in the Norwegian Sector of the Southern North Sea, in the area now referred to as the Greater Ekofisk Area, began in 1969 with the discovery of the Ekofisk Field (Pekot and Gregory, 1987). However, the first hydrocarbon discovery in chalks of Cretaceous age was made in 1964 in the adjacent Danish Sector (Selly, 1976). This proved to be a gas field now known as the Harlingen field (Van Den Bosch, 1983). Interestingly, Van Den Bosch (1983) noted that 'The feared pore collapse in the relatively weak granular framework of the chalk following decompression did not occur during the first few weeks or few months of production. Such a phenomenon is common in most chalk fields outside the North Sea Basin. Such pore collapse on a field-wide scale usually reduces production by approximately 80%.' Unfortunately Van Den Bosch (1983) does not give any examples of where this 'common' problem has occurred.

3.2. SEDIMENTOLOGY.

The greater thicknesses of the chalk formations found in the North Sea (2000m) compared with their onshore counter-parts (200m) (Kennedy, 1987a; Watts et al., 1980) provided sedimentologists with a number of problems. How could these thickness variations have been accomplished? Equally, how could the reservoir chalks buried as they were to depths of the order of 3000m still contain matrix porosities (fracture porosities add only a negligible amount to the matrix porosities) as high as 50% (Leonard and Munns, 1987).

Until 1977 it had been assumed that the chalks in the Central Graben had accumulated by a slow rain of coccoliths in the same manner as the formation of the onshore chalks and were therefore autochthonous (Kennedy, 1987b). Allochthonous chalk units (transported to the site of deposition) had been known to exist for a long time (Nygaard

et al., 1983) but it was not generally accepted that they should be a common phenomena. Large scale re- deposited chinks are known to exist at a number of locations bordering the North Sea area, such as Haute Normandie in France (Kennedy and Juignet, 1974); Hollviken, Sweden (Brotzen, 1945); Rugen, East Germany (Steinich, 1967); and Jylland, Denmark (Hakansson et al., 1974; Ekdale and Bromley, 1984). However, re-deposition textures in the chinks of the North Sea were not recognised until the work of Perch-Nielsen et al. (1979), Kennedy (1980) and Watts et al. (1980). Scholle does not mention re- depositional features in the description of North Sea chinks in his 1977 paper. It was during the study of the nanofossils in a core from the Ekofisk field that Perch-Nielsen et al. (1979) noted that the lower half of the Ekofisk Formation reservoir (Danian age) contained mass flow deposits with faunas of Maastrichtian age.

Since then numerous studies and publications have been produced on each of the fields in the Norwegian sector (where the chalk reservoirs contain between 60% (Kennedy, 1978a) and 75% (D'Heur, 1989) of Norway's known hydrocarbon reserves) and the Danish sector. 28% of the total Norwegian oil production (Berget et al., 1989) and 35% of the total gas production (Berget et al., 1989) comes from the chalk reservoirs. It is estimated that 80% of the chinks making up the hydrocarbon reservoirs have been redeposited. The style of allochthonous deposition is consistent throughout the Central Graben, but it differs in detail from field to field due to variations in the histories of tectonic and haliokinetic events that affected the chalk.

One of the most comprehensive studies of the sedimentology of the Central Graben chalk fields was undertaken by Kennedy (1985; 1986) for the Joint Norwegian/Danish Energy Agencies Chalk Research Programme. In this study he systematically described the sedimentology of all of the important cores from each of the fields. The main sedimentological features of the North Sea chinks are briefly described below. These textures are characteristic of those present in the samples tested during this study and may account for some of the variabilities in the test results. These descriptions are also an important prerequisite for the next section of this thesis, in which the fracture

development in one of the most complete cores is analysed with reference to the sedimentology. It will be seen that the two are not independent of each other.

A brief description will now be given of the sedimentological features of the original autochthonous deposits. These will be seen to be similar to many onshore units of the Southern England and Europe such as the Paris Basin, as well as the deep sea chalks. This will then be followed by descriptions of the sedimentological characteristics and modes of origin of the allochthonous sediments. Both will be illustrated with photographs taken of four inch diameter cores, and, of samples selected for laboratory rock mechanical testing from a number of the oil fields in the Greater Ekofisk Area.

3.2.1. Autochthonous Chalks.

Autochthonous deposits show an alternation of lithologies on a decimetre to metre scale even though most of the original depositional fabrics have been destroyed by bioturbation (plate 3.1). These alternations, usually of light and dark chalks (the periodites referred to above) (plate 3.2) are most obvious in the Hidra, Plenus Marls, parts of the Hod and the Lower Ekofisk Formations (see below). The colour changes are the result of different clay contents. The darker units have a relatively high terrigenous clay content and could strictly be called marls ($> 10\%$), while the lighter units are clay-poor. The boundaries are usually gradational and frequently burrowed, but at a number of levels they are sharp, indicating a break in sedimentation and the formation of a hard ground. Probably the most striking example of this is the surface between the top of the Tor Formation and the base of the Ekofisk Formation (see below). This has resulted in the formation of a burrowed hardground below a conglomerate (plate 3.3). The clay-rich units in the periodites are more heavily altered by pressure solution which tends to emphasise the internal laminations (plate 3.4). The clay-poor layers act as receptors for the released carbonates. Alternations in terrigenous clay input, fluctuations in carbonate production and changes in sea level have all been proposed as possible reasons for this cyclicity (see Kennedy, 1987b). Kennedy (1980) correlates the

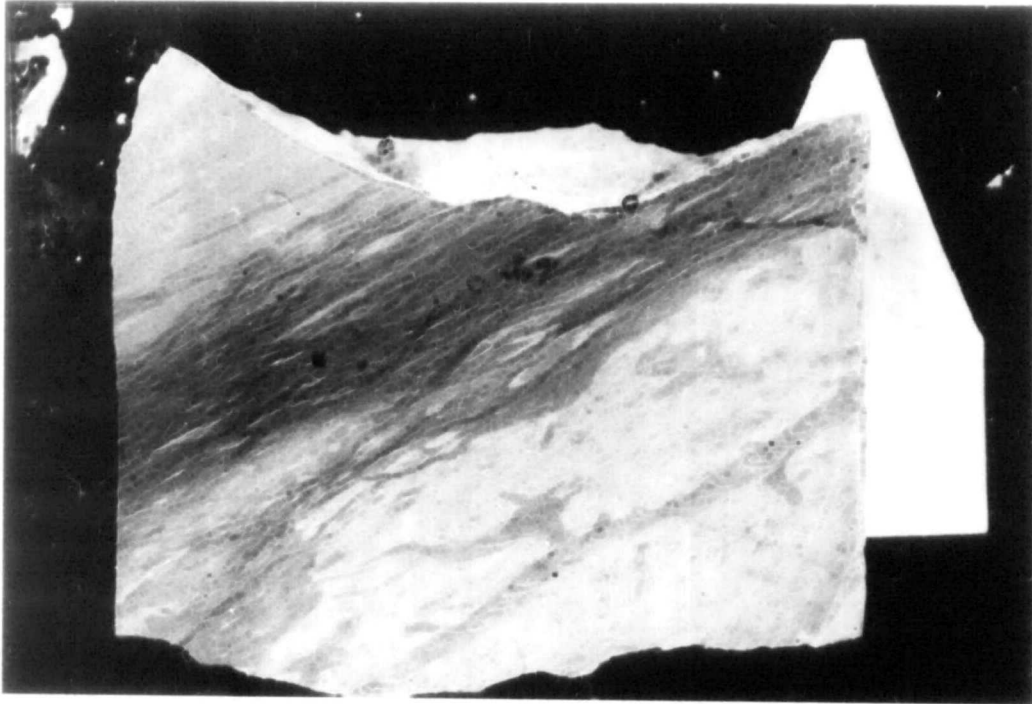


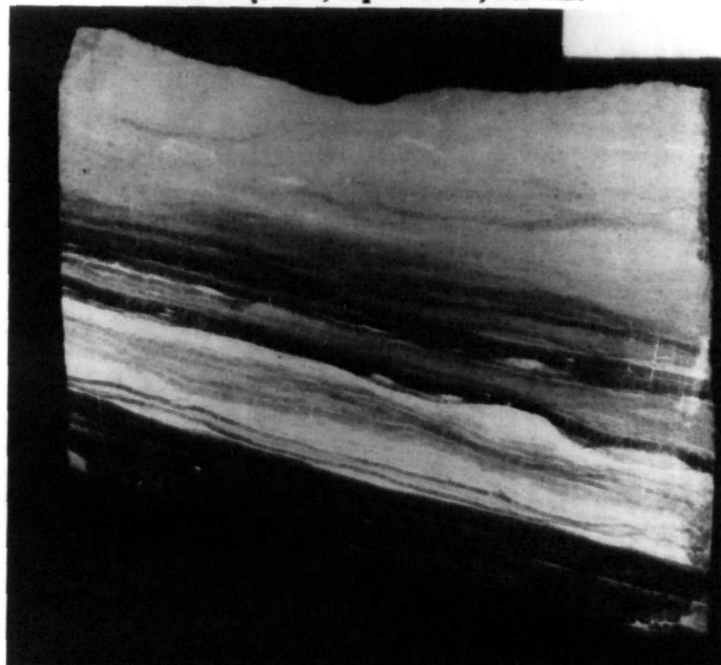
Plate 3.1 A periodite showing evidence of differential compaction and containing solution seams. Well 2\7-A20, depth 9900.5', Ekofisk Fm.



Plate 3.2 An example of the alternation depositional fabric of a periodite showing differential compaction. Well 2\7-A6, depth 9844.5', Hod Fm.



**Plate 3.3. The Ekofisk Formation basal conglomerate.
Well 2\7-B11, depth 10443', Tor Fm.**



**Plate 3.4. A periodite in which pressure solution is observed to emphasise the primary laminations.
Well 2\7-B11, depth 10593.5', Hod Fm.**

major fluctuations in terrigenous clay input into the chalk sea with peaks in the transgressive/regressive sea levels during the period of deposition.

3.2.2. Allochthonous Chalks.

Kennedy recognised six types of allochthonous deposits present in the chalk cores of the Central Graben. These are slides, slumps, debris flows, homogeneous chalks, turbidites and laminated chalks. They display a progressive degree of disaggregation and disruption of the original autochthonous sedimentological features which is governed by the distance transported after their initial deposition and pre-transport lithification.

These different phenomena are:-

- *1) Slides. A mass movement feature in which the integrity of the sediment is largely maintained and movement occurred on a basal shear.*

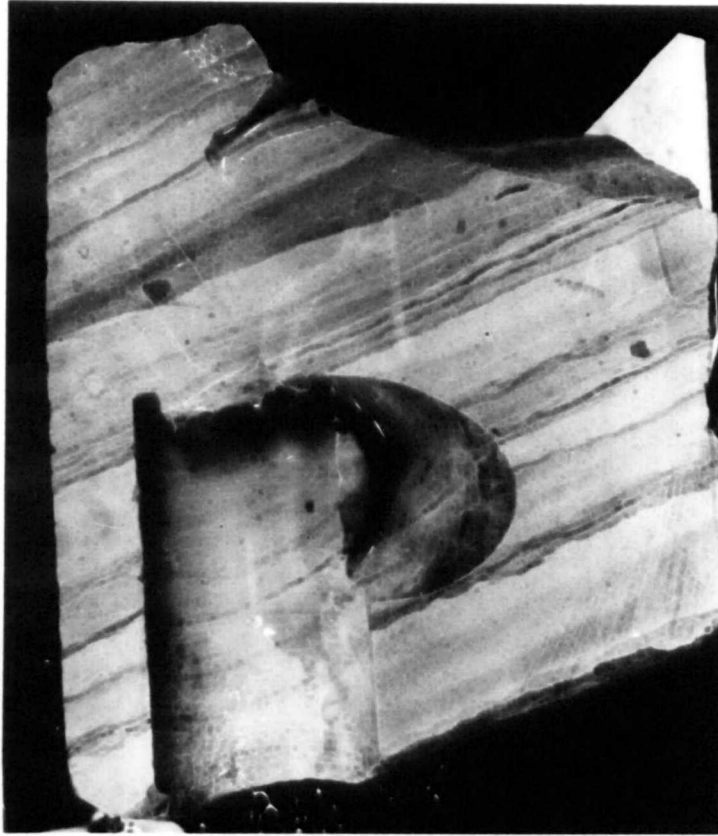
These are an important depositional feature of the Central Graben chalks especially in the Lower Ekofisk Formation of the Tor and Albuskjell fields. They are difficult to recognise in cores without the benefit of well logs showing dipmeter records. The original autochthonous pelagic cycles are retained but the dips vary from steeply inclined to near horizontal (plate 3.5). They may show only minor signs of internal disruption such as plastic deformation, in which the pelagic cycles or any burrows present are irregularly distorted. Some of the distortion associated with plastic deformation may be a result of dewatering. Frequently there is evidence of a basal shear zone. The retention of the original sedimentological fabrics and variable angles of dip in slumped chalks is an indication of limited transportation.

- *2) Slumps. Similar to slides but the sediments show greater internal disruption.*

These can vary in scale from metres to tens of metres and may include both isoclinal folds and overturned sequences such as the inverted sequences in the Albuskjell field. Plate 3.6 shows part of a small scale slump in which the fabric has been further modified



Plate 3.6. A small scale slump further deformed by small scale extension. Well 2\7-A20, depth 9837.5', Ekofisk Fm.



**Plate 3.5. Inclined strata indicating the presence of a slide.
Well 2\7-A20, depth 9857.3', Ekofisk Fm.**

by dewatering. Slumps are widespread in both the Tor and Ekofisk Formations. These are not necessarily surface features as they show internal deformations that indicate that a degree of dewatering and cementation occurred before they were transported. Taylor and Lapr   (1987) propose depths of burial before transportation which may have varied from less than 10m to almost 100m. This deformation may result in the formation of chaotic units, brecciation (plate 3.7), shearing (giving a shredded appearance which disrupted the early cement, plate 3.8) and small-scale extensional features such as faulting (plates 3.9 and 3.10). Slumping may also occur in debris flow material, emphasising the instability of allochthonous units. Plate 3.8 shows shredding produced by subsequent movement of the slumped material in which the original bedding still exists but has developed a 'fuzzy' appearance. On close inspection it can be seen that this shredded appearance is the result of micro-shearing. Plates 3.9 and 3.10 show two stages of early faulting. In 3.9 the sediments appear to have been displaced soon after dewatering, as the fault surface is indistinct. 3.10 contains a distinct fault in a more distal sediment (note the effects of pressure solution that has removed the base of the fault).

- *3) Debris flows. Pebbly redeposited chalks which show no internal structure and are poorly sorted. They may exhibit inverse grading at their base.*

The debris flows, constitute the largest proportion of the allochthonous deposits found in the North Sea chalks. They can vary from matrix supported debris flows, in which low frequency small clasts are observed to 'float' in the matrix (plate 3.11), to grain flows, in which the clasts are larger, lie in contact with each other and are surrounded by very little matrix material (plate 3.12). These two plates represent two extremes in the range of debris flows observed in the North Sea chalks. In either situation, the chalk must have been cemented before it was moved for clasts to exist.

The clast size and the clast/matrix ratio may be an indication of the distance that the debris flow has moved from its source. The further the debris flow travels, the higher the probability that the clasts and early cement would break down. If, during transportation, the original framework (due to bioturbation, dewatering and cementation) is



Plate 3.8. Small-scale shearing of a slump resulting in a shredded appearance.
Well 2\7-B11, depth 10635', Tor Fm.

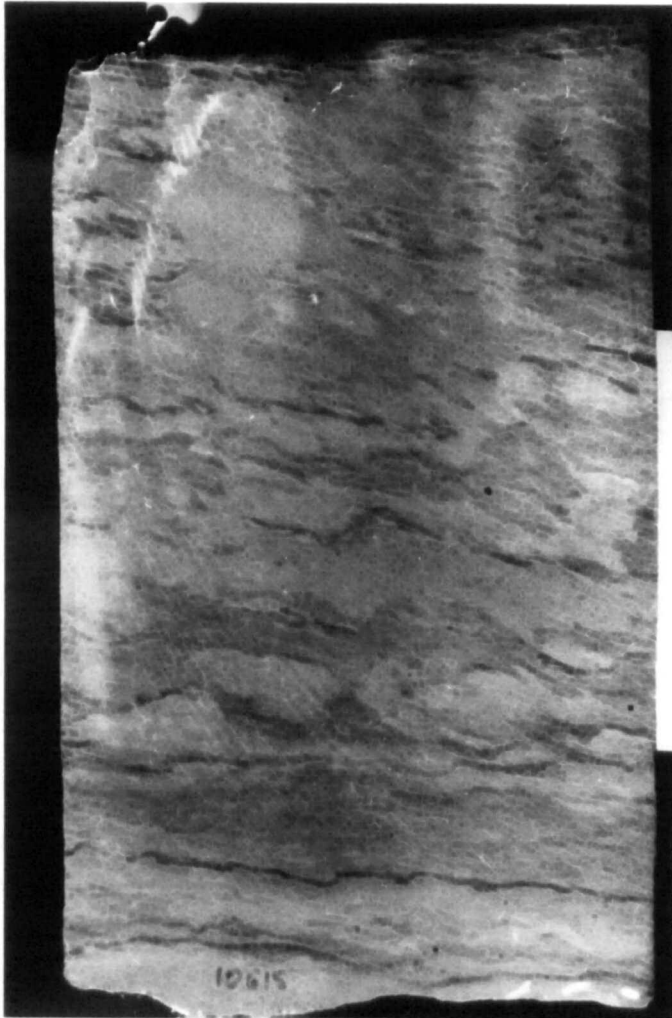


Plate 3.7. An example of post-depositional brecciation.
Well 2\7-B11, depth 10615', Hod Fm.



**Plate 3.9. Faulting in a chalk which
sustained a high fluid content at the time.
Well 2\7-B11, depth 10614', Hod Fm.**

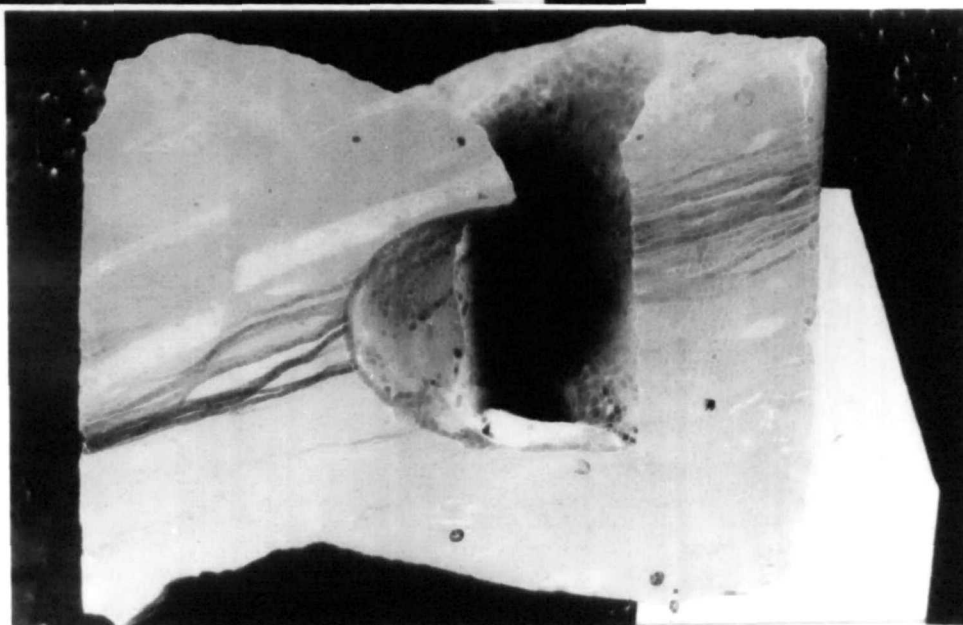
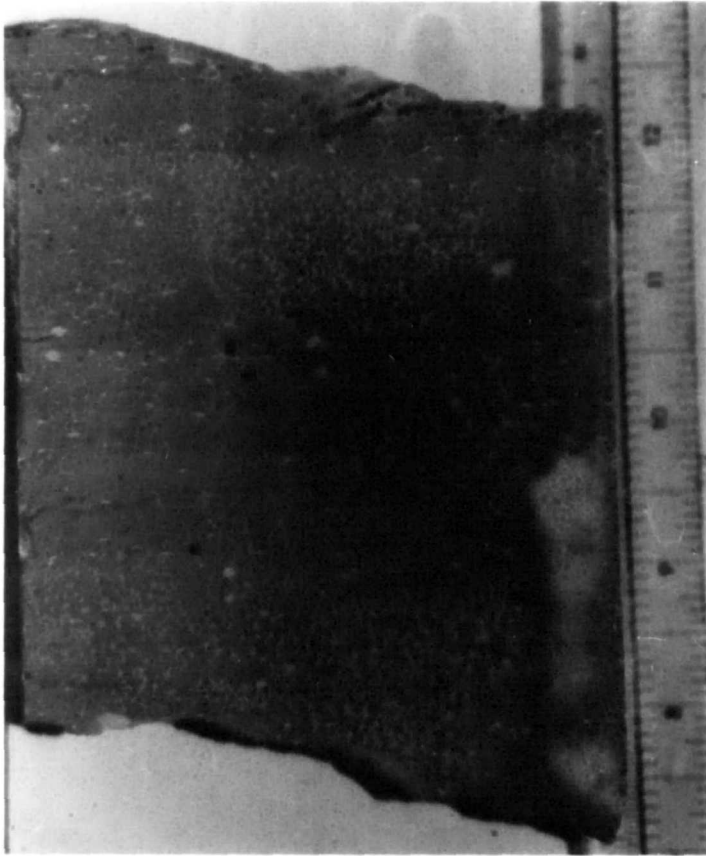
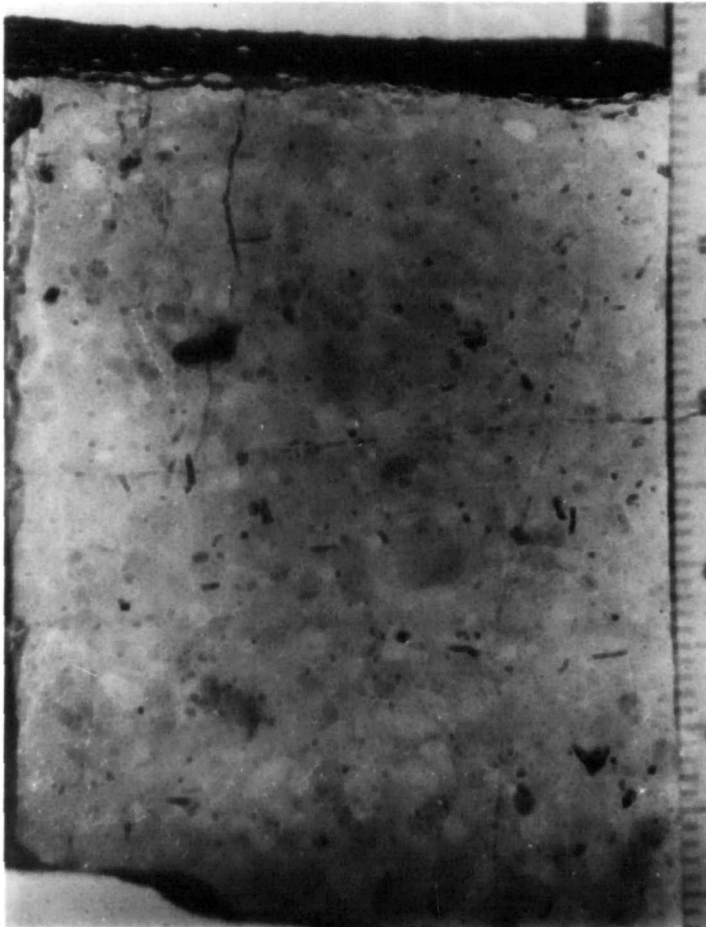


Plate 3.10. Faulting in a competent bioturbated periodite. Well 2\7-A20, depth 9895', Ekofisk Fm.



**Plate 3.11. An example of a matrix
supported debris flow.
Well 2\4-D8, depth 10744', Tor Fm.**



**Plate 3.12. An example of a coarse
debris flow in which the matrix
content is small.
Well 2\4-D8, depth 10749', Tor Fm.**

only partially destroyed, the resulting clasts will retain some of their original porosity (Taylor and Lapré, 1987). This will lead to an increase in porosity of between 5-10% (Taylor and Lapré, 1987) above that which would result from subsequent dewatering and lithification of a fully reworked sediment. The distance over which some of the debris flows travelled without the destruction of their clasts may have been substantial as Kennedy reported (1987a) that clasts have been found in some of the debris flows of the Tor Formation of chalks not known in the Central Graben today. The view that the higher porosities found in the debris flows are the result of porosity retention in the clasts is not universally accepted as, Nygaard et al. (1983) feel that the better reservoir quality of the debris flows can be attributed more to the disintegration of the matrix during re-deposition than to the early lithification of the chalk. In either case, the formation of debris flows (by rapid resedimentation) restricted the circulation of seawater to the top few metres thus restricting cementation (Taylor and Lapré, 1987) and dewatering by bioturbation.

- 4) *Homogeneous chalks.*

These are the most difficult to interpret as they show almost no internal structures apart from the occasional indication of some plastic flow and bioturbation. The tops are commonly burrowed and they often show signs of escaping water. Kennedy interprets these as being either debris flows in which the clasts have been destroyed (as in the Ekofisk 'reworked' zone), base absent turbidites, or submarine mudflows. Plate 3.13 shows a water escape structure in one of these chalk units. The chalk lacks internal features and the escape structure can be seen to be surrounded by small healed fractures.

- 5) *Turbidites. Grains carried by fluid turbulence and deposited in a fining upwards sequence.*

Turbidites have been recorded throughout the cores recovered from every field in the Greater Ekofisk Area. They consist of calcarenites grading up into finer homogeneous

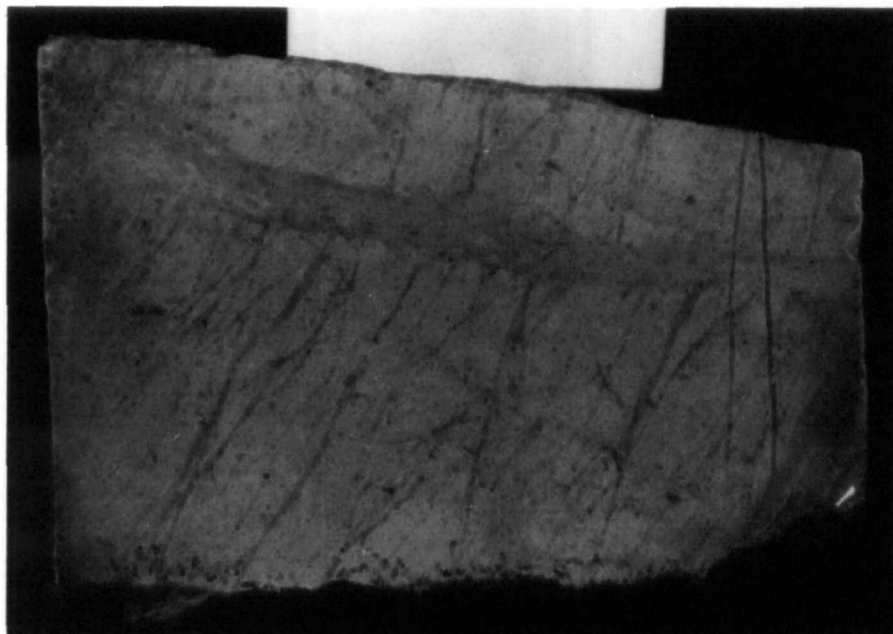
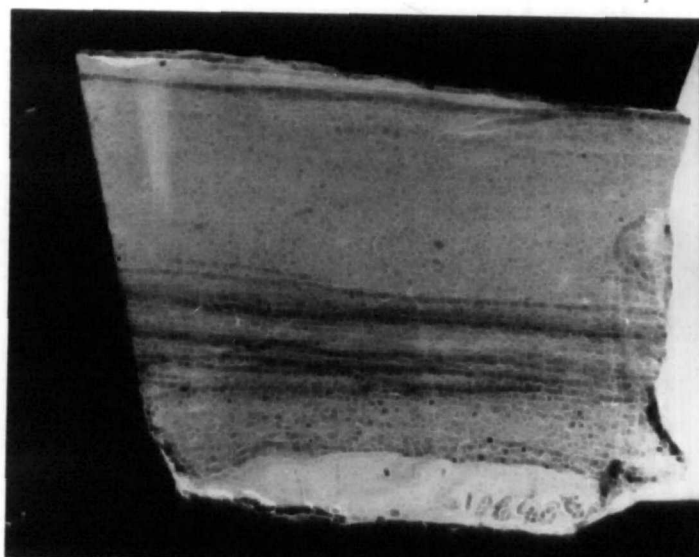


Plate 3.13. An example of a water escape structure showing two sets of high angle fractures. Well 2\7-B11, depth 10229', Tor Fm.



**Plate 3.14. An example of a thin turbidite.
Well 2\7-B11, depth 10638.3', Hod Fm.**

sediments. Occasionally the basal section may be missing. Plate 3.14 shows a small turbidite which lies over a slump. Interestingly, the effects of solution are observed to decrease in intensity upwards in this turbidite. Kennedy feels that the calcarenite sequences that appear in the Middle Hod Formation, in which the depositional fabric has been destroyed by bioturbation may also be turbidites.

- 6) *Laminated chalks. Fine centimetre, or millimetre thick laminations.*

These are small scale distal turbidites which often alternate with bioturbated chalks but do not contain the coarser elements of the proximal turbidites. The alternation in sedimentation (plate 3.15) represents impulses of allochthonous deposits into an autochthonous environment. Following the deposition of a turbidite there was a return to the deposition of pelagic sediments. This decrease in the rate of sedimentation also enabled marine organisms to re-establish themselves on the sea floor leading to bioturbation of the upper surfaces of the turbidites which continued throughout the depositions of the overlying pelagic chalks, resulting in the destruction of any internal structures. This difference in the rate of deposition and the presence of bioturbation has led to porosity differentiation in which higher porosities are found in the rapidly deposited distal turbidites and lower porosities are recorded in the pelagic sediments.

3.3. STRUCTURAL DEVELOPMENT AND OVERPRESSURING.

The fabrics described above can be related to those of similarly deposited clastic sediments (Middleton and Hampton, 1976). The areal distribution of the allochthonous chalks, indicate that their mode of deposition is different. The model proposed for the deposition of equivalent clastic sediments invokes a submarine fan. The blanket fill nature of the allochthonous chalks indicates that they were deposited as a result of variable slope profiles and changes in the intensity of tectonic activity along the boundary faults of the Central Graben (Kennedy, 1983). Hatton (1986) also feels that the synchronicity of the redeposition indicates that the triggers were earthquakes generated

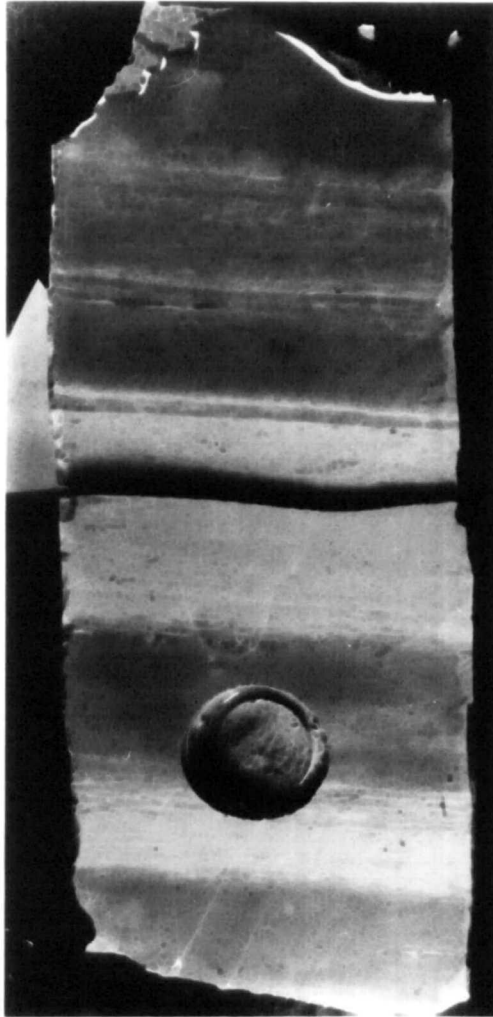


Plate 3.15. An alternating sequence of high porosity soft chinks (dark) and low porosity (light), bioturbated pelagic sediments. **Well 2\8-8, depth 9691', Hod Fm.**

by the movements of these boundary faults and not necessarily an instability on a shallow slope.

One of the most important structural features of Greater Ekofisk Area, is a fault system known as the Lindesnes Ridge (Brewster and Dangerfield, 1984). This was formed during the Jurassic period as a half-graben with a steep western fault that trends NNW-SSE. It was active throughout the Cretaceous period, during the latter part of which it developed into an inversion structure which has resulted in the formation of a half horst (Brewster and Dangerfield, 1984) (figure 3.1). Activity of the Lindesnes Ridge and the faults forming the north-eastern boundary of the Central Graben induced the instability that resulted in the resedimentation seen in the Maastrichtian and Danian chalks (see figure 3.7 for stratigraphic correlations). It also resulted in the erosion/non-deposition seen in many of the fields along the axis of the Lindesnes Ridge. This structural feature effectively divides the Greater Ekofisk area into three, with the Albuskjell, West Ekofisk, Ekofisk and Tor fields to the north-east, Tommeliten Gamma, Edda, Eldfisk, Valhall and Hod lying close to or across the Lindesnes Ridge and Tommeliten Alpha to the south-west. Movements of this fault system have played an important part in the depositional histories of each of the fields, which has resulted in significant differences between the three groups. To the south-west of the Lindesnes Ridge (Tommeliten alpha) the chalks are either distal allochthonous units or autochthonous with a total thickness for the Hod, Tor and Ekofisk Formations of 800m (Ofstad, 1983). Along the axial region (Tommeliten Gamma, Edda, Eldfisk, Valhall and Hod) the thickness of these three formations decrease to 150-200m and to the north-east they increase in thickness again to 800m (Ofstad, 1983).

The faulting therefore controlled the patterns of sedimentation. During the deposition of the Hod Formation chalks tectonic activity was slight and the majority of this formation consists of periodite facies. The Upper and Lower Hod contain minor allochthonous units which indicate some tectonic activity and slope instability. Fault activity increased during the deposition of the Tor Formation chalks (Maastrichtian). These

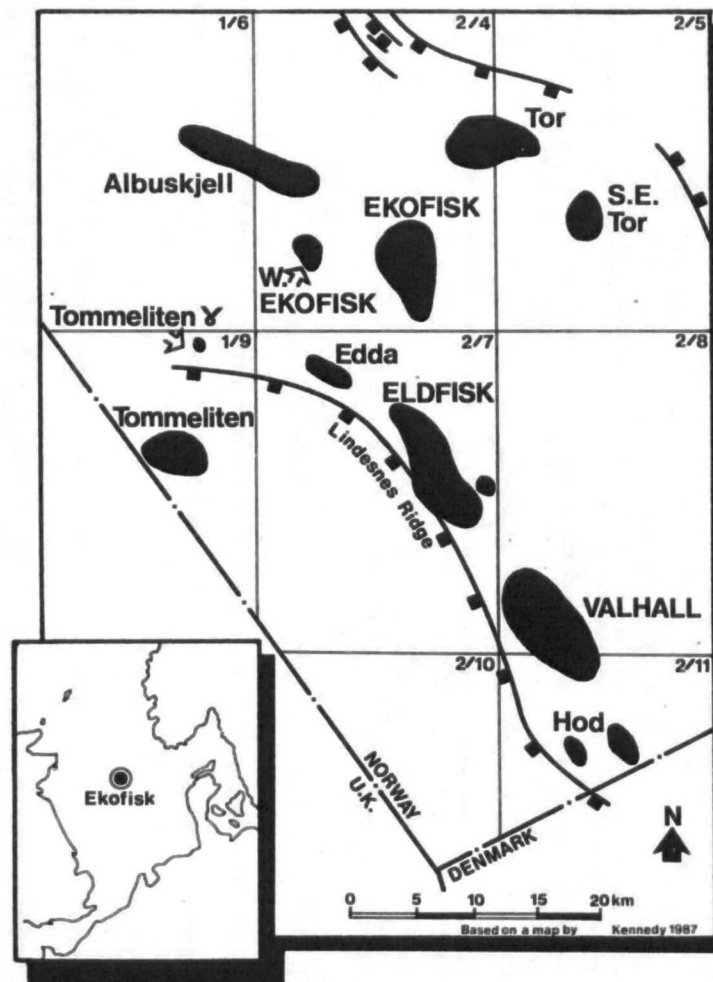


Figure. 3.1. Location map of the Greater Ekofisk Area.

movements included the uplift of the eastern flank of the Lindesnes Ridge. This resulted in the formation of an unconformity in the southern fields along the ridge (Eldfisk, Valhall and Hod) beneath which the Upper Hod is either condensed or missing. The Lower and Middle Tor Formations are absent in South Eldfisk (Brewster and Dangerfield, 1984). The area to the east became a depocentre in which extensive slump deposits developed from the area around the ridge. The slumps originating from the ridge did not reach as far east as the Tor field (figure 3.2). The source of the overlying debris flows appears to be from shallow water chalks to the north-east of the Tor field. This set of allochthonous deposits can be found throughout the north-eastern fields. To the south-west the deposits become increasingly distal in nature indicating an increasing distance from the source. Movements of the Lindesnes Ridge continued to increase towards the end of the Maastrichtian and led to an increase in the slumping even in the two Tømmeliten fields to the west. The four maps reproduced from Hatton (1986) in figure 3.3 indicate the increasing intensity of allochthonous deposition and the increasing activity of the Lindesnes Ridge. Members T4 and T10 belong to the Lower Tor, T13 is the lower member of the Middle Tor and T16 is the last Tor Member (top of the Upper Tor).

The continued growth of the Lindesnes Ridge finally resulted in the development of the erosion surface at the Tor/Ekofisk boundary and the deposition of the Ekofisk reworked zone. The reworked Tor chalk is limited to the Ekofisk and West Ekofisk fields and has originated from the increased uplift in the area of the southern fields. Indeed, the Lower Ekofisk Formation throughout the area indicates the effects of these movements (figure 3.4). To the north-east in the Tor and Albuskjell fields this formation consists of shaley periodites overlaid by slump deposits. These originated from the movements of the faults to the north. In Eldfisk, the Lower Ekofisk Formation is absent and further south in Valhall and Hod both the Upper and Lower Ekofisk Formations have been removed and transported northwards to be redeposited as slumped debris flows. Figure 3.5 shows the movement of chalks away from the Lindesnes Ridge during the deposition of the Upper Ekofisk chalks.

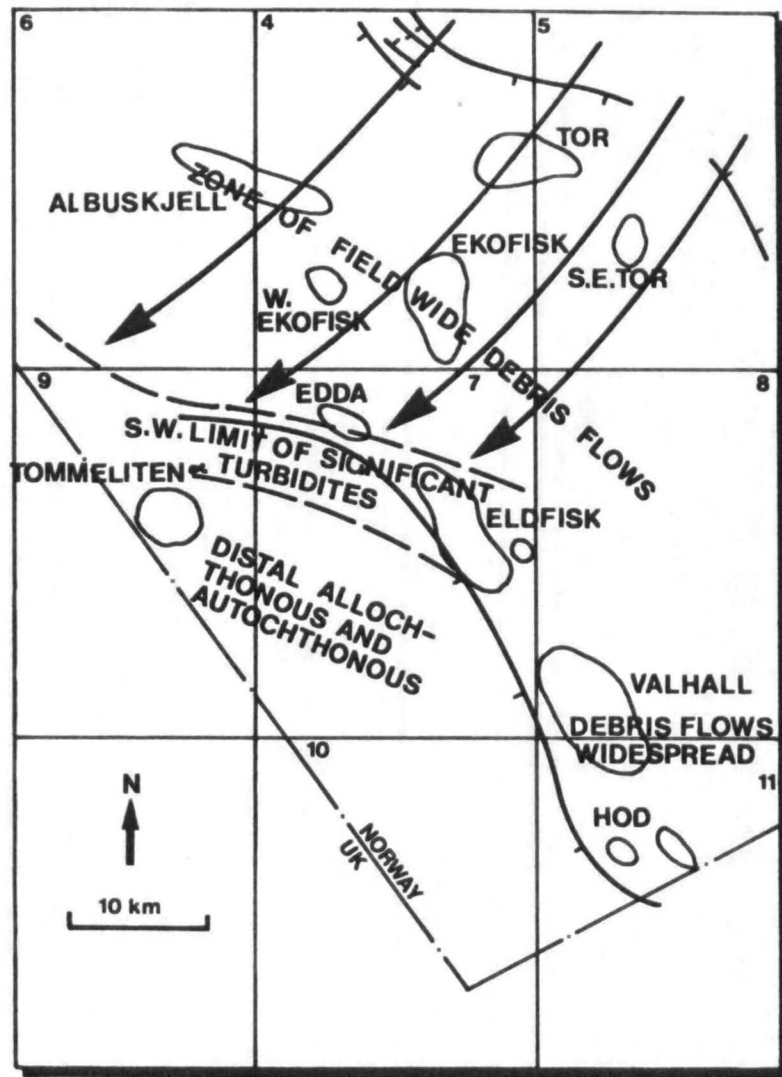


Figure. 3.2. Schematic map indicating the predominant direction of sediment transportation and re-deposition during the deposition of the Tor Formation Chalks. (After Kennedy, 1987.)

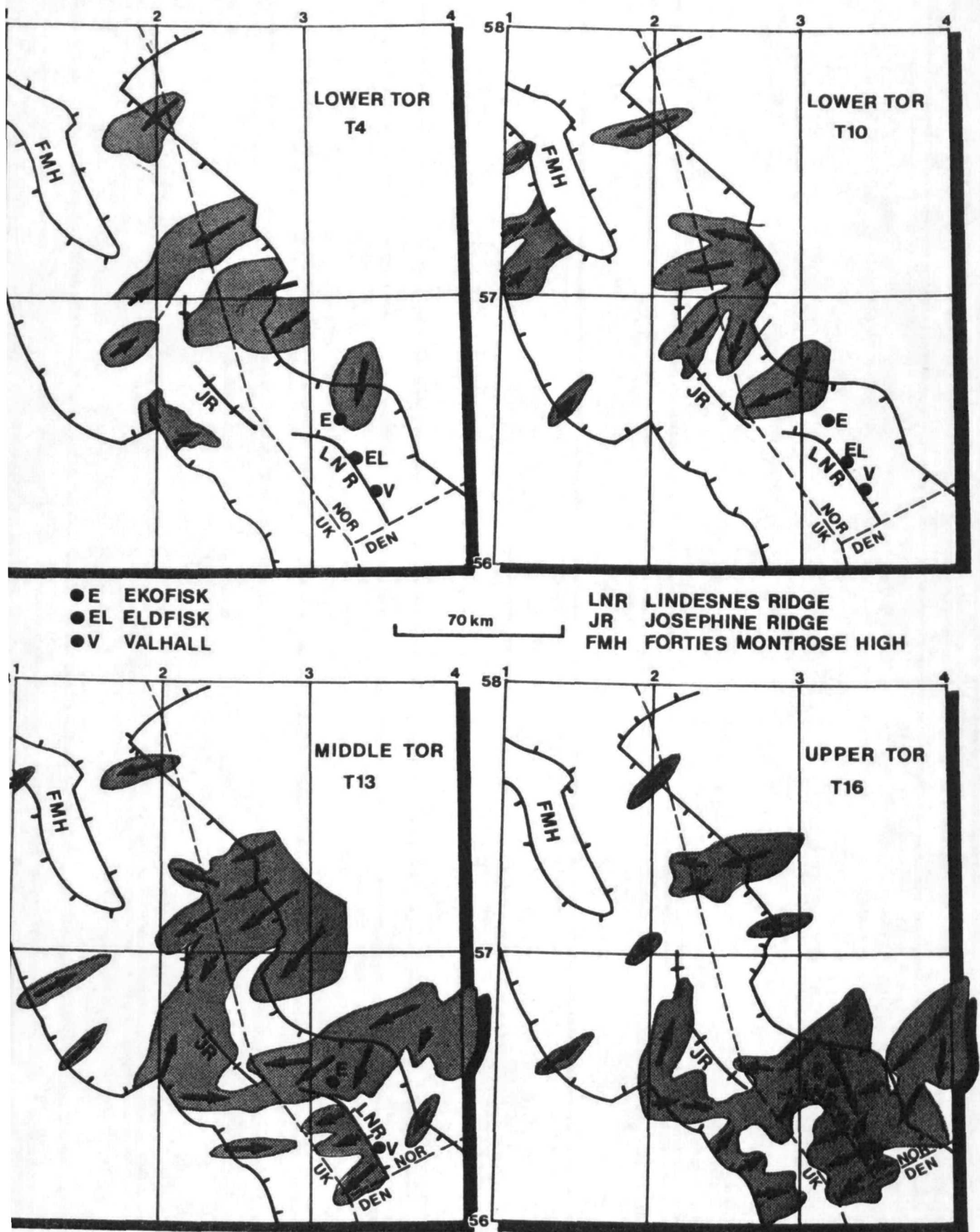


Figure. 3.3. Four maps indicating the increasing intensity of allochthonous deposition, particularly around the Lindesnes Ridge, during the deposition of the Tor Formation Chalks. (After Hatton, 1986.)

Figure 3.4. Schematic map indicating the predominant direction of sediment transportation and re-deposition during the deposition of the Lower Ekofisk Formation Chalks.
(After Kennedy, 1987.)

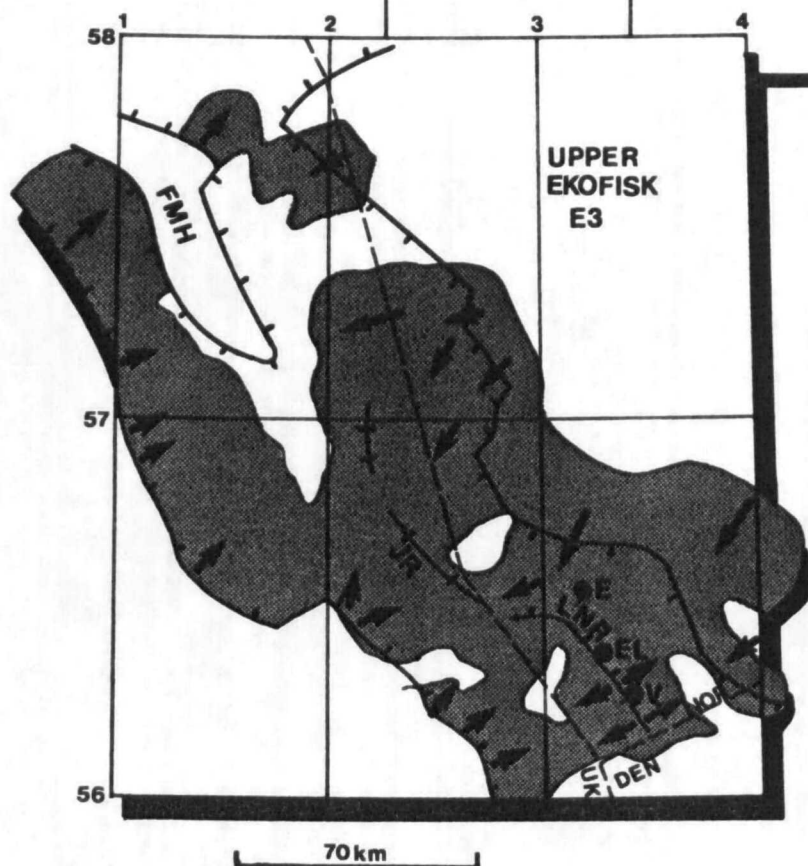
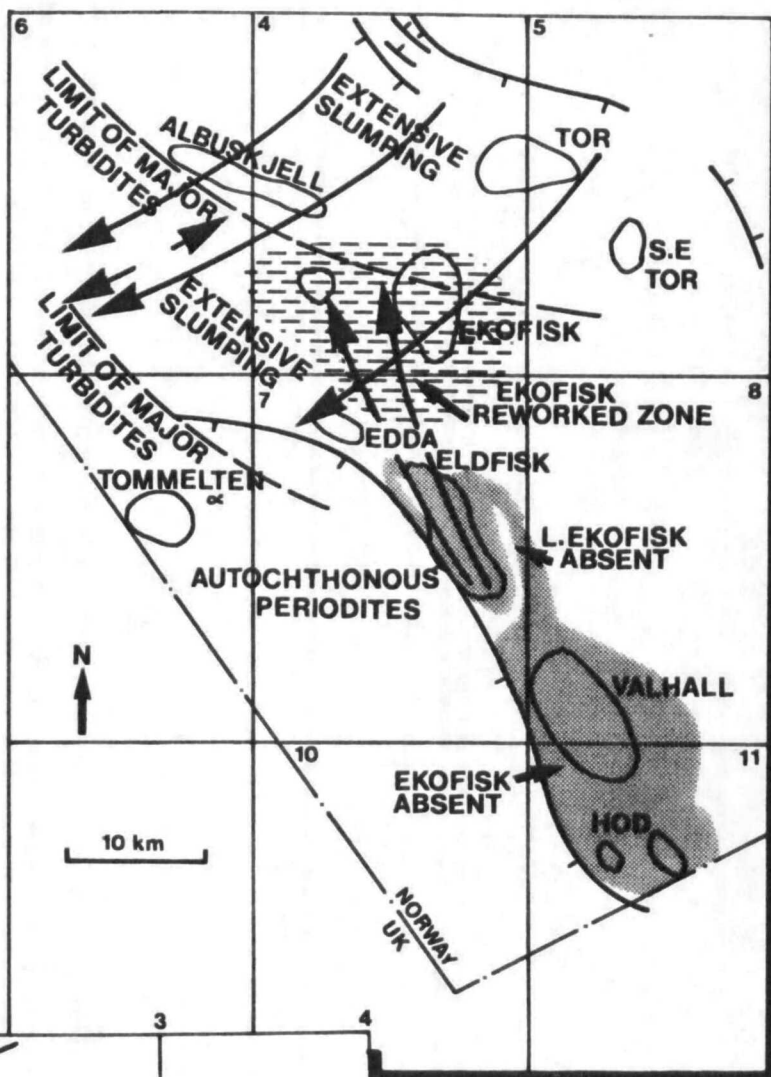


Figure 3.5. Schematic map based on isopach thicknesses indicating re-deposition during the deposition of the Upper Ekofisk Formation Chalks. (After Hatton, 1986.)

The regional tectonic activity which controlled the sedimentation in the Central Graben is further modified by the development of salt diapirs allowing a number of the fields, particularly the ones to the north-east of the Lindesnes Ridge to develop over growing structures (Ofstad, 1983; D'Heur, 1984).

Sorensen et al. (1986) indicate from their studies of high and low productivity chalks that the high productivity reservoir chalks have several features in common:

- *1) They only occur in areas where thick mature Jurassic source rocks exist (see below).*
- *2) They form either over salt structures and/or inversion features with significant relief which showed some structural growth during the Tertiary enabling a fracture network to develop.*
- *3) All the structures show significant relief, and, as the porosity of the chalk decreases, both with increasing depth and laterally away from the crest of the structures, it also forms part of the sealing system. The periodites of the Lower Ekofisk are also thought to prevent communication of oil from the Tor to the overlying Ekofisk Formation (in a number of fields these formations exhibit different pore pressures).*
- *4). There are no overlying Palaeocene sands into which the hydrocarbons would have migrated. No high porosity chalk reservoirs have been found in areas where Palaeocene sands exist. D'Heur (1984) reports that in the first exploration wells on the Ekofisk structure the target horizon was a series of Palaeocene sands. These were found to be absent, but hydrocarbon bearing chalks were discovered 15m below the estimated depth for these sands.*
- *5). The development of overpressuring before structural movement to sustain an open fracture network. Overpressuring is the key to the preservation of porosity in the reservoir chalks, but this is dependent upon the interaction of the other four points.*

The rapid resedimentation and burial of the chalks in a subsiding basin (D'Heur, 1984; Hatton, 1986) ensured that the chalks, with their natural low permeability, could not readily dewater. Equally, bioturbation, the main method by which the chalk dewater, would have also been significantly reduced by the rapid burial. Any biological activity would have been restricted to the vicinity of the upper surface of allochthonous units. The resulting restricted fluid flow in the allochthonous units meant that the increase in overburden accompanying burial would have been preferentially sustained by the pore fluid. This follows the law of effective stress and the basic theories of consolidation (see chapter 4) in which an increase in applied load (total stress) is distributed between the mineral skeleton and the pore fluid. Deformation of the mineral skeleton will only occur in response to an increase in effective stress (total stress minus the pore fluid pressure). On initial loading, this is preferentially seated in the pore fluid (as the pore fluid is less compressible than the mineral skeleton), creating an excess pore fluid pressure. If the permeability of the material is low (as in the chalk) there will be a time delay in the dissipation of this excess pore pressure. As the pore fluid escapes the pore fluid pressure decreases and the effective stress increases leading to a compression of the mineral skeleton (Atkinson and Bransby, 1978; Lambe and Whitman, 1979).

Watts (1983) has concluded from his studies of the fractures in the Albuskjell field that their open nature indicated that the generation of an overpressure occurred before the formation of the fractures, primarily as a result of the rapid burial of the sediment. He also concluded that overpressuring alone could not have been responsible for their production. The fractures he was referring to develop from the tips of stylolites. He noted that they were generally open (ie. uncemented). He used the term tension fractures for these small vertical fractures, but, it would be more appropriate to call them stylolitic fractures (they will be referred as such in section 3.5). He stated that they formed when the minimum effective stress (horizontal, if vertical fractures are formed) was reduced to a tensile stress as a result of the development of an excess pore fluid pressure and a reduction in the total horizontal stress.

During burial, as the total stresses (load) continued to increase, an excess pore pressure could have developed (due to the natural low permeability of the chalk). If this excess pore pressure became greater than the horizontal total stress the horizontal effective stress would have changed from being compressional to tensional. The formation of the stylolitic fractures does not indicate when the overpressuring, which resulted in their formation, began to develop. It is however, probable that if the high pore pressures had not been maintained after their formation, these fractures would have become cemented in a similar manner to the earlier fracture fabric (see section 3.5) seen in the core material (and also observed by Watts, 1983).

Watts (1983) discussed the various factors that led to the development of the overpressures in Albuskjell. He showed that there were three possibilities, rapid burial, early hydrocarbon migration and the influence from maturation of the underlying source rocks. From this he concluded, by back analysis leading to the production of a burial/stress curve (figure 3.6), that rapid burial was the prime cause for the development of the overpressures.

An excess pore pressure (above the hydrostatic pressure of 33.67MPa calculated for a depth of burial of 3200m) of 15.68MPa exists in the Albuskjell field. The total vertical stress has been calculated as 65.8MPa. The burial curve indicated that the effective stresses gradually increased until the chalk had been buried to a depth of 2750m, and that further burial resulted in the rapid development of the excess pore fluid pressure leading to a decrease in the horizontal and vertical effective stresses. Further modelling showed how this burial curve might have been modified by hydrocarbon emplacement which he estimated began in Early Eocene times and reached its optimum in the Early to Middle Oligocene (equal to a depth of burial of 1000m). Hydrocarbon emplacement is calculated to have produced an excess pore pressure of 1.17MPa thus producing a sudden decrease in the effective stresses. This decrease is emphasised still further as fluid pressures developed (6.62MPa) during maturation (conversion from solid kerogen to hydrocarbons just before hydrocarbon emplacement) of the source

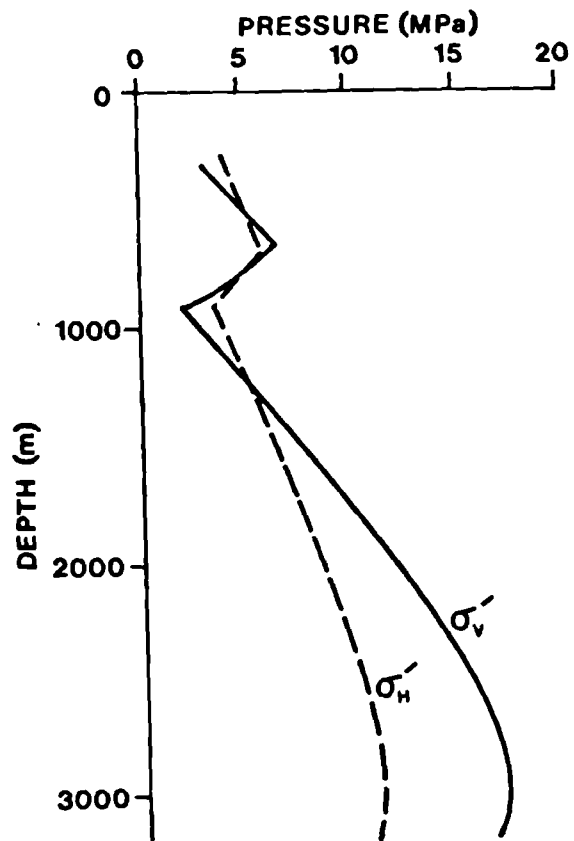


Figure. 3.6. Burial/effective stress curves assuming that overpressuring is related to burial rate, migration of hydrocarbons and increasing maturation pressure. (After Watts, 1983.)

rocks. This was estimated to have occurred at a depth of burial of between 600-1000m and would have produced an excess fluid pressure, including the excess pressure provided by hydrocarbon emplacement of 7.79MPa (Watts gives a total excess fluid pressure of 6.89MPa). The resulting burial curve (figure 3.6) shows that at the time of hydrocarbon maturation and emplacement the resulting excess pore pressure could have led to the horizontal effective stress being higher than the vertical effective stress.

The burial curve indicates that the horizontal effective stress did not reach zero, and Watts therefore concludes that the formation of stylolitic fractures could not have been due to overpressuring alone (he invokes halokinetics as the other driving mechanism). This he says is further emphasised by the fact that these fractures, if they were the result of overpressuring, should have a uniform distribution. However, their distribution can be seen to be (section 3.5) a result of variations in depositional mode, porosity and permeability (as well as differences in other factors such as quartz and clay content) which would have led to the preferential development of overpressuring in particular chalks.

The generally accepted model for the generation of the overpressures is very neat, but may simplify matters too much. For instance the timing of hydrocarbon generation in the Greater Ekofisk area is not clear. Munns (1984) states that it did not reach a significant level until the Middle to Late Miocene, but Hardman (1982) puts the period of peak generation as Late Eocene to Early Miocene. Whichever estimate is true it does not change the fact that by the time of oil invasion the chalk fields had developed into structural highs (see below). They had also been saturated with saline water for something like 50 million years, or 80% of their history, during which it has been assumed that this pore fluid had little detrimental effect on the chalk. The saline pore fluids remained in place until they were displaced by the hydrocarbons.

Although the Central Graben continued to subside throughout and after the deposition of the chalk, the Lindesnes Ridge had developed into an inversion feature and diapiric movements of the underlying salt was becoming important. During the early

Eocene period (Hardman, 1982) the tops of the chalk fields would have been at a depth of between 1000m-2000m below the sea floor. It follows that the period of peak oil generation would have coincided with the chalks reaching the depth at which a further significant reduction in porosity by the onset of additional pressure solution would have started. This indicates that oil emplacement was not essential for the development of overpressuring (Munns, 1984) but played a significant role, in retaining the high porosities by inhibiting the transfer of calcium carbonate by pressure solution. It can be seen that chalks directly above and below the base of the hydrocarbons both have high original porosities (Van den Bark and Thomas, 1979). The oil saturated chalks retained their original porosities, but, the water saturated chalks show extensive solution and cementation resulting in a loss of porosity. The hydrocarbon saturated chalks, especially the higher porosity Tor Formation chalks, also contain large dentate stylolites. These pressure solution features, indicate the dissolution of significant quantities of chalk. However, the adjacent chalks do not show a significant reduction in porosity. These stylolites imply, following the model generally accepted, a period of late stage dissolution. This is not surprising as, although the top of the chalk would have only reached a depth of 1000m-2000m during the period of oil emplacement the chalks of the Tor and Hod Formations would have been significantly lower. These would have been below the level at which pressure solution becomes a significant factor, and hence, presumably the higher frequency of stylolites. Are we to assume that pressure solution was selective, in that it resulted in the development of stylolites but did not produce the blanket reduction in porosity seen in the surrounding aquifers. The porosities of the Tor Formation chalks in particular do not appear to be significantly lower than those of the overlying Ekofisk Formation. The relative timing of the formation of stylolites and the other deformational features seen in core material will be discussed further in section 3.5.

The 1219m (4000ft) of Kimmeridge Shales, the source rocks for the hydrocarbons, are separated from the chalks by a thick sequence of Lower Cretaceous argillaceous sediments (Hardman, 1982; 1983). A growing structure was required to develop a fracture

system within these argillaceous sediments to allow the passage of the oil into the overlying chalks. For the oil to enter the chalks it needed to be at a high enough pressure (termed the entry pressure) to overcome the in situ capillary pressure and therefore be able to displace the brines from the pore spaces (Hardman, 1982; 1983). The capillary pressure represents the magnitude of the resistance to entry. Hardman (1983) indicates that there are three different factors which interact to determine the capillary pressure:

- 1) *the radius of the pore throats,*
- 2) *hydrocarbon-water interface tension,*
- 3) *wettability.*

As the chalks had low permeabilities, small pore throats and high existing pore pressures this entry pressure would have had to have been quite high. In fact, it has been proposed that this pressure became so high it ruptured the base of the overlying shales (Hardman, 1982) and hence the formation of the gas clouds in the overburden above many of the fields. This increasing pressure has been partly attributed to the structural development of the area (Hurst, 1983). Hardman (1983) and Watts (1983, see discussion above) suggested that compaction of the Kimmeridge Shales would have been able to generate some of the pressure needed to infiltrate the chalks. However, the buoyancy of oil and gas appears to be the main driving force for their migration. This increases upwards in a continuous oil column (Hardman, 1983). As the chalks fractured over the growing structures it allowed the oil to enter. Hardman, (1983), also notes that the chalks are easier to saturate with lighter oils over 36°API (gravity) such as those found in the North Sea as these lighter oils have lower hydrocarbon-water interfacial tensions and therefore the capillary pressure is lower. The fractures, which in the Valhall field are on the millimetre scale (Ofstad, 1983) provided the short drainage paths needed for the migration of oil to displace the existing pore fluids. The different pore throat

sizes of the Danian and Maastrichtian chalks may have resulted in a different level of water immobility in the chalks and different entry pressures (Hurst, 1983).

This is the usual story for the sequence of events that has led to the oil emplacement in the Greater Ekofisk area. But it does raise several problems. Firstly, Watts (1983) lists the estimated overpressure produced by burial as 1.02MPa at a depth of 1000m. He then says that the buoyancy pressure for a 183m gas column in Albuskjell is 1.17MPa. Is an excess pressure of 0.15MPa really large enough to be the main driving force needed for the hydrocarbons to be able to displace the existing pore fluids from a low permeability rock even over a long period of time? The significantly higher maturation pressures (see discussion above) combined with the above would certainly allow hydrocarbons to displace the brines. Does the pore throat size influence the permeability, thus dictating the entry pressure needed for each horizon? The study by Schatzinger (1985) concerning the pore geometry of the chalks in the Ekofisk field, indicated that the average pore throat size was 0.25 microns and that for pore throats smaller than 3 microns the permeability was independent of pore throat size.

The fracture distribution aspects of the emplacement of the oil have also been oversimplified (see section 3.5 for a detailed discussion). The fractures are neither consistent in their distribution nor preferentially open. Most appear to have been healed early in their history. If this is the case, the widely accepted theory (Van Den Bark and Thomas, 1980; D'Heur, 1984) that oil emplacement retarded cementation is not necessarily true. The distribution of the open stylolitic fractures is obviously dependent on the distribution of the stylolites, which appear to be preferentially developed in certain horizons. Pore pressure differences are now recorded between reservoirs in each of the fields resulting from different capillary and entry pressures (see above). Hardman (1983) indicated that the entry pressures for the Tor and Lower Hod of the Valhall Field were around 2.11MPa, and for the Middle Hod it would have been 7.75MPa. These differences and the lack of communication between reservoirs indicates the existence of permeability barriers (D'Heur, 1984). These must have originally been

breached by open fractures for the oil to be able to migrate from the source rocks. Why and when did these fractures close? If oil retards cementation, how were they sealed, if in fact they really do prevent communication between reservoirs? Mechanical compaction could account for this only if the effective stresses increased as the Central Graben continued to subside, and the burial curves of Watts (1983) show a continuous increase in effective stresses after hydrocarbon emplacement.

It is possible that the pore fluid was able to move out of the reservoir (even if only very slowly). After all, the gas clouds that exist above many of the fields may have developed some time after oil invasion as the pore pressure continued to increase with burial. Finally, if the oil displaced the resident brines, where did the brines go? There are few references that indicate where the water went, but, presumably it was displaced either up into the overburden, outwards into the surrounding water saturated chalks or down into the underlying tighter chalks. D'Heur (1984) says simply, 'the hydrocarbons of the lowered [porosity] zone migrated towards higher areas in the reservoir and the water invaded the lowered porous rock.' It would seem more probable that the water was displaced laterally into the surrounding chalks. This may well have been a contributing factor to the cementation of the aquifer and thus the destruction of its porosity and the sealing in of the reservoirs. The passage of such a significant amount of even partially CaCO_3 saturated water should have had a dramatic effect on the surrounding chalks even though it is widely thought that during diagenesis calcium does not migrate over large distances.

3.4. THE LITHOSTRATIGRAPHIC CHARACTERISTICS OF THE NORWEGIAN CHALK FORMATIONS.

Figure 3.7 presents a generalised stratigraphic correlation between the chalks in the Norwegian sector of the Central Graben and those exposed in South East England. The names of the different units in the Norwegian sector follow the nomenclature proposed by the joint Norwegian Petroleum Directorate / Institute of Geological Sciences report 77/25 (Deegan and Scull, 1977). The divisions used in the Danish sector fields are dif-

	STAGE	SOUTH EAST ENGLAND	NORWEGIAN NORTH SEA
TERTIARY	DANIAN	Missing	EKOFISK CHALK
CRETACEOUS	MAASTRICHTIAN		TOR CHALK
	CAMPANIAN	UPPER CHALK	HOD CHALK
	SANTONIAN		
	CONIACIAN		
	TURONIAN	MIDDLE CHALK	PLENUS MARL HIDRA CHALK
	CENOMANIAN	LOWER CHALK	

After Kennedy 1987 and
Hancock 1987

Figure. 3.7. A generalised stratigraphic correlation between the chawks of the North Sea and those found in South East England.

ferent to the Norwegian ones as the correlations are not clear (Michelsen, 1982). These chalks are labelled units one to six. They have not been included as they are not considered in this project. It will be seen that chalks equivalent to the main reservoir rocks (Tor and Ekofisk Formations) do not exist in south east England.

The chalks in the Norwegian sector of the Central Graben have been divided into five formations, namely the Hydra, Plenus Marls, Hod, Tor and Ekofisk. They are all of Cretaceous age except for the Ekofisk Formation which is Danian (Tertiary). The following is a synopsis of Kennedy's sedimentological studies reported above.

3.4.1. Hydra Formation (Cenomanian).

These autochthonous deposits closely resemble the Lower Chalk of South East England. They consist of alternations of chalk and marls with concentrations of coarser debris at the base of some of the chalks which may indicate the presence of some minor turbidites. Bioturbation is extensive. The boundary with the overlying Plenus Marl is represented by a glauconitised hardground that can be traced over the whole of the Anglo-Paris Basin.

3.4.2. Plenus Marl Formation (Cenomanian).

The Plenus Marls are also periodites in which both elements have been silicified. The limestones show some evidence of bioturbation but also contain layers in which the primary laminations still exist. There is evidence for the existence of some minor turbidites as in the Hydra Formation. The clay sequences have undergone severe post-depositional solution which has destroyed all evidence of their original depositional fabrics.

3.4.3. Hod Formation (Turonian to Upper Campanian).

This formation may be divided into three members, Upper, Middle and Lower.

The Lower Hod consists of a series of distal turbidites (and some graded calcarenites) alternating with laminated and bioturbated chalks. There are indications of plastic

deformation, which implies dewatering (see above). Towards the top of the sequence, the sedimentation changes to alternating bioturbated and laminated chalks. These represent rapidly deposited distal turbidites in which the top of each unit is bioturbated (plate 3.15). In well 2/8-8 on the Valhall structure, (Kennedy, 1987) the greenish marls and calcareous siltstones indicate the presence of bottom currents. These particular sediments clearly show the extent and nature of the slumping and folding which is present but difficult to see in the cleaner chalks (see plates).

The Middle Hod sediments represent a return to a quiescent environment with the deposition of periodites. Bioturbation is extensive and represented by the trace fossils such as *Thalassinoides*, *Zoophycos* and *Chondrites*. Cores throughout the area show little variation with a few wells showing evidence of turbidite activity.

The Upper Hod begins with periodite deposits which are gradually replaced by distal turbidites, in which laminated chalks are predominant. These are similar to the Lower Hod turbidites. The Upper Hod is either condensed or missing in the Eldfisk, Valhall and Hod Fields.

In a limited area the boundary between the Hod and the overlying Tor Formation is represented by an unconformity and conglomerate consisting of clasts from the Hod.

3.4.4. Tor Formation (Upper Campanian to Maastrichtian).

This formation represents the main reservoir in all the Central Graben fields. The Lower Tor Formation starts with a sequence of distal turbidites which show signs of later slumping (this produces a shredded texture). In the Tor, Ekofisk, West Ekofisk and Albuskjell area the Tor Formation shows a change from the deposition of distal to more proximal sediments. These develop from distal turbidites to intraclastic debris flows and, at the top of the Tor a series of slumped chalks, in which the clasts are less obvious. As noted above, many of the individual allochthonous units can be traced throughout the area. Some of the debris flows contain Bryozoans similar to those in the

onshore chalks of Denmark. The Tor/Ekofisk boundary is marked by a change in facies from clean chalks to black shales containing clasts of Maastrichtian age. In a number of fields, this boundary is also marked by a basal conglomerate and/or hardground.

3.4.5. Ekofisk Formation. (Danian, Tertiary).

The Ekofisk Formation is divided into upper and lower member. The lower member is highly variable throughout the area. To the south-west around Tommeliten Gamma the Lower Ekofisk consists of autochthonous periodites, similar to the Middle Hod. To the north-west in the Albuskjell area the sequence starts with periodites but these are gradually replaced by slides and slumps. Tor lies to the north-east beyond Ekofisk close to the Graben boundary faults. Here, the base is marked by a series of turbidites above which slide sheets of periodites are found. Ekofisk, West Ekofisk and Eldfisk are characterised by shales at the base of the Lower Ekofisk Formation followed by a thick allochthonous sequence which is generally referred to as the Ekofisk reworked zone. This consists of redeposited Maastrichtian chalks and is an important reservoir in all three fields. Reworked chalks of Maastrichtian age continue up into the overlying Maureen Formation in Eldfisk. Finally, to the south, in Valhall and Hod the Ekofisk Formation is missing. The Upper Ekofisk Formation is interpreted as a series of mud flows generally producing homogeneous, bioturbated featureless chalks.

3.5. FRACTURE STUDIES.

Having described the sedimentary processes observed in the reservoir chalks, it is important to review the types and distribution of the natural fractures. The chalk can be regarded as a dual porosity and dual permeability rock. The matrix porosity may be as high as 50% but the fracture porosity has been estimated to be less than 0.4% (Hardman, 1982). Conversely, the matrix permeability is usually less than 10mD but the fracture (effective) permeability (see table 5.1) may be as high as 200mD. This means that the fractures provide the fluid communication network that allows hydrocarbon production from this otherwise low permeability rock.

Although fracture studies will have been undertaken by oil companies involved with the chalk fields in the Greater Ekofisk Area, little information has been published on the subject. Most papers which mention the fracture system give few details (for example, Hardman and Kennedy, 1980; Van Den Bark and Thomas, 1980; Hardman, 1982; Ofstad, 1983; Munns, 1984; Sorensen et al., 1986). There are however a few exceptions such as Watts (1983); Brewster et al. (1986); and Thomas et al. (1987).

Thomas et al. (1987) recognise four types of fractures in chalk cores, whilst Brewster et al. (1986) use only three divisions and appear to include the latter two types (healed and irregular) of Thomas as one group. The classification given below is a combination of the work reported in both papers and includes details from other published work where necessary.

- *1) Stylolitic. These occur individually or in braided networks which never cross the stylolites. They are usually up to 5cm long and rarely exceed 15cm with a spacing of 0.5-5cm. They are generally restricted to the Tor Formation and the Ekofisk Reworked Zone. (See the discussion in section 3.3 on the study by Watts (1983) of the fractures in the Albuskjell field).*
- *2) Tectonic. These are planar fractures with dips that vary from 60°-75°. Displacements along these fractures vary from millimetres to a few centimetres and they represent small scale faults with surfaces that are either smooth or slickensided. They can be found as conjugate pairs, or fracture systems (a fracture system may be defined (Van Golf-Racht, 1982) as all fractures having a mutually parallel direction). These provide the most effective permeable pathways.*
- *3) Healed. These are the earliest fractures to form and are displaced by all other fractures. They occur as either single fractures or in networks (a fracture network is defined by Van Golf-Racht (1982) as a combination of a number of fracture systems) with no visible porosity and are therefore effectively impermeable. As these fractures are cemented they are stronger than the surrounding matrix. They appear to have formed as a result of brittle deformation of the partially lithified chalk and are intimately associated with reworked sediments. SEM analyses of core material from the Ekofisk field (Schatzinger, 1985) indicated that these early fractures contained whole or broken coccoliths which fell into the fractures before they were cemented while*

the chalk was still in a semi rigid state. There is evidence that the fractures were closed by the collapse of the fracture walls and that occasionally, later diagenetic processes lead to the injection of clays.

- *4) Irregular. No description of this type of fracture is provided in Thomas et al. (1987), but they are generally healed and can be described as hairline in appearance. Apart from their shape and orientation which are irregular they resemble the other early healed fractures. The calcite cement is either medium or coarse grained.*

The first two types are thought to enhance the permeability of the chalks in which they have formed as they are preferentially open. The distribution of fracture types is not consistent. Tectonic fractures are the more prominent open fractures in the Ekofisk Formation where there are fewer stylolites, and stylolitic fractures are predominant in the Tor Formation due to the higher frequency of stylolites.

Fracture distribution and intensity appears to depend on the hardness of the chalk and the structural position, and varies from well to well. Hardman and Kennedy (1980) and Hardman (1982) investigated the fracture system in the Ekofisk, Tor and Hod Formations. They found that the types and distribution of the fractures varied from formation to formation. Fracturing was most intense where the chalk was thinnest (ie. over the crests of structures) and was concentrated in the weakest (high porosity) chalks. Conversely, others have concluded that fracturing intensity is highest in the medium to hard chalks of the Ekofisk Formation and the hard chalks in the Tor Formation. Most appear to agree that fractures are less frequent in the chalks with a high clay content. The Hod Formation contained small fractures that may have been tensional (Hardman and Kennedy, 1980; Hardman, 1982). These fractures died out vertically in either direction (up and down) and were found to be associated with slumping rather than the development of the later tectonic fracturing. Fractures were found to both cut and follow some stylolites while they were also offset by other fractures indicating the presence of two sets of stylolites. Slumped zones such as the Lower Ekofisk Formation of the Ekofisk Field contain steeply dipping stylolites with associated open fractures (Pederstad et al.,

1988). High angle fractures are frequently found in the Tor Formation which contain clay coatings (Hardman and Kennedy, 1980; Hardman, 1982). This formation was the most intensely fractured of the three, with the chalks frequently being broken into 1-2cm blocks (the block size in the Hod Formation is generally in the range 5cm to several metres). The Ekofisk Formation contained fractures similar to those found in the Tor Formation.

There is some disagreement over the vertical distribution of fractures. Van Den Bark and Thomas (1980) noted that as the average porosity increased with depth in the Ekofisk Field (25- 30%, Upper Ekofisk; 30-40%, Lower Ekofisk; 35-40%, Tor) the frequency of fracturing increased, but Hardman and Kennedy (1980) and Hardman (1982) state that fracturing decreases with depth. This difference may be partly due to variations in the fracture distribution both from field to field, and well to well. Van Den Bosch (1983) felt that lack of fracturing in the crest of the Harlingen Field, compared to that of Ekofisk, was due to the less well developed structure of the former.

3.5.1. Lithological and fracture study of well 2/7-B11.

As published information was unable to provide the relationships between sedimentation, diagenesis and fracture development it was decided to produce a detailed log of the core from well 2/7-B11 from the Eldfisk Field. This particular core is one of the most complete and extensive cores recovered from the Greater Ekofisk Area (figure 3.8).

The Eldfisk field, discovered in 1969, is an elongate haliokinetic anticline lying across the Lindesnes Ridge in the south of the Greater Ekofisk area (Brewster and Dangerfield, 1984; D'Heur, 1984). The field consists of three separate reservoirs, namely North Eldfisk, South Eldfisk and East Eldfisk. The North and South reservoirs are separated by a sealed fault (Ofstad, 1981). These in turn are separated from the East Eldfisk reservoir by a saddle of low porosity chalk (Ofstad, 1981). The depth to the top of the chalk (Michaud, 1987) varies in the two major reservoirs from 2700m (South Eldfisk) to

LITHOLOGICAL AND FRACTURE LOG

Field: N. ELDFISK
Well: 2/7-B11

Sheet No. 1

Depth (feet)	Lithology	Bedding Orientation	Bedding Interval (cm)	Secondary Def.	Bioturbation	Fossils	Clay Content	Stylolites	Clay Seams	Silica Content	Pyrite	FRACTURES								Comments	
												1st Set				2nd Set					Others
												Frequency	Orientation	Spacing (cm)	Filling	Frequency	Orientation	Spacing (cm)	Filling		
9812																					
13																					Dewatering structure
14																					
9815		H	1-2		H		H/L			H		H	90	3	H						RUBBLE
16						B															
17																					Possible turbidite
18	MISSING																				
19	MISSING	H	1-2		H	B	M			H											
20	MISSING		PRESERVED																		
9820		H	2-3		H		H/L			H	✓										
21	MISSING																				
22		H	0-5		H		H/L			H	✓										
23			-3				H				✓										
24							H				✓										
25	MISSING																				
9825						B							0		O						
26		H	1-2		H ₂							L	90		H						
27	MISSING																				
28		H	1-2		H ₂		L					L	30 _R		C						
29	MISSING		PRESERVED																		
9830																					
31																					
32		H	≈				M					L	60 _R		H						
33							M					L	90	1	O	L	45 _L		O/H		
34												L	90		O					SL	
9835	F						L				✓	H	90		O						Solution
36	MISSING											L	90		H						
37	F	10			H/L		L					L	50 _R		C	L	30-60 _L	1-3	H	SL	FB

Key

Lithology		Secondary Deformation		Bioturbation		Fractures	
	Grain Flow		SR Shredded	H High	FB Fracture blocks	I Irregular	
	Coarse		ST Streaked out	L Low	SF Stylolitic fractures	V Variable	
	Medium		F Folded	2 No. of sets	SL Slickensides	HL Hairline	
	Fine		FL Faulted				
	Turbidite		P Plastic	Clay Content		Fillings	
	Homogeneous		B Shell fragments	H High	A Alternating	O Open	
				L Low	↑ Inc. downwards	H Healed	
				M Mottled	↓ Dec. downwards	C Clay	
				I Irregular		S Block surface	

Figure 3.8. A log of well 2/7-B11 constructed to indicate facies control on fracture development.

LITHOLOGICAL AND FRACTURE LOG

Field: N. ELDFISK
Well: 2/7-B11

Sheet 2
No. 2

Depth (feet)	Lithology	Bedding Orientation	Bedding Interval (cm)	Secondary Def.	Bioturbation	Fossils	Clay Content	Stylolites	Clay Seams	Silica Content	Pyrite	FRACTURES								Comments			
												1st Set				2nd Set					Others		
												Frequency	Orientation	Spacing (cm)	Filling	Frequency	Orientation	Spacing (cm)	Filling				
9837		10			L																		
38	MISSING PRESERVED																						
39	Su F	H	5		L															SL FB			
9840																					L	45 _R	H
41	Su	H	4		L	L	L	✓															
42																					L	L	✓
43																					L	L	✓
44																					L	L	✓
9845		10																					
46																							
47										L		H	90	2-3	H					FB 2-3cm			
48																							
49		20-30																					
9850	Su											H	90	2-3	H ₀					FB 2-3cm			
51																							
52	F																						
53																							
54	MISSING PRESERVED																						
9855																							
56																							
57	Su	<35						✓				H	90	0.2-0.5	H	H	90	V	H				
58																							
59																							
9860	MISSING																						
61	Su F																			RUBBLE			
62																							

Key

Lithology			
	Grain Flow		Laminated
	Coarse		Slump
	Medium		Conglomerate
	Fine		Periodite
	Turbidite		Shale
	Homogeneous		

Secondary Deformation	
SR	Shredded
ST	Streaked out
F	Folded
FL	Faulted
P	Plastic
Fossils	
B	Shell fragments

Bioturbation	
H	High
L	Low
2	No. of sets
Fractures	
FB	Fracture blocks
SF	Stylolitic fractures
SL	Slickensides
HL	Hairline
Clay Content	
H	High
L	Low
M	Mottled
I	Irregular
Fillings	
O	Open
H	Healed
C	Clay
S	Block surface

LITHOLOGICAL AND FRACTURE LOG

Field: N.ELDFISK
Well: 2/7-B11

Sheet No. 3

Depth (feet)	Lithology	Bedding Orientation	Bedding Interval (cm)	Secondary Def.	Bioturbation	Fossils	Clay Content	Stylolites	Clay Seams	Silica Content	Pyrite	FRACTURES								Comments		
												1st Set				2nd Set					Others	
												Frequency	Orientation	Spacing (cm)	Filling	Frequency	Orientation	Spacing (cm)	Filling			
9862	F											H	90	2-3	H	H	0	0.5	H		80' weak healed fractures	
63	Su				H			✓			✓	H	90	0.2-5	H							
64												H	90	0.2-5	H	H	90	0.2-5	H		RUBBLE	
9865	MISSING PRESERVED																					
66	Su M	30										L	45 _R		H							
67																						
68								✓				H	90		H							
69	Su																					
9870	F Su	H										H	90	0.5-1.5	H							
71								✓				H	90	<6	H	H	90	1-2	H			
72																					RUBBLE	
73	Su																					
74	MISSING PRESERVED																					
9875																						
76	M Su	H			ST	L						H	90	2	H							
77																						
78						SR						H	90	<0.4	H	H	70 _R		H			
79		20				ST	L	M	✓				H	90	5	H					FB	
9880								✓				L	90		H	H	90	2-6	H	FB		
81		?						✓				L	90		O							
82			2-7		L			✓				H	90		H							
83								✓				H	90	0.8	H	H	90	4x4 X16	H	SF		
84												L	50 _L		H							
9885		?			L																FB 45°	
86												H	90	1x2.5 X13	H							
87												H	40 _L	1.5-3	H							

Key

Lithology		Secondary Deformation		Bioturbation		Fractures	
	Grain Flow		Laminated	H	High	FB	Fracture blocks
	Coarse		SR Shredded	L	Low	SF	Stylolitic fractures
	Medium		ST Streaked out	2	No. of sets	SL	Slickensides
	Fine		F Folded			HL	Hairline
	Turbidite		FL Faulted	Clay Content		Fillings	
	Homogeneous		P Plastic	H	High	A	Alternating
				L	Low	↑	Inc. downwards
				M	Mottled	↓	Dec. downwards
				I	Irregular		
						S	Block surface

LITHOLOGICAL AND FRACTURE LOG

Field: N.ELDFISK
Well: 2/7-B11

Sheet No. 4

Depth (feet)	Lithology	Bedding Orientation	Bedding Interval (cm)	Secondary Def.	Bioturbation	Fossils	Clay Content	Stylolites	Clay Seams	Silica Content	Pyrite	FRACTURES								Comments	
												1st Set				2nd Set					Others
												Frequency	Orientation	Spacing (cm)	Filling	Frequency	Orientation	Spacing (cm)	Filling		
9887	Su?	<45?										H	40L		H						
88														3x7						FB	
89												H	45L		H	H	45R		H		
9890		?			✓																
91																					
92													L	45R		H					
93													L	90	V	H					
94						✓							3	10L	0.4	H	H	90	0.7	H	
9895										✓			H	90 & 80L	0.8	H	H	10R	2-7	H	10' healed fractures
													H	90	0.8	H					FB
96	MISSING PRESERVED																				
97		?			2							H	60L	1-2	H/O		70R	0.5-1	H/O		
98												L	90	weak	H	L	90	weak	H	FB	
99									S	✓		H	0	1-1.5	H					FB	
9900												H	90	3x4x6	H						
01					✓							H	90	1 x 2.5 x 3.5	H					} RUBBLE	
02																					
03																					
04			?										H	90	0.5-1	H					
9905													H	50L		H					
06																					} RUBBLE (end of core 3)
07					?							H	90	0.5	H						
08																					
09																					
9910		10			✓				✓												} Large blocks
11																					
12		MISSING PRESERVED																			

Key

Lithology		Secondary Deformation		Bioturbation		Fractures	
	Grain Flow		SR Shredded	H High		FB Fracture blocks	I Irregular
	Coarse		ST Streaked out	L Low		SF Stylolitic fractures	V Variable
	Medium		F Folded	2 No. of sets		SL Stickensides	HL Hairline
	Fine		FL Faulted	Clay Content		Fillings	
	Turbidite		P Plastic	H High	A Alternating	O Open	
	Homogeneous		B Shell fragments	L Low	↑ Inc. downwards	H Healed	
				M Mottled	↓ Dec. downwards	C Clay	
				I Irregular		S Block surface	

LITHOLOGICAL AND FRACTURE LOG

Field: N. ELDFISK
Well: 2/7-B11

Sheet No. 5

Depth (feet)	Lithology	Bedding Orientation	Bedding Interval (cm)	Secondary Def.	Bioturbation	Fossils	Clay Content	Stylolites	Clay Seams	Silica Content	Pyrite	FRACTURES								Comments																			
												1st Set				2nd Set					Others																		
												Frequency	Orientation	Spacing (cm)	Filling	Frequency	Orientation	Spacing (cm)	Filling																				
9912	MISSING	PRESERVED																																					
13		H			↑	↑	✓	HL				H	90	0.5- 2	H																								
14													I		H																								
9915																																							
16													2	20 _R		H												FB											
17	Su ?	20			✓	↓	✓		✓	S		H	90		H	H	70 _L		H																				
18													L	60 _R	0.8	H																							
19													I	90		H	H	80 _L		H	FB																		
9920												MISSING	PRESERVED																										
21	MISSING																																						
22					2	↑	✓	S				H	90	0.2	H																								
23																																							
24	MISSING	PRESERVED																																					
9925					↓				H			H	90		H	L	0	1	?																				
26																													{Escape structure										
27																																							
28																✓							H	90	HL	H	H	90	1.5- 2	H									
29	MISSING	PRESERVED																																					
9930					✓ ↑																																		
31																																							
32																																							
33																																							
34																																							
9935																											S	✓											
36																																L	45 _R		H				
37																																							

RUBBLE(end of core4)

Key

Lithology		Secondary Deformation		Bioturbation		Fractures	
	Grain Flow		SR Shredded	H High		FB Fracture blocks	I Irregular
	Coarse		ST Streaked out	L Low		SF Stylolitic fractures	V Variable
	Medium		F Folded	2 No. of sets		SL Slickensides	HL Hairline
	Fine		FL Faulted				
	Turbidite		P Plastic	Clay Content		Fillings	
	Homogeneous			H High	A Alternating	O Open	
				L Low	↑ Inc. downwards	H Healed	
				M Mottled	↓ Dec. downwards	C Clay	
				I Irregular		S Block surface	












LITHOLOGICAL AND FRACTURE LOG

Field: N.ELDFISK
Well: 2/7-B11

Sheet No. 6

Depth (feet)	Lithology	Bedding Orientation	Bedding Interval (cm)	Secondary Def.	Bioturbation	Fossils	Clay Content	Stylolites	Clay Seams	Silica Content	Pyrite	FRACTURES								Comments												
												1st Set				2nd Set					Others											
												Frequency	Orientation	Spacing (cm)	Filling	Frequency	Orientation	Spacing (cm)	Filling													
9937	Su	40			✓ 2		H ↓														} RUBBLE											
38																																
39																																
9940																					} Solution seams											
41	MISSING PRESERVED																															
42	Su	20										H	45 _L - 45 _R	3-7	H/C	H	90	0-5	H/O	FB		45°										
43																														} Leached vugs		
44																																
45																																
46																																
47																																
48																																
49																																
9950	MISSING PRESERVED																															
51	Su	20																				} Escape structure										
52																																
53																																
54																																
55																																
56																																
57																																
58																																
59																																
9960																																
61																																
62																																

Key

Lithology				Secondary Deformation		Bioturbation		Fractures				
	Grain Flow		Laminated	SR	Shredded	H	High	FB	Fracture blocks	I	Irregular	
	Coarse	} Debris Flow	 Su Slump	ST	Streaked out	L	Low	SF	Stylolitic fractures	V	Variable	
	Medium			F	Folded	2	No. of sets	SL	Slickensides		HL	Hairline
	Fine			FL	Faulted							
	Turbidite		Conglomerate	P	Plastic	Clay Content		Fillings				
	Homogeneous		Periodite	Fossils		H	High	A	Alternating	O	Open	
			Shale			L	Low		Inc. downwards	H	Healed	
				B	Shell fragments	M	Mottled		Dec. downwards	C	Clay	
						I	Irregular					
										S	Block surface	

LITHOLOGICAL AND FRACTURE LOG

Field: N.ELDFISK
Well: 2/7-B11

Sheet No. 7

Depth (feet)	Lithology	Bedding Orientation	Bedding Interval (cm)	Secondary Def.	Bioturbation	Fossils	Clay Content	Stylolites	Clay Seams	Silica Content	Pyrite	FRACTURES										Comments	
												1st Set					2nd Set						Others
												Frequency	Orientation	Spacing (cm)	Filling	Frequency	Orientation	Spacing (cm)	Filling				
9962												H	90	0.7- 1.5							FB		
63				FL			✓	✓				H	90	>0.3	H/C	2	50L			C			
64	MISSING PRESERVED																						
9965					ST	✓																	
66		H									?												
67			CR 1				S					1	90		H						SF		
68			CP 5-8	ST	✓		↓	✓				H	V	HL									
69												H	90	2	H								
9970							↑					V	80L		H								
71	Su	20			✓		↑	✓			?	L	45L		H	H	90	2	H		SL		
72		30			✓							1	45L		C								
73		H			✓				2			H	10R		?						FB		
74	MISSING PRESERVED																						
9975	Su				✓		↑	✓			?												
76							S					2	50L		C								
77		H 10					↓					H	40L		H								
78							↑		C														
79		10		SR	✓	2						L	50L		C								
9980		H							✓			L	V		C								
81	MISSING PRESERVED																						
82	Su	20				↓																	
83						2						L	60R		H/C		80L	6		FB	80°		
84				SR			H					2	45L		H/C								
9985							H																
86	Su	20		F	L	2																	
87																							

Key

Lithology			
	Grain Flow		Laminated
	Coarse		Slump
	Medium		Conglomerate
	Fine		Periodite
	Turbidite		Shale
	Homogeneous		

Secondary Deformation

SR	Shredded
ST	Streaked out
F	Folded
FL	Faulted
P	Plastic

Fossils

B	Shell fragments
---	-----------------

Bioturbation

H	High
L	Low
2	No. of sets

Clay Content

H	High
L	Low
M	Mottled
I	Irregular

Fractures

FB	Fracture blocks	I	Irregular
SF	Stylolitic fractures	V	Variable
SL	Slickensides	HL	Hairline

Fillings

O	Open
H	Healed
C	Clay
S	Block surface

LITHOLOGICAL AND FRACTURE LOG

Field: N. ELDFISK
Well: 2/7-B11










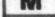

Sheet No. 8

Depth (feet)	Lithology	Bedding Orientation	Bedding Interval (cm)	Secondary Def.	Bioturbation	Fossils	Clay Content	Stylolites	Clay Seams	Silica Content	Pyrite	FRACTURES								Comments	
												1st Set				2nd Set					Others
												Frequency	Orientation	Spacing (cm)	Filling	Frequency	Orientation	Spacing (cm)	Filling		
9987																					
88		10			L				S												
89	MISSING PRESERVED																				
9990					L			S				90	0.5-3	C/O/F		70R	>1	C/O/F	FB		
91																					
9992																					

Transition zone between Ekofisk and Tor Formations is missing

10060																																																																																																																																																																																																																																																																																																																																																																																																																																																																																																																																																																																																																																																																																																																																																																																																																																																																																																																																																																																																																																																																																																																																																																																																																																																																																																																																																																																																																																																																																																																																																																														</
-------	--	--	--	--	--	--	--	--	--	--	--	--	--	--	--	--	--	--	--	--	--	--	--	--	--	--	--	--	--	--	--	--	--	--	--	--	--	--	--	--	--	--	--	--	--	--	--	--	--	--	--	--	--	--	--	--	--	--	--	--	--	--	--	--	--	--	--	--	--	--	--	--	--	--	--	--	--	--	--	--	--	--	--	--	--	--	--	--	--	--	--	--	--	--	--	--	--	--	--	--	--	--	--	--	--	--	--	--	--	--	--	--	--	--	--	--	--	--	--	--	--	--	--	--	--	--	--	--	--	--	--	--	--	--	--	--	--	--	--	--	--	--	--	--	--	--	--	--	--	--	--	--	--	--	--	--	--	--	--	--	--	--	--	--	--	--	--	--	--	--	--	--	--	--	--	--	--	--	--	--	--	--	--	--	--	--	--	--	--	--	--	--	--	--	--	--	--	--	--	--	--	--	--	--	--	--	--	--	--	--	--	--	--	--	--	--	--	--	--	--	--	--	--	--	--	--	--	--	--	--	--	--	--	--	--	--	--	--	--	--	--	--	--	--	--	--	--	--	--	--	--	--	--	--	--	--	--	--	--	--	--	--	--	--	--	--	--	--	--	--	--	--	--	--	--	--	--	--	--	--	--	--	--	--	--	--	--	--	--	--	--	--	--	--	--	--	--	--	--	--	--	--	--	--	--	--	--	--	--	--	--	--	--	--	--	--	--	--	--	--	--	--	--	--	--	--	--	--	--	--	--	--	--	--	--	--	--	--	--	--	--	--	--	--	--	--	--	--	--	--	--	--	--	--	--	--	--	--	--	--	--	--	--	--	--	--	--	--	--	--	--	--	--	--	--	--	--	--	--	--	--	--	--	--	--	--	--	--	--	--	--	--	--	--	--	--	--	--	--	--	--	--	--	--	--	--	--	--	--	--	--	--	--	--	--	--	--	--	--	--	--	--	--	--	--	--	--	--	--	--	--	--	--	--	--	--	--	--	--	--	--	--	--	--	--	--	--	--	--	--	--	--	--	--	--	--	--	--	--	--	--	--	--	--	--	--	--	--	--	--	--	--	--	--	--	--	--	--	--	--	--	--	--	--	--	--	--	--	--	--	--	--	--	--	--	--	--	--	--	--	--	--	--	--	--	--	--	--	--	--	--	--	--	--	--	--	--	--	--	--	--	--	--	--	--	--	--	--	--	--	--	--	--	--	--	--	--	--	--	--	--	--	--	--	--	--	--	--	--	--	--	--	--	--	--	--	--	--	--	--	--	--	--	--	--	--	--	--	--	--	--	--	--	--	--	--	--	--	--	--	--	--	--	--	--	--	--	--	--	--	--	--	--	--	--	--	--	--	--	--	--	--	--	--	--	--	--	--	--	--	--	--	--	--	--	--	--	--	--	--	--	--	--	--	--	--	--	--	--	--	--	--	--	--	--	--	--	--	--	--	--	--	--	--	--	--	--	--	--	--	--	--	--	--	--	--	--	--	--	--	--	--	--	--	--	--	--	--	--	--	--	--	--	--	--	--	--	--	--	--	--	--	--	--	--	--	--	--	--	--	--	--	--	--	--	--	--	--	--	--	--	--	--	--	--	--	--	--	--	--	--	--	--	--	--	--	--	--	--	--	--	--	--	--	--	--	--	--	--	--	--	--	--	--	--	--	--	--	--	--	--	--	--	--	--	--	--	--	--	--	--	--	--	--	--	--	--	--	--	--	--	--	--	--	--	--	--	--	--	--	--	--	--	--	--	--	--	--	--	--	--	--	--	--	--	--	--	--	--	--	--	--	--	--	--	--	--	--	--	--	--	--	--	--	--	--	--	--	--	--	--	--	--	--	--	--	--	--	--	--	--	--	--	--	--	--	--	--	--	--	--	--	--	--	--	--	--	--	--	--	--	--	--	--	--	--	--	--	--	--	--	--	--	--	--	--	--	--	--	--	--	--	--	--	--	--	--	--	--	--	--	--	--	--	--	--	--	--	--	--	--	--	--	--	--	--	--	--	--	--	--	--	--	--	--	--	--	--	--	--	--	--	--	--	--	--	--	--	--	--	--	--	--	--	--	--	--	--	--	--	--	--	--	--	--	--	--	--	--	--	--	--	--	--	--	--	--	--	--	--	--	--	--	--	--	--	--	--	--	--	--	--	--	--	--	--	--	--	--	--	--	--	--	--	--	--	--	--	--	--	--	--	--	--	--	--	--	--	--	--	--	--	--	--	--	--	--	--	--	--	--	--	--	--	--	--	--	--	--	--	--	--	--	--	--	--	--	--	--	--	--	--	--	--	--	--	--	--	--	--	--	--	--	--	--	--	--	--	--	--	--	--	--	--	--	--	--	--	--	--	--	--	--	--	--	--	--	--	--	--	--	--	--	--	--	--	--	--	--	--	--	--	--	--	--	--	--	--	--	--	--	--	--	--	--	--	--	--	--	--	--	--	--	--	--	--	--	--	--	--	--	--	--	--	--	--	--	--	--	--	--	--	--	--	--	--	--	--	--	--	--	--	--	--	--	--	--	--	--	--	--	--	--	--	--	--	--	--	--	--	--	--	--	--	--	--	--	--	--	--	--	--	--	--	--	--	--	--	--	--	--	--	--	--	--	--	--	--	--	--	--	--	--	--	--	--	--	--	--	--	--	--	--	--	--	--	--	--	--	--	--	--	--	--	--	--	--	--	--	--	--	--	--	--	--	--	--	--	--	--	--	--	--	--	--	--	--	--	--	--	--	--	--	--	--	--	--	--	--	--	--	--	--	--	--	--	--	--	--	--	--	--	--	--	--	--	--	--	--	--	--	--	--	--	--	--	--	--	--	--	--	--	--	--	--	--	--	--	--	--	--	--	--	--	--	--	--	--	--	--	--	--	--	--	--	--	--	--	--	--	--	--	--	--	--	--	--	--	--	--	--	--	--	--	--	--	--	--	--	--	--	--	--	--	--	--	--	--	--	--	--	--	--	--	--	--	--	--	--	--	--	--	--	--	--	--	--	--	--	--	--	--	--	--	--	--	--	--	--	--	--	--	--	--	--	--	--	--	--	--	--	--	--	--	--	--	--	--	--	--	--	--	--	--	--	--	--	--	--	--	--	--	--	--	--	--	--	--	--	--	--	--	--	--	--	--	--	--	--	--	--	--	--	--	--	--	--	--	--	--	--	--	--	--	--	--	--	--	--	--	--	--	--	--	--	--	--	--	--	--	--	--	--	--	--	--	--	--	--	--	--	--	--	--	--	--	--	--	--	--	--	--	--	--	--	--	--	--	--	--	--	--	--	--	--	--	--	--	--	--	--	--	--	--	--	--	--	--	--	--	--	--	--	--	--	--	--	--	--	--	--	--	--	--	--	--	--	--	--	--	--	--	--	--	--	--	--	--	--	--	--	--	--	--	--	--	--	--	--	--	--	--	--	--	--	--	--	----

Key

<u>Lithology</u>				<u>Secondary Deformation</u>		<u>Bioturbation</u>		<u>Fractures</u>			
	Grain Flow		Laminated	SR	Shredded	H	High	FB	Fracture blocks	I	Irregular
	Coarse	} Debris Flow	 Su Slump	ST	Streaked out	L	Low	SF	Stylolitic fractures	V	Variable
	Medium			F	Folded	2	No. of sets	SL	Slickensides	HL	Hairline
	Fine				Conglomerate	FL	Faulted				
	Turbidite		Periodite	P	Plastic	<u>Clay Content</u>		<u>Fillings</u>			
	Homogeneous		Shale	<u>Fossils</u>		H	High	A	Alternating	O	Open
						L	Low	↑	Inc. downwards	H	Healed
						M	Mottled	↓	Dec. downwards	C	Clay
				B	Shell fragments	I	Irregular			S	Block surface












LITHOLOGICAL AND FRACTURE LOG

Field: N.ELDFISK
Well: 2/7-B11

Sheet No. 9

Depth (feet)	Lithology	Bedding Orientation	Bedding Interval (cm)	Secondary Def.	Bioturbation	Fossils	Clay Cohtent	Stylolites	Clay Seams	Silica Content	Pyrite	FRACTURES								Comments		
												1st Set				2nd Set					Others	
												Frequency	Orientation	Spacing (cm)	Filling	Frequency	Orientation	Spacing (cm)	Filling			
10078								S				V	70 _R	I	H					SF		
79																						
10080												H	70 _R	>1	H					FB		
81																						
82	MISSING PRESERVED																					
83								S				H	70 _R	V	H					SF		
84																						
10085																						
86								L				H	90	0.8	H							
87					L															FB		
88																						
89												H	90	0.5	H							
10090								S														
91												H	V	HL	H						} Solution features	
92																						
93	F																					
94																						
10095												H	70 _R	0.8- 3	H							
96																						
97																						
98												H	90	0.3- 2	?					FB		
99																						
10100																					} RUBBLE regular blocks 1.5 x 2 x 3 1.5 x 3 x 4 0.5 x 1.5 x 2	
01																						
02																						
10103																						

Key

Lithology		Secondary Deformation		Bioturbation		Fractures	
	Grain Flow		Laminar	H High	FB Fracture blocks	I Irregular	
	Coarse		Slump	L Low	SF Stylolitic fractures	V Variable	
	Medium		Conglomerate	2 No. of sets	SL Slickensides	HL Hairline	
	Fine		Periodite				
	Turbidite		Shale				
	Homogeneous						
		</					

Sheet No. 10

Key

Fractures













H	High	FB	Fracture blocks	I	Irregular
L	Low	SF	Styloitic fractures	V	Variable
2	No. of sets	SL	Slickensides	HL	Hairline
<u>Clay Content</u>				<u>Fillings</u>	
H	High	A	Alternating	O	Open
L	Low	↑	Inc. downwards	H	Healed
M	Mottled	↓	Dec. downwards	C	Clay
1	Irregular				

LITHOLOGICAL AND FRACTURE LOG

Field: N. ELDFISK
Well: 2/7-B11

Sheet No. 11

Depth (feet)	Lithology	Bedding Orientation	Bedding Interval (cm)	Secondary Def.	Bioturbation	Fossils	Clay Content	Stylolites	Clay Seams	Silica Content	Pyrite	FRACTURES								Comments		
												1st Set				2nd Set					Others	
												Frequency	Orientation	Spacing (cm)	Filling	Frequency	Orientation	Spacing (cm)	Filling			
10128																						
29					?																As above	
10130																						
31																						
32	MISSING PRESERVED																					
33																						
34	F											H	60R		H	H	20-30R		H			
10135									✓													
36					L																	
37												H	90-80R	HL	H						Solution seams	
38																						
39																						
10140	MISSING PRESERVED																					
41												H	90	<0.3	H/C							
42												H	90	1-1.3	H/C							
43												H	V	HL	H/C						Solution seams	
44	C																					
10145																						
46					?							H	70R		H/C	H	70L		H/C			
47									3												Solution seams	
48																						
49									S			L	45L		H	L	45R		H		Blocks	
10150								M														
51																						
52	MISSING PRESERVED																					
53	Su F	30			✓			✓														

<u>Key</u>		<u>Lithology</u>		<u>Secondary Deformation</u>		<u>Bioturbation</u>		<u>Fractures</u>			
	Grain Flow		Laminated	SR	Shredded	H	High	FB	Fracture blocks	I	Irregular
	Coarse	} Debris Flow	 Su Slump	ST	Streaked out	L	Low	SF	Stylolitic fractures	V	Variable
	Medium			F	Folded	2	No. of sets	SL	Slickensides	HL	Hairline
	Fine			FL	Faulted						
	Turbidite		Conglomerate	P	Plastic						
			Periodite	<u>Fossils</u>							
	Homogeneous		Shale	B	Shell fragments	H	High	A	Alternating	O	Open
						L	Low	↑	Inc. downwards	H	Healed
						M	Mottled	↓	Dec. downwards	C	Clay
						I	Irregular			S	Block surface

LITHOLOGICAL AND FRACTURE LOG

Field: N. ELDFISK
Well: 2/7-B11

Sheet No. 12

Depth (feet)	Lithology	Bedding Orientation	Bedding Interval (cm)	Secondary Def.	Bioturbation	Fossils	Clay Content	Stylolites	Clay Seams	Silica Content	Pyrite	FRACTURES								Comments	
												1st Set				2nd Set					Others
												Frequency	Orientation	Spacing (cm)	Filling	Frequency	Orientation	Spacing (cm)	Filling		
10153	Su F	30			✓			✓				L 60	L		H						Blocks
54					↓																
10155																					
56																					
57												H 45	L		H	H	80	R	H		
58																					
59	F																				
10160								C				L 90			H O						
61																					
62																					
63	MISSING PRESERVED																				
64												H 90	0-2	H							
10165	F											90	V	?						FB	
66												90	V	H							
67																					
68	Su	30-40										90	V	H							
69				P?																	
10170	F							✓				H 90	1-2	H						SF	
71																					
72																					
73	MISSING PRESERVED																				
74																					
10175	C							✓													
76				P?				L													
77												L 90	HL	H							
78	F							C				H 90		H						Intense solution	

Key

Lithology		Secondary Deformation	
	Grain Flow		SR Shredded
	Coarse		ST Streaked out
	Medium		F Folded
	Fine		FL Faulted
	Turbidite		P Plastic
	Homogeneous		B Shell fragments
	Laminated		I Irregular
	Su Slump		
	Conglomerate		
	Periodite		
	Shale		

Fractures		Clay Content	
H	High	H	High
L	Low	L	Low
2	No. of sets	M	Mottled
		I	Irregular
FB	Fracture blocks	A	Alternating
SF	Stylolitic fractures	↑	Inc. downwards
SL	Slickensides	↓	Dec. downwards
HL	Hairline		
		S	Block surface

Fillings	
O	Open
H	Healed
C	Clay

LITHOLOGICAL AND FRACTURE LOG

Field: N.ELDFISK
Well: 2/7-B11

Sheet No. 13

Depth (feet)	Lithology	Bedding Orientation	Bedding Interval (cm)	Secondary Def.	Bioturbation	Fossils	Clay Content	Stylolites	Clay Seams	Silica Content	Pyrite	FRACTURES								Comments			
												1st Set				2nd Set					Others		
												Frequency	Orientation	Spacing (cm)	Filling	Frequency	Orientation	Spacing (cm)	Filling				
10178																							
79	F																						
10180	MISSING PRESERVED																						
81	F											H	90		H						} Solution		
82																							
83																							
84																							
10185												H	45 _L		H						} Solution		
86	MISSING PRESERVED																						
87	F																						
88					L							H	90	0.5- HL 3	H/C					SF	} Solution		
89					?																		
10190	MISSING PRESERVED																						} RUBBLE (end of core)
91																							
92																							
93						L	B														} Solution		
94												L	V		H								
10195	Su	40					B														} Solution		
96																							
97						L						L	V		H								
98							B																
99						L															} Soft		
10200	MISSING PRESERVED																						
1							B					L	60 _R		H	L	90 HL	0.5	H/O		} Solution		
2												L	V		H								
3																							

Key

Lithology		Secondary Deformation		Bioturbation		Fractures	
	Grain Flow		SR Shredded	H High	FB Fracture blocks	I Irregular	
	Coarse } Debris Flow		F Folded	L Low	SF Stylolitic fractures	V Variable	
	Medium } Debris Flow		FL Faulted	2 No. of sets	SL Slickensides	HL Hairline	
	Fine } Debris Flow		P Plastic	Clay Content		Fillings	
	Turbidite		B Shell fragments	H High	A Alternating	O Open	
	Homogeneous			L Low	Inc. downwards	H Healed	
				M Mottled	Dec. downwards	C Clay	
				I Irregular		S Block surface	

Sheet No. 14

Key

Page 79

Sheet No. 15

10310

Fractures

H	High	FB	Fracture blocks	I	Irregular
L	Low	SF	Stylolitic fractures	V	Variable
2	No. of sets	SL	Slickensides	HL	Hairline
<u>Clay Content</u>				<u>Fillings</u>	
H	High	A	Alternating	O	Open
L	Low	↑	Inc. downwards	H	Healed
M	Mottled			C	Clay
I	Irregular	↓	Dec. downwards	S	Block surface

LITHOLOGICAL AND FRACTURE LOG

Field: N.ELDFISK
Well: 2/7-B11

Sheet No. 16

Depth (feet)	Lithology	Bedding Orientation	Bedding Interval (cm)	Secondary Def.	Bioturbation	Fossils	Clay Content	Stylolites	Clay Seams	Silica Content	Pyrite	FRACTURES								Comments	
												1st Set				2nd Set					Others
												Frequency	Orientation	Spacing (cm)	Filling	Frequency	Orientation	Spacing (cm)	Filling		
10310																					
11						B ↓						H	V	0-9	H					FB 20°-50°	
12	C																			Clasts 0.2-0.3	
13												L	V		H						
14							1														
10315												H	60- 80L		H	H	40- 50L		H		
16																					
17								✓	✓												
18						S															
18	MISSING PRESERVED																				
19	MISSING																				
19		O																		Solution	
10320	MISSING																				
21												H	50- 60L	HL	H					} Escape structure	
22						B	S														
22												L	?	2-8	?						
23	MISSING PRESERVED																				
24												L	90	V	H						
10325																				FB 20°-50°	
26																					
27		O																		} Weak layering	
28																					
29	F					L	B					H	90	HL	H					} Escape structure	
10330	MISSING PRESERVED																				
31	MISSING																				
32													V	HL	H					FB 60°-70° & 20°-30°	
33																				} Escape structure	
33						L	B	S				L	90	V	H						
34																					
10335												H	90	V	H						

Key

Lithology	
	Grain Flow
	Laminated
	Coarse
	Medium
	Fine
	Turbidite
	Homogeneous
	Slump
	Conglomerate
	Periodite
	Shale

Secondary Deformation

SR	Shredded
ST	Streaked out
F	Folded
FL	Faulted
P	Plastic

Fossils

B	Shell fragments
---	-----------------

Bioturbation

H	High
L	Low
2	No. of sets

Clay Content

H	High
L	Low
M	Mottled
I	Irregular

Fractures

FB	Fracture blocks
SF	Stylolitic fractures
SL	Stickensides
HL	Hairline

Fillings

O	Open
H	Healed
C	Clay
S	Block surface

Sheet
No. 17

Key

Fractures








H	High	FB	Fracture blocks	I	Irregular
L	Low	SF	Styolitic fractures	V	Variable
2	No. of sets	SL	Slickensides	HL	Hairline
<u>Clay Content</u>			<u>Fillings</u>		
H	High	A	Alternating	O	Open
L	Low	↑	Inc. downwards	H	Healed
M	Mottled			C	Clay
I	Irregular	↓	Dec. downwards		
			S	Block surface	

Sheet No. 18

[illegible]

Key

Lithology

 Grain Flow <div style="display: flex; align-items: center;"> <div style="border: 1px solid black; padding: 2px; margin-right: 5px; text-align: center;">C</div> <div style="border: 1px solid black; padding: 2px; margin-right: 5px; text-align: center;">M</div> <div style="border: 1px solid black; padding: 2px; margin-right: 5px; text-align: center;">F</div> <div style="font-size: 2em; margin: 0 10px;">}</div> <div style="display: flex; flex-direction: column; align-items: center;"> <div>Coarse</div> <div>Medium</div> <div>Fine</div> </div> <div style="margin-top: 10px;">  Turbidite </div> <div style="margin-top: 10px;">  Homogeneous </div> </div>	 Laminated <div style="display: flex; align-items: center;"> <div style="border: 1px solid black; padding: 2px; margin-right: 5px; text-align: center; font-size: 1.5em;">Su</div> <div style="display: flex; flex-direction: column; align-items: center;"> <div>Slump</div> <div>Conglomerate</div> </div> </div> <div style="margin-top: 10px;">  Conglomerate </div> <div style="margin-top: 10px;">  Periodite </div> <div style="margin-top: 10px;">  Shale </div>
---	---

Secondary Deformation

SR Shredded
ST Streaked out
F Folded
FL Faulted
P Plastic

Fossils

B Shell fragments
Ec Crushed Echinoid

Bioturbation

H	High	FB	Fracture blocks	I	Irregular
L	Low	SF	Styloitic fractures	V	Variable
2	No. of sets	SL	Slickensides	HL	Hairline

Clay Content

H	High	A	Alternating
L	Low	↑	Inc. downwards
M	Mottled	↓	Dec. downwards
I	Irregular		

Fractures

FB	Fracture blocks	I	Irregular
SF	Styolitic fractures	V	Variable
SL	Slickensides	HL	Hairline

Fillings

O Open
H Healed
C Clay
S Block surface

LITHOLOGICAL AND FRACTURE LOG

Field: N.ELDFISK
Well: 2/7-B11

Sheet No. 19

Depth (feet)	Lithology	Bedding Orientation	Bedding Interval (cm)	Secondary Def.	Bioturbation	Fossils	Clay Content	Stylolites	Clay Seams	Silica Content	Pyrite	FRACTURES								Comments	
												1st Set				2nd Set					Others
												Frequency	Orientation	Spacing (cm)	Filling	Frequency	Orientation	Spacing (cm)	Filling		
10385	C																				
86	F											H	80 _L		H						
87																					
88																					
89																					
10390								✓													
91																					
92	C											H	90	0.5	H					FB	
93	MISSING PRESERVED																				
94	C											H	90	0.5	H					FB	
10395																					
96	M											H	20- 45 _R		H	H	50- 60 _L		H		
97																					
98	MISSING PRESERVED																				
99	F											H	20- 40 _R		H	H	50- 60 _L		H		
10400																					
1												H	20- 45 _R		H	H	50- 60 _L		H		
2	MISSING PRESERVED																				
3												H	60 _R		H					Solution	
4	F																				
10405																					
6																					
7																					
8																					
9										S	1		H	70 _R	HL	H					
10410	C											L	70 _R		H						

Key

Lithology			
	Grain Flow		Laminated
	Coarse		Slump
	Medium		Conglomerate
	Fine		Periodite
	Turbidite		Shale
	Homogeneous		

Secondary Deformation	
SR	Shredded
ST	Streaked out
F	Folded
FL	Faulted
P	Plastic

Fossils	
B	Shell fragments
I	Irregular

Bioturbation

H	High
L	Low
2	No. of sets

Clay Content

H	High
L	Low
M	Mottled
I	Irregular

Fractures

FB	Fracture blocks
SF	Stylolitic fractures
SL	Slickensides
I	Irregular
V	Variable
HL	Hairline

Fillings

O	Open
H	Healed
C	Clay
S	Block surface

LITHOLOGICAL AND FRACTURE LOG

Field: N. ELDFISK
Well: 2/7-B11

Sheet No. 20

Depth (feet)	Lithology	Bedding Orientation	Bedding Interval (cm)	Secondary Def.	Bioturbation	Fossils	Clay Content	Stylolites	Clay Seams	Silica Content	Pyrite	FRACTURES								Comments	
												1st Set				2nd Set					Others
												Frequency	Orientation	Spacing (cm)	Filling	Frequency	Orientation	Spacing (cm)	Filling		
10410																					
11	C											L	90		H						
12								✓													
13												L	90		H						
14	F																				
10415							M			✓											
16																					
17	MISSING PRESERVED																				
18																					
19	F _{Su}	10				B		C	✓			L	70R	I	H					Heavy solution	
10420							↑	S	✓												
21	M				✓		M			✓											
22							M					L	70R		H						
23																					
24	MISSING PRESERVED																				
10425					✓		M					L	70R		H					SL	
26	M						↓														
27								✓	✓												
28																					
29								✓													
10430	MISSING PRESERVED																				
31								✓				H	90	V	H	H	O	V	H		
32																					
33												1	80R	V	H						
34										✓		L	90	V	H	L	O	V	H		
10435																					

Key

Lithology		Secondary Deformation		Bioturbation		Fractures	
	Grain Flow		SR Shredded	H High	FB Fracture blocks	I Irregular	
	Coarse		ST Streaked out	L Low	SF Stylolitic fractures	V Variable	
	Medium		F Folded	2 No. of sets	SL Slickensides	HL Hairline	
	Fine		FL Faulted				
	Turbidite		P Plastic	Clay Content		Fillings	
	Homogeneous		B Shell fragments	H High	A Alternating	O Open	
				L Low	↑ Inc. downwards	H Healed	
				M Mottled	↓ Dec. downwards	C Clay	
				I Irregular		S Block surface	












LITHOLOGICAL AND FRACTURE LOG

Field: N.ELDFISK
Well: 2/7-B11

Sheet No. 21

Depth (feet)	Lithology	Bedding Orientation	Bedding Interval (cm)	Secondary Def.	Bioturbation	Fossils	Clay Content	Stylolites	Clay Seams	Silica Content	Pyrite	FRACTURES								Comments	
												1st Set				2nd Set					Others
												Frequency	Orientation	Spacing (cm)	Filling	Frequency	Orientation	Spacing (cm)	Filling		
10435	Su?	20						✓													
36																					
37								↓													
38								↑				L	90	V	H						
39								↓							L	0	V	H			
10440						↑	↑													Clasts > 0.4	
41	MISSING PRESERVED																				
42						↑	↑														
43							↓	↑													
44						✓	↓														
10445						✓	↑	✓													
46																					
47						✓		✓	✓												
48							↑	✓													
49																					
10450							↑					Trellaced fractures									
51																					
52						✓															
53	MISSING PRESERVED																				
54			0.1-0.2									L	50L		H	6					
10455			0.3-0.4				↓														
56			CR 2-9 CP 3-10																		
57							↓	✓													
58												H	0		H						
59							↓														
10460																					

Key

Lithology			Secondary Deformation		Bioturbation		Fractures				
	Grain Flow		SR	Shredded	H	High	FB	Fracture blocks	I	Irregular	
	Coarse	} Debris Flow	ST	Streaked out	L	Low	SF	Stylolitic fractures	V	Variable	
	Medium			Su	Slump	2	No. of sets	SL	Slickensides	HL	Hairline
	Fine			FL	Faulted						
	Turbidite		P	Plastic							
	Homogeneous				Clay Content		Fillings				
			Fossils		H	High	A	Alternating	O	Open	
					L	Low	↑	Inc. downwards	H	Healed	
					M	Mottled			C	Clay	
					I	Irregular	↓	Dec. downwards			
									S	Block surface	












LITHOLOGICAL AND FRACTURE LOG

Field: N.ELDFISK
Well: 2/7-B11

Sheet No. 22

Depth (feet)	Lithology	Bedding Orientation	Bedding Interval (cm)	Secondary Def.	Bioturbation	Fossils	Clay Content	Stylolites	Clay Seams	Silica Content	Pyrite	FRACTURES								Comments		
												1st Set				2nd Set					Others	
												Frequency	Orientation	Spacing (cm)	Filling	Frequency	Orientation	Spacing (cm)	Filling			
10460																						
61					✓					↑	✓											
62																						
63	MISSING PRESERVED																					
64			0.5- 1.2							↑												
10465										↓												
66					✓		↑					L 90		C								
67							↑	✓														
68							↑	↓				L 90		C								
69							↑															
10470	MISSING PRESERVED																					
71			0.1- 1				↑	2				L 70R 90	HL	H/O								
72	Su?	10																			Solution	
73																						
74			2																			
10475												L 90	HL	H								
76					✓																	
77																						
78			1-2																			
79						✓	✓															
10480																						
81												2 90		H/O L	0			H/O				
82	MISSING PRESERVED																					
83			0.2- 1																			
84					✓			2	✓													
10485												L 70R		H								

Key

<u>Lithology</u>		<u>Secondary Deformation</u>		<u>Bioturbation</u>		<u>Fractures</u>	
	Grain Flow		Laminated	H High	FB Fracture blocks	I Irregular	
	Coarse	 Su Slump	SR Shredded	L Low	SF Stylolitic fractures	V Variable	
	Medium		ST Streaked out	2 No. of sets	SL Slickensides	HL Hairline	
	Fine		F Folded				
	Turbidite		FL Faulted				
			P Plastic				
	Homogeneous		Shale				
				<u>Clay Content</u>		<u>Fillings</u>	
				H High	A Alternating	O Open	
				L Low	↑ Inc. downwards	H Healed	
				M Mottled	↓ Dec. downwards	C Clay	
				I Irregular			
						S Block surface	









LITHOLOGICAL AND FRACTURE LOG

Field: N.ELDFISK
Well: 2/7-B11

Sheet No. 23

Depth (feet)	Lithology	Bedding Orientation	Bedding Interval (cm)	Secondary Def.	Bioturbation	Fossils	Clay Content	Stylolites	Clay Seams	Silica Content	Pyrite	FRACTURES								Comments	
												1st Set				2nd Set					Others
												Frequency	Orientation	Spacing (cm)	Filling	Frequency	Orientation	Spacing (cm)	Filling		
10485																					
86																					
87								S	✓												
88					✓																
89												2	90		H/O						
10490	MISSING PRESERVED																				
91								✓	✓			H	90	Short	L	0	Long				
92																					
93																					
94																					
10495												2	90		H						
96																					
97					✓			1				H	90	V	H					Dewatering	
98																					
99																					
10500												H	90	4-6	H	H	0	4-6	H		
1																					
2								1				L	90		H						
3	MISSING PRESERVED																				
4					✓																
10505																					
6									✓												
7									✓											Solution	
8					✓																
9																					
10510																					

Key

<u>Lithology</u>		<u>Secondary Deformation</u>		<u>Bioturbation</u>		<u>Fractures</u>	
	Grain Flow		Laminated	H High	FB Fracture blocks	I Irregular	
	Coarse	 Su Slump	SR Shredded	L Low	SF Stylolitic fractures	V Variable	
	Medium		ST Streaked out	2 No. of sets	SL Slickensides	HL Hairline	
	Fine		F Folded				
	Turbidite	FL Faulted	<u>Clay Content</u>		<u>Fillings</u>		
		P Plastic	H High	A Alternating	O Open		
	Homogeneous	<u>Fossils</u>	L Low	↑ Inc. downwards	H Healed		
		B Shell fragments	M Mottled	↓ Dec. downwards	C Clay		
			I Irregular		S Block surface		

LITHOLOGICAL AND FRACTURE LOG

Field: N. ELDFISK
Well: 2/7-B11

Sheet No. 24

Depth (feet)	Lithology	Bedding Orientation	Bedding Interval (cm)	Secondary Def.	Bioturbation	Fossils	Clay Content	Stylolites	Clay Seams	Silica Content	Pyrite	FRACTURES								Comments			
												1st Set				2nd Set					Others		
												Frequency	Orientation	Spacing (cm)	Filling	Frequency	Orientation	Spacing (cm)	Filling				
10510																							
11								✓															
12																							
13										✓		2	70- 80	V	H								
14																							
10515																							
16																							
17					✓																		
18																							
19																							
10520																							
21																							
22																							
23	MISSING PRESERVED																						
24								✓															
10525					✓			✓		✓													
26								S															
27	MISSING PRESERVED																						
28			2					✓															
29					✓																		
10530										✓	✓												
31				P				S															
32					✓																		
33								✓		✓													
34								✓															
10535	MISSING PRESERVED																						

Key

Lithology	
	Grain Flow
	Laminated
	Coarse
	Medium
	Fine
	Turbidite
	Homogeneous
	Debris Flow
	Slump
	Conglomerate
	Periodite
	Shale

Secondary Deformation	
SR	Shredded
ST	Streaked out
F	Folded
FL	Faulted
P	Plastic
Fossils	
B	Shell fragments

Bioturbation	
H	High
L	Low
2	No. of sets
Clay Content	
H	High
L	Low
M	Mottled
I	Irregular
Fractures	
FB	Fracture blocks
SF	Stylolitic fractures
SL	Slickensides
I	Irregular
V	Variable
HL	Hairline
Fillings	
O	Open
H	Healed
C	Clay
S	Block surface

Sheet No. 25

Key

Page 90

LITHOLOGICAL AND FRACTURE LOG

Field: N.ELDFISK
Well: 2/7-B11

Sheet No. 26

Depth (feet)	Lithology	Bedding Orientation	Bedding Interval (cm)	Secondary Def.	Bioturbation	Fossils	Clay Content	Stylolites	Clay Seams	Silica Content	Pyrite	FRACTURES								Comments		
												1st Set				2nd Set					Others	
												Frequency	Orientation	Spacing (cm)	Filling	Frequency	Orientation	Spacing (cm)	Filling			
10560																						
61																						
62												H	90	V	?	H	0	V	?			
63																						
64																						
10565																						
66																						
67																				SF		
68																						
69						✓																
10570								✓				H	90	V	H/O							
71																						
72																						
73																						
74																						
10575												H	80-90	V	H/O	H	0	V	H/O			
76																						
77	MISSING PRESERVED																					
78																						
79																						
10580												H	90	V	H/O							
81																						
82						✓																
83												H	90	V	H/O							
84												H	90	V	H							
10585																						

Key

Lithology		Secondary Deformation		Bioturbation		Fractures	
	Grain Flow		SR Shredded	H High	FB Fracture blocks	I Irregular	
	C Coarse		ST Streaked out	L Low	SF Stylolitic fractures	V Variable	
	M Medium		F Folded	2 No. of sets	SL Slickensides	HL Hairline	
	F Fine		FL Faulted	Clay Content		Fillings	
	Turbidite		P Plastic	H High	A Alternating	O Open	
	Homogeneous		B Shell fragments	L Low	↑ Inc. downwards	H Healed	
				M Mottled	↓ Dec. downwards	C Clay	
				I Irregular		S Block surface	

LITHOLOGICAL AND FRACTURE LOG

Field: N. ELDFISK
Well: 2/7-B11

Sheet 27
No. 27

Depth (feet)	Lithology	Bedding Orientation	Bedding Interval (cm)	Secondary Def.	Bioturbation	Fossils	Clay Content	Stylolites	Clay Seams	Silica Content	Pyrite	FRACTURES								Comments	
												1st Set				2nd Set					Others
												Frequency	Orientation	Spacing (cm)	Filling	Frequency	Orientation	Spacing (cm)	Filling		
10585																					
86												H	90	V	H						
87																					
88												2	90	V	H						
89																					
10590					L																
91																					
92		0.5-1			F/SR		↑														
93	MISSING PRESERVED																				
94		0.5-1																			
10595							↓					H	90	V	H						
96					F		↓	S													
97					P		↓														
98						L															
99																					
10600												H	90	V	H/O						
1																					
2	MISSING PRESERVED																				
3																					
4																					
10605							↓					H	90	1-3	H/O						
6					L																
7																					
8					ST		↓													Solution	
9							↓	M													
10610	MISSING PRESERVED																				

Key

Lithology				Secondary Deformation		Bioturbation		Fractures	
	Grain Flow		Laminated	SR	Shredded	H	High	FB	Fracture blocks
	Coarse		Slump	ST	Streaked out	L	Low	SF	Stylolitic fractures
	Medium		Conglomerate	F	Folded	2	No. of sets	SL	Slickensides
	Fine		Periodite	FL	Faulted				
	Turbidite		Shale	P	Plastic				
	Homogeneous								
				Fossils		Clay Content		Fillings	
				B	Shell fragments	H	High	A	Alternating
						L	Low	↑	Inc. downwards
						M	Mottled	↓	Dec. downwards
						I	Irregular		
								O	Open
								H	Healed
								C	Clay
								S	Block surface

LITHOLOGICAL AND FRACTURE LOG

Field: N.ELDFISK
Well: 2/7-B11

Sheet No. 28

Depth (feet)	Lithology	Bedding Orientation	Bedding Interval (cm)	Secondary Def.	Bioturbation	Fossils	Clay Content	Stylolites	Clay Seams	Silica Content	Pyrite	FRACTURES								Comments		
												1st Set				2nd Set					Others	
												Frequency	Orientation	Spacing (cm)	Filling	Frequency	Orientation	Spacing (cm)	Filling			
10610																						
11																						
12																						
13																						
14																						
10615																						
16																						
17																						
18																						
19																						
10620	MISSING PRESERVED																					
21																						
22																						
23																						
24																						
10625																						
26																						
27																						
28																						
29																						
10630																						
31																						
32																						
33	MISSING PRESERVED																					
34																						
10635																						


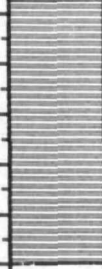
Key

Lithology				Secondary Deformation		Bioturbation		Fractures	
	Grain Flow		Laminated	SR	Shredded	H	High	FB	Fracture blocks
	Coarse		Slump	ST	Streaked out	L	Low	SF	Stylolitic fractures
	Medium		Conglomerate	F	Folded	2	No. of sets	SL	Slickensides
	Fine		Periodite	FL	Faulted				
	Turbidite		Shale	P	Plastic	Clay Content		Fillings	
	Homogeneous			Fossils		H	High	A	Alternating
				B	Shell fragments	L	Low	↑	Inc. downwards
						M	Mottled	↓	Dec. downwards
						I	Irregular		
								O	Open
								H	Healed
								C	Clay
								S	Block surface

LITHOLOGICAL AND FRACTURE LOG

Field: N.ELDFISK
Well: 2/7-B11

Sheet No. 29

Depth (feet)	Lithology	Bedding Orientation	Bedding Interval (cm)	Secondary Def.	Bioturbation	Fossils	Clay Content	Stylolites	Clay Seams	Silica Content	Pyrite	FRACTURES								Comments																	
												1st Set				2nd Set					Others																
												Frequency	Orientation	Spacing (cm)	Filling	Frequency	Orientation	Spacing (cm)	Filling																		
10635			1-1.5 & 3-10	F/P								H	90	V	H																						
36																																					
37																																					
38																		✓																			
39																L																					
10640																																					
41																																					
42																							H	70- 80 _R	V	H											
43												MISSING PRESERVED																									
44																L																					
10645																																					
46																																					
47																																					
48			>1																																		
49	MISSING PRESERVED																																				
10650	END OF CORE 2/7-B11																																				

Key

Lithology				Secondary Deformation		Bioturbation		Fractures	
	Grain Flow		Laminated	SR	Shredded	H	High	FB	Fracture blocks
	Coarse		Slump	ST	Streaked out	L	Low	SF	Stylolitic fractures
	Medium		Conglomerate	F	Folded	2	No. of sets	SL	Slickensides
	Fine		Periodite	FL	Faulted	Clay Content		Fillings	
	Turbidite		Shale	P	Plastic	H	High	A	Alternating
	Homogeneous			Fossils		L	Low	↑	Inc. downwards
				B	Shell fragments	M	Mottled	↓	Dec. downwards
				I	Irregular				
								O	Open
								H	Healed
								C	Clay
								S	Block surface

2800m (North Eldfisk). The porosities of the three producing formations also vary from 18-40% for Ekofisk, 14-42% for Tor and 8-29% for the Hod Formation (Michaud, 1987). Two production platforms were installed, 2/7 Alpha (South Eldfisk) and 2/7 Bravo (North Eldfisk) from which development drilling began in 1978 and 1979 respectively.

Well 2/7-B11 is situated to the south-east of the Bravo platform on the North Eldfisk reservoir. Chalk recovered from this well, contains an almost continuous succession from 2990.6m (9812') in the transition zone between the Ekofisk Formation chalks and the overlying shales of the Maureen Formation to 3245.8m (10649') in the Lower Hod Formation. The Middle Hod is well represented but the boundary between the Hod and Tor Formations at 3185.3m (10450.5') appears to be just above the boundary between the Middle and Upper Hod. This indicates that virtually all the Upper Hod Formation had been removed before the deposition of the Tor Formation chalks occurred. The upper surface of the Hod chalk is represented by an erosion surface below a Tor Formation basal conglomerate.

The Tor Formation is also well represented, but, the boundary between the Tor and Ekofisk Formations (at approximately 3065m (10056')) including the basal conglomerate and Ekofisk Tight Zone is also missing.

The Upper and Lower Ekofisk Formations are otherwise complete (Michaud, 1987) although much reduced in thickness compared with the fields to the north. The top of the core (2990.6m (9812')) is located in the gradational boundary between reworked chalks of the Ekofisk Formation and the overlying heavily bioturbated shales of the Maureen Formation.

The photographs in section 3.4 used to illustrate good examples of the different lithologies within the chalk. Much of the core consists of chalk that initially appears to be homogeneous in which the more subtle features and relationships, that provide clues

to the origins of the chalks, are difficult to see. These can only be observed on the smooth surface of slabbed cores (as the outer surface of whole core is too rough) using a vital piece of equipment, a wet sponge!

The log is designed to show the relationships between the types of fractures and their distribution with respect to lithological changes. Depths on the log are presented in the imperial units to conform with the units used on the core. Where specific features are discussed in the text the depths are given in metric units with the original imperial units in brackets. All other measurements are in metric units.

The lithologies have been divided into Grain flows; coarse, medium and fine grained debris flows; turbidites; homogeneous; laminated; conglomerates; slumps; periodites; and shale. This varies slightly from Kennedy's (1987a) classification, in that the slumped deposits are not strictly treated as separate lithologies but are included, via the use of initials, under their original lithological divisions. The transitional zone between the Ekofisk and Maureen Formations may contain debris flows as well as periodites and turbidites, but they are sufficiently different from the finer laminated periodites found elsewhere in the core that they are represented by the symbols for homogeneous chalks and shales. If they are periodites the primary laminations in the clay rich layers have been destroyed by bioturbation and there is little evidence of pressure solution. Shortly after coring, sections of chalk were removed, preserved and put into storage. The locations of these sections are represented on the log as 'missing preserved'. Other sections of core are removed from time to time for experimental and analytical purposes. On completion of the programme all unused core is returned to the core store. This means that at any time the core held in the Norwegian Petroleum Directorate core store may not be complete. Where sections of core had been taken for such purposes during the recording of this log, their locations are indicated by the word 'missing'.

The log has been used to indicate the relative ages of the fractures recorded (1st set being the youngest) their orientation and spacing. The fractures are recorded as either

being open healed or filled with clay. Healed fractures represent those filled with calcite or other cements.

Throughout the more porous sections of the core there exists a network of fine vertical or near vertical healed fractures. They are the earliest fractures formed (Thomas et al., 1987) and have a spacing of 0.5-1cm. These fractures can be seen to cut and are cut themselves by various systems of burrows. The burrows indicate two periods of bioturbation, the earliest being the spiral type called Zoophycos. The second set are generally the more tubular Chondrites. The early fractures consistently cut the Zoophycos burrows, from which it can be inferred that they formed after an initial period of bioturbation. The Chondrites over-print the Zoophycos burrows and frequently cut the early fractures. This is, however, not consistent, as occasionally the Chondrites burrows are cut by the fractures.

The above relationships give the relative timing for the formation of the early fractures. Firstly, the burrowing organisms could not have existed on the substrate until it had compacted to a density strong enough to support them. Once these burrowing organisms were able to establish themselves on the chalk, bioturbation (initially by Zoophycos) then continued the processes of dewatering and compaction. As the thickness of the overburden increased, the substrate continued to compact gradually becoming stiffer. However it remained relatively unstable. It was this instability which led to the formation of the early fractures. The development of this fracture network began either before, or was concurrent with a second phase of burrowing by organisms. These organisms are thought to extend their burrowing activities to a depth below that of Zoophycos (Nygaard et al., 1983).

Identification of these early fractures is important in the debris flows of the Tor Formation, in which burrows, if they exist are difficult to identify. Here, if we assume a limited period of surface exposure due to rapid burial by subsequent allochthonous deposits, the sediments dewatered without the assistance of large-scale bioturbation.

This lack of biological activity may have resulted in less effective dewatering. The dewatering process appears to have been achieved by the development of these early, closely spaced, healed fractures which are such a prominent feature of the high porosity chalks. It is not a coincidence that the rubble zones in the Tor Formation occur in some of the highest known porosity layers. To discount these rubble zones as a result of coring may not be fully justified. Much of the rubble can be seen to have flat faces with block sizes consistent with the spacing of these early fractures. Indeed, where larger slabbed blocks are found within the rubble zones they reveal the same closely-spaced network of fractures. The only question that therefore needs to be addressed is, do the rubble zones exist as such in the reservoir? It is possible that they do. If they don't then why are the other horizons in which this consistent fracturing pattern is observed not broken into rubble zones as well?

Lithology appears to exert some control on both the formation and style of fracturing. Where the clay content is found to increase, the number of fractures formed is low (Hardman and Kennedy, 1980). Many fractures in lithologies with a high clay content are either partly open or are clay filled. Indeed, the escape structure found at the top of the core (in the transition zone between the Maureen and Ekofisk Formations) clearly shows that the fracture network has formed by a gradual combination of finer fractures into a larger one (plate 3.16). Towards the top of this feature clays have been rotated and moved up the fracture. The remainder of the Maureen/Ekofisk boundary does not contain an early fracture network.

Where the grain size increases, as in the grain flows, turbidites and the conglomerates, the degree of fracturing is substantially reduced. Indeed, most of the turbidites do not contain any fractures. Those present appear to have either developed from the underlying sediments or are associated with solution features. Some of the matrix material in the conglomerates shows clear evidence of flow around the clasts which may be the result of movement (or possibly dewatering) following deposition.

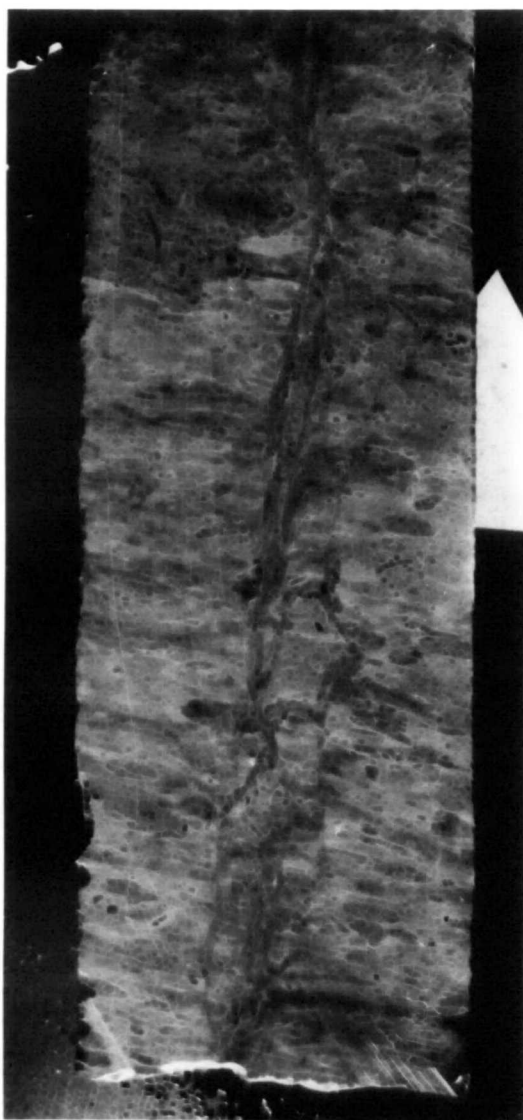
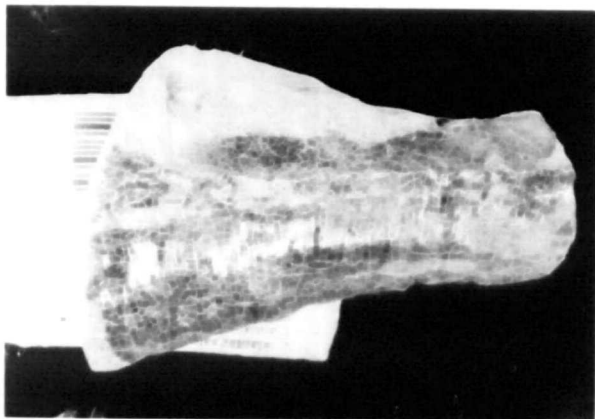


Plate 3.16. A water escape structure in a bioturbated marly chalk which has been modified by pressure solution. Well 2\7-B11, depth 9813', Maureen/Ekofisk Fm boundary.



**Plate 3.17. An example of slickensides of a fracture face.
Well 2\8-8, depth 8186', Tor Fm.**

The laminated chinks of the Lower Hod Formation also show that fracture development is controlled by the lithology. These laminated chinks contain layers of low porosity, high silica, oil free chinks which alternate with higher porosity, low silica, oil stained layers. The softer layers contain evidence of bioturbation and development of an early fracture network, whereas the harder, silica-rich laminae do not. The fractures that have developed in the harder layers form an open, oil stained, trellised network.

The slump deposits, which are a prominent feature of the Ekofisk Formation in this well, contain either the high frequency early fractures or less frequent inclined fractures. The latter vary in both their orientation (between 10° and 80°) and their cement (many are either partially open or partly clay filled). The relationship between the angle of the fractures and the dip of the strata is poor. It appears that the beds with the highest dips contain the fractures with the lowest angles. Equally, the beds with the lowest dips contain the majority of the vertical and near vertical fractures. The highly deformed beds of the Lower Hod Formation contain very few fractures. This is probably due to the higher clay content and the silty grain size of these sediments.

As the core has broken up into a series of blocks, the upper and lower surfaces are worthy of examination. In the Tor Formation these blocks are often bounded by stylolites or clay seams. Although these do have the consistent angle of the tectonic fractures as defined above, they contain slickensides (plate 3.17) and other features that indicate movement of the chalk leading to its breakup and indicate that they were at least partly open when in situ. This later fracturing appears to have formed during or sometime after the onset of pressure solution. The relationships between the fractures and the stylolites agrees with that proposed by Hardman and Kennedy (1980) (reported above). The fractures appear to both follow and cut across the stylolites. As the fractures developed they would have allowed more water to pass through the chalk, which may have enhanced pressure solution before the emplacement of the hydrocarbons.

The final feature worth noting from this core is a series of vugs in the Ekofisk Formation (3030.6-3030.9m (9943'-9944')) indicating intense (local) solution. No evidence could be found as to why they formed at that particular depth.

The sedimentological and fracture characteristics of this core tend to agree with much of the previously published work, but, they also highlight how variable the chalks of the North Sea can be. The slickensided fractures are well represented in the Ekofisk Formation and decrease in frequency downwards throughout the core. They generally have a steep dip although some can be found with dips as low as 45° . They form fracture blocks that are significant features of both the Ekofisk and Tor Formation chalks and can be found in each of the Eldfisk cores (2/7-B12, 2/7-A6, 2/7-A20, 2/7-1X and 2/7-3X). Where the chalks are particularly soft they disintegrate into rubble, but the component blocks of this rubble appear to have a consistent shape and size distribution. Most of the fractures in the Hod Formation are partially open, but recognisable fracture blocks are rare. When undertaking modelling or analytical studies, such as the experimental programme described in the following chapters. These differences should be considered (see chapter five), even if they cannot be included in the modelling process or specifically investigated, as they may account for a number of the unusual features seen in the results of such studies.

PART 2

EXPERIMENTAL STUDIES.

CHAPTER 4

UNIAXIAL EXPERIMENTS.

4. UNIAXIAL EXPERIMENTS.

4.1. INTRODUCTION.

Reservoir compaction resulting from hydrocarbon production has been identified as a significant problem in a number of oil and gas fields throughout the World (see Jones et al., 1987). Compaction may have both beneficial and detrimental effects on hydrocarbon production. One of the main advantages is the instigation of compaction drive (Botter, 1985; Ruddy et al., 1988; Berget et al., 1989) which has led to an increase in the estimated recoverable reserves in a number of fields. Compaction however has many negative features associated with it. These include a decrease in reservoir porosity, a possible decrease in rock permeability, development of new faults and the reactivation of existing ones (see Jones et al., 1987), and well casing failures (Botter, 1985; Berget et al., 1989). A further problem associated with reservoir compaction is that of surface subsidence. This phenomenon, in particular, is well documented and has led to ground instability, failure of dikes and dams and large-scale flooding. It is inappropriate to present a detailed discussion of examples of reservoir compaction and surface subsidence here, but a review of a number of significant examples can be found in Jones et al. (1987).

Reservoir compaction and surface subsidence has been recognised at several of the chalk fields in the Norwegian Sector of the North Sea, in particular at Ekofisk (Wiborg and Jewhurst, 1986; Sulak and Danielsen, 1988; Rentsch and Mes, 1988; Jewhurst and Wiborg, 1988). Compaction is a consequence of pore pressure depletion. As the pore fluid pressure is reduced, stress is transferred from the pore fluid to the mineral skeleton. It is this transference of stress that leads to the deformation of the reservoir rock. The stress regime generally considered to be present in most large hydrocarbon reservoirs means that compactional deformations occur under conditions of no lateral strain. A series of laboratory experiments were undertaken to investigate the magnitude of these deformations in order to determine whether this behaviour followed a predictable pattern. The results from a number of these experiments are reported in this chap-

ter. Table 4.1 contains a list of all the uniaxial strain experiments conducted during this part of the study. The remaining uniaxial strain experimental results are reported in chapter five.

Table 4.1.
UNIAXIAL STRAIN EXPERIMENTAL DATA.

EXP. No.	TYPE OF EXP.	FMN. INITIAL PORO %	EXP No.	TYPE OF EXP.	FMN. INITIAL PORO %
WEC2	S/S	U. EKO. 29.8	VOHC3	REL	L. HOD 26.0
WEC3	S/S	U. EKO. 38.2	VOTC1	REL	L. TOR 42.0
WEC8	S/S	U. TOR 38.0	ELOTC1	S/S	L. TOR 34.0
EC18/26A	INJ	L. EKO. 38.0	ELOTC2	S/S	L. TOR 34.0
EC18/26B	INJ	L. EKO. 38.0	ELOTC3	S/S	L. TOR 36.0
EC25/29	INJ	L. EKO. 40.7	ELOTC4	S/S	L. TOR 39.0
EC2/24	REL	L. EKO. 39.2	ELOHC1	S/S	L. HOD 28.0
VOAC2	S/S	S. KNT. 49.6	ELOUEC1	S/S	U. EKO. 38.0
VOBC3	S/S	S. KNT. 49.2	ELOUEC2	S/S	L. EKO. 40.0
VOBC5	REL	S. KNT. 49.2	ELONGC1	SR	L. EKO. 36.3
VOBC7	REL	S. KNT. 49.2	ELONGC2	SR	L. EKO. 41.9
VOCC1	S/S	S. KNT 48.2	ELONGC3	SR	L. EKO. 38.1
VOHC1	S/S	L. HOD 41.0	ELONGC4	SR	L. EKO. 36.7
VOHC2	REL	L. HOD 26.0			

S/S = Stress/strain experiments.

INJ = Water injection experiments.

REL = Stress relaxation experiments.

SR = Strain rate experiments.

Note: The experimental data presented in chapter five were also conducted under conditions of uniaxial strain. For the sake of brevity, the full data for each experiment are not necessarily included but were used to construct figure 4.76

A comprehensive study of the mechanical behaviour of both onshore and offshore chalks was undertaken by Addis (1987). This present study was designed to expand the uniaxial strain dataset of Addis (1987) and to investigate a number of aspects of chalk deformation not included in that study. As much of the 'ground work' has been covered in the study undertaken by Addis (1987), the following section will provide only a brief resume of the theory. Most of the examples given are from the experiments conducted

during the present study, but where appropriate data from Addis (1987) will be included.

4.2. RESUME OF UNIAXIAL STRAIN: THEORY AND PRACTICE.

Porous sediments such as the chalk are multi-phase systems consisting of a mineral skeleton with pore spaces which contain various fluids. Deformations within this system will occur in response to changes in the effective stress, defined by Terzaghi (1943) as:

$$\sigma' = \sigma - U \quad 4.1$$

where σ' is the effective stress; σ is the total stress; and U is the pore fluid pressure. Effective stress can therefore be increased by either an increase in the total stress, a decrease in the pore fluid pressure or a combination of the two processes. Various other forms have been proposed for the effective stress principle which take into account the compressibility of the mineral grains, the mineral skeleton as a whole and the compressibility of the pore fluid (see Addis, 1987 for further discussions). In most hydrocarbon reservoirs the effective stress increases due to a reduction in the pore fluid pressure which is a consequence of hydrocarbon production. In the experiments reported here, and in Addis (1987), effective stress was increased by increasing the total vertical and horizontal stresses whilst maintaining a low (approximately 1.8MPa) constant pore fluid pressure.

Janbu (1985) introduced the concept that effective stress is a consequence of the ability of the mineral skeleton to resist shape changes and the ability of the system to dissipate excess pore fluid pressures. This resistance may be considered to comprise of three different components:

$$\sigma' = r_c + r_i + r_m \quad 4.2$$

where r_c is a cementation resistance; r_i is an intergranular frictional resistance; and r_m is an intergranular molecular bonding resistance. In the chalk it can be envisaged (Jones and Leddra, 1989) that whilst the elastic bonding remains intact cementation resistance is the dominant element of the equation. However, once yield has been attained and the cement structure begins to break down intergranular frictional resistance becomes the dominant process. Intergranular molecular bonding resistance is considered to be important with regard to clays.

In passive tectonic areas, or in large sedimentary basins, deformation of the rocks may be regarded as a one dimensional (vertical) process. In order to simulate the deformations expected to occur in rocks under such conditions, experiments are usually conducted in such a manner that a condition of no lateral strain exists. The stress ratio (between the horizontal and vertical effective stresses) required to maintain this condition is generally referred to as the K_0 condition or the coefficient of earth pressure at rest.

$$K_0 = \sigma_h' / \sigma_v' \quad 4.3$$

Various K_0 values are observed for normally consolidated sediments, 0.3-0.5 for sands and 0.5-0.7 for clays. In a cemented material such as the chalk the ratio between the horizontal and vertical effective stresses which is required to maintain a condition of no lateral strain is observed to vary in a predictable manner. This behaviour has been well documented by Addis (1987), Jones et al. (1987), Addis and Jones (1989), Jones and Leddra (1989) and the K_0 experimental results presented in this study. The effective stress ratio shows three distinct values (figure 4.1). These different values represent changes in the deformational behaviour of the chalk. At low stresses the cemented structure of the chalk is observed to deform in an elastic manner, in which the effective stress ratio is low, typically around 0.3. As the effective stresses increase this cementation begins to break down (this breakdown is observed to be a progressive process) and the material undergoes yield. During yield, the compressibility of the structure in-

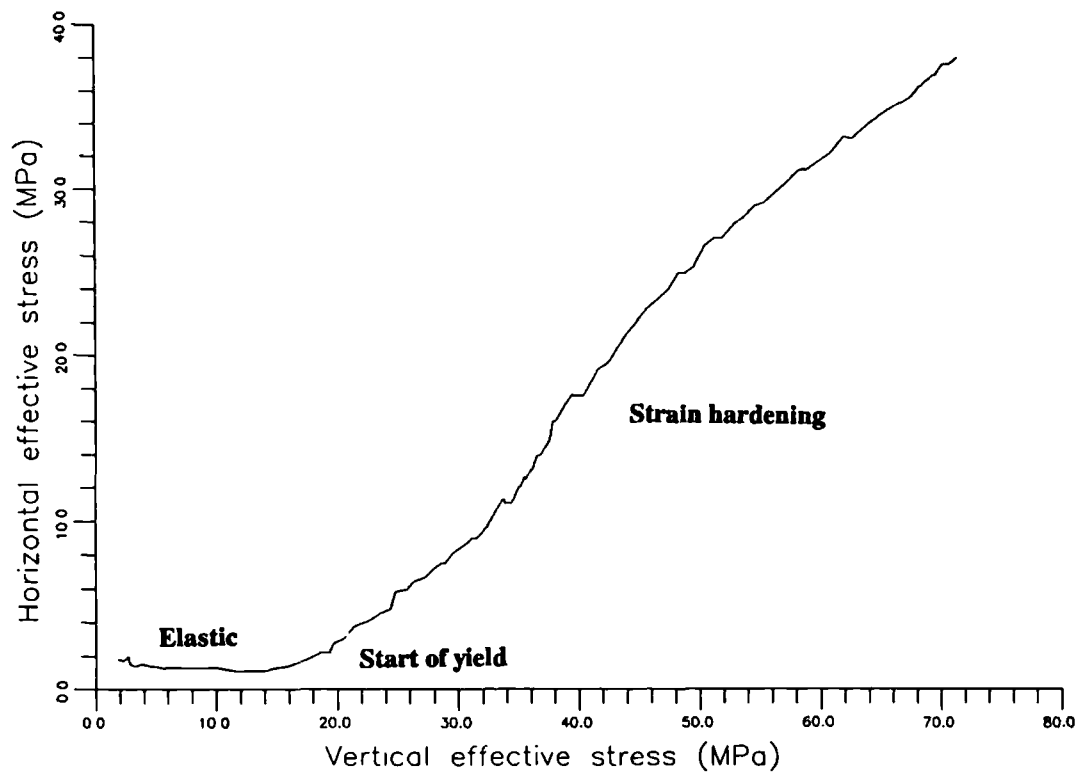


Figure. 4.1. Graph of horizontal effective stress/vertical effective stress for a 38% porosity chalk.

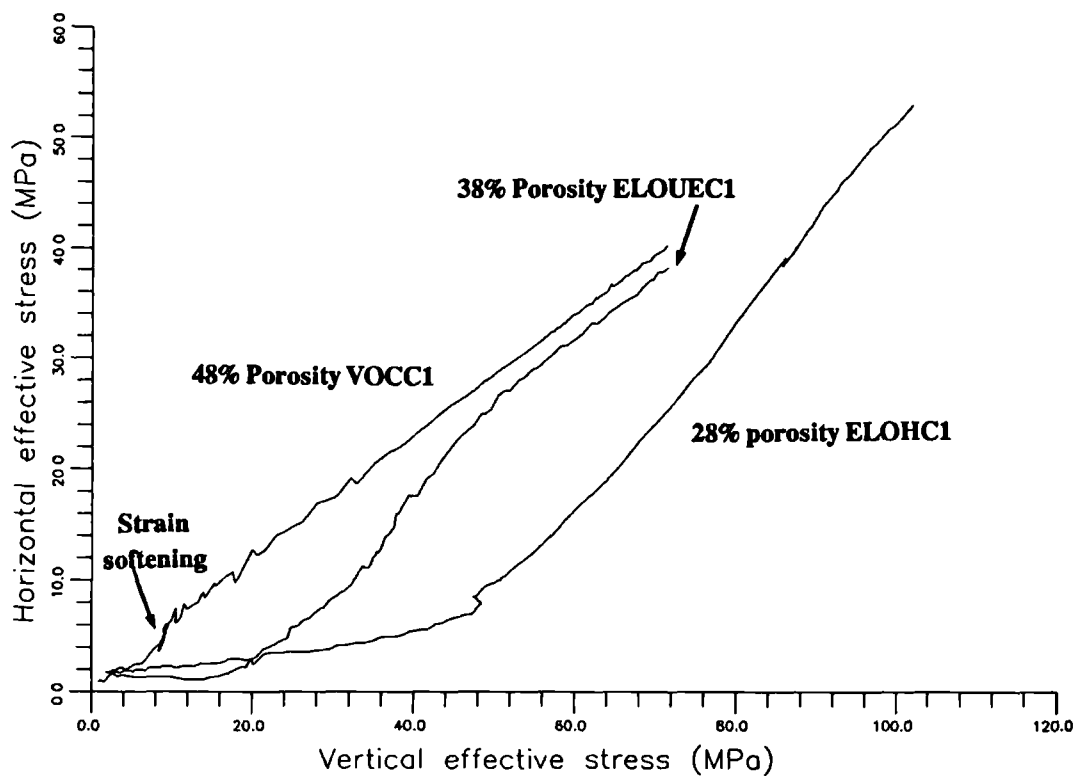


Figure. 4.2. Graph of horizontal effective stress/vertical effective stress for three sample with different initial porosities (28, 38 and 48%).

creases (Addis, 1987) and the stress ratio increases to approximately 0.9-1.0. Yield is followed by strain softening (the term is used here when the deviatoric stress decreases or remains constant) and/or strain hardening. The relative importance of the strain softening behaviour is governed by the initial porosity of the material. During this phase of the deformation the stress ratio remains high. The onset of strain hardening is accompanied by a decrease in the effective stress ratio to approximately 0.6 and a reduction in compressibility (Addis, 1987).

This three stage deformational behaviour has been observed in all of the medium and high porosity chalks deformed during K_0 experiments in this study and that of Addis (1987). The stresses at which the transitions between the three stages of deformation occur are dependent on the initial porosity of the sample (figure 4.2). As the initial porosity decreases the yield stress is observed to increase and the importance of strain softening decreases.

Changes in effective stress and sample volume can be represented in graphical form in the axes mean effective stress, deviatoric stress and void ratio. These three parameters are defined as:

$$\text{Mean effective stress} \quad = p' = (\sigma_1' + 2\sigma_3')/3 \quad 4.4$$

$$\text{Deviatoric stress} \quad = q = \sigma_1' - \sigma_3' \quad 4.5$$

$$\text{Void ratio} \quad = e = \text{Volume of voids}/\text{Volume of the solids} \quad 4.6$$

Where the principal effective stresses: σ_1' represents the greatest (axial) effective stress; σ_3' represents the least (lateral) effective stress. The third (intermediate) principle effective stress, σ_2 cannot be independently controlled in a triaxial system and is equal to σ_3 .

These three axes have been wisely used to present the results of deformation experiments (ie. Roscoe et al., 1958; Sangrey, 1972; Atkinson and Bransby, 1978; Addis 1987, 1989; Carter et al., 1988; Dobry et al., 1988; Fahey, 1988; Golightly and Hyde, 1988; Bressani and Vaughan, 1989; Goldsmith, 1989; Goldsmith et al., 1989; Jones and Leddra, 1989; Leddra and Jones, 1989). Data plotted against the two stress axes are referred to as stress paths. An effective stress path may be defined as 'the line joining all the points of instantaneous states of effective stress' (Atkinson and Bransby, 1987). Stress paths representing uniaxial strain deformation of chalk samples show the behaviour described above. Figure 4.3 presents a single chalk stress path. The initial straight section of this plot indicates the elastic deformation. As the effective stresses increase, elastic deformation is replaced by yield. The shape of the yield curve indicates that it is a gradual process, during which the sample loses deformation resistance, preventing further increase in shear stress (figure 4.3). Yield is followed in higher porosity samples by strain softening, where shear strength decreases (figure 4.4). In chalks with lower initial porosities, yield is observed to be a more gradual process and strain softening is insignificant (figure 4.5). The influence of initial porosity is again clearly seen in the multiple plot presented in figure 4.6. It should be noted that all the graphs presented in this section represent the results of experiments on chalks containing very little silica. Increased silica content has a similar influence on the experimental data as decreasing porosity.

As effective stress increases an excess pore pressure is generated and pore fluid is expelled (Lambe and Whitman, 1979). The expulsion of pore fluid is accompanied by a shortening of the sample (K_0 tests may also be termed uniaxial strain experiments). However, this relationship is seen to be modified by the presence of cementation. The structure of the material is able to sustain higher effective stresses with little volume change compared to an uncemented material. The manner in which this volume change is accomplished has been fully described in Lambe and Whitman (1979) and is briefly described in section 4.4. Changes in volume resulting from increasing effective stress may be represented by plots of void ratio against mean effective stress. Figure 4.7 rep-

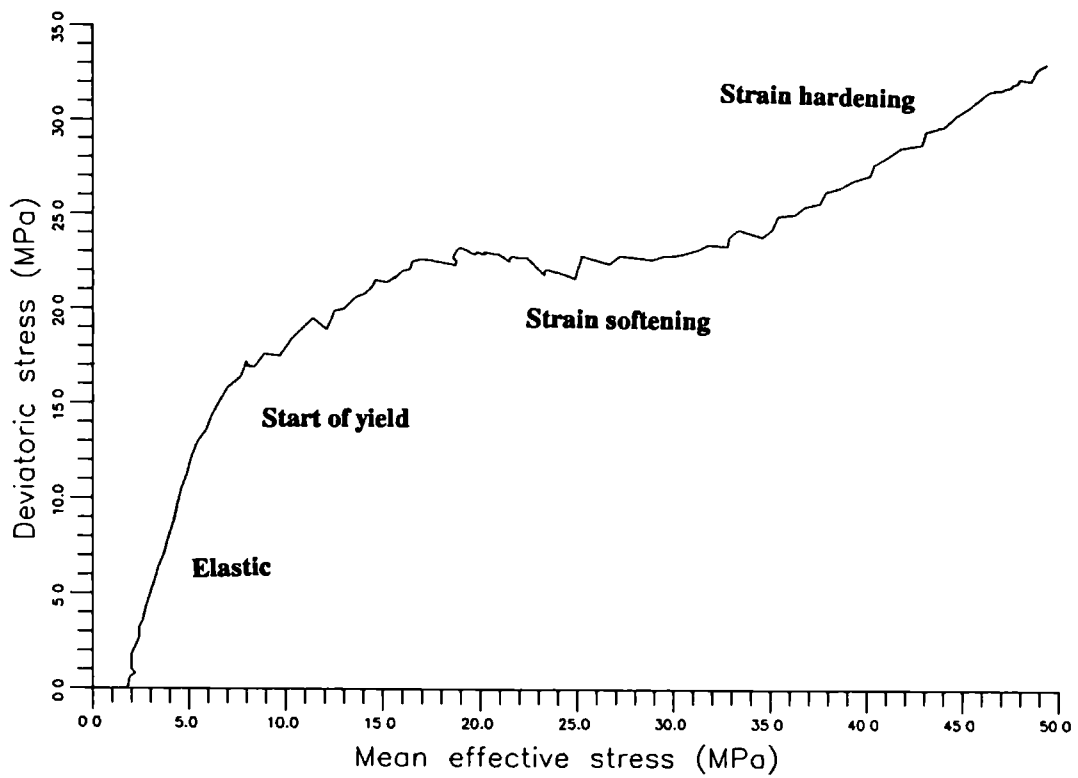


Figure. 4.3. Graph of deviatoric stress/mean effective stress for a 38% porosity chalk.

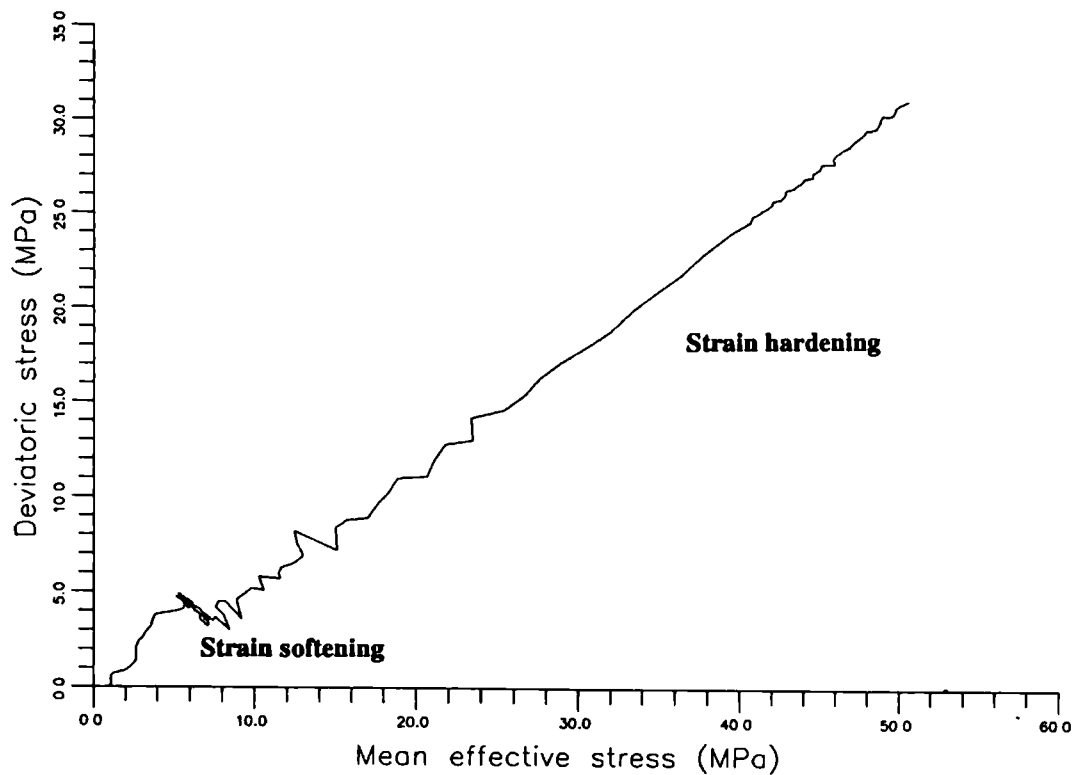


Figure. 4.4. Graph of deviatoric stress/mean effective stress for a 48% porosity chalk.

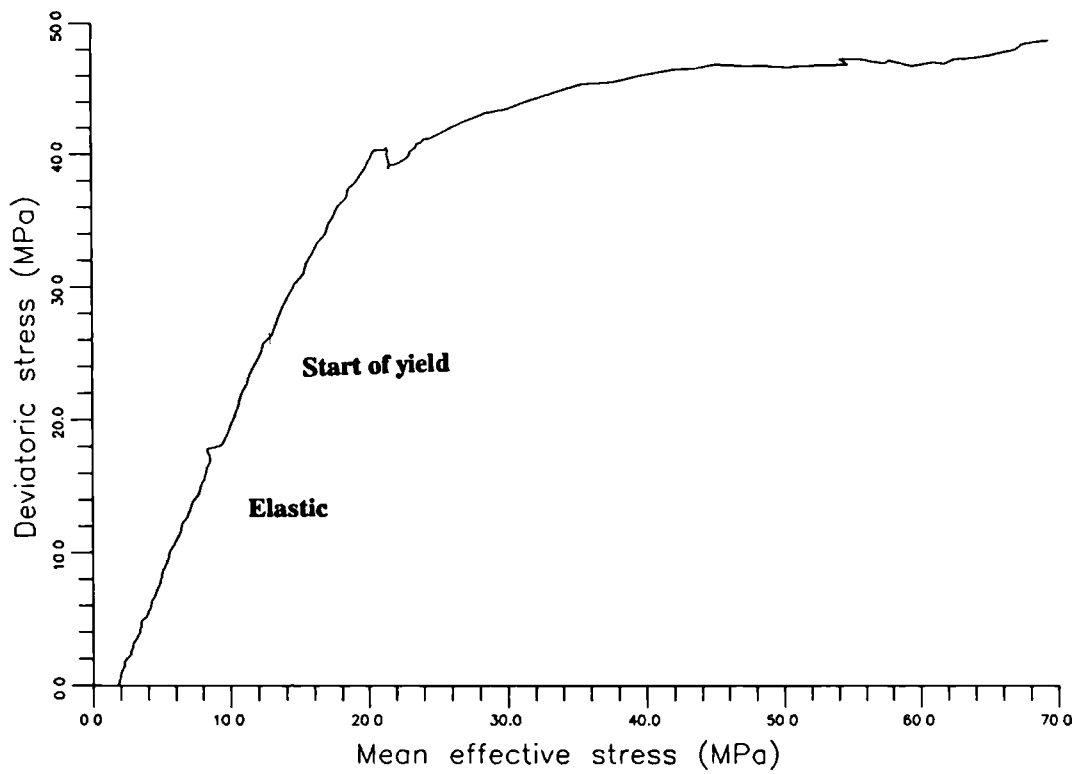


Figure. 4.5. Graph of deviatoric stress/mean effective stress for a 28% porosity chalk.

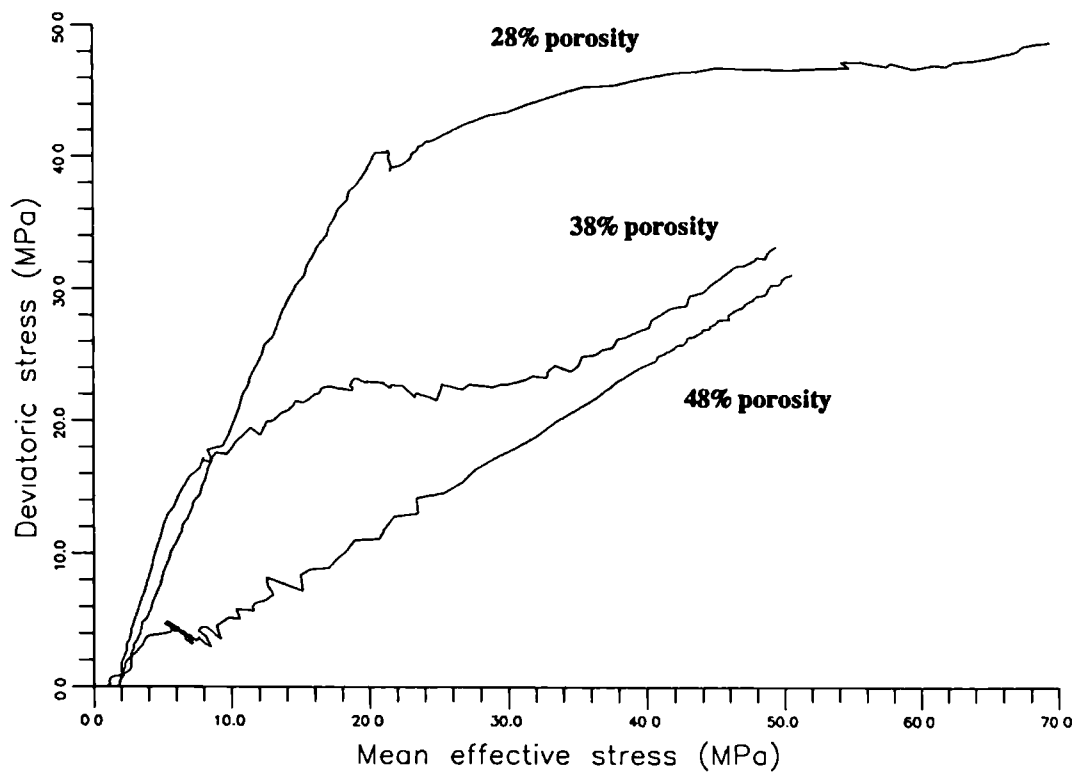


Figure. 4.6. Graph of deviatoric stress/mean effective stress for three samples with different initial porosities (28, 38% and 48%).

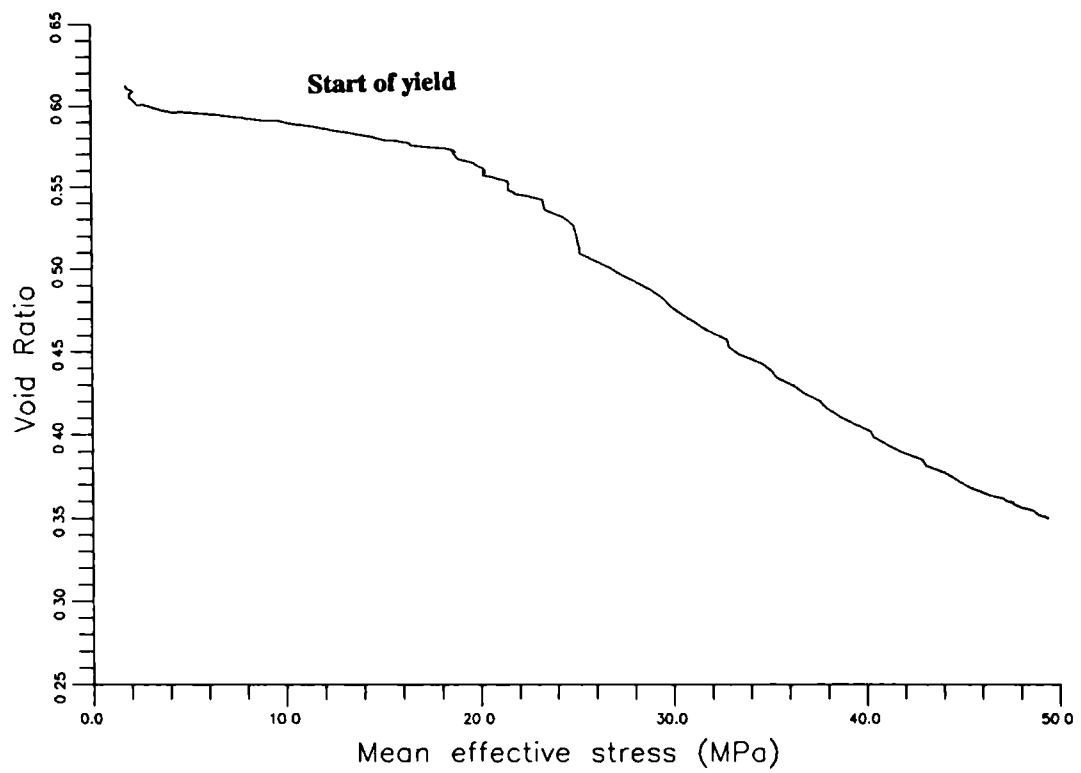


Figure. 4.7. Graph of void ratio/mean effective stress for a 38% porosity chalk.

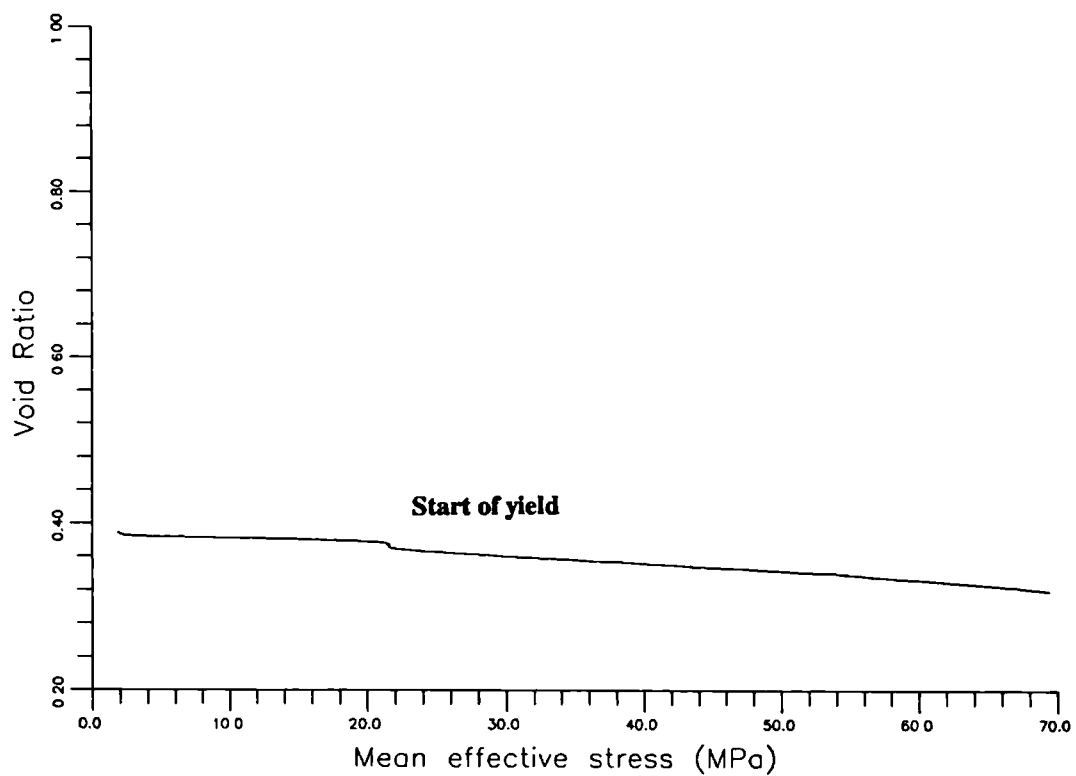


Figure. 4.8. Graph of void ratio/mean effective stress for a 28% porosity chalk.

resents a typical void ratio/mean effective stress plot. This plot may be divided into three sections. During the initial (elastic) phase of deformation very little volume change is observed. At a stress, dictated primarily by the porosity, larger volume changes are initiated. As porosity (and therefore void ratio) decreases the mean effective stress range over which very small changes in volume are recorded increases. In high porosity samples this trend in decrease of void ratio is observed to flatten out, indicating a gradual strengthening of the sample. Figure 4.8 represents the plot of a low porosity sample and figure 4.9 shows the pattern of volume changes in a high porosity sample. Figure 4.10 shows a combined plot of several experiments representing a range of initial porosities.

A model termed the Cam Clay Model may be presented in terms of the three parameters defined above, namely deviatoric stress (q), mean effective stress (p') and void ratio (e) (figure 4.11). This model can be used to define the yield surface for a sediment in which the Normal Consolidation Line represents the path followed by a sediment consolidated without the application of shear stress in mean effective stress/void ratio space. The Roscoe Surface represents a surface defining the maximum ratio's of q , p' and e for a normally consolidated sediment during compaction and shear. This surface is bounded by the Normal Consolidation Line and the Critical State Line. Critical State refers to the style of behaviour at failure where the sediment continues to strain at constant stress and constant void ratio. The Hvorslev Surface is defined as the yield surface for overconsolidated sediments. An explanation of the Critical State concept can be found in chapter 6 and full descriptions may be found in Atkinson and Bransby (1987) and Schofield and Wroth (1968). The results of the experimental study presented in this thesis and those reported in Addis (1978) are portrayed with respect to this model which is an appropriate description of the observed style of deformation.

During his experimental study of the mechanisms of sediment compaction, and, in particular, the behaviour of chalk, Addis (1987) investigated the way in which, sample size, elevated temperatures, and differing strain rates may affect the results of uniaxial strain

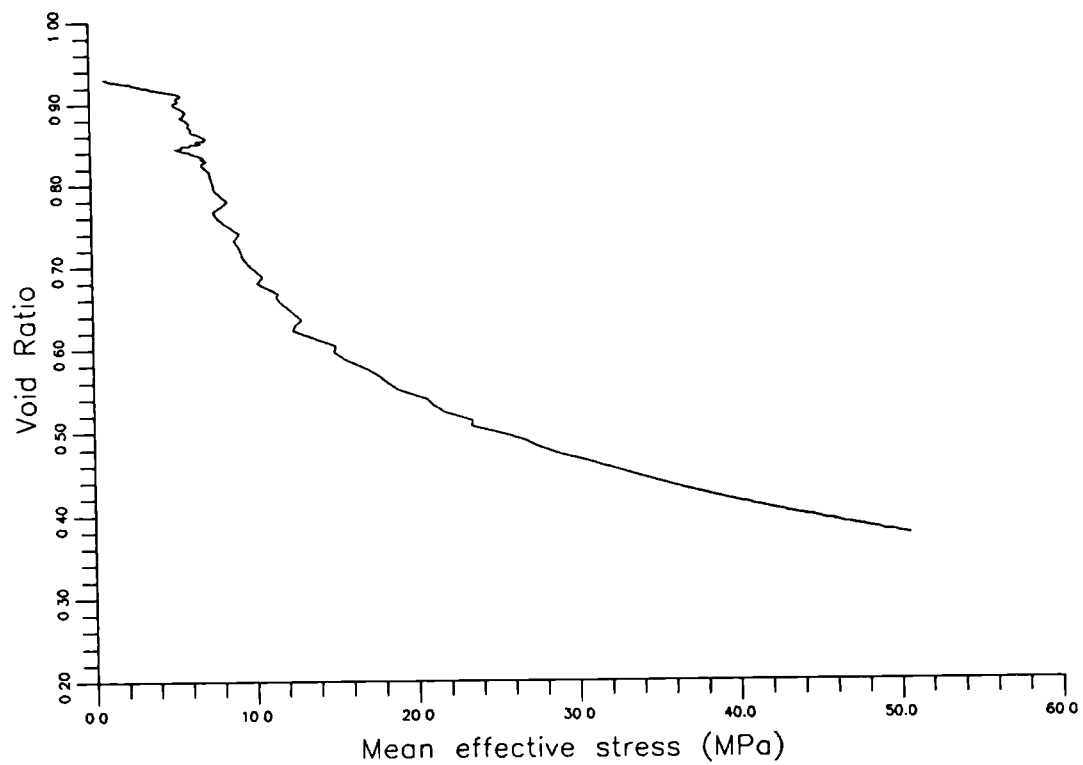


Figure. 4.9. Graph of void ratio/mean effective stress for a 48% porosity chalk.

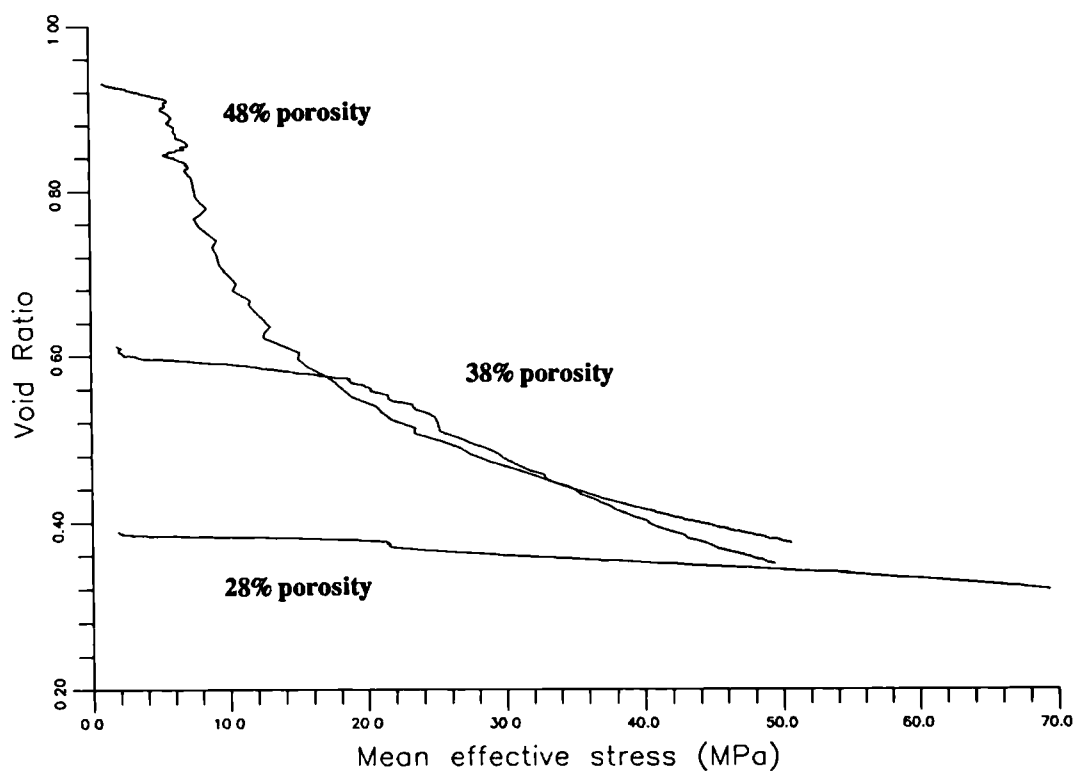


Figure. 4.10. Graph of void ratio/mean effective stress for three samples with different initial porosities (28, 38 and 48%).

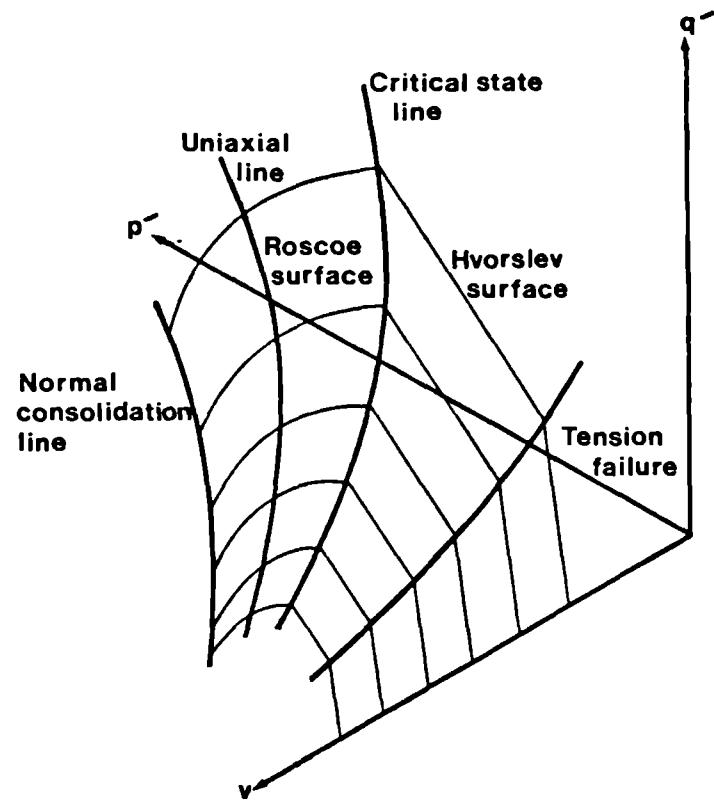


Figure. 4.11. Cam Clay model (After Atkinson and Bransby, 1978).

experiments. A discussion of the latter of these three parameters can be found in section 4.4. Addis (1987) conducted a number of experiments, in which he used samples of outcrop chalk cut to three different length/diameter ratio's (1.9, 1.3 and 0.6). He found that although the stress paths were not affected by sample size, vertical effective stress/axial strain and deviatoric stress/axial strain curves indicated that strain increased as the ratio of the sample's dimensions decreased. Uniaxial strain experiments were also conducted on outcrop samples at different temperatures (20, 60 and 100°C). Although increasing temperature appeared to have some effect on the test results, no relationship was identified within the reproducibility of the experiments. He concluded that any temperature effects would be masked by those resulting from differences in the initial porosity of the samples.

4.3. EXPERIMENTAL EQUIPMENT AND SAMPLE PREPARATION METHODOLOGY.

The uniaxial strain experiments reported in both this chapter and chapter five were undertaken using a high pressure, high temperature triaxial cell located in the Soil Mechanics Laboratory, Department of Civil Engineering, Imperial College of Science and Technology, University of London. A brief description of the cell, the load frame and the ancillary equipment used to perform uniaxial strain experiments is provided in this section and a full description can be found in Addis (1987).

4.3.1. The triaxial cell.

The triaxial cell which was designed by Dr Angus Skinner from the Department of Civil Engineering at Imperial College, is composed of three main sub-assemblies, namely the ram, cylinder and pedestal (figure 4.12).

Figure 4.13 shows a detailed drawing of the ram section of the triaxial cell. The ram, termed a balanced ram, consists of a shaft with a central flange, the surface area of which is equal to the cross-sectional area of the shaft. The ram contains a number of drainage holes which allow fluid communication between the cylinder and the chamber above the flange. These holes have two functions:

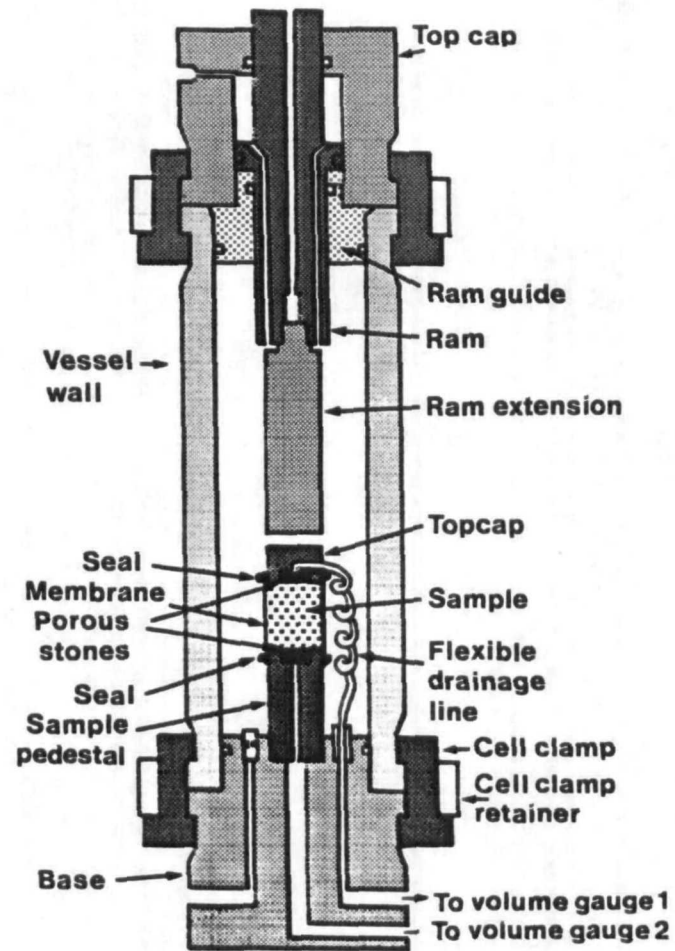


Figure. 4.12. Schematic representation of the high triaxial cell used during this study.

- *1) they allow the volume of the confining fluid to remain constant (this does not include volume changes resulting from compaction of the sample) by allowing fluid to flow from the cylinder into the top of the cell as the ram is displaced, and,*
- *2) the confining fluid is able to exert an equal pressure on either side of the ram (ie. on the bottom of the ram and the top of the flange) so that only the deviatoric component of the vertical stress has to be applied by the load frame.*

The pedestal section of the cell contains a series of holes (capped off with 'O' ring sealed steel plugs when not in use) through which communication with the sample and the cell is achieved. The sample is placed on the pedestal which contains a drainage line that allows pore fluids to be expelled from the base of the sample. Further fluid communication with the top of the sample is provided by a drainage line which passes through one of the communication ports and is connected to a top cap which sits between the sample and the ram. Other entry ports are used for a thermocouple to measure the temperature of the confining fluid and a radial strain belt which is used to record changes in the radial dimensions of the sample in the mid-height position.

4.3.2. Measurement of horizontal and vertical displacements.

The strain belt consists of a thin metal band on which four strain gauges have been glued in a full bridge configuration (figure 4.14). It is attached by screws through the strain belt to two brass pads which are held in contact with the sides of the sample (see section 4.3.6). The strain belt can be linked to a control system (see Addis, 1987) so that changes in the voltage output from the strain belt can be used to drive an electric motor which is attached to the confining pressure system. This allows uniaxial strain experiments to be conducted in a semi- automatic manner.

Axial displacements are measured by a displacement transducer located on the outside the cell. The transducer is attached to the ram by a clamp and sits on a brass rod which

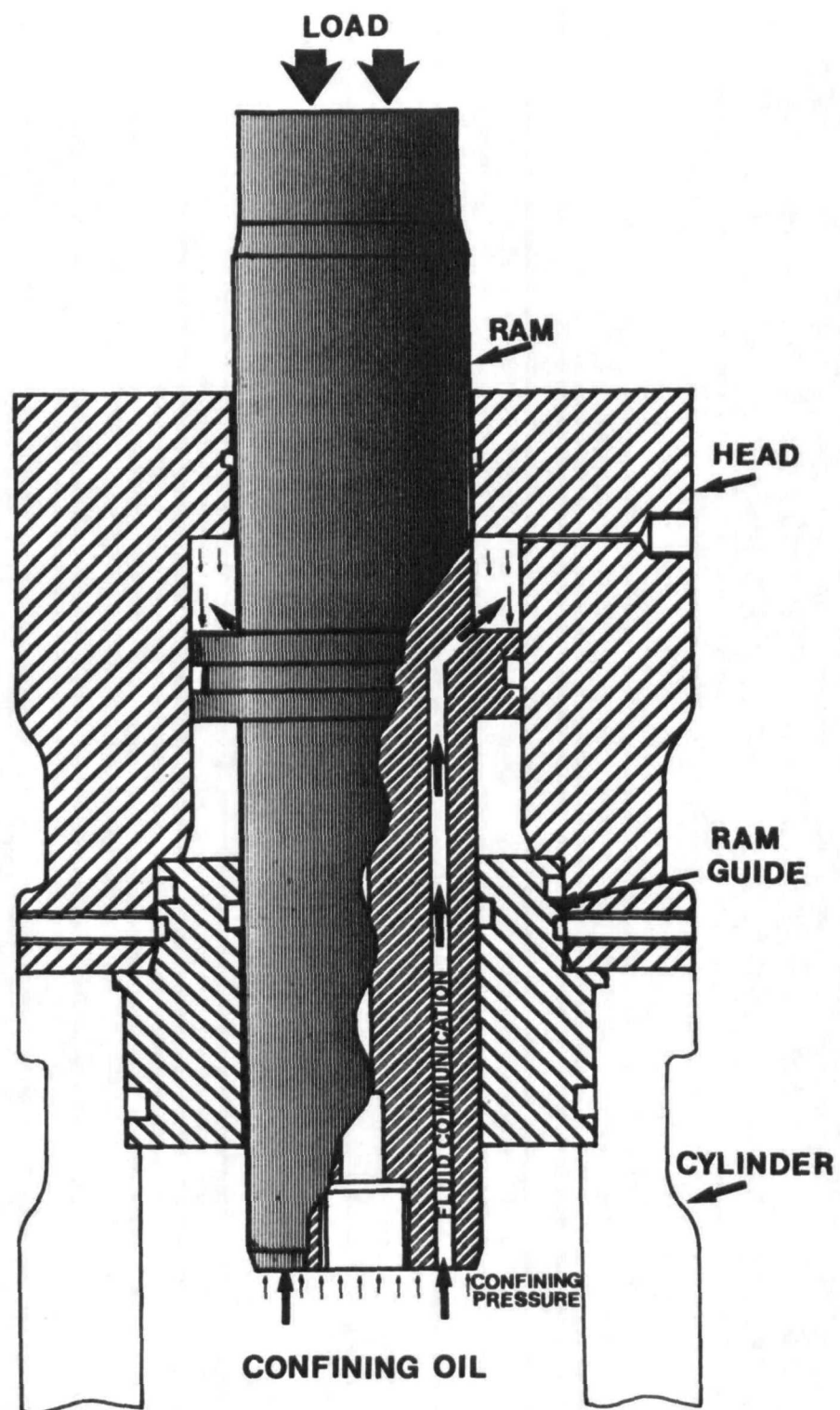


Figure. 4.13. Sectioned drawing of a balanced ram.

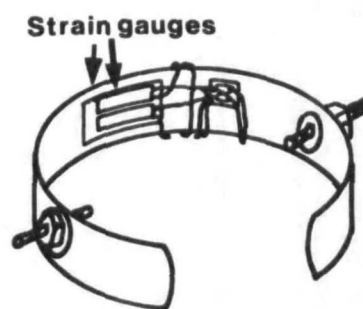


Figure. 4.14. Schematic representation of a radial strain belt.

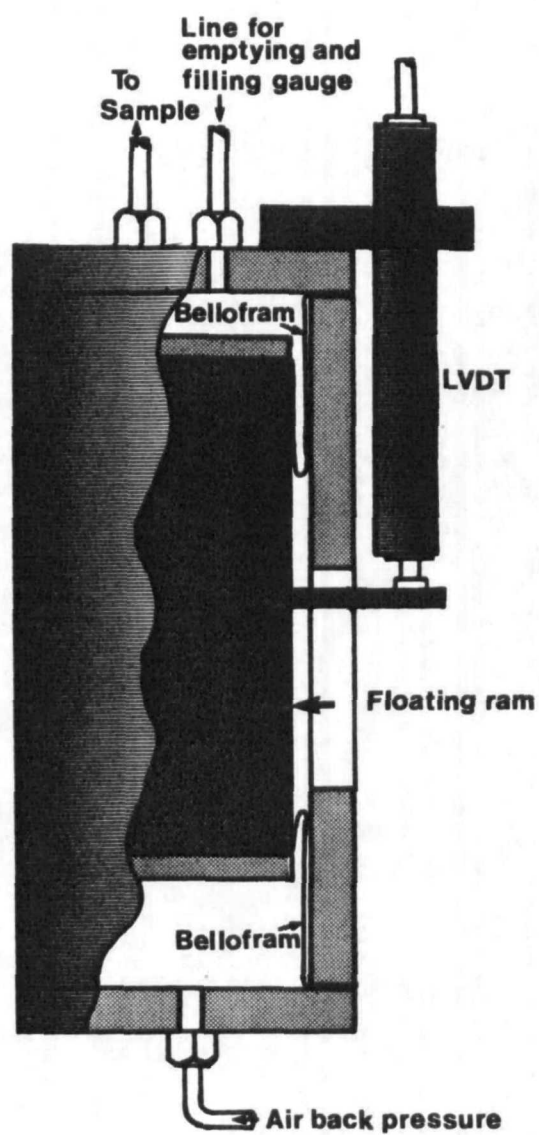


Figure. 4.15. Sectioned drawing of an Imperial College volume gauge.

is attached to the base of the cell. This is used to measure the movement of the ram with respect to the body of the cell.

4.3.3. The load frame.

The triaxial cell has been installed in a Clockhouse Engineering Ltd. 500kN (50tons) load frame. This is capable of supplying a constant displacement rate which can vary from 9.99×10^{-1} mm/min to 1×10^{-6} mm/min.

4.3.4. The drainage system.

Fluids may be passed into and drained from either end of the sample through two independent drainage lines. These lines are connected to Imperial College volume gauges (figure 4.15). Each volume gauge is divided into two sections separated by a floating piston which is held between two belloframs. This allows the volume gauges to be operated as fluid/air interfaces, in which an air pressure is supplied to the bottom of the volume gauge which is used to apply a back pressure to the drainage system attached to the upper part of the volume gauge. Manostat constant leak air regulators allow a constant air pressure to be applied which can be adjusted to control the fluid back pressure supplied to either end of the sample. A vertical displacement transducer is attached to each volume gauge which is calibrated so that displacement represents a change in volume. Pressure transducers are attached to the drainage lines between the sample and the volume gauges in order to determine the fluid pressures at either end of the sample. The drainage lines are designed so that both volume gauges may be isolated from the sample to allow them to be drained or refilled at any time during an experiment. This means that if required, the fluid entering or contained in, the sample may be changed during an experiment.

4.3.5. Data logging.

Data monitoring, logging and reduction is provided by a computer program (written by Dr David Toll) which is run on a Prime 250 computer. This program allows simultaneous monitoring and logging of nine transducers connected to the equipment described above. These consist of: the radial strain belt; three displacement transducers

(one measuring displacement of the ram and two calibrated to determine changes in volume in the volume gauges); three pressure transducers (one to determine the cell pressure and one connected to each drainage line); the load cell; and a thermocouple (located inside the cell) to determine the temperature of the confining fluid and sample. Transducers may be monitored individually or in groups of four at three second intervals. The data may be written to a computer disc at selected (logging) intervals between 3 seconds and two hours. For details of the computer facilities and their use see Toll (1988).

4.3.6. Sample preparation and installation procedures.

38mm diameter right cylindrical samples are cut from core material and blocks of chalk using a diamond-edged rotary coring tool which is used in a pillar-drill. The ends of the samples are then planed off to the required length (approximately 76mm) in a flat-bed surface grinder.

Once the samples have been cored and faced, they are placed in a desiccator to be saturated, under vacuum, with the chosen pore fluid. Following saturation, they are stored submerged in this fluid until required for testing.

When a sample is to be tested, it is firstly weighed (to determine the saturated weight) and measured. These parameters are required for subsequent data analysis. The sample is normally held in two Neoprene rubber membranes (37mm diameter, 0.5mm thick and 150mm long). These are pressure tested for leaks and then trimmed to a length of 130mm. Once trimmed, two small round holes are cut in one of the membranes. These holes are located on opposite sides of the membrane in the mid-height position. Two brass pads (to which the strain belt will subsequently be attached) are then sealed into these holes with super glue. When the glue is dry, a further coating of glue is applied to the other side of the membrane to act as a seal.

When a sample is ready to be located in the test cell it is removed from the fluid in which it has been stored. The two short sections of membrane are then placed around either end of the sample in such a way that they overlap the ends. Usually a piece of filter paper, soaked in the pore fluid, is then placed inside either membrane in contact with the ends of the sample. Highly permeable porous discs are then placed on top of the filter papers. Thus the short (inner) membranes are used to hold the entire 'sub-assembly' together. This sub-assembly is then fitted into the full membrane containing the brass pads (which is expanded in a suction tube). The second membrane is then added in the same manner, and once it is in place, holes are cut into it to allow the outer ends of the brass strain belt pads to pass through. Glue is applied to seal the brass pads to this outer membrane. The sample is then ready to be assembled on the pedestal in the test cell. The membranes are fitted around the pedestal and are then held in place by three 37mm diameter 'O' rings. Super glue is again applied to the contact between the strain belt pads and the outer membranes. When the glue has dried, the strain belt is screwed into the brass pads and the top-cap placed on the top of the sample assembly (this is also held in position by three 'O' rings). Figure 4.16 is a sectioned drawing of the sample assembled in the triaxial cell.

Once the cell has been assembled and filled with the confining fluid, it may be heated if necessary to the required temperature.

4.4. SLOW STRAIN-RATE EXPERIMENTS.

4.4.1. Introduction.

The relationship between stress and strain in most rock and soil materials is known to exhibit a time dependency. If the results of deformation experiments are to be used as input data for deformation analyses, such as those undertaken for Ekofisk (Boade et al., 1988) this time dependency needs to be correctly specified. In soil mechanics this is known as primary and secondary consolidation and in rock mechanics similar effects are often termed creep.

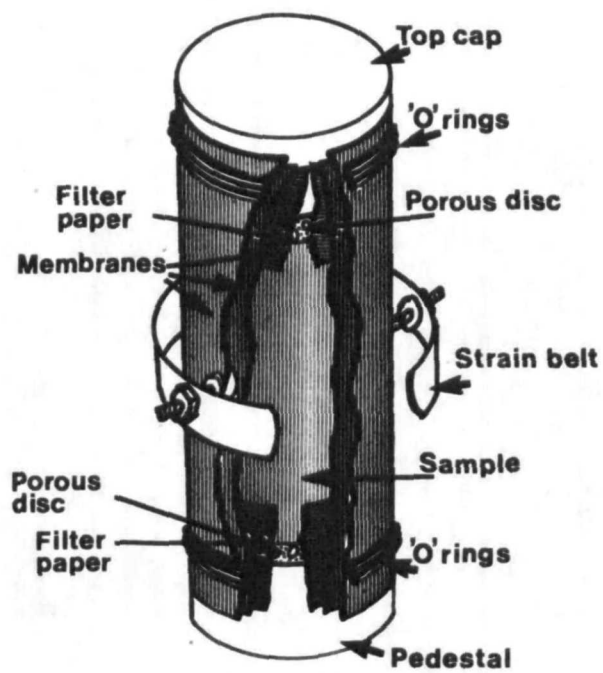


Figure. 4.16. Schematic drawing of a sample assembled in the triaxial cell.

The volume changes in a sediment associated with an equilibration of effective stresses to changes in the boundary stress state is described as compression, and the time dependent change in volume associated with the approach to stress equilibrium is termed consolidation (Lambe and Whitman, 1979).

The dissipation of an excess pore fluid pressure generated as a result of an increase in the total stress acting on a soil is referred to as primary consolidation (Lambe and Whitman, 1979). The time required for primary consolidation to create an equilibrium pore pressure, and therefore an equilibrium strain state in a soil, will be dependent on its permeability, the hydraulic gradient and the length of the drainage path. This is referred to as the hydrodynamic time lag (Lambe and Whitman, 1979). The time required for consolidation to occur is related to two factors (Lambe and Whitman, 1979): a) the volume of the soil and the compressibility of the mineral skeleton will determine the volume of pore fluid expelled from a soil resulting from an increase in stress; b) it is inversely proportional to the rate of flow of pore fluid through the soil.

Secondary compression is described as the slow, continued compression that occurs after excess pore pressures have substantially dissipated (Lambe and Whitman, 1979). In reality Lambe and Whitman (1979) observed that there must be an excess pore pressure present during secondary compression to cause the pore fluid to move. This excess pore pressure is however considered to be immeasurably small or transient. The deformation of the mineral skeleton may also have time-dependent stress-strain properties apart from reorientation and grain crushing. Such properties have been recognised in stronger rock and minerals (where temperature effects are also important). They include plasticity of the mineral grains, atomic diffusion through and around mineral grains, pressure solution and cataclasis (time dependent fracture propagation).

The relative importance of primary and secondary compression varies with the type of soil and also with the ratio of stress increment to initial stress. The ratio of secondary

to primary compression is largest when the ratio of the applied stress increment to initial stress is small. In an initially elastic material such as the chalk, the relatively incompressible cement structure will resist the deformation which results from an increase in effective stress, and therefore strain energy will be stored in the structure of the sample. At the elastic limit, the cement structure begins to fail, the compressibility of the chalk starts to increase (Addis, 1987) and the stored strain energy will be gradually released. Experiments described in the following sections indicate that at yield, the cement structure begins to breakdown in a limited number of discrete centres of failure. As yield progresses these areas spread. The deformation is effectively cataclastic, although the large pore spaces in the chalk allow cataclasis to progress in a contractant rather than a dilatant manner. Part of the time dependent behaviour expected to be observed in the deformational behaviour of the chalk could therefore be a result of this gradual propagation of individual fractures. This would lead to a transfer of stress from the failed mineral structure to the pore fluid and the generation of an excess pore pressure. Gradual dissipation of this pore pressure leads to a strain in the rock as the released grains are able to move and an increase in effective stress in the intact structure at the margins of the failed regions which in turn results in a further breakdown of the mineral structure etc. The presence of failure centres and areas of relatively undeformed chalk existing in samples deformed to nearly 30% axial strain can be seen in plates 4.1-4.3 (section 4.5).

4.4.2. Experimental methodology and results.

The majority of the deformation experiments undertaken on chalk reported in this thesis and by Addis (1987) were conducted at approximately the same constant displacement rates (10^{-6} sec^{-1}). Therefore the magnitude of deformations resulting from the use of different strain rates could not be recognised.

In order to quantify whether the chalk would be subject to strain rate effects, Addis (1987) conducted a series of experiments, using outcrop chalk from Pegwell Bay. Two different experimental methods were employed, namely, deforming a number of



Plate 4.1. Scanning electron micrograph for a sample of Stevn's Klint chalk subject to approximately 28% axial strain.

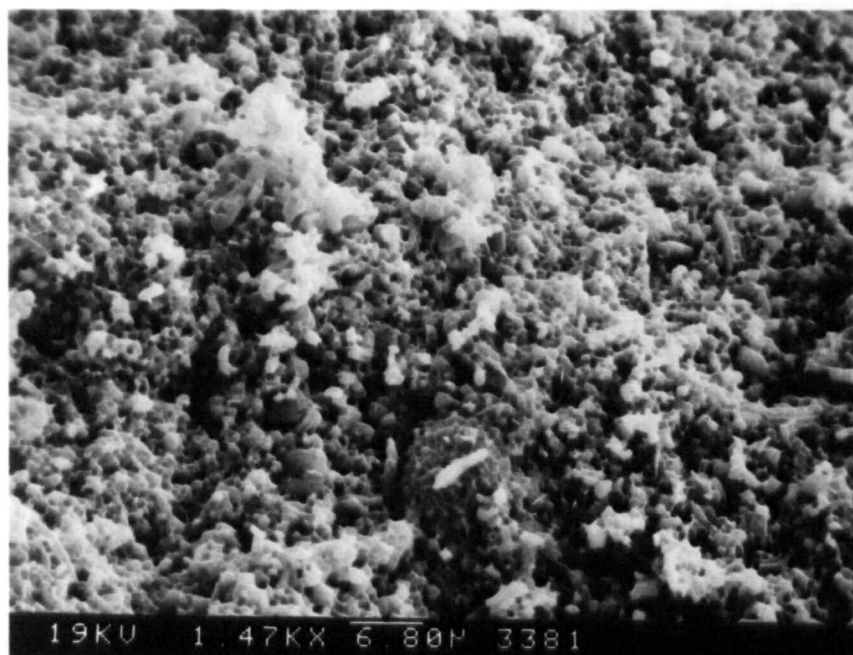


Plate 4.2. Scanning electron micrograph for a sample of Stevn's Klint chalk subject to approximately 28% axial strain.

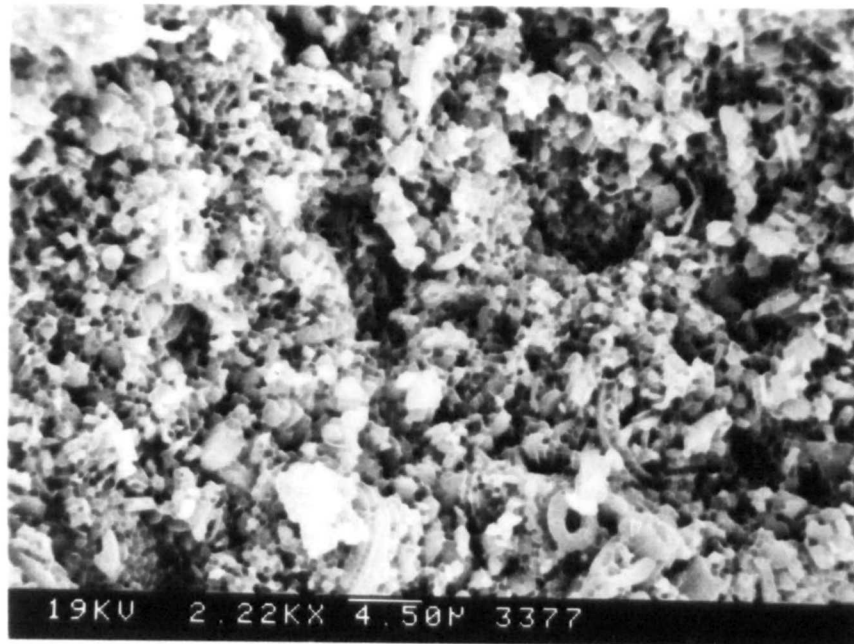


Plate 4.3. Scanning electron micrograph for a sample of Stevn's Klint chalk subject to approximately 28% axial strain.

samples cut from the same block of outcrop chalk at different displacement rates, and deforming a single sample of the same chalk whilst varying the displacement rate during the experiment. This latter experiment was based on a method developed by Leroueil et al. (1985) for investigating the strain-rate effects recorded during the deformation of Canadian sensitive clays. The deformation curves were normalised with respect to the stress at the start of normal consolidation in order to remove any rate effects that were associated with the elastic and pore collapse sections of the stress/strain data. Addis (1987) noted that the strain at the start of normal consolidation was observed to increase as the strain rate decreased.

It was noted in Addis and Jones (1989) that a strain rate dependency was not observed in the series of tests using the first method described above. They conclude that this could have been a result of the limited range of strain rates to which the samples were subject ($6.5 \times 10^{-7} \text{ sec}^{-1}$ to $1.7 \times 10^{-5} \text{ sec}^{-1}$), a large variation in the samples used (even though the samples were cut from outcrop chalk considered to be relatively homogeneous) and that the strain rates used were too low. The latter point is interesting, as it is generally considered that laboratory imposed strain rates are too fast compared to those found in nature (where strain rate effects are though to be significant). They also observed that in the experiment in which the displacement rate was varied during the experiment, strain-rate effects were more distinguishable.

The experiments described below were conducted using offshore chalk samples from the Ekofisk Field. The tests were designed to identify whether samples subject to constant rates of displacement (which lead to nearly constant rates of strain) slower than those used by Addis (1987) would reveal the strain-rate effects he was trying to identify. The strain rates and the initial porosities are given in table 4.2 for the four samples tested.

Table 4.2.

DATA FOR THE SLOW STRAIN-RATE EXPERIMENTS.

EXPERIMENT NUMBER	INITIAL POROSITY %	STRAIN RATE
ELONGC1	37	$3.8 \cdot 10^{-9} \text{ SEC}^{-1}$
ELONGC2	42	$1.1 \cdot 10^{-8} \text{ SEC}^{-1}$
ELONGC3	38.1	$1.1 \cdot 10^{-8} \text{ SEC}^{-1}$
ELONGC4	36.7	$4.2 \cdot 10^{-8} \text{ SEC}^{-1}$

Measurements of sea floor subsidence conducted around the Ekofisk complex have indicated a discrepancy between the subsidence that is actually occurring (Rentsch and Mes, 1988) and that predicted by computer simulations (Leddra et al., 1989). One of the primary reasons for this difference is the lack of data concerning the long-term creep response of the chalk.

Four slow strain-rate experiments are described separately below. Only two samples (ELONGC2 and ELONGC4) were taken to large strains due to the time periods involved with operating at such slow displacement rates. Essential maintenance of various elements of the equipment used, as well as break downs in the data logging system during long term experiments has resulted in a degree of scatter in the data. The transducers used in the study are subject to a certain amount of drift in their outputs. Where possible, these have been taken into account when data processing. Following the difficulty of maintaining K_0 conditions during ELONGC1 it was decided that the automatic system described in Addis (1987) was not capable of reliably controlling the confining pressure required during these experiments, for such long periods of time. It was therefore decided to adjust the confining pressure manually.

4.4.2.1. ELONGC1.

This experiment was conducted at an initial strain rate of $3.8 \cdot 10^{-9} \text{ sec}^{-1}$. This was the slowest rate used in these experiments. The sample was observed to shorten by 0.3% in about 350 hours (when a seal in the ram failed). A change in the slope of the verti-

cal effective stress/axial strain curve (figure 4.17) is observed at approximately 10MPa. Similar changes are observed in figures 4.18 (horizontal effective stress/vertical effective stress) and 4.19 (deviatoric/mean effective stress). These indicate the onset of yield, even though the stress/strain curve (figure 4.17) does not show a significant deviation from an elastic behaviour, particularly as the value of K_0 changes from 0.36 to 0.98 in figure 4.18. Figure 4.20 illustrates the decrease in void ratio resulting from the increase in mean effective stress during the experiment. The volume of the sample does not appear to change significantly even though both effective stress plots (figure 4.18 and 4.19) indicate the onset of yield. The irregularity of the data for this experiment is a result of drifting in the zero position of the radial strain belt controller.

4.4.2.2. *ELONGC2*.

Experiment ELONGC2 had a duration of approximately 3000 hours and an initial rate of strain of $1.1 \cdot 10^{-8} \text{ sec}^{-1}$. Figure 4.21 shows the vertical effective stress/axial strain curve for this experiment. The sample begins to yield at approximately 8MPa and 0.5% axial strain. Following yield the sample appears to strain harden. The sections of the curve, which consist of straight lines represent periods when the data logging system was not operational (although records were still taken by hand as the monitoring facilities were still available). The effective stress ratio plot (figure 4.22) also indicates that yield began at approximately 8MPa (where a break in the slope from a K_0 value of 0.2 to 0.89 occurred) and was not completed until a vertical effective stress of greater than 20MPa had been achieved. Although pore collapse is not observed in the stress/strain curve, the stress path diagram (figure 4.23) indicates a decrease in the shear resistance which is normally associated with pore collapse. This behaviour is also observed in figure 4.24 (void ratio/mean effective stress) where significant changes in void ratio are observed to occur at approximately 13MPa (p'). This occurs at same value of p' in the stress path (figure 4.23) which indicated that the sample was starting strain hardening.

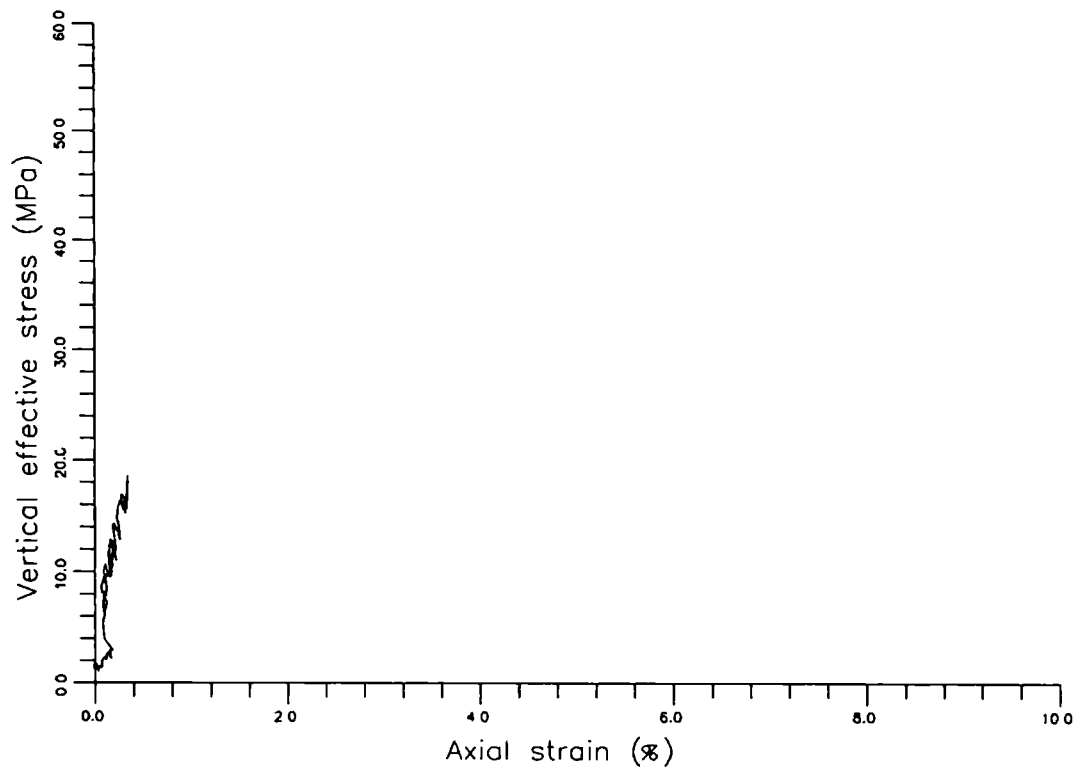


Figure. 4.17. Graph of vertical effective stress/axial strain for slow strain-rate experiment **ELONGC1**.

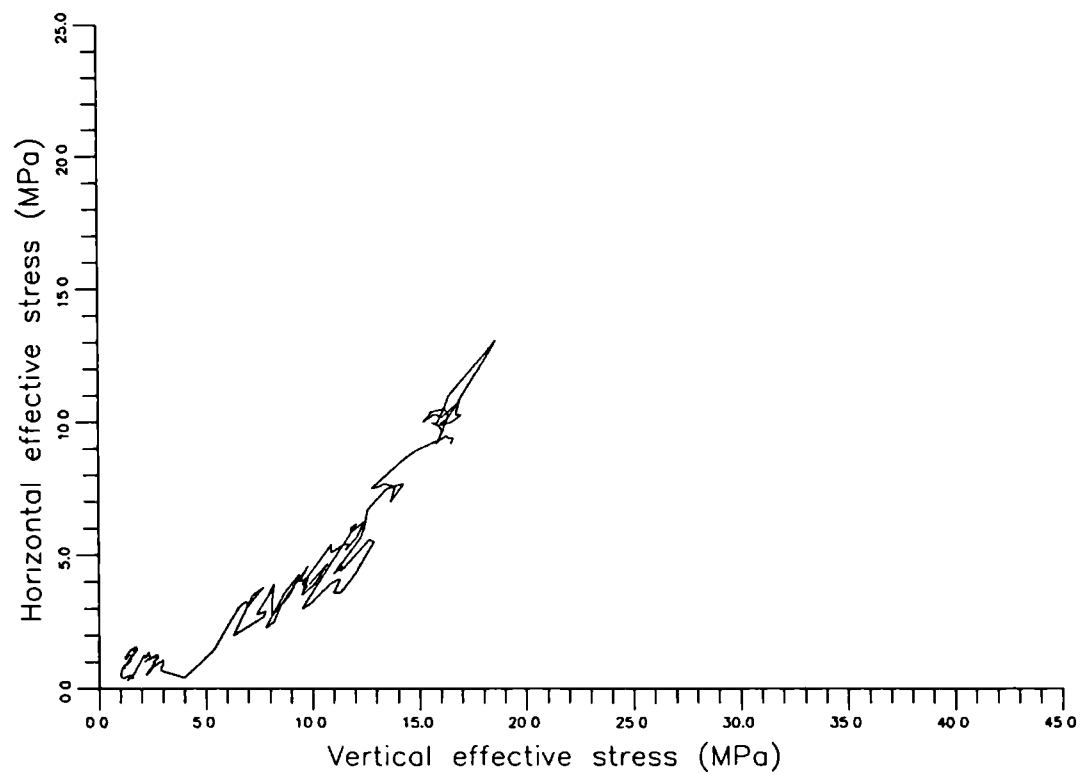


Figure. 4.18. Graph of horizontal effective stress/vertical effective stress for slow strain-rate experiment **ELONGC1**.

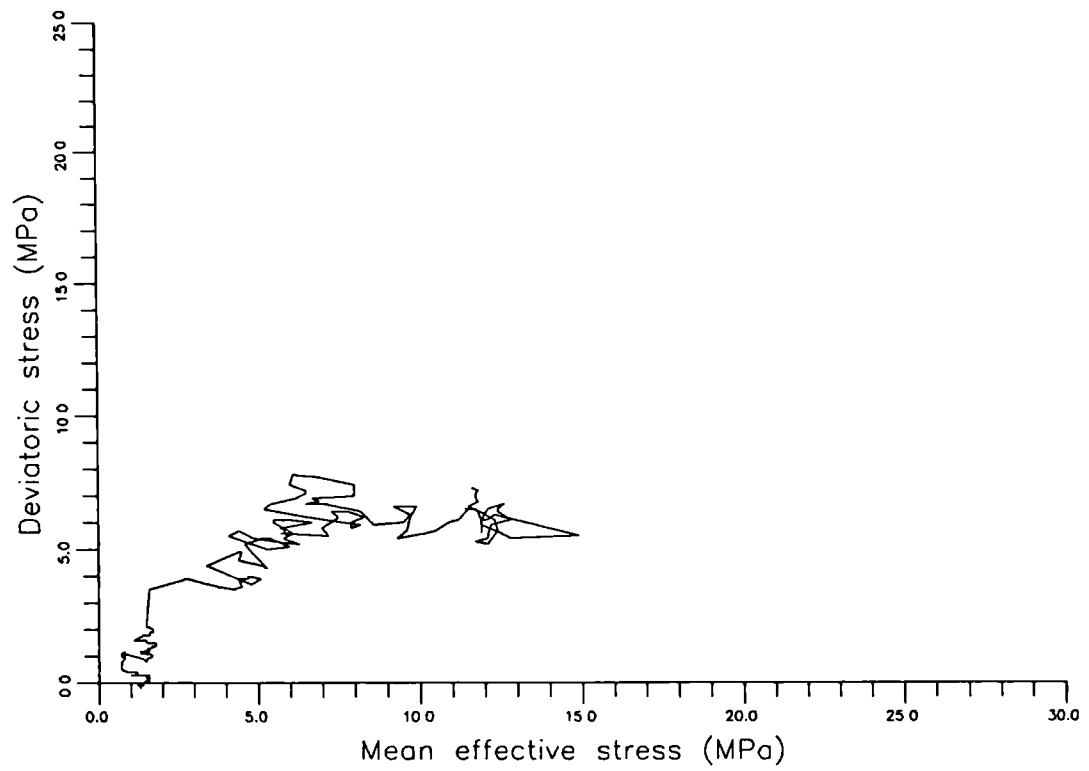


Figure. 4.19. Graph of deviatoric stress/mean effective stress for slow strain-rate experiment ELONGC1.

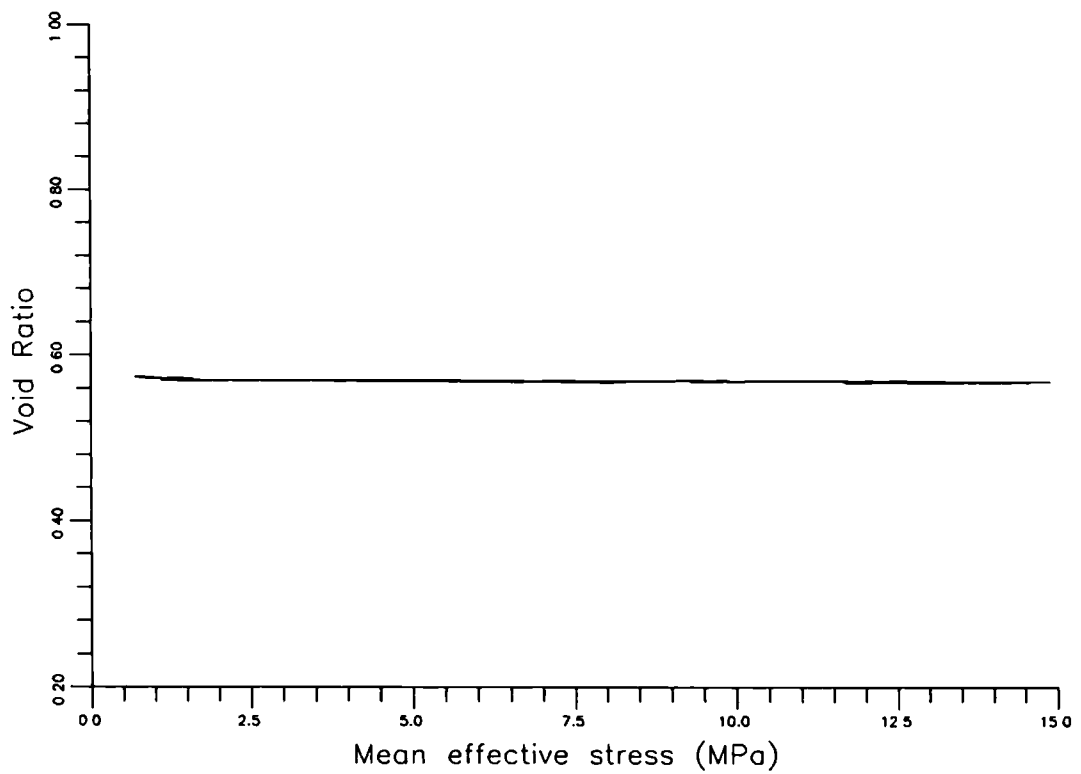


Figure. 4.20. Graph of void ratio/mean effective stress for slow strain-rate experiment ELONGC1.

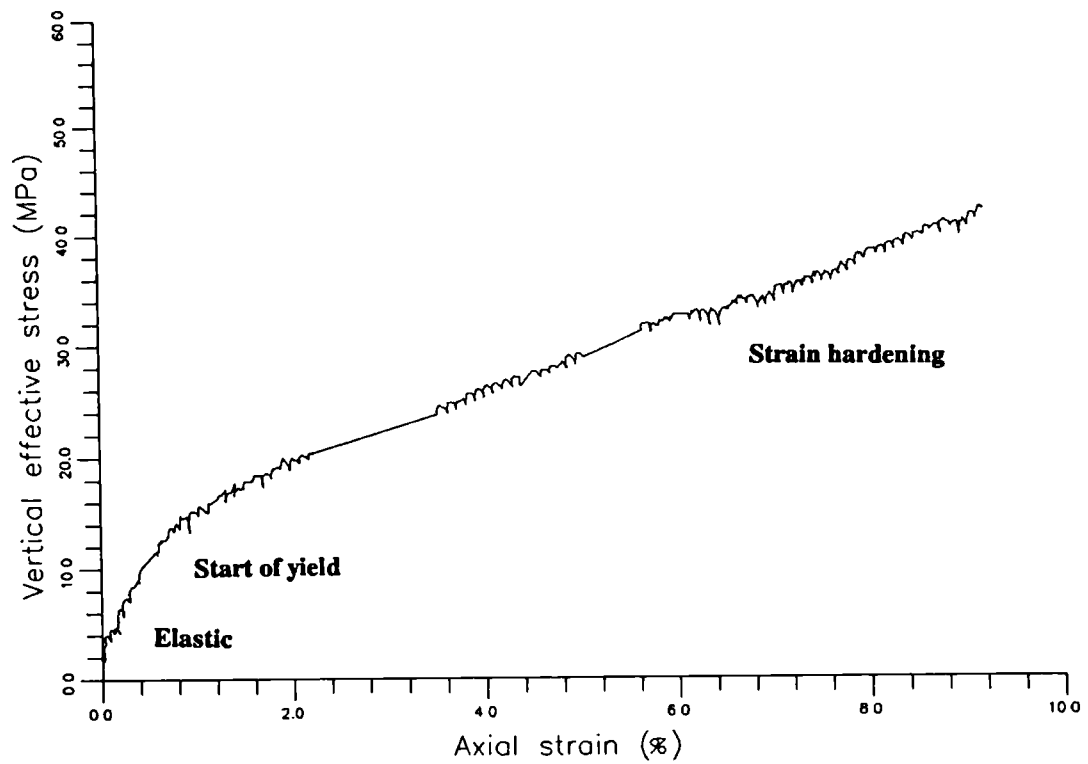


Figure. 4.21. Graph of vertical effective stress/axial strain for slow strain-rate experiment ELONGC2.

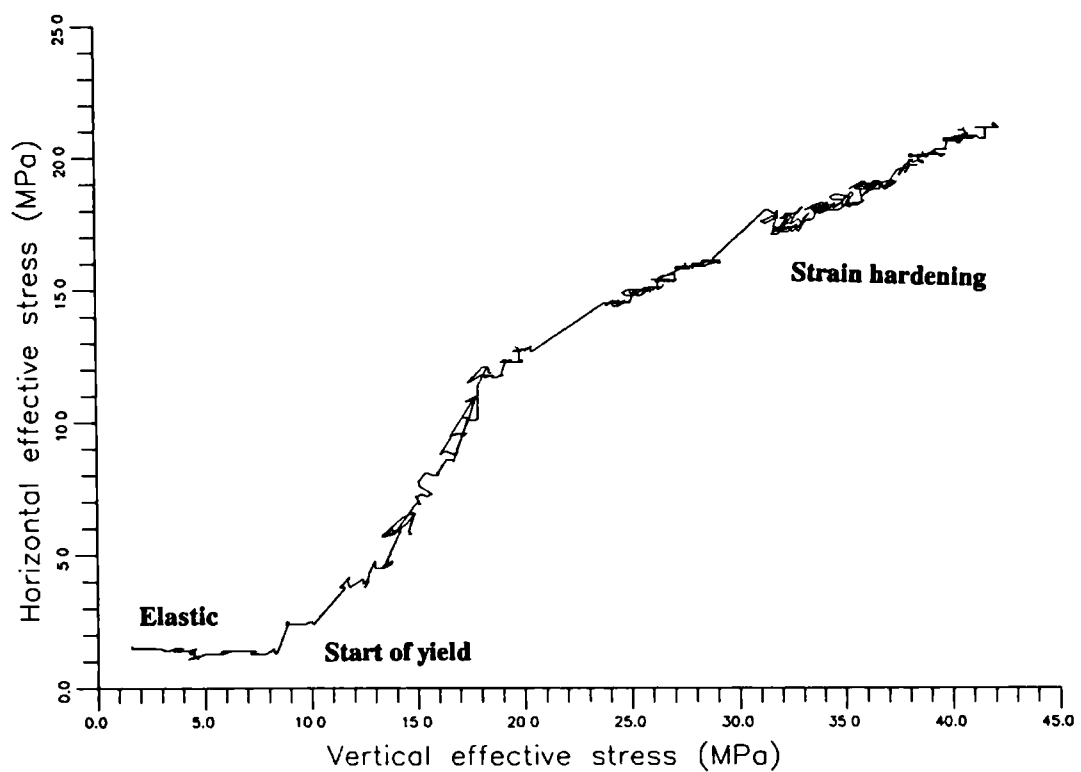


Figure. 4.22. Graph of horizontal effective stress/vertical effective stress for slow strain-rate experiment ELONGC2.

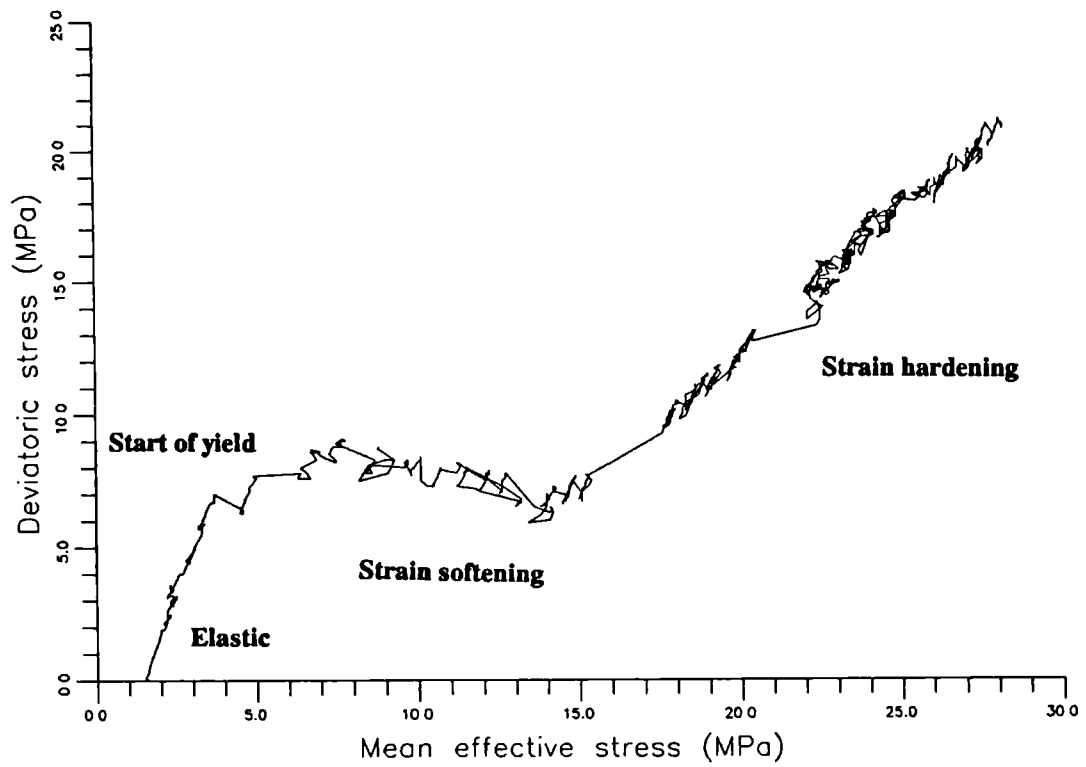


Figure. 4.23. Graph of deviatoric stress/mean effective stress for slow strain-rate experiment ELONGC2.

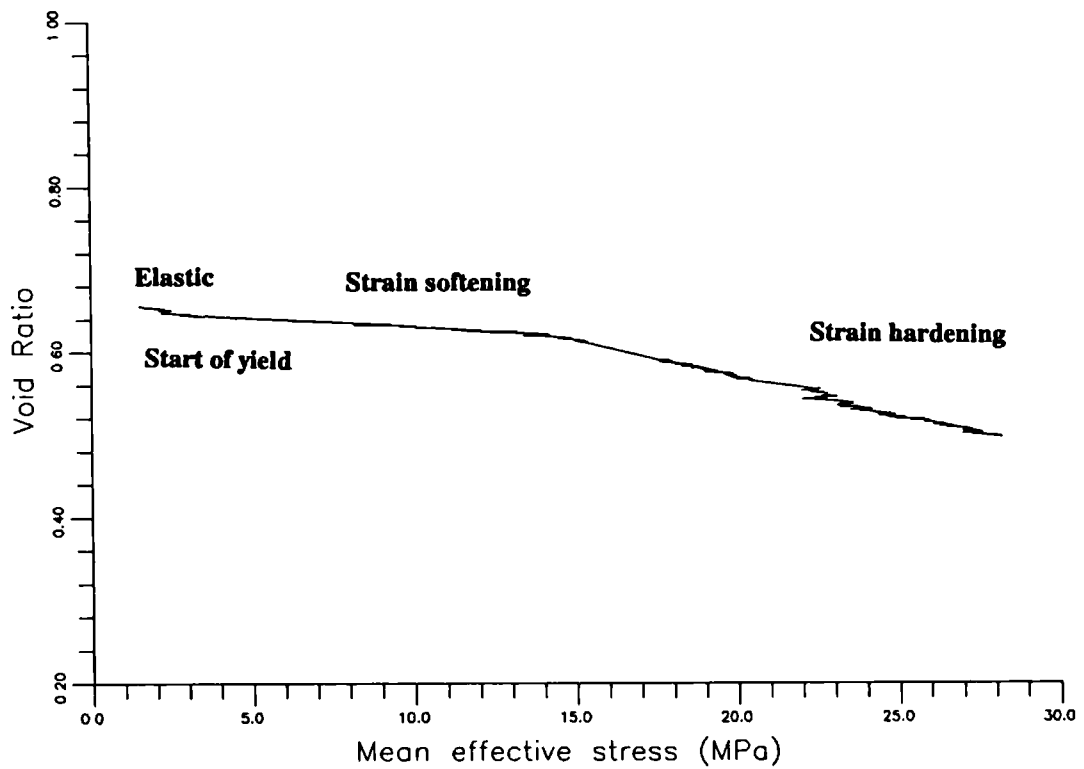


Figure. 4.24. Graph of void ratio/mean effective stress for slow strain-rate experiment ELONGC2.

4.4.2.3. *ELONGC3.*

This experiment had a duration of approximately 700 hours and an initial rate of strain of $1.1 \cdot 10^{-8} \text{ sec}^{-1}$ (the same as *ELONGC2*). Figure 4.25 indicates that the sample yielded at 10MPa and this is confirmed by the data in figure 4.26 (effective stress ratio plot). The apparatus failed (leading to the termination of the experiment) shortly after the start of strain hardening. The stress path diagram (figure 4.27) and the void ratio/mean effective stress plot (figure 4.28) also indicate the onset of strain hardening towards the end of the experiment.

4.4.2.4. *ELONGC4.*

This experiment also lasted for approximately 700 hours, but was conducted at a faster initial rate of strain ($4.2 \cdot 10^{-8} \text{ sec}^{-1}$). The K_0 part of the experiment was terminated by the application of undrained shear. In both figure 4.29 (vertical effective stress/axial strain) and 4.30 (effective stress ratio plot), yield is observed to be a gradual process that was initiated at a vertical effective stress of approximately 15MPa. Following yield, the sample started to strain hardening. During undrained shear, the sample was observed to strain soften (figure 4.31). Figure 4.32 (void ratio/mean effective stress) indicates that although the sample began to yield at a mean effective stress of less than 10MPa, the volume of the sample did not start to decrease significantly until the mean effective stress had increased to approximately 20MPa.

4.4.3. Discussion.

The experiments reported above were performed to evaluate the effect of reducing the rate of strain on the magnitudes of the deformations developed in samples of North Sea chalk subject to K_0 compaction. As the samples were taken from different cores and exhibit different initial porosities, the experimental results are not directly comparable. Each result therefore, will have to be compared with data from experiments conducted on similar samples. These comparative data are presented in figures 4.33 to 4.36. Only *ELONGC3* shows any significant weakening when compared to the results obtained from samples with similar initial porosities. The other three slow rate of strain results fall within the scatter of previous experiments and show no clear evidence of a strain

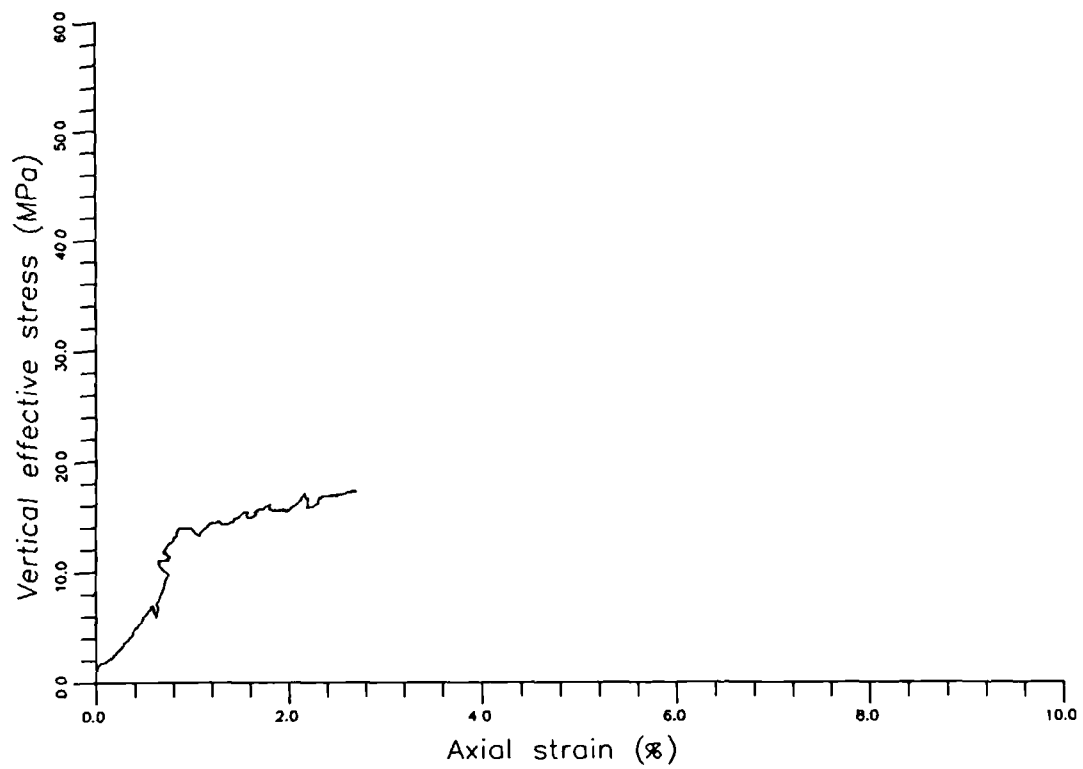


Figure. 4.25. Graph of vertical effective stress/axial strain for slow strain-rate experiment ELONGC3.

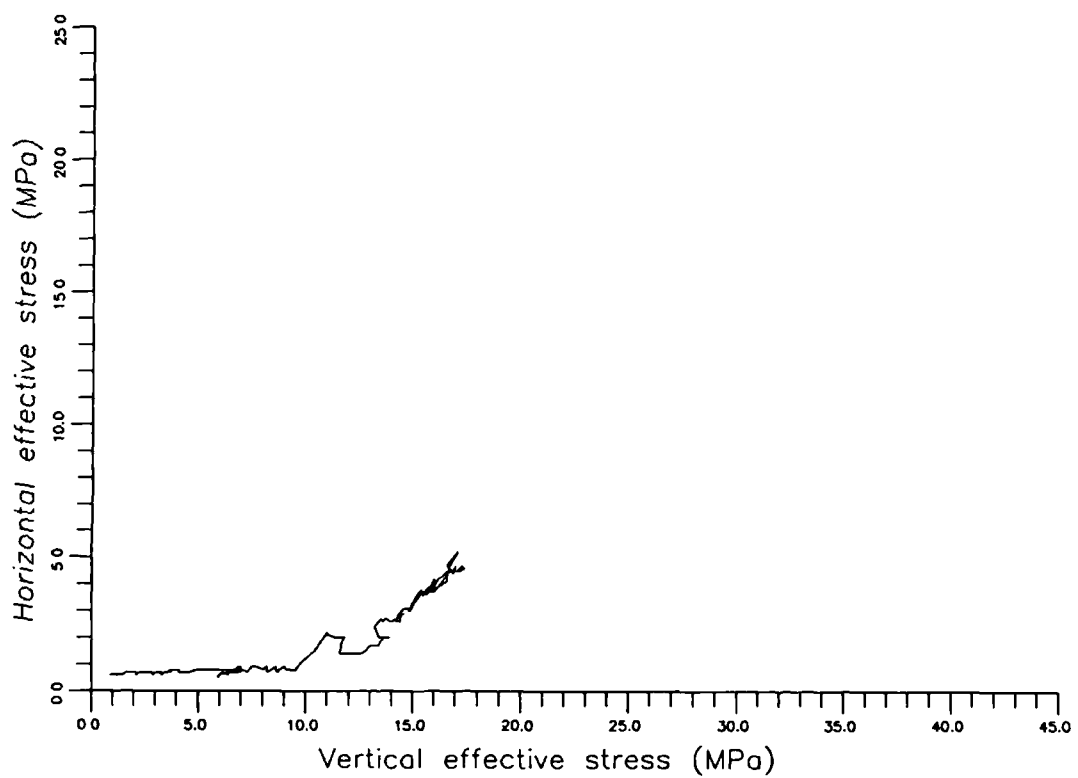


Figure. 4.26. Graph of horizontal effective stress/vertical slow strain-rate effective stress for experiment ELONGC3.

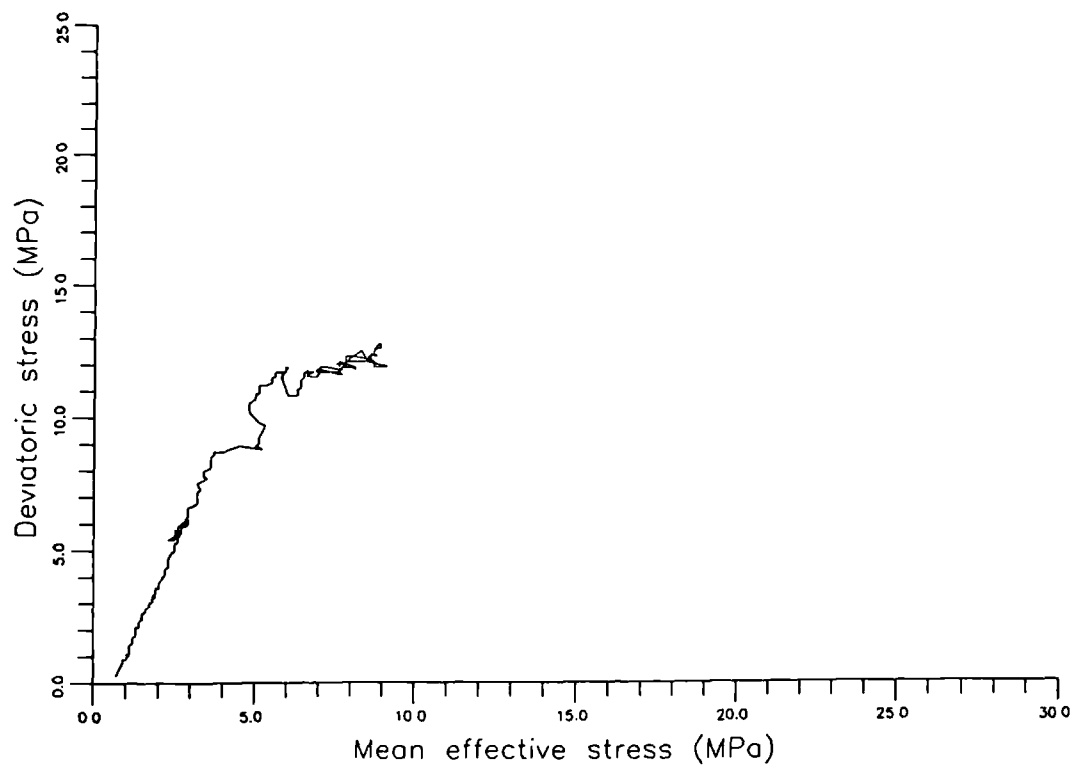


Figure. 4.27. Graph of deviatoric stress/mean effective stress for slow strain-rate experiment ELONGC3.

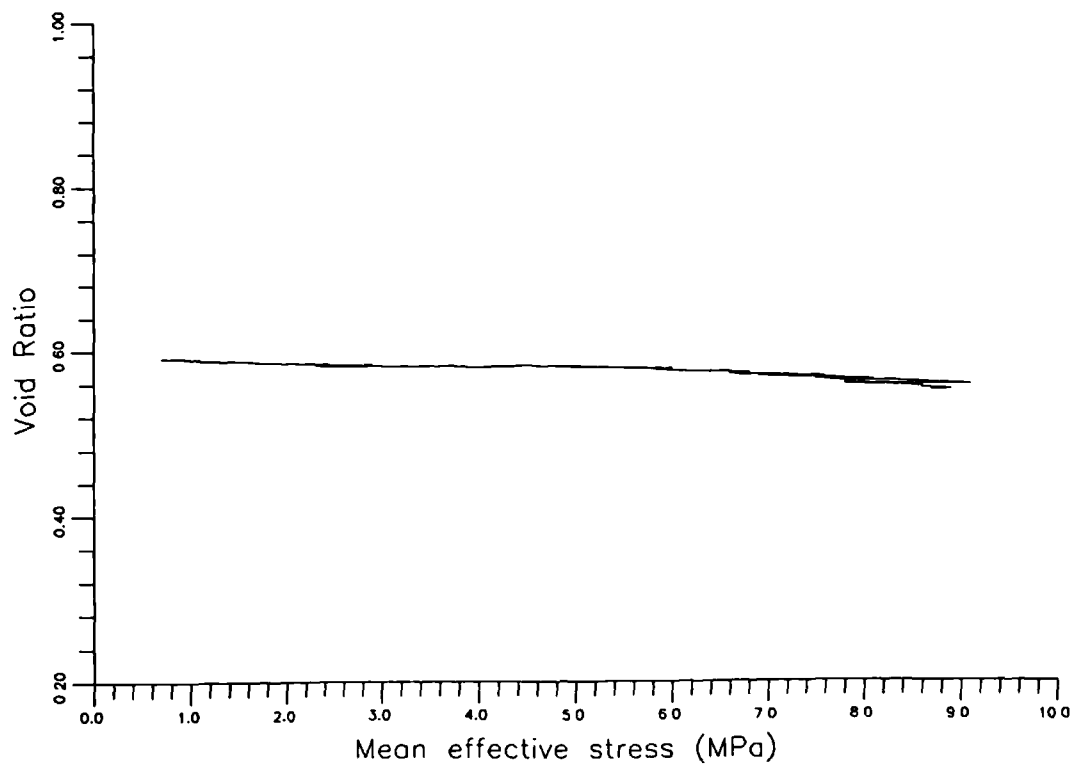


Figure. 4.28. Graph of void ratio/mean effective stress for slow strain-rate experiment ELONGC3.

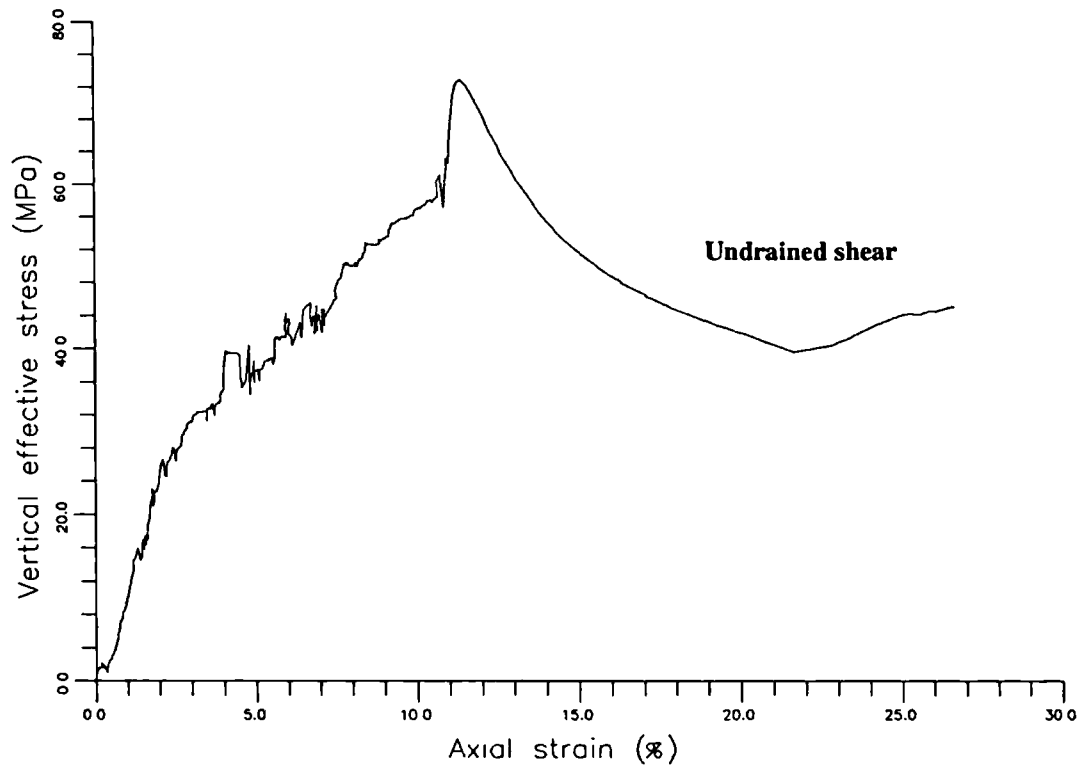


Figure. 4.29. Graph of vertical effective stress/axial strain for slow strain-rate experiment ELONGC4.

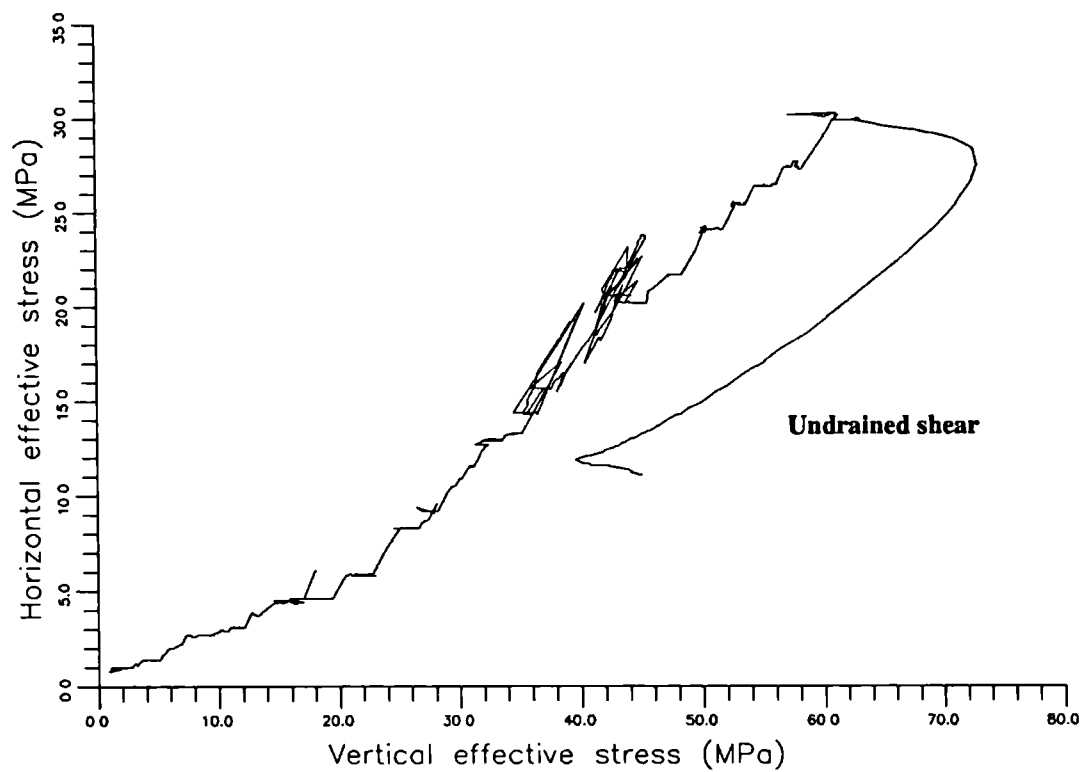


Figure. 4.30. Graph of horizontal effective stress/vertical effective stress for slow strain-rate experiment ELONGC4.

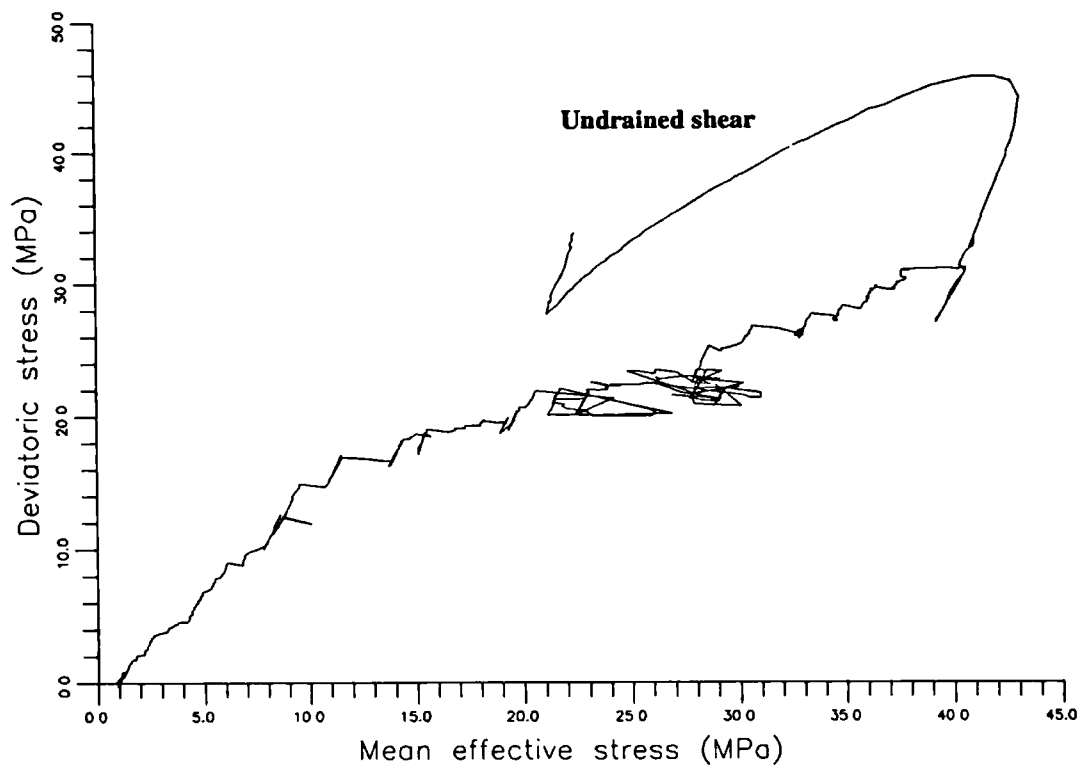


Figure. 4.31. Graph of deviatoric stress/mean effective stress for slow strain-rate experiment ELONGC4.

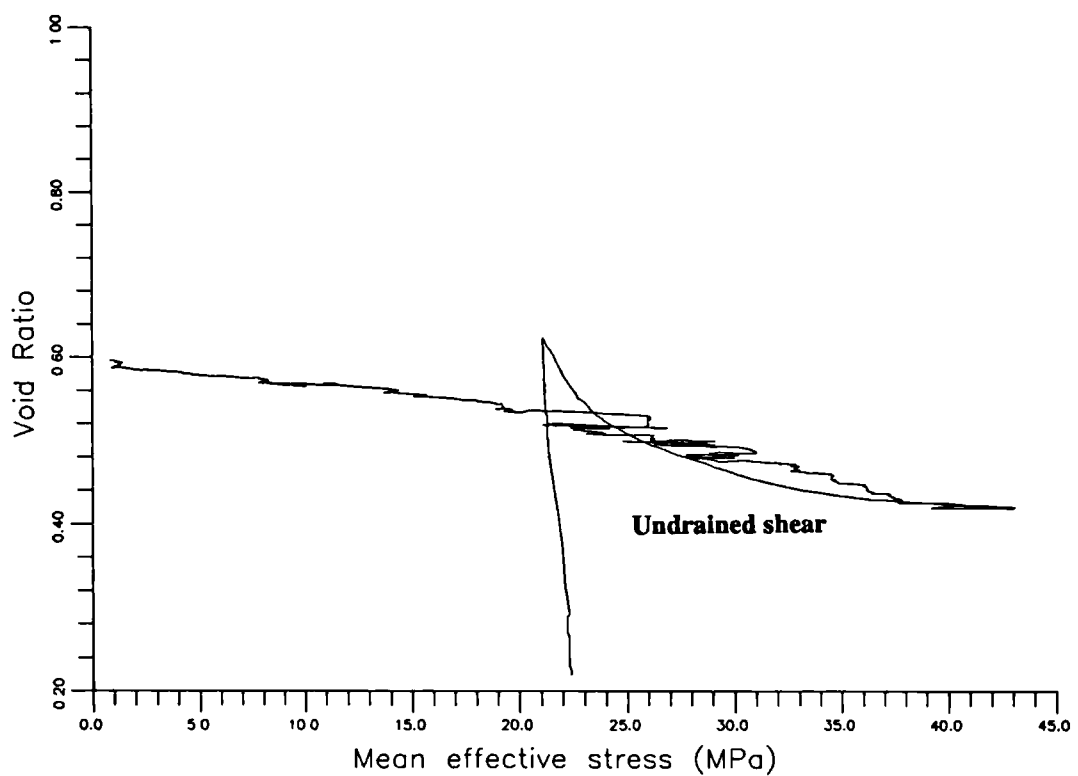


Figure. 4.32. Graph of void ratio/mean effective stress for slow strain-rate experiment ELONGC4.

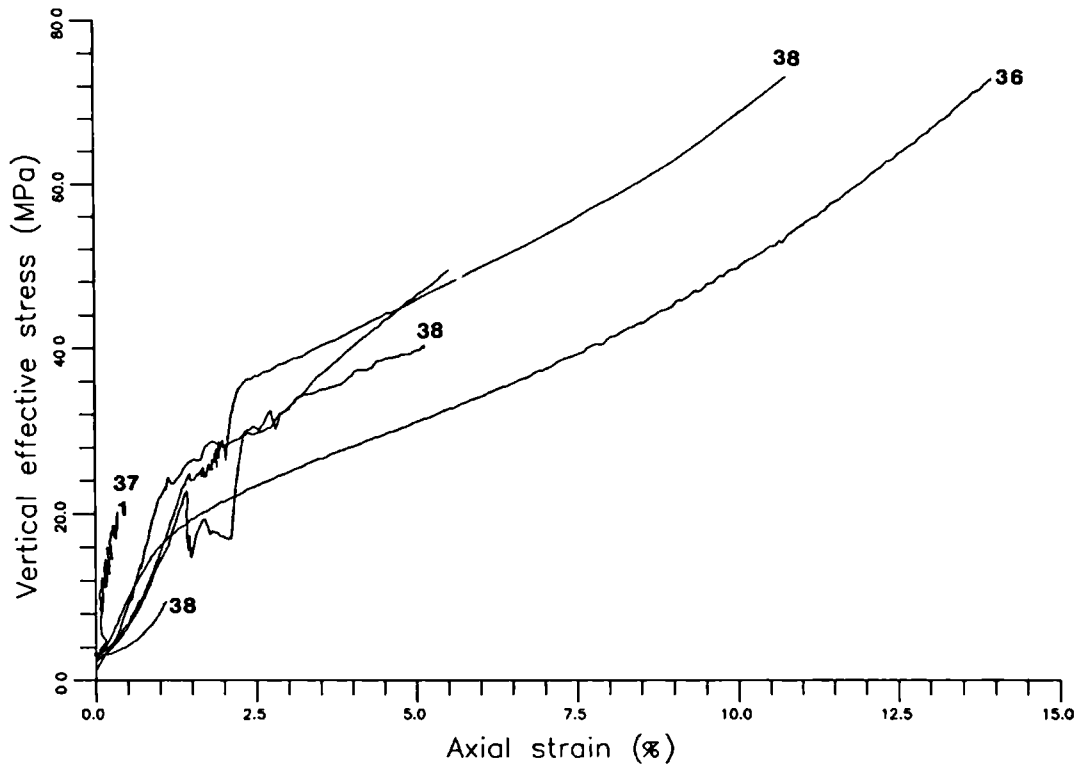


Figure. 4.33. Graph of vertical effective stress/axial strain which compares the result of slow strain-rate experiment ELONGC1 with samples of equivalent initial porosities.

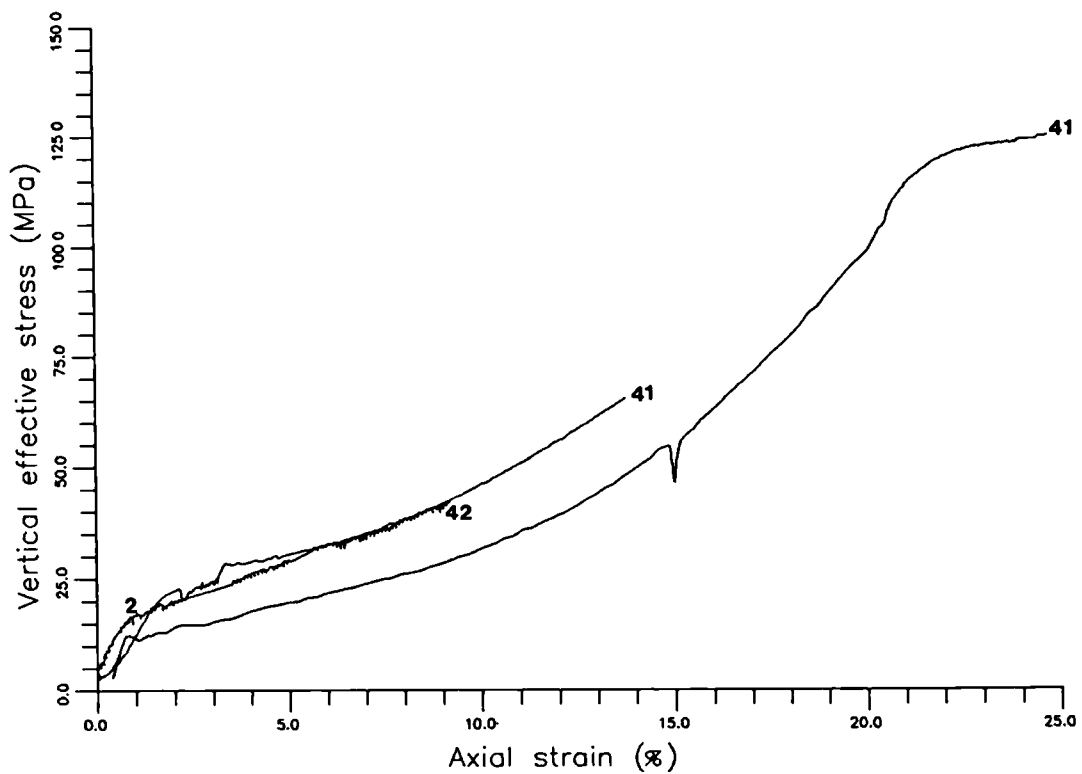


Figure. 4.34. Graph of vertical effective stress/axial strain which compares the result of slow strain-rate experiment ELONGC2 with samples of equivalent initial porosities.

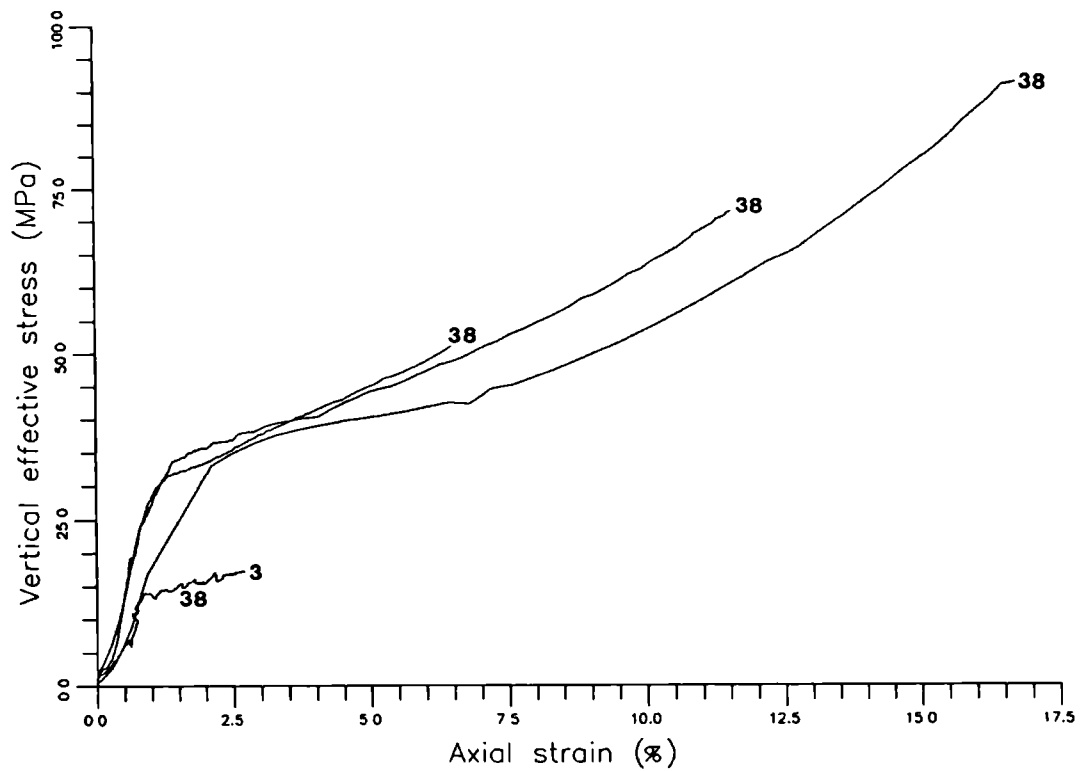


Figure. 4.35. Graph of vertical effective stress/axial strain which compares the result of slow strain-rate experiment ELONGC3 with samples of equivalent initial porosities.

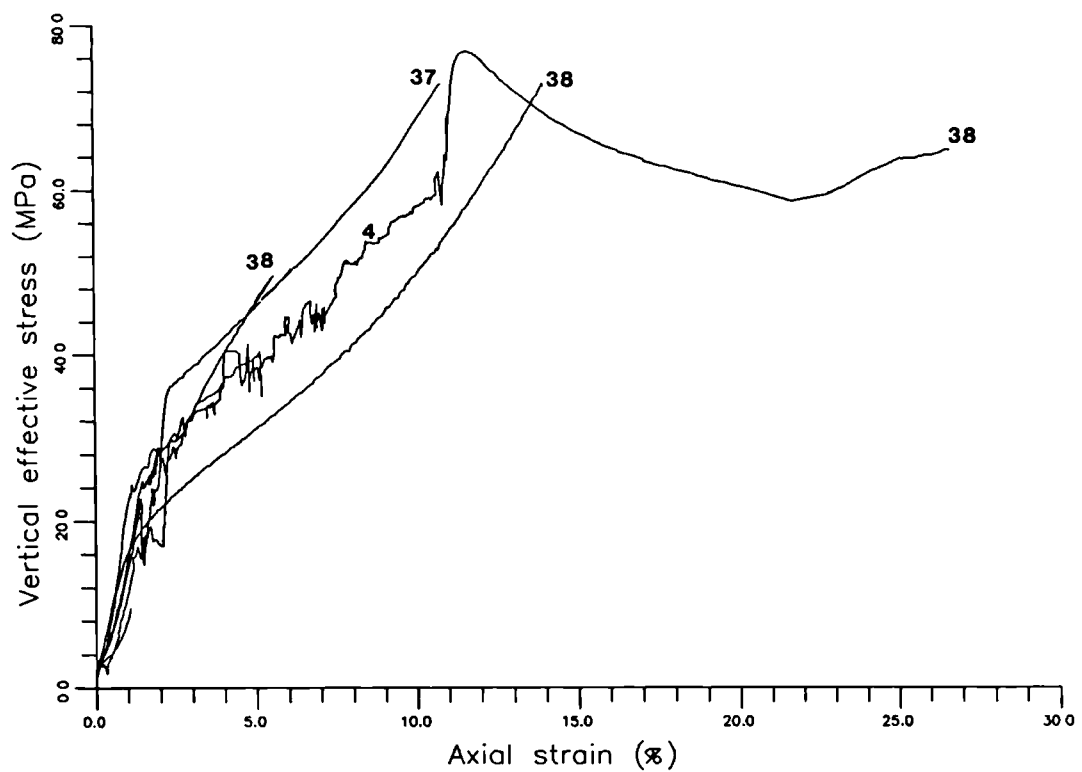


Figure. 4.36. Graph of vertical effective stress/axial strain which compares the result of slow strain-rate experiment ELONGC4 with samples of equivalent initial porosities.

rate effect. It would therefore appear that even by conducting these experiments at significantly slower strain-rates, determining the magnitude of secondary consolidation is extremely difficult when different samples are used. Unfortunately, the proposal by Addis (1987) to extend this type of experiment into shorter term tests is not entirely practical. If strain rates significantly faster than those already employed are used, the low permeability of the chalk will result in the generation of excess pore fluid pressures (which will restrict the primary consolidation of the samples). The results presented above would appear to confirm that the only way to determine whether the deformation of the chalk is influenced by rate of strain, is to use a method similar to that employed by Addis (1987) based on that of Leroueil et al. (1985) (Skinner pers. comm., 1989).

It is also important to note that the data reported above show similar characteristics to those presented in section 4.2. This indicates that the onset of significant changes in pore volume coinciding with the end of yield is not a product of the strain rates used in the majority of the experiments reported in this chapter and chapter five. Further discussion of this aspect of the deformational behaviour may be found in section 4.7.

4.5. STRESS RELAXATION EXPERIMENTS.

4.5.1. Introduction.

Five of the uniaxial strain experiments undertaken as part of this study were allowed to 'relax' during testing. These five experiments (see table 4.1 for details) represent two samples cut from a block of Stevn's Klint outcrop chalk and three samples taken from North Sea core material (two samples from the Hod Formation and one from the Tor Formation).

These experiments were designed to determine whether, by allowing the samples to relax for a period of time, the process of relaxation would lead to a change in the form of the deformation curves. If secondary consolidation was inhibited by the speed at

which the majority of the uniaxial strain experiments were conducted during the present study, relaxation, with full drainage would enable this process to operate and the deformation curve should reflect the additional strain.

During relaxation, ram displacement was stopped, the cell pressure was held constant at the pressure required to maintain the K_0 condition prior to the cessation of loading and the sample was allowed to strain laterally. Following a period of relaxation, the sample was reloaded vertically until the radial strain measurement returned to the pretest (zero) value without altering the confining pressure (except in VOHC2). Once the original value of radial strain had been attained, the K_0 experiment continued.

4.5.2. Experimental results.

The results of the stress relaxation experiments are presented in four sub-sections (with respect to four sets of axes) in order to allow comparisons to be made.

4.5.2.1. Vertical effective stress/axial strain.

Each period of relaxation is represented by a break in the vertical stress/axial strain curves (figures 4.37-4.41). Although active vertical displacement was stopped during the process of relaxation, these figures indicate that axial strain continued. It is observed that once loading was restarted and the radial strain value had returned to the original 'zero' value, each axial stress/strain curve continued on its original trend although there is an offset of that trend either side of the section representing relaxation (figure 4.37-4.41). This offset is similar to those recorded by Addis (1987) during his strain rate experiments and indicates that each sample has been subject to increased secondary consolidation during the process of relaxation. During the K_0 part of each experiment, these curves indicate typical behaviour for low silica chalks with similar initial porosities.

Plates 4.1 to 4.3 show scanning electron micrographs of parts of samples VOBC5 and VOBC7 after testing. The axial stress/strain curves record that both samples (which were 'soft' Stevn's Klint chalk) were subject to 25% axial strain. However, plates 4.1 to

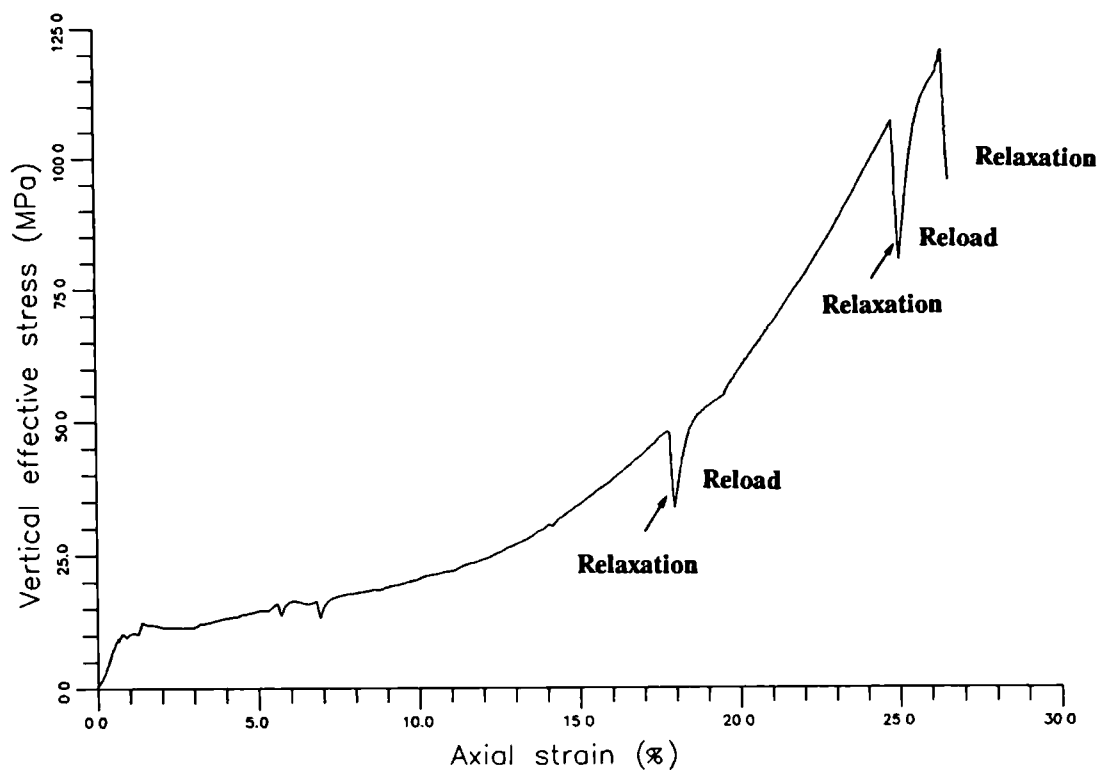


Figure. 437. Graph of vertical effective stress/axial strain for stress relaxation experiment VOBC5.

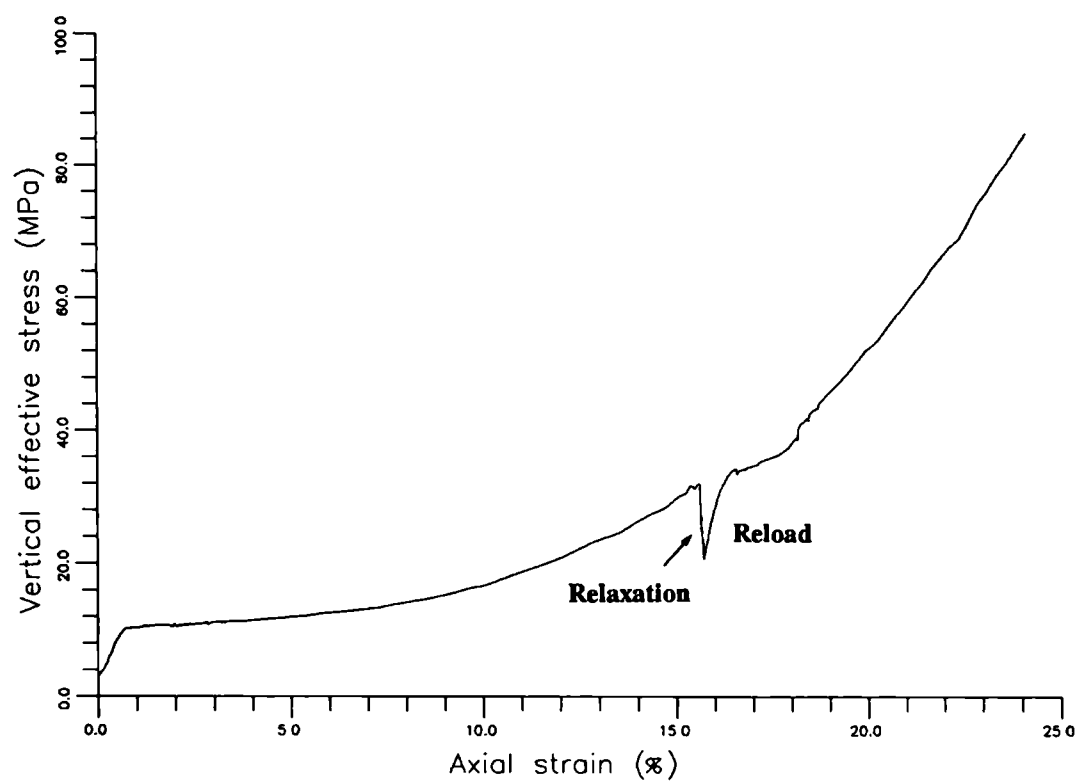


Figure. 438. Graph of vertical effective stress/axial strain for stress relaxation experiment VOBC7.

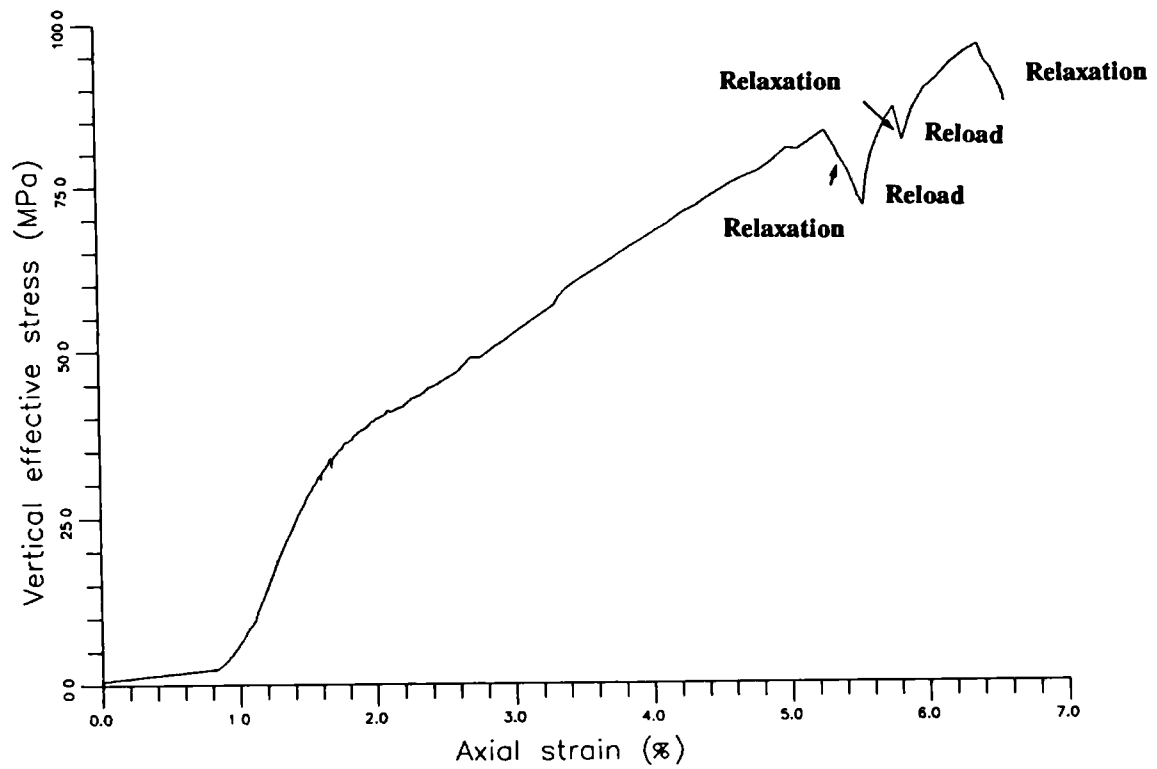


Figure. 4.39. Graph of vertical effective stress/axial strain for stress relaxation experiment VOHC2.

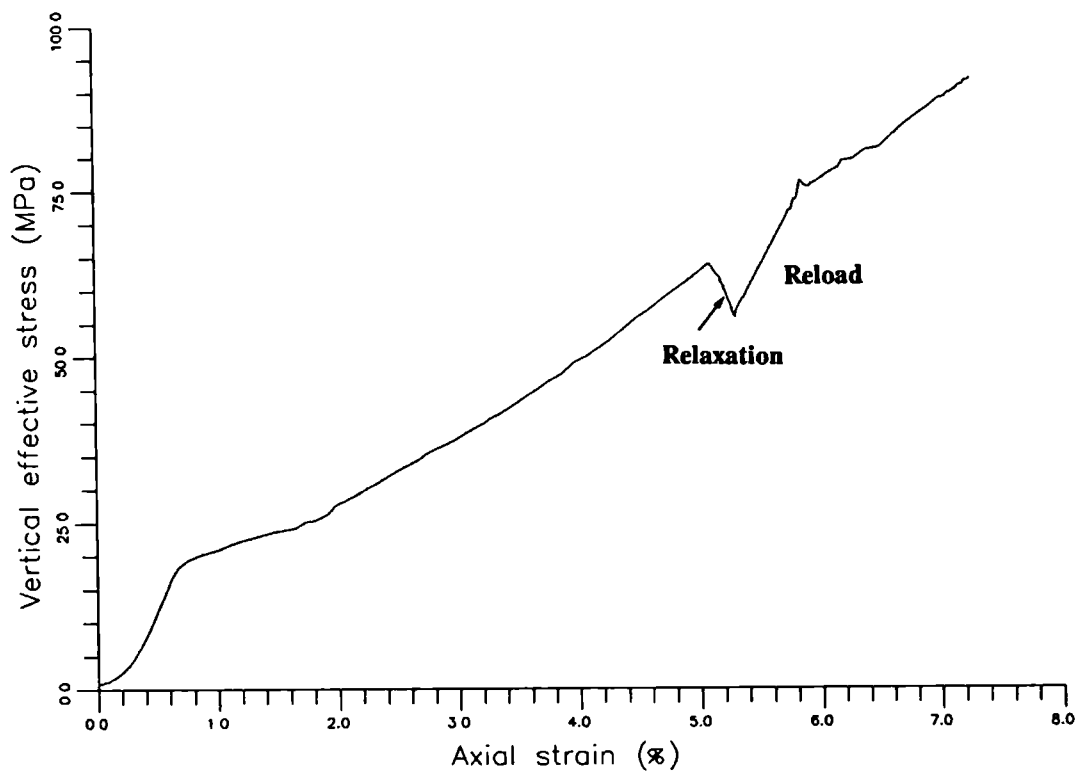


Figure. 4.40. Graph of vertical effective stress/axial strain for stress relaxation experiment VOHC3.

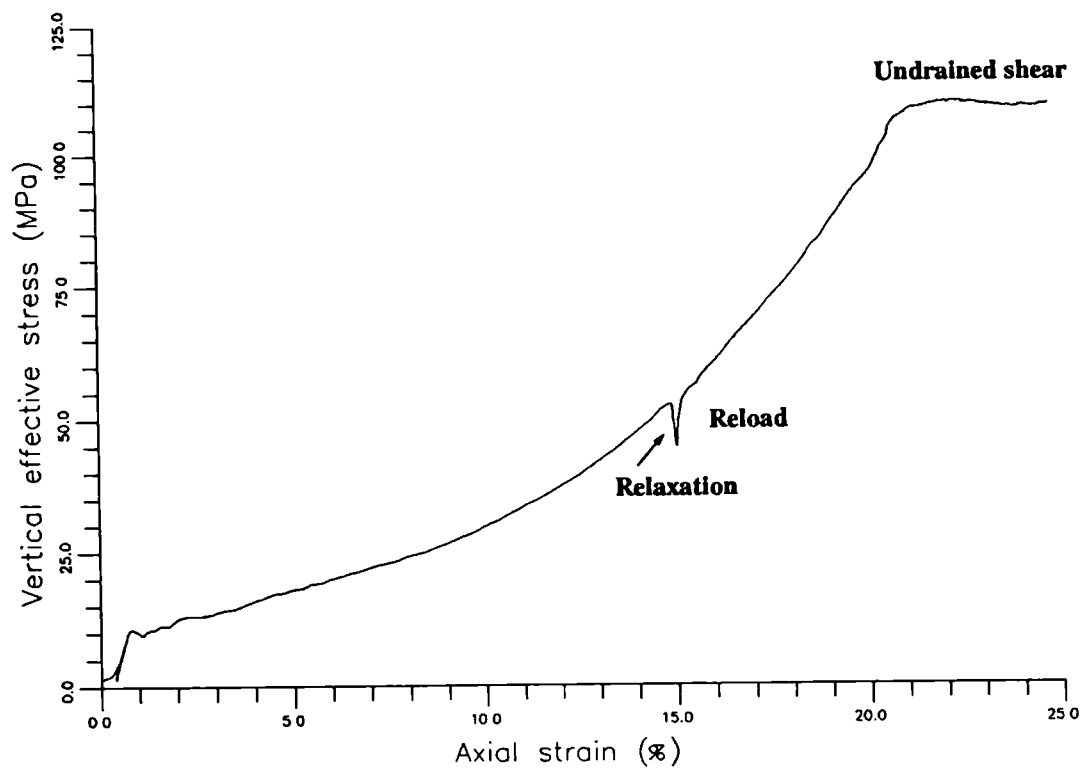


Figure. 4.41. Graph of vertical effective stress/axial strain for stress relaxation experiment VOTC1.

4.3 indicate that even though this deformation resulted in a loss of half of the original sample porosity (figures 4.52 and 4.53) large pore spaces still exist. It may also be observed that the chalk still contained apparently undamaged coccoliths. The experiment conducted on sample VOTC1 was terminated by loading under conditions of undrained shear (see chapter six for an explanation of this type of experiment).

4.5.2.2. Horizontal and vertical effective stress.

Figures 4.42 to 4.46 present plots of changes in horizontal and vertical effective stress during each experiment. Problems were encountered with the lower porosity Hod Formation samples (figures 4.44 and 4.45). Although both experiments were conducted at substantially slower displacement rates (0.008 and 0.005mm/min respectively) than that used for the other samples in this series of tests (0.02mm/min), significant excess pore pressures were generated. These pore pressures were gradually dissipated as the samples relaxed, hence, although the confining pressure remained constant during this process, the horizontal effective stress was observed to increase. Pore pressure generation was insignificant in the other samples. This is reflected by a lack of change in the horizontal effective stress during relaxation.

Reloading of the samples to regain the original zero radial strain condition required a larger vertical effective stress than the maximum value achieved before relaxation. This increase in load reflects the increase in strength achieved by the sample whilst it continued to strain during the period of relaxation and initial reloading. Although the radial strain then returned to its original value, these plots indicate that the ratio between the two effective stresses had changed.

The effective stresses did not return to their pre-relaxation ratio until after the K_0 test had restarted (this re-equilibration is reflected by the curvature in the reloading sections of the stress/strain curves).

4.5.2.3. Deviatoric/mean effective stress.

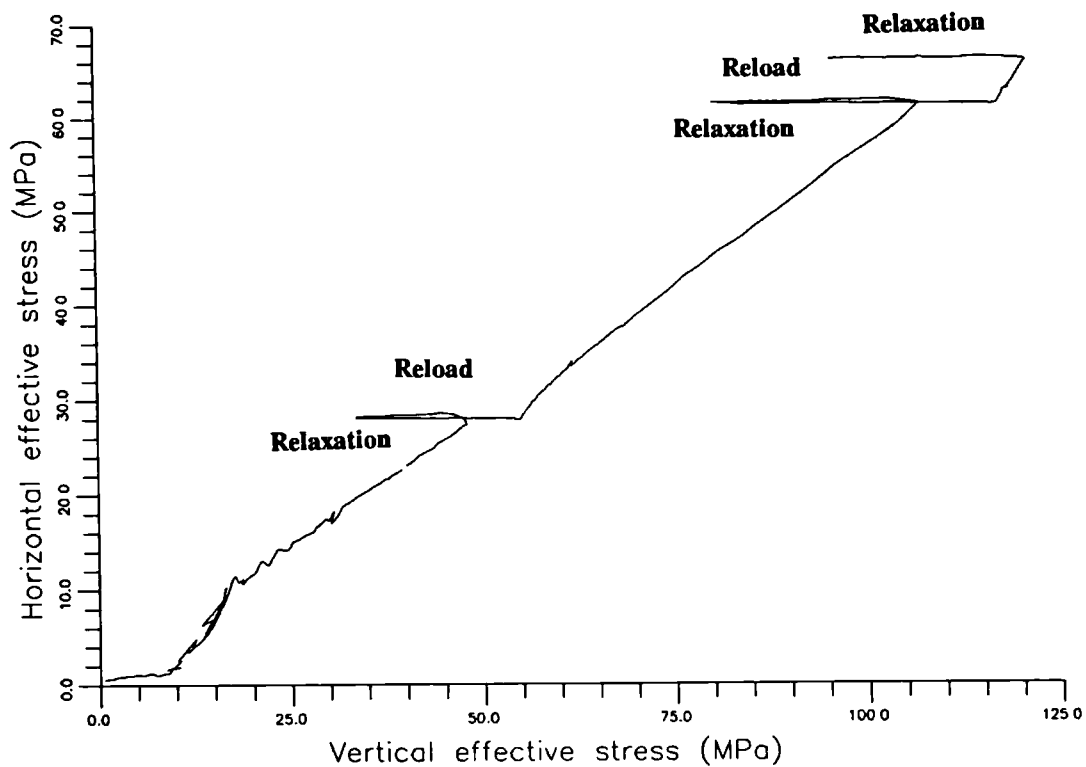


Figure. 4.42. Graph of horizontal effective stress/vertical effective stress for stress relaxation experiment VOB5.

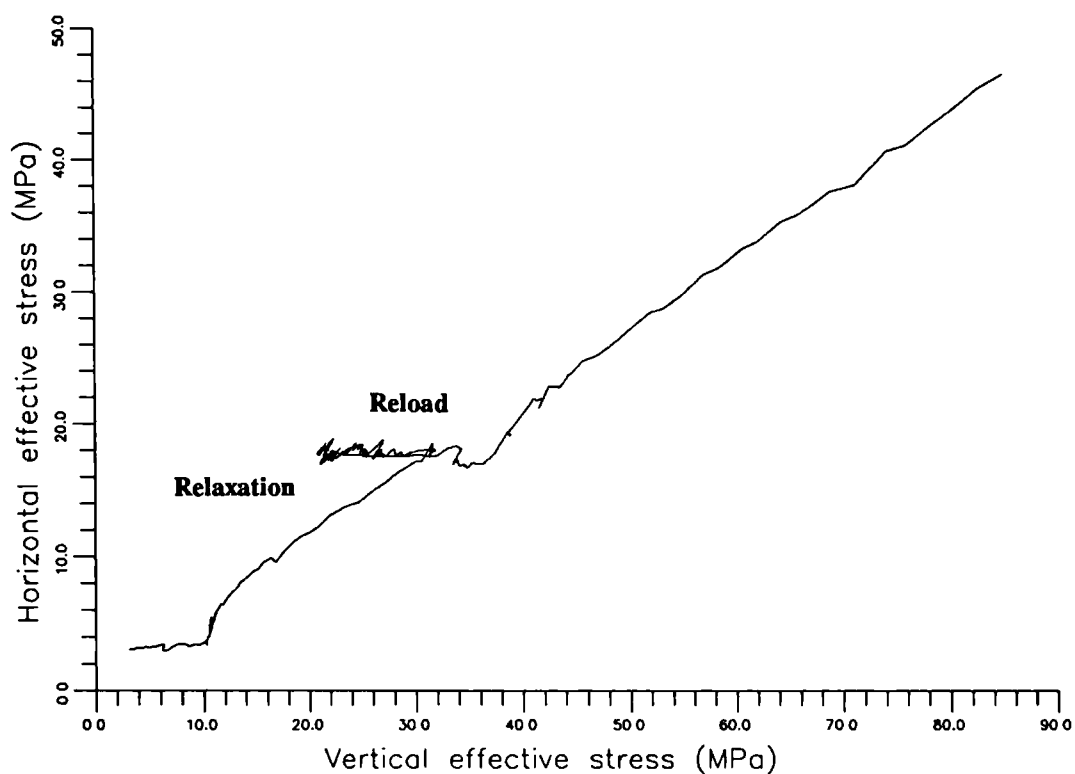


Figure. 4.43. Graph of horizontal effective stress/vertical effective stress for stress relaxation experiment VOB7.

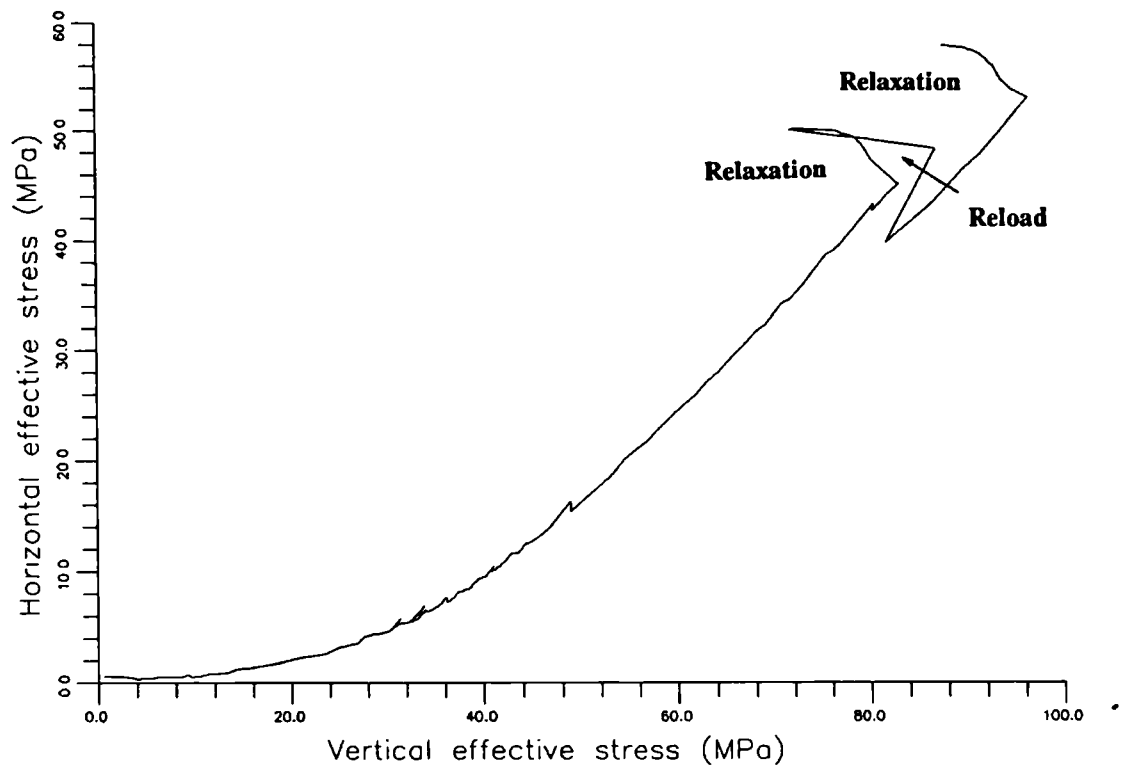


Figure. 4.44. Graph of horizontal effective stress/vertical effective stress for stress relaxation experiment VOHC2.

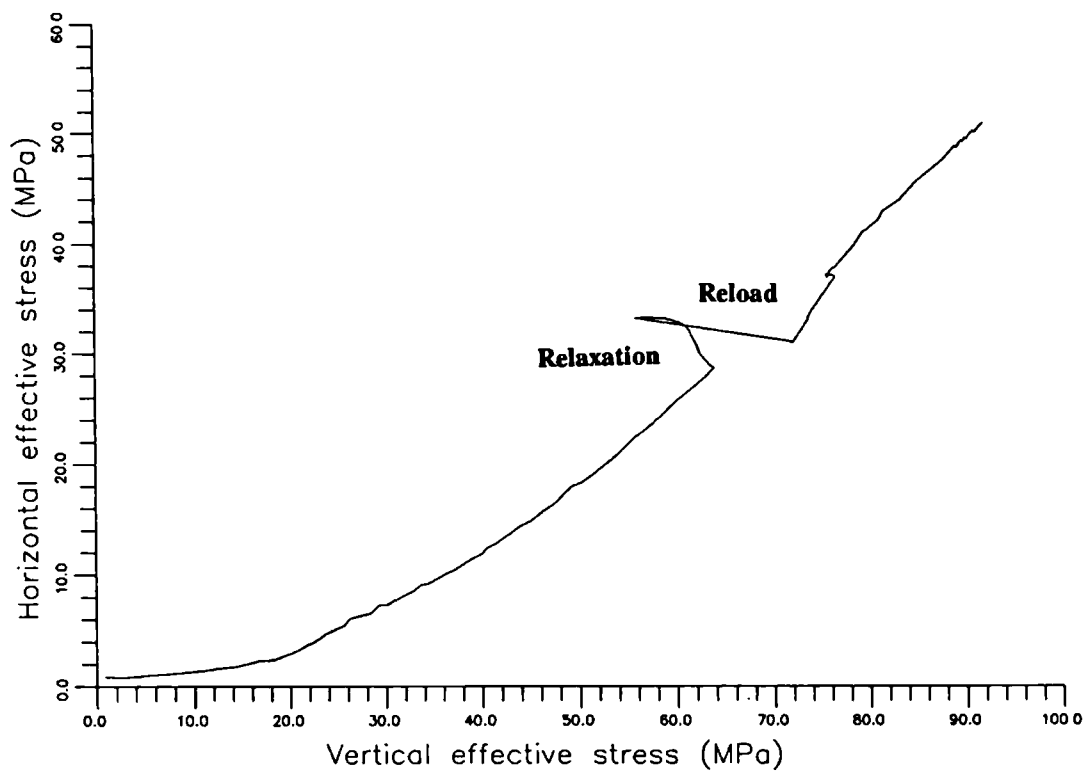


Figure. 4.45. Graph of horizontal effective stress/vertical effective stress for stress relaxation experiment VOHC3.

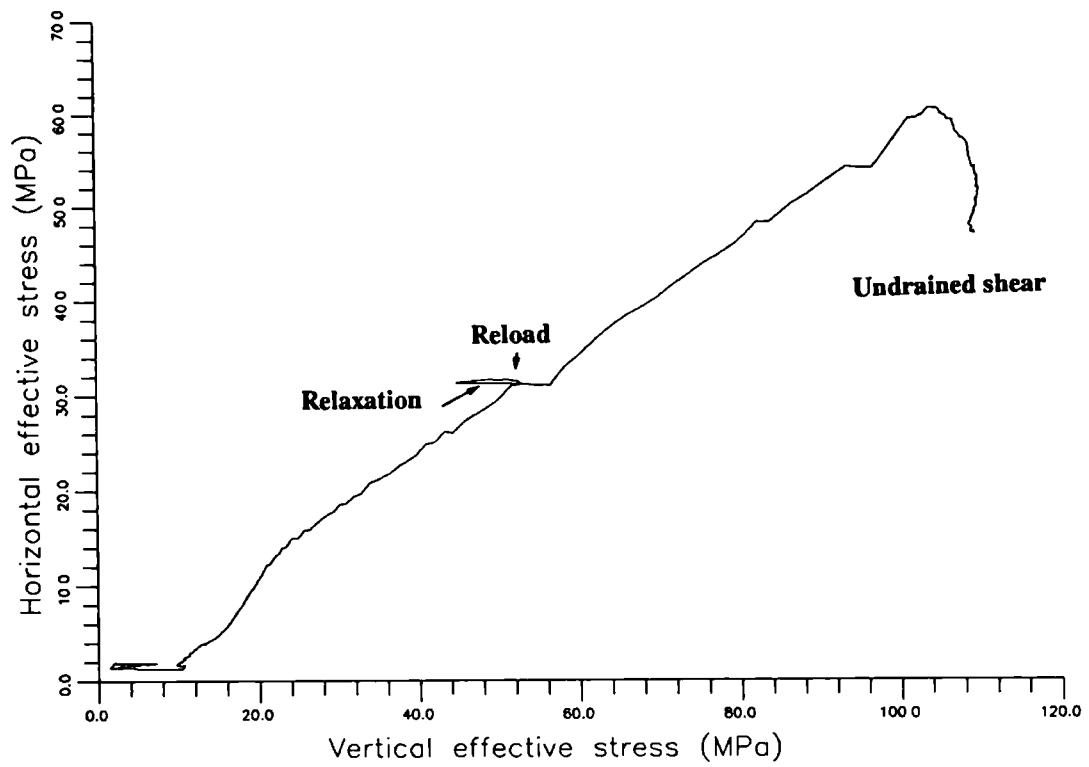


Figure. 4.46. Graph of horizontal effective stress/vertical effective stress for stress relaxation experiment VOTC1.

The changes in the deviatoric/mean effective stress plots (figures 4.47 to 4.51) reflect those changes already discussed above. The inclinations of the unloading/reloading paths in each of the higher porosity sample (figures 4.47, 4.48 and 4.51) are observed to be at the same angle (71.5°) as the elastic sections of their stress paths. The equivalent paths for the two lower porosity samples (figures 4.49 and 4.50) have a greater inclination (77.3°) than the elastic sections of their stress paths.

Carter et al. (1988) noted that the slope of the unloading/reload loops in experiments conducted on weakly cemented carbonates recovered from the North Rankin 'A' site in Australia (see chapter six for details) did not change either side of the preconsolidation pressure. He also noted that all of the loops were parallel to each other. He says 'it is surprising [the consistent angle] since it is natural to assume that some of the stiffness was due to cementation which would have been destroyed on reaching the preconsolidation pressure. It is therefore more likely that the stiffness is due more to the interlocking of the grains than to cementation and so it is not affected by the breakdown'.

A similar grain interlocking behaviour may account for the parallel nature of the unloading/reloading trends observed in figures 4.47, 4.48 and 4.51 during which unloading/reloading was initiated after the samples had yielded and were in the process of strain hardening. Under these conditions the cemented structure of the samples is normally considered to have been destroyed. If complete destruction of the cement bonding is achieved during yield, the samples should behave in a similar manner to that of a normally consolidated material. Unloading/reloading was conducted on the harder, lower porosity samples before the process of yield had been completed. The difference in the inclination of the two sets of unloading/ reloading data reflect the existence of the cement bonding in the low porosity samples.

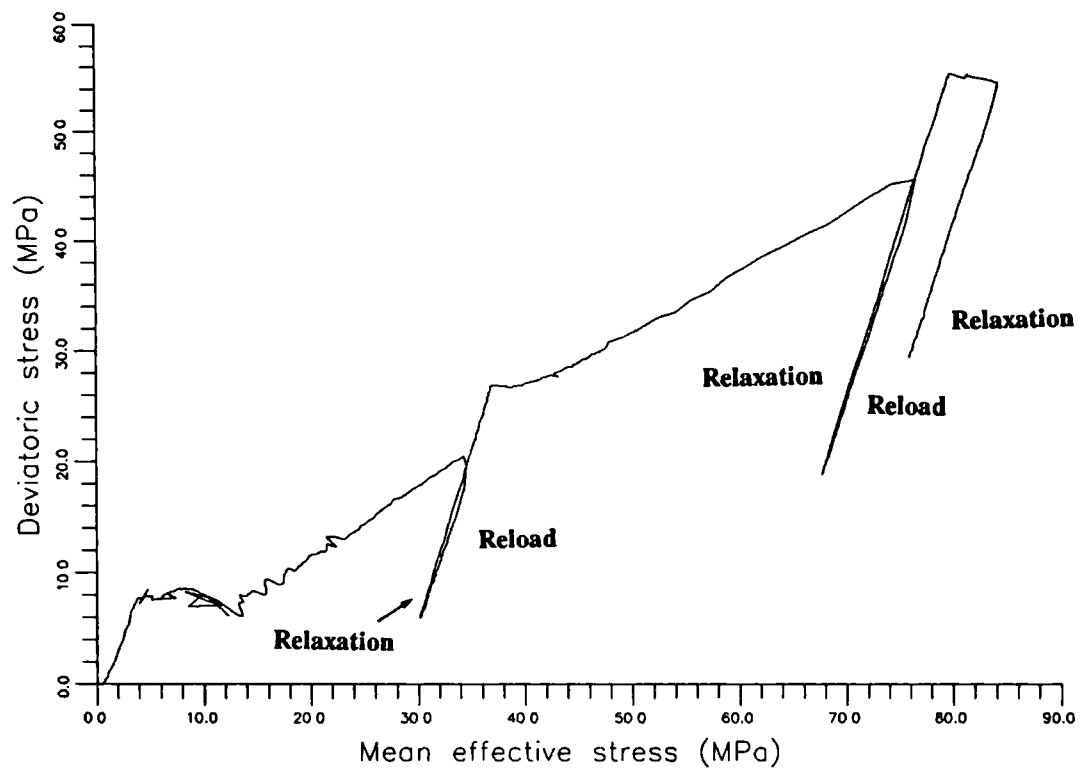


Figure. 4.47. Graph of deviatoric stress/mean effective stress for stress relaxation experiment VOBC5.

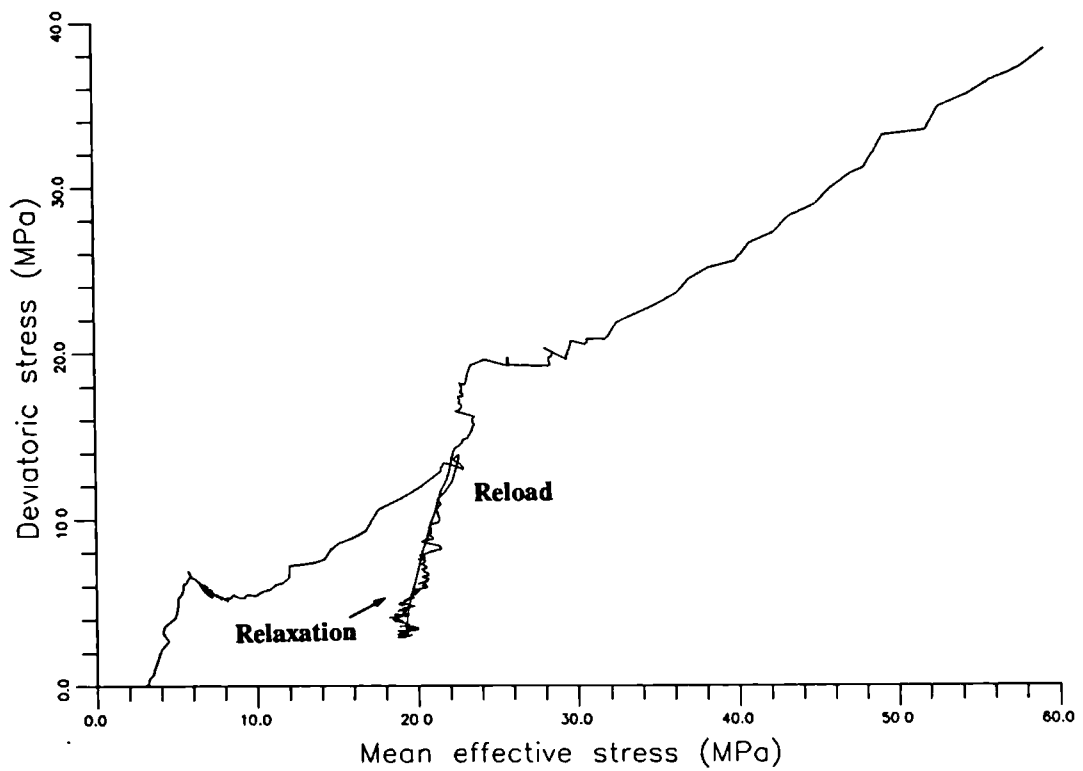


Figure. 4.48. Graph of deviatoric stress/mean effective stress for stress relaxation experiment VOBC7.

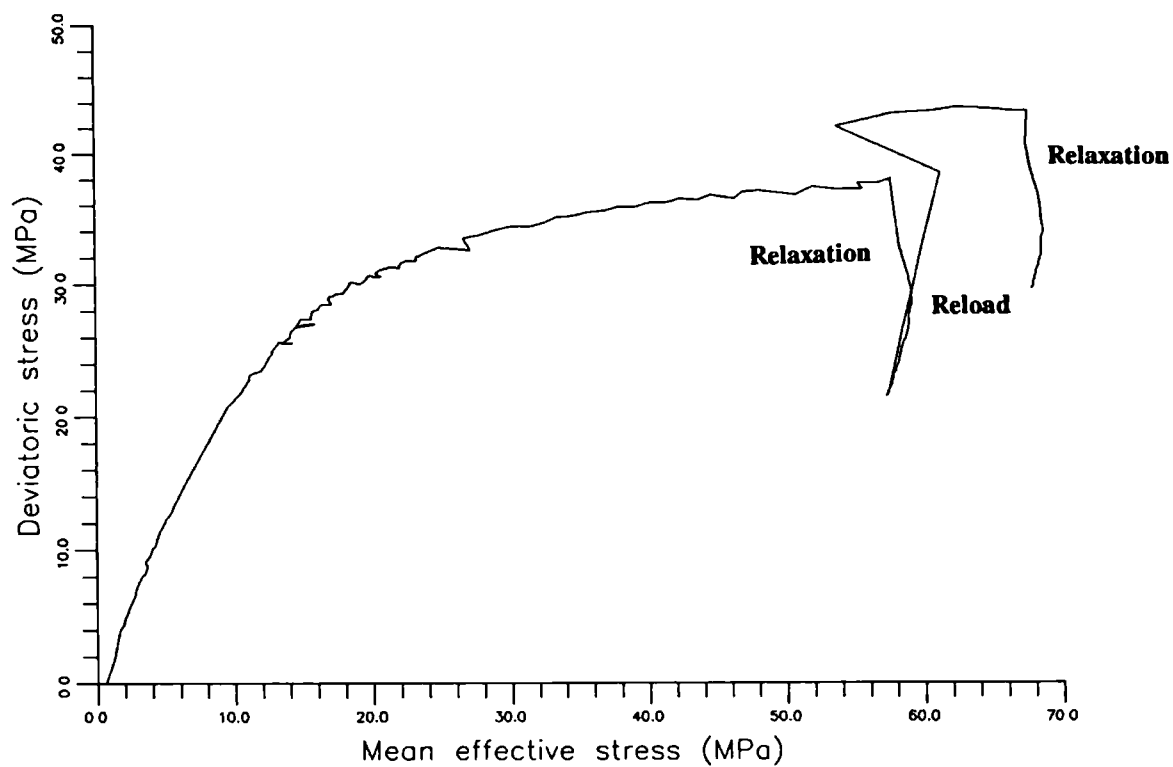


Figure. 4.49. Graph of deviatoric stress/mean effective stress for stress relaxation experiment VOHC2.

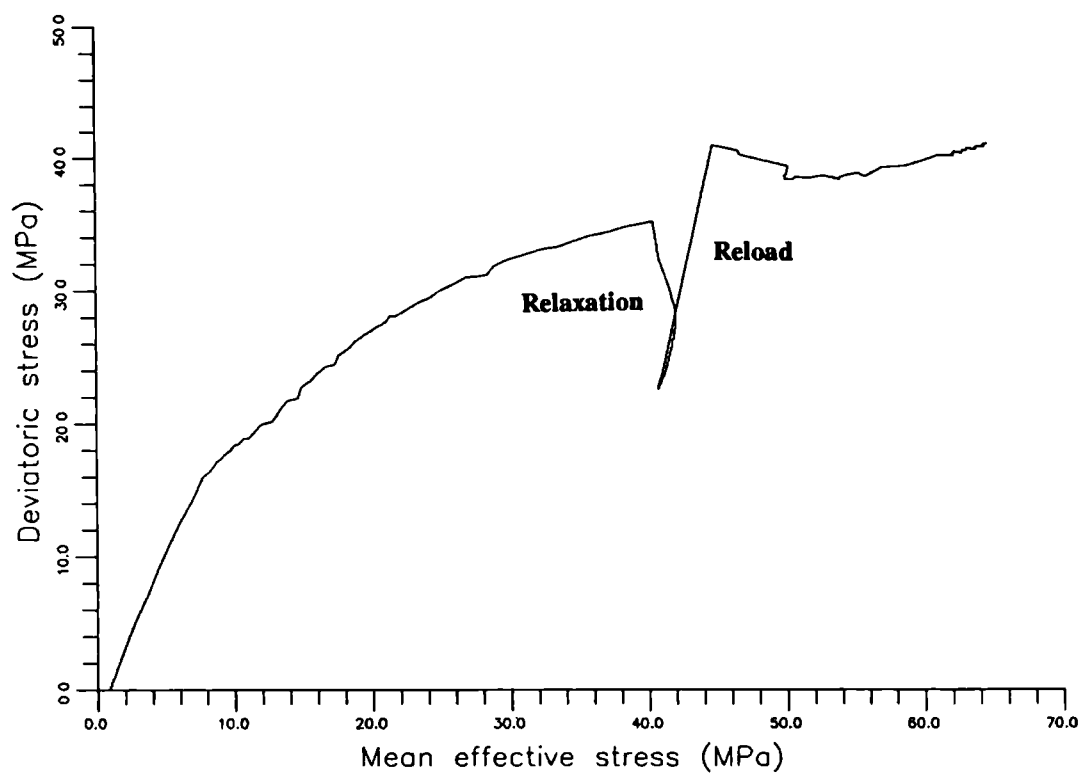


Figure. 4.50. Graph of deviatoric stress/mean effective stress for stress relaxation experiment VOHC3.

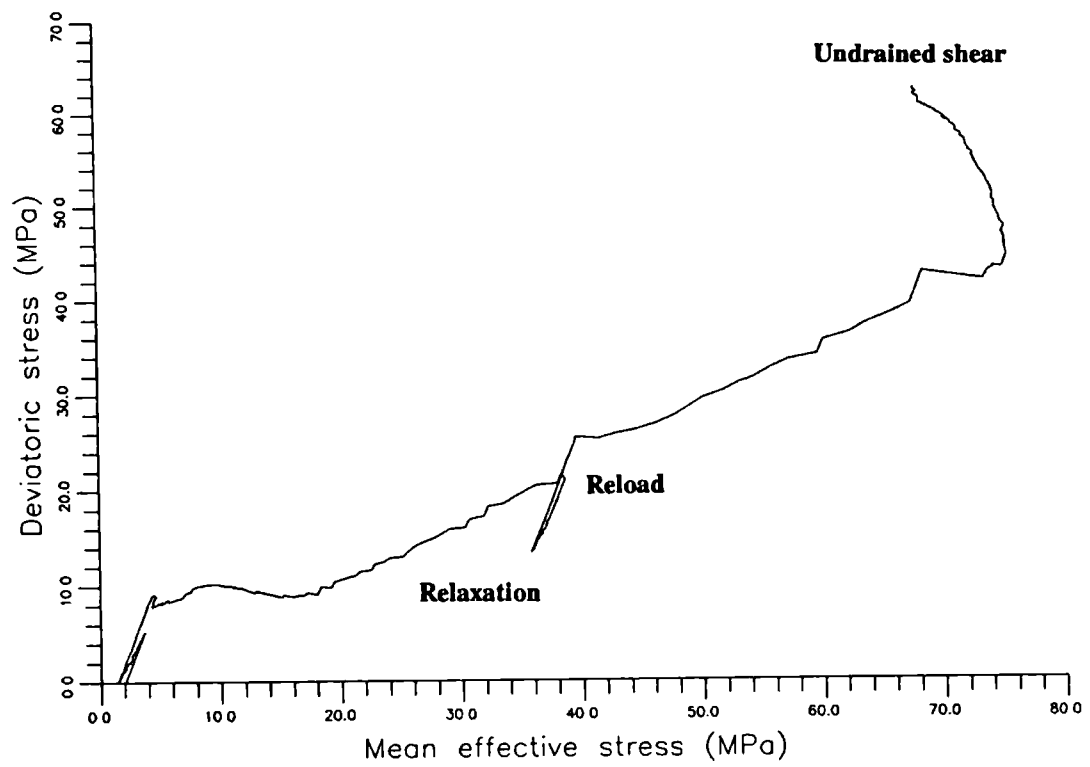


Figure. 4.51. Graph of deviatoric stress/mean effective stress for stress relaxation experiment VOTC1.

4.5.2.4. Void ratio/mean effective stress.

The void ratio/mean effective stress plots (figure 4.52 to 4.56) indicate the volume changes experienced by each sample during uniaxial compaction. The three high porosity outcrop samples (VOBC5, VOBC7 and VOTC1) show significant reductions in porosity (figures 4.52, 4.53 and 4.56). The two low porosity Hod Formation samples (figures 4.54 and 4.55) are observed to be stronger and the reductions in porosity which are a consequence of broadly similar increases in mean effective stress are smaller.

Periods of relaxation are indicated by decreases in mean effective stress. During each experiment, the process of relaxation was accompanied by further reductions in porosity. Decreasing mean effective stress did not result in swelling of the samples. Following a period of relaxation and the recovery of the K_0 condition, each sample is observed to return to a consistent trend in porosity decline resulting from increasing mean effective stress. However these trends are offset, confirming the observations reported for the vertical effective stress/axial strain plots in sub-section 4.5.2.1. During each period of relaxation the samples were able to develop an additional increment of strain that was not recoverable once the K_0 condition was re-established.

4.6. WATER INJECTION EXPERIMENTS.

4.6.1. Introduction.

Three uniaxial experiments were conducted on high porosity North Sea core samples to determine whether the introduction of conditioned sea water during the experiment would affect the mechanical behaviour of the chalk. In each of these experiments, the sea water was introduced into the sample once the vertical effective stress had reached a value of approximately 25MPa. During the flooding process, the displacement rate was slowed down (in a similar manner to that described above) and approximately 10 pore volumes (between 323 and 348cc) of water were allowed to pass through the samples. Each sample was initially saturated with Ekofisk crude oil in the manner described in section 4.3.6.

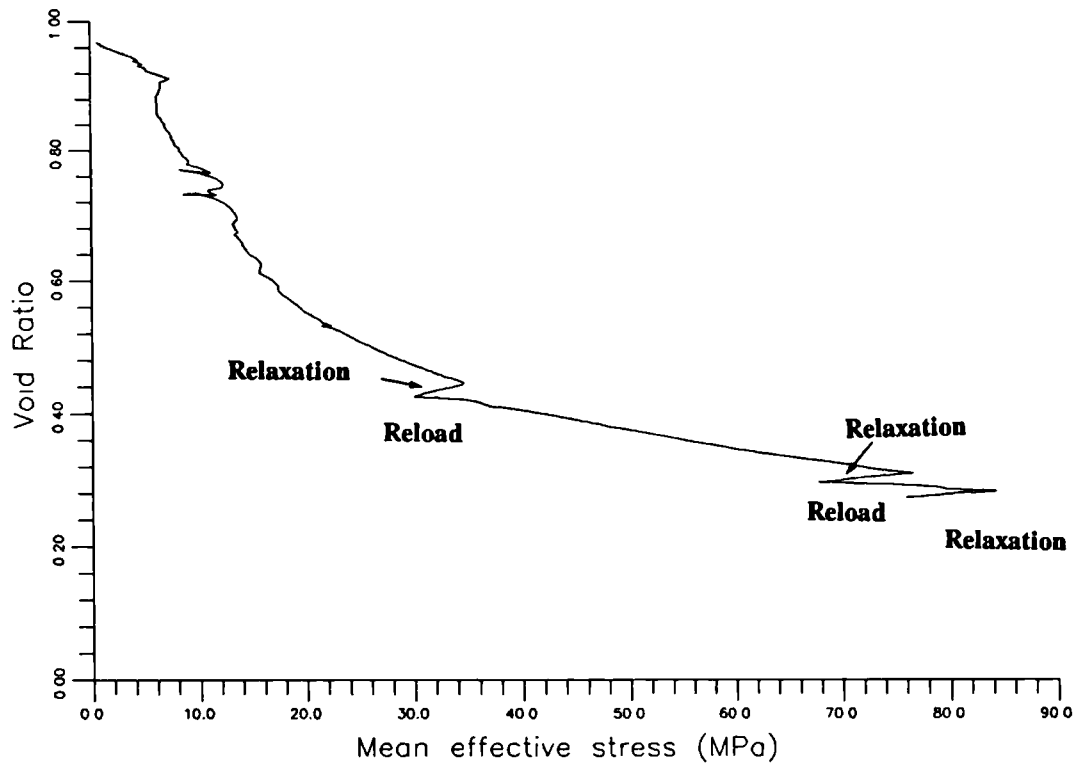


Figure. 4.52. Graph of void ratio/mean effective stress for stress relaxation experiment VOBC5.

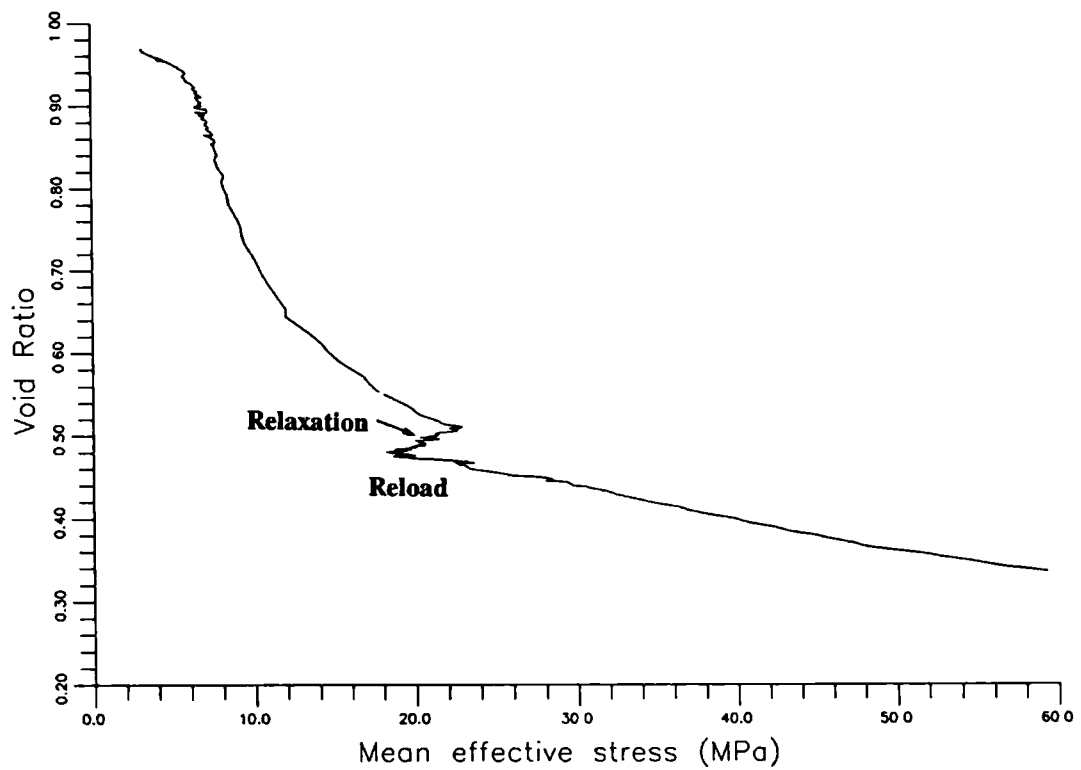


Figure. 4.53. Graph of void ratio/mean effective stress for stress relaxation experiment VOBC7.

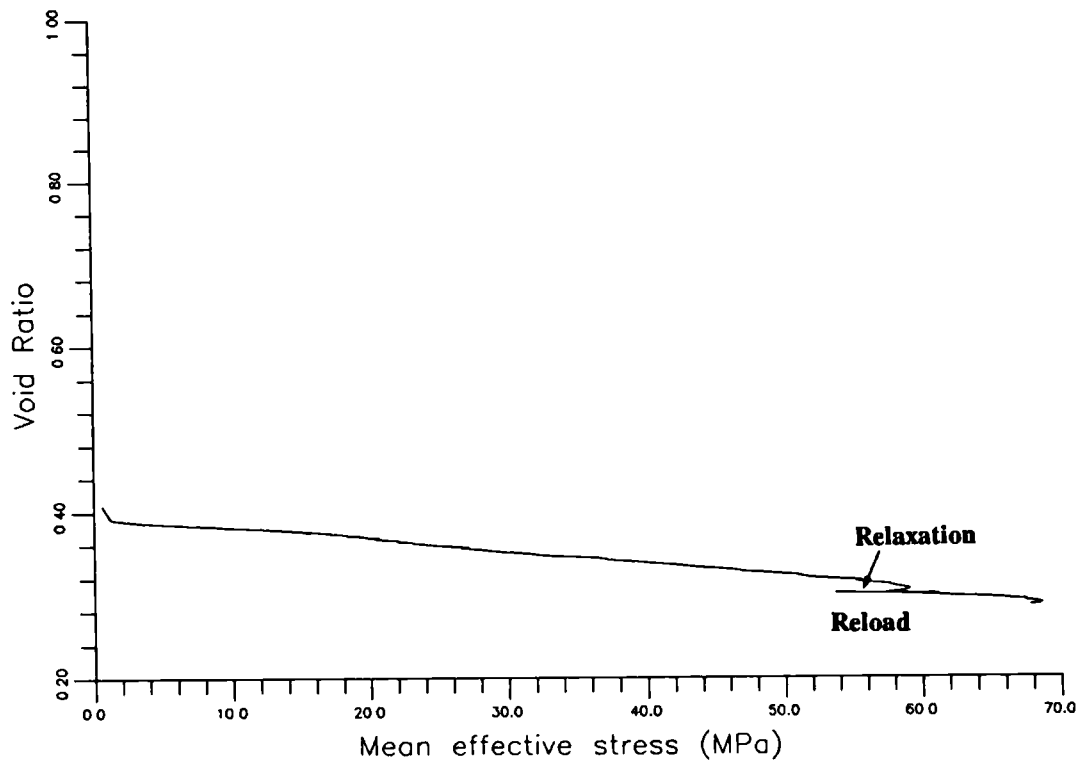


Figure. 4.54. Graph of void ratio/mean effective stress for stress relaxation experiment VOHC2.

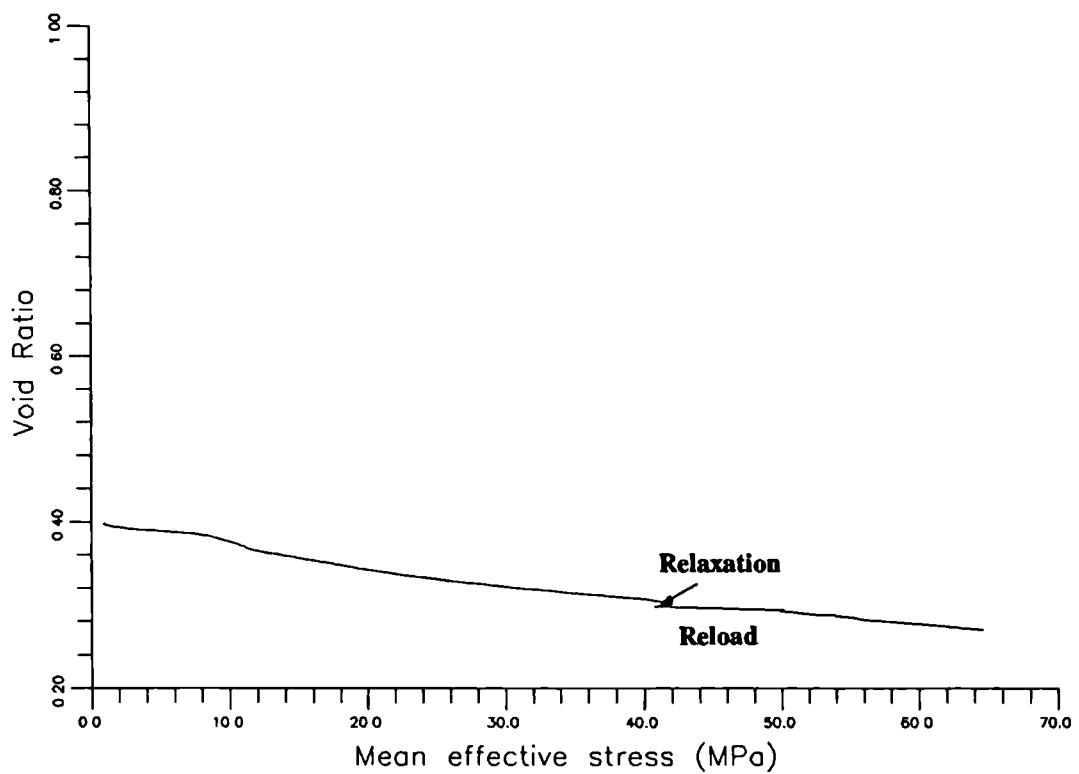


Figure. 4.55. Graph of void ratio/mean effective stress for stress relaxation experiment VOHC3.

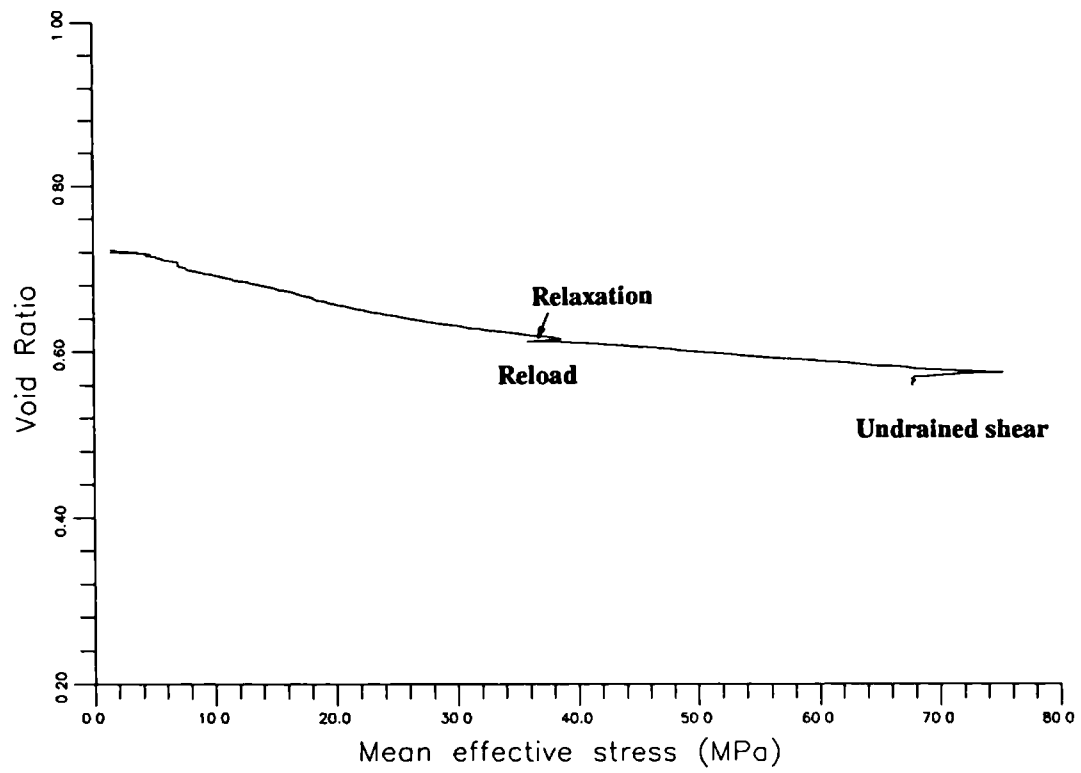


Figure. 4.56. Graph of void ratio/mean effective stress for stress relaxation experiment VOTC1.

Table 4.3.
WATER INJECTION EXPERIMENTAL DATA

EXPERIMENT NAME	POROSITY (%)	FORMATION	VOLUME OF WATER (cc)
EC18/26A	38	L. EKO.	323
EC18/26B	38	L. EKO.	344
EC25/29	40.7	L. EKO.	348

4.6.2. Experimental results.

The vertical effective stress/axial strain plots for each of the experiments (figures 4.57 to 4.59) are typically of the form described throughout this chapter, except during the periods of water injection. These sections of the stress/strain curves indicate an instability in the sample which appears to have been recovered once the period of injection had been terminated. The observed decrease in vertical effective stress was not the result of introducing a head difference across the sample. A similar process for fluid injection was used for the permeability determinations reported in chapter five (a description of the methodology used can also be found in that chapter). Although the displacement rate was decreased during the period of injection, deformation of each sample was difficult to control (ie. to maintain the K_o condition). This instability is reflected in the plot of effective stress ratio (figures 4.60 to 4.62), the complex stress paths (figures 4.63 to 4.65) and the changes in radial strain (figures 4.66 to 4.68) that occurred during the process of injection. It can be seen in each set of data that once injection of water had been terminated, the experiments returned to a normal behaviour.

Figures 4.57, 4.60, 4.63, 4.66 and 4.69 indicate that during the period of water injection, sample EC18/26A was the most unstable of the three experiments. This instability reflects changes in the diameter of the sample. These changes were too rapid for the automatic controller attached to the cell pressure system to react to. Similar large variations were prevented in the other two experiments (EC18/26B and EC25/29) by adjusting the cell pressure manually. This large deviation in radial strain resulted in the

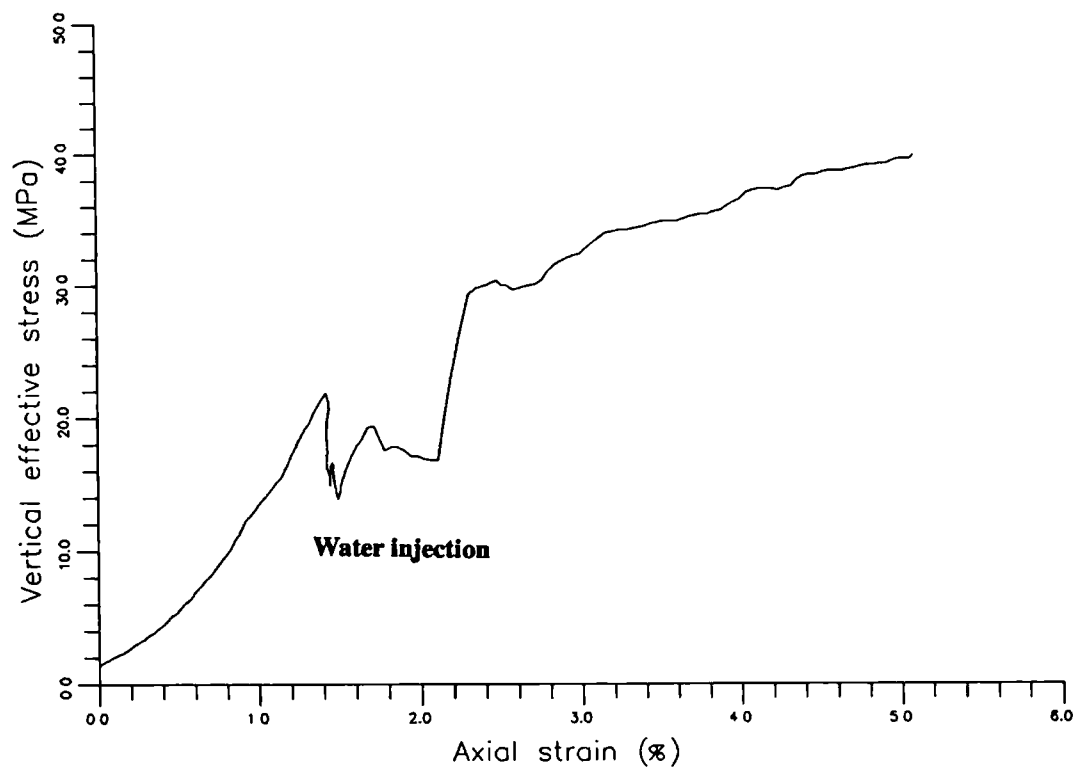


Figure. 4.57. Graph of vertical effective stress/axial strain for water injection experiment EC18/26A.

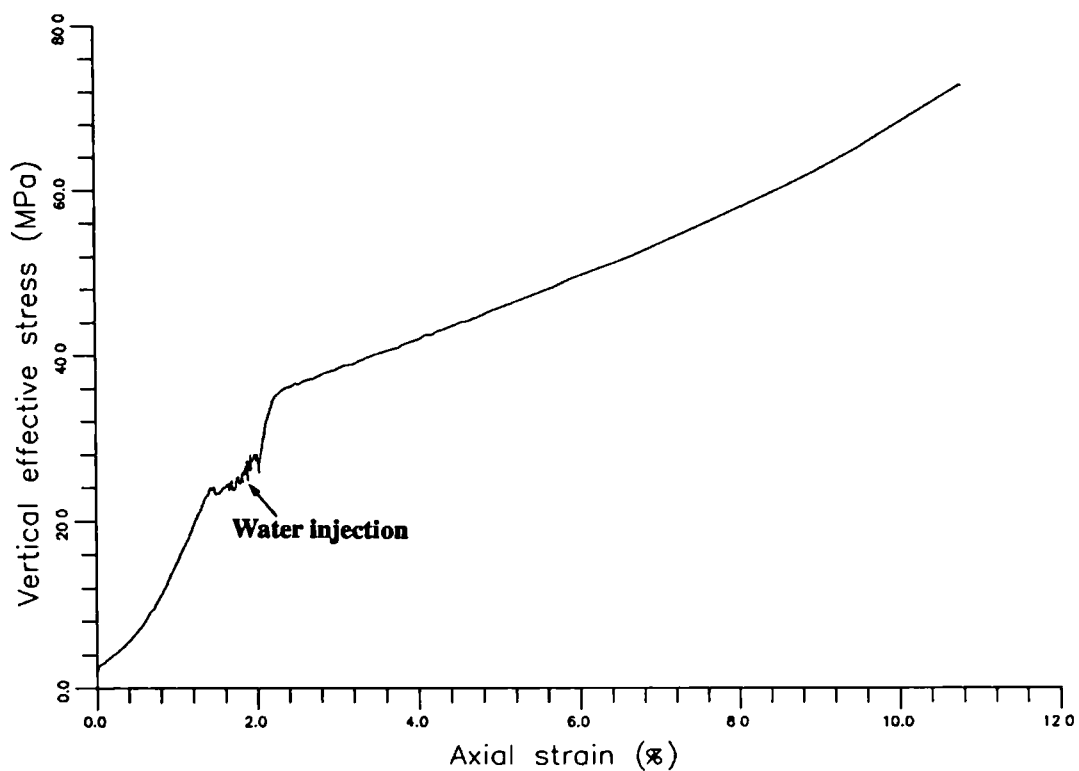


Figure. 4.58. Graph of vertical effective stress/axial strain for water injection experiment EC18/26B.

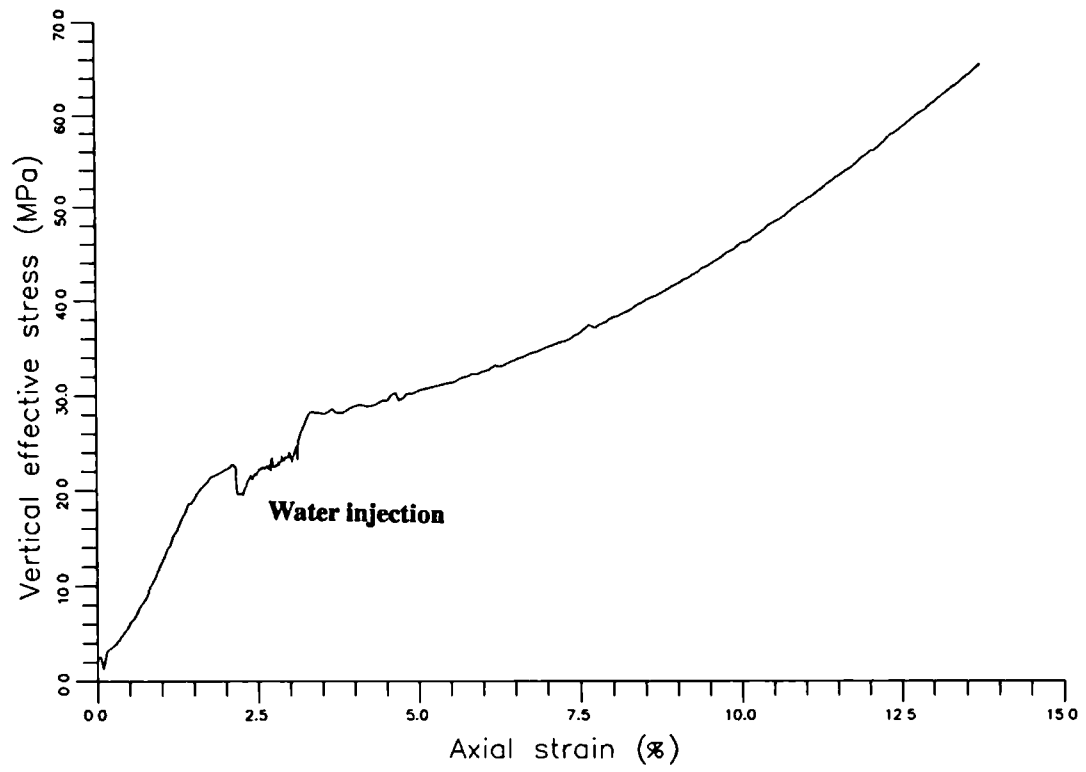


Figure. 4.59. Graph of vertical effective stress/axial strain for water injection experiment EC25/29.

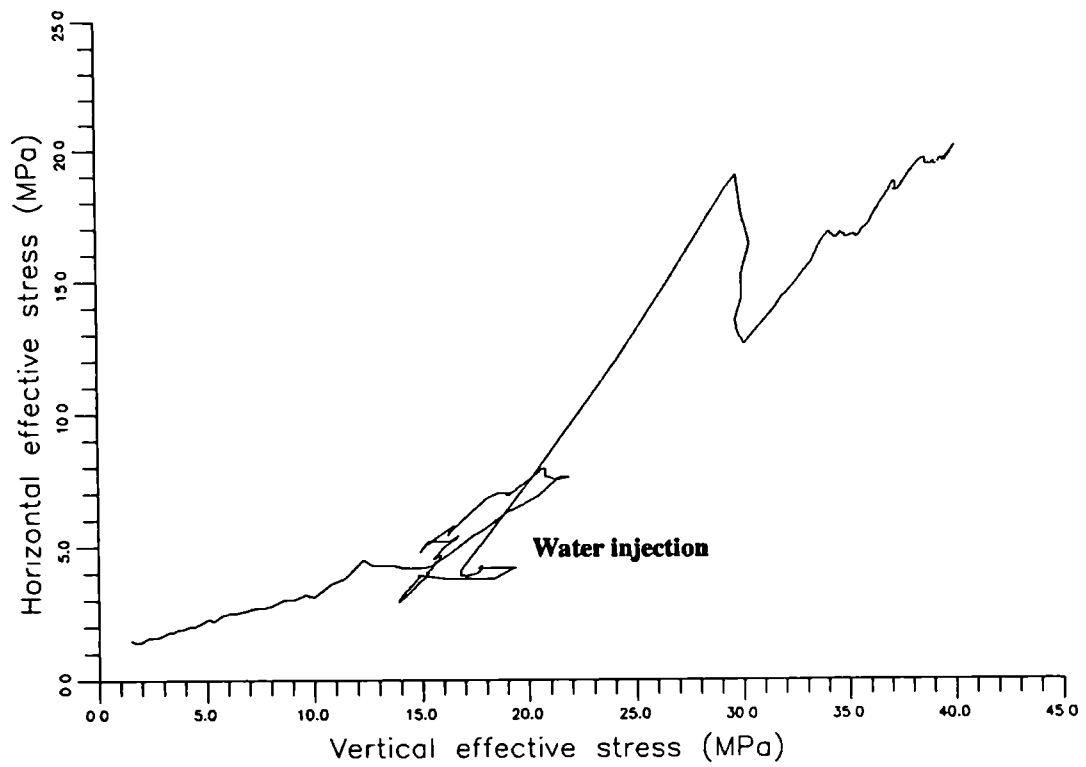


Figure. 4.60. Graph of horizontal effective stress/vertical effective stress for water injection experiment EC18/26A.

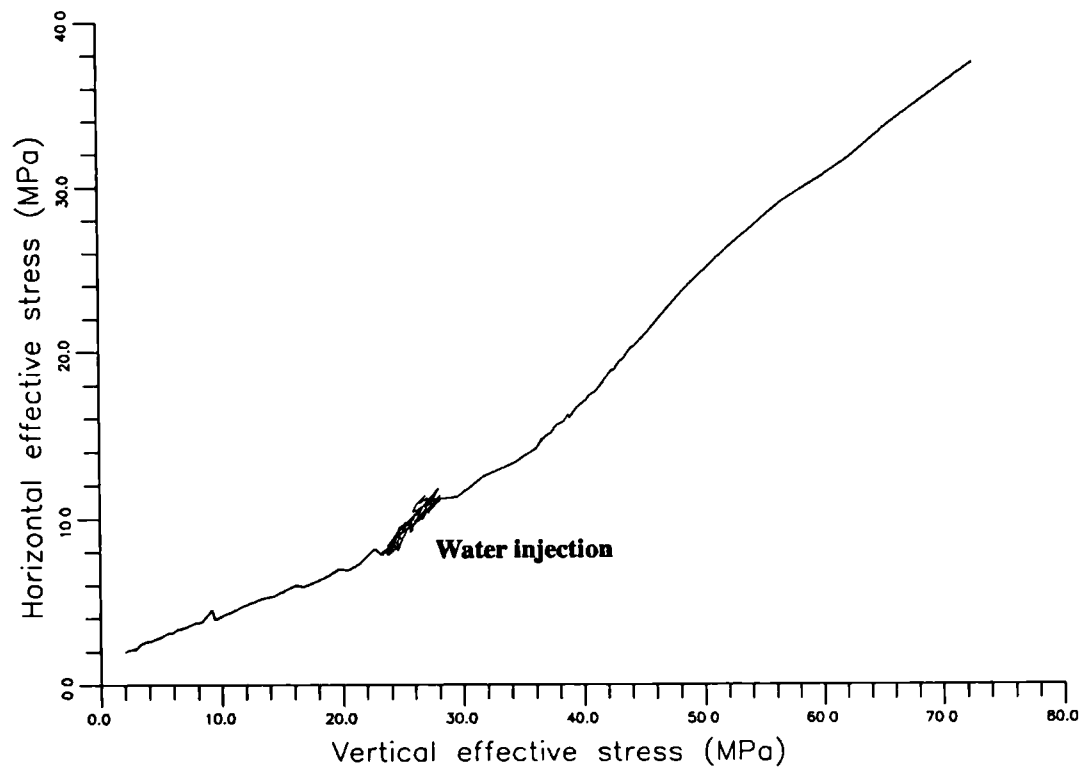


Figure. 4.61. Graph of horizontal effective stress/vertical effective stress for water injection experiment EC18/26B.

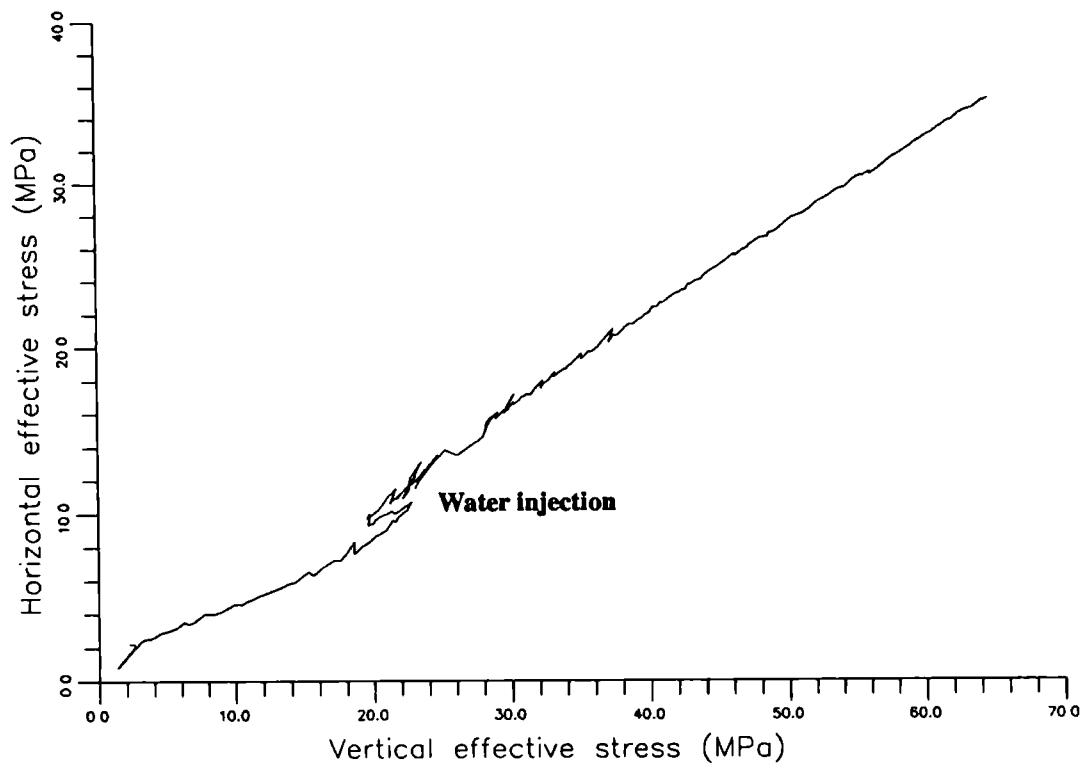


Figure. 4.62. Graph of horizontal effective stress/vertical effective stress for water injection experiment EC25/29.

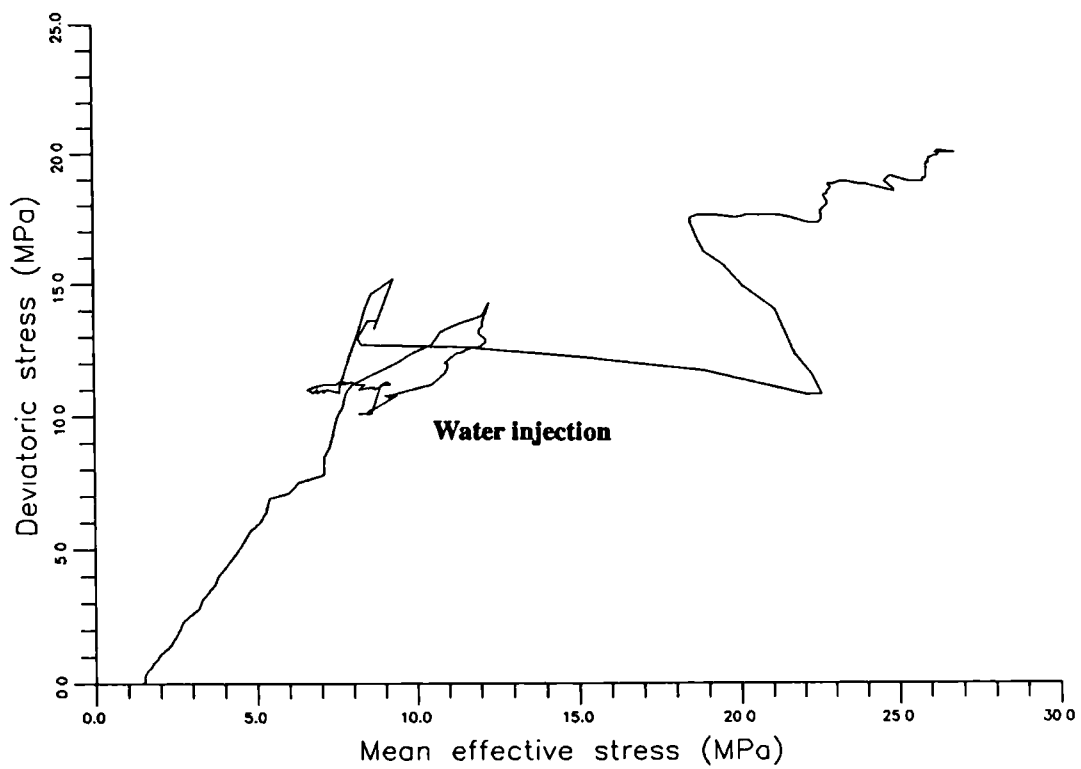


Figure. 4.63. Graph of deviatoric stress/mean effective stress for water injection experiment EC18/26A.

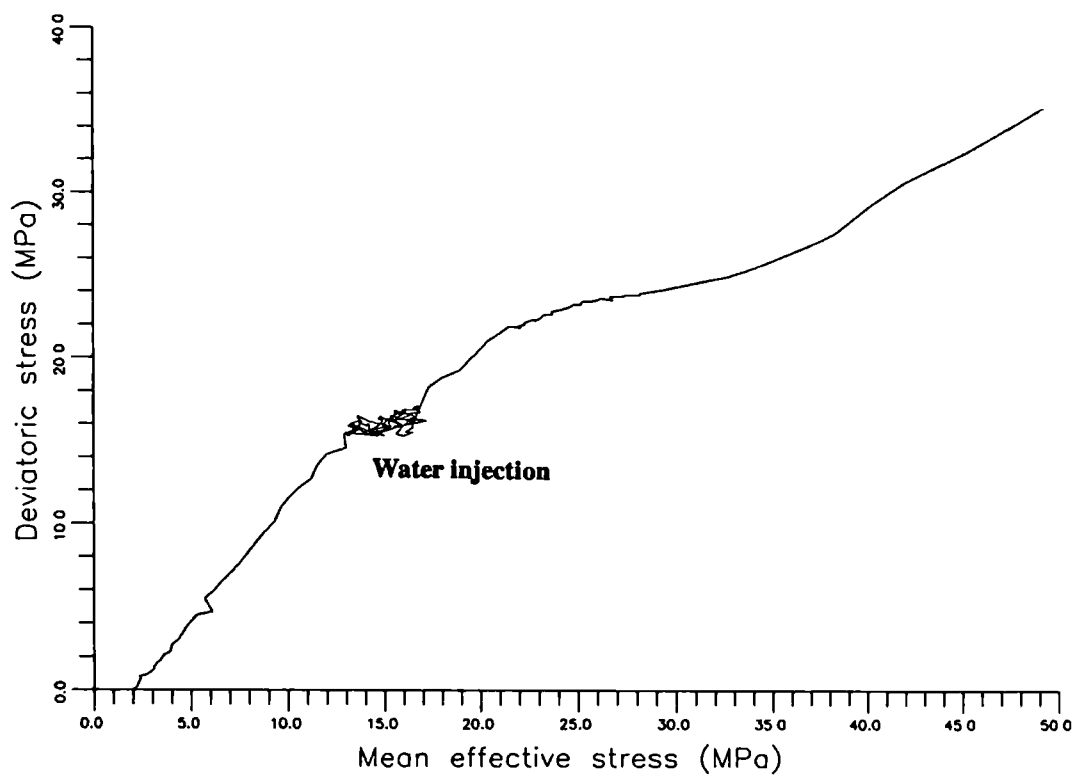


Figure. 4.64. Graph of deviatoric stress/mean effective stress for water injection experiment EC18/26B.

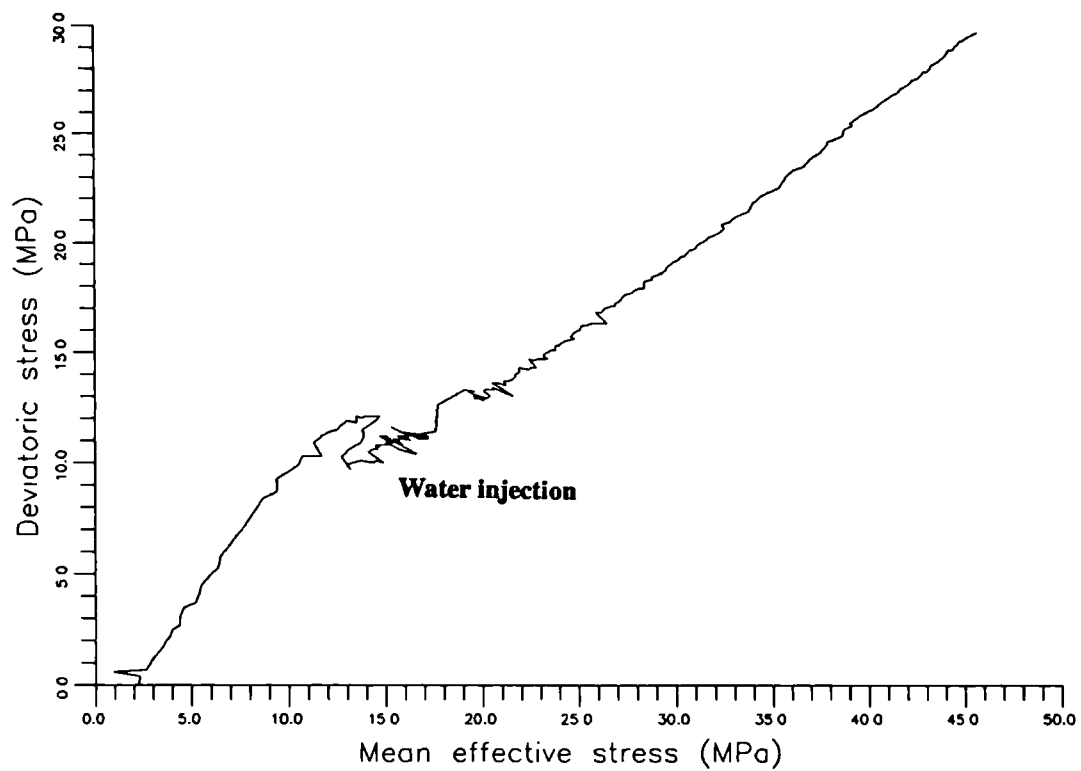


Figure. 4.65. Graph of deviatoric stress/mean effective stress for water Injection experiment EC25/29.

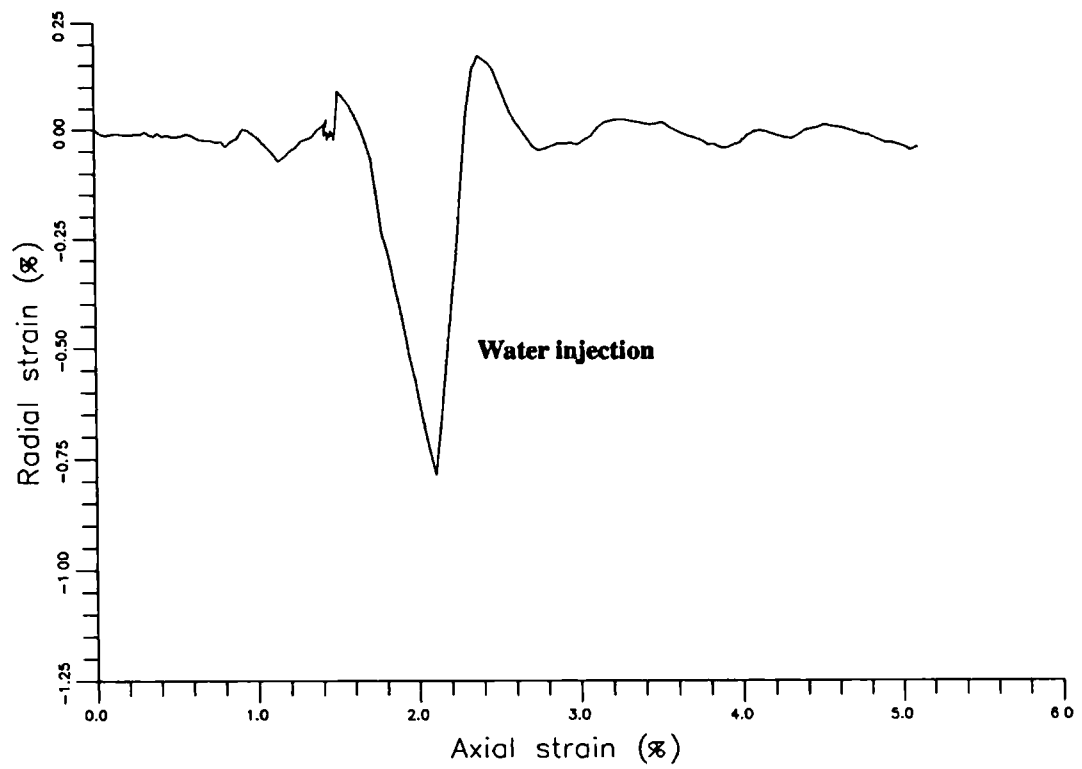


Figure. 4.66. Graph of radial strain/axial strain for water injection experiment EC18/26A.

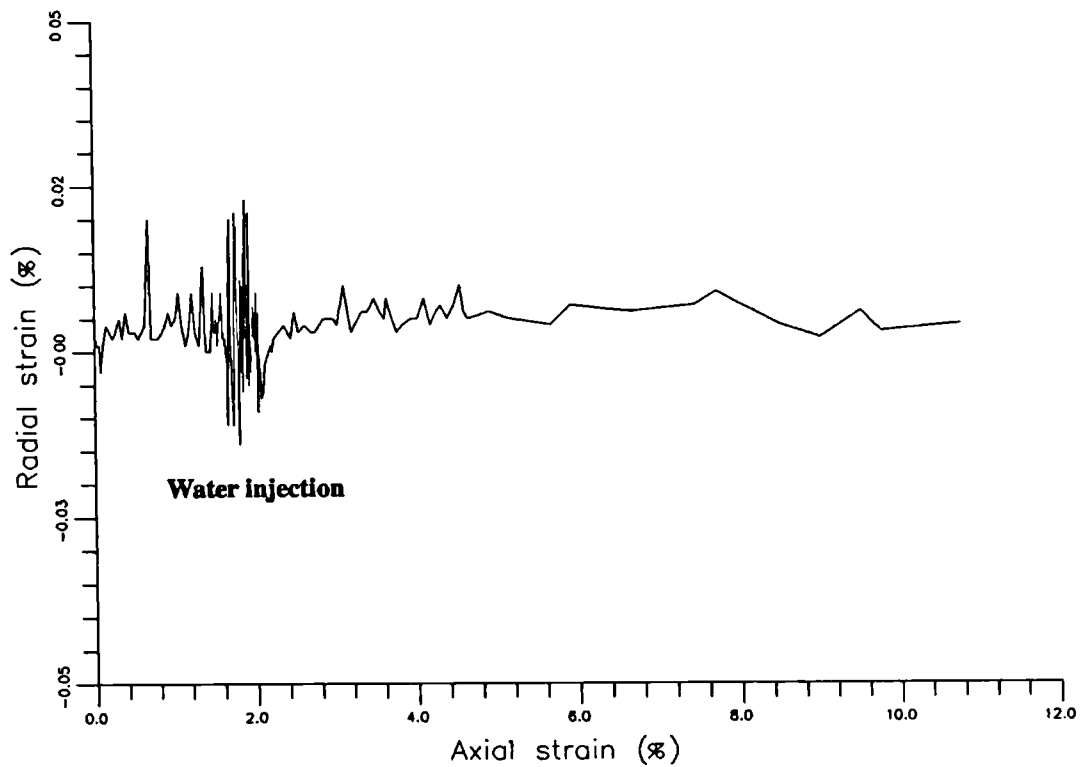


Figure. 4.67. Graph of radial strain/axial strain for water injection experiment EC18/26B.

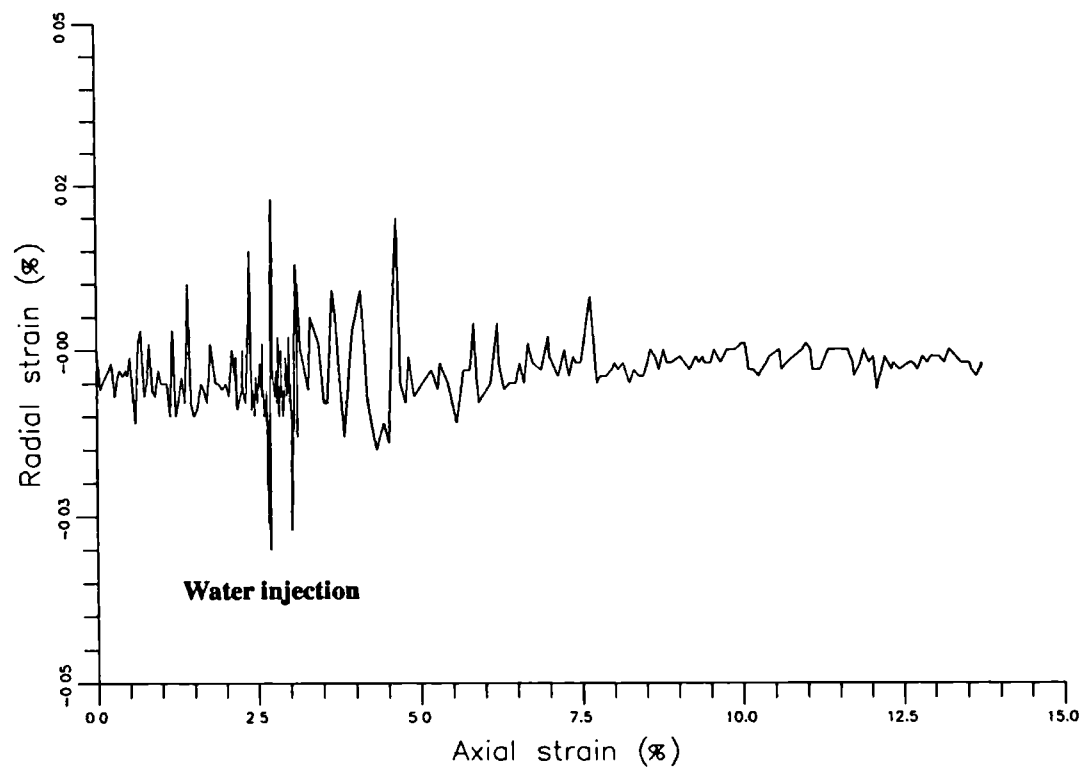


Figure. 4.68. Graph of radial strain/axial strain for water injection experiment EC25/29.

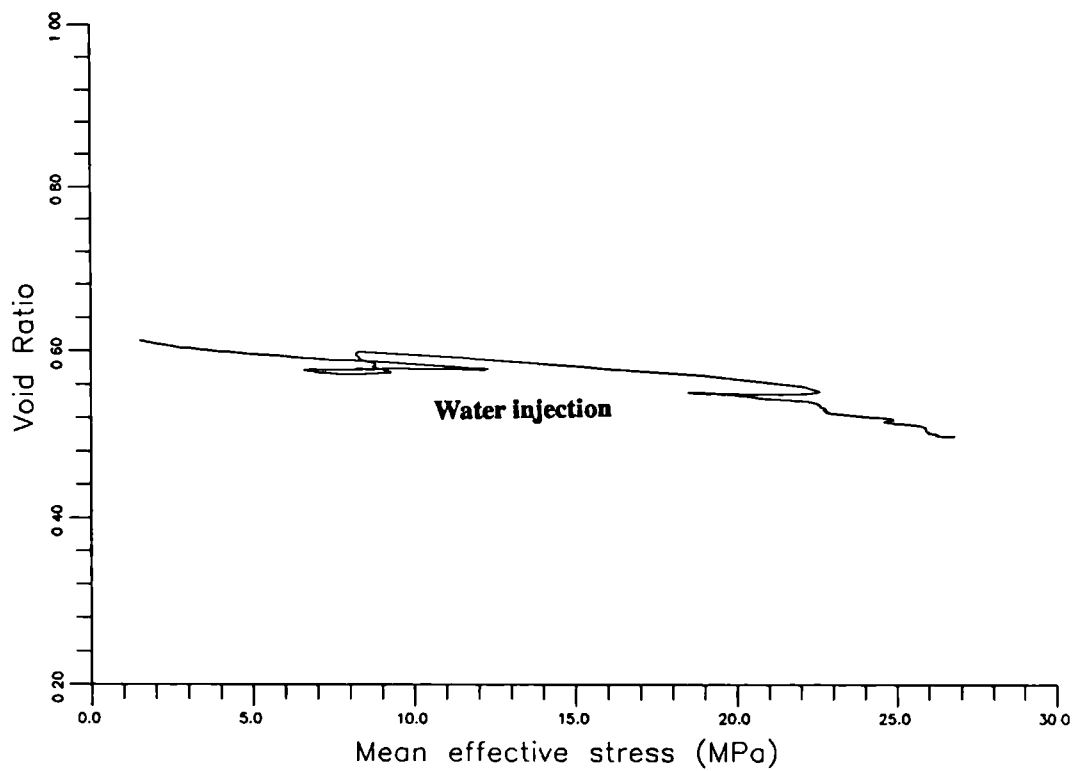


Figure. 4.69. Graph of void ratio/mean effective stress for water injection experiment EC18/26A.

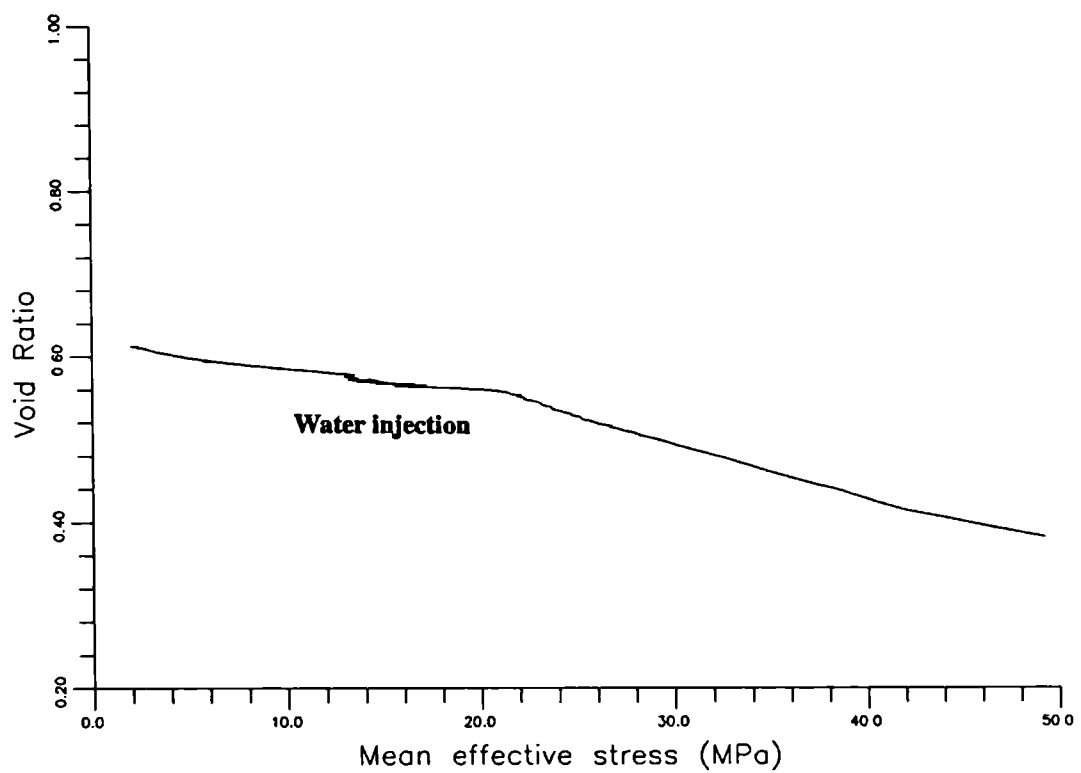


Figure. 4.70. Graph of void ratio/mean effective stress for water injection experiment EC18/26B.

extreme variations observed in the effective stress ratio and stress path plots of this particular experiment.

As a result of the experience gained from the first test, samples EC18/26B and EC25/29 show a more controlled and regular variation in confining pressure and radial strain during the period of injection. Each time the diameter of the samples began to expand or contract, the confining pressure was adjusted to bring the strain belt back to its zero value. Once this had been achieved, zero radial strain was only maintained for a short period of time before a further deviation developed.

Figures 4.57 to 4.65 indicate that when water injection was terminated, each sample had undergone yield. It may be a coincidence that injection began close to the yield point of each sample (as they had very similar initial porosities) or it is possible that the process of injection led to the samples yielding prematurely. Newman (1981) found that samples tested with brine as a pore fluid tended to fail at a lower stress than those saturated with oil, whereas Johnson et al. (1988) reported that they found no weakening of the chalk following water flood experiments. The radial strain plots for the second and third experiments (figures 4.67 and 4.68) show a similar pulsating type behaviour to that observed during partial liquefaction (Taylor, pers. comm., 1987). The undrained shear data presented in chapter six also indicates that the chalk can be a very unstable material when close to its yield stress.

Figures 4.69 to 4.71 represent the changes in void ratio that occurred during each of the three water injection experiments. The latter two figures indicate that the instabilities recorded during injection had no significant affect on volumetric reduction compared to experimental results obtained from chinks of similar porosities.

Each of these experiments indicate that during the process of water injection, the chalk became extremely unstable. This instability does not appear to be the result of head difference imposed across the samples (generally 0.5MPa), as a similar head difference

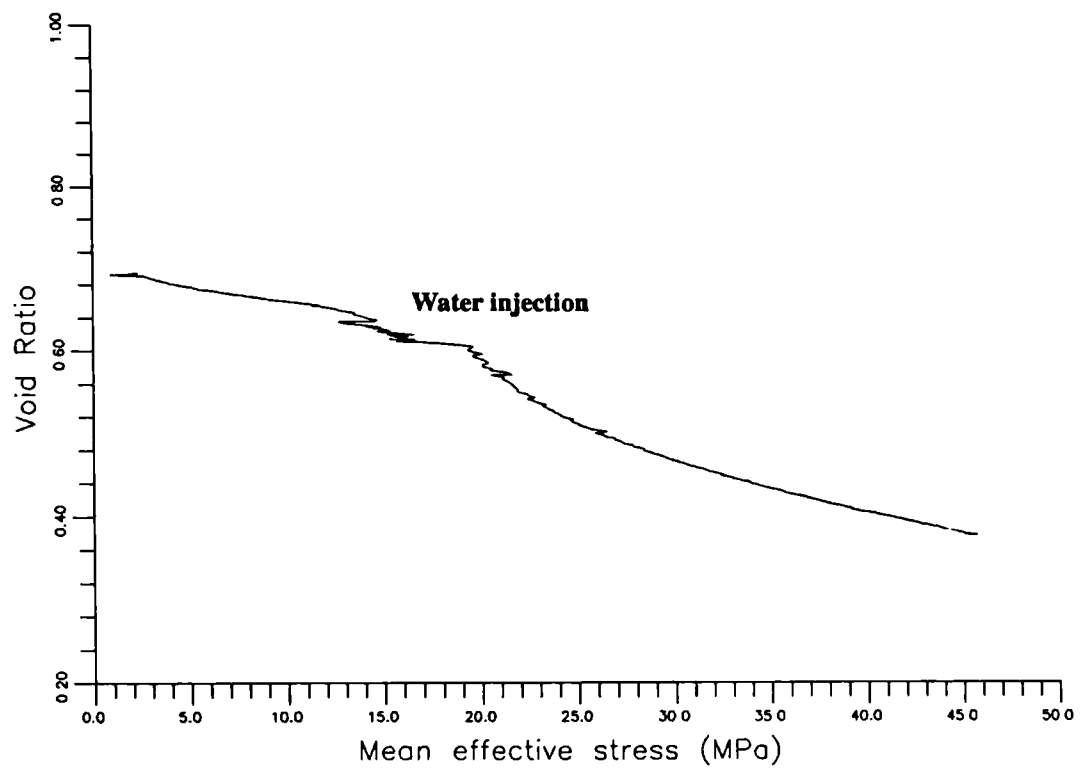


Figure. 4.71. Graph of void ratio/mean effective stress for water injection experiment EC25/29.

was used during the permeability studies reported in the following chapter (where oil was used as a permeant and no instabilities were recorded). The unstable nature of the chalk does not appear to be a result of the presence of the water, as following the completion of the injection process, water remained in the sample as the pore fluid. It is difficult to determine from these three experiments whether the samples were significantly weakened as a result of water injection, however, the results imply that serious stability problems may be encountered during the process of water injection.

4.6. DISCUSSION.

Results from experimental investigations such as those described above may be incorporated into a model depicting the behaviour of a particular material. Such a model has been proposed by Addis (1987, 1989) and Addis and Jones (1989) for chalk behaviour based on their experimental results using the Cam Clay concept. This model is presented in figure 4.72.

The conceptual model presented in figure 4.73 is based on data collected during the present study. Figure 4.74 represents a collection of some of the data on which figure 4.73 is based. With the aid of the three dimensional plotting routines developed by Goldsmith and described in Goldsmith et al. (1989) it is possible to present these data together with their projections onto the three planes, namely, void ratio/mean effective stress, deviatoric stress/mean effective stress and deviatoric stress/void ratio. Such a plot is presented in figure 4.75. This figure clearly indicates how these three dimensional data appear in the more conventionally used two dimensional graphs. It also highlights how misleading it may be to consider such three dimensional data only as a series of two dimensional graphs. This is particularly true when changes in void ratio, as observed on the void ratio/mean effective stress surface, are related to a three dimensional trace. The experimental data from which these multiple plots (figure 4.74 and 4.75) were compiled included a slow strain-rate experiment (ELONGC2, conducted at an average strain rate of $1.1 \times 10^{-8} \text{ sec}^{-1}$), a water injection experiment (EC25/29) and a stress relaxation experiment (VOBC7). These data clearly show the consistent non-linear behaviour

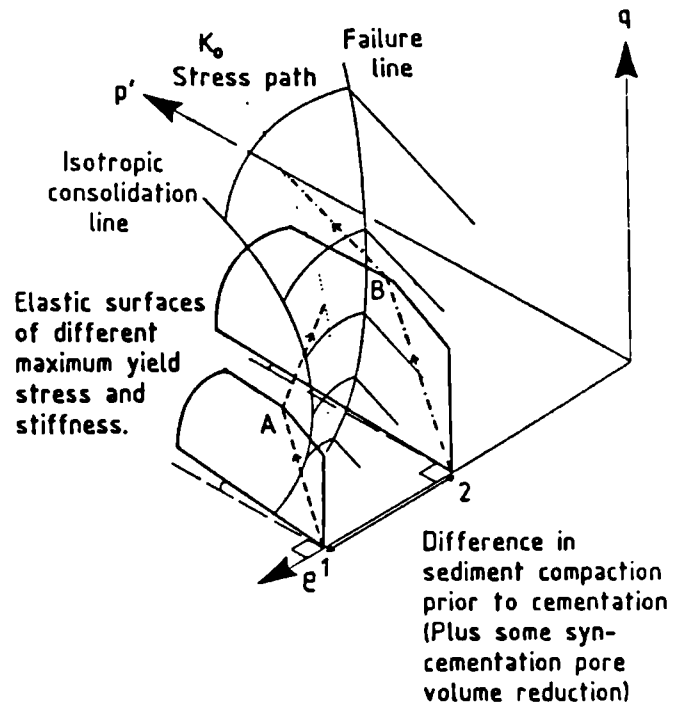


Figure. 4.72. Schematic effective stress/void ratio diagram indicating the compactional behaviour of two chinks (After Addis and Jones, 1989).

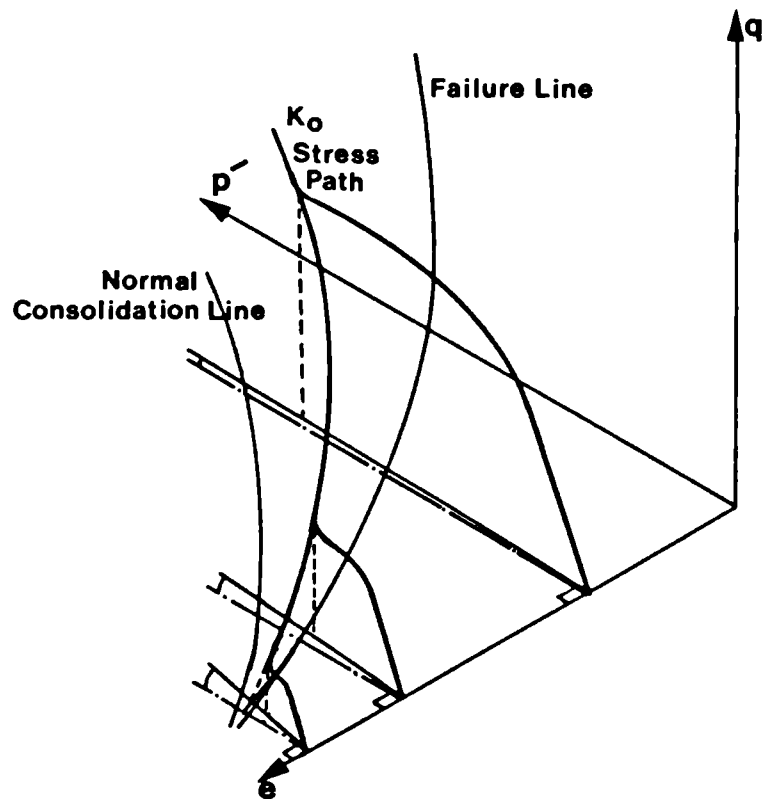


Figure. 4.73. Schematic effective stress/void ratio diagram indicating the compactional behaviour of three chinks proposed from the results of the current study.

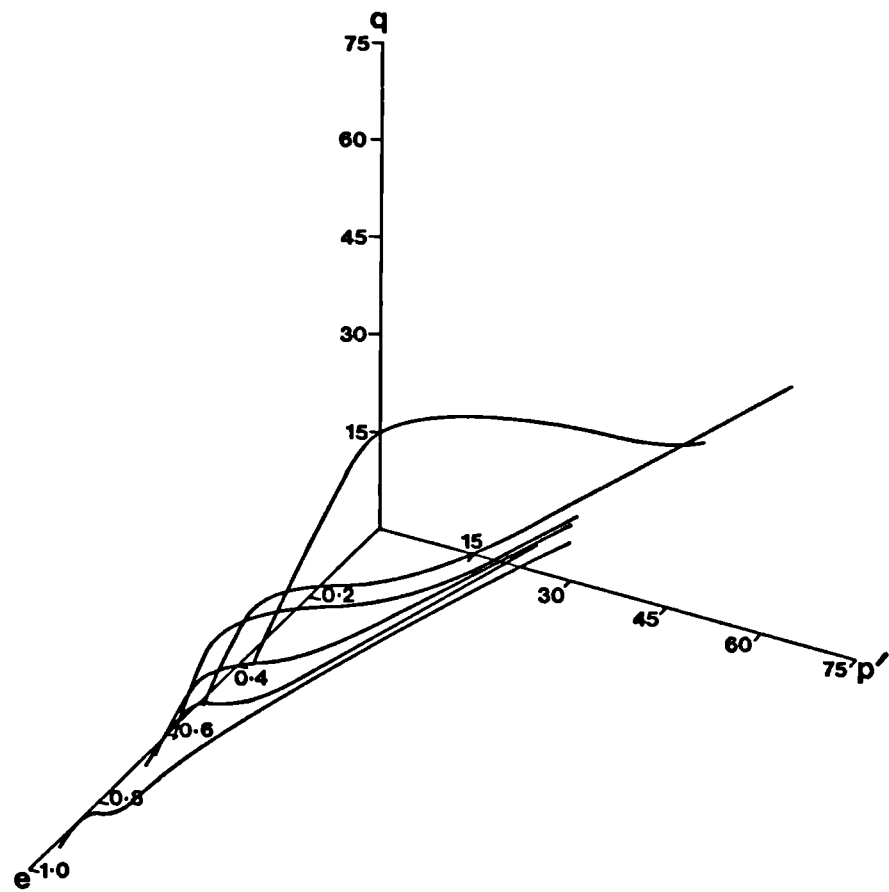


Figure. 4.74. Effective stress/void ratio plot of a group of uniaxial strain experiments.

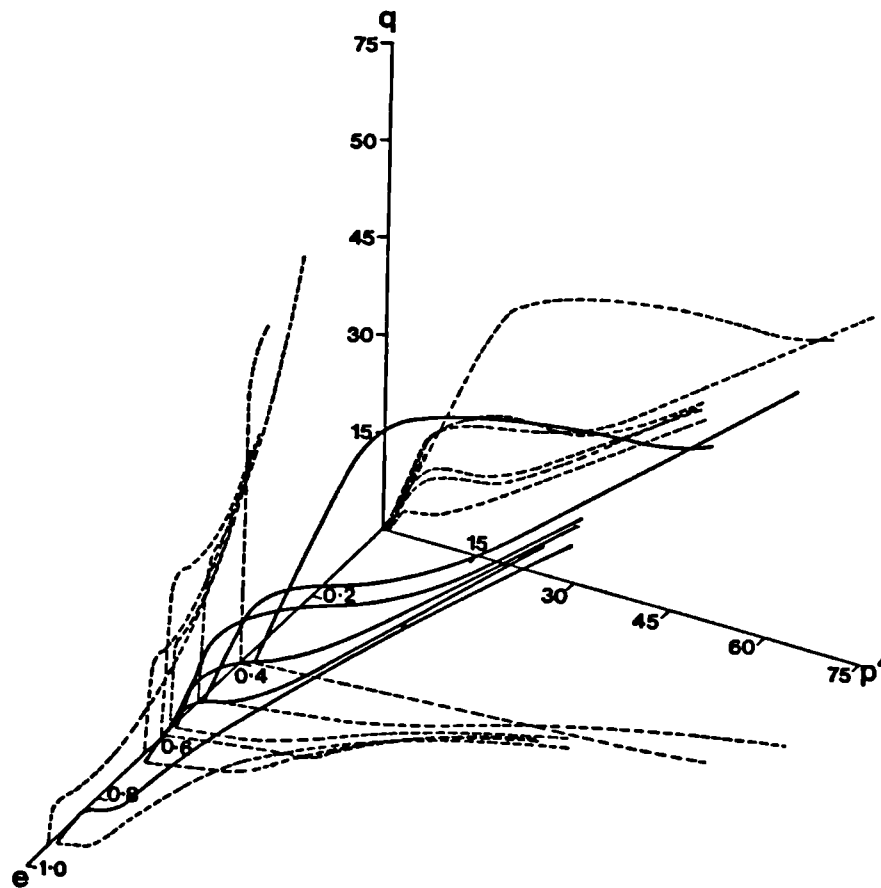


Figure. 4.75. The same data as shown in figure 4.74 but with the data projected on to the effective stress/void ratio planes.

described throughout this chapter. It is also clear, that as the initial void ratio of the chalk decreases, the yield stress is observed to increase, and the range of effective stress over which yield occurs also increases (Jones and Leddra, 1989). Equally, strain softening becomes less significant as the initial void ratio decreases. This relationship is demonstrated in figure 4.76, which presents a series of vertical stress/axial strain curves compiled from all of the uniaxial strain experiments conducted during this study.

Changes in void ratio are small during the elastic phase of deformation (figures 4.72 and 4.73). Figures 4.72 to 4.75 indicate that although volume changes are small whilst the chalk is deforming in an elastic manner, the inclination of this wall decreases as the initial porosity of the chalk decreases. This implies that, in samples with a high initial porosity, such as the Stevn's Klint outcrop chalk, the volume decrease during the elastic phase of the deformation process is greater for an increment of mean effective stress than that observed for low porosity samples. This is to be expected. As the grain size of the chalk is reported to be fairly constant (see chapter two) high porosity chalks will have fewer grain contacts and therefore less cement for a given volume than in a low porosity sample. This means that increases in stress are concentrated on fewer cemented grain contacts in the high porosity chalks. The observed decrease in yield strength with increasing porosity confirms this. It is also possible that these high porosity chalks may begin to yield earlier than their stress paths indicate. It may equally indicate that the open nature of the high porosity chalks allows a certain amount of flexibility in the structure before yield develops. The smaller volume changes associated with elastic deformation of lower porosity chalks implies the reverse situation. In the low porosity chalks, more cemented grain contacts exist per unit volume, and the observed increase in yield strength indicates that this makes them stronger materials. Equally, as their density is higher and any flexibility that may exist in their structure is significantly reduced. These differences are also reflected in the yield and post-yield behaviour of the chalk.

The chalk is generally observed to yield at an axial strain of 1% or less. Figure 4.76 is a composite vertical effective stress/axial strain diagram representing a combination of all of the uniaxial strain experiments conducted during this present study. This figure indicates that as yield strength increases with decreasing porosity, the gradient of the elastic section of the stress/strain curve increases. During yield, resistance to increasing shear stress is reduced and the deformation behaviour changes. Figures 4.73 to 4.75 clearly demonstrate that in each experiment the processes of yield resulted in changes in void ratio similar to those observed during the elastic phase of deformation. This relationship is more easily recognisable in lower porosity samples. In these samples yield is observed to be a gradual process, during which deformation resistance decreases as mean effective stress continues to increase. It can be envisaged that yield progresses by the spreading out of areas of deformation as the random orientation of the coccoliths means that stress will inevitably be concentrated in certain areas. As the effective stress increases, the cement bonds in those areas will break first. This will lead to a strain which will transfer the stress to surrounding coccoliths, and the process will continue. Lower porosity samples contain a higher density of grains and therefore a larger number of cemented contacts. Therefore, increases in stress are more evenly distributed, the breakdown of the bonding is slower, movements of the grains are more restricted and the resulting volume changes are smaller.

In high porosity chalk samples, yield is followed by strain softening (during which the mean effective stress continues to increase whilst the deviatoric either remains fairly constant or decreases). Strain softening becomes a less significant part of the deformational process as the initial porosity of the chalk decreases, until samples with a low initial porosity are observed to deform without strain softening.

Strain softening behaviour, following the onset of yield and prior to the development of strain hardening has been termed pore collapse. Botter (1985) described pore collapse as a large irreversible deformation induced at high stresses as the compressibility of the material increased.

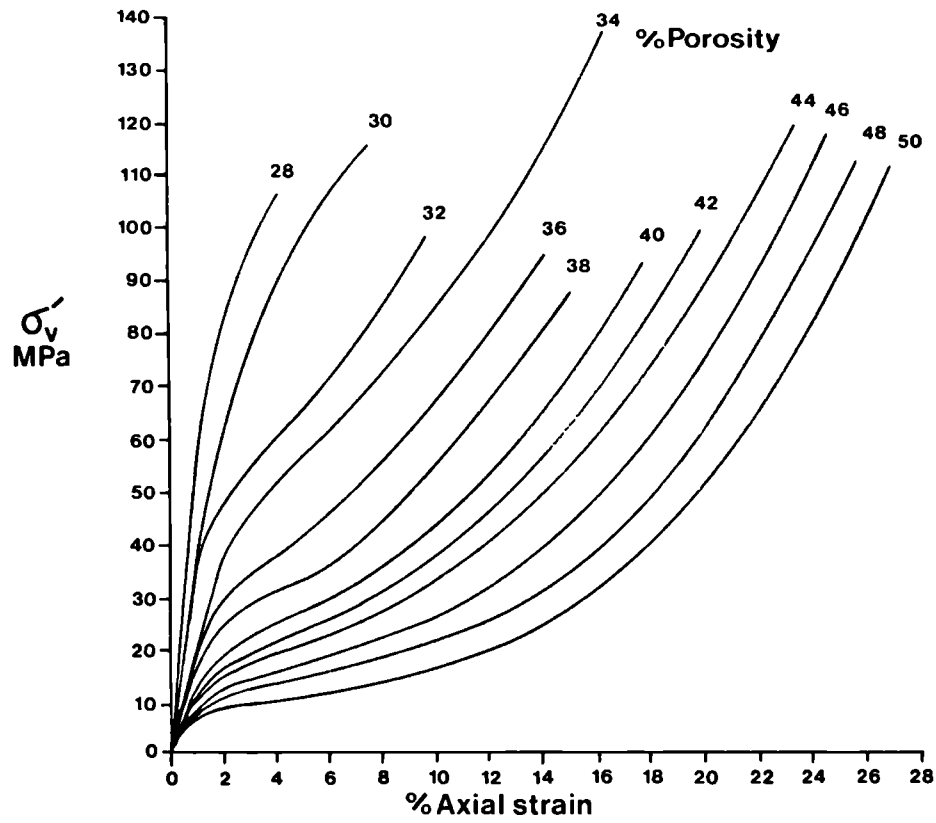


Figure. 4.76. A set of vertical effective stress/axial strain curves compiled from data determined during the present study.

The timing of this change in the rate of volume decrease is therefore of importance, particularly in relation to changes in effective stress that are a consequence of hydrocarbon production in the chalk fields of the North Sea. It has already been stated that the timing of significant changes in volume proposed from this present study are at a variance with that proposed by Addis (1987, 1989) and Addis and Jones (1989). Both models indicate that the deformation behaviour of the chalk will follow an elastic wall until yield (figures 4.72 and 4.73). In the Addis (1987, 1989) and Addis and Jones (1989) model, the initiation of yield in high porosity (high void ratio) chalks results in a rapid decrease in void ratio. This model indicates that, for samples with a high porosity, cementation allows the effective stress/void ratio path to pass outside of the Roscoe Surface. The onset of yield then leads to significant volume changes which result in the effective stress/void ratio path joining the Roscoe Surface. However, since proposing this model, Addis (pers. comm., 1989) has determined that his data do not pass outside of the Roscoe Surface.

Vaughan (1985), Vaughan et al. (1988) and Vaughan pers. comm. (1989) have noted that artificially cemented materials which have extremely high initial void ratio's are able to sustain stresses that take them outside of permissible stress states for an equivalent unbonded (normally consolidated) material (figure 4.77). This data also indicates that as the initial void ratio decreases the yield point of the material moves closer to normal consolidation curve of the unbonded material. Following yield, the stress/void ratio path for the bonded material decreases until it joins that of the unbonded example. The concept shown in the model drawn by Addis (1987; 1989) and Addis and Jones (1989), in which yield is shown to occur outside permissible space is therefore not necessarily wrong. However, the implications noted above from Vaughan et al. (1988) indicate that the chalk is incapable of achieving this state. Figure 4.78 consists of two sets consolidation curves obtained from Butser Hill chalk samples. Two of the curves represent samples consolidated under conditions of uniaxial strain and the others are isotropically consolidated samples. Following consolidation each sample was subjected to undrained shear (see chapter six). These data indicate that changes in void ratio for

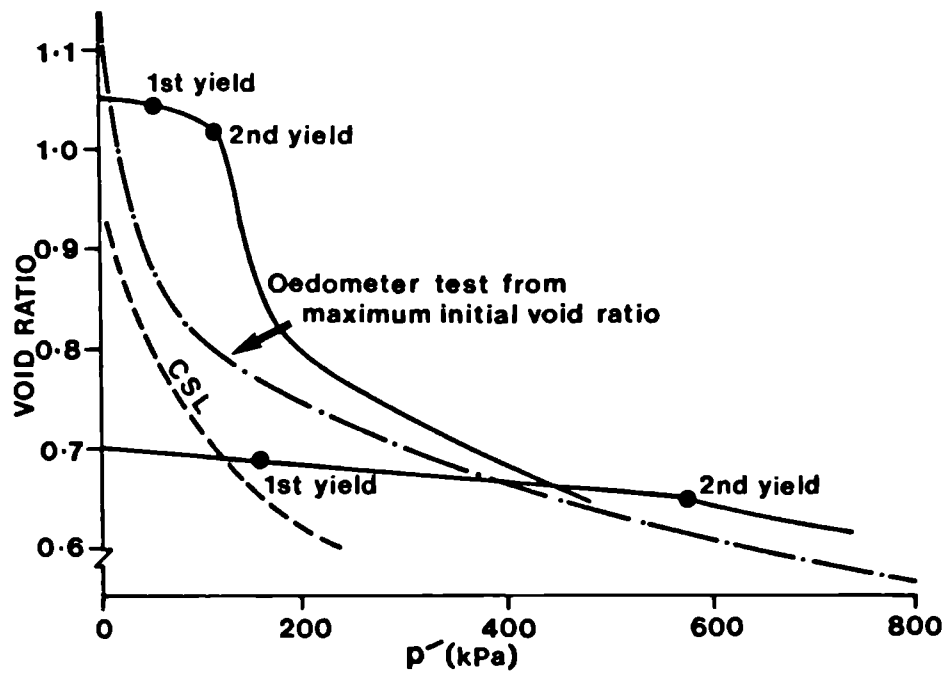


Figure 4.77. Plot of the yield behaviour of an artificially bonded material deformed under uniaxial strain conditions compared to that of a similar unbonded sample. (After Vaughan, et al.1988.)

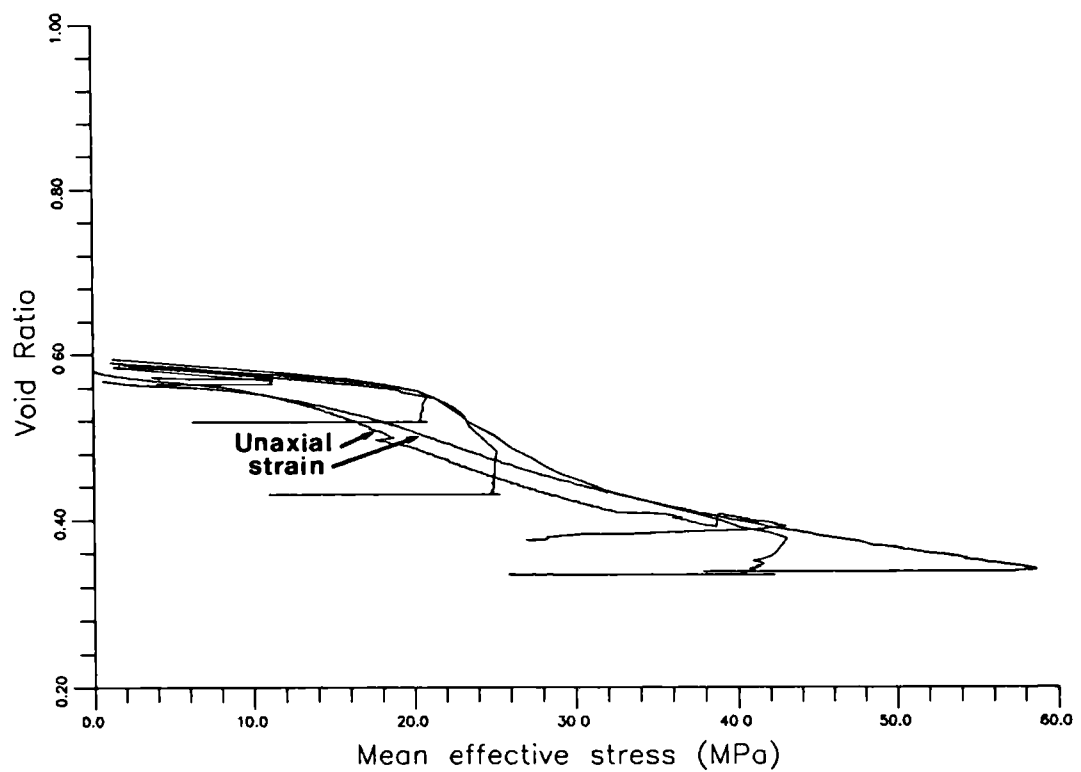


Figure 4.78. Uniaxial and isotropically consolidated Butser Hill chalks presented in void ratio/mean effective stress space.

the uniaxial consolidated samples fall inside of those for samples consolidated isotropically. Both are seen to converge indicating that as mean effective stress increases, chalks subjected to uniaxial strain consolidation behave more like isotropically (normally) consolidated chalk.

It has been shown that the reservoirs consist of a complicated distribution of high, medium and low porosity chalks (see chapter three) (figure 4.79). Each of these different porosity chalks will react in a different manner to increases in effective stress. The relationship between changes in effective stress and void ratio are therefore critical. As the effective stress increases, the data presented in figures 4.74, 4.75 and 4.76 indicate that the higher porosity chalks will quickly reach their respective yield stresses. Further increases in effective stress will lead to a rapid decrease in porosity (void ratio). The yield stresses of the low porosity chalks are considered to be outside of the effective stress changes expected to occur in the reservoirs (see chapter three for details). It is the volume changes that are likely to occur in the medium porosity (34-40%) chalks that are therefore important, as they represent the most significant proportion of the reservoir rocks. Reservoir chalks with this range of initial porosities will behave elastically and may undergo yield when subject to the changes in effective stress which are a consequence of pore pressure depletion. Deformation may, however, not progress beyond the completion of yield. If the model proposed by Addis (1987; 1989) and Addis and Jones (1989) (figure 4.72) is accepted, as soon as medium porosity chalks begin to yield, significant changes in volume are likely to occur in the reservoir. If however the data and model represented in figures 4.73 to 4.75 are correct, significant volume changes will not occur. These two models represent important differences in the increases in effective stress that may be tolerated before large deformations develop in the reservoirs.

This problem may be partly resolved by the use of graphs showing the change in void ratio plotted against changes in mean effective stress. The changes in void ratio/mean effective stress data presented in figures 4.74 and 4.75 represent a series of chalks which

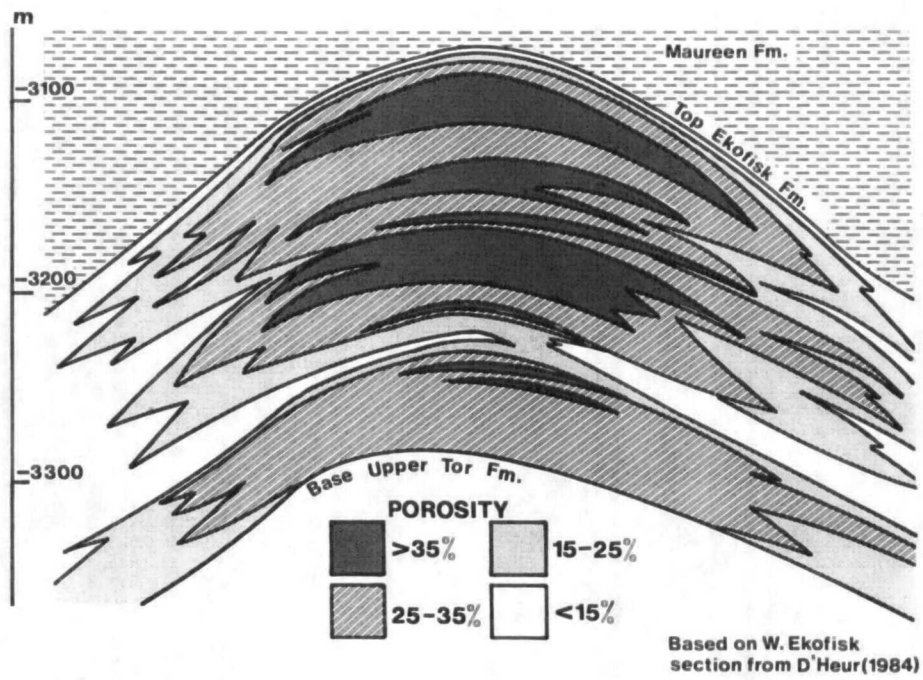


Figure. 4.79. Schematic porosity cross-section.

follow a particular trend (frequently referred to as a porosity trendline). It has been observed by several authors (Botter, 1985; Johnson and Rhett, 1986; Johnson et al., 1988) that chalks from different reservoirs, or chalks which contain increased quantities of silica or clay, result in different porosity trendlines. This would seem a plausible proposition based on the data available. However, it should be noted that figures 4.74 and 4.75 contain data representing chalks from onshore Denmark and the North Sea, from several different formations.

Although porosity trendlines are not an ideal representation of variations in mechanical behaviour, as they represent changes in porosity against a single effective stress parameter. They, however, provide evidence that the behaviour observed in effective stress/void ratio space will vary, depending on the specific chalk under investigation. The model proposed in this thesis indicates that the change in gradient of the void ratio/mean effective stress plot does not represent the onset of yield (often equated with pre-consolidation pressure (see chapter six)), but rather, it indicates the completion of the yielding process.

Significantly, the data presented in Vaughan et al. (1988) (figure 4.77) indicate the presence of two yield points. It is possible that the onset of yield in the present model represents an equivalent to the first yield of Vaughan et al. (1988) and the completion of yield in the proposed model is equivalent to the second yield in Vaughan et al. (1988). This may be an oversimplification as the two materials may not be analogous.

CHAPTER 5

DETERMINATION OF RESERVOIR ROCK PERMEABILITY.

5. DETERMINATION OF RESERVOIR ROCK PERMEABILITY.

5.1. INTRODUCTION.

Determination of reservoir rock permeability is one of the most important factors required for evaluating production potential and simulating reservoir performance. A knowledge of the distribution of variations in permeability is particularly important in North Sea reservoir chalks as, although these rocks commonly have high porosities (often in the range 35-45%), they invariably exhibit low matrix permeabilities (table 5.1). In the reservoirs, matrix permeability is generally enhanced by naturally occurring fractures and other discontinuities. This higher permeability, termed effective permeability (table 5.1), which can be up to 500 larger than the matrix permeability, enables the hydrocarbons to be produced from the chalks of the North Sea. The chalk can therefore be classified as a dual porosity and permeability reservoir rock.

The chalks which form hydrocarbon reservoirs in the Greater Ekofisk Area (Jones et al., 1989) exhibit wide variations in porosity (D'Heur, 1984, 1989) and permeability (table 5.1). For permeability data to be useful in reservoir evaluation and production planning exercises it should be collected from a range of samples representative of the rock types present in the reservoir (Morgan and Gordon, 1970). These authors indicate that there are a range of rock properties that may affect pore geometry and matrix permeability, these include; grain shape; grain size; sorting; pressure solution; cementation; intergranular clay; clay seams. To this list may also be added the initial void ratio (Lambe and Whitman, 1979) and changes in effective stress. A change in any one of these parameters will seldom have an equivalent effect on permeability in different rock types. In this study two variables (variations in fabric and changes in the applied effective stress), which may affect the permeability of the chalk are investigated. These two variables were selected because it has been widely observed that the fabric of the chalk will influence its permeability (D'Heur, 1984; Hardman, 1982; Thomas et al., 1984). Similarly, the large compactional strains experienced by the reservoir rock during

production (Addis, 1987; Potts et al., 1988; Jones et al., 1987; 1989; Johnson and Rhett, 1986; Johnson et al., 1988) might be surmised to cause a change in permeability. No permeability decline of this type has, as yet, been reported from the chalk fields.

Table 5.1.

PUBLISHED PERMEABILITY DATA FOR THE CHALKS OF THE NORTH SEA.

Field	Matrix Permeability (mD)			Effective Permeability (mD)	Reference
	Formation				
	Eko.	Tor	Hod		
EDDA	1.0			24	D'Heur & Michaud, 1987
EKOFISK	0.06- 8.0	0.1- 8.0		150	Pekot & Gresib, 1987
	0.1- 1.0	1.0- 10.0			Johnson & Rhett, 1986
	0.1 - 10.0				Van Den Bark & Thomas, 1980
	0.1 - 10.0				Thomas et al., 1984
	0.1 - 10.0				Taylor & Lapr�, 1987
ELDFISK	0.01 -	35		140	Michaud, 1987
HOD	0.5 -	6.5		200	Norbury, 1987
TOMMELITEN	0.1- 0.5- 0.5- 1.0-				D'Heur & Pekot, 1987
TOR	0.04- 3.0	0.04- 5.0		20-90	D'Heur, 1987
VALHALL	2.0- 10.0	2.0-		20-90	Leonard & Munns, 1987
	1.0- 1.0-	0.03-			Hardman, 1982
	2.7- 4.8	0.4- 1.9			Munns, 1985
(Norwegian in general)	3..0			12	Scholle, 1977
	1.0-10.0				Sorensen et al., 1986
GORM (Danish)	0.6- 11.0	0.3- 8.0			Hurst, 1983
HALINGEN (Danish in general)	0.7-10.0				Van Den Bosch, 1983
	0.03-1.5			0.1-20	Michelsen, 1982
	0.02-15.0				Nygaard et al., 1983

The experimental studies reported in chapter 4, and the work of Addis (1987) and Johnson et al. (1988) confirm that the compactional response of North Sea reservoir chalks to increasing effective stress as a consequence of pore pressure draw-down is primarily dependent on the initial porosity. In low porosity chalks, compaction is entirely elastic, but in chalks of intermediate or high porosity, compaction results in a gradual breakdown of the cement bonding, a closing of pore spaces and a distortion of fractures. This chapter reports the results of an experimental programme, designed to investigate how these processes may affect the permeability of the chalk. The experimental investigation was part of a study, conducted jointly with Norsk Hydro, to provide permeability data for a major new reservoir engineering analysis of the Ekofisk oilfield and to evaluate the risk of a reduction in permeability due to compaction of the reservoir chalks.

Chalks from the Upper Ekofisk, Lower Ekofisk and Tor Formations were chosen from core material held in the Norwegian Petroleum Directorate's core store in Stavanger. Samples were selected which were representative of diagenetic and sedimentological features found throughout the North Sea chalk succession. These included, stylolites; stylolitic fractures; tectonic fractures; irregular fractures; clay seams; debris flows; plastically deformed chalks; and burrowed chalks. A full explanation of the origin of these features can be found in chapter 3.

In general, the chalk samples were only subjected to the range of effective stress changes (36MPa) expected to occur in the reservoirs during hydrocarbon production. The initial porosity of the samples used in this study varied from 18.7-41.4% (table 5.3). In the vertical effective stress range applied, the stronger, low porosity chalks remained elastic, but a vertical effective stress of 36MPa was observed to be close to, or larger than the yield stress for a number of the weaker, high porosity chalks.

At the time of this study the experimental equipment currently available in our laboratory was not capable of investigating the influence of compaction on the effec-

tive permeability, but new equipment, under construction, will be able to test full core size samples containing both fractures and diagenetic features, restored to the physical conditions existing in the reservoir.

Results of petrographic analyses, undertaken by Norsk Hydro on the samples tested in this study which were reported in Leddra et al. (1989) are also included in this chapter. This part of the study was designed to identify the geological parameters which control matrix permeability so that permeability data obtained from core samples could be extrapolated to other horizons within the reservoir without the need for further experimental studies. The parameters investigated included, lithofacies, calcite and silica cementation and local variations in grain composition and texture.

Experiments such as those reported in this chapter also serve the additional purpose of calibrating routine matrix permeability data used in reservoir modelling. These data are usually based on measurements made under conditions of low confining stress, and are seen to give permeabilities in excess of those determined under restored state reservoir conditions.

5.2. ROUTINE PERMEABILITY ANALYSIS.

Permeability constitutes one of the most important parameters measured during routine core analysis. It is generally considered difficult to obtain representative values of total fracture and matrix permeability (Van Golf-Racht, 1982). If the fractures, which are such an important constituent within the reservoir, do not have a random orientation and distribution, the method used for evaluating permeability has to be modified. Most conventional permeameters are insufficiently flexible to allow modifications of test procedures to take account of specific requirements and are therefore inadequate for determining the true permeability of a rock (Van Golf-Racht, 1982). These analyses are usually undertaken using a low pressure Hassler Cell consisting of a steel cylinder with two end caps in which the sample is placed inside a rubber membrane. A confining pressure of between 1.5 and 1.8MPa is usually applied to prevent the permeant from flowing down the sides of the sample. The permeant is then passed, under a constant

pressure-head, through the sample (typically 25mm diameter and 38mm long) to atmospheric pressure at the bottom. Before testing, the samples are generally cleaned with Toluene to remove any residual hydrocarbons and Methanol to remove both water and residual salts. Morgan and Gordon (1970) point out that once a core has dried out it is not always possible to clean out oil that has dried onto the surface of the grains. Cuiec (1975) indicates that similar problems may exist with the cleaning of preserved samples. Once they have been cleaned they are then dried in an oven at temperatures of between 70°C and 100°C. Various permeants are used. These include, dry nitrogen, helium, air, conditioned water, brine and hydrocarbons. The permeabilities determined from these types of tests are usually higher than the true permeability (Archer and Wall, 1986) and require the application of a 'Klinkenberg correction'. This involves conducting a series of tests at different inlet pressures. Mean permeability is then determined and the calculated permeabilities are plotted on a graph against 1/mean permeability (Archer and Wall, 1986). These values are then corrected using a set of empirical tables to determine the true permeability.

The routine method used for permeability determination has several disadvantages. Firstly, the confining pressure and effective stresses are usually small compared with those prevailing in the reservoir. Results presented in section 5.7 indicate that under low confining pressures fractures may remain open in the samples that would be closed at the pressures existing in the reservoirs while others are closed that may be partially open under reservoir conditions. Van Golf-Ract (1982) noted that the results from tests using Hassler cells indicated that fracture permeability was severely reduced as the confining pressure increased, and that fracture permeability compared to matrix permeability was very sensitive to changes in effective stress. The low pressures associated with testing using a Hassler Cell may therefore result in an artificially high permeability. It was shown in chapter 3 that the distribution and orientation of fractures and stylolites was closely linked to porosity distribution. The strength and degree of deformation, in the chalk, resulting from increasing effective stress, is dependent on the initial porosity (Addis, 1987; Jones and Leddra, 1989). This relationship may be modified by the

presence of discontinuities, such as fractures and stylolites and variations in sedimentology. This implies that as the effective stress increases changes in permeability within reservoir units of the same porosity may not be uniform. If the range of effective stresses that can be applied to a sample is not large enough to explore the full range of deformations that may be activated in the reservoir, the resulting permeabilities may be seriously in error.

Drainage of pore fluids to atmospheric pressure at one end of the sample may prevent the maintenance of full sample saturation during the experiment (Carpenter and Stephenson, 1986). If hydrocarbons or water (which has not been deaired) are used as a permeant, or if the drainage system has not been totally deaired, gasses may exist in the sample or drainage system, which, under reservoir pressures would be held in solution.

A further disadvantage with the routine method of permeability measurement concerns the manner in which stresses are applied to the sample. Most routine experiments are conducted under isotropic stress conditions. The stress system acting in the reservoir is considered to be heterogeneous, often approximating to the K_0 condition (Jones et al., 1987). This anisotropic stress system, which was also effective during burial, led to the development a non-uniform fabric in the reservoir rock. The data presented in section 5.7 indicate that such a fabric may dilate or contract when subject to anisotropic loading during laboratory experiments giving rise to an increase or decrease in permeability. Fabric changes resulting from the application of an isotropic stress will be different from those which develop under conditions of anisotropic stress.

Two other problems exist which are not confined to routine testing methods. Scale factors are important. The length and diameter of the sample required for testing may not contain the full range of fractures and other diagenetic features representative of those existing in the reservoir. The orientation of the fractures and other discontinuities may prevent successful preparation of samples, particularly when a coring tool is used.

Therefore a bias may exist in the permeability data that can be obtained from laboratory experiments.

To avoid some of these problems, the permeabilities measured in this study were determined under reservoir effective stress conditions following K_0 loading in a triaxial deformation system (Jones et al., 1987). Unfortunately, the equipment used requires relatively small sized samples (76mm long and 38mm diameter), and the permeant can only be passed vertically through the sample.

5.3 HIGH PRESSURE FALLING-HEAD METHODOLOGY.

Experimental programmes designed to investigate changes in permeability as a consequence of increasing effective stresses have been conducted by a number of authors including Marek (1979); Newman (1981); Carpenter and Stephenson (1986); Addis (1987). Each of these studies used the falling head methodology, employing one of two techniques. One technique, used by Addis (1987), proceeded by loading the sample at a displacement rate which led to the generation of an excess pore pressure at the top (undrained end) of the sample. This excess pore pressure resulted in a flow of pore fluid from the bottom sample to a measuring device. In the second technique an excess pressure was introduced in the drainage line at one end of the sample which was allowed to dissipate and drain through the sample to a measuring device (Remy, 1973). Very little fluid movement is involved in both methods.

5.4. HIGH PRESSURE CONSTANT-HEAD EQUIPMENT.

The experimental programme reported in the remainder of this chapter was conducted using the high pressure triaxial cell described in chapter 4. Two 50cc Imperial College volume gauges were connected to the drainage lines from the top and bottom of the sample. These volume gauges, which act as air-fluid interfaces, can be used to supply different back pressures (using Manostat constant leak air regulators) to either end of the sample. This system means that a constant head (pressure) difference can be established across the sample. It also allows a degree of flexibility in the head difference

applied during permeability determination. This is important as individual samples exhibit very different flow rates, and the duration of each determination can only be standardised by adjusting the head difference. Further fluid lines from the volume gauges allow both volume gauges to be recharged or emptied independently during a test. This allowed volumes of the chosen permeant, larger than 50cc, to be passed through the sample during each permeability determination.

5.5. HIGH PRESSURE CONSTANT-HEAD METHODOLOGY.

Two sets of experiments (table 5.3) were conducted under conditions of uniaxial strain in which permeability was determined at specific values of vertical effective stress. The initial set of eight experiments (prefixed by NHEC) were designed to determine changes in the permeabilities of chalks containing both fractures and stylolites at vertical effective stresses of approximately 14, 24 and 36MPa, typical of those expected to occur in the North Sea chalk oil fields. The second set of sixteen experiments (with the prefix NEOC) used broadly similar samples chosen because they exhibit specific depositional and diagenetic fabrics. Vertical effective stresses of approximately 2.4, 14, 24 and 36MPa were applied in the second set of experiments followed by unloading of the sample (still under uniaxial conditions) to a vertical effective stress of 14MPa. The second experimental programme was designed to extend the original permeability data set and define the degree of permeability recovery that might be expected if pressure maintenance in the reservoir was introduced. An additional permeability determination was also introduced at a low effective stress in the latter experiments to establish whether the higher permeabilities, recorded from routine tests, using the methods described above, were the result of using low confining stresses.

Displacement rates were adjusted, whilst maintaining the condition of uniaxial strain, so that excess pore pressures did not develop within the samples. When a vertical effective stress was attained at which a permeability determination was to be conducted the stresses were held constant. Constant axial and radial stresses were achieved by maintaining the same confining pressure, and slowing the loading rate down substantially until there was virtually no displacement during the period of the determination.

Different back pressures were established in the top and bottom volume gauges. The top pressure being approximately 0.5MPa higher so that when the top drainage line was opened to the sample, oil would flow through the sample under a constant pressure gradient. Flow was sustained for approximately 2 hours or until 30 pore volumes of fluid had passed through the sample. On completion of a permeability determination, the deformation experiment was resumed allowing the axial load to increase until the vertical effective stress required for the next permeability determination was attained. In both the experimental programmes one experiment was conducted at a temperature of 100 °C in order to investigate whether permeability was affected by temperature. All other determinations were made at ambient temperature ($\sim 23^{\circ}\text{C}$).

Hydraulic conductivities were determined using the relationship:-

$$Q = AkI \quad (5.1)$$

where Q is the volume of pore fluid passed per unit time, A is the cross sectional area of the sample, k is the hydraulic conductivity, and I is the difference in hydraulic head per unit length of the flow path.

Hydraulic conductivity in cm/sec is converted into absolute permeability using the relationship:-

$$K = k.\gamma/\rho \quad (5.2)$$

Where K is the absolute permeability, γ is the viscosity of the pore fluid, and ρ is the density of the pore fluid.

Table 5.2.

VALUES TAKEN FOR THE VISCOSITY AND DENSITY OF THE HYDROCARBON USED AS THE PERMEANT.

TEMPERATURE (centipoise)	γ VISCOSITY (gm/cc)	ρ DENSITY
Ambient Temp.	8.00	0.86
100°C.	0.22	0.42

To convert from K in cm to millidarcies, a factor of 1.013×10^{11} was used (Lambe and Whitman, 1979).

In reservoir evaluation, it is generally considered that horizontal permeability is a more important variable than vertical permeability. Unfortunately, the apparatus used in this study does not permit the determination of permeability normal to the axis of the sample and, because of the restored-state stress system employed, all plugs have to be cut with their long axes in the natural vertical orientation. Equipment currently under construction in our laboratory has been designed to permit determination of both vertical and horizontal permeabilities in a vertically orientated whole core sample under uniaxial strain conditions.

5.6. SAMPLE MORPHOLOGY.

It can be seen from table 5.3 that the distribution of porosities (18.7-41.4%) exhibited by the samples chosen, spans the volumetrically important part of the porosity range encountered in the reservoirs (10-45%). The samples prepared for testing contained a number of post-depositional features, including, healed, partially open and open fractures with various orientations; stylolitic fractures; solution seams; clay seams; and stylolites. Samples which contain natural discontinuities cause difficulties during preparation and are therefore not normally selected for routine analysis. In this study

these materials were deliberately sampled to determine whether the various fabric elements effect the permeability of the samples.

Table 5.3.

PERMEABILITY EXPERIMENTAL DATA.

EXP.	Fm.	POROSITY	EXP.	Fm.	POROSITY
No.		%	No.		%
NHEC2B	U.EKO.	31.0	NEOC8	U.EKO.	41.4
NHEC3B	U.EKO.	35.9	NEOC9	U.EKO.	36.2
NHEC6	L.EKO.	36.5	NEOC11	M.TOR	18.7
NHEC10	L.EKO.	37.5	NEOC12	U.EKO.	26.0
NHEC21B	U/M.TOR	19.0	NEOC14	L.EKO.	37.8
NHEC24	U.EKO.	27.5	NEOC15	L.EKO.	28.1
NHEC1	U.EKO.	40.8	NEOC16	U.TOR	19.0
NHEC5	U.EKO.	28.9	NEOC17	L.EKO.	22.8
NEOC18	L.EKO.	25.5			
NEOC1	U.EKO.	28.5	NEOC19	U.EKO.	33.4
NEOC3	U.EKO.	32.1	NEOC21	M.TOR	31.9
NEOC6	L.EKO.	37.9	NEOC22	L.EKO.	30.6
NEOC7	U.TOR	35.3			

5.7. EXPERIMENTAL RESULTS.

In this section each experiment is represented by a photograph of the sample, an annotated drawing, a graph of the determined permeability plotted against mean effective stress and the vertical effective stress/axial strain curve. The permeability/mean effective stress and vertical effective stress/axial strain graphs are plotted to common scales to enable comparisons between samples to be made.

- *NHEC1. (figure 5.1)*

Formation: Upper Ekofisk.

Initial porosity: 40.8%.

Sample morphology: Featureless.

Changes in permeability: This sample was tested for comparative purposes. All determinations were made after the sample had passed its yield stress. Permeability increased between 15MPa (0.2708mD) and 24MPa (0.2815mD) and then decreased to 0.2129mD when loaded to 30MPa.

- *NHEC2B. (figure 5.2)*

Formation: Upper Ekofisk.

Initial porosity: 31.0%.

Sample morphology: Slump facies; inclined healed fractures.

Changes in permeability: At the initial reservoir stress, the permeability was determined as 0.3028mD. Loading to a stress just above the maximum effective stress (36MPa) expected in the reservoir resulted in a slight increase in permeability to 0.3363mD. The sample was observed to fail during the latter determination. Additional loading led to a decrease in permeability, until at 112MPa it had increased to 0.2142mD. Although the sample was subject to a large increase in vertical effective stress, the change in permeability, particularly prior to failure were small.

NHEC1: U. Ekofisk Fm., Depth 3165.3m, Featureless chalk.

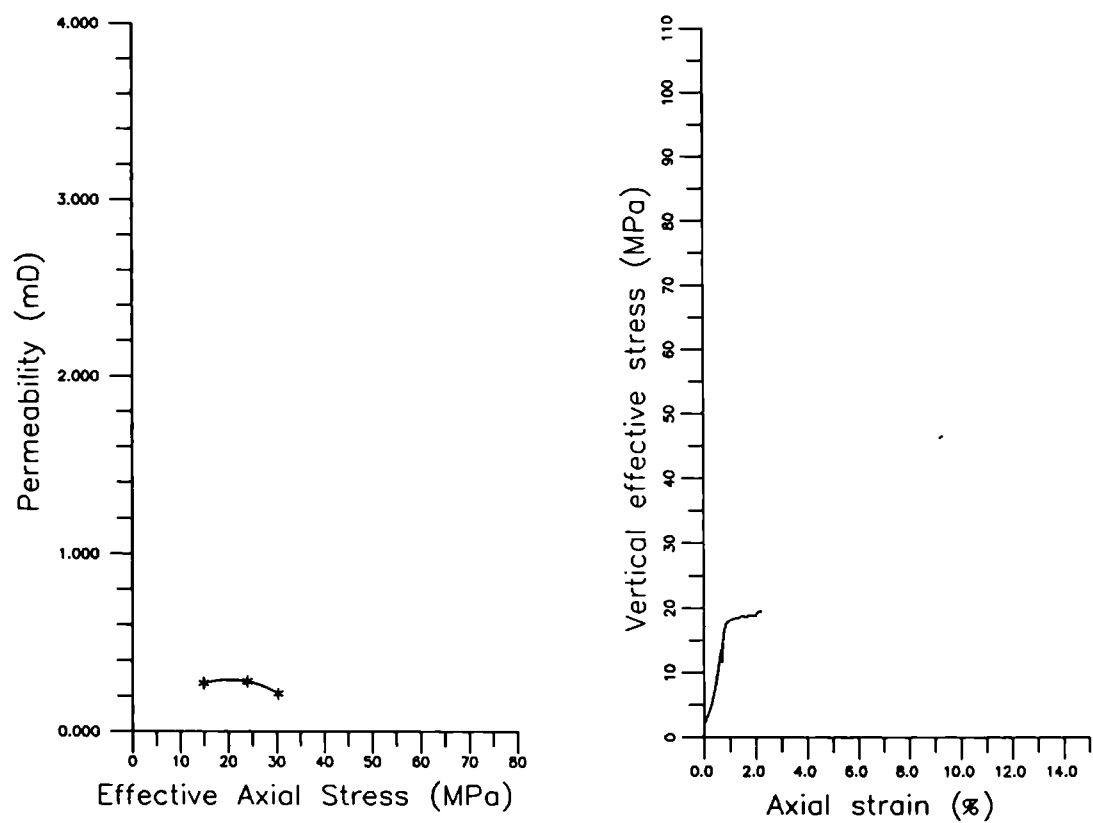
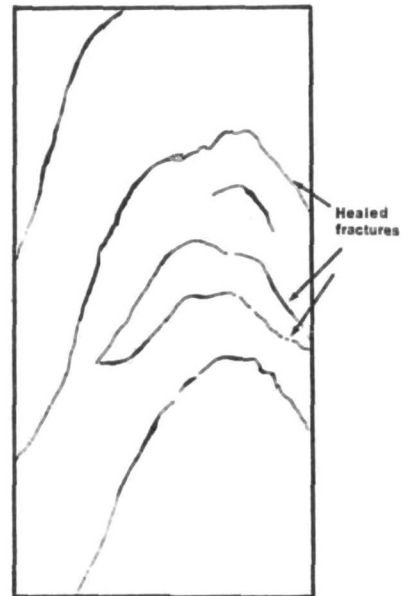
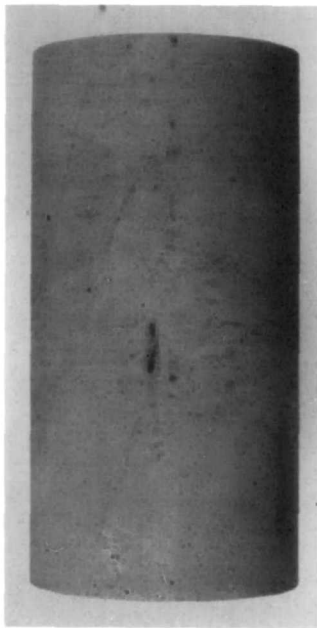


Figure. 5.1. Data sheet for permeability experiment NHEC1.



NHEC2B: U. Ekofisk Fm., Depth 3135.4m, Slumped, bioturbated, homogeneous chalk.

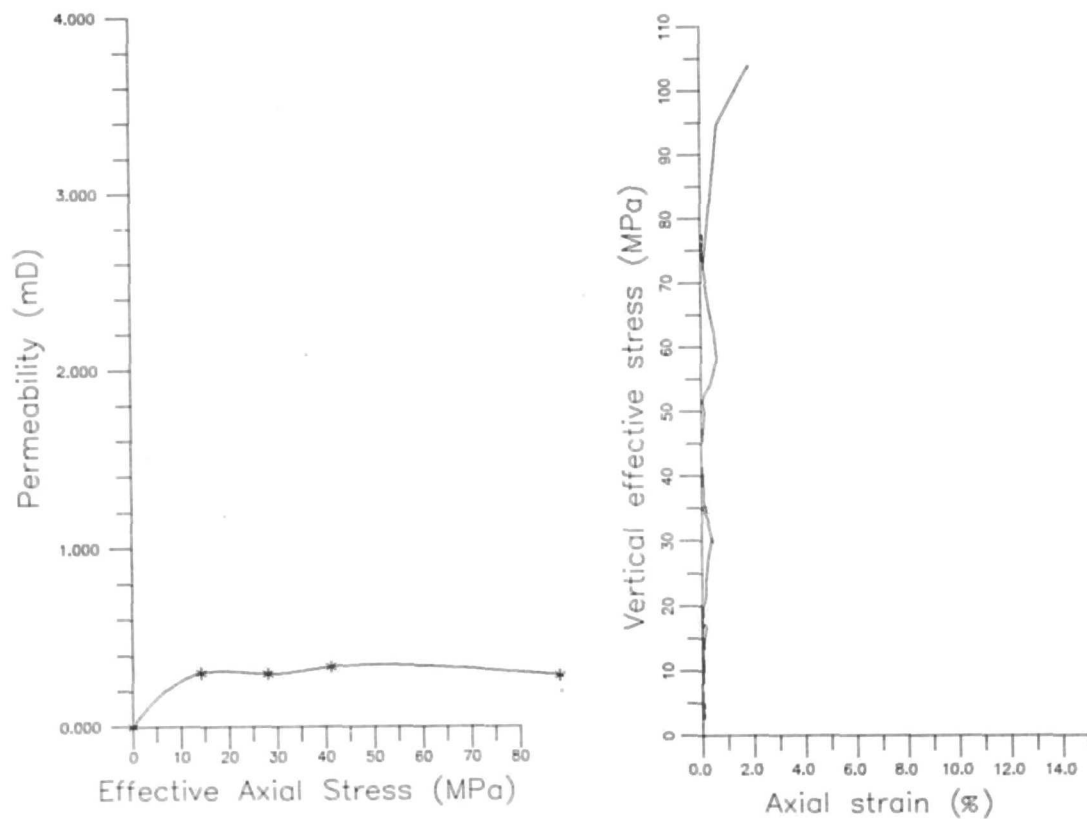


Figure. 5.2. Data sheet for permeability experiment NHEC2B.

Note: The photographs and annotated drawings of the samples are not necessarily in the same orientation.

- *NHEC3B. (figure 5.3)*

Formation: Upper Ekofisk.

Initial porosity: 35.9%.

Sample morphology: Slump facies; weak clay filled stylolites; two early vertical healed fractures.

Changes in permeability: During loading this sample showed only a slight decrease in permeability from 0.6388mD at 14.8MPa to 0.5967mD at 37.4MPa.

- *NHEC5. (figure 5.4)*

Formation: Upper Ekofisk.

Initial porosity: 28.9%.

Sample morphology: Featureless.

Changes in permeability: This sample was tested for comparative purposes. All permeability determinations were performed at stresses below the sample's yield stress. A remarkably high permeability of 2.1443mD was recorded for such a low porosity sample. During loading permeability increased to 2.5464mD at 24MPa, but decreased dramatically thereafter to 0.7801mD at 49MPa.

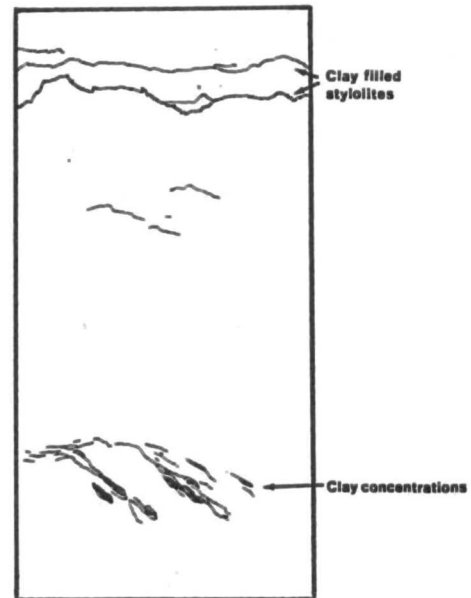
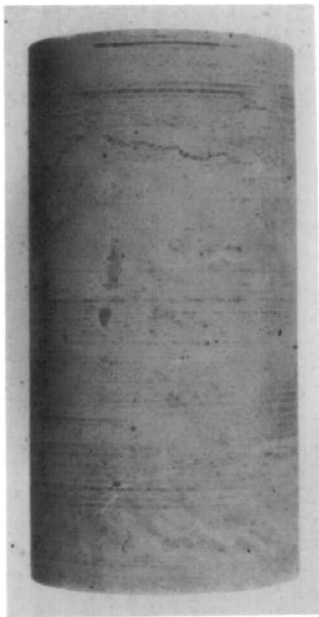
- *NHEC6. (figure 5.5)*

Formation: Lower Ekofisk.

Initial porosity: 36.5%.

Sample morphology: Clay filled stylolites; stylolitic fractures; inclined healed fractures.

Changes in permeability: Permeability decreased throughout the experiment and the rate of decrease was observed to accelerated following yield. The first determination was performed at a vertical effective stress of 14.5MPa (0.6365mD) and the final determination was made at 50.8MPa (0.3635mD). The closing of fractures, particularly the stylolitic ones, appears to have played a significant part in the permeability decreases recorded.



NHEC3B: U. Ekofisk Fm., Depth 3145.8m, Slumped chalk.

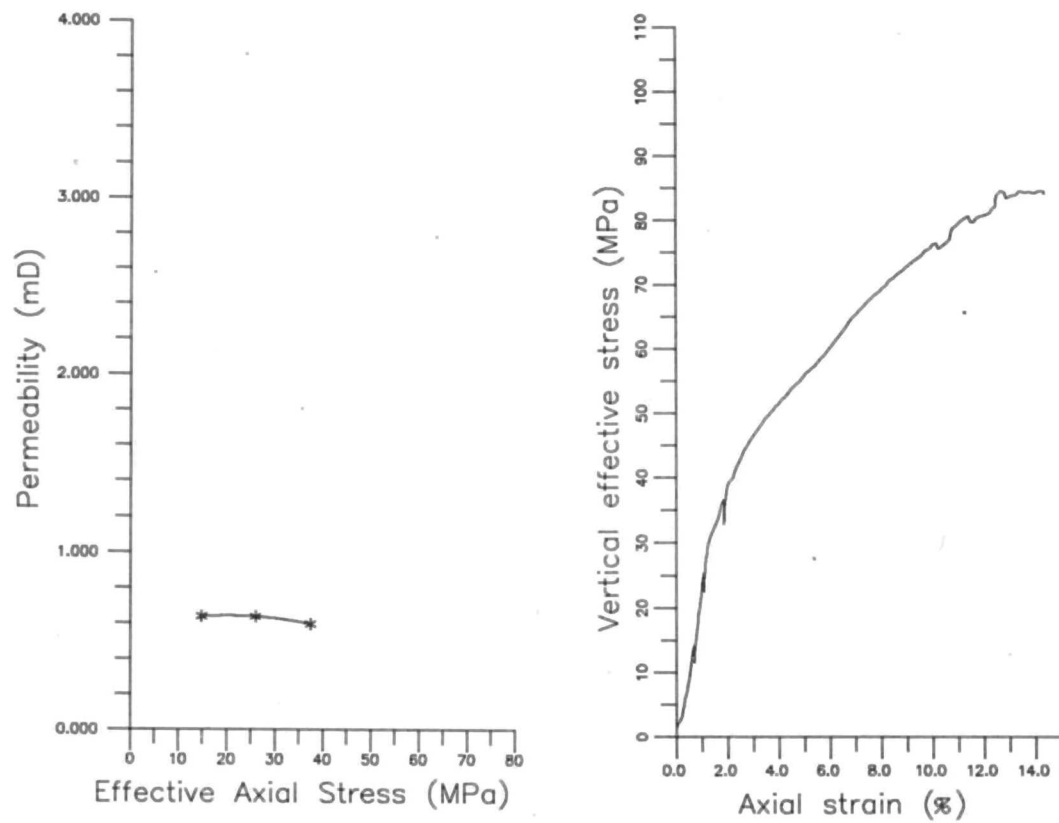


Figure. 5.3. Data sheet for permeability experiment NHEC3B.

NHEC5: U. Ekofisk Fm., Depth 3126.2m, Featureless chalk.

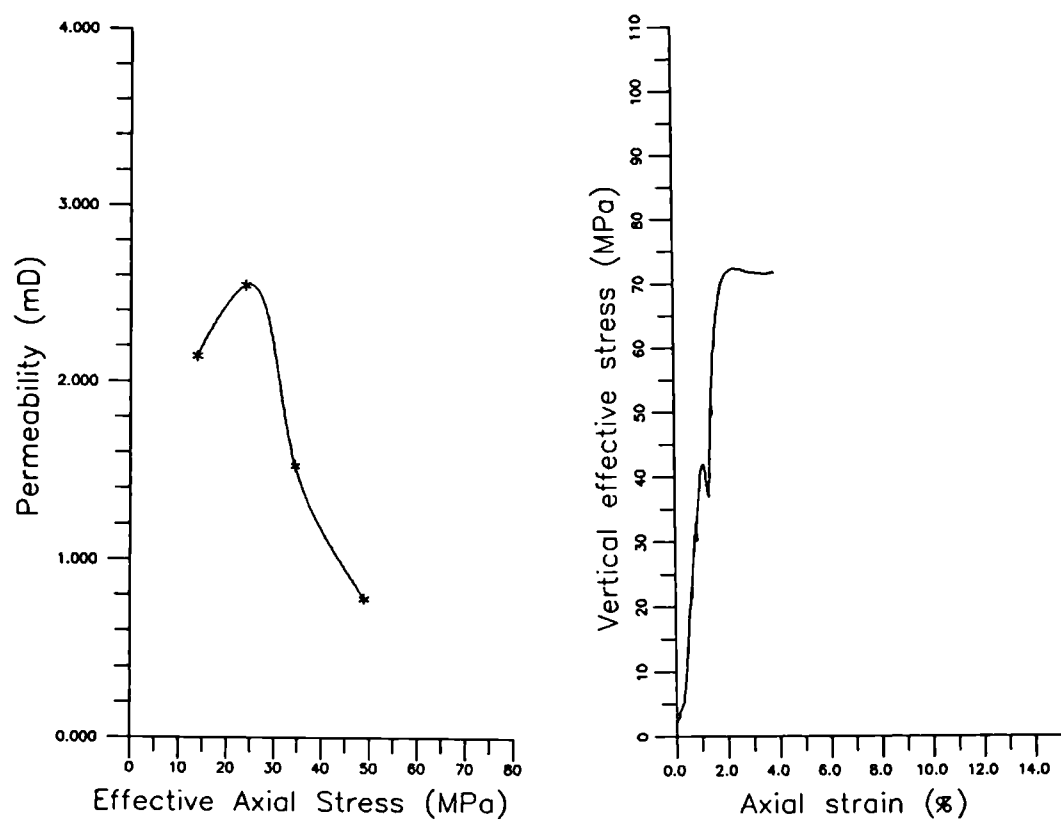
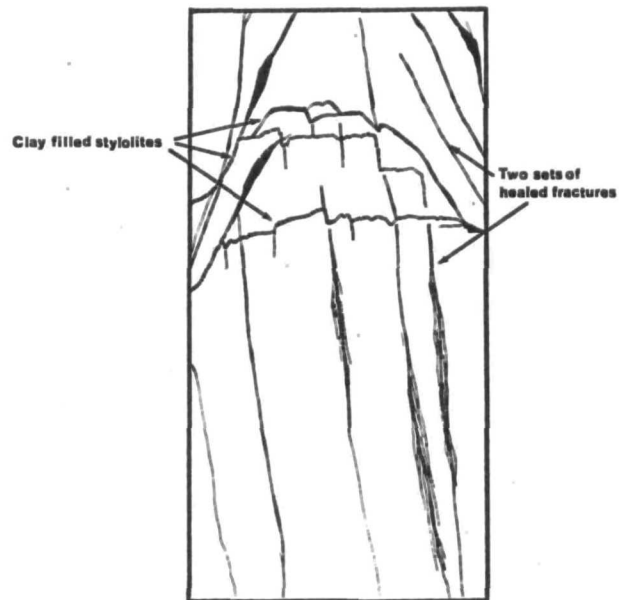
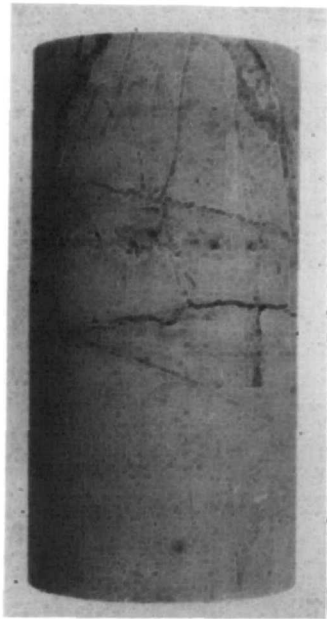


Figure. 5.4. Data sheet for permeability experiment NHEC5.



NHEC6: L. Ekofisk Fm., Depth 3176.1m, Homogeneous chalk.

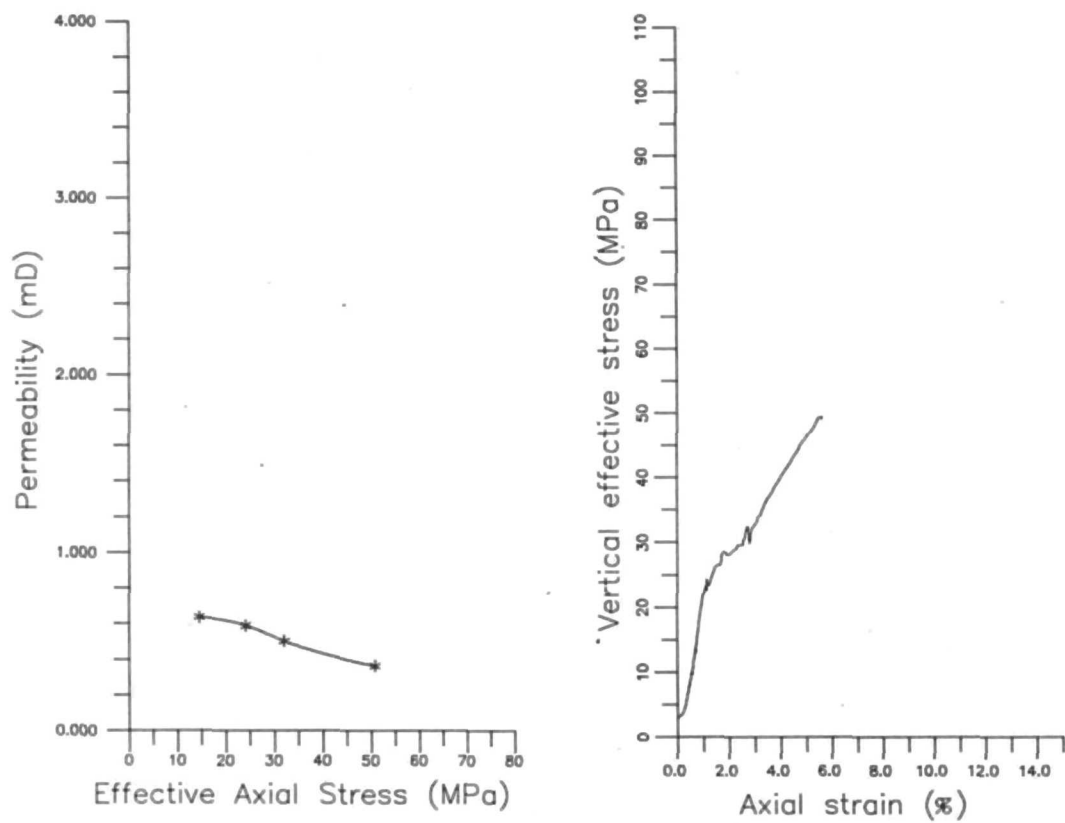


Figure. 5.5. Data sheet for permeability experiment NHEC6.

- ***NHEC10. (figure 5.6)***

Formation: Lower Ekofisk.

Initial porosity: 37.5%.

Sample morphology: Slump facies; one clay filled stylolite; conjugate healed fractures; minor stylolitic fractures; occasional open vertical fractures.

Changes in permeability: This highly fractured sample suffered a significant decrease in permeability during the experiment. At 14MPa the permeability was determined as 3.263mD, the highest value recorded from any sample used in this study. At 24MPa the permeability had fallen dramatically to 1.84mD. At the final expected reservoir vertical effective stress of 37.7MPa the permeability had decrease still further to 1.002mD. Yield occurred between the second and third determinations.

- ***NHEC21B. (figure 5.7)***

Formation: Middle/Upper Tor.

Initial porosity: 19.0%.

Sample morphology: Debris flow; four weak horizontal stylolites; one inclined healed fracture.

Changes in permeability: This low porosity sample remained elastic throughout the experiment and had a correspondingly low permeability which showed little change from an initial value of 0.0306mD to a final value (at 69.5MPa) of 0.0357mD.

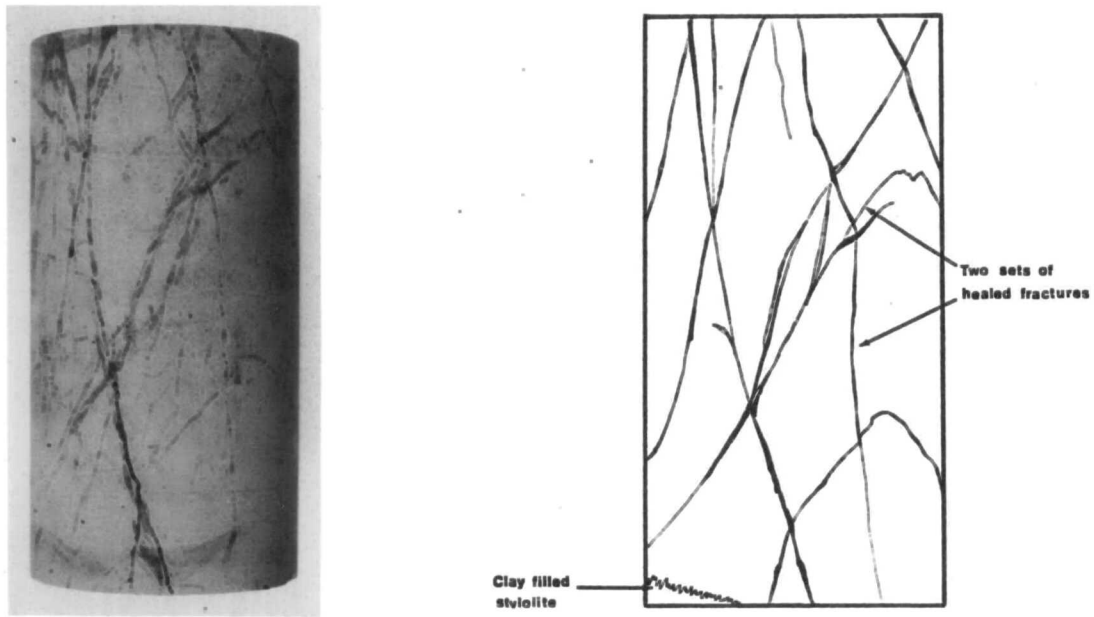
- ***NHEC24. (figure 5.8)***

Formation: Upper Ekofisk.

Initial porosity: 27.5%.

Sample morphology: Debris flow; two sets of steeply inclined healed fractures.

Changes in permeability: The closure of the inclined fractures led to a decrease in permeability during loading from 0.8556mD (15.65MPa) to 0.7822mD (26.7MPa). A slight increase in permeability (0.7959mD) was recorded at 40MPa which may have been due to yielding of the sample.



NHEC10: L. Ekofisk Fm., Depth 3184.5m, Slumped chalk.

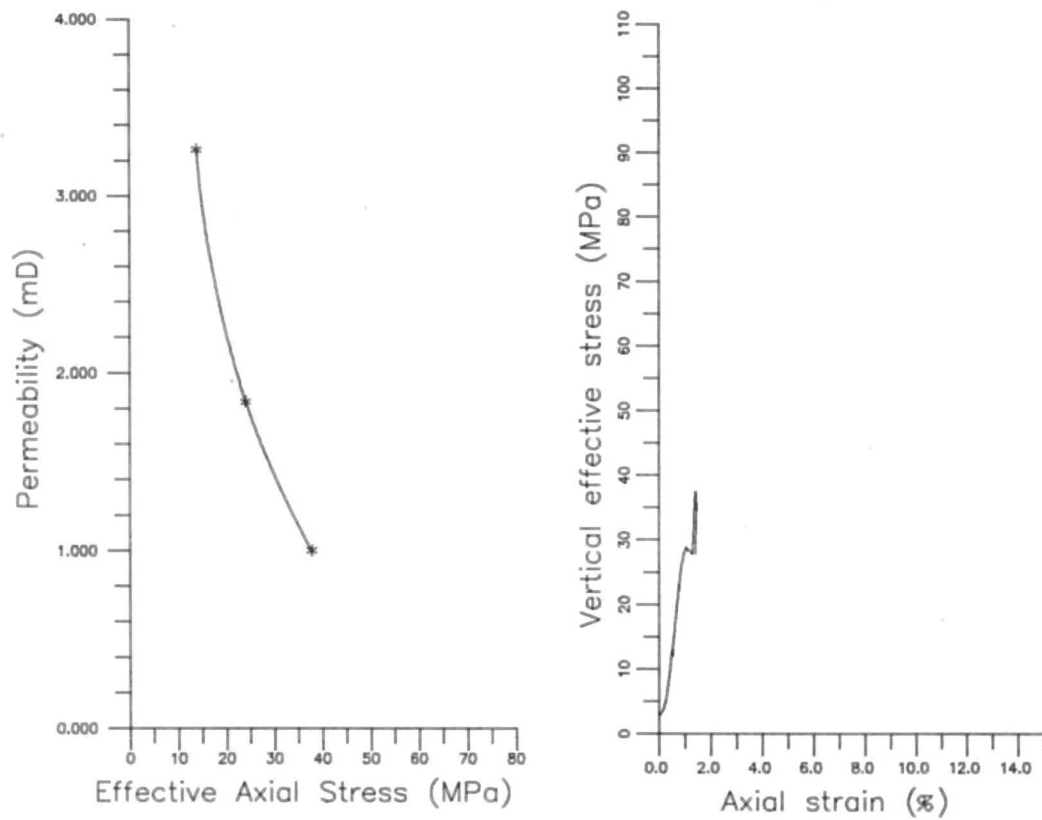
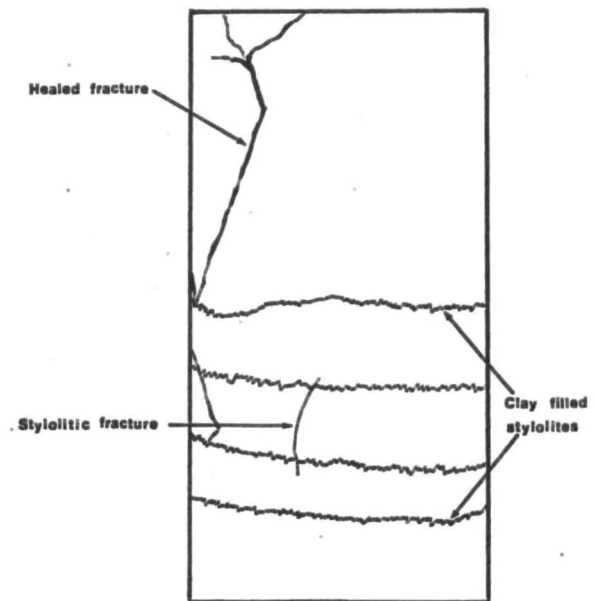
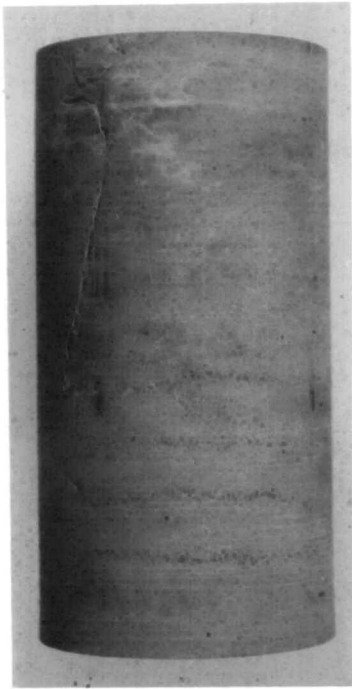


Figure. 5.6. Data sheet for permeability experiment NHEC10.



NHEC21B: M. Tor Fm., Depth 3274.0m, Debris flow.

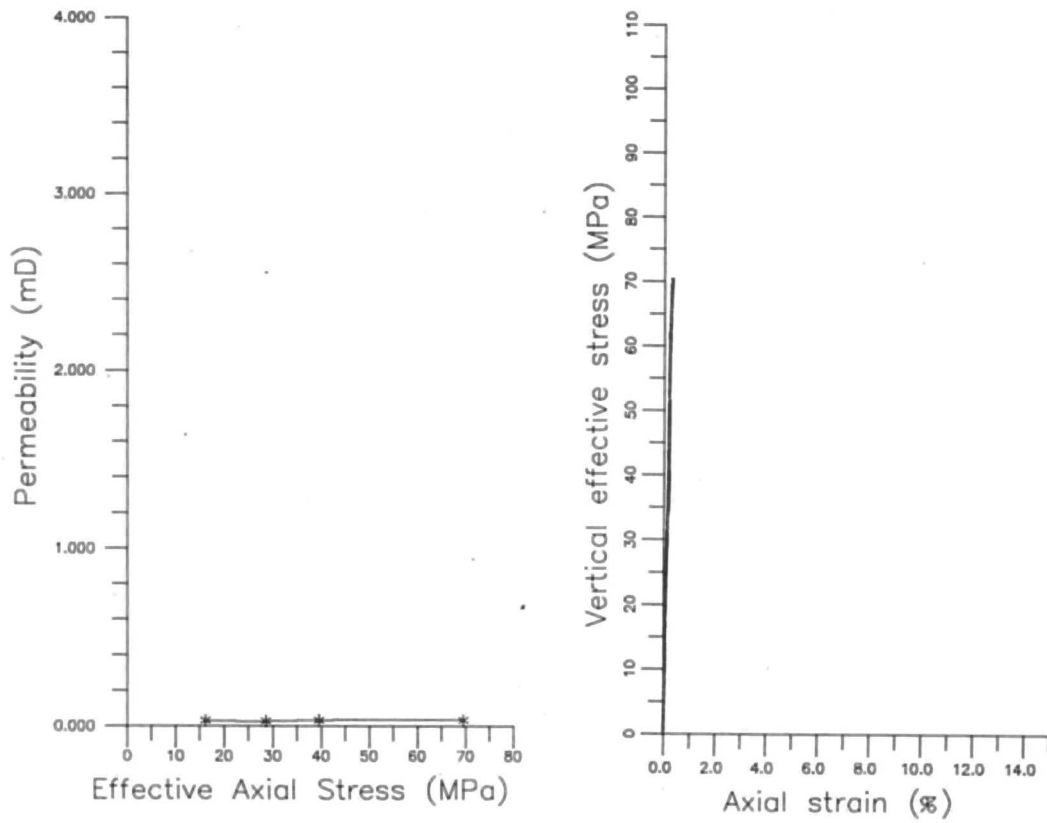
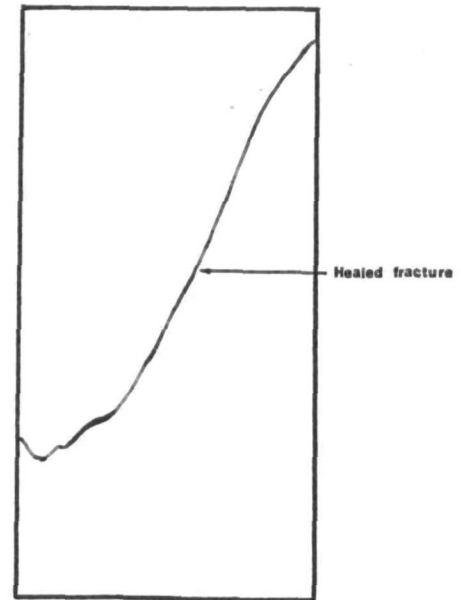
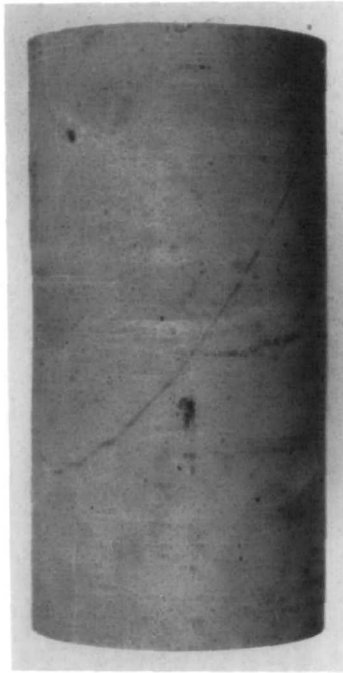


Figure. 5.7. Data sheet for permeability experiment NHEC21B.



NHEC24: U. Ekofisk Fm., Depth 3124.5m, Debris flow.

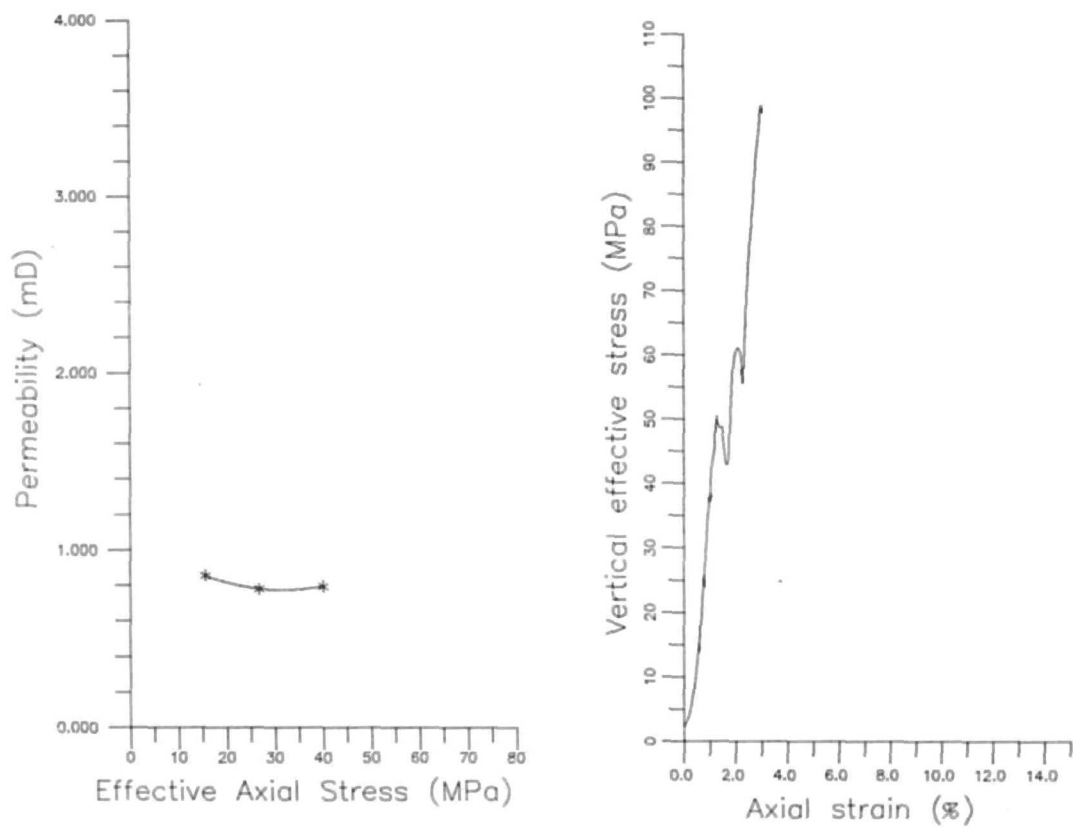


Figure. 5.8. Data sheet for permeability experiment NHEC24.

- *NEOC1. (figure 5.9)*

Formation: Upper Ekofisk.

Initial porosity: 28.5%.

Sample morphology: Burrowed; vertical healed fractures.

Changes in permeability: A slight increase in permeability from 0.1368mD to 0.1384mD was detected as the initial reservoir vertical effective stress was attained. As the effective stress continued to increase, permeability decreased, until at 40MPa, when the sample appears to have failed, permeability had fallen to 0.128mD. During unloading, axial strain was not recovered and the permeability continued to decrease (0.1152mD).

- *NEOC3. (figure 5.10)*

Formation: Upper Ekofisk.

Initial porosity: 32.1%.

Sample morphology: One large open fracture at the top of the sample; short stylolite; four short vertical healed fractures.

Changes in permeability: This sample showed a dramatic loss of permeability (from 1.8mD to 1.0mD) upon reaching the initial reservoir stress conditions. This large reduction in permeability was due to the closure of the open fracture at the top of the sample. During further loading the permeability continued to decline. No permeability recovery was measured following unloading. The presence of the open fracture caused the sample, which had a moderate to low initial porosity to deform in a similar manner to that of a higher porosity chalk.

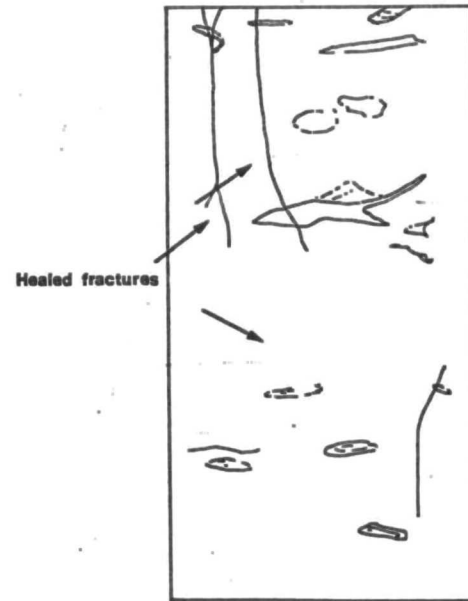
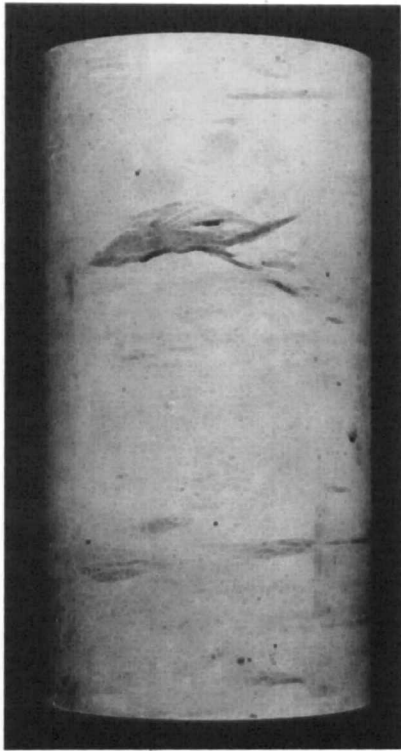
- *NEOC6. (figure 5.11)*

Formation: Lower Ekofisk.

Initial porosity: 37.9%.

Sample morphology: Highly fractured; numerous stylolites.

Changes in permeability: A high initial permeability was recorded for this sample (1.8359mD) which decreased to 1.7580mD at the initial reservoir effective stress conditions. Permeability continued to decrease throughout the experiment. The sample



NEOC1: U. Ekofisk Fm., Depth 3093.3m, Bioturbated chalk.

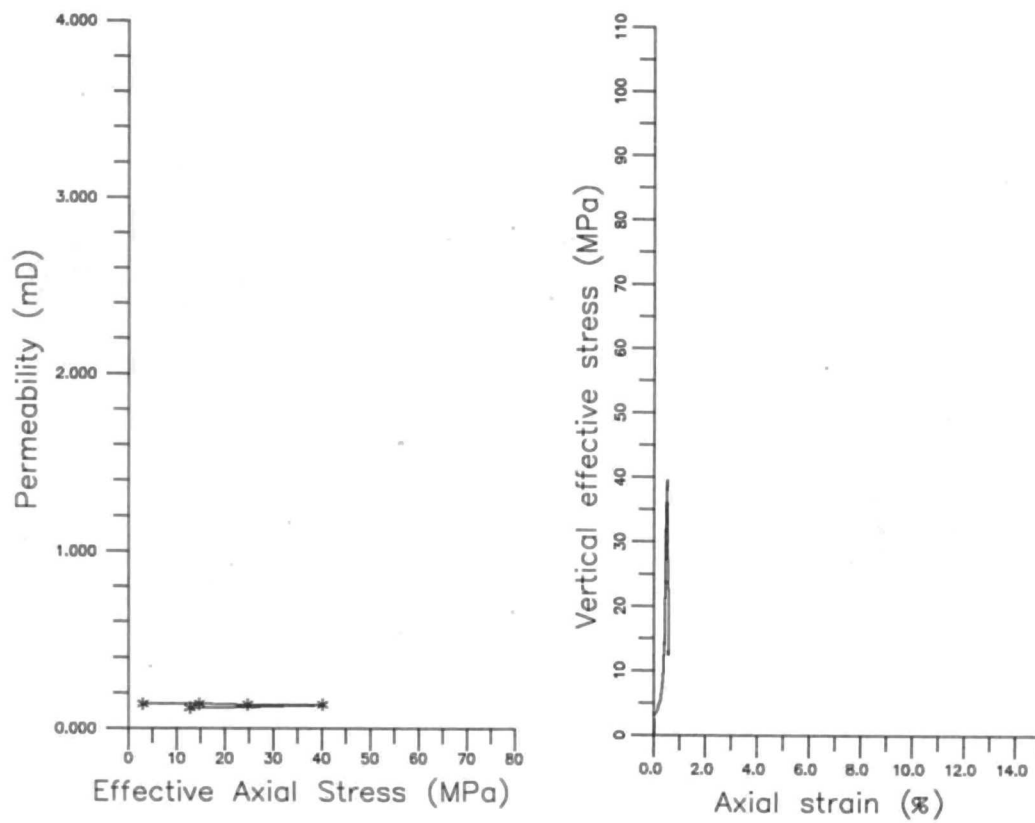
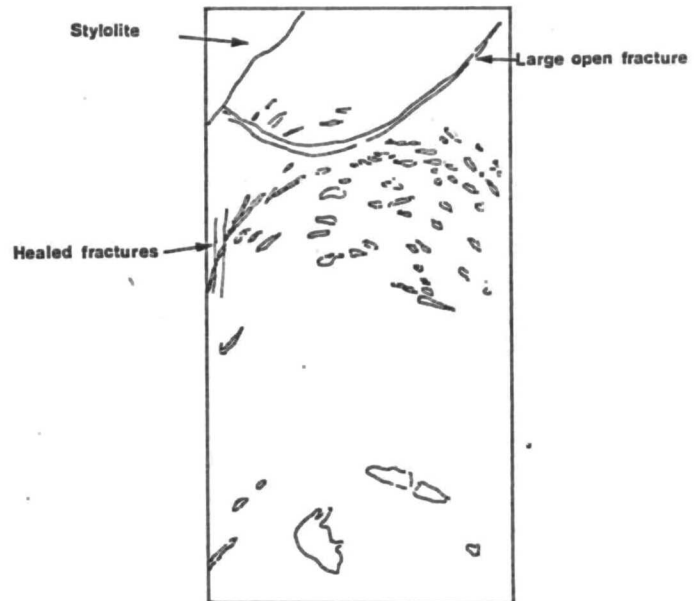


Figure. 5.9. Data sheet for permeability experiment NEOC1.



NEOC3: U. Ekofisk Fm., Depth 3126.6m, Steeply dipping periodite.

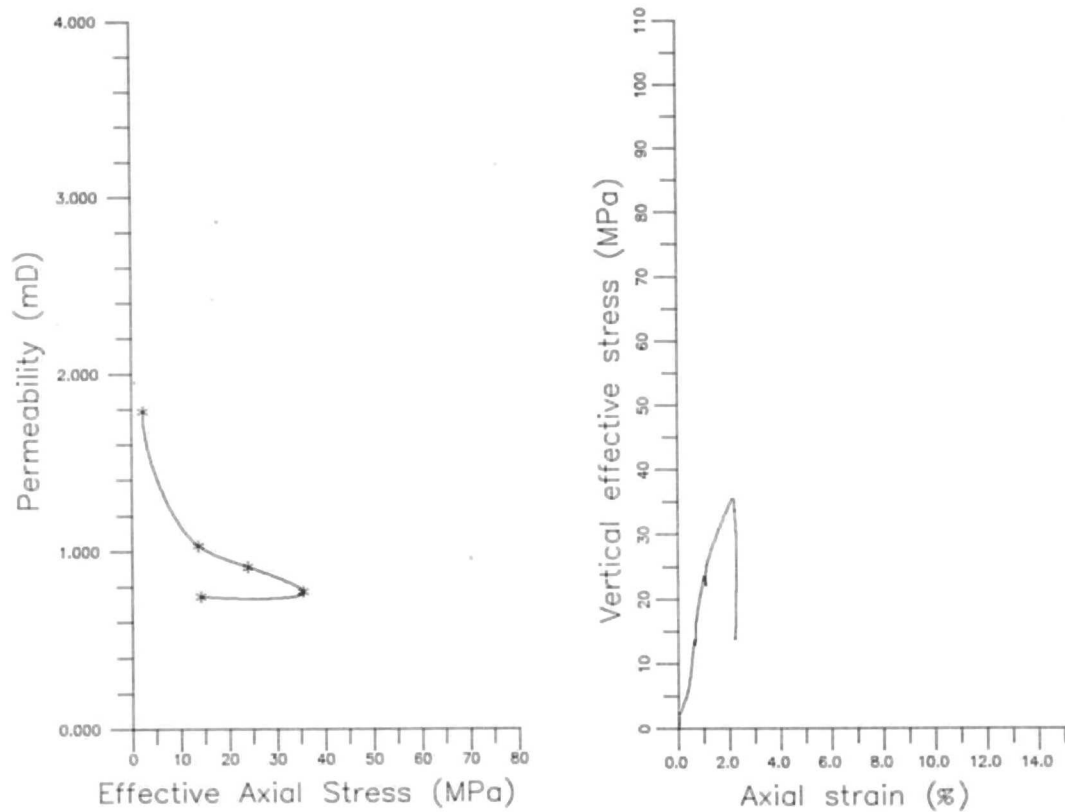
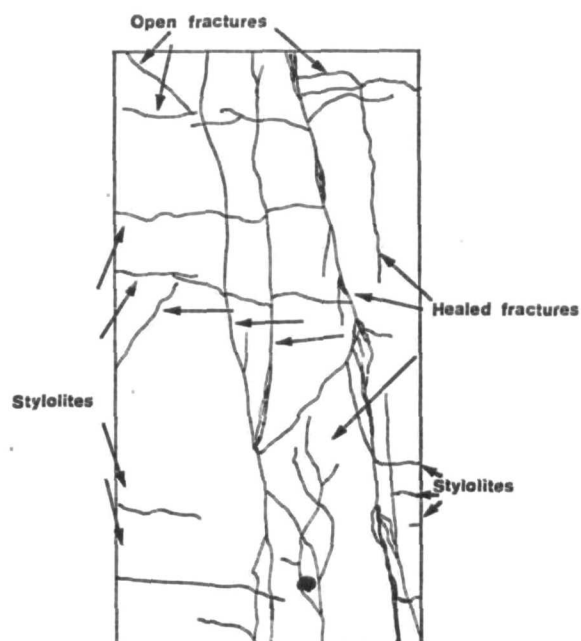
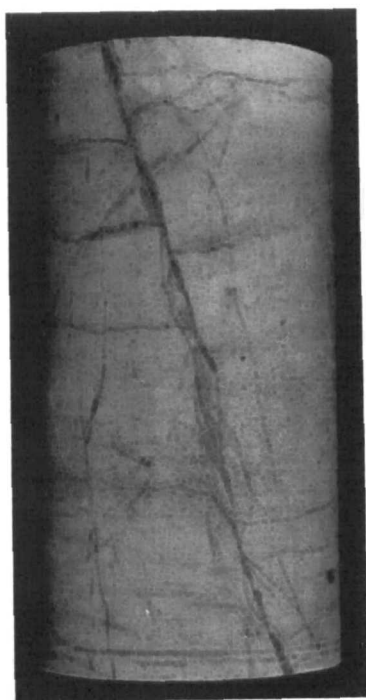


Figure. 5.10. Data sheet for permeability experiment NEOC3.



NEOC6: L. Ekofisk Fm., Depth 3201.3m, Featureless allochthonous chalk.

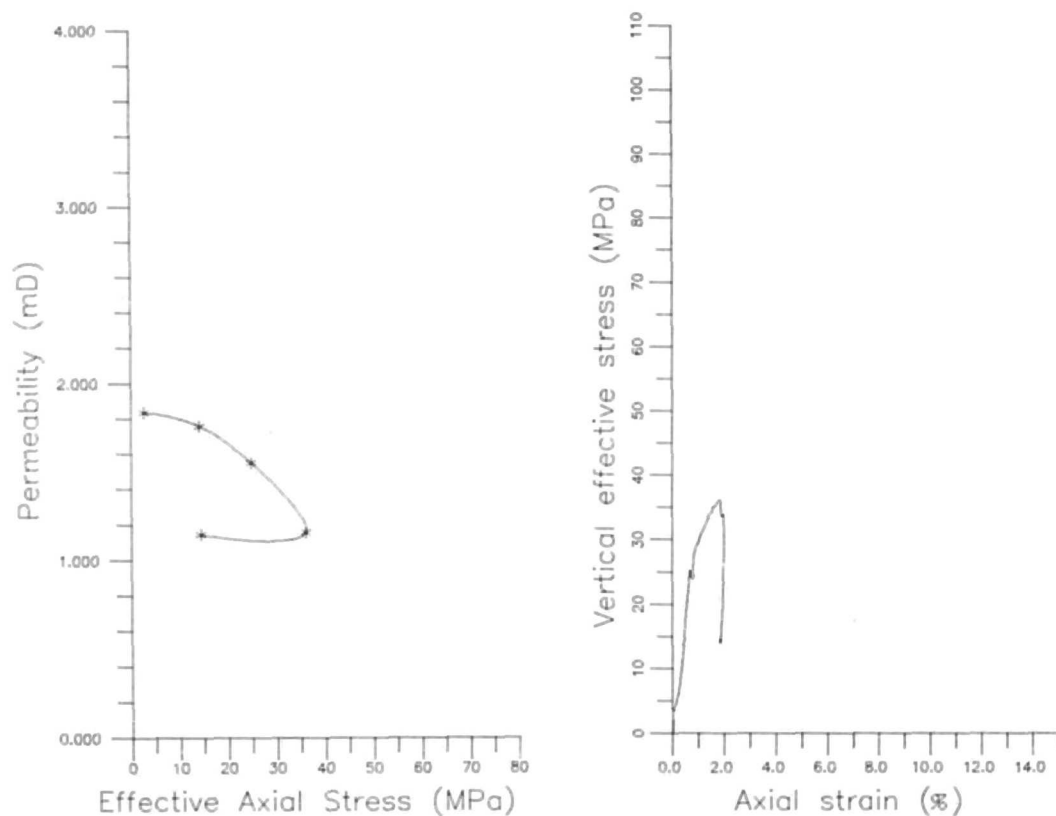


Figure 5.11. Data sheet for permeability experiment NEOC6.

was observed to yield at a vertical effective stress of approximately 24MPa. After yield, the rate of decrease in permeability increased. Very little change in permeability was observed during unloading. The high initial permeability was considered to be due to the presence of open vertical fractures. The presence of stylolites appears to have had no discernible affect on the samples permeability.

- *NEOC7 (figure 5.12)*

Formation: Upper Tor.

Initial porosity: 35.3%.

Sample morphology: Inclined healed fractures; thin inclined stylolites.

Changes in permeability: Permeability increased throughout the experiment from an initial value of 0.1046mD to 0.1458mD at 36MPa. Unloading resulted in a further increase to 0.1543mD.

- *NEOC8. (figure 5.13)*

Formation: Upper Ekofisk.

Initial porosity: 41.4%.

Sample morphology: Debris flow; single partially open fracture.

Changes in permeability: This high porosity sample showed a steady decrease in permeability from 1.035mD to 0.8417mD at 37MPa. After the onset of yield (approximately 16MPa) the rate of permeability loss was observed to increase. During the unloading part of the experiment the permeability recovered slightly to 0.8588mD.

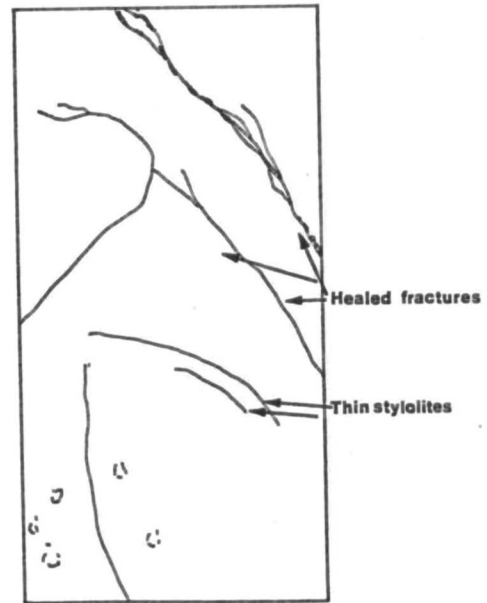
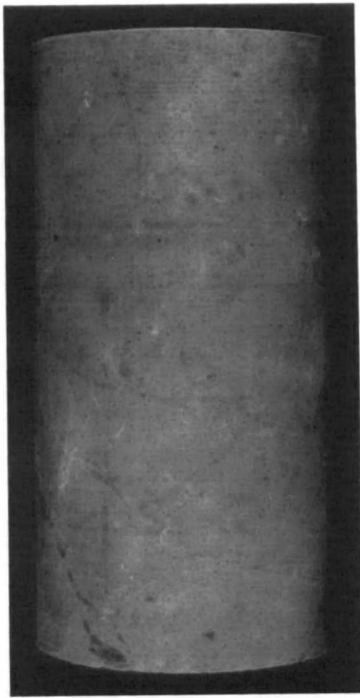
- *NEOC9. (figure 5.14)*

Formation: Upper Ekofisk.

Initial porosity: 36.2%.

Sample morphology: Debris flow; weak inclined healed and open fractures.

Changes in permeability: Very little change in permeability occurred between the initial value of 0.4969mD and that at 14MPa (0.5056mD). Permeability continued to in-



NEOC7: U. Tor Fm., Depth 3231.0m, Debris flow.

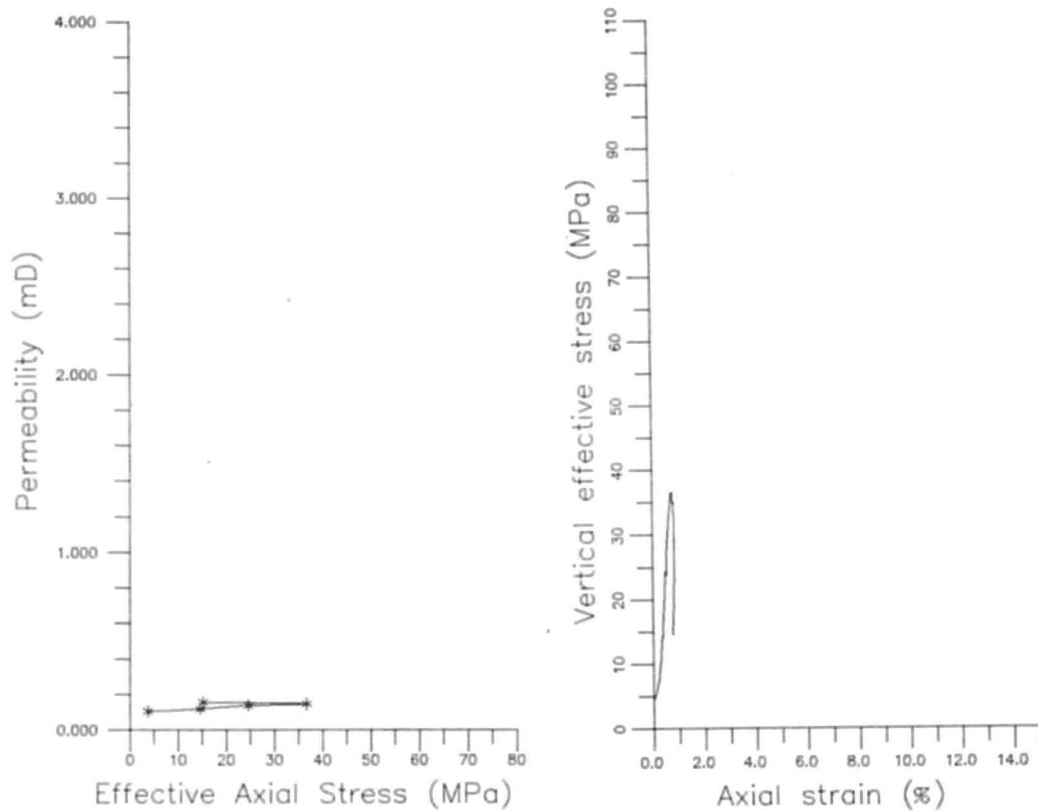
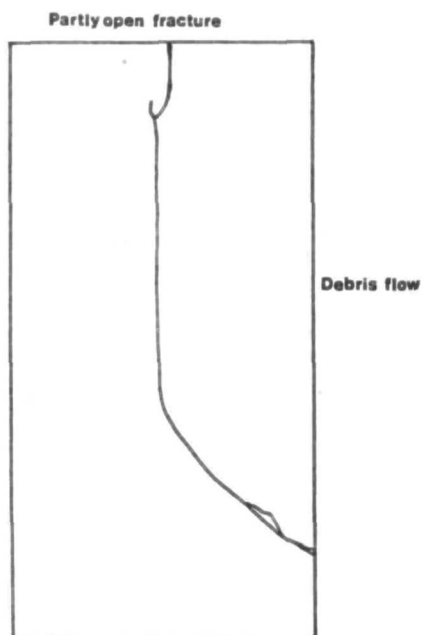
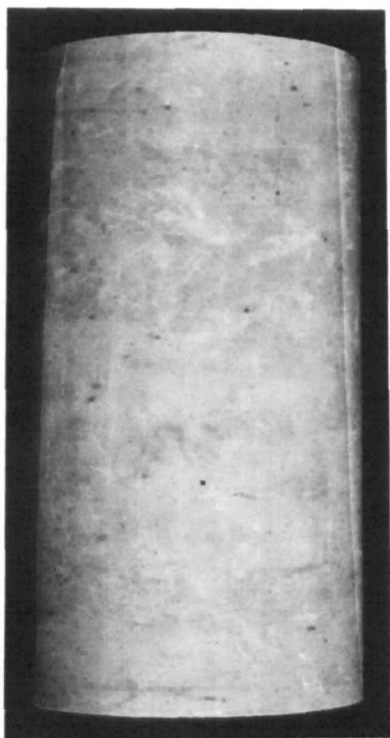


Figure. 5.12. Data sheet for permeability experiment NEOC7.



NEOC8: U. Ekofisk Fm., Depth 2931.4m, Debris flow.

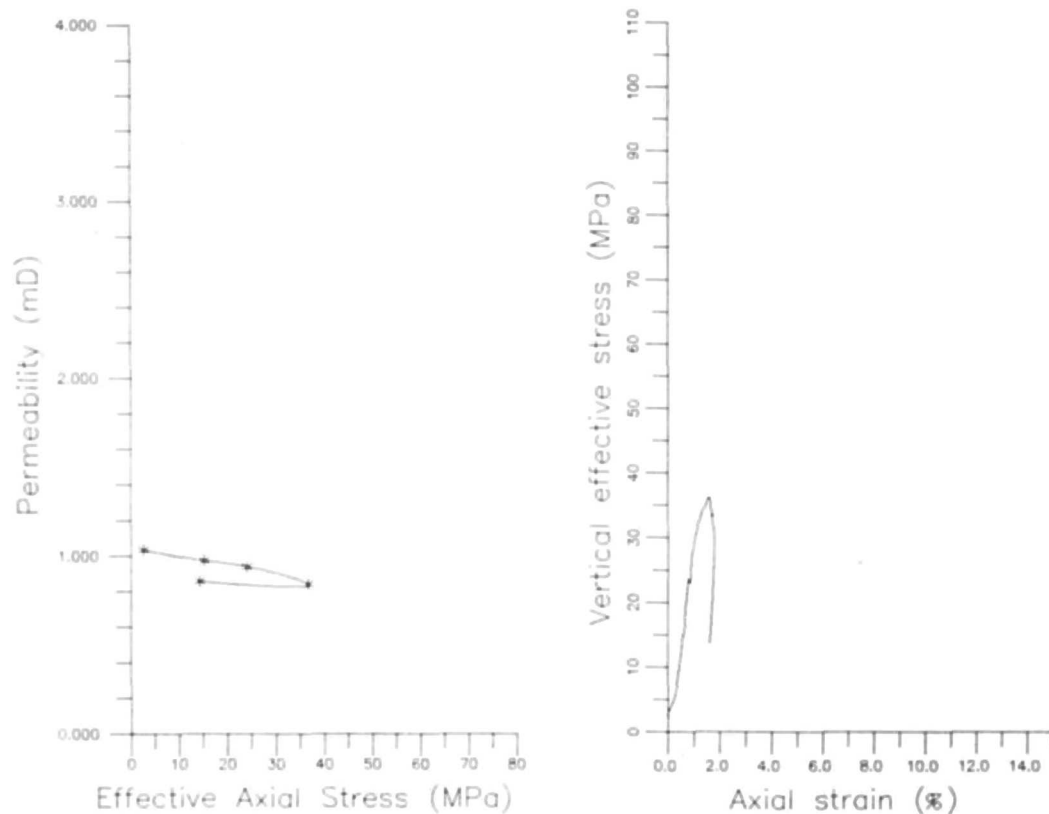
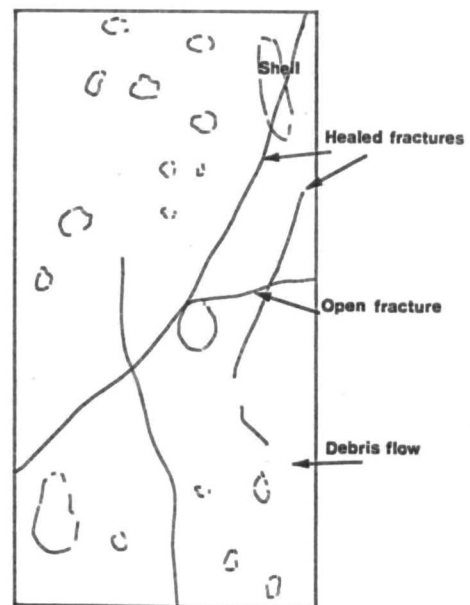


Figure. 5.13. Data sheet for permeability experiment NEOC8.



NEOC9: U. Ekofisk Fm., Depth 2966.6m, Debris flow.

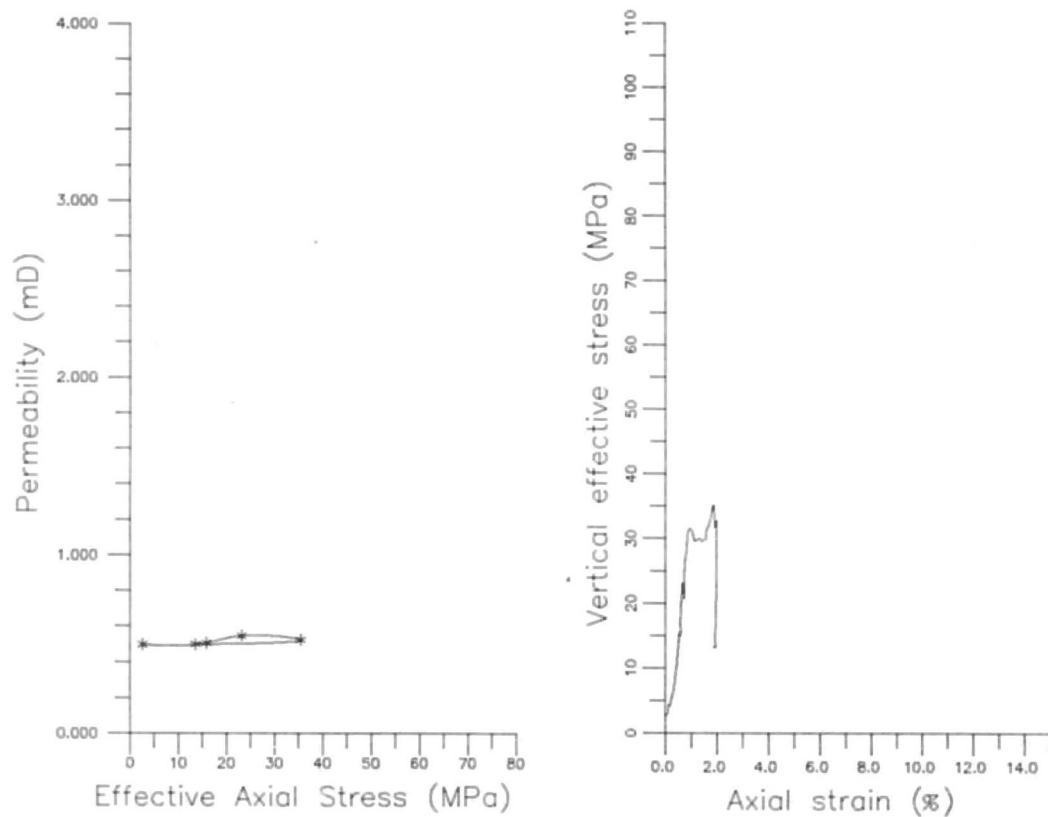


Figure. 5.14. Data sheet for permeability experiment NEOC9.

crease prior to yield (0.5465mD at 24MPa), but decreased afterwards (0.5237mD at 35.5MPa). Following unloading, the permeability increased to 0.4977mD.

- *NEOC11. (figure 5.15)*

Formation: Middle Tor.

Initial porosity: 18.7%.

Sample morphology: Debris flow; stylolites; stylolitic fractures.

Changes in permeability: This experiment failed before reaching the initial reservoir conditions. Only one determination was successfully achieved (0.0344mD at 2.4MPa).

- *NEOC12. (figure 5.16)*

Formation: Upper Ekofisk.

Initial porosity: 26.0%.

Sample morphology: Rare healed fractures; shell fragments.

Changes in permeability: This low porosity sample showed only small change in permeability during the experiment. A slight increase was detected during the initial stages (0.0372mD at 2.4MPa to 0.0510mD at 23MPa), followed by a decrease to 0.0257mD at 36MPa and a subsequent small recovery after unloading to 0.0273mD.

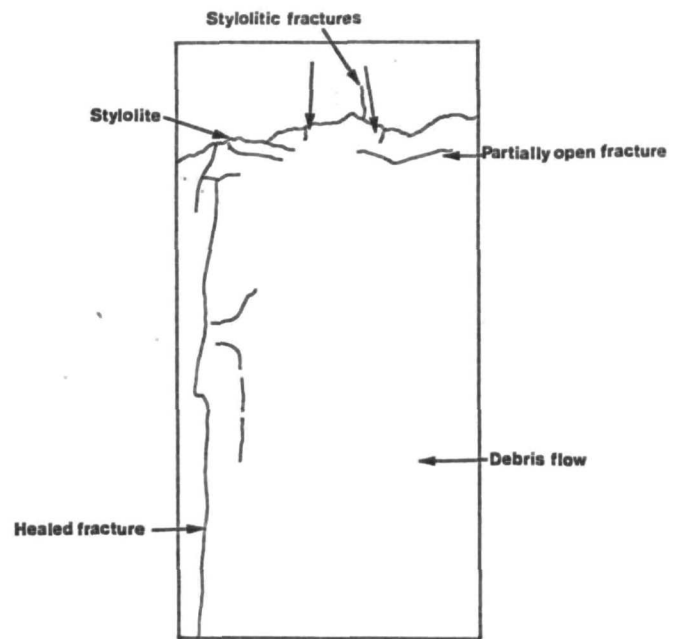
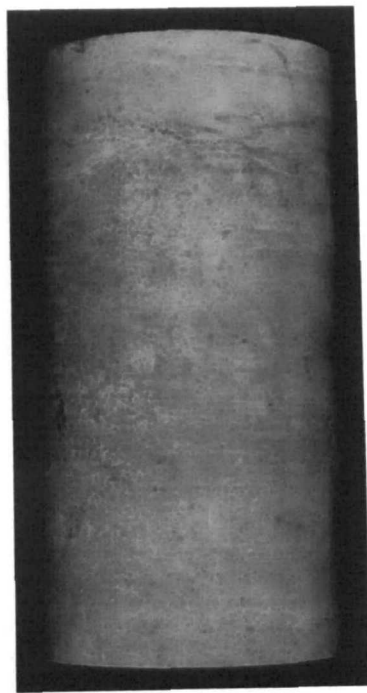
- *NEOC14. (figure 5.17)*

Formation: Lower Ekofisk.

Initial porosity: 37.8%.

Sample morphology: Debris flow and burrowed chalk; weak inclined healed fractures.

Changes in permeability: This medium porosity sample had a high initial permeability of 1.8788mD. During loading to pre-production reservoir effective stresses this increased to 1.9064mD. Thereafter as the vertical effective stress continued to increase, permeability decreased. Yield occurred at approximately 36MPa and was followed by a partial failure of the sample. This failure was recovered and the vertical effective stress continued to increase until a further permeability determination was conducted at 41.6MPa (1.4714mD). Neither yield or the partial failure appeared to influence the



NEOC11: Tor Fm., Depth 3207.6m, Debris flow.

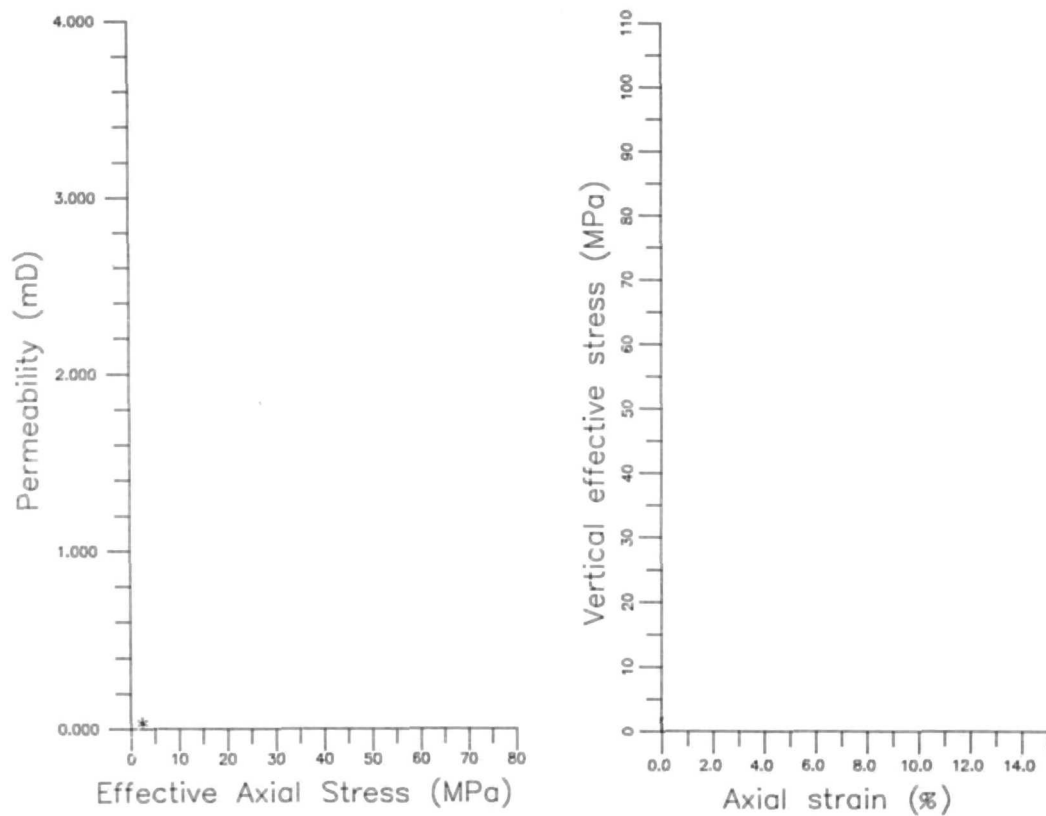
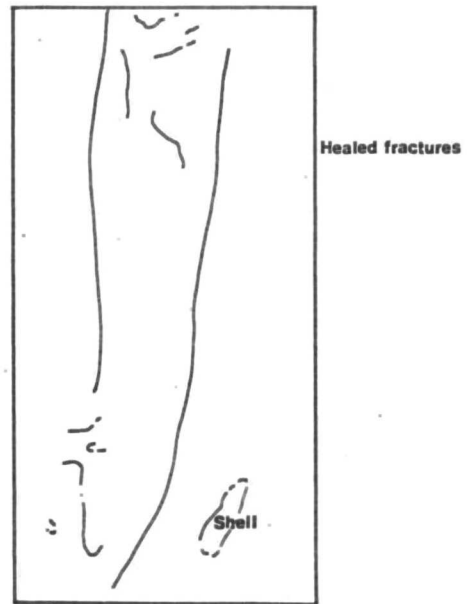
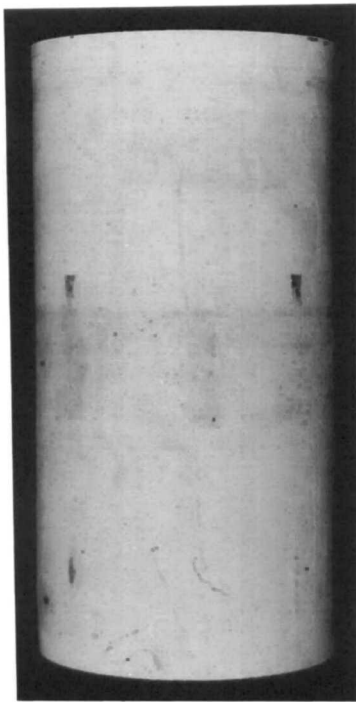


Figure. 5.15. Data sheet for permeability experiment NEOC11.



NEOC12: U. Ekofisk Fm., Depth 3146.3m, Bioturbated chalk.

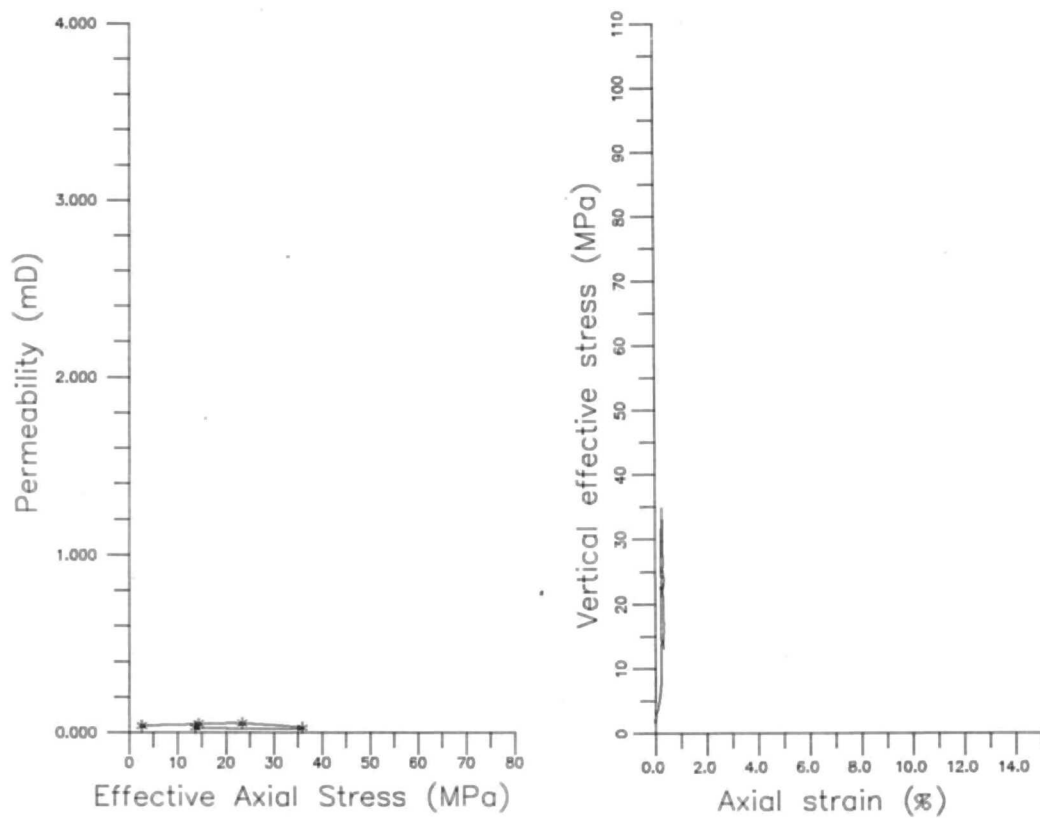
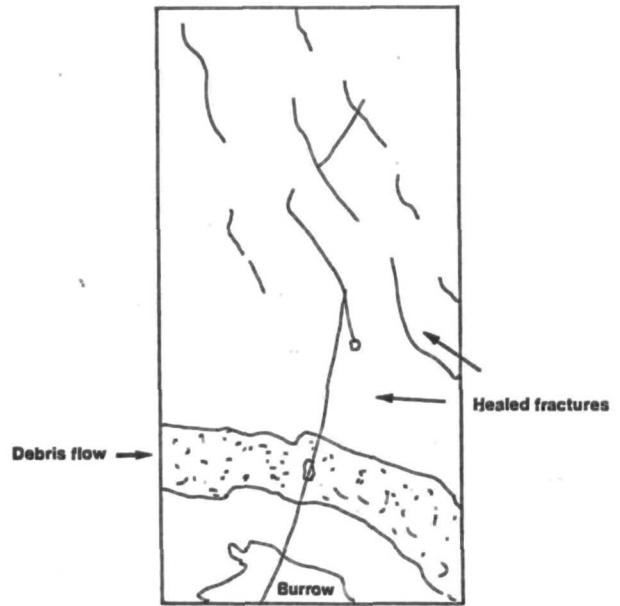
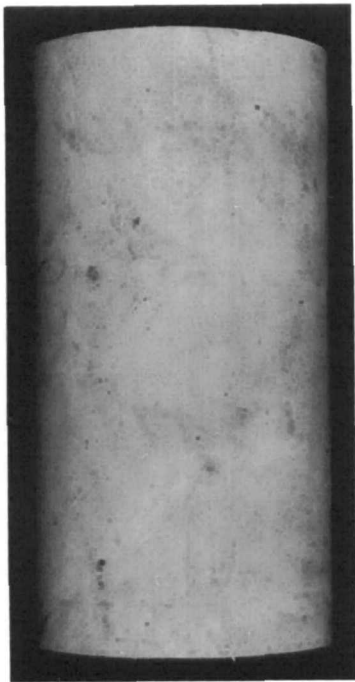


Figure. 5.16. Data sheet for permeability experiment NEOC12.



NEOC14 L. Ekofisk Fm., Depth 3197.4m, Bioturbated debris flow.

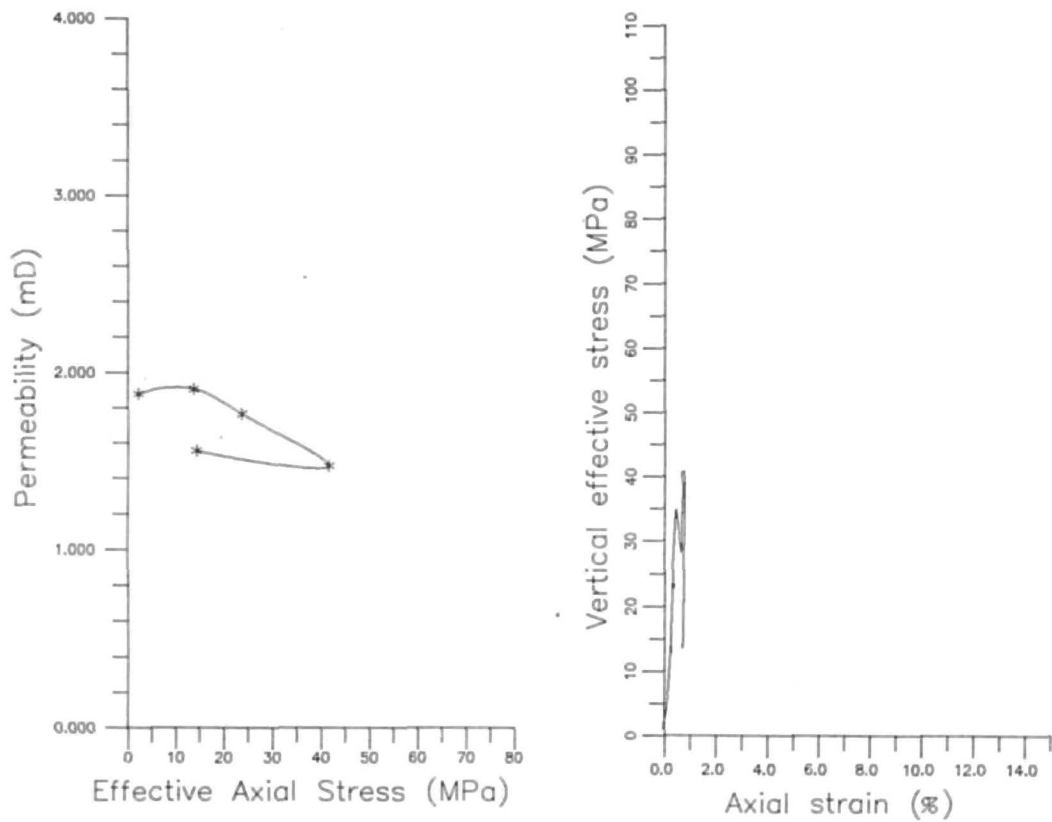


Figure. 5.17. Data sheet for permeability experiment NEOC14.

decline in permeability. However, following stress recovery to 14.3MPa an increase in permeability (1.5564mD) was recorded.

- *NEOC15. (figure 5.18)*

Formation: Lower Ekofisk.

Initial porosity: 28.1%.

Sample morphology: Plastic deformation.

Changes in permeability: This relatively low porosity sample displayed complicated changes in permeability throughout the experiment, which although small, cannot easily be explained. At 2.4MPa the permeability was determined as 0.1740mD. This increased to 0.2304mD at 14MPa but fell to 0.1666mD at 24MPa. At 36MPa the permeability had again decreased to 0.1518mD but the rate of decrease had reduced. Following unloading, permeability was observed to recover (0.1798mD) to a value slightly higher than the initial reading. The permeability/mean effective stress graph indicates that permeability recovery had the same gradient as the decline during the final stages of loading. As the sample contained a series of vertical and steeply inclined healed fractures, it is considered that movements of these fractures dictated the observed changes in permeability. Although the sample did not yield, it would appear, from the final permeability recovery, that some permanent deformation of the fractures, however small, must have occurred.

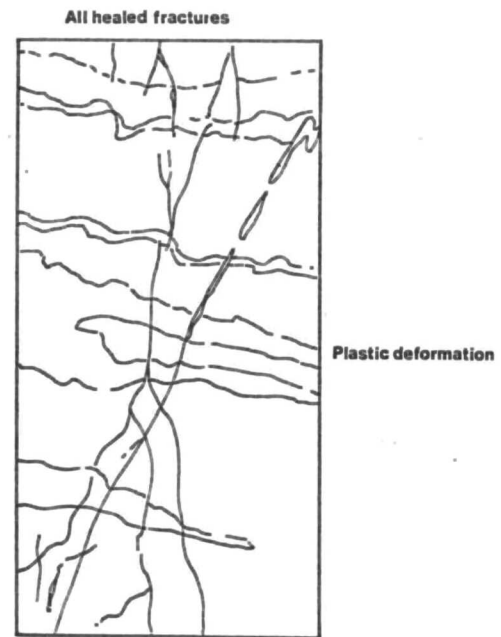
- *NEOC16. (figure 5.19)*

Formation: Upper Tor.

Initial porosity: 19.0%.

Sample morphology: Short inclined healed fractures; stylolites.

Changes in permeability: A low porosity sample in which vertical strain, throughout the applied stress range, was insignificant. However, although the sample was stiff the permeability changed. A gradual decrease occurred during loading from 0.0957mD (2.6MPa) to 0.0364mD (35.5MPa). Unloading to 14MPa resulted in a recovery of per-



NEOC15: L. Ekofisk Fm., Depth 3215.2m, Slumped, plastically deformed chalk.

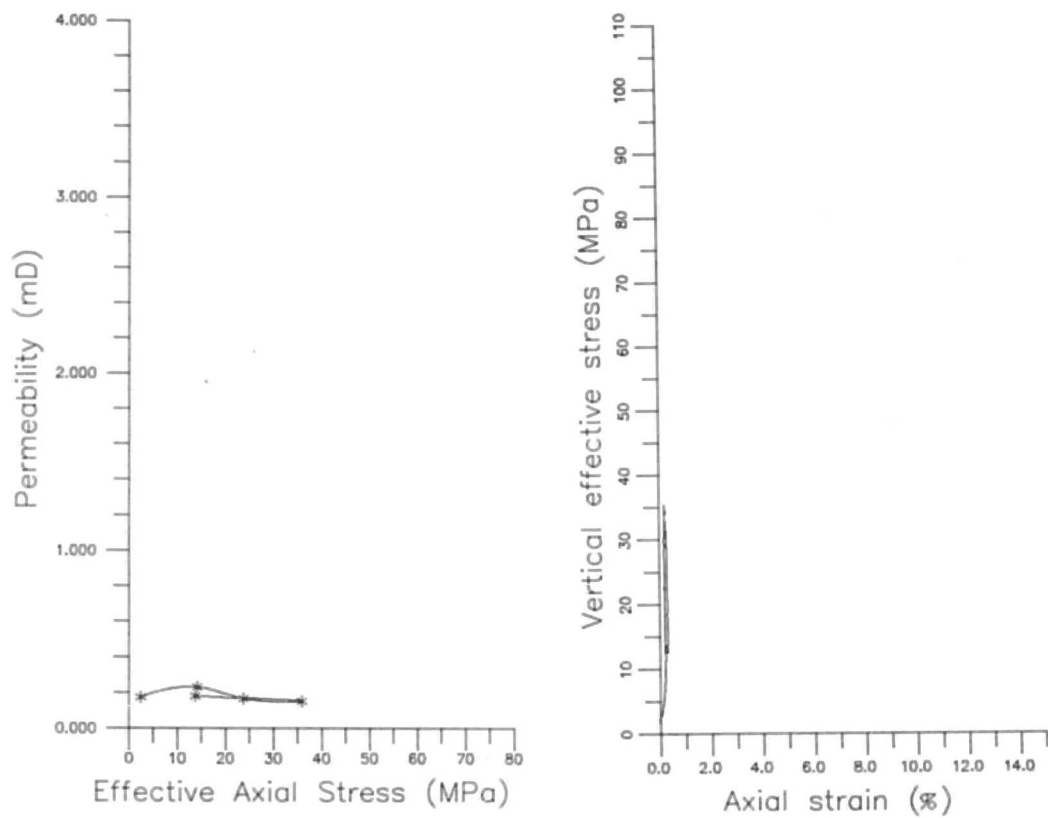
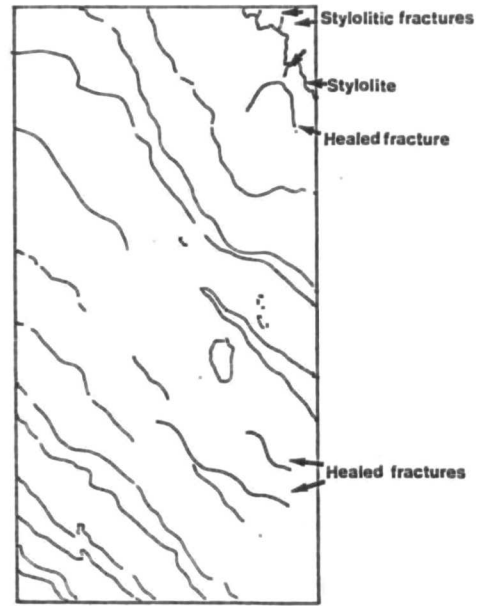
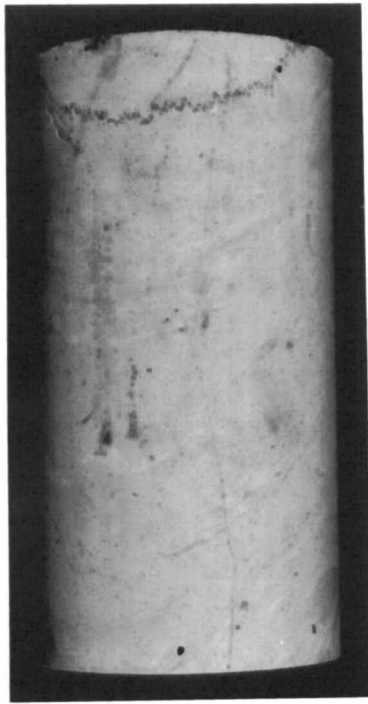


Figure. 5.18. Data sheet for permeability experiment NEOC15.



NEOC16: U. Tor Fm., Depth 3275.7m, Slumped debris flow.

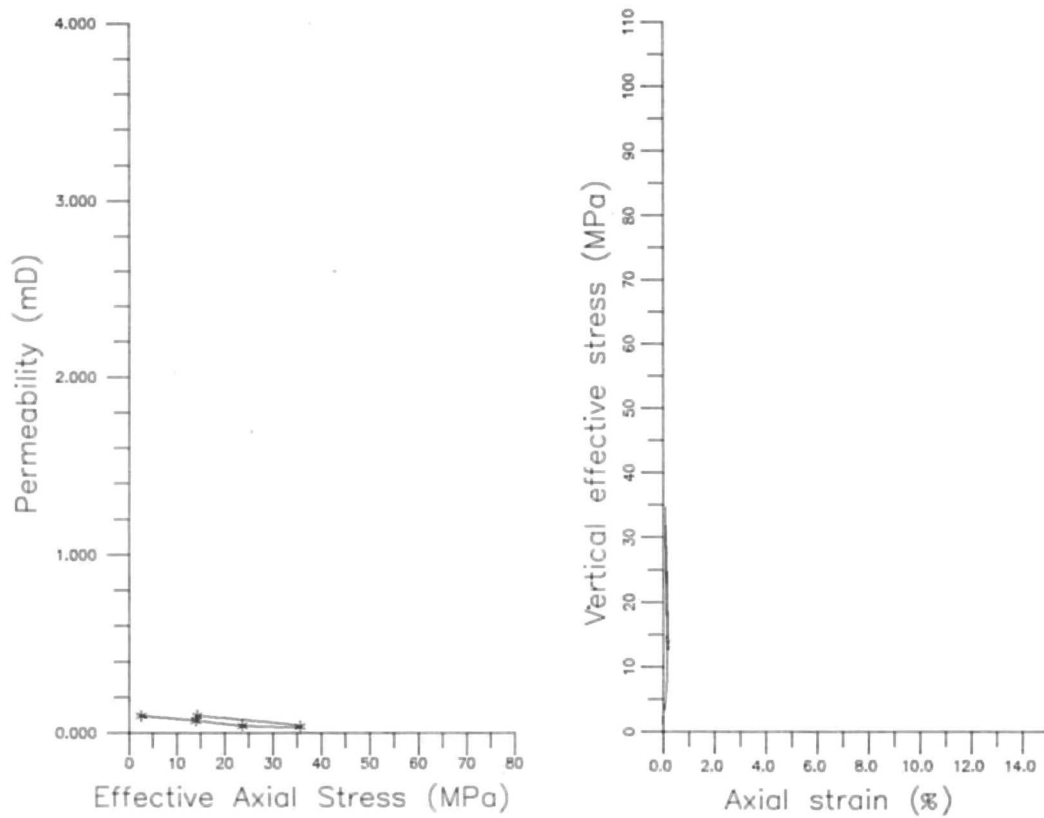


Figure. 5.19. Data sheet for permeability experiment NEOC16.

meability to a value of 0.971mD, which was marginally higher than the initial permeability.

- *NEOC17. (figure 5.20)*

Formation: Lower Ekofisk.

Initial porosity: 22.8%.

Sample morphology: Series of large vertical and inclined healed fractures.

Changes in permeability: A marginal increase in permeability was recorded between the initial value of 0.4321mD (2.4MPa) and 0.4385mD (13.7MPa). As the vertical effective stress continued to increase, permeability decreased (0.2296mD at 36.8MPa).

Unloading led to a small recovery (0.2655mD). The overall decrease in permeability must reflect some permanent damage to the chalk structure, even though the sample appeared to have deformed essentially in an elastic manner. This deformation may have been restricted to a closure of the inclined fractures. The slight increase in permeability observed at the start of the experiment may have been due to flexing of the vertical fractures.

- *NEOC18. (figure 5.21)*

Formation: Lower Ekofisk.

Initial porosity: 25.5%.

Sample morphology: Debris flow; single vertical healed fracture.

Changes in permeability: As this sample did not achieve its yield stress during the experiment, all changes in permeability are probably due to movements of the single vertical healed fracture. Permeability increased slightly from the initial value of 0.3171mD (2.7MPa) to 0.4174mD at 23.4MPa, but fell with further loading to 0.3832mD (36MPa).

Unloading resulted in a final permeability which was significantly higher (0.3988mD) than the initial value.



NEOC17: L. Ekofisk Fm., Depth 3156.2m, Lithological variations picked out by syn-sedimentary fractures.

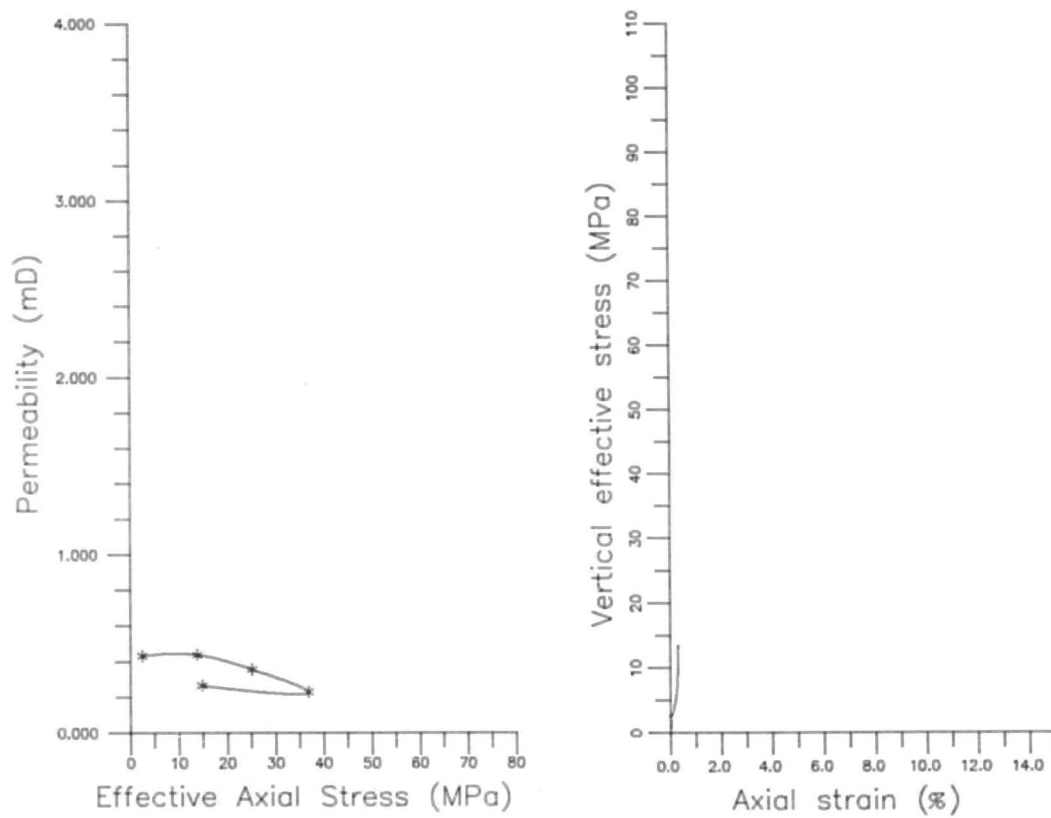
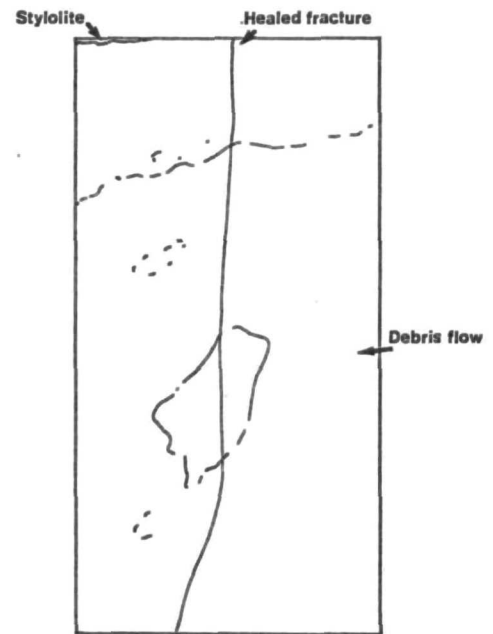
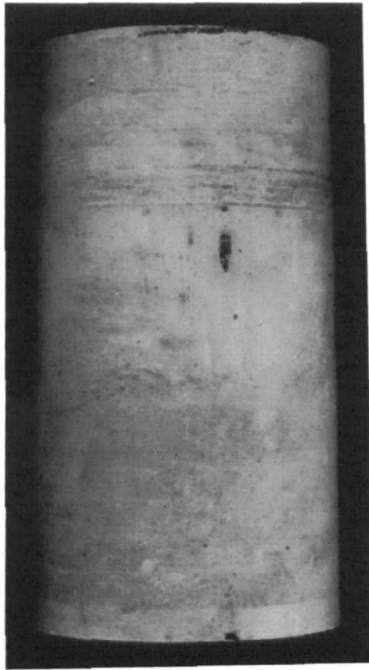


Figure. 5.20. Data sheet for permeability experiment NEOC17.



NEOC18: L. Ekofisk Fm., Depth 3165.3m, Debris flow.

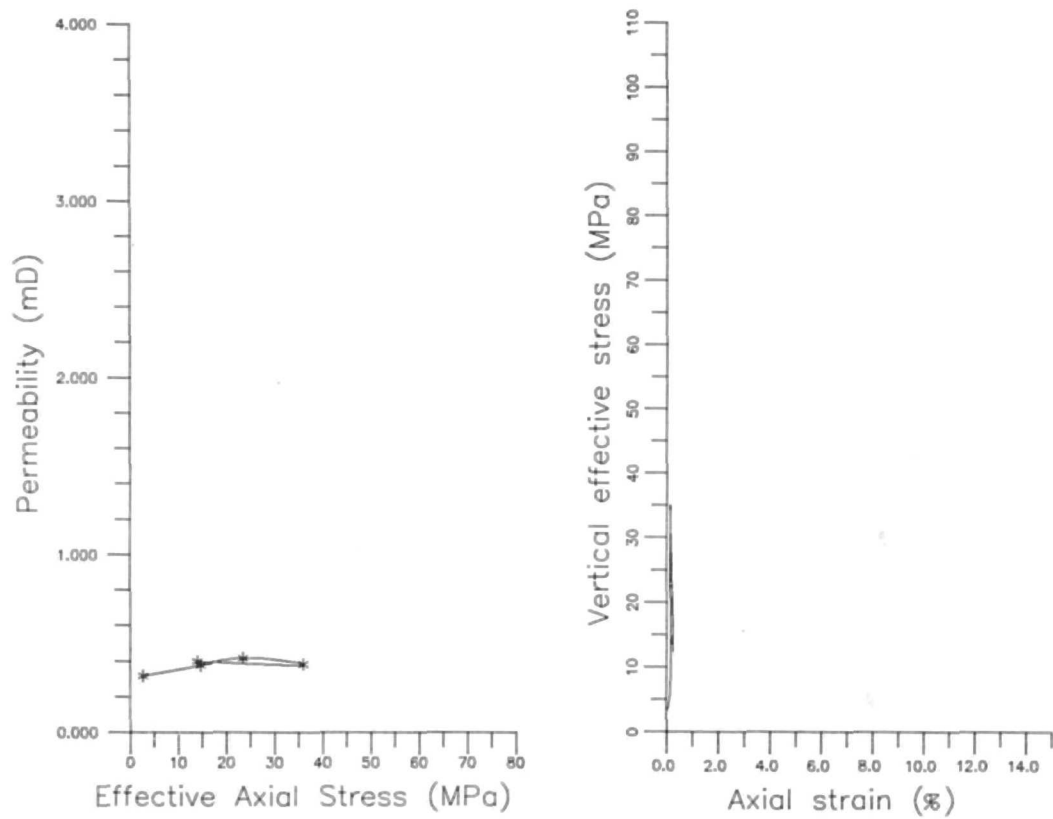


Figure. 5.21. Data sheet for permeability experiment NEOC18.

- *NEOC19. (figure 5.22)*

Formation: Upper Ekofisk.

Initial porosity: 33.4%.

Sample morphology: Small deformed burrows; Solution/high clay content on partially open near vertical fractures.

Changes in permeability: This sample contained a high, initial permeability (1.8207mD) which decreased significantly to 0.928mD as the vertical effective stress increased to 28MPa. Permeability was observed to increase as the sample approached yield. Following yield however, permeability continued to decrease (0.7646mD at 75MPa) and did not recover during unloading (0.6298mD at 39.6MPa). This sample was subjected to effective stresses beyond those expected during production to determine how permeability may be effected by larger changes in effective stress.

- *NEOC21. (figure 5.23)*

Formation: Middle Tor.

Initial porosity: 31.9%.

Sample morphology: Series of large nearly vertical healed fractures.

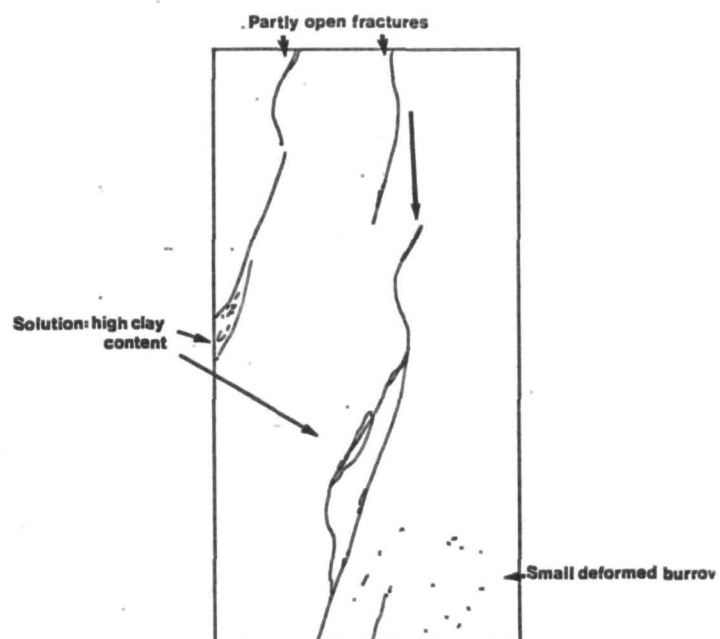
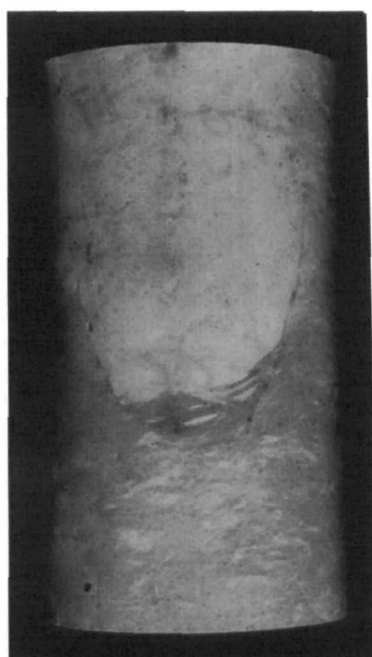
Changes in permeability: Dilation of these fractures during the initial loading phase of the experiment to reservoir stresses produced a large increase in permeability (from 0.1072mD to 1.6202mD). Although the sample did not progress beyond the stage of elastic deformation, the subsequent decreases in permeability (1.3209mD at 24.4MPa and 1.2960mD at 36.6MPa) appear to be a consequence of the gradual closing of the these fractures. Permeability fell following unloading to 1.0438mD, however, this value was still significantly larger than the initial value.

- *NEOC22. (figure 5.24)*

Formation: Lower Ekofisk.

Initial porosity: 30.6%.

Sample morphology: Plastically deformed; horizontal solution feature; steeply inclined and nearly horizontal healed fractures.



NEOC19: U. Ekofisk Fm., Depth 3121.5m, Bioturbated periodite.

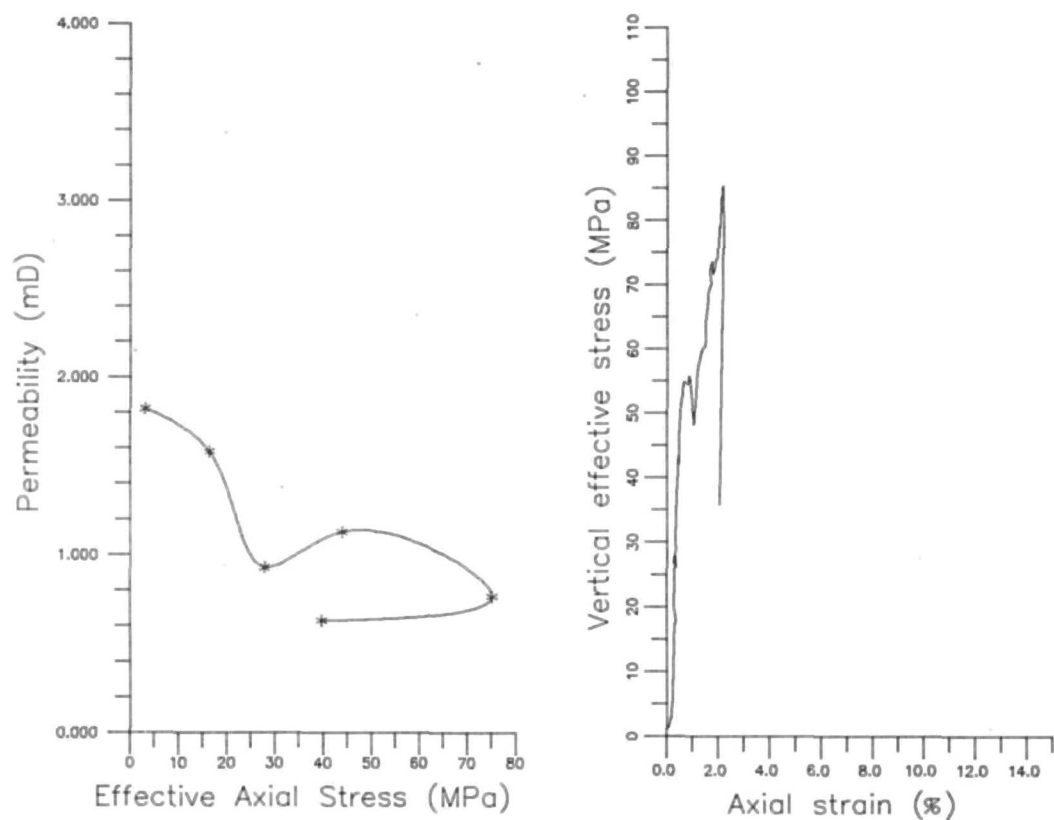
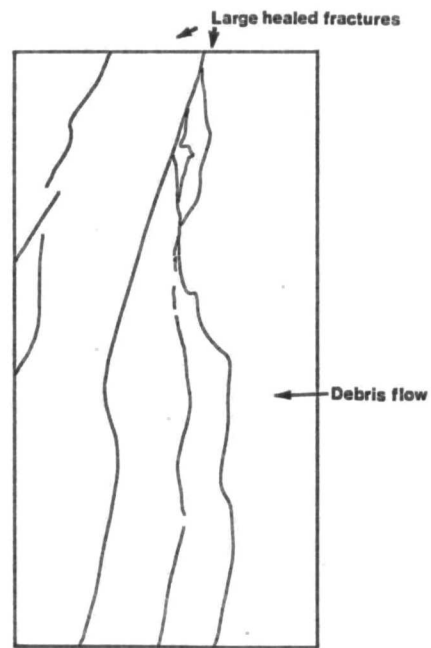
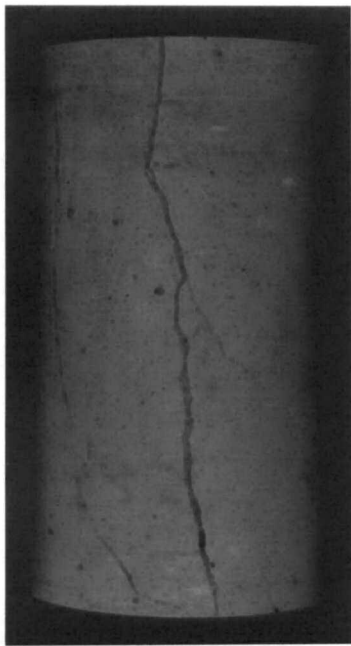


Figure. 5.22. Data sheet for permeability experiment NEOC19.



NEOC21: Tor Fm., Depth 3216.6m, Debris flow.

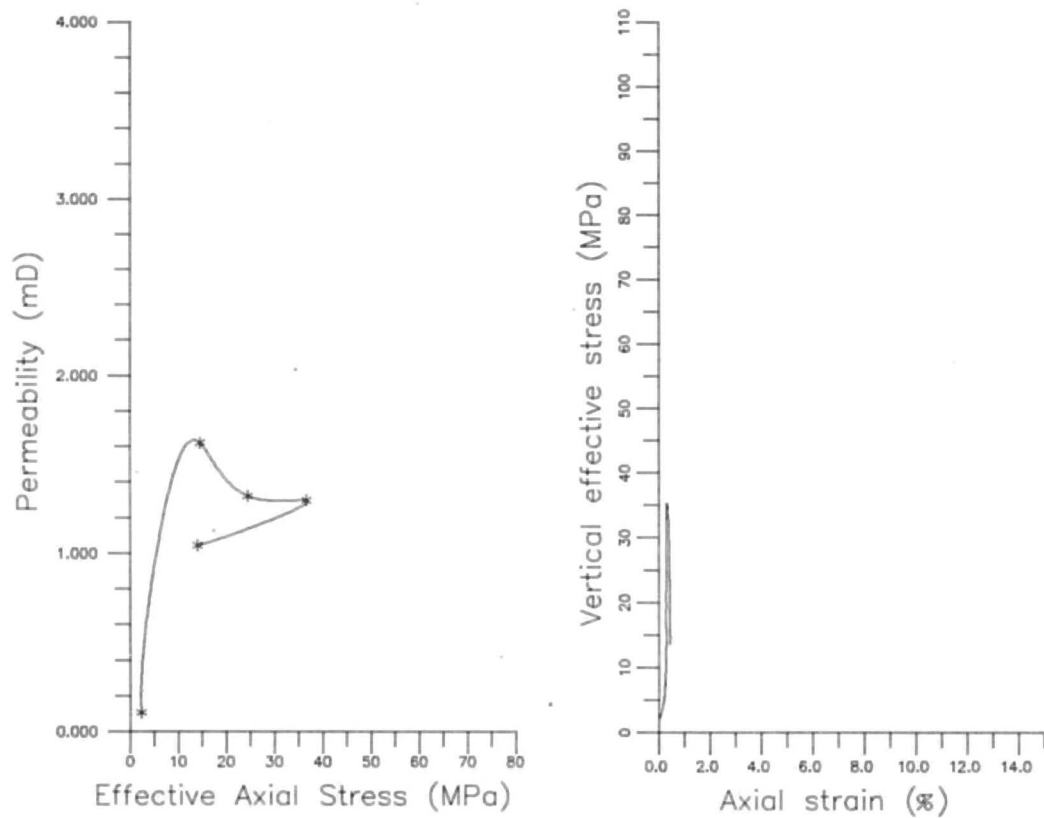
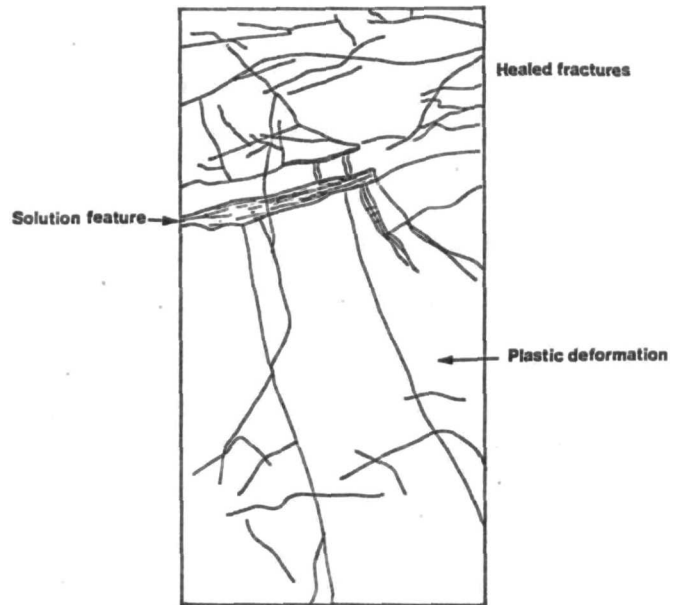
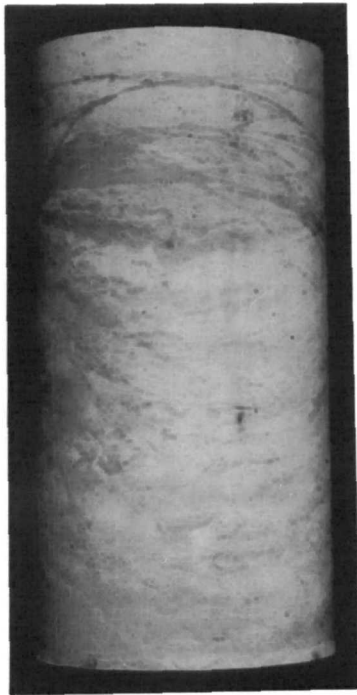


Figure. 5.23. Data sheet for permeability experiment NEOC21.



NEOC22: L. Ekofisk Fm., Depth 3201.6m, Brecciated slump.

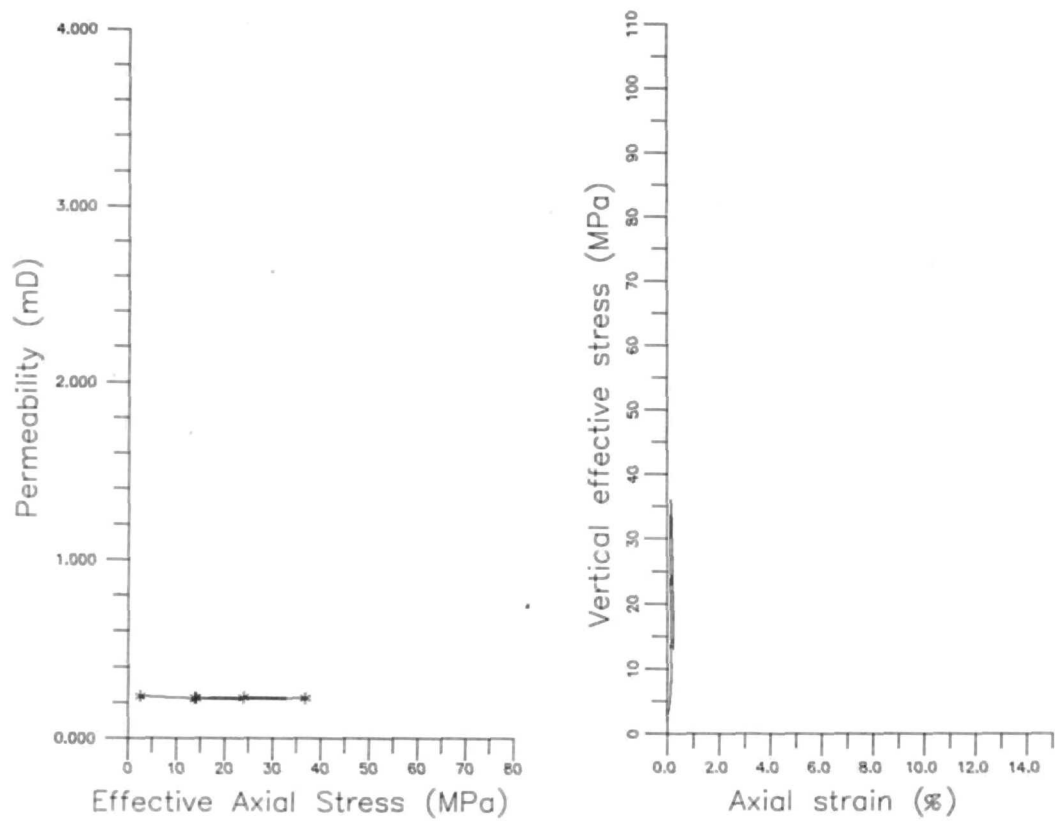


Figure. 5.24. Data sheet for permeability experiment NEOC22.

Changes in permeability: This sample displayed a small decrease in permeability throughout the experiment. The initial, low- stress permeability was calculated to be 0.2357mD and the final value after unloading was 0.2224mD. This decrease was probably the result of closure of the short horizontal fractures observed in the sample.

5.8. MICROFACIES ANALYSIS.

Re-sedimented chalks provide the best (preserved) porosities (D'Heur, 1984, 1989; Kennedy, 1985, 1986, 1987a; Pederstad et al., 1988) and therefore constitute the best reservoirs. Core material recovered from the chalk reservoirs (see the log constructed for core from well 2/4-B11 in chapter 3) indicates that partly consolidated chalks, broken up during transportation, represent an important part of the allochthonous units. The highest quality reservoir rocks are those that show evidence of rapid sedimentation, slumping, and a lack of burrowing. The characteristics of these allochthonous sediments have been described in chapter 3.

From well logs (figure 5.25) and core data (such as that presented in chapter 3) it is evident that the reservoirs are layered in a complex manner, in terms of their lithofacies, porosity and permeability (D'Heur, 1984, 1989). The allochthonous units which contain the highest preserved porosities (frequently over 40%) alternate with, and are surrounded by, low-porosity and low-permeability chalks. Figure 5.25 presents a log which clearly identifies a link between porosity, permeability and sedimentology.

It was noted in Leddra et al. (1989b) that the petrography of the chalk exerted an influence on both the pre-production permeability and on the extent of any permeability reduction resulting from compaction. The primary controls appeared to be lithofacies, fracture density and type, calcite and silica cementation, clay content and locally, variations in grain composition and primary depositional texture (Leddra et al., 1989). The highest permeabilities occur in samples with wackestone or packstone textures which exhibit low cementation and clay content.

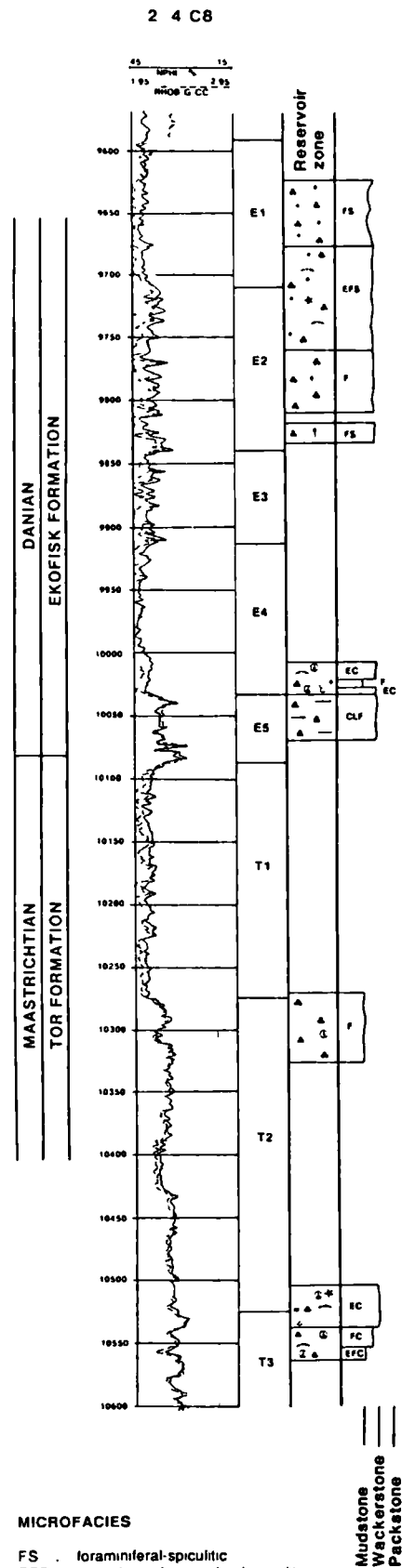
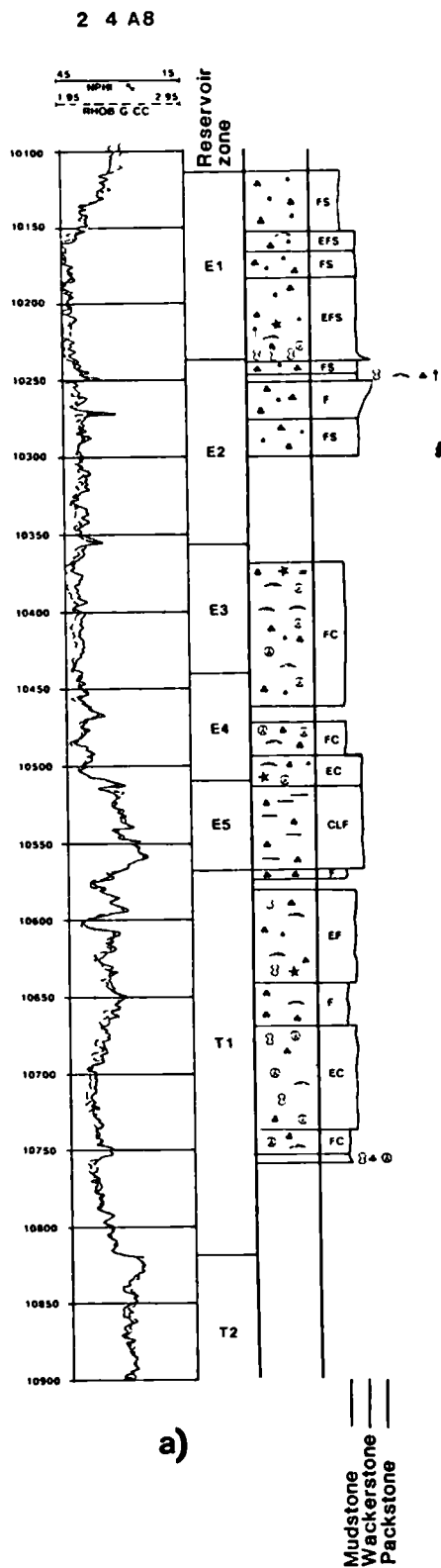


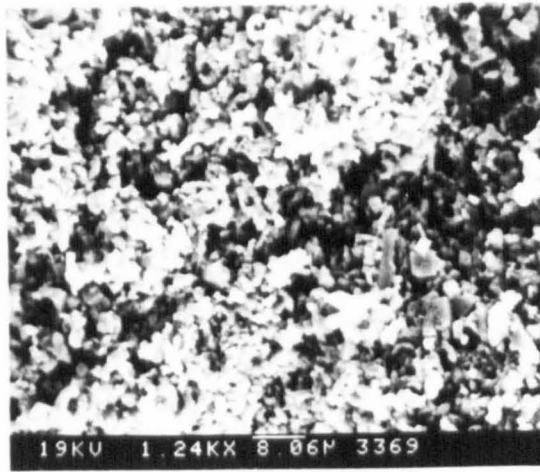
Figure. 5.25. Sedimentology versus FDC/CNL logs, porosity and permeability data in wells a) 2/4-A8, and b) 2/4-C8.

5.9. DISCUSSIONS AND CONCLUSIONS.

Permeability analysis of the North Sea reservoir chinks using a high pressure triaxial cell allowed the assessment of permeability changes, that were a consequence of the expected changes in the effective stress regime acting within the reservoir. The measured values of permeability from the samples provided a consistent view of low matrix permeability, especially in the Tor Formation. Rarely did the matrix permeability exceed 3mD, even in the most porous layers of the Ekofisk Formation. The use of samples which contained discontinuities such as fractures and stylolites, that are a common occurrence within the reservoir rocks, may have provided more representative permeabilities for the chinks that constitute the majority of the reservoirs. It should be noted that samples taken from better quality rocks without these features may give matrix permeabilities which could lead to an optimistic view of the overall reservoir quality.

Permeability reduction during uniaxial strain experiments was most severe in the samples with the highest initial permeabilities and low cementation. Scanning electron micrographs were taken of two samples prior to, and following uniaxial strain deformation experiments to determine the extent to which the structure of the chalk was altered. Plates 5.1 and 5.2 indicate that during the experiments the chalk deformed in an irregular manner. In high porosity chinks individual faunal constituents are loosely bound and therefore permeability reduction can be expected to be more severe. Cementation, particularly silica cement (as in the upper part of the Ekofisk Formation), increases the strength of the chalk and results in lower, but more stable permeabilities. (Calcite cement, which is most abundant in the Ekofisk Tight Zone, the Tor Formation and the flanks of the Ekofisk Structure is observed to have an effect similar to that of silica.) The distribution of such cements is controlled by depth of burial, structural position and water saturation history.

Although the data presented in figure 5.25 would appear to indicate that there is a link between porosity and permeability, this link is not clear. Addis (1987) constructed a



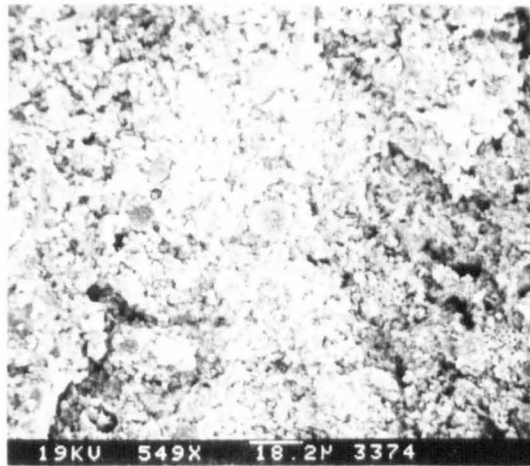
a)

Plate 5.1. a) Scanning electron micrographs of sample NEOC19 (figure 5.23) before uniaxial deformation, b) Scanning electron micrograph of sample NEOC19 following uniaxial deformation to an effective stress of 75MPa. Note the irregularity in the distribution of the deformation.



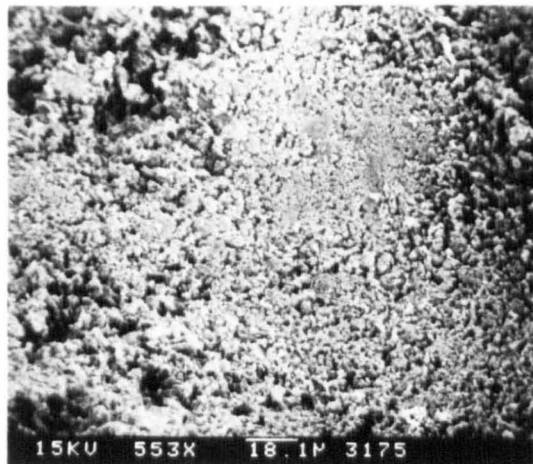
b)

Lower scanning electron micrograph illustrates the differential breakdown of the structure of the chalk associated with compaction.



a)

Plate 5.2. a) Scanning electron micrograph of sample NEOC6 (figure 5.11) before uniaxial deformation, b) Scanning electron micrograph of sample NEOC6 following uniaxial deformation to a vertical effective stress of 36MPa.



b)

Lower scanning electron micrograph illustrates the differential breakdown of the structure of the chalk associated with compaction.

graph (reproduced in figure 5.26) in which he plotted the changes in permeability calculated during his experiments with respect to the decrease in porosity. He added to this data a trendline established by Scholle (1977) for pure chalk. The permeability/porosity data (at 14MPa σ_v) from each of the experiments conducted during the present study have been added to this information. These new data show a wide scatter. None of the new data points fall below the trendline of Scholle (1977), although a number of the Tor Formation samples plot close to it.

Scholle (1977) clearly indicates that a link exists between porosity and permeability but this relationship is disputed by a number of authors. Schatzinger (1985) defined a non-linear trend in permeability for the chalk which he considered to be dependent on pore size distribution. It has been recognised (Schatzinger, 1985) that the pores in the top of the Tor Formation are smaller than those in the Ekofisk Formation. This is related to a change in the size of the Coccoliths. As the Lower Ekofisk Formation in the Ekofisk Field contains a large proportion of resedimented Tor Formation chalk, this may account for the apparent distribution observed in figure 5.26. Although this graph shows a large scatter in the data, there appears to be some kind of trend developing for the results from the three formations. The Tor Formation samples have a higher permeability for a given porosity than any of the Ekofisk Formation samples. The Upper Ekofisk chalks have the lowest permeabilities per porosity and the Lower Ekofisk samples lie somewhere in between. This would indicate that a relationship does exist between porosity and permeability, but the dataset on which this was based is too small to be definitive. In order to expand this data set further experiments would have to be conducted on a large number of samples with an equally large range of initial porosities, diagenetic and sedimentological fabrics. This would not be a practical use of valuable core material.

A number of studies have been conducted to investigate permeability changes that are a result of increasing effective stress (Fatt and Davis, 1952; McLatchie et al., 1958; Brighenti, 1967; Marek, 1979; Gobran et al., 1981; Addis, 1987; Goldsmith, 1989).

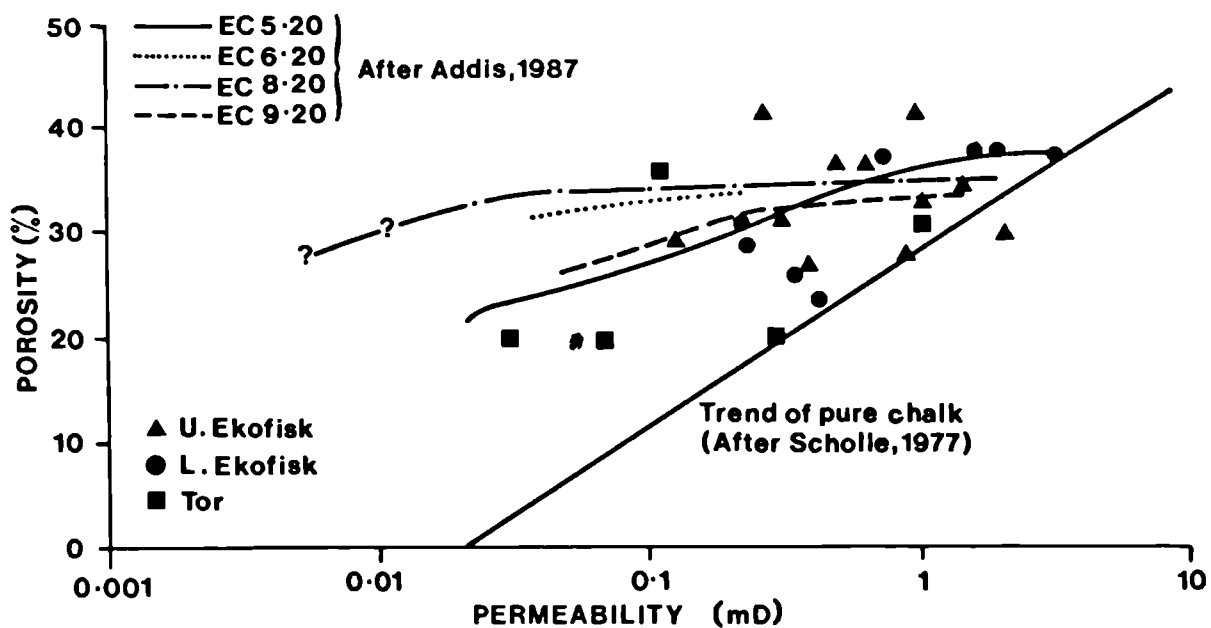


Figure.5.26. A graph of porosity/permeability for each of the samples tested during the present experimental programme. The points represent the porosity and permeability recorded at a vertical effective stress of 14MPa. This graph also includes the porosity/permeability decreases observed by Addis (1987) during uniaxial experiments conducted on North Sea chalk samples and the trendline established by Scholle (1977) for pure chalk. (Based on Addis (1987.))

Most of these studies used sands or sandstones, but Addis (1987) and Marek (1979) studied these effects in chalk and chalk-like limestones. Pore collapse and a decrease in permeability in high porosity carbonates was recognised by Marek (1979) and Newman (1981). Experiments were undertaken by Marek (1979) on whole-core samples (152mm long and 89mm diameter) of carbonates from the Middle East. These materials were subject to large isotropic confining pressures (up to 40.8MPa) in a high pressure triaxial cell. A decrease in porosity and permeability was observed during pore collapse that was greater than would have been predicted using published correlations. Similar results have been obtained by Sarda (1985) at high isotropic pressures for North Sea chalks. Newman (1981) found that the type of pore fluid used affected permeability. During a study on the effects of water chemistry on the permeability characteristics of North Sea chalks, he found that, samples tested with brine as a pore fluid tended to fail at lower stresses than those in which oil was used. A number of experiments were conducted where samples were saturated with oil and loaded to over 41MPa. They were then unloading to 28MPa and then injected with brine. It was found that compaction began with no further increase in load and the injected water contained increased levels of CaCO_3 .

Well test analyses indicate that effective permeabilities in the chalk are greater than the measured matrix permeabilities (table 5.1). This difference is a result of the fracture system, which is stratigraphically controlled. Core studies have shown that an alternation exists throughout the reservoir between tight and porous rocks, and that the latter are preferentially fractured. It also appears that stylolites, matrix porosity and clay content all exert some control on fracture development. Therefore the highest effective permeabilities should develop in chalks with the highest matrix porosities. The Ekofisk Field core and log data establish the complexity of lithofacies, porosity, diagenesis and pore development (figure 5.25). The allochthonous sediments above the oil/water interface appear to have high pre- production porosities. These sediments have retained high porosities and resisted cementation during burial (Sorensen et al., 1986). Sediments below the oil/water contact nearly always show increased cementa-

tion. In the flank areas of the field the reservoir quality has been reduced by diagenetic phenomena. However, it is important to note that high porosities (up to 35%) are also seen within the aquifer zone in several wells. This porosity preservation cannot be easily explained by the introduction of oil into the reservoir (see chapter 3).



There did not appear to be a strong correlation between any of the variables listed in section 5.1 and the changes in permeability observed during this study. For instance, stylolites and high clay contents were observed in samples covering the entire range of permeabilities recorded. This is equally true for sedimentological fabrics. Debris flows and samples containing plastically deformed sediments also exhibited a wide range of permeabilities. The presence of vertical or inclined fractures appears not to have unduly influenced sample (ie. pre-test) permeability. However a number of general conclusions can be drawn from the experimental results.

- *1) There was a weak correlation between permeability and porosity. A scatter existed in the data which appeared to indicate a link between the porosity and permeability within each stratigraphic unit. This link may be dependent on variations in pore size.*
- *2) In the experiments conducted during this study, the low porosity samples tended to exhibit a slight increase in permeability before reaching initial reservoir stress conditions. Generally, further changes in permeability were small, but increases or decreases were observed which appeared to have been controlled by the orientation and nature of the fractures present. During the deformation experiments, vertical fractures usually led to an increase in permeability even though radial strain was generally kept to within ± 2 microns, and inclined fractures resulted in a decrease. This indicated that only very small movements of these fractures were necessary to influence the sample's permeability.*
- *3) High porosity samples followed a different pattern of behaviour to that exhibited by the lower porosity ones. They behaved initially in an elastic manner, but beyond a certain stress level (governed by the initial porosity) they underwent yield and strain softening. It was assumed that microfractures would close during the initial loading. As a consequence of closure of both fractures and primary pore spaces the permeability decreases throughout the experiment. There is little or no recovery of the lost permeability during the*

unloading stage of the experiments conducted on the higher porosity samples.

- *4) Stylolites and other clay filled features are thought to suppress the initial permeabilities of moderate and high porosity samples, but appear to play a passive role in changes that are a consequence of experimentally induced deformations.*
- *5) Generally, samples which contained vertical fractures showed no signs of permeability recovery following unloading.*
- *6) No definitive correlation could be found between the sedimentological and diagenetic fabrics present and permeability.*

Experiments of the type described in this chapter may give a more realistic appreciation of the changes in permeability that could occur within the reservoir rocks during production. By conducting permeability analyses using the constant-head method significant quantities of the chosen permeant can be passed through the sample. The permeant can also be changed during the experiment to determine whether such changes may influence the permeability. As the volumes of the permeant introduced and expelled from the sample are both measured a consistent permeability can be determined for a particular effective stress.

Addis (1987) noted that the falling-head method employed during his study allowed constant changes in permeability to be determined throughout each experiment by allowing a small excess pore pressure to develop in the sample. Continuous measurements could also be made using the constant-head method described in section 5.5, as emptying and recharging of the volume gauges can be achieved throughout the experiment. This method would retain the flexibility described in the previous paragraph and would also allow a constant head difference to be established across the sample throughout the experiment which would be independent of the loading rate (rather than dependent upon it as in the method used by Addis (1987)).

CHAPTER 6
•
UNDRAINED SHEAR EXPERIMENTS.

6. UNDRAINED SHEAR EXPERIMENTS.

6.1. INTRODUCTION.

Chapters 4 and 5 presented data from a series of experiments designed to investigate the mechanical behaviour of North Sea reservoir chalks under conditions of uniaxial strain. These experiments were primarily concerned with the determination of physical parameters, such as, changes in permeability, the effects of loading at different strain-rates and the nature of the deformation of these chalks.

The experimental study presented in this chapter was designed to investigate a different aspect of chalk behaviour, namely, the behaviour of high porosity chalk during undrained triaxial shear. This type of experiment provides data which defines the Critical State Line (Atkinson and Bransby, 1978) in pore volume/stress space. This data cannot be determined from uniaxial strain experiments as materials following this stress path do not attain their critical state (defined as the condition where strain continues at constant stress and constant void ratio). Data that establishes the position of the Critical State Line, (which can be regarded as a state boundary), in stress/void ratio space, provides the necessary refinement for the construction of a constitutive model for chalk behaviour. To determine the position of this line, high porosity onshore chalks from Denmark (Stevn's Klint) and South East England (Butser Hill) were used. These were initially consolidated, under either isotropic or uniaxial strain conditions to various mean effective stresses, and then sheared (undrained) until failure occurred.

Chalk may be subject to conditions of undrained shear in a variety of environments including, cliff falls, rapid draw-down of hydrocarbon production wells following a period of shut-in and the construction of chalk embankments. In each of these examples, large, rapid changes in applied stress may induce conditions of undrained shear (due to the low permeability of the chalk), which may result in collapse of the cement structure and possibly, flow of material.

It has been observed by Hutchinson (1980) that rockfalls from chalk cliffs with large elevations (over 130m) behave in a different manner from those affecting lower ones. Examples of the latter, such as those along the South Foreland in Kent (80m), which come to rest on an essentially flat surface (their wave-cut platform), have a run-out 1.1 times the height of the cliff. The debris is seen to collect in a similar manner to that of a scree slope. It has been noted that further south however, at Abbots Cliff (north of Folkestone), where the cliffs are approximately 130m high and the rock-falls also impact on a wave-cut platform, that the run-out distance is significantly larger (X5) (Hutchinson, 1988, 1989) and the debris exhibits many of the characteristics observed in a debris flow. Hutchinson (1988) refers to these as impact-collapse flow slides. One of these flow slides, from Abbots Cliff, is illustrated in plate 6.1 and is accompanied by an annotated cross-section in figure 6.1. The full extent of this flow slide is difficult to determine as much of it is below sea level. Figure 6.1 represents only the area visible at low tide. It can be seen from this illustration that it contains many of the diagnostic features observed in debris flows and other types of failure in which the material disintegrates on impact (Brunsden, 1979). These include: an arcuate front and a pressure ridge, where the chalk spread outward from the point of impact; a ponding of fluid behind the pressure ridge; and blocks of intact material (including a brick ventilation shaft) transported on top of the disaggregated material. Hutchinson (1980, 1983, 1989) proposed that these more dramatic failures were the result of undrained loading, in which high porosity chalks attain a sudden loss of strength, which causes them to behave in a semi-fluid manner.

Further studies (Hutchinson pers. comm., 1989) have indicated that the more dramatic chalk failures are restricted to high cliffs (which therefore have higher potential energy available in the chalk as it impacts on the wave-cut-platform) formed of high porosity chalks. At Abbots Cliff, where they occur most frequently, the porosity of the chalk varies from 45-48%. This porosity distribution is amongst the highest recorded in South-east England (where the porosity generally varies from between 35-47% (Hancock, 1985)).

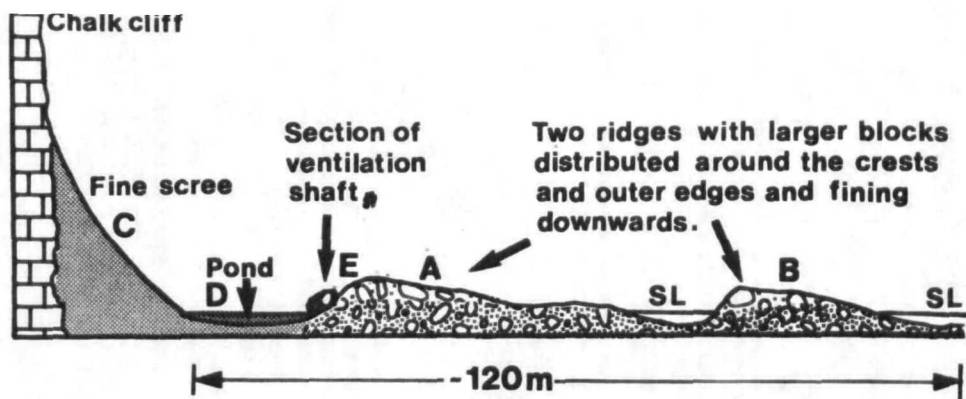


Figure. 6.1. Annotated, schematic cross-section of the chalk-flow at Abbots Cliff.

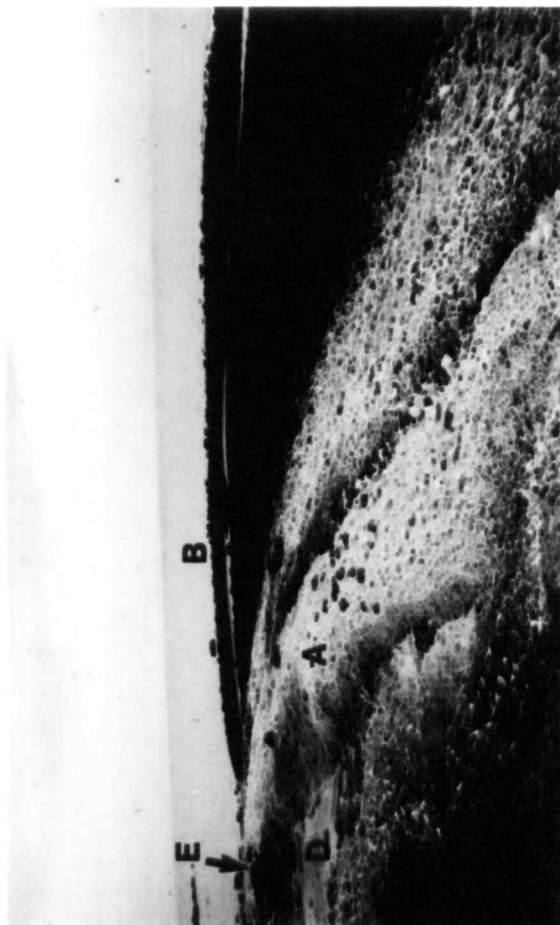


Plate 6.1. The chalk-flow at Abbotts Cliff which exhibits a form similar to a typical mudflow.

Failure and flow fabrics formed during re-deposition of the high porosity chalks, which constitute the hydrocarbon reservoirs in the North Sea are well documented (see chapter 3). During hydrocarbon production these high porosity reservoir chalks, can be mobilised and flow through the well perforations to partially fill the well bore. Well invasion nearly always occurs after a well has been shut-in. When a well is brought back into production, the high fluid pressures that have developed in the well-bore are rapidly reduced. This reduction in pressure removes the support provided by the fluid in the well-bore before the pore pressure gradient in the reservoir chalk can be reestablished (a result of the time delay imposed by the low permeability of the chalk) inducing large shear stresses in the chalk (figure 6.2).

Chalk fill material, used in the construction of embankments, may also be subject to undrained loading (Ingoldby, 1978; Perry, 1978) resulting in the formation of 'putty chalk'. Putty chalk is a particularly common problem in the soft Upper Chalk, where crushing of the chalk during excavation and subsequent compaction in the embankment results in the breakdown of the cement structure. This break-down releases the in-situ pore fluid which leads to the development of excess pore fluid pressures (Ingoldby, 1978; Perry, 1978). The embankment may become so unstable that it is unable to bear the weight of the construction equipment. Further work may then have to be suspended to allow the dissipation of the fluid pressures and consolidation of the chalk. The fill material is observed to be a mixture of intact lumps of chalk, chalk fines and water. It is the proportions of the latter two, resulting from crushing of the material during excavation and compaction, that determines the stability of the embankment (Puig, 1973). Excessive handling (Clayton, 1989) and vibration (Thomson and Buthee, 1989) are also known to be responsible for the disaggregation of chalk. Lewis and Parsons (1973) reported an incident where chalk was transported from a quarry near Portsmouth for four kilometres on a conveyor belt to a reclamation site. The vibration caused by movement along the conveyor belt led to a break-down of the chalk and turned it into a chalk slurry. Once this had drained, however, it became a stable fill material.

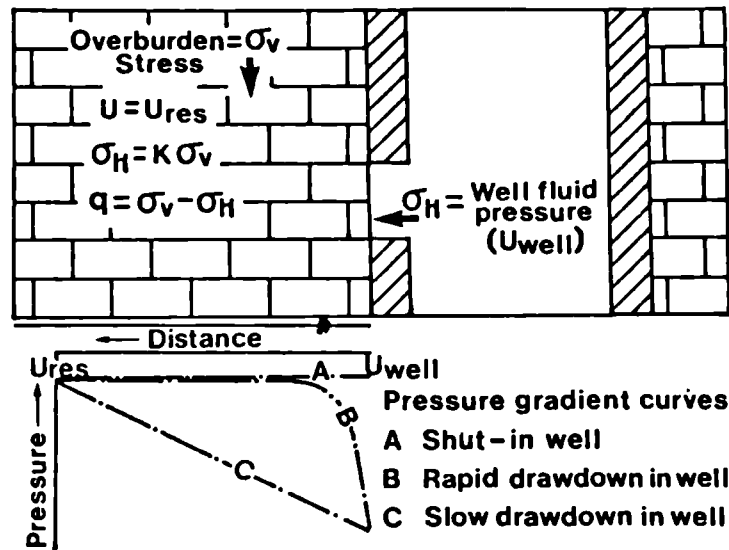


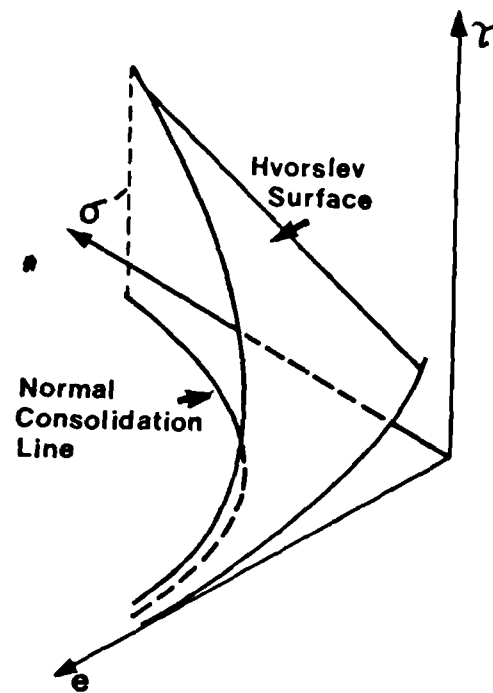
Figure. 6.2. A schematic representation of the fluid and stress changes around a well perforation during a "shut-in".

High porosity chalks in both the onshore and offshore environments therefore have the ability, under specific circumstances, to generate high excess pore fluid pressures and behave in a ductile manner. This ductile behaviour will only exist whilst the high pore fluid pressures are maintained. Once the excess pore pressures have been dissipated, the chalk is observed to revert back to a rigid structure. Evidence for this can be provided for each of the three examples that have been described in this section. Following a well invasion down-hole tools are often encased in reconstituted chalk which is strong enough to prevent the recovery of the tool. In chalk embankments, the dissipation of excess pore fluid pressures following the formation of putty chalk increases the strength of the embankment to allow construction work to begin again. Chalk flow material rapidly returns to being a rigid structure with an ability to resist marine erosion that is almost equal to that of the intact material.

Similar mechanical and pore pressure conditions prevail in each of the examples described above. They all involve rapid, and effectively undrained, loading with development of large shear stresses. Once the shear stresses are released and the pore pressure is allowed to dissipate the chalk reverts back to a coherent material.

6.2. RESUMÉ OF UNDRAINED SHEAR: THEORY AND PRACTICE.

Hvorslev (1937), as reported in Roscoe et al. (1958), showed that for a remolded, saturated, cohesive soil, the peak shear (deviatoric) stress (q) was a function of the normal (mean) effective stress (p') and the void ratio (e) in the plane of failure at the moment of failure. It was also independent of the samples previous stress history. He was able to define a surface, in stress/void ratio space, using drained, stress controlled, shear box data from experiments conducted on overconsolidated clays, termed the Hvorslev Surface (figure 6.3). The area below this surface is termed the Hvorslev Domain (Roscoe et al., 1958). However, Hvorslev could not investigate the condition of samples after attaining their peak shear strength by using this stress controlled equipment. To extend the Hvorslev data to clays that sustained large shear strains before realising their peak



**Figure. 6.3. An isometric diagram of the Hvorslev Surface as defined by undrained shear box experiments
(After Roscoe et al., 1958.)**

shear strength, and to investigate the behaviour of materials beyond that state, Roscoe (1953) developed a shear box that would impose large, uniform shear strains on soil samples.

If a number of similar, uncemented samples are subject to undrained shear conditions following consolidation to different mean effective stresses, the resulting stress paths define lines on a curved surface (in stress/void ratio space) generally referred as the Roscoe Surface (Atkinson and Bransby, 1978). This surface, in soil mechanics, is defined by the maximum achievable ratio's of p' , q and e for a normally consolidated particulate material (Atkinson and Bransby, 1978). The Critical State Line and the Normal Consolidation line (Atkinson and Bransby, 1978) (figure 6.3) form the upper and lower boundaries to this curved surface. The former represents the line of intersection between the Roscoe and Hvorslev Surfaces where a sample is deemed to have attained its critical state. The latter depicts the stress/void ratio path followed by a particulate sample during isotropic consolidation (i.e. with no deviatoric component of stress).

The most common and simplest method used for conducting undrained shear tests using a triaxial cell involves consolidating the sample under isotropic conditions to a specified mean effective stress then closing off the drainage line and loading the sample axially whilst maintaining a constant confining pressure until the critical state has been achieved. The same ultimate condition can also be attained by following a number of other loading paths. These include:

- *1) Maintaining a constant vertical stress and decreasing the confining pressure (known as compression unloading).*
- *2) Increasing the vertical stress whilst at the same time decreasing the horizontal stress, so that the mean stress remains constant (similar to that used by Crawford, 1963).*
- *3) Cyclic loading of one or both of the principle stresses (eg. Dobry et al., 1988).*

- 4) *Drained triaxial.*



Samples of the same material, consolidated to the same mean effective stress, with the same void ratio, loaded, undrained, along any of the above stress paths will follow the same effective stress path and achieve the same undrained shear strength (the highest attained shear stress (Lambe and Whitman, 1979)). This indicates that the effective stress path resulting from undrained shear is only dependent on the stress/void ratio conditions which existed immediately prior to the start of shear. It has been found that undrained shear strength will increase with:

- 1) *Decreasing Void ratio.*
- 2) *Increasing Consolidation pressure.*
- 3) *Increasing pre-consolidation pressure (or cementation).*
- 4) *Increasing rate of strain.*
- 5) *Increasing time allowed for consolidation (associated with secondary consolidation).*

The degree of pore pressure generation, resulting from an increase in either the horizontal or vertical total stress can be expressed in terms of a pore pressure parameter. Each pore pressure parameter relates the change in the pore pressure to a change in a particular stress (Skempton, 1954). Pore pressure parameters A and B are only valid for isotropically consolidated samples.

1) Pore pressure parameter A

This term relates a change in the pore pressure to an increase the total vertical stress in an undrained experiment where σ_3 is held constant

$$A = \frac{dU}{d\sigma_1} \quad \# \quad 6.1$$

or, where the triaxial apparatus uses a balanced ram (in which part of the vertical load is provided by the cell pressure) the change in σ_1 is equal to the change in deviatoric stress (q), as the cell pressure remains constant, thus,

$$A = \frac{dU}{dq} \quad 6.2$$

2) Pore pressure parameter B

This term relates pore pressure development to an incremental change in isotropic stress (using the step-wise method of loading). B is considered to be equal to 1 when the sample is fully saturated

$$B = \frac{dU}{d\sigma} \quad 6.3$$

3) Pore pressure parameter C

This parameter is used with uniaxial strain experiments (generally Oedometer tests) and defines the pore pressure developed by an increment of uniaxial stress.

$$C = \frac{dU}{d\sigma_1} \quad 6.4$$

or

$$C = \frac{1}{1 + n(C_w/C_{cl})} \quad 6.5$$

where n = porosity, C_w = compressibility of pore fluid, and C_{cl} = compressibility of the soil skeleton. As the pore fluid is generally considered to be incompressible compared to the compressibility of the soil skeleton, the value for parameter C is usually considered to be one. However, the compressibility of the pore fluid may increase at high fluid pressures (Skinner pers. comm., 1989).

Consolidation theory (Lambe and Whitman, 1979) indicates that volume changes are a consequence of an increase or decrease in effective stress. Fluid flow from the sample is prevented during undrained shear experiments and therefore any changes in effective stress cannot be accompanied by changes in the volume of the pore fluid (unless it is compressible). The development of shear will also lead to changes in volume (Lambe and Whitman, 1979). In order to indicate the manner in which these two processes of volume change interact to maintain constant volume during undrained shear experiments, the volume changes developed in normally consolidated and overconsolidated samples are described below.

In a fully saturated, normally consolidated material (defined for a soil element when it is at equilibrium under the maximum stress it has ever experienced (Lambe and Whitman, 1979)), an increase of total stress leads to consolidation. In undrained shear experiments, the process of consolidation is inhibited. Increases in stress therefore lead to the generation of excess pore fluid pressure and a decrease in mean effective stress. Decreasing mean effective stress is associated with an increase in volume. Lambe and Whitman (1979) indicate that the application of shear stress results in a decrease volume which compensates for the volumetric increases described above so that there is no net change in volume. If the net volume has not changed the density of the sample must also be the same, so that the strain necessary to achieve failure in an undrained shear experiment will be less than that required in a drained experiment where an in-

crease in effective stress leads to a reduction in volume and an increase in density (Lambe and Whitman, 1979). When a heavily overconsolidated material (a soil that is at equilibrium under a stress less than that to which it was once consolidated (Lambe and Whitman, 1979)), is subjected to undrained shear the volume should also remain constant (Lambe and Whitman, 1979). As the vertical displacement increases the grains are less able to move past each other, than in a normally consolidated material, so that the pore spaces have a tendency to expand resulting in the generation of a negative pore pressure and an increase in the mean effective stress. This volume decrease is compensated by an equivalent increase in volume due to shearing. The behaviour of overconsolidated materials is further complicated by a greater variation in the size and distribution of the pore spaces (Roscoe et al., 1958). This means that areas within the material in which there is a concentration of large pore spaces will tend to reach their Critical State before those dominated by smaller pore spaces. This leads to a complicated distribution of stresses and strains in which the stress paths for different regions within the sample will gradually diverge (Roscoe et al., 1958).

Sensitive clays and very loose sands behave in a completely different manner. The Canadian sensitive clays are strong and brittle in their undisturbed state (Crawford, 1963; Mitchell, 1970), due to cement bonding of the clay particles. Once the strength of this cement has been exceeded they are easily deformed and remolded. During the initial stages of undrained shear, when the cemented structure is still intact, large pore pressures are developed and a peak shear stress is usually attained at an axial strain of approximately 1%. Further strain leads to a breakdown of the cement bonds which results in a decrease in shear strength. During shearing, two different trends develop. The potential energy available from friction increases and the effective stresses decrease. In these types of materials peak shear strength is attained before the full frictional resistance has been realised. At large strains, when frictional resistance would lead to a strengthening of the material, the actual shear resistance is observed to be small because of the decrease in effective stress. This loss of strength during straining and remolding accounts for the phenomenon of liquefaction (Lambe and Whitman,

1979; Taylor, 1987). The ratio between the undisturbed and the remolded strength is referred to as the material's sensitivity. The cement bonding provides sensitive clays with an artificial strength which they would not have if they were an uncemented, particulate material of equivalent void ratio. This sensitivity becomes more critical if the grains of the material are also deformable. When a cemented quartz sand is subject to undrained shear the cement bonds break following the attainment of a peak shear strength, but remolding allows the sand grains to move together until they are able lock. Once this has occurred the sand grains are able to resist further deformation. Remolding, under elevated stresses, may also lead to a breakdown of the grains if they are composed of a deformable material such as calcite.

6.3. PREVIOUS STUDIES ON THE UNDRAINED SHEAR BEHAVIOUR OF CALCAREOUS SEDIMENTS.

A number of papers from the proceedings of a conference on Engineering for Calcareous Sediments, held in Perth Australia during 1988, report the results of undrained triaxial experiments conducted on cemented carbonate sediments (Price, 1988b; Carter et al., 1988; Tsuchida et al., 1988; Golightly and Hyde, 1988; Fahey, 1988; Dunbavan, 1988; Dorby et al., 1988).

Golightly and Hyde (1988) conducted both drained and undrained experiments on four different sands. They compared the behaviour of sub-angular quartzitic Leighton Buzzard sand, which contained very little CaCO_3 , to sands with a high CaCO_3 content (70-95%), such as the molluscan carbonate sands from Dogs Bay (Eire), the coralline/algal Ballyconneely Sand (Eire), and the Bombay Mix, which consisted of marine siliceous carbonate sand from the western continental shelf of India. They found that the skeletal carbonate sands, which have large intra-particle voids tended to exhibit a large volumetric contraction, and the early generation of large positive pore pressures during undrained shearing (figure 6.4). The siliceous Leighton Buzzard sands, and to a lesser extent the Bombay Mix, behaved in a similar manner to a dense siliceous sand. Both materials generated small initial excess pore pressures, but further deformation led to

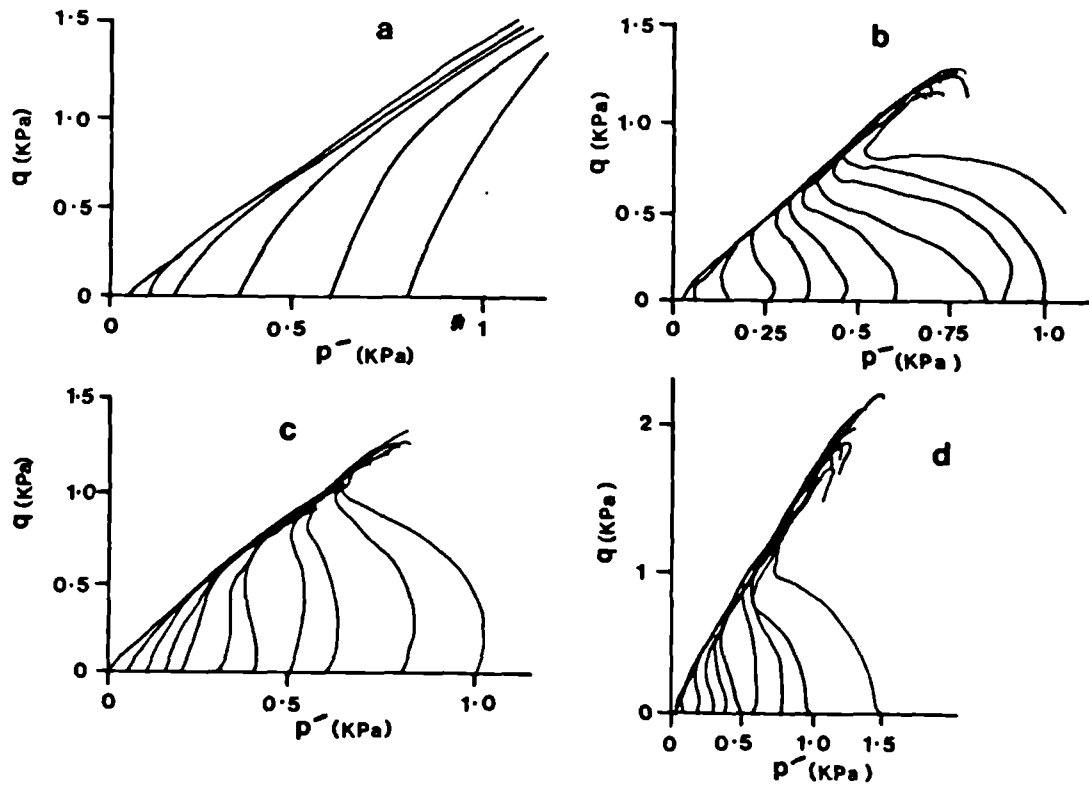


Figure 6.4. Deviatoric stress/mean effective stress plots for undrained shear experiments on, a) Leighton Buzzard Sand, b) Dogs Bay carbonate sand, c) Ballyconneely Sand, d) Bombay Mix. (After Golightly and Hyde, 1988.)

a grain rearrangement (with minimal grain shearing), and the development of large negative pore pressures.

Drained and undrained experiments were conducted by Fahey (1988) on weakly cemented, shallow carbonates from the North Rankin 'A' site in Australia. Samples were consolidated under isotropic and anisotropic conditions to pressures (150-550KPa) above and below their pre-consolidation pressure (P_c) (defined as the maximum consolidation stress to which the material has previously been subject). He considered that the observed pre-consolidation pressure to be a function of cementation. During the experiments, in which the samples were loaded under anisotropic consolidation conditions, Fahey found that a K value (stress ratio) of 0.4 applied either side of the pre-consolidation pressure. At the pre-consolidation pressure there was an increase in this stress ratio (this increase in the ratio between σ_H and σ_V is also observed during uniaxial experiments conducted on chalk, see chapter 4). Each sample was observed to reach the critical state line at an axial strain of 1%. Three results are presented for isotropically consolidated undrained shear experiments (figure 6.5). These indicate the difference between samples consolidated to pressures which were considered to be above and below the materials pre-consolidation pressure (0.5MPa). The stress path for the sample consolidated beyond this pressure is observed to behave like a normally consolidated material until reaching the critical state line followed by strain softening. The other two samples (figure 6.5) were regarded as being overconsolidated. The stress paths for both of these samples indicate strain hardening after the Critical State Line was reached. Three results are also provided for anisotropically consolidated samples. These reveal similar behaviour for samples consolidated above and below the pre-consolidation pressure. During one of these experiments, the sample (figure 6.5) was initially consolidated to a pressure above pre-consolidation pressure in order to destroy the cement bonds. Axial load was then reduced to allow the sample to become overconsolidated again and the sample was then sheared (undrained). The stress path indicates the strain hardening behaviour expected from an overconsolidated sample. A similar experiment was conducted by Fahey (1988) (figure 6.5), in which the sample

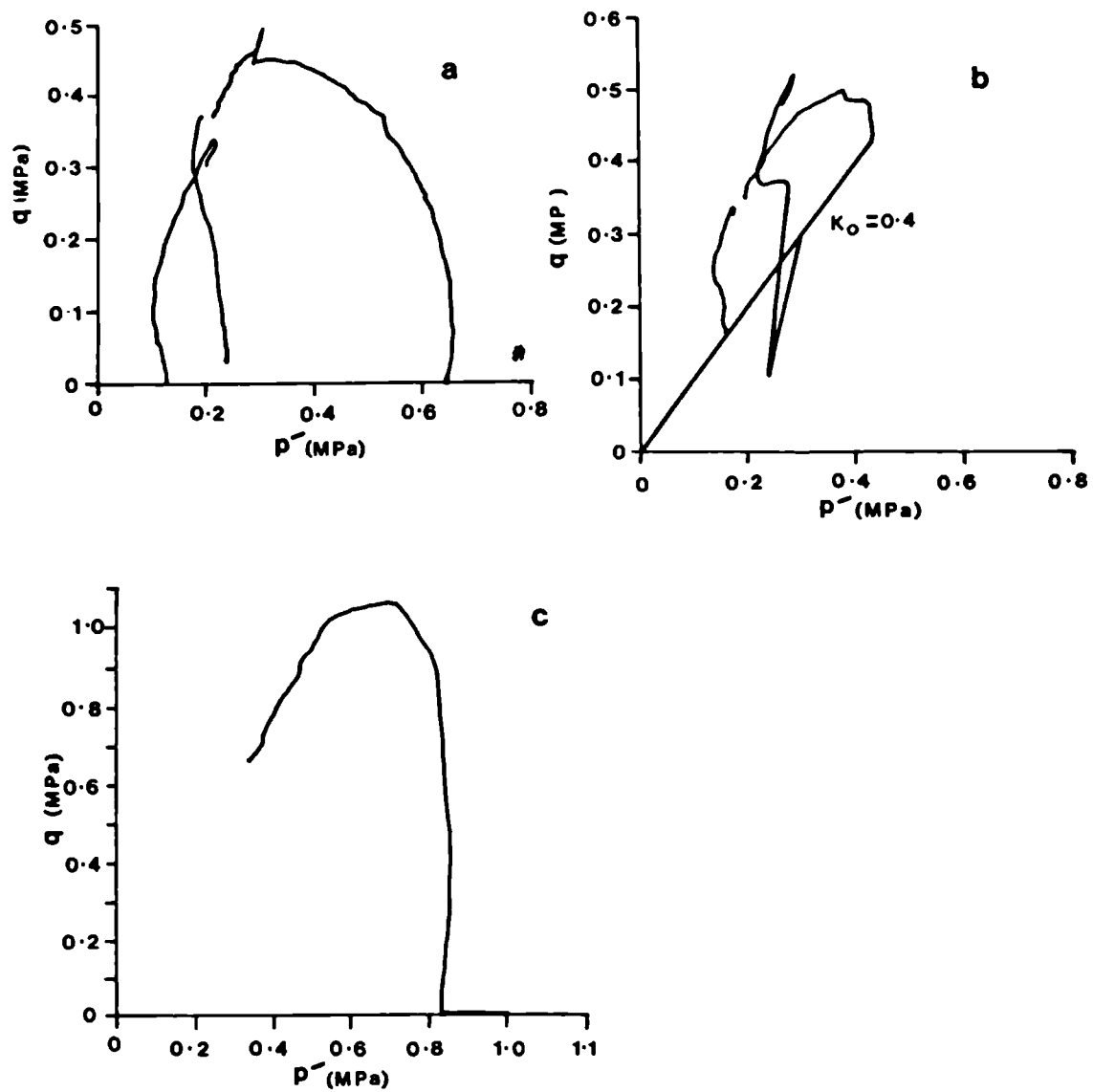


Figure 6.5. Deviatoric stress/mean effective stress plots of calcarenites from the North Rankin 'A' site, Australia. a) Three isotropically consolidated undrained shear experiments, b) anisotropically consolidated undrained shear experiments, c) an isotropically consolidated sample that was allowed to swell back to a lower pressure before being subject to undrained shear. (After Fahey, 1988.)

was initially consolidated to 1MPa isotropically (ie. above p'_c). The sample was then allowed to swell back to 0.8MPa. During undrained shear, this sample was observed to strain soften after reaching the Critical State Line at a point on the yield surface for the pre-consolidation pressure. Its behaviour was described as being similar to that of a lightly overconsolidated sample. *

Carter et al. (1988) reported the results of a large experimental programme (112 samples) conducted on calcarenites recovered from the North Rankin 'A' site. During isotropic consolidation every sample showed an initial stiffness. Samples taken to pressures above their pre-consolidation pressure showed a marked increase in compressibility, which was associated with damage to the cement structure and possibly the carbonate grains themselves. They also found that these materials attained their peak deviatoric (shear) stress at approximately 1% axial strain. During the undrained shear experiments this peak was always followed by an increase in pore pressure, and generally by a decrease in deviatoric stress, resulting in the typical strain softening/contractant behaviour observed in figure 6.6. The results indicate that the manner in which the material responded to the imposition of deviatoric stress depended on its consolidation history. Peak deviatoric stress was found to increase with increasing mean effective stress. There was also a strong correlation between the pre-consolidation pressure and the dry unit weight of the material.

Dobry et al. (1988) conducted a set of cyclic (strain controlled), undrained shear experiments using shallow buried (9-34m) uncemented or weakly-cemented calcareous sediments collected from the North Rankin 'A' site. These experiments were designed to investigate the lateral response of piles, particularly with regard to the development of excess pore pressures in the sediments adjacent to the piles due to storm action. A further static undrained triaxial experiment was also undertaken, using a similar sample under the same pressures, in order to provide a comparison with the results of the cyclic experiments. The authors discovered that cyclic loading reduced the strength of the material at low strains in comparison to the static test results, but at higher strains the

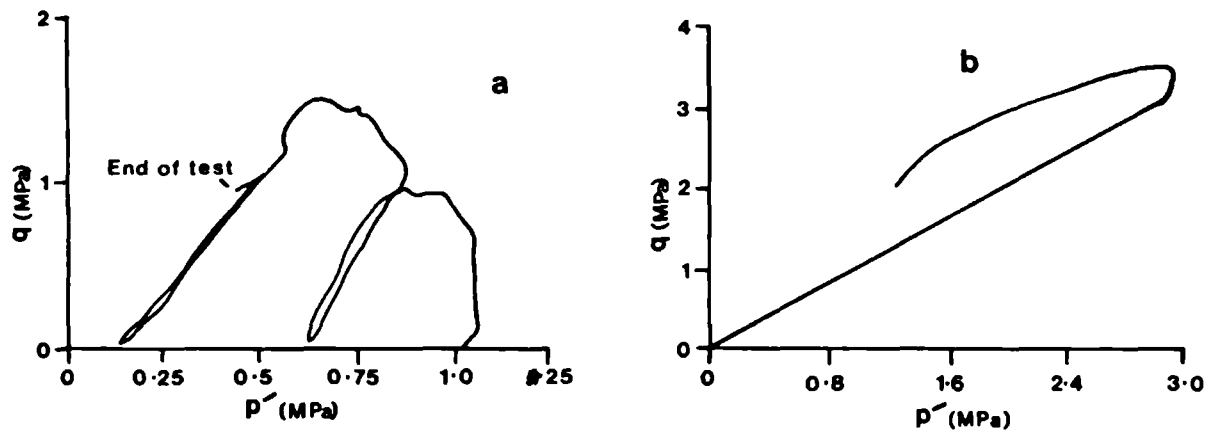


Figure. 6.6. Deviatoric stress/mean effective stress plots of calcarenites from the North Rankin 'A' site, Australia. a) An isotropically consolidated undrained shear experiment in which unload/reload cycles of the deviatoric stress were performed, b) an anisotropically consolidated undrained shear experiment. (After Carter et al., 1988.)

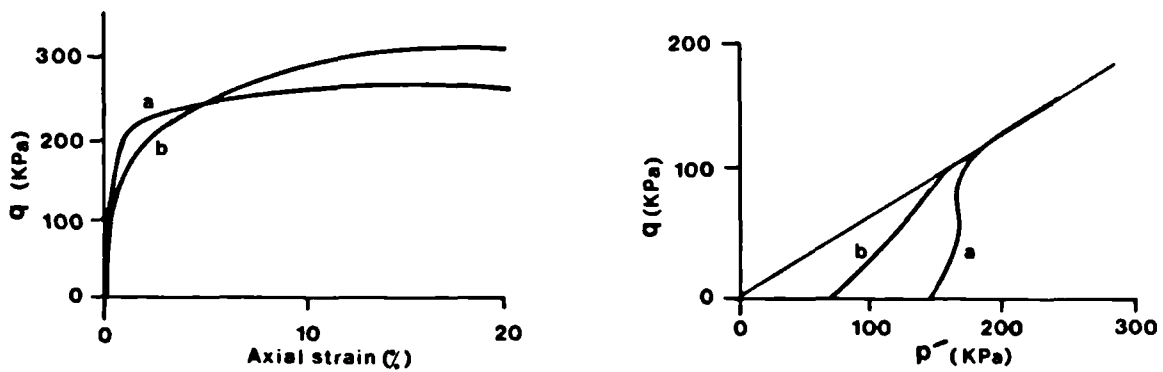


Figure. 6.7. Static undrained shear tests a) before and b) after cyclic loading. (After Dobry et al., 1988.)

cyclically loaded materials attained a higher ultimate strength (figure 6.7). The static test developed only a moderate positive pore pressure and behaved in a similar manner to a medium-dense sand or moderately overconsolidated clay (figure 6.7). The stress path for the cyclically loaded sample presented in figure 6.7 indicates that there was very little pore pressure development in this sample, which was seen to behave like a dense sand or a heavily over-consolidated clay. This data indicated that the degree of cementation, and presumably the degree of consolidation, played an important role in determining the undrained shear behaviour of the calcareous sediments. The shallow (9m-34m), less cemented sediments from the North Rankin 'A' site behave in a different manner to the deeper (110m-220m), more heavily cemented sediments tested by Carter et al. (1988) and Fahey (1988). The former are seen to develop only moderate pore pressures and behave in a dilatant (strain hardening) manner during shear. The latter, developed a significant excess pore pressure and reached a peak strength, beyond which the materials were seen to deform in a contractant (strain softening) manner.

Dunbaven (1988) also reports the results from drained and undrained shear experiments conducted on weakly-cemented, highly porous, calcareous silty sands from the North Rankin 'A' site. These consisted of skeletal fragments and pelletoids of organically bound fine carbonates. The mechanical response of these sediments to the application of load was dominated by large volumetric strains at low stress (yield (1-2MPa)) followed by plastic work hardening during drained experiments and the generation of excess pore fluid pressures in undrained experiments. A failure surface was proposed which consists of a cylinder with a radius of 0.6MPa and a hemispherical end cap (figure 6.8). A sample subjected to a stress outside this failure surface will work harden. After yield, drained and undrained tests produced very different results. Brittle failure is observed after yield at low confining pressures whilst ductile (described as diffuse shear) behaviour occurred at higher pressures.

Tsuchida et al. (1988) investigated the engineering properties of coral sands from Okinawa Island, Japan. These sediments, which have a grain size distribution ranging

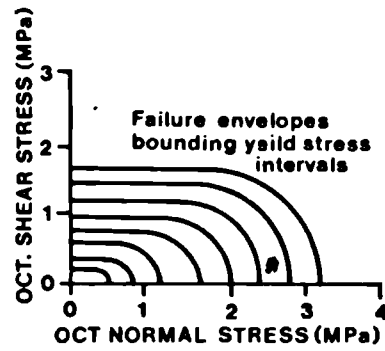


Figure. 6.8. Yield surface proposed by Dunbaven (1988).

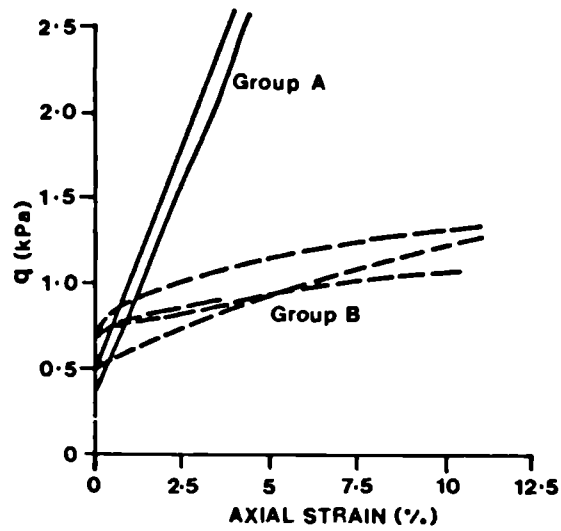


Figure. 6.9. Deviatoric stress/axial strain plot showing the effects of different grain size distributions during undrained shear. a) Uniform grain size distribution from clay size to gravel, b) grain size concentrated between fine sand and silt. (After Tsuchida et al., 1988.)

from clays to gravels (2mm), were divided into two groups. The first group contained sediments with a uniform grain size distribution over the entire range. The second group was predominantly silt and fine sand. In experimental studies both types of sediment were consolidated anisotropically to the in-situ stress conditions, and then subject to undrained shear. In the sediments with the uniform grain size distribution, deviatoric stress increased continuously with increasing strain. In the sediments dominated by the silt and fine sand grades the deviatoric stress reached a peak at a shear strain of 0.2-0.5% and remained almost constant thereafter (figure 6.9). The first group therefore behaved like a medium to dense sand, whilst the second group reacted in a similar manner to a loose sand or slightly overconsolidated clay.

Price (1988a; 1988b) studied the fabrics of the North Rankin 'A' sediments prior to, and after drained and undrained shear to identify mechanically significant fabric elements and the deformation mechanisms that govern the mechanical behaviour of these sediments. Part of this study involved the shearing of a number of samples to different shear strains and one dimensional consolidation under a variety of normal loads, in order to determine the progressive fabric changes that occurred during deformation. These sediments, recovered from a depth of between 112-220m (Price, 1988a), consisted of either well-cemented, coarse-grained, calcarenites and calcareous gravels, or weakly-cemented bioclastic sands (calcarenites) and silts (calcsiltites). This latter group have several features in common with the higher porosity chalks. For instance, although the average porosity of these well sorted carbonates was 20-30%, it could be as high as 50%. Like the high porosity chalks they were poorly cemented. The grains were found to touch at only three or four points, which reduced the size of the pore throats and resulted in low permeabilities (10^{-7} - 10^{-10} m/sec). Similarly, bioturbation has led to pelleting of the original carbonates, which, as with the chalk, has resulted in areas of increased grain size and porosity. Price (1988a) predicted that the initial response to the application of load would be governed by the elasticity of the cement at the grain contacts. He determined that the cementation, which was considered to be weak, would under increased loading, progressively fail through the sequential breaking of bonds,

starting at the points where the stress concentration was greatest. He felt that yielding of the material would therefore be a gradual process. As individual grains were released by the breakdown of their cement bonds, they would be free to move. This indicated that following yield, the material would tend to behave in a similar manner to an unconsolidated, unconsolidated sand. Initially, movement of grains was easy due to the large pore spaces, and large changes in volume (collapse) were expected. As the number of 'free' grains increased, further movement became more difficult. Friction increased and stress concentrations were high enough to lead to grain fracturing. The structure would then begin to strain harden. However, the fabrics observed by Price (1988b) in the test samples, indicated the development of not one (as he had predicted) but two different types of deformation fabric, following yield, in what were essentially similar samples tested under similar conditions. Price (1988b) described the deformation mechanisms present as displaying either a consolidation or shear type behaviour. He found that specimens which deformed by localised shear did not exhibit the predicted behaviour (see above). Unfortunately, the stress conditions that led to the formation of the fabrics described (other than yield beginning at 1MPa, 0.5% strain) are not defined. In the samples which deformed in the homogeneous manner as predicted in Price (1988a) the fabric changed progressively throughout the experiment by the release of grains and their subsequent repacking. This fabric change resulted at higher pressures in the formation of barrel shaped samples. Further deformation could only develop as a result of increased grain crushing. The second (shear) fabric, did not exhibit the predicted, progressive, homogeneous fabric changes. These samples were found to deform by the formation of discrete localised shear surfaces, in which changes were confined to restricted regions, whilst the rest of the sample remained essentially undisturbed (including the cement structure). At low stresses, large numbers of individual grains were observed to disintegrate. These were then squashed between the remaining larger grains. Discrete shears developed rapidly and continued to be active for the remainder of the test. The pore fluid which was described as a fluidised carbonate mud (resulting from grain crushing) assisted the deformation by lubricating the surrounding grains.

These studies indicate that there are a number of similarities in the manner in which cemented carbonates deform when subject to large shear stresses. These similarities can be summarised as:

- *1) Their behaviour varies from that of a loose sand or wet clay to a dense sand. This appears to be dependent on various physical characteristics, including:-*
- *a) the depth of burial and therefore the amount of cementation (Dunbaven (1988); Fahey (1988); Carter et al. (1988)),*
- *b) their constituent materials (Golightly and Hyde (1988)),*
- *c) the grain size and grain size distribution (Tsuchida et al. (1988); Golightly and Hyde (1988)),*

The weakly cemented and uncemented, shallow (9-34m) samples tested by Dobry et al. (1988) were observed to behave like a dense sand, whereas the deeper (110-220m), slightly more cemented samples reported in Fahey (1988) behaved like a loose sand or wet clay. This indicates that the degree of cementation is an important factor in determining the manner of failure. The stress range over which these experiments were conducted increased with increasing depth of recovery of the samples. The cement in the sediments used by Dobry et al. (1988) may not have been developed sufficiently to provide a rigid structure. This lack of cementation compared to the samples used by Fahey (1988) is reflected in the lower stresses required to fail the samples in Dobry et al. (1988). These stresses would have also been too low to induce shearing of the constituent grains, and hence they behaved like a dense (quartz) sand. The results reported in Price (1988b) for highly cemented North Rankin calcarenites indicate that there is an upper limit to the degree of cementation over which the weaker style of behaviour will develop. It would appear that there exists a range of cementation that may develop in which carbonates will behave like loose sands. This range is bounded by weakly cemented, high porosity carbonates, in which the cement has not sufficiently developed

to provide a rigid structure, and heavily cemented carbonates in which the cement is too pervasive and the porosity too low to allow collapse of the structure.

Deformation behaviour is further influenced by the constituent materials. The results in Golightly and Hyde (1988) clearly show that there is a range of behaviour from the Leighton Buzzard quartz sands which behave like a dense sand, through that of the Bombay Mix (a mixture of siliceous and carbonate grains) to the calcareous Ballyconneely and Dogs Bay sands which behave like a medium/weak sand. Variations in grain size are also seen to exert an influence on the style of deformation. Tsuchida et al. (1988) found that the Japanese sediments with a wide variation in grain size behaved like a dense/medium sand, whereas the sediments which were dominantly of sand and silt grade behaved in a similar manner to a medium/loose sand. The results of Golightly and Hyde (1988) indicate that grading may exert only a subordinate influence on the style of behaviour, as the well graded Bombay Mix and Dogs Bay show different styles of behaviour to the medium graded Ballyconneely and Leighton Buzzard sediments.

- *2) Two different styles of deformation are developed by the application of shear stress, namely:-*
 - *a) brittle deformation,*
 - *b) ductile deformation.*

Experiments reported by Dunbaven (1988) indicated that low pressures resulted in brittle deformation and high pressures led to the development of ductile failure, but Price (1988b) found that both types of behaviour occurred at similar stresses. The former behaviour was also reported by Fahey (1988) and Carter et al. (1988), who both concluded that this represented a difference in deformation for sediments when subject to pressures below or above their pre-consolidation pressure. It is difficult from the data provided to see why the behaviour observed by Price (1988b) does not agree with Fahey and Carter et al.

- 3) *These studies have several other features in common. For example:-*
 - a) *Fahey (1988) and Carter et al. (1988) found that unloading/reloading during shear did not effect the undrained stress path and plotted as straight lines in log stress space irrespective of whether they occurred above or below the pre- consolidation pressure. This straight line behaviour was felt to represent an elastic type response (Fahey, 1988) resulting from the interlocking of grains.*
 - b) *Yield was observed at an axial strain of less than 3% and usually less than 1% in studies by Fahey (1988), Carter et al. (1988), Dobry et al. (1988) and Golightly and Hyde (1988). Yield at low strain was also observed by Tsuchida et al. (1988) in the sand and silt dominated sediments, but grain size distribution may modify this behaviour, as the deviatoric stress/axial strain plot for the second group of sediments (gravels-silt) do not contain a yield point. The stress/strain data presented by Golightly and Hyde (1988) indicate that yield strain is increased as the confining pressure increases.*

The data reported in these studies provide a basis for the analysis of the results of the undrained shear experiments conducted on outcrop chalks that comprise the remainder of this chapter. In particular they relate changes in stress, strain and void ratio recorded during undrained shear experiments to physical changes in the materials. Similar changes have been observed in the chalk experiments reported below.

6.4. METHODOLOGY.

A description of sample preparation and the high pressure triaxial equipment used for these experiments can be found in chapter 4. Initially, each sample was subjected to drained consolidation under either isotropic or anisotropic (K_0) stress conditions. There are two methods by which isotropic consolidation can be achieved (Lambe and Whitman, 1979). In the first and most frequently used method, the confining pressure is increased in incremental steps. During the application of each increment, drainage from the sample is prevented. Once the desired pressure had been achieved, drainage from one or both ends of the sample is then re-established thus allowing consolidation

to proceed. Once consolidation is complete the drainage lines are once again closed and the confining pressure is increased to the next increment. (The pressure is usually doubled with each successive increment). This method of consolidation creates a pressure gradient between the excess pore fluid which has developed in the sample and the fluid in the drainage line when drainage is re-established from the sample. In a low permeability rock such as clay or chalk this pressure gradient gradually migrates through the sample until consolidation is complete and the pore pressures in the sample are equal to the applied back pressure. As the confining pressure is increased with each increment, the pore pressure gradient that develops (between the back pressure and the induced pore pressure) becomes larger. In sediments of low permeability this could lead to a sustainable pressure difference between either end of the sample. Drainage results in an uneven stress distribution (including induced shear stresses), preferential consolidation at the drained end of the sample and a weakening of the sample (Skinner pers. comm., 1989).

The second method, described as the ramped method in Fahey (1988), was the one adopted in this experimental programme. In this method, the confining pressure is increased in small, almost continuous steps until the required mean effective stress has been attained. The bottom drainage line from the sample remains open to the back pressure (usually 1.8MPa) throughout the period of consolidation. This method therefore helps avoid the development of an uneven distribution of stress in the sample during consolidation. The rate of pressure increase is determined by the permeability of the sample, and is controlled to prevent the development of excess pore pressures (determined from the pore pressure response at the top of the sample). The same method of pressure increase was used for the K_0 experiments reported in chapters four and five therefore the results should be comparable. One sample was consolidated using the step method and the results are presented for comparison in section 6.6.

Once the sample has been consolidated to the desired mean effective stress (p') (table 6.1), this pressure was maintained and the bottom drainage line was closed. The

balanced ram was then advanced to contact the sample, after which the loading was continued (for all but two samples (table 6.1)) with a constant displacement rate of 0.1mm/min. The samples were generally shortened by approximately 25%. During loading, measurements of the applied deviatoric stress, pore pressures at either end of the sample, the confining pressure, and in the case of the uniaxial strain experiments the radial strain were recorded.

Table 6.1.

UNDRAINED SHEAR EXPERIMENTAL DATA.

EXP.	P'	DISPLACEMENT	EXP	P'	DISPLACEMENT
No.	(MPa)	RATE	No.	(MPa)	RATE
		(mm/min)			(mm/min)
BHWC1	50	0.1	SKWC1	40	0.1
BHWC2	20	0.1	SKWC3	10.4	0.1
BHWC3	10.2	0.1	SKWC4	22	K_O
BHWC4	42.9	0.1	SKWC5	19.4	0.1
BHWC5	30	0.1	SKWC6	1	0.1
BHWC6	10	0.01	SKWC7	5.3	0.1
BHWC7	10	1.0	SKWC8	2.8	0.1
BHWC8	3	0.1	SKWC9	10.6	K_O
BHWC9	25	0.1	SKWC10	9.5	0.1

6.5. EXPERIMENTAL RESULTS.

This section has been divided into three sub-sections. The first, describes the results for the samples that were consolidated under isotropic stress conditions prior to undrained shear. The second, details the results of those experiments in which the samples were anisotropically (K_0) consolidated before undrained shear. The third, presents in

greater detail, data included in the first sub-section, obtained during a limited number of isotropically consolidated experiments conducted at different rates of strain.

6.5.1. Isotropically consolidated samples.

Deviatoric stress/axial strain curves for the two sets of experiments where the chalk was isotropically consolidated are illustrated in figures 6.10 (Butser Hill) and 6.11 (Stevn's Klint). These two graphs indicate the influence exerted by the consolidation pressure in determining the magnitude of the shear stress at yield (see tables 6.3a and 6.3b). Figures 6.10 and 6.11 indicate that all but two experiments conducted on the Butser Hill chalk and one experiment involving a Stevn's Klint sample experience strain softening after yield. The other three samples (figure 6.10) and (figure 6.11) were consolidated to higher pressures. These three samples are seen to strain harden after yield. The behaviour of the Butser Hill chalks (figure 6.10) show this division between strain softening and hardening more clearly than the Stevn's Klint chalks. The samples consolidated to 42.9MPa (BHWC4) and 51.6MPa (BHWC1) both appear to fail and recover before reaching yield. This apparent failure and recovery is actually the result of a temporary drop in the confining pressure. The other samples, consolidated to pressures below 30MPa (table 6.1), have all undergone strain softening following yield. Yield is observed in both sets of data to occur at progressively higher axial strains (albeit below 2% (table 6.3a)) as the consolidation pressure increases. A failure of the back pressure system and problems with the drainage system during the experiment conducted on sample BHWC4 (figure 6.10) have resulted in an anomalous result. Yield began at approximately 1% axial shortening but was not completed (due to continued partial drainage from the sample) until an axial strain of 5.72% had been attained. Ultimately, this does not appear to have affected the final $p'/q/e$ values to any significant degree (table 6.3a).

The Stevn's Klint chalks (figure 6.11) are seen (with the exception of sample SKWC1) to strain soften after yield. The lack of data during the pre-yield section of experiment SKWC5 was caused by a problem with the logging device. The final deviatoric stresses

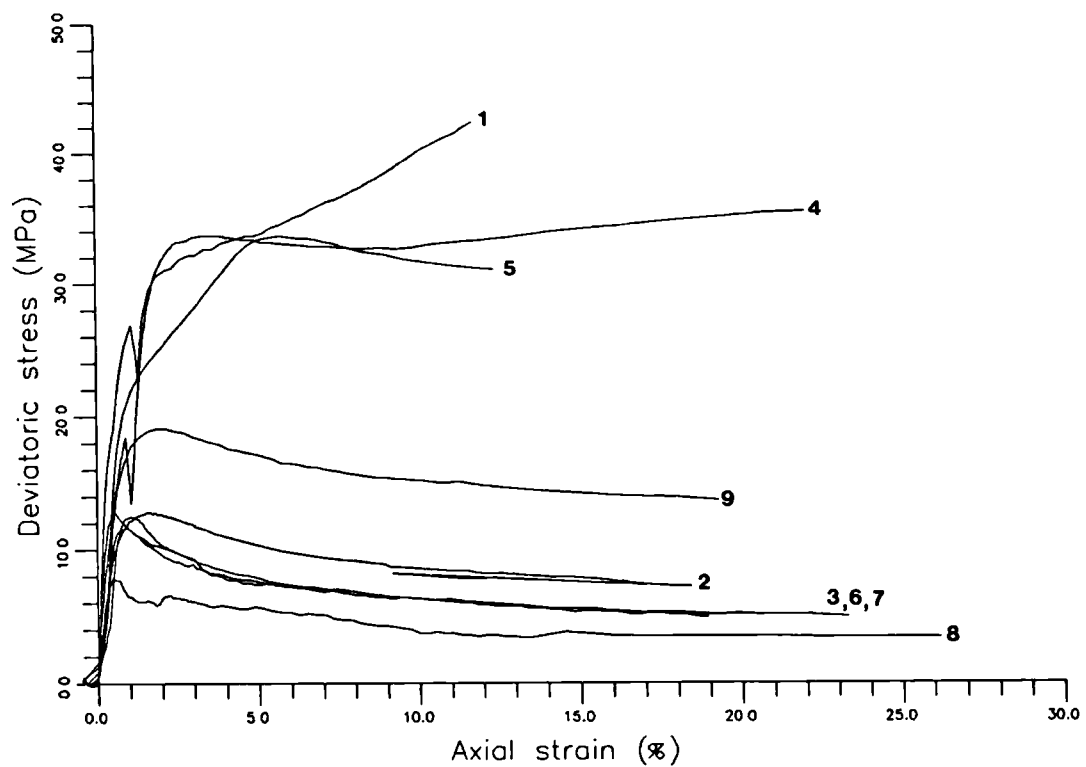


Figure. 6.10. Graph of deviatoric stress/axial strain for isotropically consolidated undrained shear experiments on Butser Hill outcrop samples.

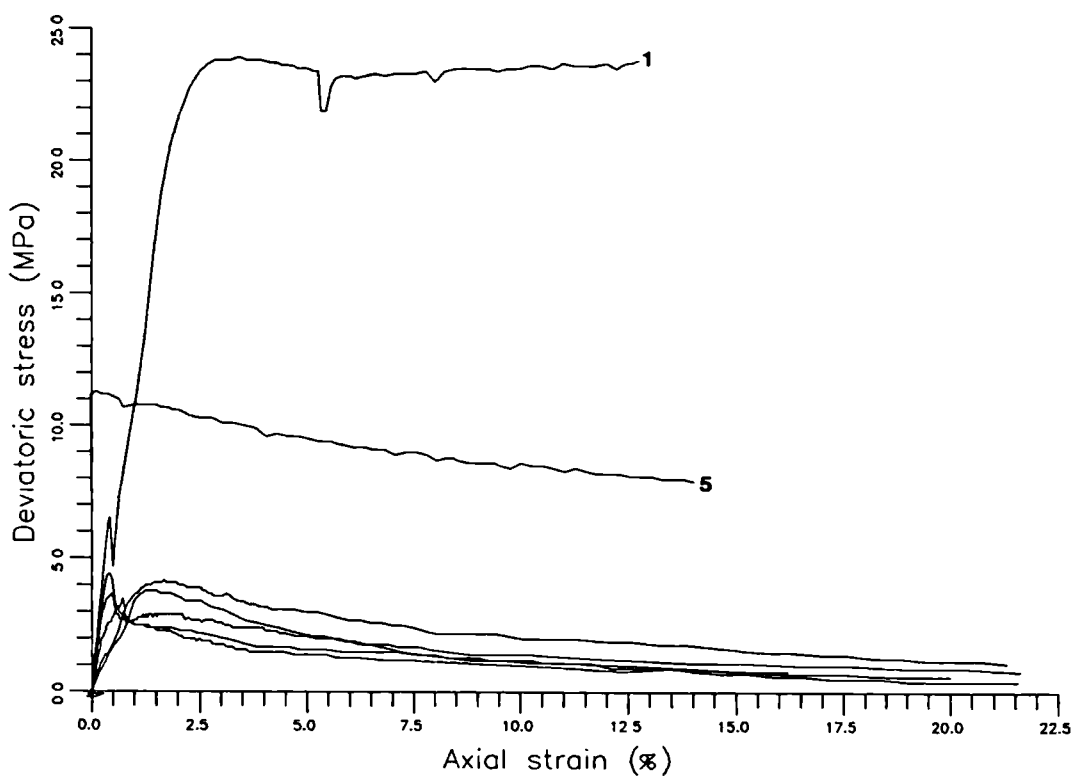


Figure. 6.11. Graph of deviatoric stress/axial strain for isotropically consolidated undrained shear experiments on Stevn's Klint outcrop samples.

(q_f) are presented in table 6.3b as a percentage of the peak deviatoric stress (at yield). This percentage can be used to represent the degree of strain softening experienced during shear (ie. the lower the percentage the greater the strain softening). These data indicate that the Stevn's Klint chalks are subject to more severe strain softening under lower confining pressures than the Butser Hill chalks.

Figures 6.12 and 6.13 present the pore pressure/mean effective stress response for the undrained section of each experiment. It can be seen that during shear each sample develops a substantial excess pore pressure (tables 6.3a and 6.3b). Figures 6.14 and 6.15 present pore pressure/axial strain plots. These indicate that in each experiment (excluding sample BHWC5 in figure 6.14) significant pore pressure generation had been achieved within the first 4% axial strain. As axial strain continued to increase, further pore pressure changes are observed to be fairly small.

The relationships between pore pressure generation and changes in deviatoric stress are presented graphically in figures 6.16 and 6.17 and as a percentage in table 6.3b. The application of a shear stress leads to an increase in pore pressure. However, both figures indicate that prior to yield, the deviatoric stress increases faster than the corresponding increase in pore pressure. At yield, the deviatoric stress stops increasing but pore pressures continue to rise. Following yield, strain softening is represented by a decrease in deviatoric stress and further increase in pore pressure, and strain hardening results in an increase in deviatoric stress and a decrease in pore pressure.

Figures 6.18 and 6.19 indicate how the generation of an excess pore fluid pressure changes the effective stress paths followed during each experiment. The difference between strain hardening and strain softening is clearly visible in figure 6.18. The plot of each experiment ends on a straight failure line that passes through the origin of the graph. This failure line appears to be the equivalent of the Critical State Line. However, the Critical State Line only exists as a line in three dimensional stress/void ratio space. The plots of the experiments in figures 6.18 and 6.19 represent a series of individual stress

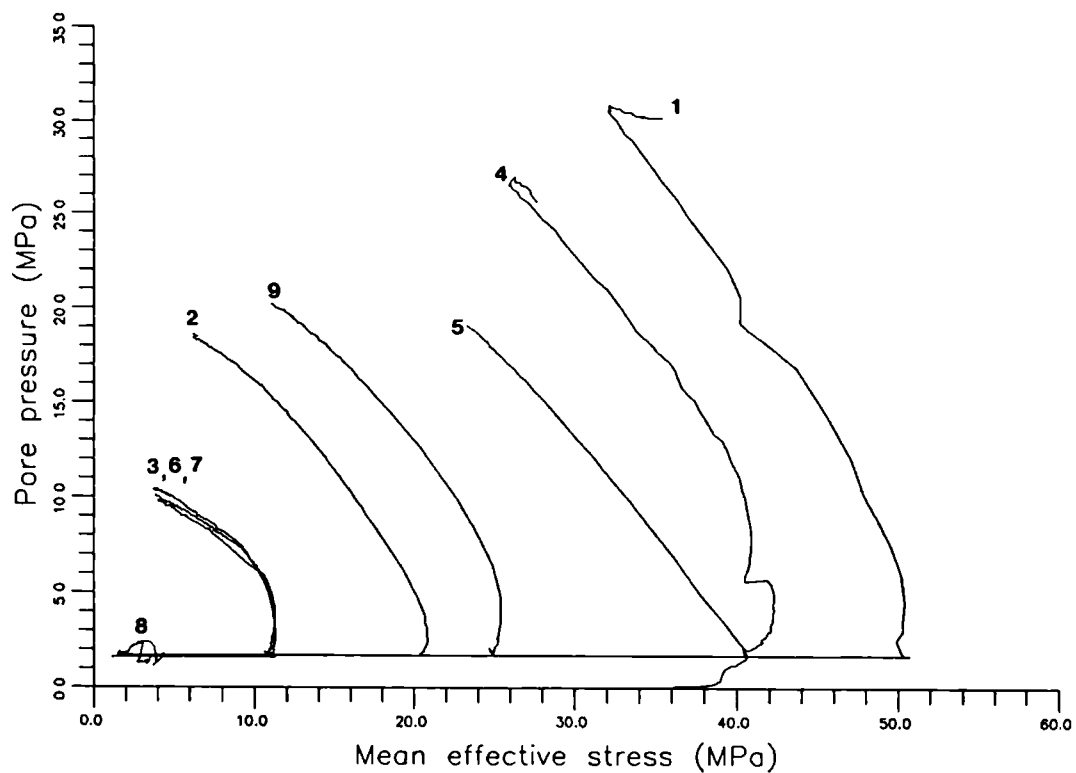


Figure 6.12. Graph of pore pressure/mean effective stress for isotropically consolidated undrained shear experiments on Butser Hill samples.

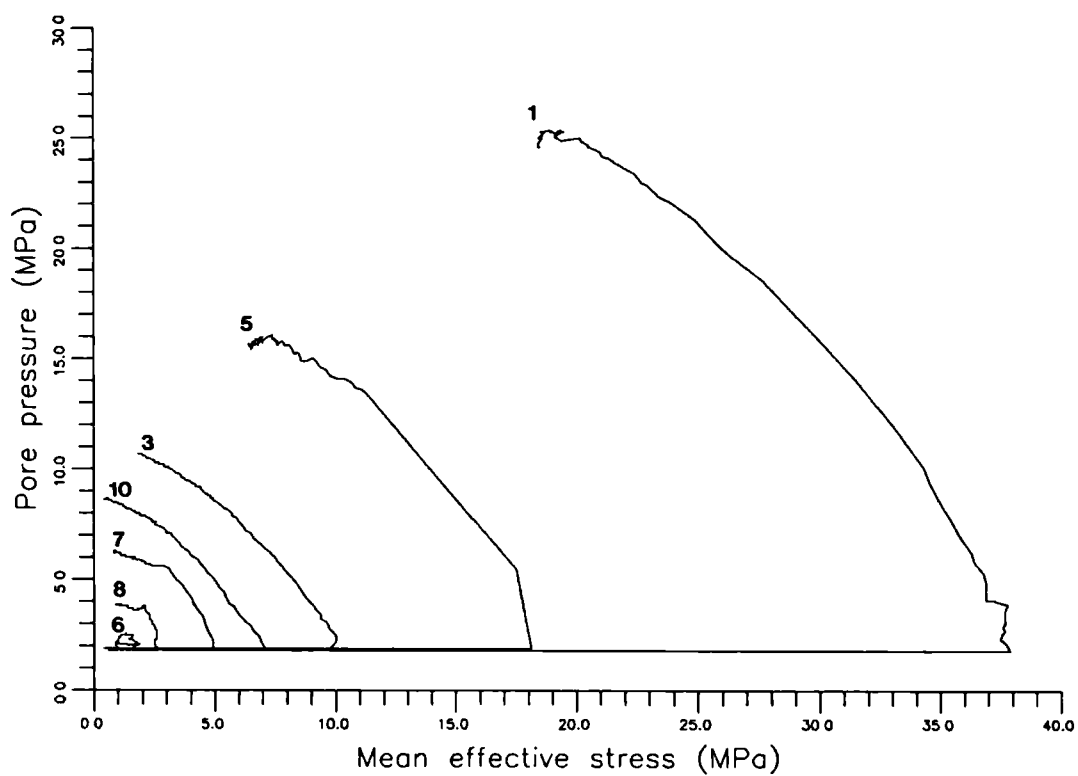


Figure 6.13. Graph of pore pressure/mean effective stress for isotropically consolidated undrained shear experiments on Stevn's Klint samples.

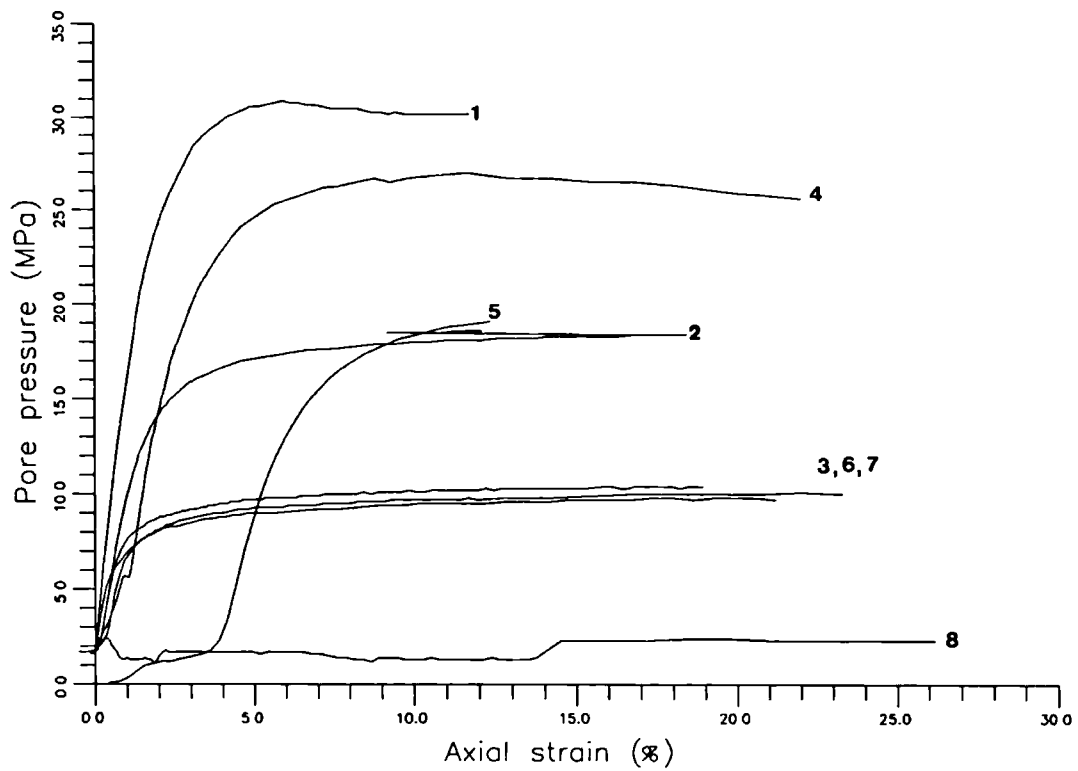


Figure 6.14. Graph of pore pressure/axial strain for isotropically consolidated undrained shear experiments on Butser Hill samples.

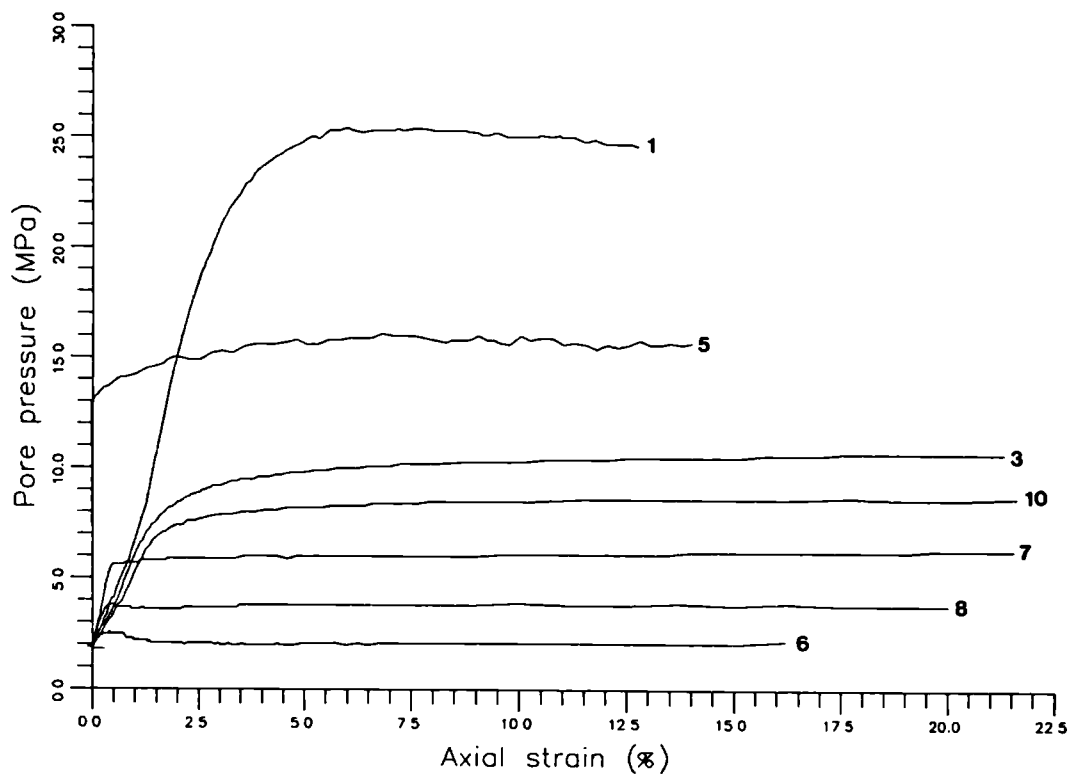


Figure 6.15. Graph of pore pressure/axial strain for isotropically consolidated undrained shear experiments on Stevn's Klint samples.

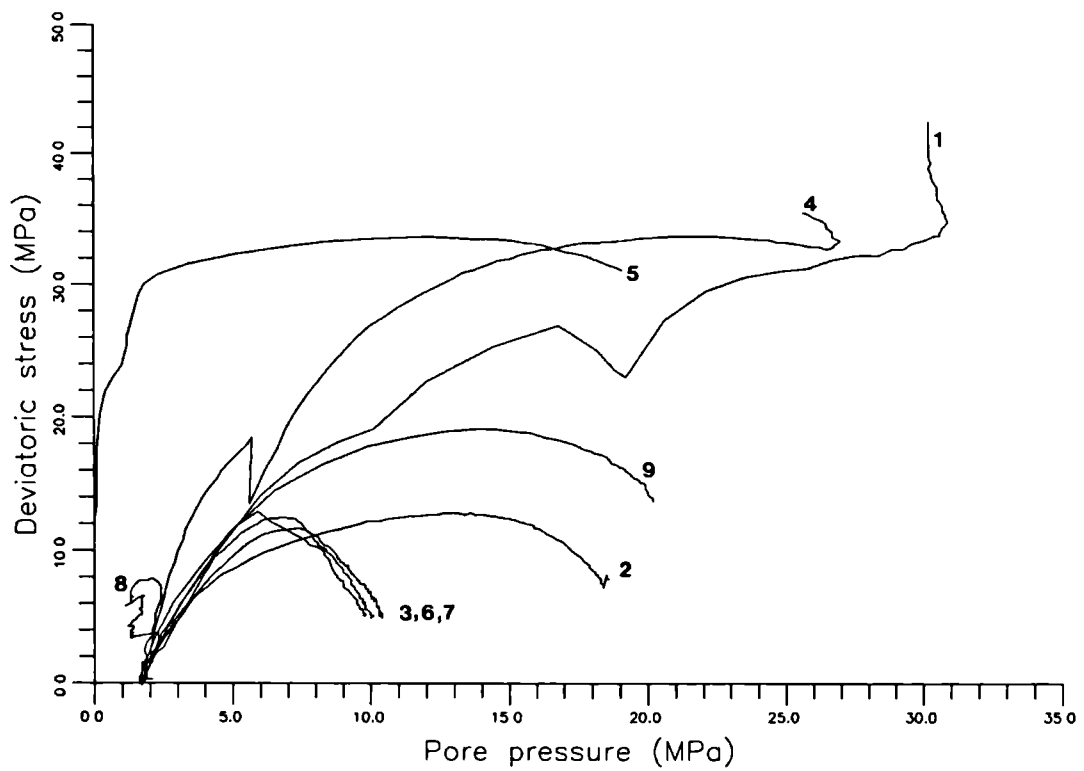


Figure. 6.16. Graph of deviatoric stress/pore pressure for isotropically consolidated undrained shear experiments on Butser Hill samples.

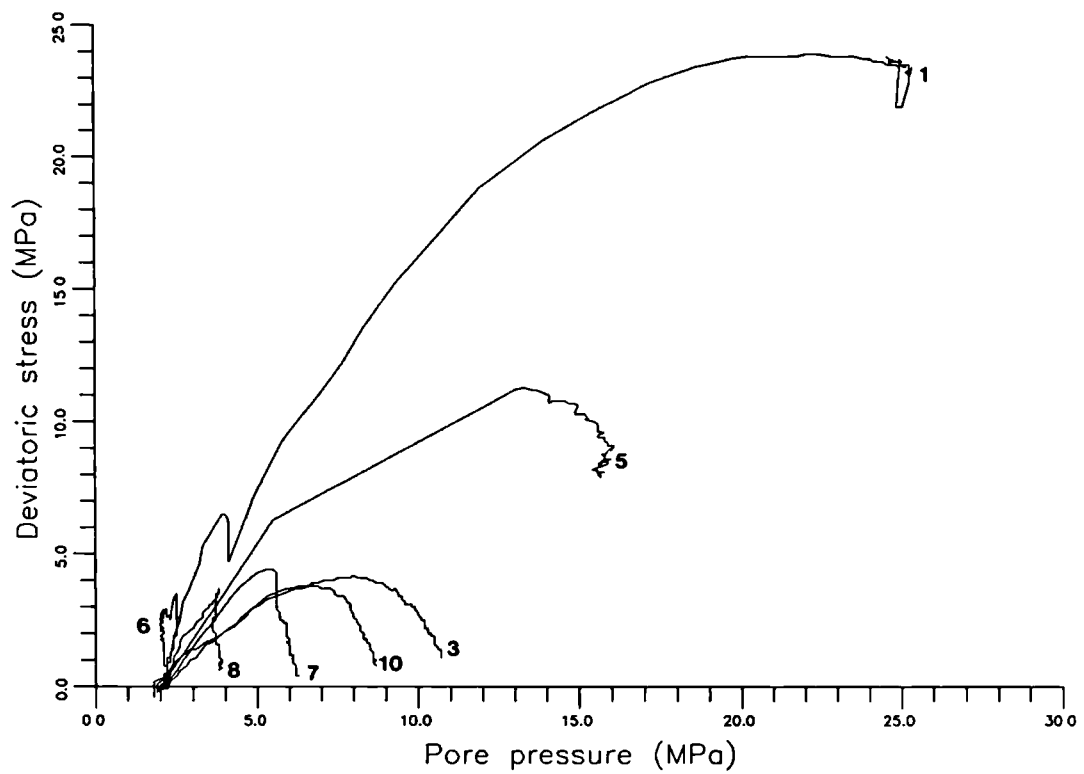


Figure. 6.17. Graph of deviatoric stress/pore pressure for isotropically consolidated undrained shear experiments on Stevn's Klint samples.

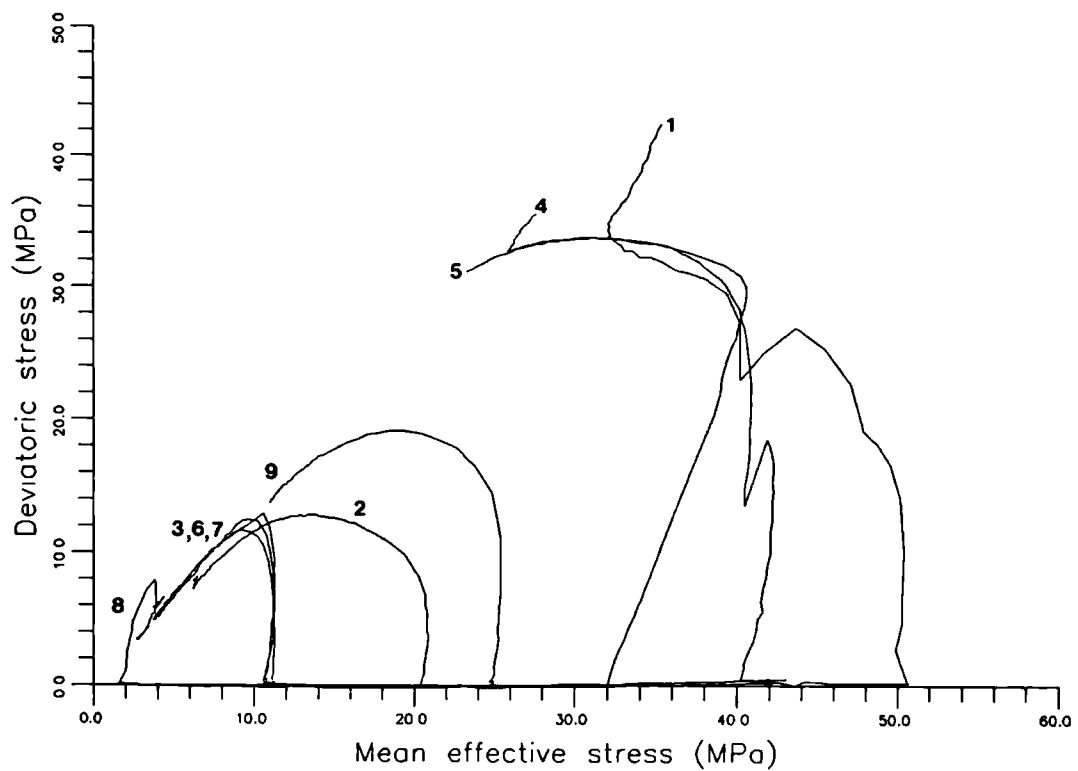


Figure. 6.18. Deviatoric stress/mean effective stress graph for isotropically consolidated undrained shear experiments on Butser Hill samples.

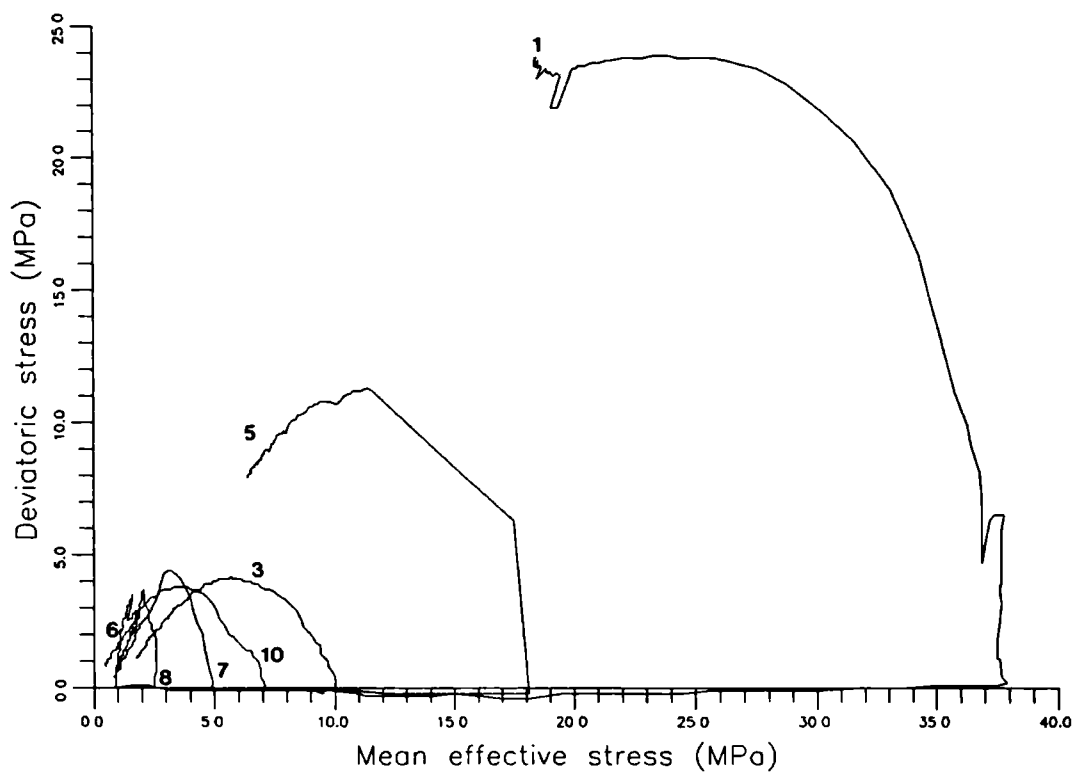


Figure. 6.19. Deviatoric stress/mean effective stress graph for isotropically consolidated undrained shear experiments on Stevn's Klint samples.

paths in two dimensional effective stress space. Each stress path exists on a different constant void ratio plane and, on such a plane, the critical state only exists as a single point. This means that when a stress path (plotted on a graph with axes of effective stress) is described as moving up or down the Critical State Line it is in fact only moving along a two dimensional projection of that line (unless the volume is changing during undrained shear).

The effective stress path for BHW C8 (figure 6.18), which was consolidated to 1MPa, is observed to pass above the projection of the Critical State Line, to yield at a deviatoric stress of 7.9MPa. This increase in deviatoric stress is accompanied by a slight increase in mean effective stress. Following yield, the sample is observed to rapidly strain soften, as indicated by the significant decrease in deviatoric stress. Deviatoric stress continues to decrease until the stress path coincides with the projection of the Critical State Line. The rate of strain softening decreases and the stress path is observed to pass down the projection of the Critical State Line. The stress paths for the three samples consolidated to approximately 10MPa (BHW C3, 6 and 7) climb steeply towards this projection before they yield and follow it. The stress paths for the two samples consolidated under pressures of 20MPa and 25MPa (BHW C2 and 9) also indicate an initial increase in deviatoric stress with very little change in mean effective stress. But as the deviatoric stress continues to increase, higher pore pressures are generated. This results in a gradual decrease in mean effective stress until yield. Following yield, these stress paths also follow down the projection of the Critical State Line, indicating strain softening. The samples consolidated to pressures above 30MPa all yield at approximately the same deviatoric stress. Following yield, BHW C5 is observed to strain soften and the other two (BHW C1 and 4), which were subject to the largest consolidation pressures, strain harden. In figure 6.19, all the samples except sample SKWC1, which was consolidated to the highest pressure (37.9MPa) are seen to strain soften after yield. This sample (SKWC1) begins to strain soften after yield, but as the stress path approaches the projection of the Critical State Line, the behaviour changes to one of strain hardening.

Figures 6.20 and 6.21 present the changes in void ratio plotted against mean effective stress. The two parts of each experiment can be clearly distinguished. The initial section indicates the decrease in void ratio associated with consolidation, and the straight line indicates a constant volume (as no volume changes are recorded and the accepted theories for undrained shear state that the volume of the sample does not change) during the undrained part of each experiment. Figure 6.20 shows the changes in void ratio for the Butser Hill chinks. Once the required mean effective stress had been attained, each plot shows a deviation (decrease in void ratio) from the consolidation curve. As no excess pore pressures were generated during consolidation, these subsequent volume changes must represent the effects of secondary consolidation. The Stevn's Klint results (figure 6.21) indicate that shearing proceeded as soon as the required mean effective stress had been achieved (hence there are no volume changes due to secondary consolidation). The variation in the initial void ratio (figure 6.21) indicates a variation of 2.7% porosity in the Stevn's Klint samples.

6.5.2. Anisotropically consolidated samples.

Four samples were anisotropically consolidated. The results of these experiments are presented in figures 6.22 through to 6.35. The two experiments performed on Butser Hill chalk were conducted by Addis (1987) whilst at University College. These are now held in a chalk experimental database (Goldsmith et al., 1989). The second pair of experiments, using Stevn's Klint chalk, were conducted as part of the experimental programme for this thesis. In each experiment, the sample was consolidated under K_0 conditions (see chapter 4 for details of uniaxial experimental procedure) following the ramped method described in section 6.4.

Figures 6.22 and 6.23 (deviatoric stress/axial strain) clearly indicate the typical uniaxial strain behaviour of both chinks (see chapter 4). The Butser Hill samples (figure 6.22) were consolidated to greater effective stresses than the Stevn's Klint samples (figure 6.23). Figure 6.22 indicates that in the Butser Hill samples, yield, which occurred at approximately 1% axial shortening, was followed by strain softening (for a further 5%

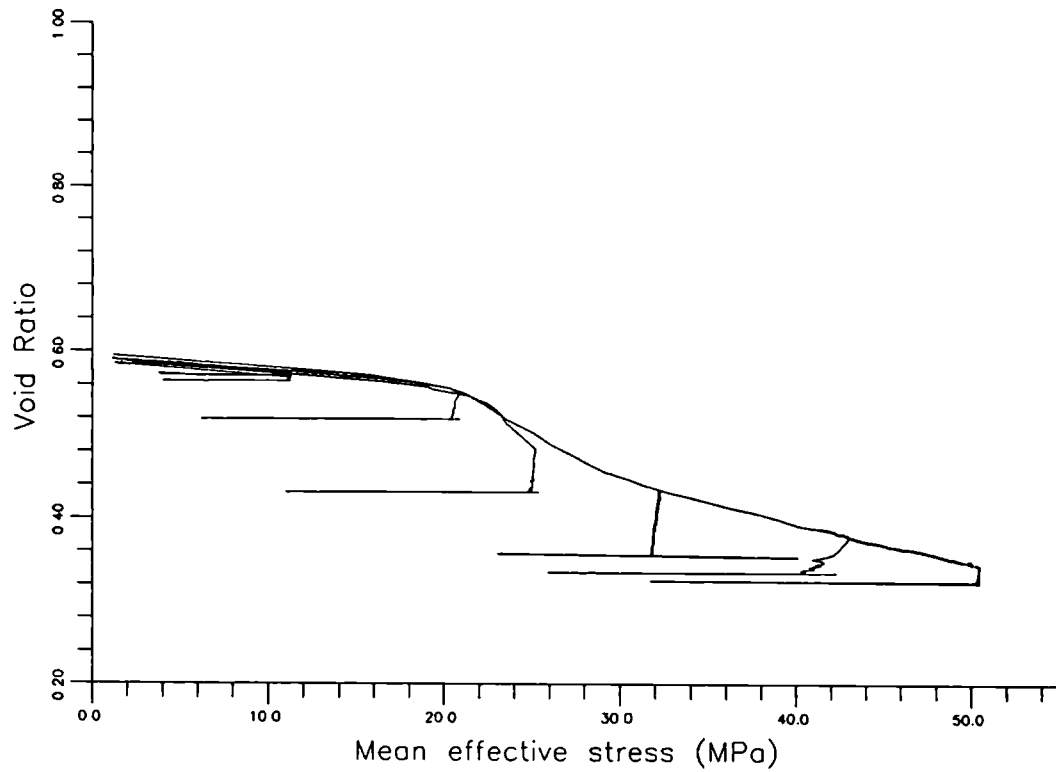


Figure. 6.20. Graph of void ratio/mean effective stress for isotropically consolidated undrained shear experiments on Butser Hill samples.

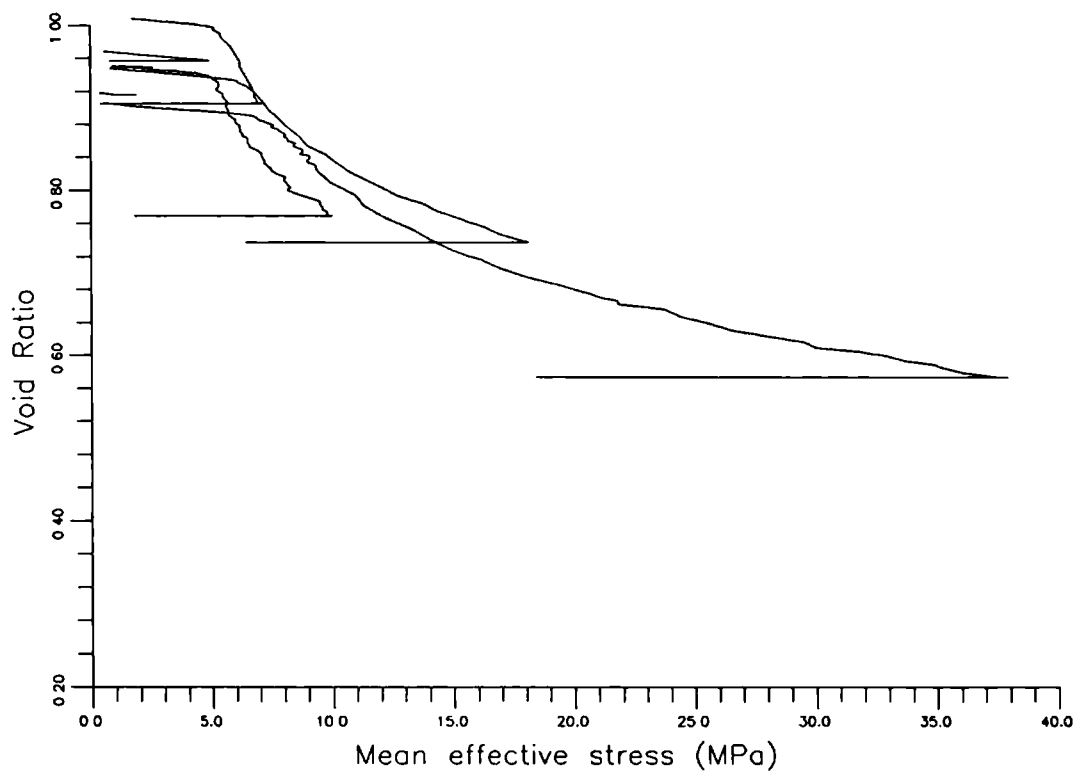


Figure. 6.21. Graph of void ratio/mean effective stress for isotropically consolidated undrained shear experiments on Stevn's Klint samples.

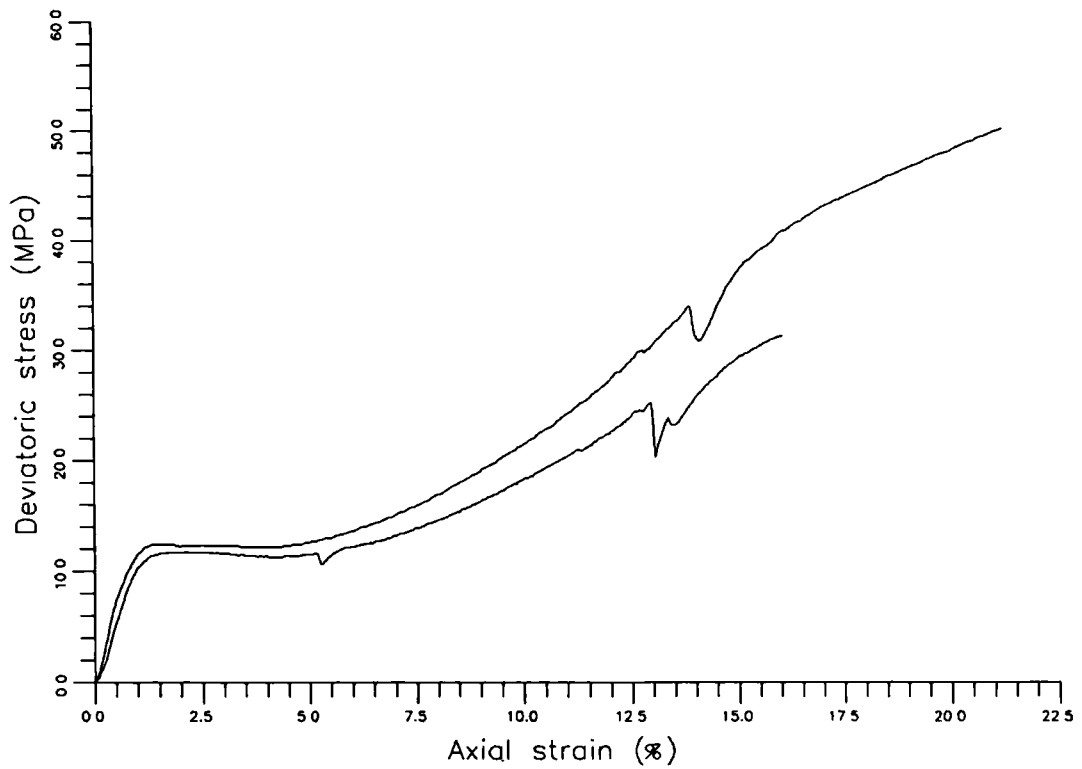


Figure. 6.22. Graph of deviatoric stress/axial strain for anisotropically (K_0) consolidated undrained shear experiments on Butser Hill samples. (After Addis, 1987.)

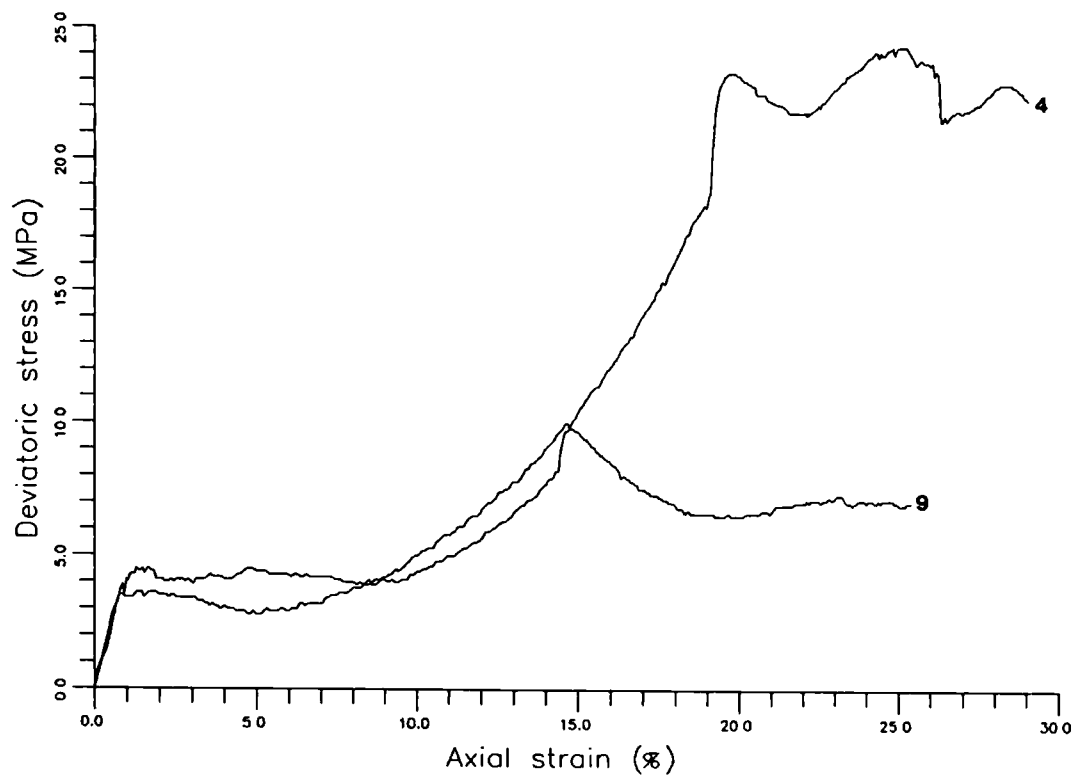


Figure. 6.23. Graph of deviatoric stress/axial strain for anisotropically (K_0) consolidated undrained shear experiments on Stevn's Klint samples.

axial strain) and eventually strain hardening. The undrained shear part of these two experiments began at an axial strain of between 13% and 14% during the strain hardening phase. Prior to undrained shear there was decrease in differential stress. However, this decrease was recovered during shear and both samples are then seen to continue strain hardening. Addis (1987) explained that the initial decrease in deviatoric stress (and mean effective stress) resulted from problems with the confining pressure system. The higher initial porosities of the Stevn's Klint samples (figure 6.23) are observed to have a marked affect on their stress/strain curves, compared to those for the Butser Hill chalks. Following yield (figure 6.23) at approximately 1% axial shortening, strain softening continued for approximately 7-8% axial strain and was then replaced by strain hardening. Both Stevn's Klint samples were in the process of strain hardening when undrained shear was initiated. Their undrained shear behaviour was quite different from that observed for the Butser Hill samples. During undrained shear, both Stevn's Klint samples were seen to revert to a strain softening behaviour.

Figures 6.24 and 6.25 are graphs of pore pressure generation against mean effective stress. Pore pressure is also plotted against axial strain in figures 6.26 and 6.27 and against deviatoric stress in figures 6.28 and 6.29. It can be seen from figures 6.24-6.29, that pore pressure generation was more rapid in the stronger Butser Hill chalks than in the Stevn's Klint samples. The onset of strain hardening led to a gradual decrease in pore pressure in the Butser Hill samples, whilst strain softening led to further increases in pore pressure in the Stevn's Klint samples.

The style of deformation behaviour (strain softening or hardening) and the speed of pore pressure generation are both seen to significantly affect the deviatoric/mean effective stress graphs (figures 6.30 and 6.31). The stress paths in figure 6.30 (Butser Hill) show the effects of the decrease in confining pressure prior to shear. The initial stage of shear was marked by an increase in pore pressure (decrease in mean effective stress) that was faster than the increase in deviatoric stress. This behaviour was replaced, eventually, by more typical strain hardening stress paths. Figure 6.31 indicates that un-

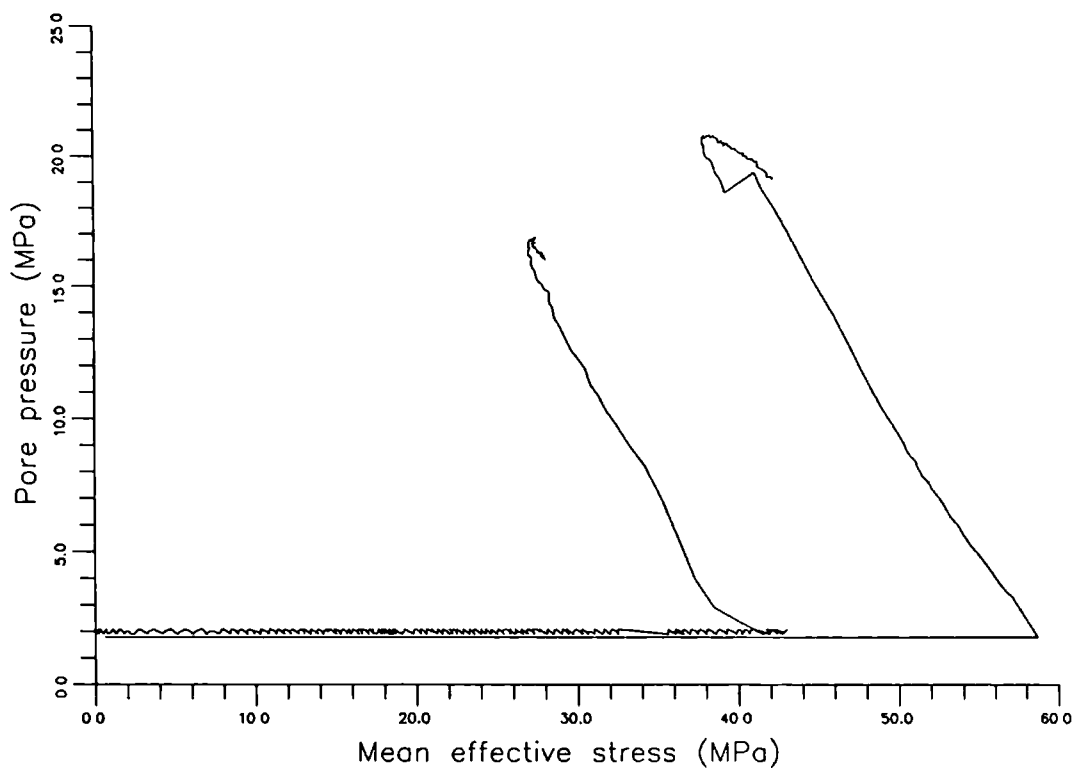


Figure. 6.24. Graph of pore pressure/mean effective stress for anisotropically (K_0) consolidated undrained shear experiments on Butser Hill samples. (After Addis, 1987.)

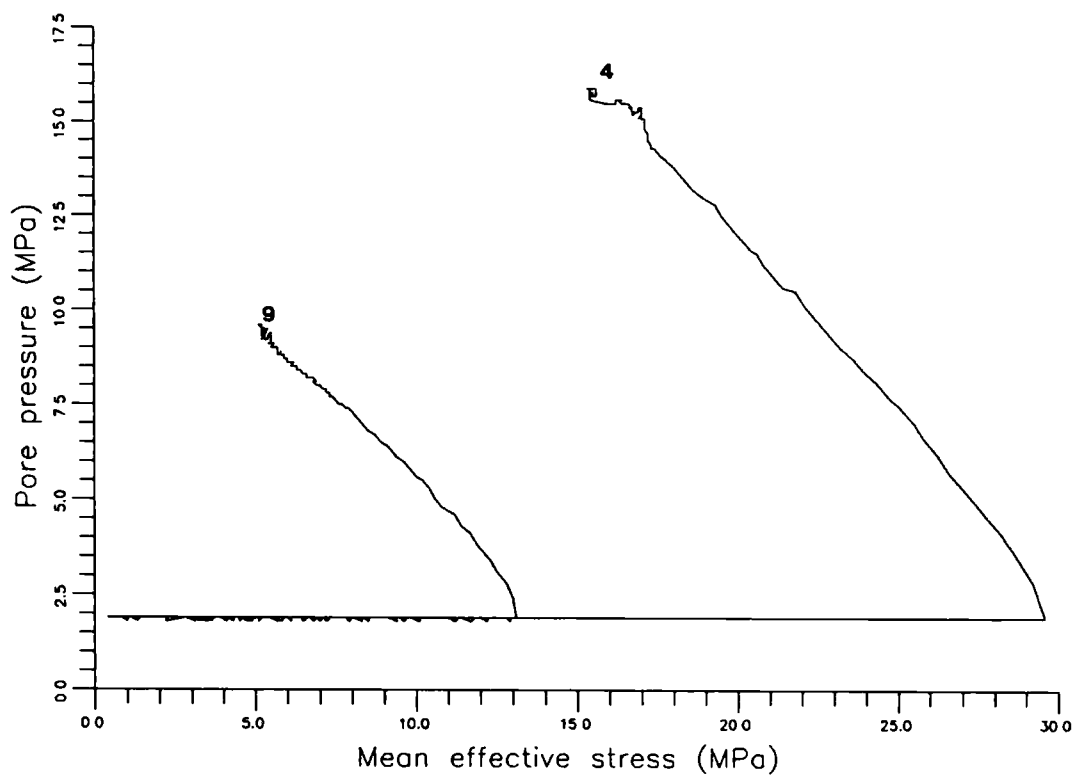


Figure. 6.25. Graph of pore pressure/mean effective stress for anisotropically (K_0) consolidated undrained shear experiments on Stevn's Klint samples.

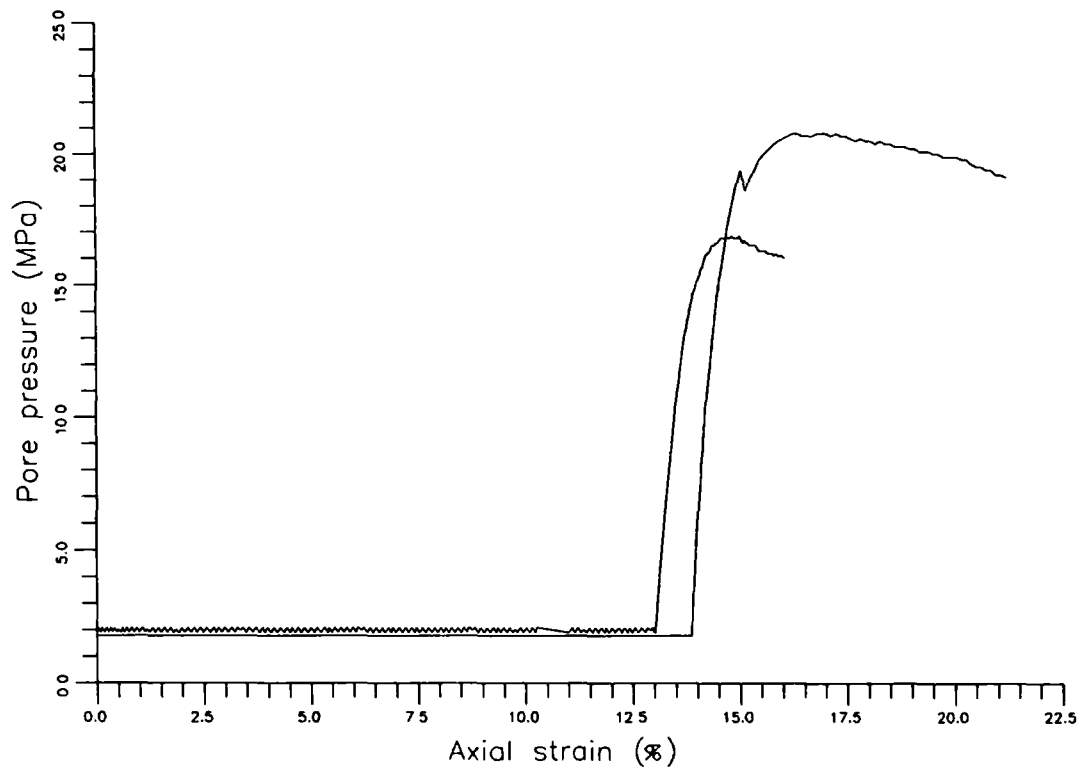


Figure. 6.26. Graph of pore pressure/axial strain for anisotropically (K_o) consolidated undrained shear experiments on Butser Hill samples. (After Addis, 1987.)

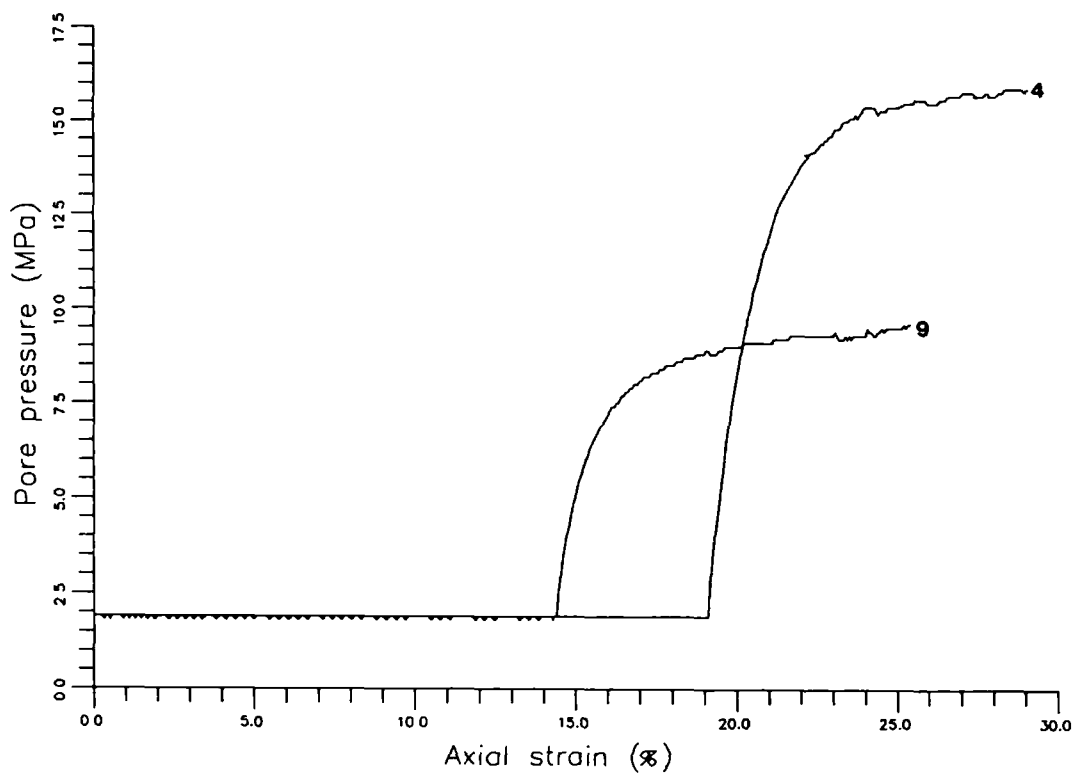


Figure. 6.27. Graph of pore pressure/axial strain for anisotropically (K_o) consolidated undrained shear experiments on Stevn's Klint samples.

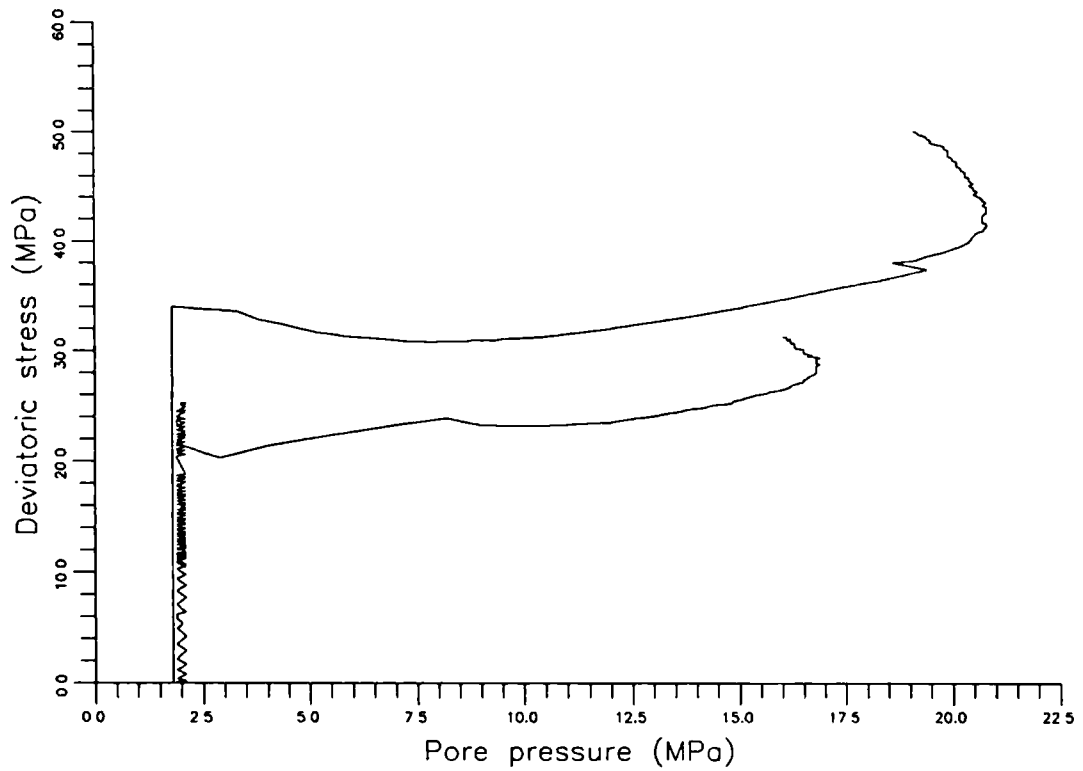


Figure. 6.28. Graph of deviatoric stress/pore pressure for anisotropically (K_0) consolidated undrained shear experiments on Butser Hill sample. (After Addis, 1987.)

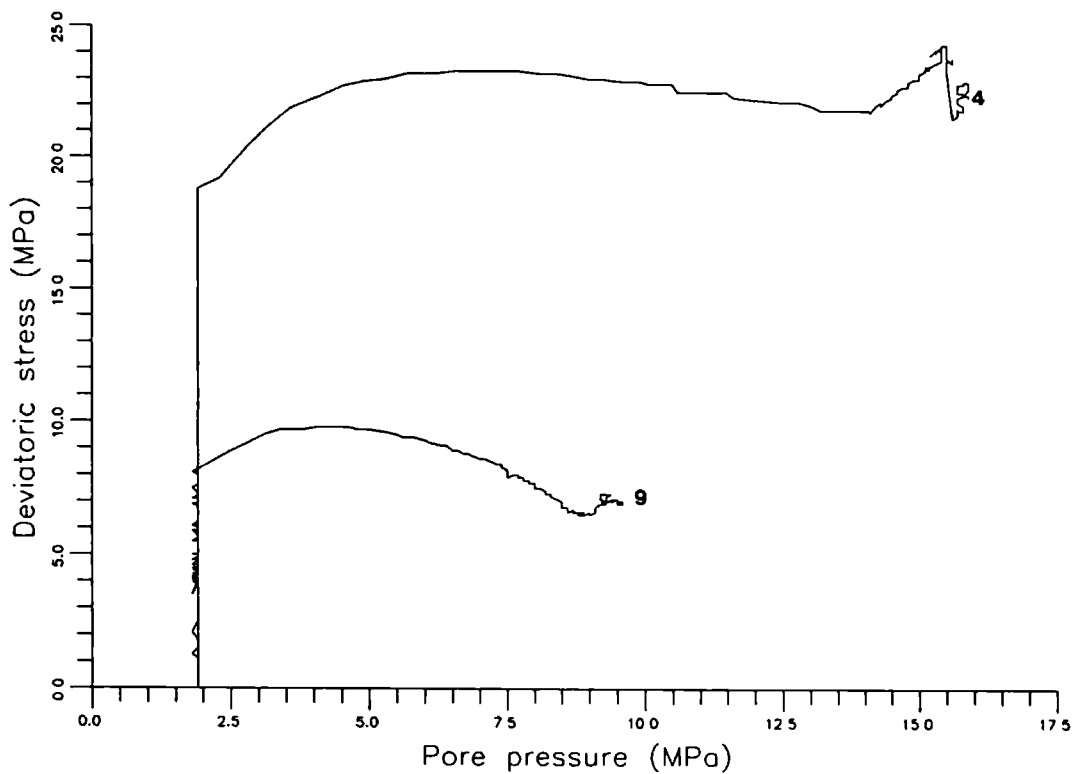


Figure. 6.29. Graph of deviatoric stress/pore pressure for anisotropically (K_0) consolidated undrained shear experiments on Stevn's Klint samples.

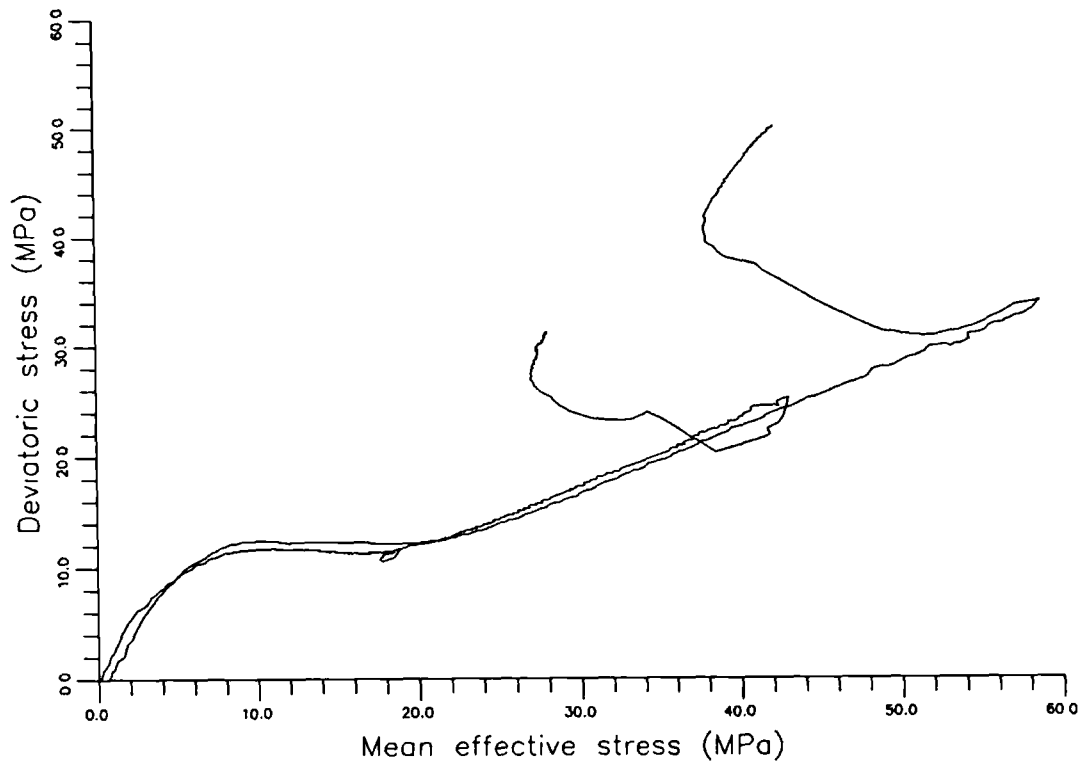


Figure. 6.30. Deviatoric stress/mean effective stress graph for anisotropically (K_o) consolidated undrained shear experiments on Butser Hill samples. (After Addis, 1987.)

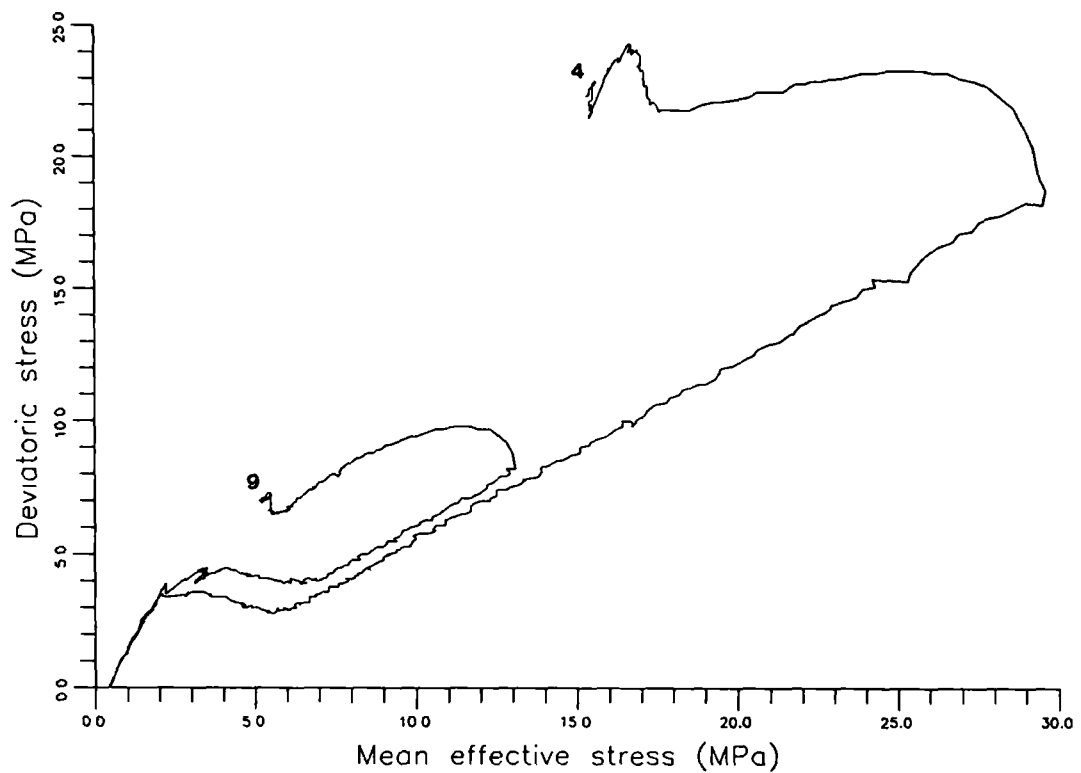


Figure. 6.31. Deviatoric stress/mean effective stress graph for anisotropically (K_o) consolidated undrained shear experiments on Stevn's Klint samples.

drained shear of the anisotropically consolidated Stevn's Klint samples resulted in typical undrained stress paths, in which initially, the deviatoric stress increased more rapidly than pore pressure. Both samples are observed to strain soften.

Figures 6.32 and 6.33 indicate the change in void ratio as a function of mean effective stress. For both sets of data the change in void ratio was calculated from recorded changes in radial and axial strain. During data processing of the Butser Hill experiments (figure 6.32) the void ratio was 'frozen' at the start of undrained shear. For comparison, the data in figure 6.33 (Stevn's Klint) represent volume changes calculated from radial and axial strain measurements before and during shear. The volume changes calculated during the K_0 consolidation part of each experiment can be verified, as axial strain will be equal to volumetric strain. The void ratio changes (equivalent to changes in volume) calculated for the undrained shear part of the two Stevn's Klint experiments cannot be verified by the volume of pore fluid expelled and are probably too large (see below). The radial strain data (figure 6.35) indicate that very large changes in mid-height diameter of both samples occurred during shear.

Radial strain/axial strain data are presented in figures 6.34 and 6.35. Radial strains are determined, using a strain belt secured in a mid-height position on the sample (see chapter 4 for details). The mid-height diameters of the Butser Hill samples are seen to increase at an almost uniform rate during shear. This would be expected for samples that strain harden. There was evidence from the surface of the samples that the strain belt moved during shearing (Addis pers. comm., 1989) so this radial strain data may not be representative of shape changes that occurred in the samples. The radial strain data for the strain softening Stevn's Klint samples are substantially different. In both experiments, the start of shear led to an increase in diameter. Following this initial increase the centres of both samples collapsed. This unusual behaviour was observed in the first experiment (SKWC4), but when the sample was removed from the test apparatus its diameter was significantly larger than that calculated from the radial strain belt data. There were no indications from the sample that the strain belt had moved during the

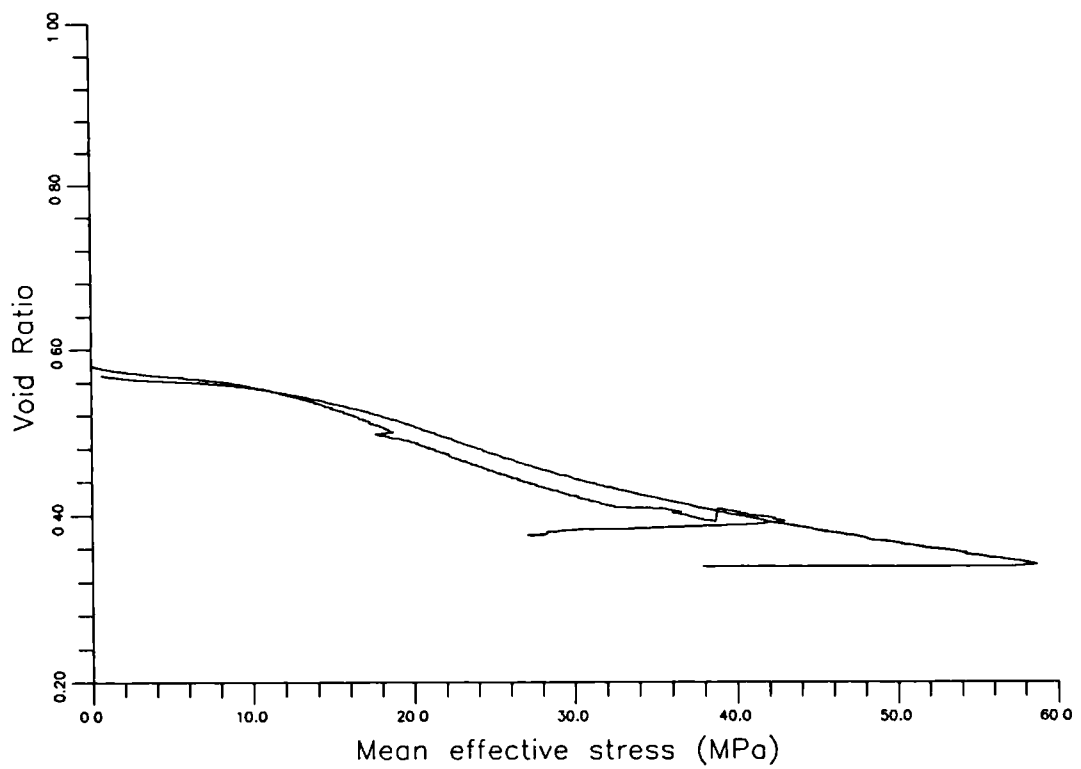


Figure. 6.32. Graph of void ratio/mean effective stress for anisotropically (K_o) consolidated undrained shear experiments on Butser Hill samples. (After Addis, 1987.)

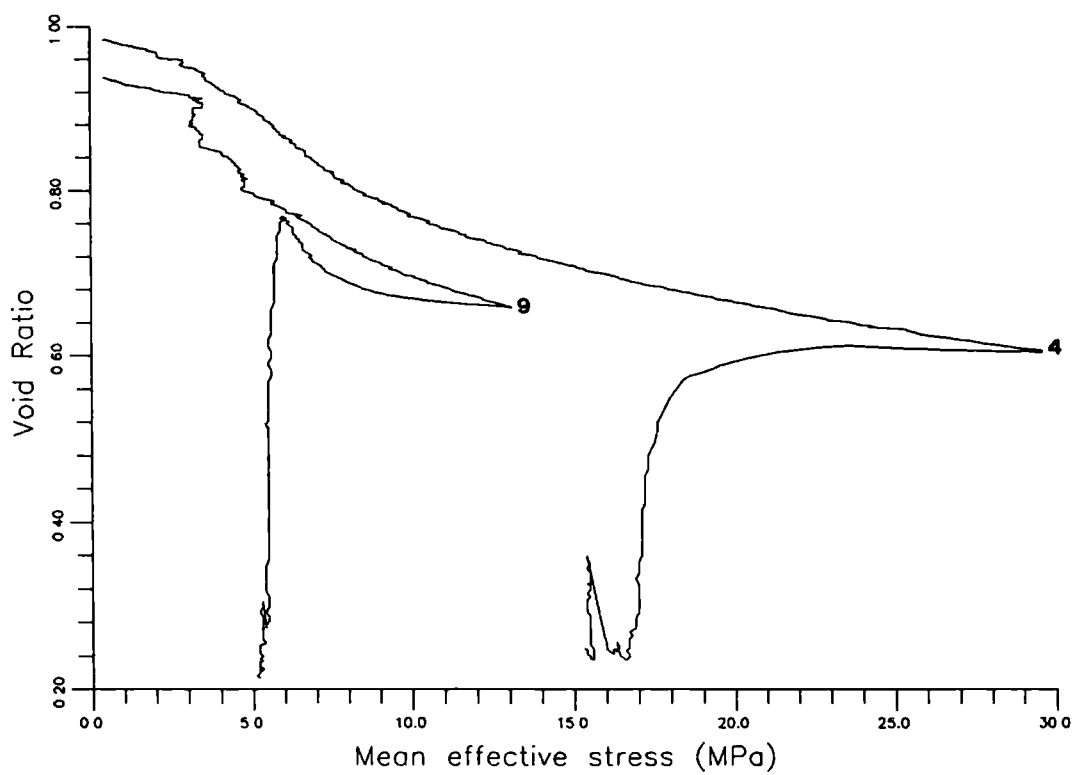


Figure. 6.33. Graph of void ratio/mean effective stress for anisotropically (K_o) consolidated undrained shear experiments on Stevn's Klint samples.

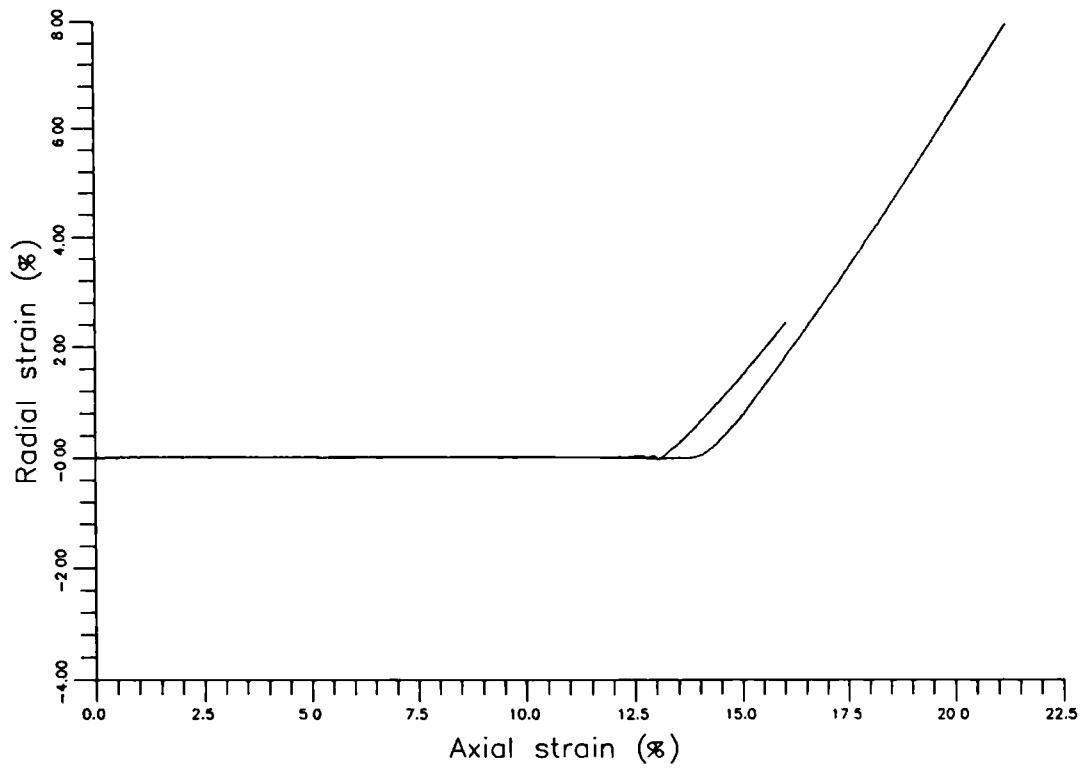


Figure. 6.34. Graph of radial strain/axial strain for anisotropically (K_0) consolidated undrained shear experiments on Butser Hill samples. (After Addis, 1987.)

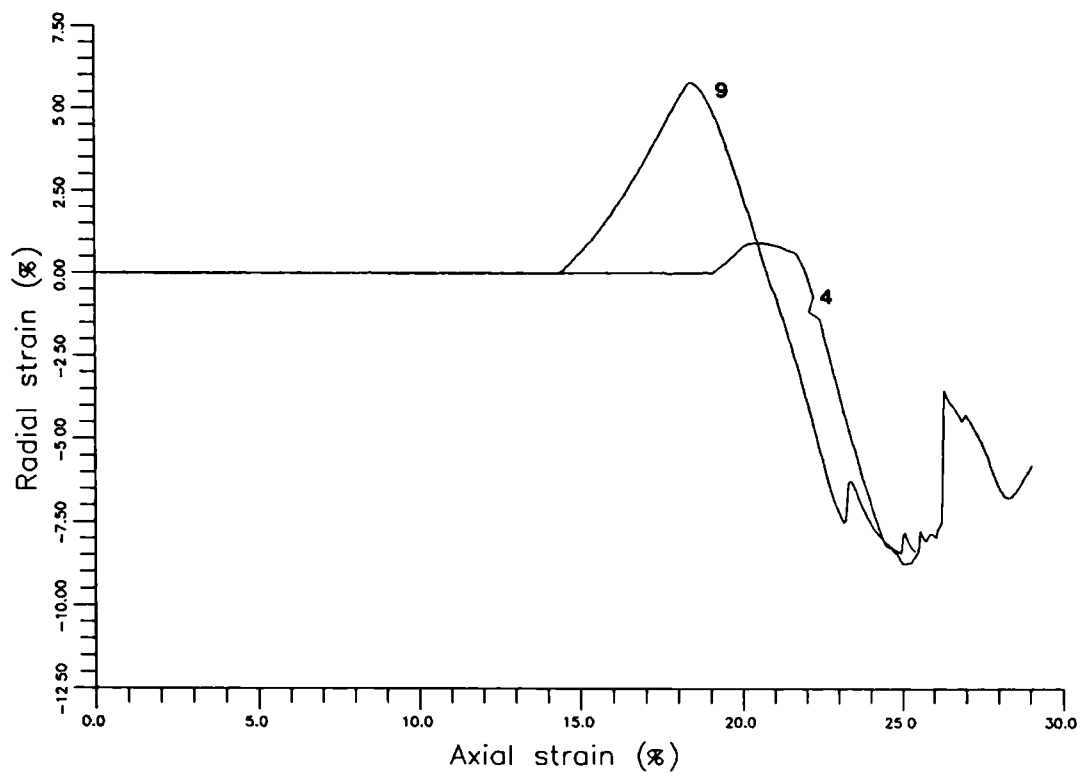


Figure. 6.35. Graph of radial strain/axial strain for anisotropically (K_0) consolidated undrained shear experiments on Stevn's Klint samples.

experiment. (The pads which hold the strain belt against the sample (see chapter 4 for details) make very small indentations in the surface of these soft chinks). The calibration of the strain belt was checked and found to be correct. When a similar collapse behaviour was observed during testing of the second sample (SKWC9) a note was made of the radial strain measurements after the test had been terminated. It can be seen from the figure 6.35 that during shear the diameter of the second experiment (SKWC9) expanded by +0.376mm (measurements given with respect to the initial diameter), then contracted to -3.38mm, expanded again to -1.127mm, contracted to -2.25mm then finally re-expanded to -1.878mm. Radial strain measurements were continued after the termination of this experiment to try to determine from this sample why there was such a discrepancy between the calculated diameter of sample SKWC4 determined from the radial strain belt and the measured diameter once the sample had been removed from the test apparatus. Following the end of experiment SKWC9 the entire cell assembly was lowered away from the cross-head in order to remove the vertical load from the sample. (The load cell was also removed, but ram friction meant that with the ram still in contact with the sample, the sample would have been under a load of approximately 0.3MPa.) This did not result in a change in diameter. However, as the confining fluid (zero pressure) was emptied from the triaxial cell the radial strain belt recorded an expansion in the diameter of the sample of 1.343mm (to 36.723mm). When the top of the cell was removed, so that the ram was no longer in contact with the top of the sample, the diameter expanded again by 3.893mm to a final diameter of 40.616mm (this was confirmed by measuring the sample after it had been removed from the test cell). It would appear from this that similar changes occurred during experiment SKWC4 and this therefore accounts for the discrepancy in the calculated and measured final diameters of that sample. Further discussions of the possible significance of these large changes in diameter will be presented in the next section.

6.5.3. Strain rate data.

Figures 6.36 to 6.39 present data from three experiments already included in section 6.5.1 but on expanded scales. These graphs represent three samples consolidated isotropically under approximately the same confining pressure but sheared at three different strain rates (see table 6.2).

Table 6.2.

UNDRAINED SHEAR, STRAIN-RATE EXPERIMENT DATA.

Experiment	Length	Displacement	Strain	Peak shear	Residual shear
		rate	rate	strength	strength
name	(mm)	(mm/min)	(mm/sec)	(MPa)	(MPa)
BHWC6	75.50	0.01	2.20 *10 ⁻⁶	11.7	4.9
BHWC3	75.05	0.10	2.22 *10 ⁻⁵	12.5	4.9
BHWC7	76.68	1.00	2.17 *10 ⁻⁴	12.9	5.1

Although this is a limited data set, the results of these three experiments seem to indicate that little change occurs in mechanical behaviour when the strain rate is varied over three orders of magnitude. It can be seen from figure 6.36 and table 6.2, that, the peak shear strength increases with increasing strain rate, but following yield, residual strength for all three samples is virtually identical. The difference in pore pressure generation resulting from shear (figure 6.37) also shows little variation for all three experiments. This similarity is reflected again in the stress path diagram (figure 6.38). Although the highest strain rate used (BHWC7) has produced a more pronounced peak than observed in the other two experiments, the pre- and post-yield behaviour, including critical state, are again almost identical. It is also observed from figure 6.39 that the void ratio's of all three samples show little variation throughout the experiments. These data indicate that changes in strain rate do not have a significant effect on the mechani-

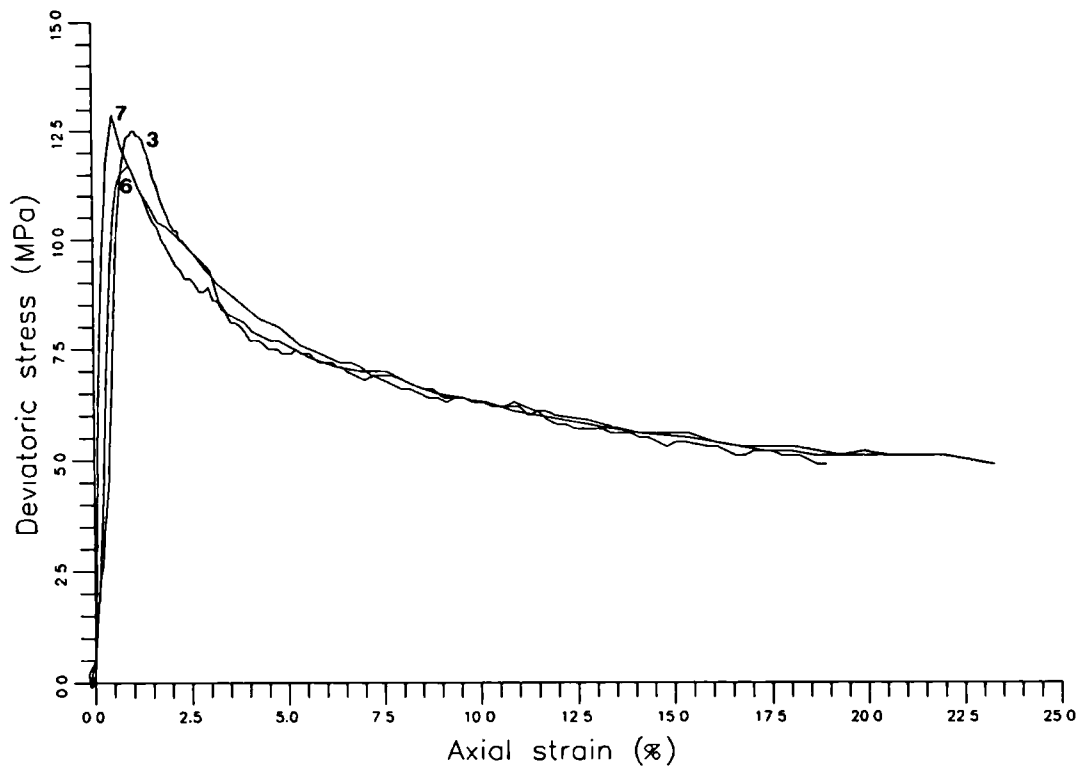


Figure 6.36. Graph of deviatoric stress/axial strain for undrained shear experiments conducted at three different strain rates on samples of Butser Hill outcrop chalk.

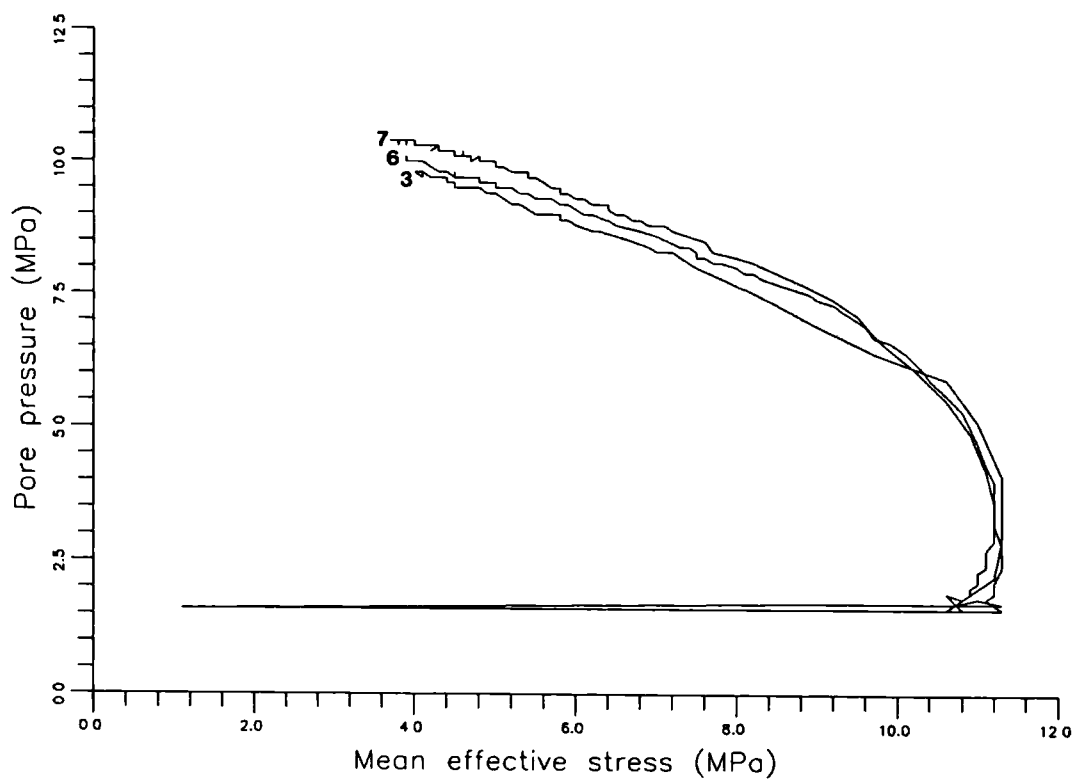


Figure 6.37. Graph of pore pressure/mean effective stress for undrained shear experiments conducted at three different strain rates on Butser Hill outcrop chalk.

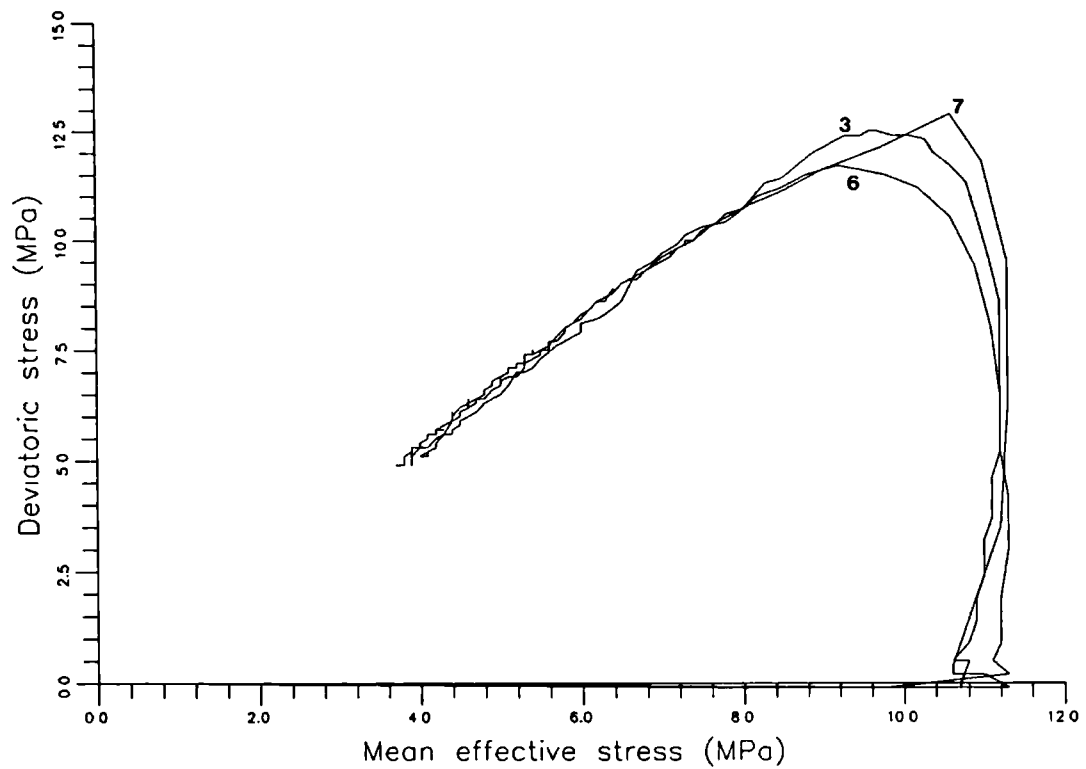


Figure. 6.38. Deviatoric stress/mean effective stress graph for undrained shear experiments conducted at three different strain rates on Butser Hill outcrop chalk.

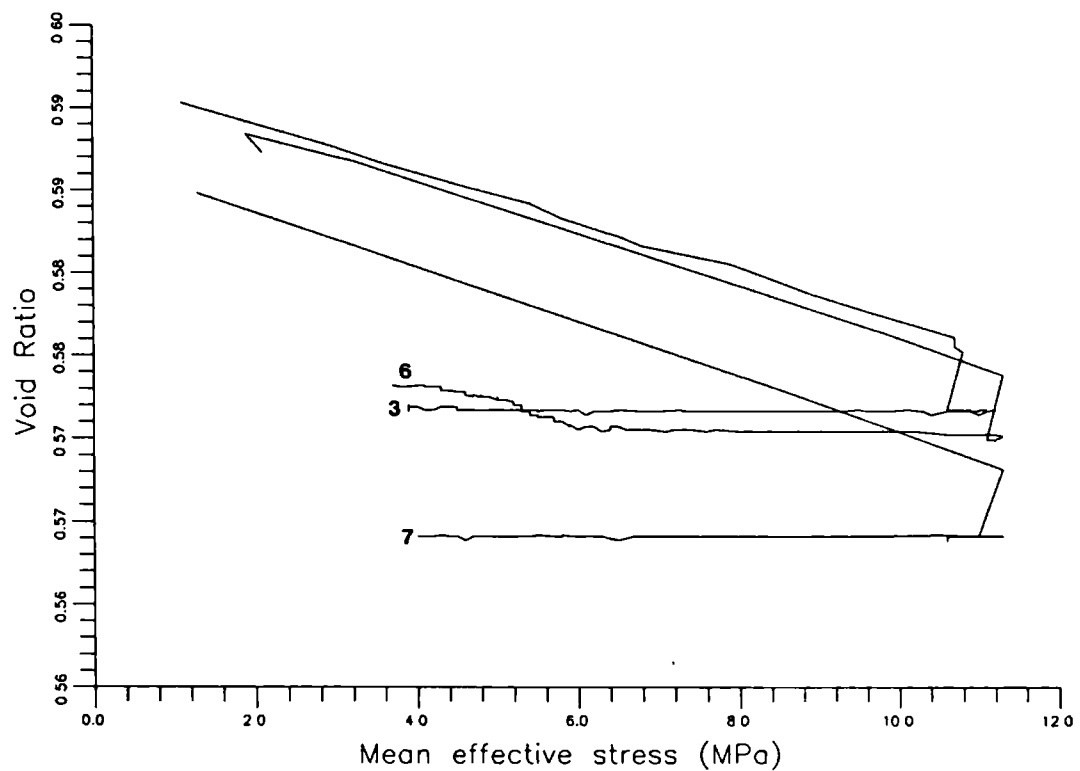


Figure. 6.39. Graph of void ratio/mean effective stress for undrained shear experiments conducted at three different strain rates on Butser Hill outcrop chalk.

cal behaviour of outcrop chalks. Further discussions on strain rate affects will be presented in the next section.

Table 6.3.a

EFFECTS OF INCREASING CONSOLIDATION PRESSURE (σ_3').

σ_3' (MPa)	Exp Name	Peak shear					Final shear		
		qp (MPa)	Ev %	Up (MPa)	pp' (MPa)	Um (MPa)	qf (MPa)	pf (MPa)	Uf (MPa)
1.0	SKWC6	3.2	0.60	2.5	1.5	2.6*	0.8	1.0	2.2
2.6	SKWC8	3.7	0.47	3.8	2.1	3.8	0.6	0.9	3.8
4.7	SKWC7	4.3	0.35	5.0	3.4	6.3	0.8	0.4	6.3
7.0	SKWC10	3.8	1.25	6.3	3.9	8.9	0.8	0.5	8.7
9.9	SKWC3	4.2	1.68	8.0	5.7	10.7	1.1	1.8	10.7
18.0	SKWC5	11.3	0.11	13.3	11.4	16.1	7.9	6.4	15.7
37.9	SKWC1	23.8	2.86	20.2	25.8	25.4	23.8	18.4	24.6
1.6	BHWC8	7.9	0.49	2.1	3.8	2.4	3.4	2.8	2.3
10.7	BHWC3	12.5	1.02	6.7	9.7	10.1	4.9	3.9	10.0
11.2	BHWC6	11.7	0.93	7.4	9.2	10.4	4.9	3.7	10.4
11.2	BHWC7	12.9	0.53	5.9	10.6	9.8	5.1	4.1	9.7
22.1	BHWC2	12.8	1.53	12.6	13.9	18.6	7.8	6.2	18.6
25.0	BHWC9	19.1	1.85	13.7	19.3	20.2	13.7	11.0	20.2
31.9	BHWC5	33.7	5.72	12.1	31.2	19.1	31.1	23.2	19.1
42.9	BHWC4	35.4	20.7	25.8	27.5	25.8	35.4	27.5	25.8
51.6	BHWC1	42.5	11.7	30.2	35.4	30.2	42.5	35.4	30.2
10.4	SKWC9	9.8	0.34	4.1	11.7	9.6	7.0	5.2	9.6
23.4	SKWC4	24.3	5.71	15.4	16.7	15.9	22.3	15.3	15.9
36.2	BH3.20	31.3	16.0	16.0	28.1	16.0	31.3	28.1	16.0
47.4	BH18.30	50.1	21.2	19.1	42.2	20.8	50.1	42.2	19.1

* Maximum pore pressure achieved before peak deviatoric stress attained.

Table 6.3.b**EFFECTS OF INCREASING CONSOLIDATION PRESSURE (σ'_3).**

σ'_3 (MPa)	Exp. Name	% Up/Uf	% qf/qp	% p'f/p'p	% Uf/03f	% Uf/01f	% Uf/p'f	% Uf/qf
1.0	SKWC6	113.64	25.00	66.67	78.57	61.11	133.69	275.00
2.6	SKWC8	100.00	16.22	42.86	84.44	76.00	422.22	633.33
4.7	SKWC7	79.37	18.60	11.76	92.65	86.30	1575.00	787.50
7.0	SKWC10	72.41	21.05	12.82	97.75	90.63	1740.00	108.75
9.9	SKWC3	74.77	26.19	31.58	91.45	81.06	594.44	972.73
18.0	SKWC5	84.71	69.91	56.14	78.11	57.51	254.31	198.73
37.9	SKWC1	100.00	100.00	71.32	61.96	41.84	133.70	103.36
1.6	BHWC8	91.30	43.04	73.68	69.70	31.51	82.14	67.65
10.7	BHWC3	67.00	39.20	50.52	81.30	58.48	256.41	204.08
11.2	BHWC6	71.15	41.88	40.22	81.89	60.12	281.08	212.24
11.2	BHWC7	60.82	39.53	38.68	80.16	56.73	236.58	190.20
22.1	BHWC2	67.74	60.94	44.60	84.16	62.42	300.00	238.46
25.0	BHWC9	67.82	71.73	56.99	75.94	50.25	183.64	147.45
31.9	BHWC5	63.35	92.28	74.68	59.87	30.31	84.97	61.41
42.9	BHWC4	100.00	100.00	100.00	60.14	29.73	93.82	72.88
51.6	BHWC1	100.00	100.00	100.00	58.53	32.20	85.30	71.06
10.4	SKWC9	42.71	71.43	44.44	78.05	49.48	184.62	137.14
23.4	SKWC4	96.86	91.77	91.62	63.10	34.57	103.92	71.30
36.2	BH3.20	100.00	100.00	100.00	44.20	24.62	56.94	51.12
47.4	BH18.30	100.00	100.00	100.00	40.30	20.19	45.26	38.12

These data indicate that both chalks generate large pore pressures during undrained loading. In samples consolidated under low pressures, yield is followed by a strain softening response, with significant decreases in both mean effective and deviatoric stresses. This type of behaviour has been recognised for other geotechnical materials and is

generally associated with liquefaction. Samples subject to high consolidation pressures also generate significant pore pressures, but mean effective and deviatoric stresses increase throughout shear, indicating strain hardening. There is also evidence from radial strain measurements and observation of the samples following testing, that large and irregular shape changes may occur in these weak materials during undrained shear. These shape changes may reflect deviations from the more usual (symmetrical barrelling) behaviour seen in cemented soils and weak rocks under conditions of undrained shear.

6.6. DISCUSSION.

It has been shown in a number of studies (Jones and Addis, 1986; Addis, 1987; Johnson et al., 1988; see also chapter 4 of this study) that the chalk behaves as an elastic material at low stresses, but, as stress increases the cement bonds start to yield and as the stress increases the cement bonds start to yield and the structure begins to deform in a ductile manner. This ductile behaviour (strain softening) continues, though the rearrangement of grains, until the structure becomes dense enough that further movement of individual grains gradually becomes more restricted and frictional resistance starts to increase. Increasing friction leads to a gradual increase in strength of the material (strain hardening). The data presented in Addis (1987), Johnson et al. (1988) and chapter 4 of this study, indicate that as the initial porosity of the chalk increases, strain softening became a more important factor in the deformational processes and larger strains were required before repacking of the grains led to an increase in frictional resistance and the onset of strain hardening.

The majority of the experimental studies that have been conducted on chalk (Addis, 1987; Johnson et al., 1988), have been designed to reveal the values of stress and strain at which the different elements of this characteristic deformational behaviour develop (for further discussion see chapter 4). These studies (including the data presented in chapter 4), followed either the uniaxial (K_0) and/or the isotropic stress paths. They were primarily devoted to understanding the compactional characteristics of chalk and

provided little information on chalk behaviour when subject to large shear stresses, particularly at low confining pressures. The data presented in the preceding section are therefore unusual, even when compared to other investigations of weak, cemented carbonates (section 6.3) (Vaughan, pers. comm., 1989).

The range of consolidation pressures used in these undrained shear experiments (table 6.3a) cross the yield surfaces for the two chalks studied. Both sets of experiments therefore contain undrained shear data for high porosity chalks during the initial pre-yield elastic phase, post-yield strain softening and large axial strain, strain hardening conditions (figures 6.20-6.25 and 6.28-6.29).

When the stress paths (figures 6.18 and 6.19) are examined, it is seen that for each set of experiments, all stress paths end close to or on a common line which passes through the origin of the plot (figure 6.40). Although it is a failure envelope (often referred to as the failure line), it is not the elastic envelope (some of the undrained experiments that define this line begin at consolidation pressures beyond the elastic yield envelope). It appears from figure 6.40 that this line has the same stress coordinates for both chalks investigated. From the data obtained the failure line is described by the equation:

$$e = A - B \ln p' \quad 6.6$$

$$q = M p \quad 6.7$$

where e is void ratio and A and B are constants, with values $A = 1.24$, $B = 0.243$ and $M = 1.2$. This equation may be used to calculate the value of mean effective stress (p') at which a chalk of a particular initial void ratio will reach the failure line.

Studies in soil mechanics have revealed that inelastic particulate materials produce a failure envelope of similar geometry to that determined here for chalk. This envelope, which is part of a figure (figure 6.3) consisting of the Roscoe, Hvorslev and Tension

surfaces is normally regarded as a state boundary between those effective stress states where the material can exist and those where it cannot (Atkinson and Bransby, 1978). If the material is subject to any stress state outside of this envelope, its structure and geometry evolves until a permissible stress state is again attained. At the failure line (the boundary between the Roscoe and Hvorslev surfaces), particulate materials are observed to be very weak and to deform to large strains at constant effective stress. This failure line which is therefore also part of the state boundary, is normally referred to as the Critical State Line (Atkinson and Bransby, 1978). The failure line defined for the chalks in this study (figure 6.40) has the same characteristics in stress space as a Critical State Line, suggesting that this is also a state boundary surface. It is therefore reasonable to attribute this state boundary for the chalk with the same properties as the critical state. However, this comparison may not be strictly analogous, as, the cement bonding, which provides the chalk with a rigid structure, allows stress paths at low confining pressures to pass outside of this state boundary (figure 6.40).

The identification that a locus of stress states exists, which defines a Critical State Line for any particular porous chalk, provides the explanation for the three problems of chalk flow and loss of strength discussed at the beginning of this chapter. In both the rock fall and the well invasion examples, these chalks were able to sustain large strains at some stress level, and can therefore be regarded as having reached their critical states. Figures 6.18 and 6.19 indicated however, that although each sample attained its critical state, the physical state of the sample following consolidation and prior to shearing had a profound affect on whether it approached the Critical State Line under conditions of strain softening or hardening. It is also evident from figures 6.18 and 6.19 that the more dramatic failures are found in samples in which cementation was either intact or only partially destroyed during the consolidation process. The behaviour of the chalk as an elastic material should therefore be reviewed.

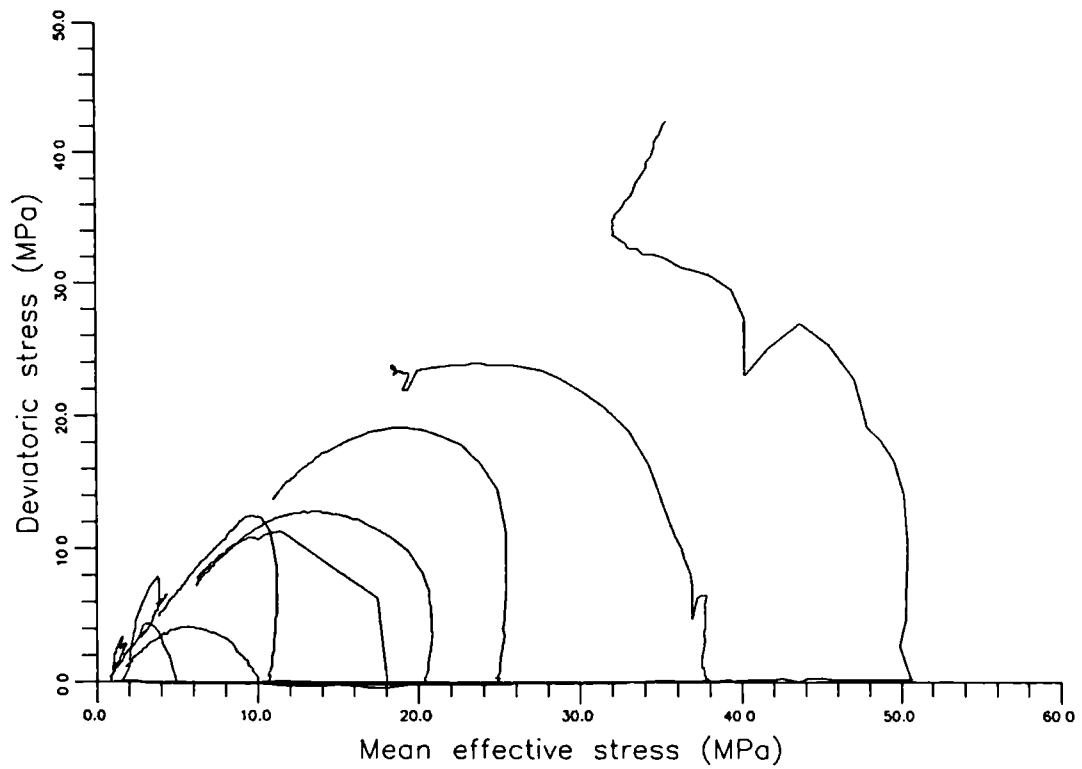


Figure. 6.40. Combined stress path diagram for both the Butser Hill and Stevn's Klint isotropically consolidated samples.

6.6.1. The Critical State for an Elastic Material.

The critical state is a property of particulate (inelastic) materials, and all chalks behave in an elastic manner at low stresses. It therefore follows, that if the chalk is to attain the critical state at low stresses, it must first fail at its elastic yield envelope and undergo the necessary structural changes to become a particulate material. This aspect of the behaviour is well illustrated in figures 6.18, 6.19 and 6.40.

In each of these figures, the samples that were consolidated to the lowest stresses prior to undrained shear, have stress paths which pass above the projection of the Critical State Line and then return to it. At these low consolidation stresses, the chalk is still an elastic material. It is therefore stronger than its particulate equivalent, which means that before it can attain its critical state it must attain and fail at stresses on the elastic yield envelope. The relative positions of the two envelopes for the Butser Hill and Stevn's Klint chalks are shown in figures 6.41 and 6.42. It can be envisaged that, these two envelopes are expressions of an elastic surface that increases in size above the Hvorslev Surface as the porosity (void ratio) decreases and cementation increases. It follows that low porosity chalks will experience a larger decrease in deviatoric stress after elastic yield than will high porosity chalks. At low consolidation pressures, the elastic yield can be regarded as a peak strength and the critical state as a residual strength (table 6.3a). With increasing consolidation pressure, the stress decrease is progressively eliminated until the peak and residual strengths are the same (table 6.3a).

If the uniaxial (K_0) and isotropically consolidated data are combined (figures 6.43 and 6.44) the low pressure undrained experiments are seen to coincide with the yield part of the uniaxial experiments. This is further evidence that prior to yield, the cemented structure of the chalk allows it to deform in a stress regime that is not related to its particulate state. The fact that, in these low pressure, undrained shear experiments, shear stress decreases following yield and the stress path is observed to follow the projection of the Critical State Line, indicates that the elastic envelope lies above the particulate Hvorslev Surface at low pressures.

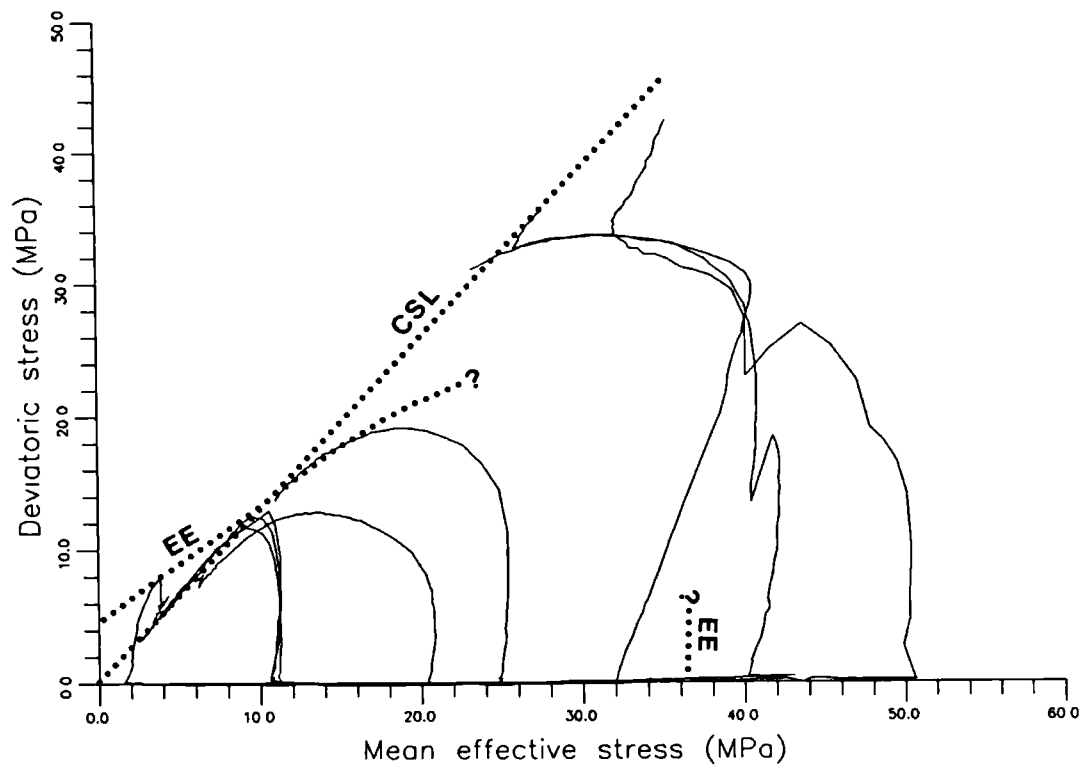


Figure. 6.41. Stress path diagram indicating the proposed position of the elastic yield envelope for the Butser Hill samples.

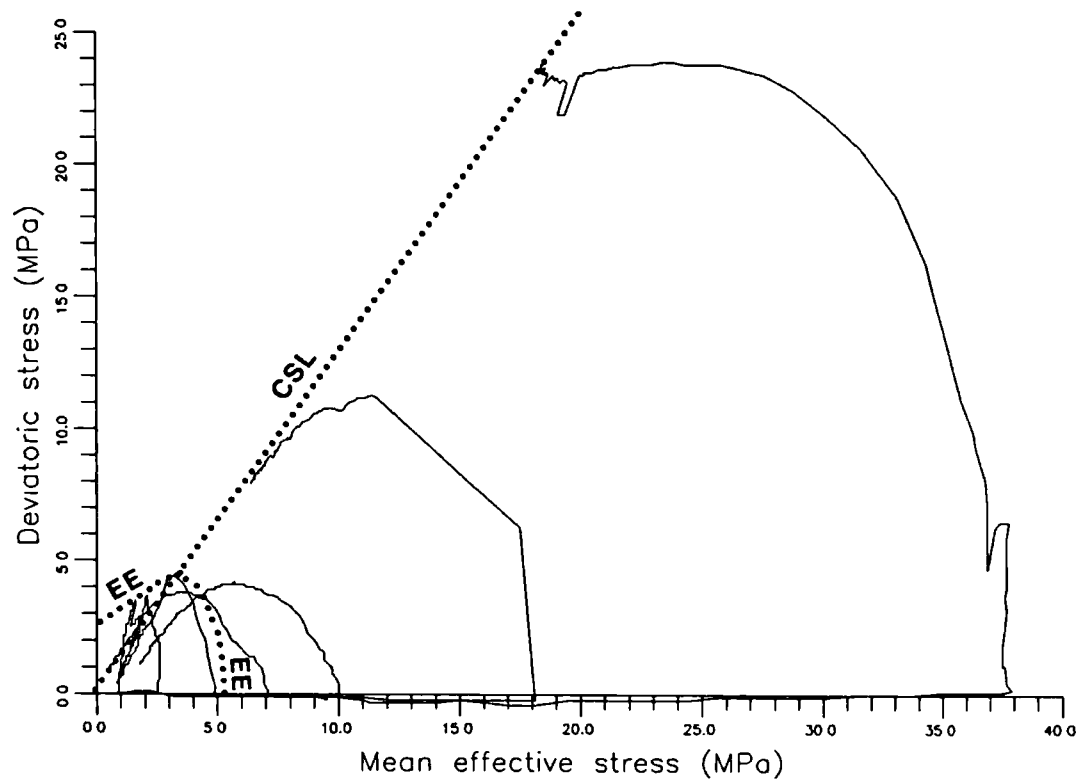


Figure. 6.42. Stress path diagram indicating the proposed position of the elastic yield envelope for the Stevn's Klint samples.

6.6.2. Influence of Consolidation Pressure on failure.

The consolidation pressure will determine to what extent the cement structure is broken down, the degree of compaction and hence the density of the sample before it is subject to undrained shear. It has already been shown in uniaxial experiments (see chapter 4) that even at large strains, areas of the sample may still contain large voids. Yield during shear, whether it is due to the breakdown of the cement bonds (under low consolidation pressures) or the overcoming of frictional resistance (at higher consolidation pressures) is observed to occur below 2% axial strain. This is consistent with the observations of Allman and Poulos (1988), Fahey (1988), Tsuchida et al. (1988), and Sangrey (1972) who all found that yield always occurred at an axial strain of less than 2%, and generally less than 1%.

The stress paths in figures 6.18 and 6.19 clearly show that the response of the chalk during shear depends on the consolidation pressure. At low consolidation pressures, the stress path is observed to move down the projection of the Critical State Line. This is a strain softening response associated with major shear deformations. This condition is known for some silts, sands and sensitive clays in soil mechanics (Crawford, 1963; Mitchell, 1970). It is also the stress path followed when materials become liquefact (Taylor, 1987). Materials of this type deform plastically to large strains (Mitchell, 1970). Under higher consolidation pressures, the samples strain harden before reaching their critical state.

The Canadian sensitive clays (Crawford, 1963; Mitchell, 1970) are considered to be strong and brittle in their undisturbed state. This strength results from the development of cement bonding between the clay particles. The bonding allows these clays to behave in a similar manner to other cemented materials (such as the chalk and weakly cemented sandstones), in which strains are fully recoverable below a distinct yield stress. During yield, in which the cement bonds begin to rupture, compressibility increases dramatically. Mitchell (1970) attributes this increase in compressibility to the onset of second-

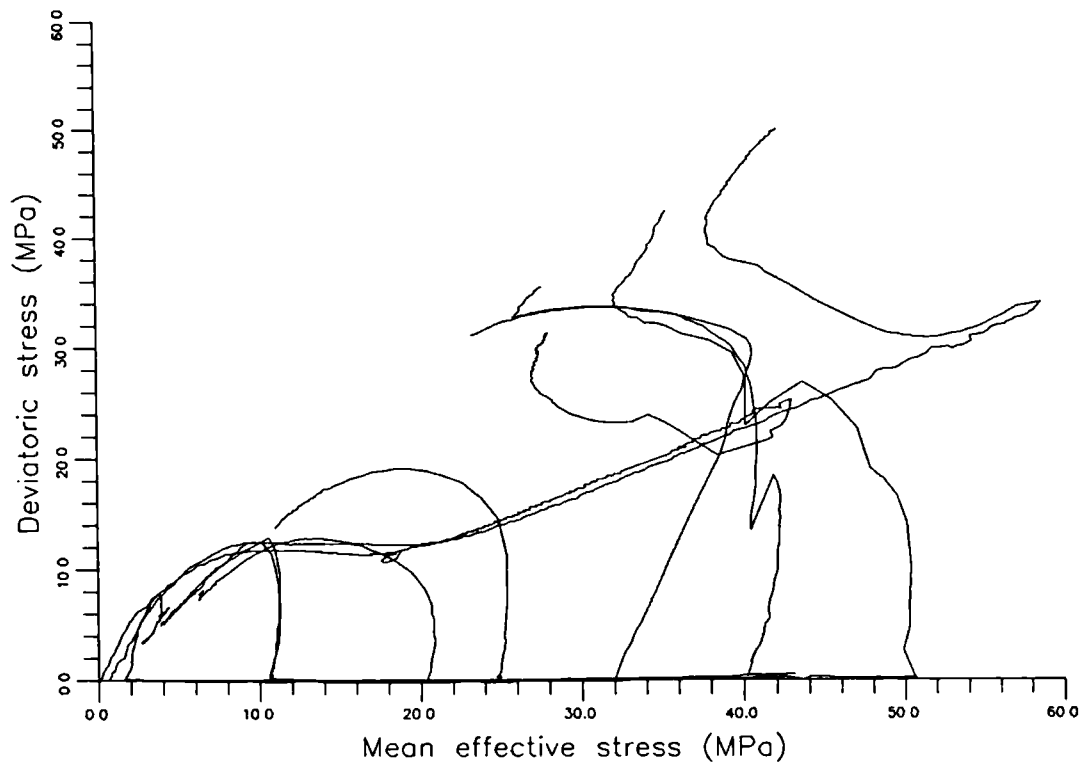


Figure. 6.43. Combined stress path diagram for isotropically and anisotropically consolidated Butser Hill samples. (Anisotropically consolidated samples, after Addis, 1987.)

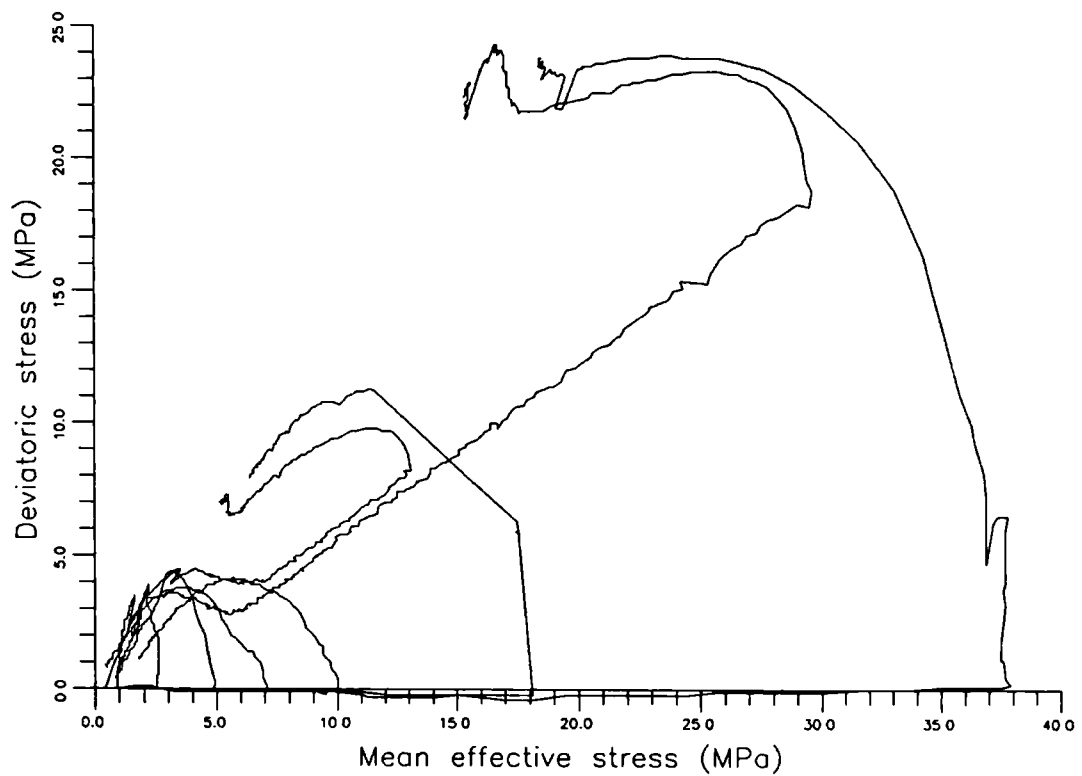


Figure. 6.44. Combined stress path diagram for isotropically and anisotropically consolidated Stevn's Klint samples.

dary creep as it is not associated with the dissipation of excess pore pressures. Although yield corresponds to the initial breaking of the cement bonds, the post yield strain softening behaviour can also be regarded as a result of continued cement breakdown (Mitchell, 1970), until the clay is reduced to the conditions of a normally consolidated material.

Although continued deformation, particularly strain hardening, results in the development of a barrel shaped sample, this increasing eccentricity may contribute to stiffening in the experimentally deformed materials. This work hardening may be less pronounced in nature.

The strain softening and strain hardening failures are accompanied by rather different physical responses in the materials. This pattern of deformation, detailed below, reflects to some extent that found by Price (1988b) in the North Rankin 'A' carbonates. However, as would be expected, due to differences in the depositional environment, subsequent burial history and the nature of the carbonate materials themselves, they do not provide a direct analogy.

6.6.2.1. Butser Hill.

In the Butser Hill samples, the degree of 'flow' and fracture distortion is seen to be dependant on the consolidation pressure. As the consolidation pressure is increased, the shape of the sample becomes more regular and fractures less pronounced, until at the highest consolidation pressures no disruption of the structure is visible. Under the lowest consolidation pressure used (3MPa) the sample (BHW C8) is observed to develop a pair of simple conjugate shear fractures (plate 6.2). The chalk between the shears is soft, but, the ends of the sample are relatively undisturbed. When the consolidation pressure is increased to 10MPa, the samples (BHW C3, 6, 7) continue to strain soften (figures 6.36-6.38) and develop fractures. These fractures form high frequency conjugate sets which divide all the sample up into small discrete blocks of ductile material (plate 6.3). The surface of the chalk is again very soft. In each of the three

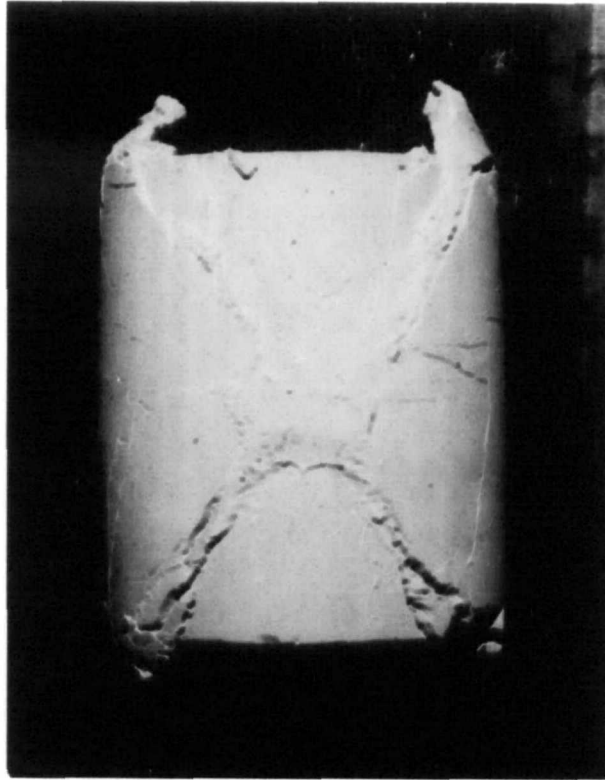


Plate 6.2. Sample BHWC8 isotropically consolidated to 3MPa before being subject to undrained shear.
Note the formation of large discrete shear planes.

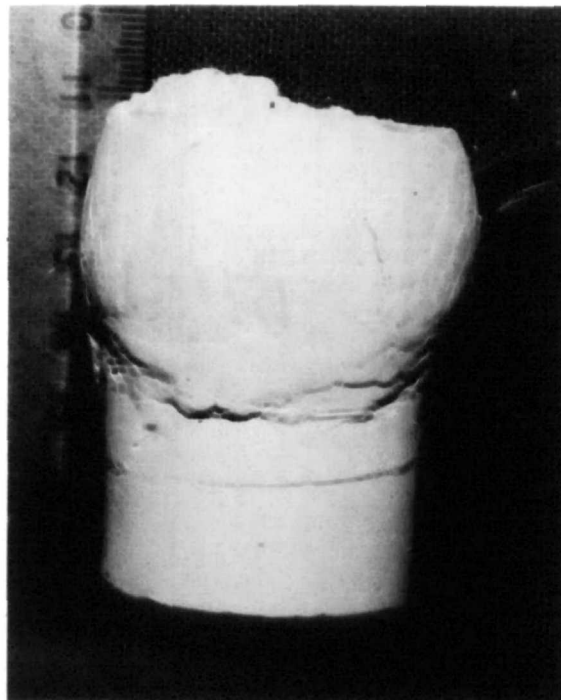


Plate 6.3. Sample BHWC3 isotropically consolidated to 10MPa before being subject to undrained shear.
Note the formation of small discrete blocks that appear to have 'flowed' in a ductile manner.

samples tested at a consolidation pressure of 10MPa, the breakdown of the structure is irregular and is restricted to the upper half of the sample. The lower half of each sample appears to be relatively undeformed. Similar deformations have been observed in weakly cemented sandstones (Goldsmith, pers. comm., 1989). The fracture bounded blocks appear to have moved past one another as sheets to produce the texture shown in plate 6.3. The reason for this uneven deformation is unclear. It may reflect the irregular breakdown of the chalk observed in chapter 4. In each experiment, the sample was subject to shear before its original cement structure had been completely destroyed. The sample consolidated at the lowest pressure developed individual fracture blocks which may have remained stiff and deformation was concentrated on a few well defined fractures (plate 6.2). As the consolidation pressure increased, fracturing became more diverse, but the material between the fractures still remained essentially undeformed (plate 6.3) (Price, 1988b).

Figure 6.20 indicates that as the consolidation pressure increased, the volume of the sample changes in a systematic manner. The pre- and post-yield area shows little change in volume as the cemented structure begins to breakdown. Continued structural deformation leads to a larger decrease in volume and strain softening, until eventually the rate of volume loss decreases and strain hardening increases again. This three phase behaviour is also reflected in the relative distortion of the samples during shear. It can be seen in figure 6.18 that in the samples (BHCW3, 6-8) subjected to the lowest consolidation pressures (3 and 10MPa), the cement structure is largely undisturbed (as indicated by the small volume changes, figure 6.20) and they deformed by shearing and 'flow' (plates 6.2 and 6.3). The remaining samples sheared whilst still in the strain softening phase (BHCW2, 9) of consolidation do not develop these pronounced shears. These two samples were observed to have distorted around the tops of the inner membranes in a ductile manner with no discernible fracturing present (plate 6.4). The surfaces of both samples were sufficiently soft to be marked with finger print during removal from the membranes. The style of deformation has gradually become more ubiquitous and fracturing less pronounced as the consolidation pressure has increased.



Plate 6.4. A Butser Hill sample isotropically consolidated to 20MPa (BHWC2). The sample contains no visible shears but has distorted around the tops of the inner membranes.



Plate 6.5. Sample BHWC4, isotropically consolidated to 40MPa. Undrained shear has resulted in a barrel shaped sample.

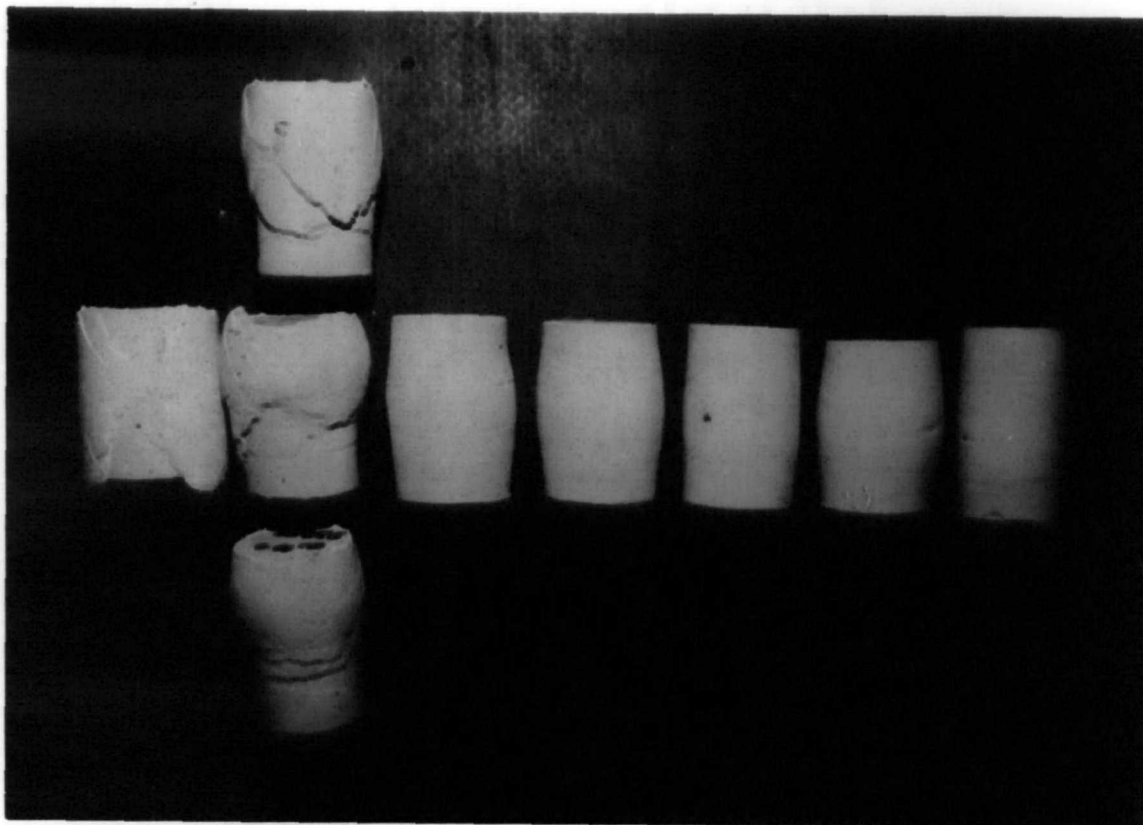


Plate 6.6. All of the isotropically consolidated Butser Hill samples showing a progressive change in the style of deformation with increasing consolidation pressure (left to right).

This change in the style of deformation continues throughout the remaining pressure range. With the onset of strain hardening, the surfaces of the samples gradually become harder until they can be handled with ease without leaving any imprints. The distortion at the junctions of the inner membranes are less obvious and the samples became increasingly barrel shaped (plate 6.5). Plate 6.6 shows all of the Butser Hill samples together in order of increasing consolidation pressure. The progressive change in the style of deformation is clearly seen.

6.6.2.2. *Stevn's Klint.*

These higher porosity chalks were also subject to undrained shear at a range of consolidation pressures (1-37.9MPa) (table 6.3a) during which shearing was initiated whilst the samples were either still elastic (SKWC6), undergoing post-yield strain softening (SKWC3, 5, 7, 8, and 10) or strain hardening (SKWC1). As with the Butser Hill chalks, these samples also show a variation in the style of deformation in response to increasing consolidation pressure, but it was observed that the styles of deformation were not necessarily the same. Three samples (SKWC6- 8) were sheared following consolidation to low pressures (1- 4.7MPa) during which only small changes in volume were recorded (figure 6.21). All three samples developed a small number of conjugate shear fractures (plate 6.7). A consolidation pressure of 1MPa was applied to sample SKWC6 to ensure that it was still in its elastic, pre-yield state, before being subject to undrained shear. During shear, large conjugate fractures developed which appeared to be comparable to the fractures that developed in the Butser Hill sample (BHWC8) which was also sheared whilst still elastic. All the remaining samples were consolidated to pressures beyond the yield stress for this material. The other two samples (SKWC7 and 8) in which only small changes in volume were recorded following yield also developed large conjugate fractures. This behaviour is not comparable to the Butser Hill samples consolidated under similar conditions, in which a large number of conjugate shears developed in a 'flow' pattern.

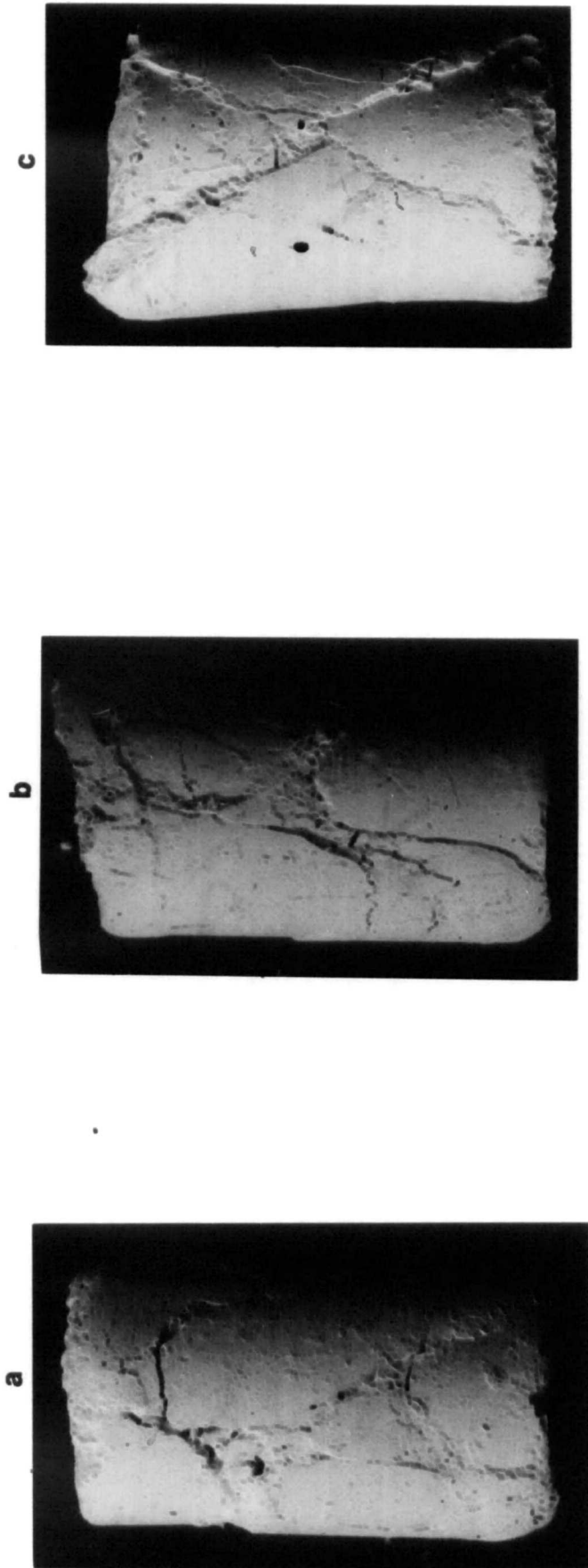


Plate 6.7. Three Stevn's Klint samples subject to undrained shear following isotropic consolidation to a) 1MPa (SKWC6), b) 2.8MPa (SKWC8), and c) 5.3MPa (SKWC7). Note all three sample have developed conjugate shears.

Samples SKWC3, 5 and 10 were also observed to be deforming by strain softening during consolidation. However, these three samples were subject to consolidation pressures that were high enough to lead to significant volume changes (figure 6.21). They behaved in a similar manner to the equivalent Butser Hill samples (BHCW2 and 9). They were extremely soft (easily marked with finger prints), showed no evidence of fracturing, and had clearly distorted at the junctions of the inner membranes (plate 6.8). These samples had clearly formed 'putty chalk' (Vaughan, pers. comm., 1989) and were sufficiently malleable, that once they had been taken out of the test cell and rubber membranes had been removed, squeezing them by hand led to the expulsion of pore fluids, whilst stretching allowed this water to be reabsorbed. This plasticity was not uniform. The ends and the centre of the samples were stiffer than the areas adjacent to the tops of the inner membranes around which deformation had been concentrated (plate 6.8).

As the initial porosity of the chalk increases, strain softening plays a more important role in the deformational process.

Only one sample (SKWC1) of Stevn's Klint chalk was consolidated to a pressure large enough to allow strain hardening to develop. Unlike the Butser Hill samples (BHCW1 and 4), this did not result in the formation of a barrel shaped sample. Like the other Stevn's Klint samples, deformation was still concentrated around the tops of the inner membranes (plate 6.9) and the surface of the sample was soft enough to be marked by finger prints.

6.6.3. Influence of the method of consolidation on the stress path.

Figure 6.45 provides evidence that the method of consolidation may influence the undrained shear behaviour of a material. This graph represents an experiment in which a sample of Butser Hill chalk (BHCW11), was consolidated isotropically using the step method (see section 6.4). This stress path shows substantial decrease in mean effective stress compared to the stress path for sample BHCW4 which was consolidated to

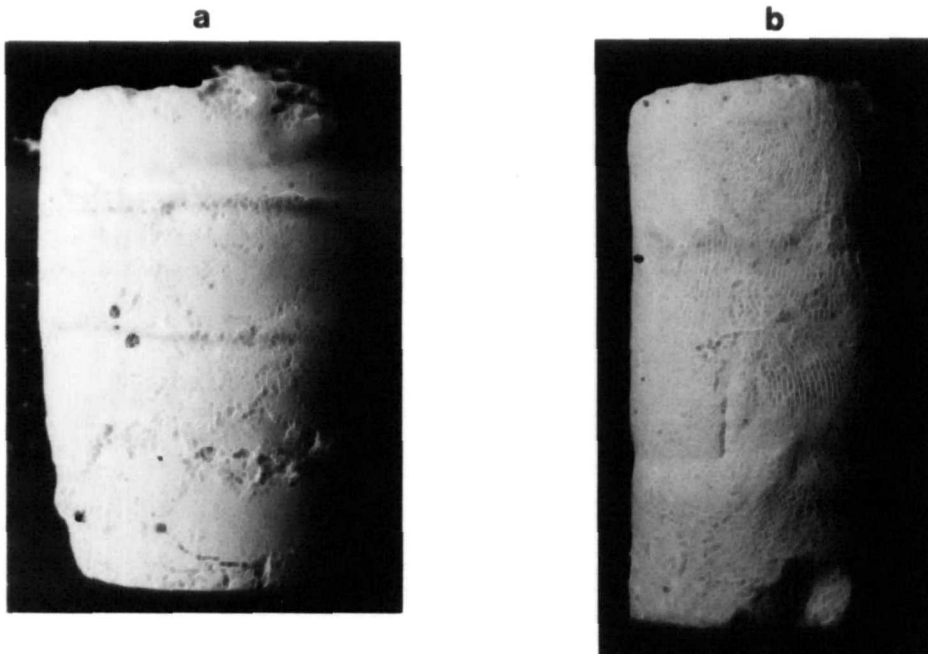


Plate 6.8. Two Stevn's Klint samples subject to undrained shear following isotropic consolidation to a) 9.5MPa (SKWC10) and b) 19.4MPa (SKWC5). These samples were observed to be extremely soft and had clearly distorted around the edges of the inner membranes.



Plate 6.9. Sample SKWC1, isotropically consolidated to 40MPa before shearing.

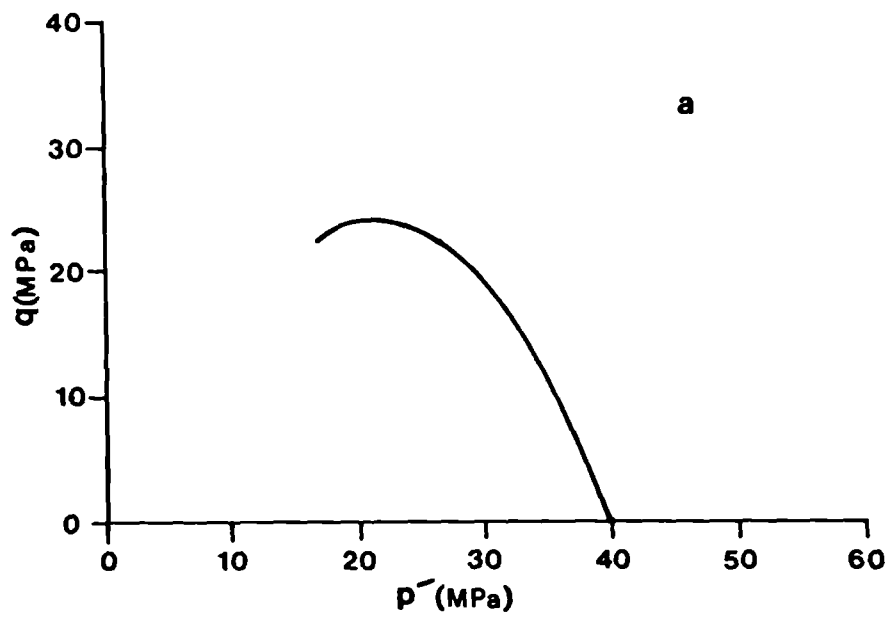
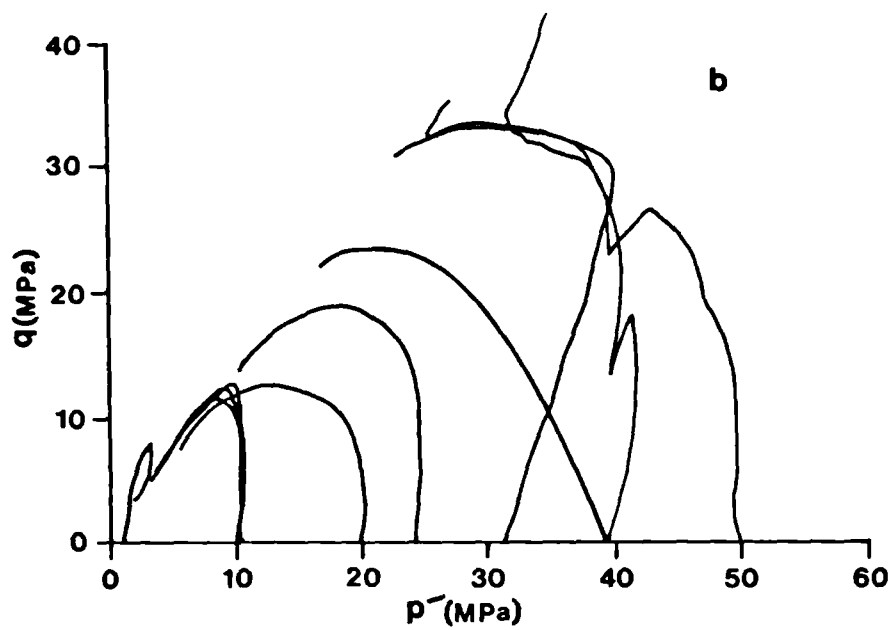


Figure. 6.45. a) A Butser Hill sample consolidated using the step-wise method. b) The same curve in relation to the other Butser Hill samples isotropically consolidated using the ramp method.



approximately the same pressure using the 'ramp' method. There is also a significant difference in the two peak shear stresses. Sample BHWC4 attained a peak shear strength of 35.4MPa, but sample BHWC11 is observed to sustain a peak shear stress of only 25MPa. The behaviour of the two samples once their stress paths have reached the projection of the Critical State Line is also different. Sample BHWC4 is observed to strain harden, whereas sample BHWC11 clearly deformed by strain softening.

It therefore appears, from this limited data, that the method of consolidation may have a profound affect on the nature of the stress path followed, even though the ultimate conditions may not be affected.

6.6.4. Influence of consolidation pressure on pore pressure generation.

It has been shown that increasing the consolidation pressure leads to an increase in the peak shear stress, and may have a profound affect on the stress path. It is also observed that increasing the consolidation pressure leads to higher pore pressures (tables 6.3a and 6.3b). Figure 6.46 and 6.47 present typical top and bottom pore pressure curves for two Stev's Klint samples. In each experiment except for BHWC5 in which drainage problems were encountered, the difference between the top and bottom pore pressures during shear remained within 2% of the total pore pressure. The pore pressure measured at the bottom of the sample remained marginally higher than the top pore pressure in all but one experiment (BHWC1). In sample BHWC1, the top pore pressure briefly rose above the bottom one towards the end of the shearing process, after which it reverted back to a pressure lower than the bottom pore pressure.

The significance of pore pressure generation during undrained shear can be represented by Skempton's pore pressure parameter 'A' (equation 6.2, section 6.2). This parameter may be used to represent the physical state of the sample at failure (table 6.4).

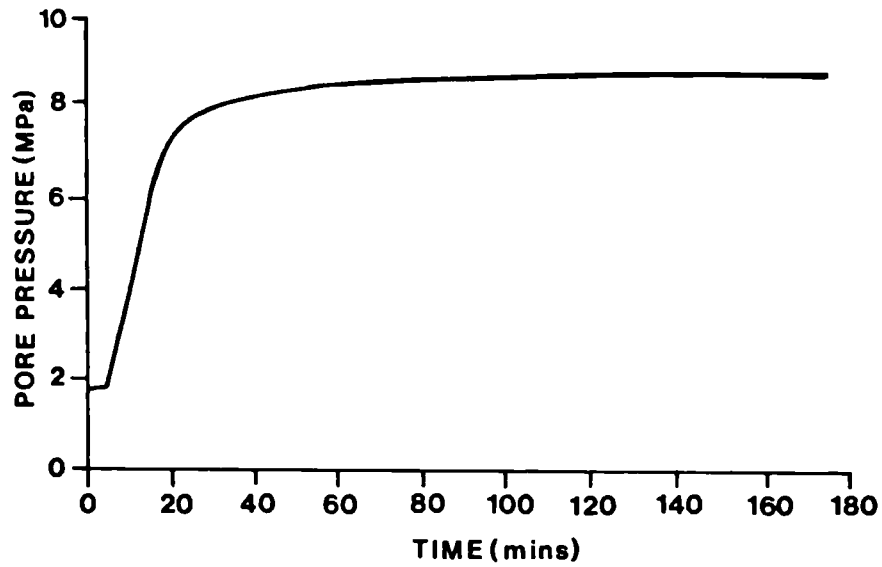


Figure. 6.46. Top and bottom pore pressures generated during undrained shear for isotropically consolidated Stevn's Klint sample SKWC10.

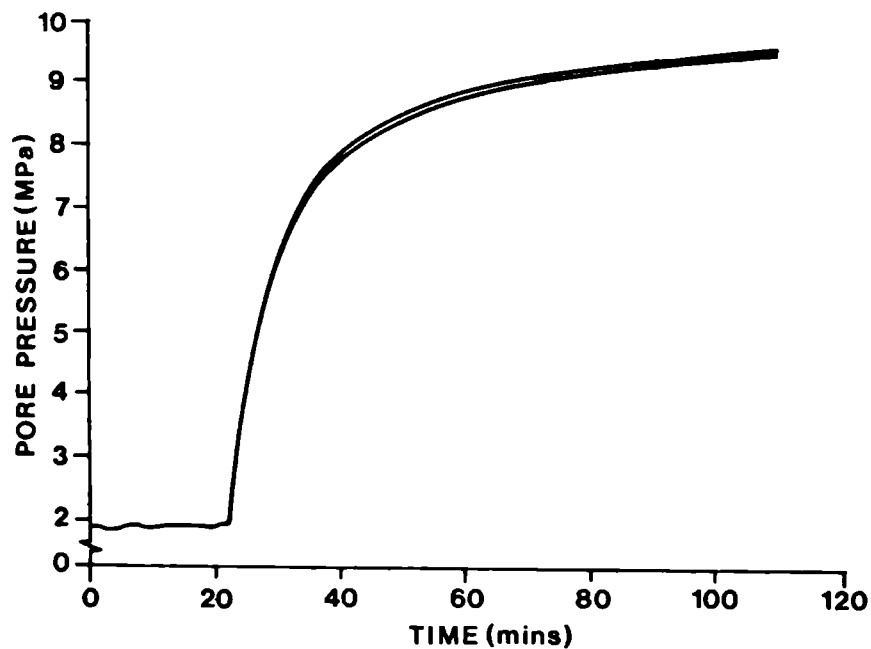


Figure. 6.47. Top and bottom pore pressures generated during undrained shear of anisotropically (K_0 consolidated Stevn's Klint sample SKWC9.

Table 6.4

**TYPICAL VALUES OF PORE PRESSURE PARAMETER A
IN A FULLY SATURATED SOIL (after Lambe and Whitman, 1979)**

Material	Value of A at failure line
----------	-------------------------------

- | | |
|----------------------------------|------------|
| a) Very loose fine sand | 2 to 3 |
| b) Sensitive clay | 1.5 to 2.5 |
| c) Normally consolidated clay | 0.7 to 1.3 |
| d) Lightly overconsolidated clay | 0.3 to 0.7 |
| e) Heavily overconsolidated clay | -0.5 to 0 |

Table 6.5 details the final 'A' values for each of the isotropically consolidated samples in relation to the consolidation stress.

Table 6.5

PORE PRESSURE PARAMETER 'A' DATA CALCULATED FOR CHALK SAMPLES AT FAILURE

Exp. name	P' (MPa)	Displace- ment rate (mm/min)	Parameter 'A'	Exp. name	P' (MPa)	Displace- ment rate (mm/min)	Parameter 'A'
BHWC1	50	0.1	0.67(d)	SKWC1	40	0.1	0.96(c)
BHWC4	41	0.1	0.67(d)	SKWC5	19.4	0.1	1.75(b)
BHWC5	30	0.1	0.61(d)	SKWC3	10.4	0.1	8.8 (a +)
BHWC9	25	0.1	1.35(c)	SKWC10	9.5	0.1	8.5 (a +)
BHWC2	20	0.1	2.16(a)	SKWC7	5.3	0.1	11.0 (a +)
BHWC6	10	0.01	1.8 (b)	SKWC8	2.8	0.1	3.17(a +)
BHWC3	10.2	0.1	1.71(b)	SKWC6	1	0.1	0.38(d)
BHWC7	10	1.0	1.59(b)				
BHWC 8	3	0.1	0.18*(e)				

*** Note at peak shear strength the 'A' value was -0.11.**

Letters after the A values correspond to categories in table

6.4. A + indicates that these values of A are higher than those presented in table 6.4.

The values of parameter 'A' presented in table 6.5 provides further evidence for a change in the nature of both chalks with increasing consolidation pressure. Although an analogy between these high porosity chalks and the materials listed in table 6.4 may not be fully justified, the table may provide a basis for discussion. The data in table 6.5 indicate that deformation during undrained shear of the Stevn's klint chalk represents a more extreme type of behaviour than deformation of the Butser Hill chalks. However, the change in the style of material behaviour during shear follows a similar pattern for both chalks. If the chalks are subject to undrained shear whilst still elastic, they behave in a similar manner to an overconsolidated clay. As the consolidation pressure is increased the chalks are observed to yield. Following yield they strain soften. If they are subject to shear during this post-yield, strain softening phase of deformation they behave in a similar manner to a sensitive clay or loose sand. Further consolidation leads to compaction of the structure and strain hardening. Samples subject to undrained shear during this phase of the consolidation process result in 'A' values consistent with that of an overconsolidated clay.

It is possible to extend the use of the 'A' value, with certain reservations, to examine the behaviour of both types of chalk throughout the shearing process (Skinner, pers. comm., 1989). Figures 6.48 and 6.49 represent this pore pressure parameter plotted against the maximum consolidation pressure for each sample. This provides a further indication of the physical changes induced in the samples during shearing. It is observed from these data that similar changes to those recorded in table 6.5 which are the result of increased consolidation pressure are experienced by the chalks during shear.

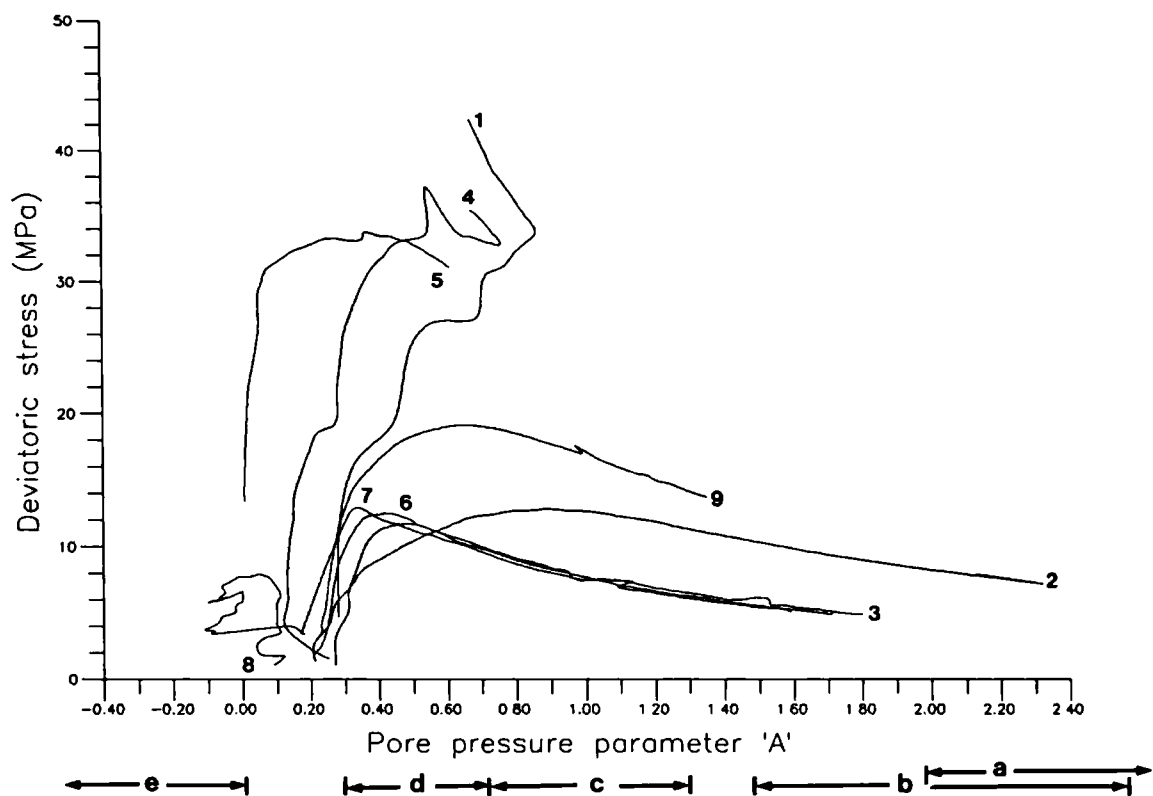


Figure. 6.48. Values of Skempton's pore pressure parameter 'A' plotted against the maximum consolidation pressure for each of the Butser Hill isotropically consolidated samples.

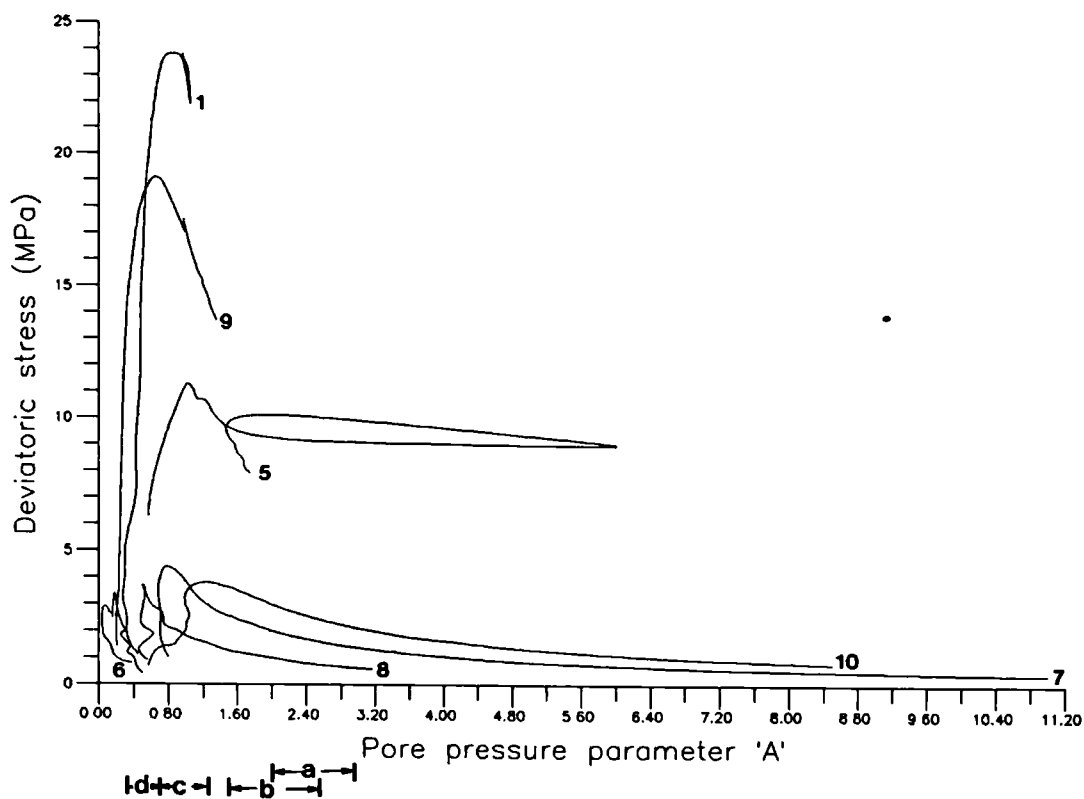


Figure. 6.49. Values of Skempton's pore pressure parameter 'A' plotted against the maximum consolidation pressure for each of the Stevn's Klint isotropically consolidated samples.

6.6.5. The influence of strain rate.

Lambe and Whitman (1979) record that during shear, as the rate of strain is increased, the undrained shear strength also increases. There is however, little agreement (Lambe and Whitman, 1979) on the magnitude of this rate effect. The data in figures 6.36-6.39, and tables 6.2 and 6.5, indicate that by varying the strain rate over three orders of magnitude the peak shear strength increases by approximately 10%. Peak shear strength will increase with increasing rate of strain as there appears to be a time dependency in the breakdown of the cement bonds. But, although peak shear strength increases, the residual shear stress and the pore pressure response for all three samples are virtually the same (table 6.3a). The 'A' pore pressure parameter data (table 6.5) for these three strain rate experiments (BHW3, 6, and 7) appear to contradict the view that the chalks should become stronger as the strain rate is increased. These data (table 6.5) indicate that the chalk is marginally weakened by an increase in the rate of strain.

6.6.6. Failure Surface and Consolidation Path.

Critical state soil mechanics (Atkinson and Bransby, 1978) demonstrates that the stress state at failure depends upon the pore volume of the material. As consolidation pressure increases, the pore volume is observed to decrease (figures 6.20, 6.21, 6.32 and 6.33), the density of the sample increases and friction between grains becomes a significant factor in increasing the strength of the rock. To represent changes in volume during consolidation the data in figures 6.18 and 6.19 should be replotted with the axes of void ratio (porosity), mean effective stress and deviatoric (shear) stress (figures 6.50 and 6.51). These graphs show the geometry of the Critical State Line and the effect of the different initial consolidation pressures are clearly seen.

It is interesting to compare the effects of different consolidation paths on the undrained shear behaviour. Figures 6.52 and 6.53 show that experiments, where undrained shear follows K_0 consolidation, end on the Critical State Line in the same manner as experiments consolidated under isotropic conditions. This is to be expected. What is more interesting is that the path followed during K_0 consolidation passes close to the Critical State Line at elastic yield. Following the onset of yield, the stress path passes back

into permissible stress space. This indicates that chalk, consolidating under K_0 conditions, comes very close to a critical state failure as it passes through its elastic yield. The material is therefore potentially unstable at this condition if it is to be subjected to small variations in shear stress.

Chalk in hydrocarbon reservoirs is close to the K_0 stress condition. The data in figures 6.52 and 6.53 indicate that if the chalk adjacent to a well perforation is close to its elastic limit, small changes in well pressure may be all that is needed to promote the critical state failure responsible for well invasion. This will mean that in a reservoir, where chinks exhibiting a range of porosities are present, invasion of solids into wells may occur at different times during the production history, as chinks of different porosity approach their elastic limit. Generally, chinks with the greater pore volumes, which will fail after smaller changes in reservoir pressure might be expected to give the most dramatic deformations. This is because only a small increase in stress is necessary for the material to transfer from the elastic envelope to the Critical State Line.

Computer data processing employed during this study assumed a Poisson's Ratio of 0.5 (Lambe and Whitman, 1979) so that the void ratio, during undrained shear, remained constant and that the mid height diameter of the sample increases by half the axial shortening. Figure 6.34 and 6.35 showed changes in radial strain plotted against axial strain during undrained loading following K_0 consolidation. The two Stevn's Klint experiments (figure 6.35) show that initial increases in radial strain, consistent with the assumption of increasing mid-height diameter were followed by dramatic decreases. This indicated, that during strain softening the Stevn's Klint samples underwent significant non-uniform radial deformations which finally led to a total breakdown in their structure. If a constant void ratio is assumed, these plots must represent a zonation in the break-down of the chalk, in which some areas will be decreasing in void ratio while others are increasing to compensate for the volume changes (allowing the average void ratio to remain constant). (See also section 6.2 for another explanation of the maintenance of constant volume). The two Butser Hill samples were observed to strain hard-

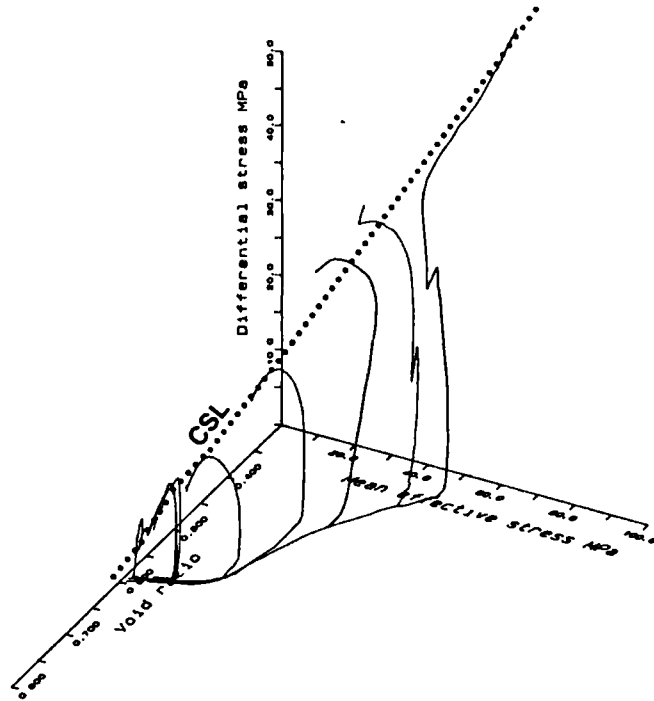


Figure. 6.50. The isotropically consolidated Butser Hill experiments plotted against axes of void ratio/mean effective and deviatoric stress.

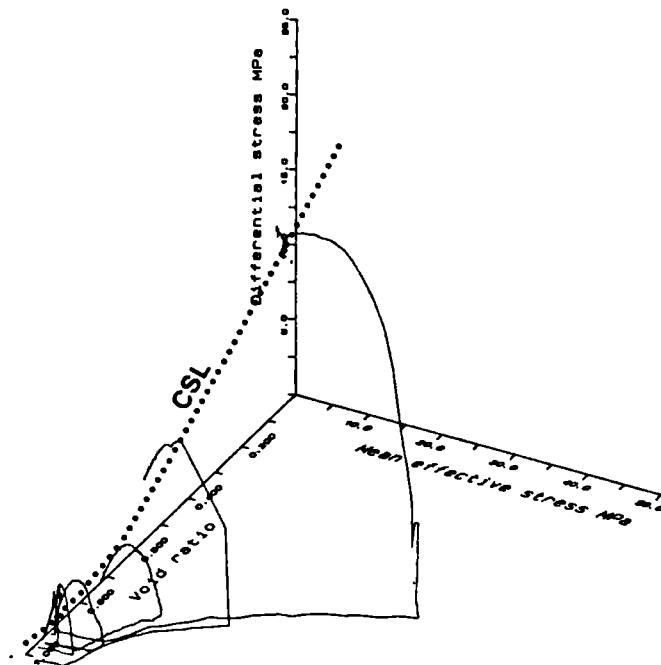


Figure. 6.51. The isotropically consolidated Stevn's Klint experiments plotted against axes of void ratio/mean effective and deviatoric stress.

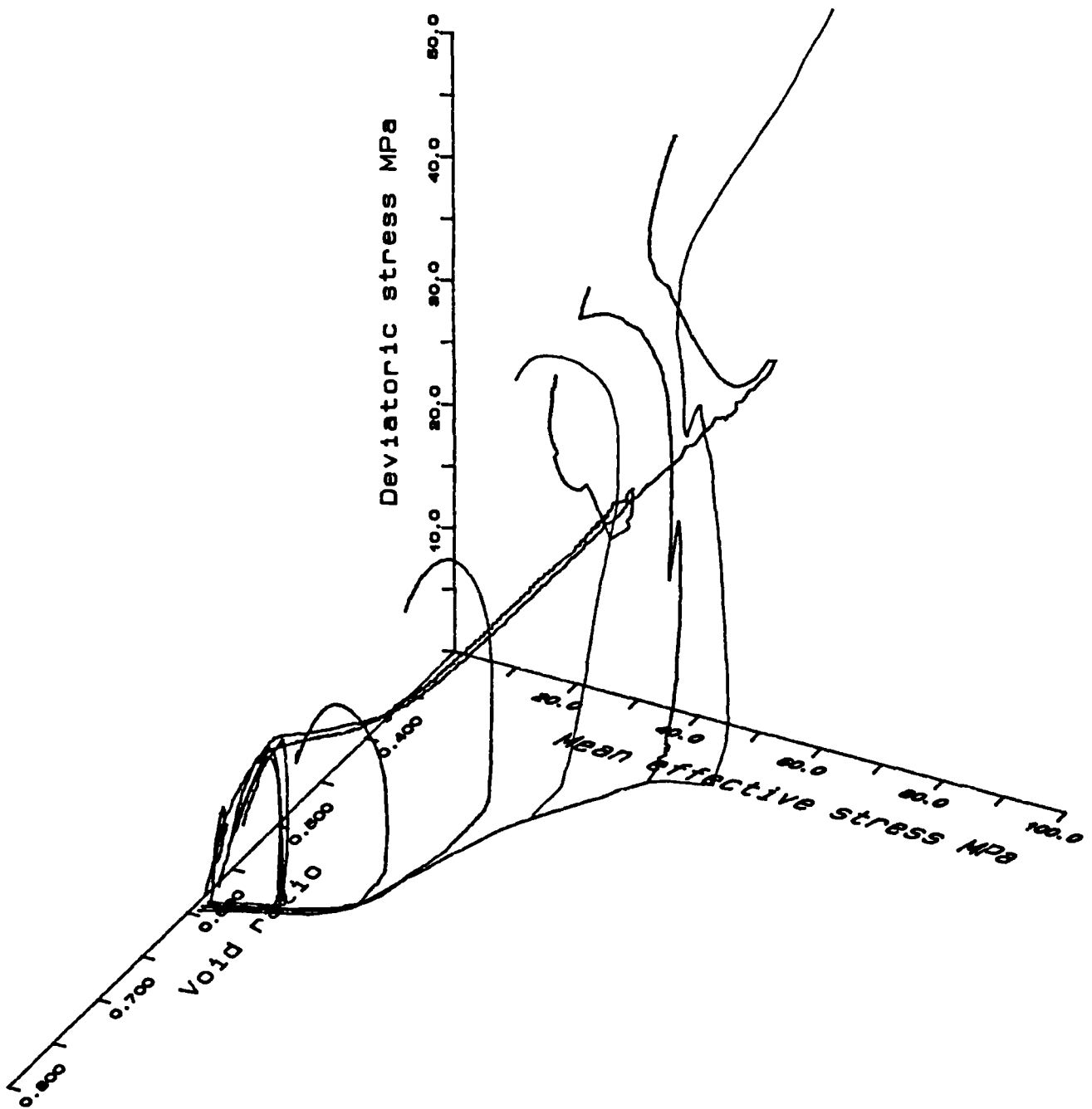


Figure. 6.52. The isotropically and anisotropically (K_0) consolidated Butser Hill experiments plotted against axes of void ratio/mean effective and deviatoric stress.

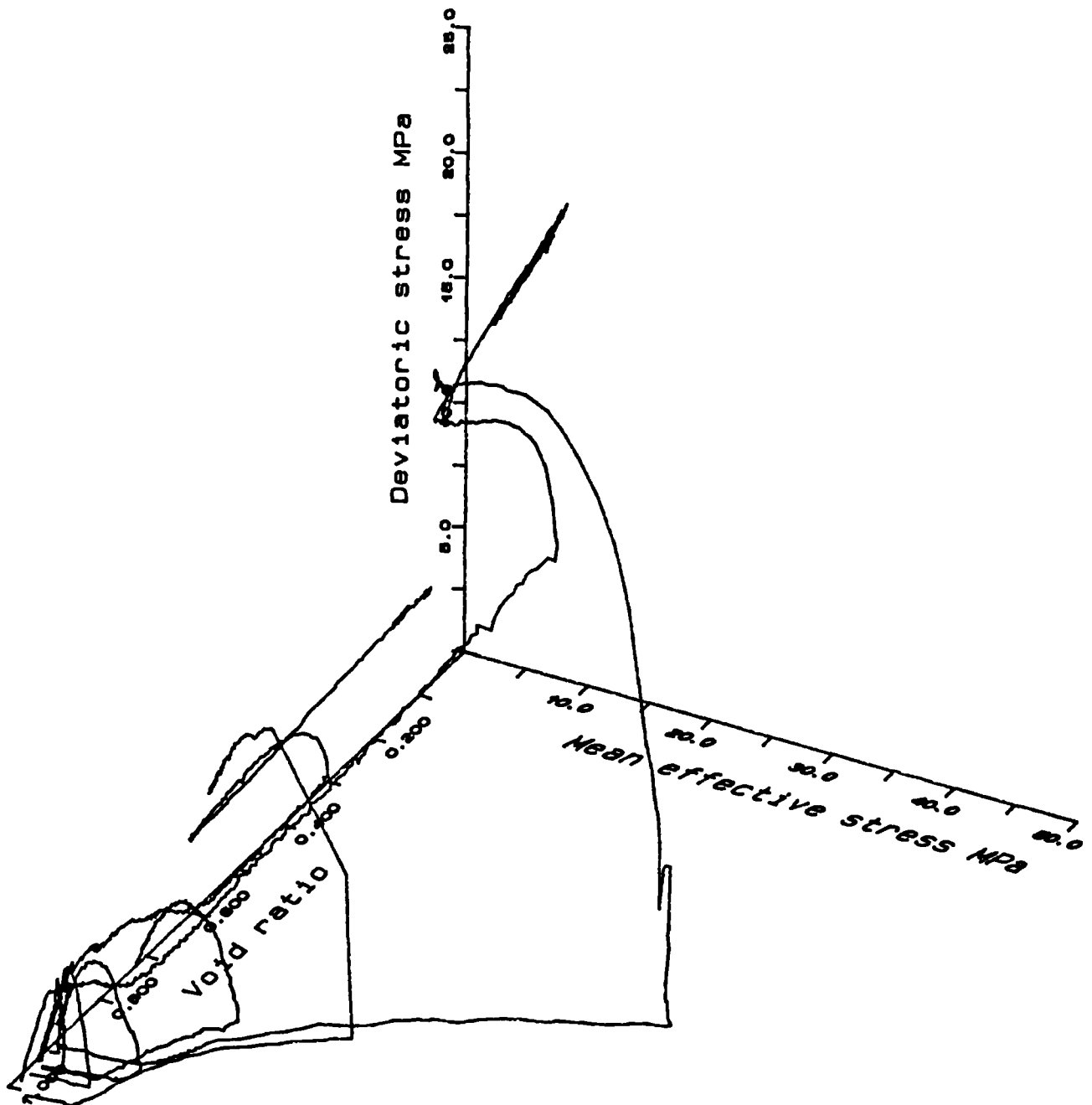


Figure. 6.53. The isotropically and anisotropically consolidated Stevn's Klint experiments plotted against axes of void ratio/mean effective and deviatoric stress.

en during shear. The radial strain graph for these two experiments (figure 6.34) indicates that the mid-height diameter increased in a manner consistent with the assumption stated above. These two sets of data therefore do not agree as to the radial strain changes during the process of undrained shear. These differences may be due to variations in the initial porosity and cementation of the two chalks.

It has been noted by a number of authors (see Seed et al., 1989) that membrane compliance can significantly alter the volume of samples during the application of undrained shear. As the pressure increases during the drained consolidation part of the experiment, the membrane is pushed into the surface voids of the sample. This leads to an overestimation of the volume changes occurring in the sample, if such changes are only determined from volume of pore fluid displaced. As the effective stress decreases during undrained shear, membrane penetration decreases and the volume of the sample changes. It has been noted that this process can lead to a serious overestimation of the resistance of the sample to liquefaction (Seed et al., 1989). However, it is not considered to be a problem that could account for the volume changes recorded above, as the grain size of the chalk is small.

Elliott and Brown (1985) found, by instrumenting samples of oolitic Bath Stone with strain gauges, that the distribution of strain within the samples varied with consolidation pressure. The limestones were sheared under drained conditions, but the pattern of behaviour shows many similarities with the undrained shear experiments described here. At low stresses, there was a rapid strain relief in the undeformed parts of the sample. As the consolidation pressure increased, the formation of microfractures ceased and the samples tended to deform by barrelling. At these higher pressures the strain gauges indicated a uniform distribution of strain.

If the assumption of a constant void ratio during undrained shear (Atkinson and Bransby, 1978; Lambe and Whitman, 1979) is not valid, the variations in radial strain recorded during shear of the two anisotropically consolidated Stevn's Klint samples

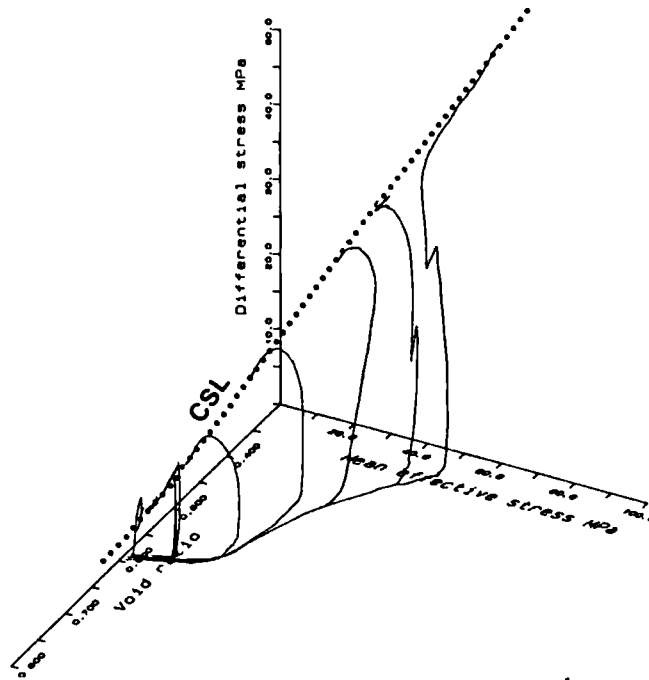


Figure. 6.54. The isotropically consolidated Butser Hill experiments plotted against axes of void ratio/mean effective and deviatoric stress, in which volume changes have been allowed during data processing, so that the stress paths follow the Critical State Line.

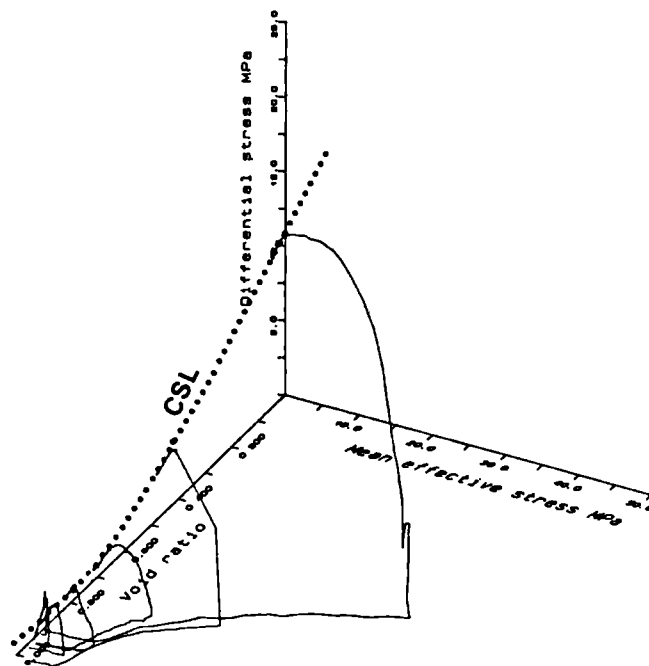


Figure. 6.55. The isotropically consolidated Stevn's Klint experiments plotted against axes of void ratio/mean effective and deviatoric stress, in which volume changes have been allowed during data processing, so that the stress paths follow the Critical State Line.

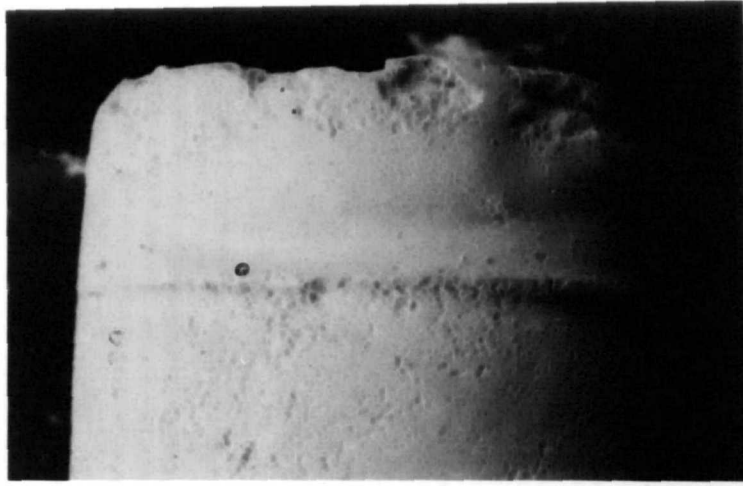


Plate 6.10. Enlargement showing the distortion around the top of the inner membranes on a Stevn's Klint sample.

may be significant. Changes in volume during undrained shear could allow dilation or contraction of samples to follow the Critical State Line in stress/void ratio space (figures 6.54 and 6.55). Although the mid-height diameter may change significantly (figure 6.35), other areas within the sample may also undergo equally large shape changes, so that the total change in volume, if any exists, may be small. Deformations in many of the Stevn's Klint samples appear to have been concentrated in zones adjacent to the ends of the inner membranes (plates 6.9 and 6.10). Two explanations may be proposed for the existence of these two zones of deformation. Firstly, it is possible that the changes recorded by the radial strain belt may have been restricted to bulging and collapse of the samples between these zones so that the ends of the samples remained comparatively unaffected by the deformation. Secondly, these areas may represent transition zones in which an expansion in the centres of the samples were compensated for by contraction of the ends. Equally, when the centres were observed to collapse, the ends of the samples may have expanded. There is no evidence for the existence of these narrow zones of deformation in the Butser Hill samples where deformation was concentrated at one end of the sample.

It is evident that measurements of radial strain across the centre of a sample are not sufficient to determine whether volume changes occur during undrained shear. But measurements over the entire length of a sample have proved to be extremely difficult (Skinner, pers. comm., 1989). One method that has been tried involved the placing of lead shot inside the rubber membrane. X-rays were then used to determine shape changes during shear (Skinner, pers. comm., 1989). This method failed as changes in the total volume were found to be too small to be recorded. Another method which may be useful is the measurement of changes in the volume of the confining fluid which results from changes in the volume of the sample.

If volume changes do occur, and the radial strain measurements given here are not sufficient to determine this, then a number of definitions may be called into question. For instance, strain softening or contractant behaviour, seen with changing pore volume

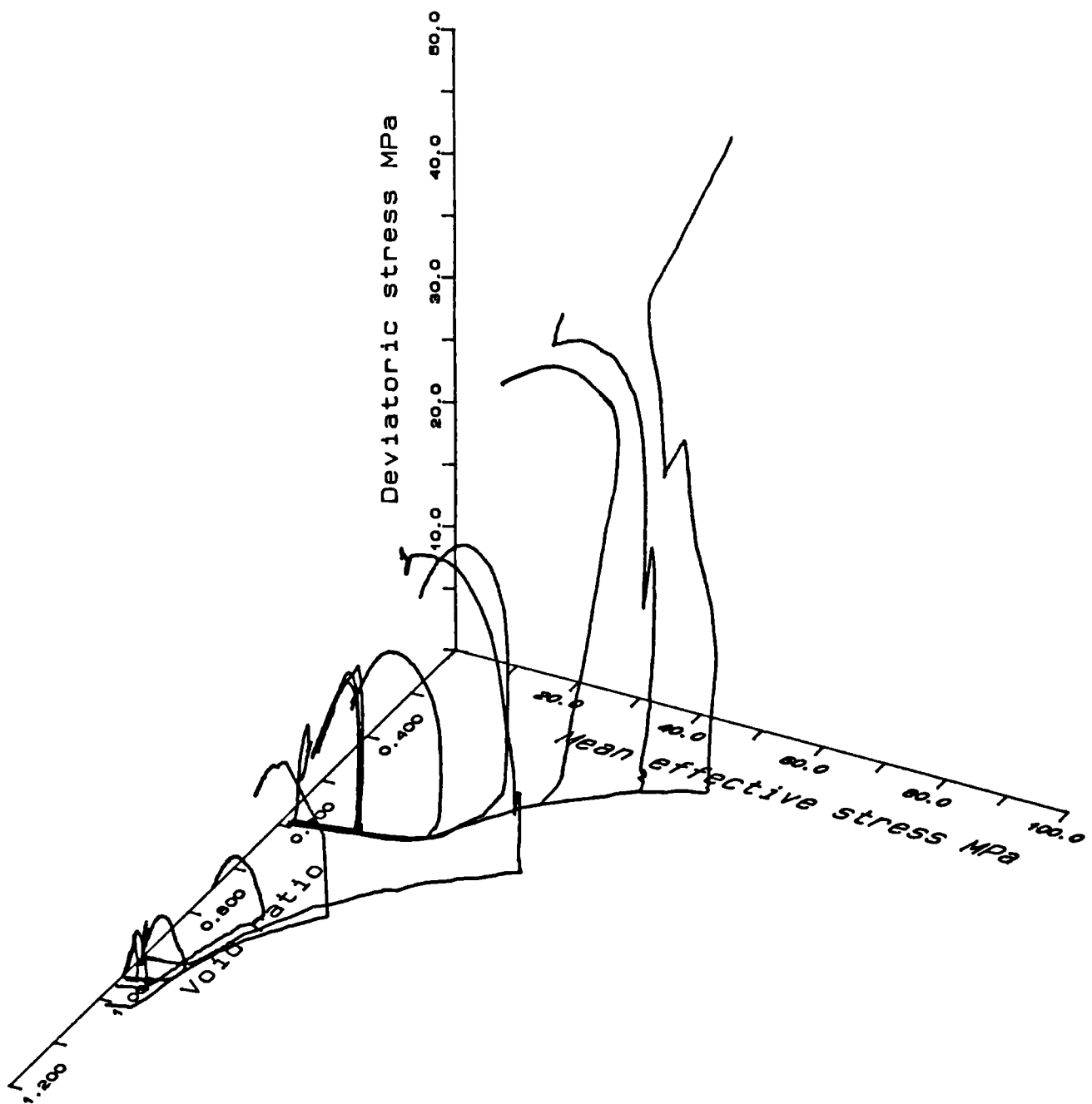


Figure. 6.56. Both sets of isotropically consolidated experiments plotted together in void ratio/mean effective and deviatoric stress space.

shows an increase in volume rather than a decrease. Conversely, dilatancy or strain hardening would produce a decrease in volume. The two terms themselves, namely contractant and dilatant, imply volume changes but are often used for undrained shear results in which zero volume change is an implicit requirement.

Figure 6.56 shows the two sets of isotropically consolidated data together in stress/void ratio space. This plot emphasises the individual nature of the behaviour of both chalks. Although they both have a common Critical State Line (figure 6.40) differences in initial void ratio and volume changes resulting from consolidation mean that the stress paths for both chalks do not coincide in stress/void ratio space (figure 6.56). The plots of the lower porosity Butser Hill samples are seen to lie 'inside' that of the higher porosity Stevn's Klint chalks. This indicates that the mechanical behaviour of any particular chalk will depend on a combination of the initial void ratio and the consolidation pressure prior to shearing. These data further confirm that a single porosity trendline does not exist for the chalk as demonstrated by Ruddy et al. (1988).

6.7. CONCLUSIONS.

This experimental investigation has shown that under specific conditions of mean effective and deviatoric stress, 1) high porosity chalk will become weak and can deform in a manner equivalent to a loose sand or a sensitive clay at the critical state condition. It is observed that chalk will 2) change from a strain softening to a strain hardening behaviour in response to increasing consolidation pressure. 3) A chalk subject to undrained shear whilst still elastic is observed to yield at a shear stress outside critical state space. This yield stress represents the position of an elastic yield surface which exists above the Hvorslev Surface (of the Cam Clay model). Following yield, the chalk will strain soften until the critical state is achieved. 4) Strain softening and collapse is also observed in chalks sheared when they are in the post-yield, strain softening phase of deformation (during the consolidation process). 5) At higher consolidation pressures, the density of the chalk increases sufficiently for frictional resistance and strain harden-

ing to develop. If chalks are subject to undrained shear under these conditions, the chalk will tend to continue to strain harden until it attains its critical state.

6) As the consolidation pressure increases, peak shear strength and pore pressure generated during undrained shear are observed to increase.

7) At yield, under conditions of K_0 consolidation, the chalk lies close to its critical state. Change in shear stress, under these conditions may well lead to structural collapse. This situation may be particularly important in reservoir chalks which exhibit a range of different porosities (as yield strength appears to be dependent on the initial porosity (Jones and Leddra, 1989)). Pore pressure draw-down in high porosity chalks may lead to an increase in effective stress that takes the chalk close to its yield strength. An increase in shear stress, resulting from a shut-in well being brought back on-stream, may be sufficient to take the weakened chalk to its critical state, causing it to flow into the well bore.

8) When the results of these undrained shear experiments are plotted together in stress/void ratio space, it was observed that strain hardening or strain softening depends not only on the pre-shear consolidation pressure, but also on the initial void ratio. These data indicate that changes in void ratio for each chalk do not reduce to a single trendline.

Radial strain data, recorded during anisotropic consolidation experiments on both chalks reveal significant differences in their response to undrained shear. The weaker, higher porosity, Stevn's Klint chalks, undergo large changes in diameter at the mid-height position during shear. These data indicate that careful measurements of sample volume are required during undrained shear, as it is possible that the assumption of constant volume may not be valid.

Deformation mechanisms, similar to those recorded during shear experiments conducted on weakly cemented carbonates from offshore Australia are observed to operate during deformation of these chalks.

CHAPTER 7.

GENERAL DISCUSSION AND CONCLUSIONS.

7. GENERAL DISCUSSION AND CONCLUSIONS.

7.1 INTRODUCTION.

The chalk in the North Sea shows evidence of having deformed through natural compaction and shear due to the processes of burial diagenesis and redeposition. Today, the same chalk is again deforming in compaction due to pore pressure reduction during hydrocarbon production, and in shear due to failures in the vicinity of well perforations. The experimental study reported in this thesis provides the means to describe and quantify these deformations.

The results of the experiments reported, reveal that the characteristics of both compaction and shear deformation of the chalk is dominated by one feature, the presence of cement bonding. The mechanical behaviour of bonded porous rock materials has received little attention even though Vaughan (1985) and Vaughan et al. (1988) have demonstrated the importance of cement bonding in altering the mechanical behaviour of soil materials. The importance of understanding the role of cement bonding in understanding the mechanical behaviour of porous rocks forms a major subject of this thesis and has been described in the literature (Jones and Leddra, 1989).

The presence of bonding (mineral cement bridges between individual carbonate grains) introduces a unique style of deformation behaviour. The cement bonds tend to freeze the structure with a pore volume which is not equilibrated to the active stress system. This means that in the case of high porosity chalks, the pore volume exceeds that in equilibrium with the effective stress state whilst in low porosity chalks the pore volume is significantly smaller than the equilibrium volume for the chalk as a particulate material. Deformation to small strains is accommodated by this structure and relatively large but recoverable stresses are maintained. Deformation to larger strains is dominated by progressive failure of the bonded structure and its conversion to a particulate material. In the short term, all subsequent behaviour is substantially that of the particulate material, but in the natural geological situation, cementation may re-establish the bonded state.

7.2. BURIAL COMPACTION AND SHEAR DEFORMATION DURING REDEPOSITION.

Chalk compaction probably progresses in a series of steps, with periods when compression (grain boundary sliding) will dominate and periods when pressure solution will recement the structure. Each cycle of compression/pressure solution/recementation will permit an increase in the magnitude of the effective stress as the weight of the overburden increases through geological time. The chalk will thus compact by progressively concentrating stress in the intergranular bonds, until they fail by fracturing whence the stress is transferred to the post fracture grain contacts leading to pressure solution and formation of new cement bonds. During burial, the process will be continuously repeated, progressively reducing the porosity and permeability of the chalk as the proportion of cement in the sediment increases. With increased burial the rock becomes stronger and the compactional events less frequent as the cement produced by pressure solution infills more of the pore space (figure 7.1). Nonetheless, it seems probable that the prime mechanism of compaction is compression, not pressure solution. A similar process has been proposed by McClay (1977).

The process of compaction can be arrested in a number of ways. Firstly, as the fracturing of cement bonds is effective stress driven, the establishment of a cement structure of large strength will prevent further fracturing and therefore a further increase in density, so the compaction rate will slow. Secondly, the establishment of a high pore fluid pressure will serve to reduce the effective stress. This pressure may be established by the reducing permeability of the compacting chalk and will prevent further fracturing of cement bonds (as this is solely dependent on effective stress). Pressure solution may continue at a reduced rate as this is probably less dependent on effective stress (Rutter, 1983). Thirdly, the arrival of oil, or other inert pore fluids, will serve to prevent further pressure solution, and, if at sufficiently high pressure will also terminate mechanical compaction.

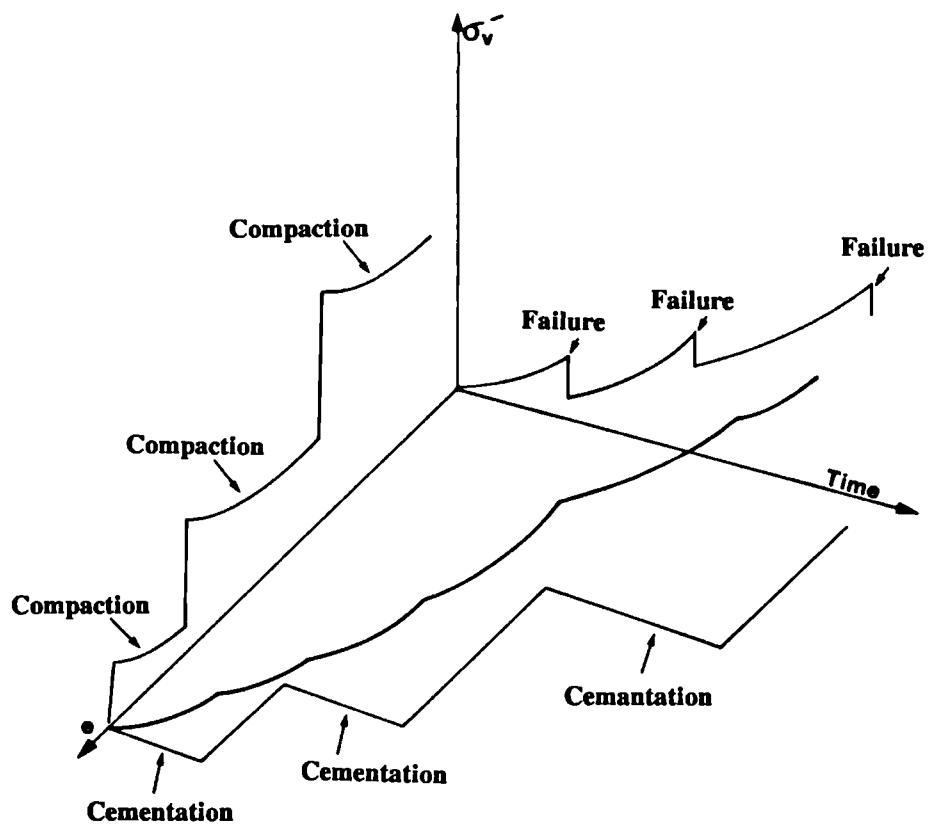


Figure. 7.1. Idealised compaction path for the North Sea Chalk.

The compaction history of the chalk is therefore one in which mechanical compaction (compression) dominates until large fluid pressures are established. When this occurs the rate of porosity loss is greatly reduced and becomes a consequence of pressure solution. Where hydrocarbons become concentrated, pressure solution is also prevented, thereby preserving porosity.

The data presented in this thesis indicate that chalks with porosities of the order 45-50% yield at a vertical effective stress of approximately 5MPa (which is equivalent to a minimum burial depth of 300-400m). Yield is followed by a significant decrease in pore volume as stress is transferred into the pore fluid and then into a strain as consolidation occurs. In nature it seems probable that the times for the dissipation of the excess pressures produced by the collapse of the mineral skeleton are somewhat longer, due to the low permeability of the system, and where dissipation is prevented, these excess pressures will contribute to the overpressuring recorded today in the chalk reservoirs. The highest preserved porosities in the North Sea chalks are of the order of 45-50%. These chalks have never experienced an effective stress greater than 5MPa, indicating the preservation of early porosity.

The highest preserved chalk porosity varies from field to field (Jones, 1989), and the yield stress for these chalks is always close to the recorded in-situ vertical stress prevailing at the start of production (Jones, 1989). The highest porosities preserved in the chalks of each reservoir therefore give an indication of the maximum vertical effective stress experienced by the reservoir rock during burial (5MPa for Valhall, 11MPa for Eldfisk, 14MPa for Ekofisk and West Ekofisk), and the chalks with these porosities lie close to yield under in-situ stress conditions. The porosity and effective stress state have therefore evolved together. Other chalks within each reservoir have experienced more pressure solution and now support lower porosities. The highest preserved porosity is therefore that resulting from compression with a minimal stiffening due to pressure solution/cementation.

The reason why the action of pressure solution has been selective, leading to variable porosities in each of the reservoirs is still unclear. In part it will be due to variations in grain size and shape controlling the susceptibility of any particular stratum to solution. But another and more profound influence may be bifurcation of the compaction paths for different stratigraphic units. Those units most susceptible to early pressure solution will be protected from later compression by the elasticity of the early cement bonds. Layers not subject to early pressure solution will compress to a lower porosity prior to their first pressure solution event. Different parts of the reservoir will therefore be subject to different fracturing/compression, pressure solution/cementation, event histories. The transfer of stress from region to region within the reservoir as regions variously experience these softening and hardening events will serve to further diversify the number of compaction paths. It is interesting to note that even at the scale of a laboratory test sample, variations in cement density serve to localise regions of failure (plates 5.1, 5.2, 4.1, 4.2 and 4.3). Bifurcation of compaction paths therefore occurs across a wide range of scales.

Undrained shear experiments have indicated that at low effective stresses high porosity chalks will collapse (strain soften) and flow. These results are significant, with respect to the burial history of the North Sea chalks, as they define a mechanism by which the slump structures observed in the redeposited chalks and the early healed fracture networks which are often associated with the slumps were formed.

The North Sea chalks exhibit a wide range of deformational fabrics which are considered to have been formed by processes of mass movement in either unconsolidated, consolidated or early cemented states. Many of these structures are related to superficial movement (turbidites) whilst others indicate a high degree of plasticity (debris flows and some slumps) but one group of structures is invariably associated with a complex network of healed fractures. These appear to be brittle slumps. The experimental results indicate that cemented chalks subject to undrained shear after consolidation to effective stresses equivalent to shallow burial depths (300m-600m) (effective stresses

between 5MPa and 10MPa) will deform by brittle shear and strain soften producing a fabric of dilatant fractures with a 1mm to 1cm spacing. This is equivalent to the fabric seen in the brittle slumps. If the same chalk is deformed in undrained shear at lower consolidation pressures conjugate fracture sets are formed, whilst at high consolidation pressures plasticity occurs. These data appear to define the depth range in which brittle slumping of the chalk can occur.

There is some evidence that healed fractures are sometimes cut by trace fossil burrows. If, as the experimental results indicate, the pervasive fracture fabric cannot be generated without an overburden exceeding 300 metres, it must follow that the overburden itself is then progressively reworked eventually exposing the upper part of the brittle slump. This does not present any major difficulty, because the frequency of landslip activity is typically two or three orders faster (Brundsdon and Prior, 1984) than the rate of chalk deposition, so remobilising chalk slumps in large landslip/debris flow systems is quite possible.

The picture presented in the previous paragraphs is important on two counts. Firstly, it indicates that the early diagenetic history may have exerted a major influence on the distribution of reservoir rock quality. Secondly, slump structures within the chalk may be of large size, even if the displacements at depth were localised compared with the turbidity flows that were active at the surface. Reworking of the chalk is not therefore just a superficial process.

It is possible that the importance of pressure solution as the major mechanism of chalk compaction has been previously overstated.

7.3. RESERVOIR COMPACTION AND SEAFLOOR SUBSIDENCE.

Sea floor subsidence and reservoir compaction have proved to be a major feature of North Sea chalk hydrocarbon production. In this section, these problems are reviewed and the application of laboratory experimental data to the analysis of subsidence is outlined.

7.3.1 Introduction.

Subsidence of the sea-floor over the Ekofisk Oil Field (figure 3.1), was first recognised by Phillips Petroleum Co. Norway in 1984 who identified that it was a consequence of the reducing pore fluid pressure in the two reservoirs (Wiborg and Jewhurst, 1986; Sulak and Danielsen, 1988). This subsidence posed a serious threat to the stability of the surface installations. Final mitigation of this threat was achieved in 1987 through simultaneous jacking, and permanent extension of the legs of the entire production complex by 6 metres (Aam, 1988).

When the subsidence was first recognised, its extent and rate were uncertain but qualitative observations of the rate of immersion of the large concrete oil storage tank in the centre of the production complex, indicated the severity of the problem. In 1984, no quantitative settlement data existed for Ekofisk, and land subsidence over deeper oil fields like Ekofisk was so uncommon as to have been regarded as impossible (Potts et al., 1988; Jones et al., 1987). A programme of displacement measurements and a number of independent analytical studies designed to quantify and predict the rate and extent of the subsidence were initiated at this time.

Following the initial investigations for Ekofisk, attention turned to the other chalk oil fields in the Greater Ekofisk Area. This was necessary for two reasons. Firstly, to establish that the production platforms on the Tor, Edda and Albusjkell fields were stable, and suitable reference base-stations for the Ekofisk subsidence survey. Secondly, to identify any other fields that might develop sea-floor subsidence on a comparable scale to that observed at Ekofisk. Early in 1986, a small subsidence of the sea floor was recorded over West Ekofisk, and in 1987, subsidence was also recognised over Valhall.

The Eldfisk Oil Field, although not exhibiting subsidence, was shown to have a subsidence potential. This section of the thesis reports the results of studies of the chalk oil field subsidence problem, commissioned by the Norwegian Petroleum Directorate. Detailed studies of the subsidence at Ekofisk were undertaken by Phillips Petroleum Company (Boade, et al., 1988) and at Valhall, by Amoco Norway Oil Co. (Ruddy et al., 1988).

7.3.2. SURFACE SUBSIDENCE OVER CHALK OIL FIELDS.

Two important factors contribute to the Ekofisk oilfield being an unexpected candidate for a major sea-floor subsidence problem (Potts et al., 1988). Firstly, no other case of land surface subsidence arising from compaction of a reservoir located at depths of the order of 3000 metres had been recognised. Thus, no historical precedent existed for the Ekofisk problem. Secondly, the chalk, unlike most hydrocarbon reservoir rocks, exhibits strongly non-linear deformation characteristics when subject to the effective stress changes typically encountered during hydrocarbon production (Potts et al., 1988; Addis, 1987; Jones & Addis, 1986; Johnson et al., 1988).

7.3.2.1. History of the Ekofisk Subsidence.

After recognition of sea-floor subsidence at Ekofisk a number of different survey activities were instigated. Chief amongst these were satellite surveys, analysis of the water depth and air gap (the distance between mean sea level and the lowest deck on the platform) and bathymetry. Sub-sea pressure measurements were started following the main jacking operation in the autumn of 1987. Prior to the sub-sea pressure survey, satellite measurements were the major dataset for subsidence. A continuous record of the subsidence measurement has been established (figure 7.2) (Rentsch and Mes, 1988) which has provided reliable estimates of the subsidence rate. The maximum rate was 0.5 metres per year and it has now diminished to about 0.3 metres per year (Rentsch and Mes, 1988). Unfortunately, the combined record from satellite and sub-sea pressure measurements does not exist from the onset of subsidence, and as the subsidence rate is highly variable, these techniques cannot give an absolute magnitude for the displace

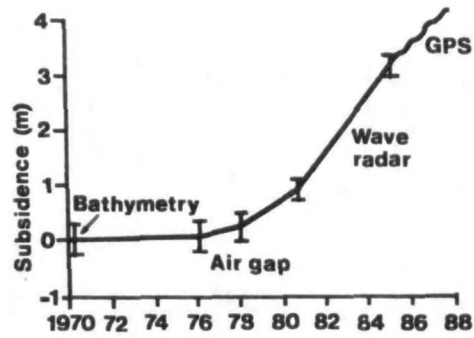


Figure. 7.2 Ekofisk subsidence history.

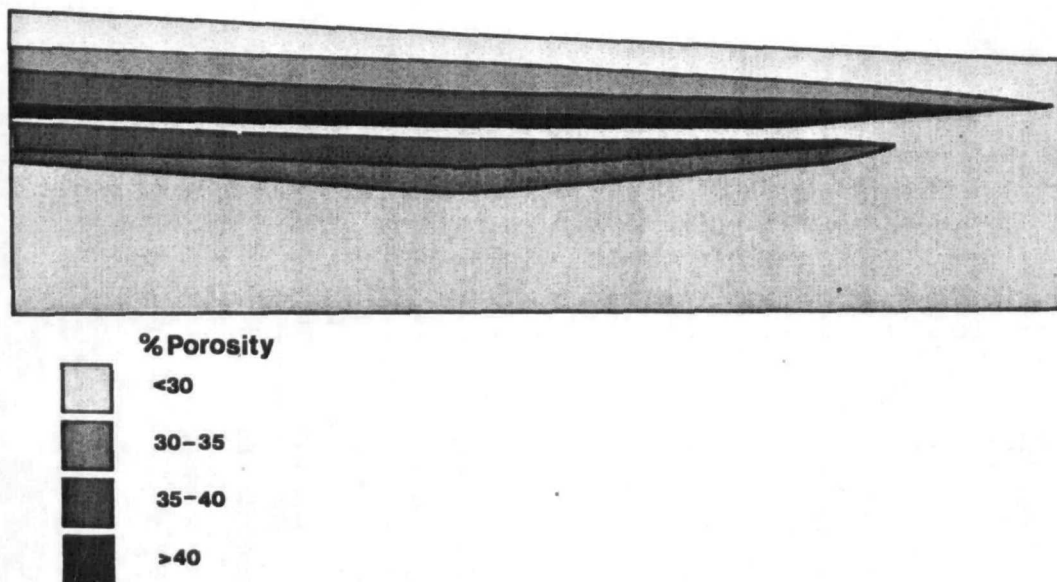


Figure. 7.3. The Ekofisk reservoir model showing the layered porosity structure that was determined from the well-logs.

ment, without including the less precise bathymetric and air gap data (Rentsch and Mes, 1988; Jewhurst and Wiborg, 1988).

7.232.2. Subsidence history at West Ekofisk.

Subsidence over the West Ekofisk reservoirs was first noticed in 1986. Satellite measurements indicated a slow rate of settlement was occurring and bathymetric measurements confirmed that the subsidence bowl was very small (Rentsch and Mes, 1988; Jewhurst and Wiborg, 1988). This subsidence and subsidence rate is not expected to cause problems with the platform on West Ekofisk, because, with the advanced state of the pressure depletion in this reservoir, it is anticipated that the subsidence rate will become negligible in the near future.

7.3.2.3. Subsidence history at Valhall.

In mid-1986, Amoco (Norway) reported that satellite survey measurements for Valhall revealed subsidence. Early measurements were uncertain, but it soon became apparent that the subsidence rate, although greater than West Ekofisk, was less than that which would necessitate modifications to the platforms during production of the field. This subsidence (Ruddy et al., 1988) is currently proceeding at a rate of about 0.25 metres per year, but is expected to decrease, giving a maximum settlement at the end of production of the order of 1.75 metres. The recorded subsidence history for the Valhall platforms started after monitoring was initiated and is therefore not subject to the same baseline uncertainty as Ekofisk and West Ekofisk.

7.3.2.4. Causes of the sea-floor subsidence.

Subsidence of the sea-floor over the Greater Ekofisk Area oil fields occurs because the reservoirs themselves undergo a reduction in volume. This volume reduction is a consequence of a reduction in the pore fluid pressure due to hydrocarbon extraction which leads to an increase in the vertical and horizontal effective stresses acting on the reservoir. As the reservoirs are laterally extensive, and confined by rocks of equivalent, or greater stiffness, deformations in response to effective stress changes are dominantly expressed as a reduction in the vertical dimension of the reservoirs. Pore fluid pressure

change will therefore lead to a downward displacement of the roof of a reservoir. Depending on such factors as geometry of the reservoir, its surface area, depth and the material properties of the overburden, a proportion of this displacement may be transmitted to the sea floor. See Jones et al. (1987) for an extensive discussion of subsidence.

The magnitude of the displacement of the base of the overburden will itself depend largely on the effective stress change in the reservoir and the reservoir rock compressibility. The effective stress change is dependent upon the change in pore pressure, and changes in total stress acting on the reservoir due to the previous displacements (often termed the stress arch). The magnitude of this arch is dependent on the overburden strength and the surface area and geometry of the reservoir.

The Greater Ekofisk Area chalk reservoirs exhibit variable mechanical properties, and, in many cases, they will become highly compressible after modest changes in the reservoir fluid pressure. Compaction should therefore be present in many of these reservoirs. The variable size of the reservoirs, and to a lesser degree their variable shape are seen to have a profound influence of the magnitude of any subsidence at the sea floor.

Compactional volume change will only occur where removal of fluids from the reservoir leads to changes in pore pressure. Reservoirs which do not experience pressure support from adjacent aquifers will be particularly prone to compaction if pressure is not maintained through fluid injection. The Greater Ekofisk Area chalk reservoirs are all effectively sealed, and, because of their very high initial fluid pressures (Potts et al., 1988; Ruddy et al., 1988; Sorensen et al., 1986), all have been produced (prior to 1986) by pressure depletion (with some reinjection of natural gas during periods of low demand). Any of these reservoirs could therefore have been a candidate for major volume changes and consequent subsidence.

7.3.3. ANALYSIS AND PREDICTION OF SUBSIDENCE.

Analyses of the deformations occurring in the Chalk reservoirs, and the transfer of the resulting displacements to the sea-floor, were undertaken using the finite element method. This was necessary because the reservoirs contain a complicated distribution of chalks with different material properties, and because the change in pore pressure through time varies with spatial position (Potts et al., 1988).

7.3.3.1. The Finite Element Models.

Use of the finite element method required that a number of different datasets be obtained for each field to be analysed. These datasets are: 1, the geometry and distribution of the different material types in the reservoir and adjacent formations; 2, the material behaviour of the various chalks; 3, the material properties of the rocks lying between the reservoir and the sea floor (the overburden); 4, observed and predicted reservoir fluid pressures.

In the case of Ekofisk, the analyses reported below were undertaken with the express intent of identifying the maximum subsidence that would occur as a result of depletion of the pore pressures in one or both reservoirs, and of the possible mitigating influence of maintaining pore pressure through the injection of sea water and the reinjection of natural gas.

7.3.3.1.1. The Geology and Model Geometries.

The hydrocarbon reservoirs examined have a number of features in common. Firstly, they exist entirely in chalks of Cretaceous or Palaeocene age which are effectively sealed from other formations by a shale/low porosity chalk cap rock and by flanking and underlying low porosity chalks. Secondly, they contain a complex distribution of chalks with different porosities, although generally, the highest porosities are preserved over the crest of each structure (D'Heur, 1984). Thirdly, each reservoir is developed in a structure that is either a dome, or an elongated dome. Finally, each oil field consists of two or more reservoir horizons (developed in chalks of higher porosities) separated by low porosity/low permeability chalks. Fluid pressure communication between the in-

dividual reservoirs is generally restricted by these low permeability chalks (D'Heur, 1984).

The finite element models created for the oil fields investigated were all based on pseudo-geological cross-sections constructed in a manner that preserved the correct structural shape of a particular part of the field, but with the complex distribution of porosities simplified into a series of porosity bands in each reservoir. Depending upon the shape of the field, the analyses were conducted axi-symmetrically, or in plane strain, and this influenced the choice of the cross-section. In West Ekofisk, which closely approximates a dome, a single section was taken from the crest to the flanks of the structure and the analysis was then conducted in an axi-symmetric manner. For Ekofisk, which is elongated, models were constructed based on the short axis, for plane strain analysis, and the long axis for axi-symmetric analysis (figure 7.3). For Eldfisk and Valhall, only short axis sections for plane strain analysis were constructed.

For Ekofisk, the chalk forming each reservoir was divided into four porosity bands in which spatial variations were based on available well-log information. The finite element mesh used to represent this geological model (figure 7.4) consisted of 400 eight noded isoparametric elements. Each element was assigned the material properties appropriate to the strata it represented. Displacement restraints, as indicated in figure 7.4 were applied to the base and sides of the mesh. Pore pressure drawdown, as a result of hydrocarbon production, was simulated by specifying changes in pore pressure to the elements representing reservoir materials, and the first 200m of overlying shales.

7.3.3.1.2. Mechanical Behaviour of the Reservoir Rock.

The hydrocarbon reservoirs under investigation are variously formed in chalks from the Ekofisk, Tor and Hod Formations. The chalks in each of the reservoirs exhibit porosities ranging from less than 25% to greater than 40%. Their behaviour was characterised in the experimental programme described above.

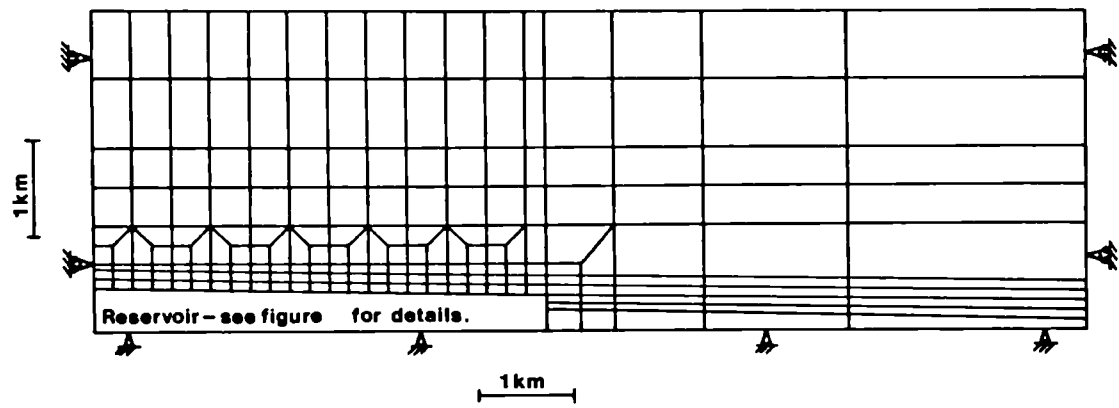
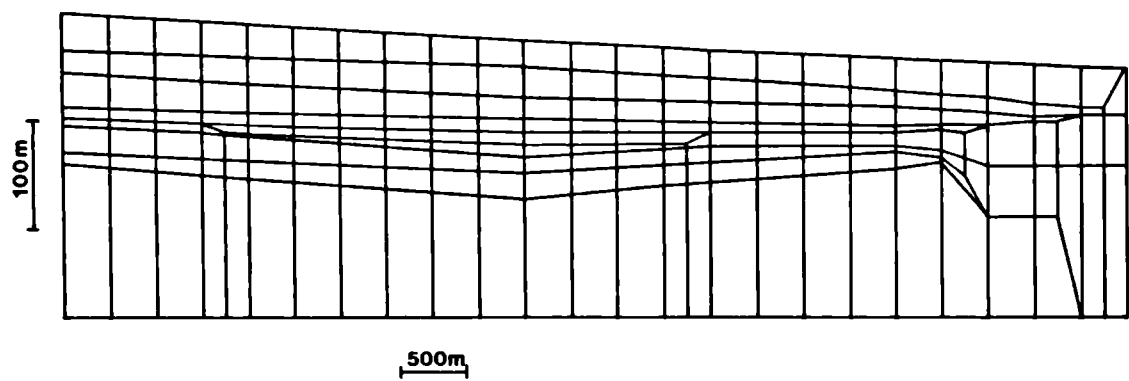


Figure. 7.4. The Ekofisk finite element mesh, with an expanded scale diagram for the reservoir section.



A number of assumptions were made concerning the nature of the deformation in the reservoirs. 1), that the lateral dimensions of the reservoir, or of any of its component parts will remain unchanged during the deformation. 2), that normal effective stresses would be mobilised in the horizontal direction to maintain this no lateral deformation condition. 3), that the fracture system in the chalk played a passive role in the deformation (Potts et al., 1988). With this rather simple picture of the deformation as a one-dimensional consolidation of the reservoir rock, and as, the reservoir is fairly permeable, a majority of the experiments on the chalk were one dimensional compression tests (see chapters 4 and 5 above). The results of the experiments were used to provide a constitutive model for the chalk, by simply normalising curves representative of chalks of different porosities to zero strain at initial reservoir pressure. Typical experimental results have been reported above and the family of standard curves is shown in figure 4.76. The results confirm that the strength of the chalk is inversely dependent on its porosity and, that its behaviour is markedly non-linear over the stress range of interest.

7.3.3.1.3. Mechanical Behaviour of the Overburden Rocks.

The thick sequence of shales and mudrocks that overlie each of the chalk reservoirs (D,Heur, 1986) are overpressured for a considerable distance above the top of the chalk (figure 7.5). The detailed stratigraphy of these overburden materials is not well known neither is their structure. Description of the overburden therefore posed a number of problems. 1), what materials are present, and what are their thicknesses? 2), what are the material properties of these different rock units? 3), as the pressure profile from the overburden into the reservoir becomes modified (figure 7.5), is it possible that the overburden could compact due to under drainage into the reservoir? These problems were largely insurmountable, so the overburden was treated as an elastic sheet with stratified material properties and limited under-drainage (Potts et al., 1988).

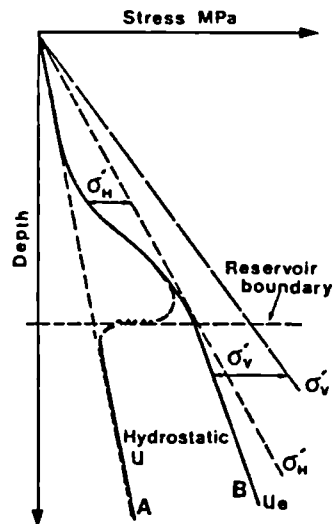


Figure. 7.5. Schematic representation of the variation of pore fluid pressure with depth over the Ekofisk Area chalk reservoirs, before (curve B), and after (curve A) a period of production. The geometry of the dotted part of the profile is unknown, but is widely held to be confined to narrow depth interval.

7.3.3.1.4. Pore Fluid Pressures.

The finite element analyses were conducted by reducing the pore fluid pressure in each element of the reservoir rock. To achieve this, it was necessary to obtain historical records of the fluid pressures measured in production wells along the line of the cross-section chosen for the model. For subsidence predictions, fluid pressures predicted by reservoir simulation were used. By controlling the analyses in this manner, it was simple to check the influence of a revised production scenario (water or gas injection for example) on the subsidence (Potts et al., 1988).

7.3.3.2. Running the Analysis.

In Ekofisk, axi-symmetric analyses were conducted using two sets of pore pressure data, corresponding to two different production scenarios. In the first (Analysis A), no injection of sea water or gas was assumed for the Ekofisk Formation reservoir. In the second (Analysis B), the pore pressure data accounted for the injection of a considerable volume of gas into the Ekofisk Formation reservoir from 1986 onwards. In both cases water injection into the Tor Formation reservoir was started in 1986, and pressure communication between the Ekofisk and Tor reservoirs was taken to be very restricted (Potts et al., 1988).

In each analysis, the pore pressure history from the beginning of production until the year 2010 was simulated incrementally. Each increment refers to a specific date and the results therefore predict the changes in stresses and associated displacements as the hydrocarbon reserves are depleted.

7.3.4. RESULTS.

Subsidence analyses have been conducted for the Ekofisk, West Ekofisk, Eldfisk and Valhall Oil Fields. In the case of Ekofisk, three results are considered. These represent a long axis axi-symmetric analysis comparing two different pore pressure reduction scenarios, and a short axis plane strain analysis. For West Ekofisk, Eldfisk and Valhall only one analysis was conducted for each field. These analyses were designed

to investigate 'worst possible cases' and indicated that subsidence would not constitute a significant risk.

7.3.4.1. Ekofisk Subsidence.

For the two axi-symmetric analyses, vertical movements at a depth of 2700m below sea level (just above the reservoir) and sea bed subsidence troughs are illustrated in figures 7.6 and 7.7 respectively. Results are given at various stages during the period of hydrocarbon production. Comparison of the surface settlements with those occurring immediately above the reservoir indicate that the former were significantly smaller. This reduction in magnitude of vertical movements with height above the reservoir is accompanied by an increase in the width of the subsidence trough (figure 7.8). Such behaviour is a result of a stress distribution (arching) over the reservoir and would not have been predicted from an analysis assuming a one-dimensional situation. The pattern of changes in the vertical total stress acting over the reservoir is illustrated in figure 7.9. Comparison of the results from analyses A and B indicate the influence that gas injection has in reducing vertical settlement. From figure 7.7 it can be seen that injection of gas reduces the sea floor settlement from 6.4m to 4.8m.

Figure 7.10 illustrates the predicted compaction and subsidence profiles for a short axis model of the Ekofisk Field, analysed using plane strain. It is seen that the compaction and subsidence are broadly comparable with the no-injection axi-symmetric long axis case. This result is important because it indicates that an axi-symmetric long axis model is a valid model for Ekofisk. This is because in the real system, the arching stress contribution from the short axis will only be in the plane of that axis, i.e. the natural system approximates to a short axis plane strain case, with a component of stiffening due to the finite length of the long axis.

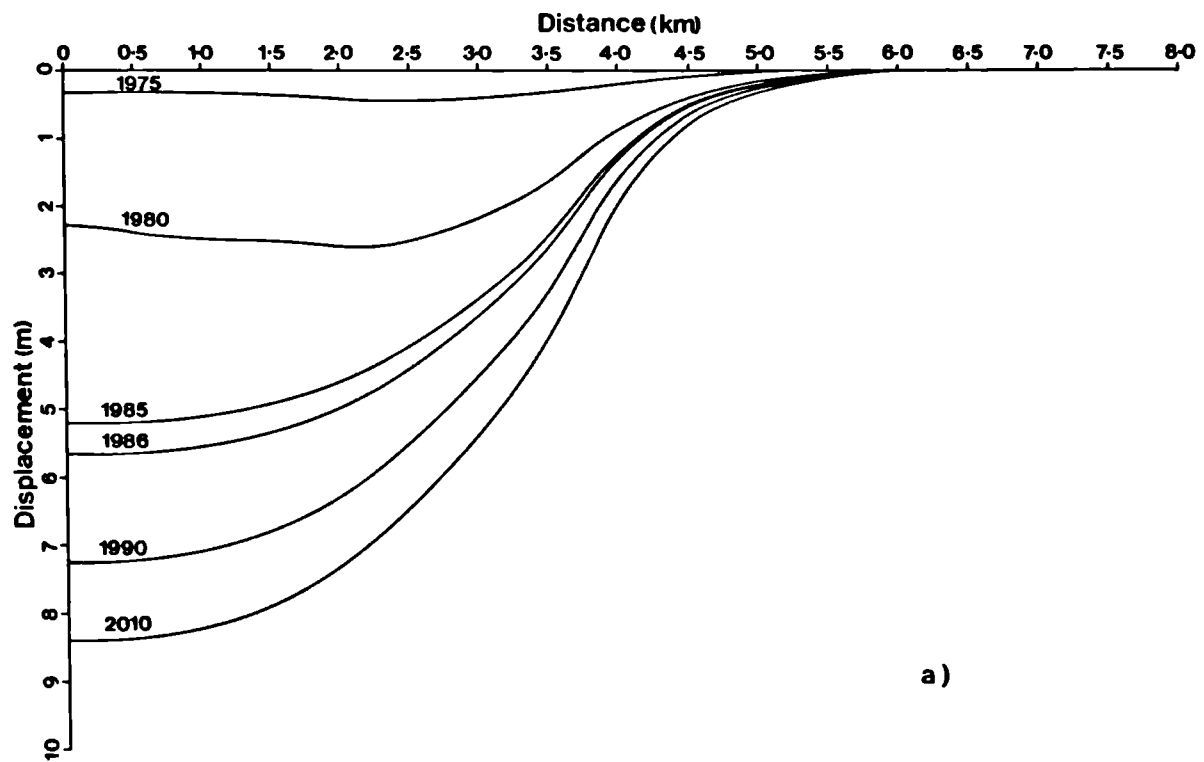
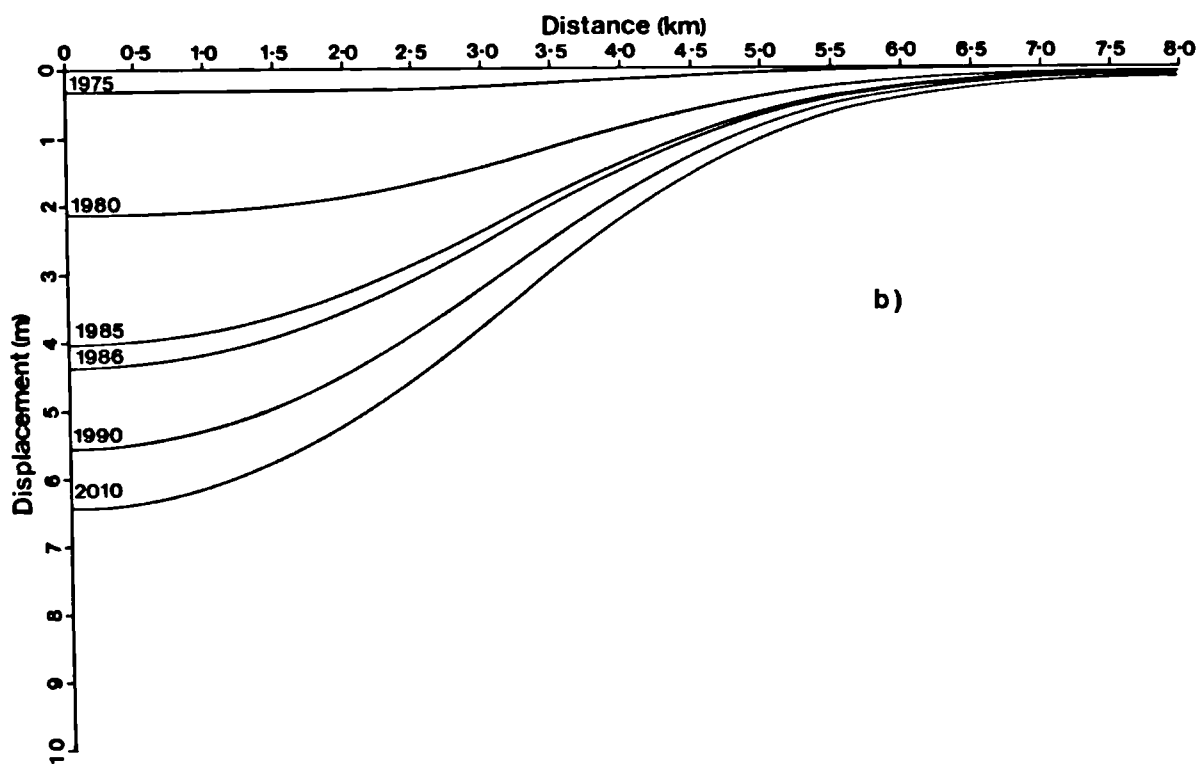


Figure. 7.6. Predicted reservoir compaction for the no gas injection (a) and gas injection (b) analyses for Ekofisk.



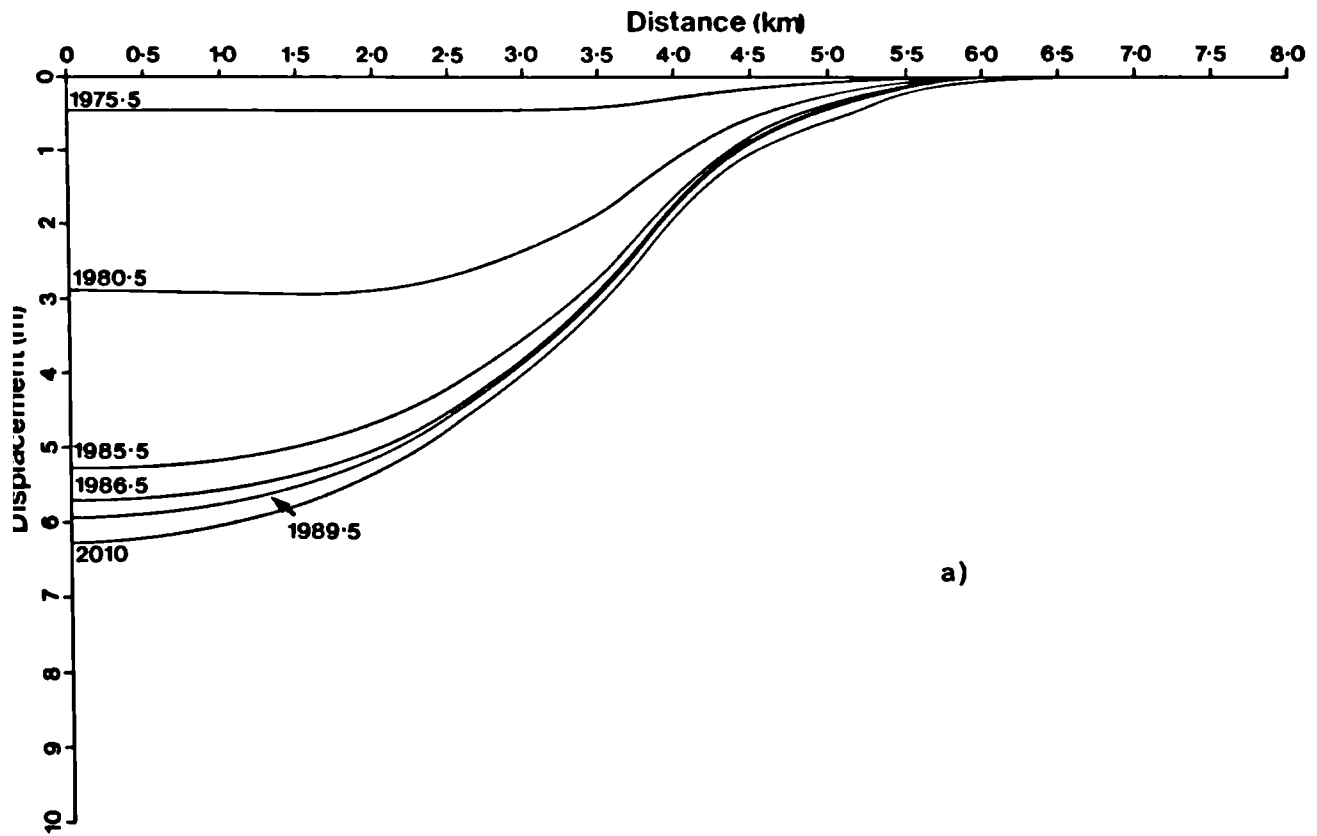
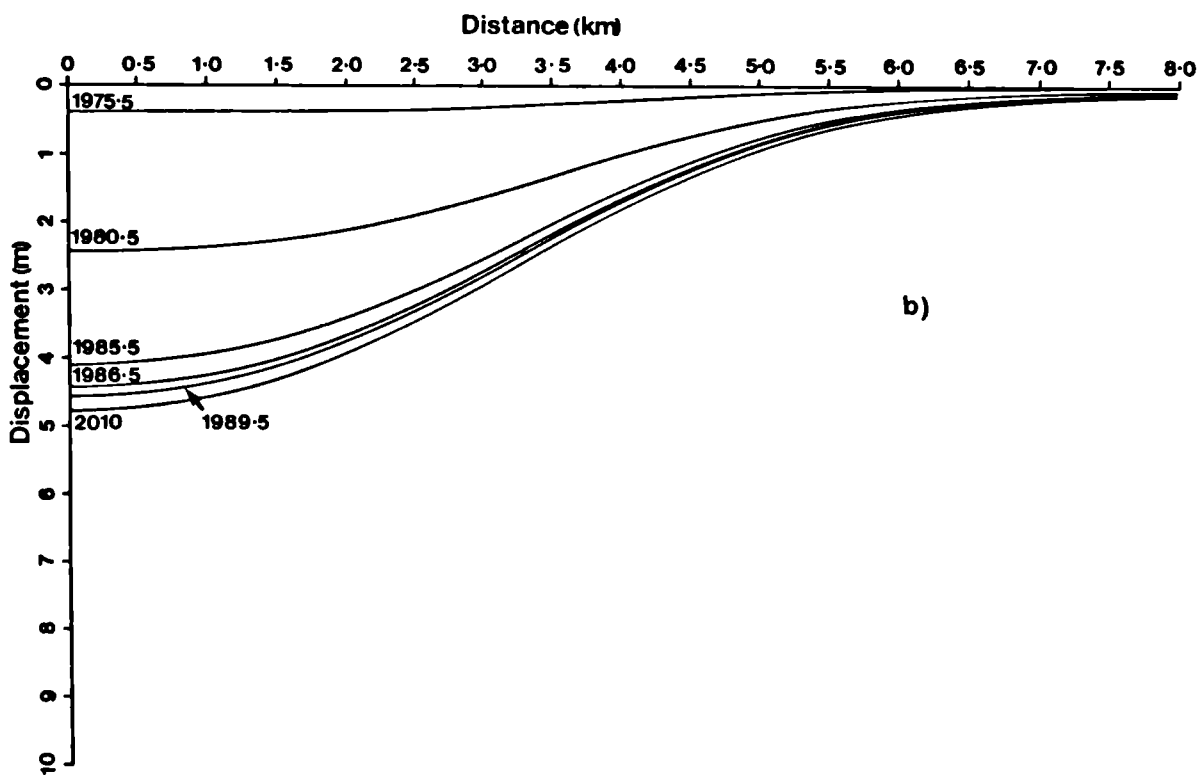


Figure. 7.7. Predicted sea floor subsidence for the no gas injection (a) and gas injection (b) cases for Ekofisk.



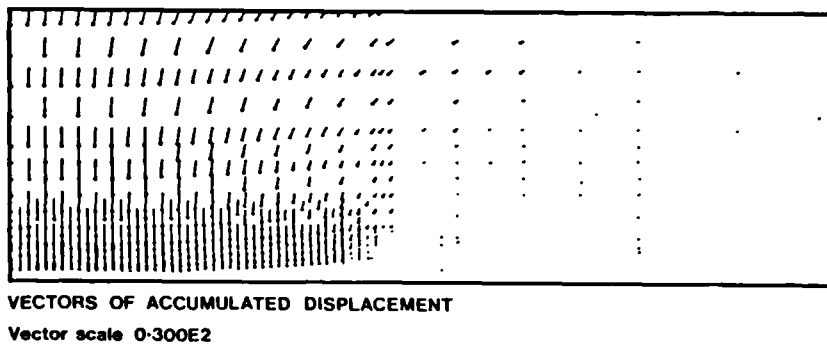


Figure. 7.8. Pattern of displacements that develops over the Ekofisk Oil field as a result of reservoir compaction.

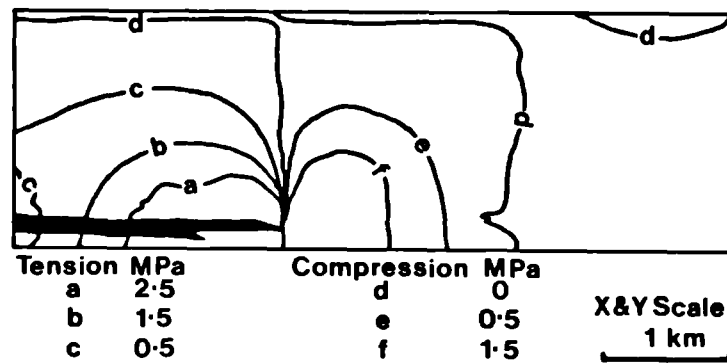


Figure. 7.9. The changes in total vertical stress that occurs over the Ekofisk Oil Field as a consequence of reservoir compaction.

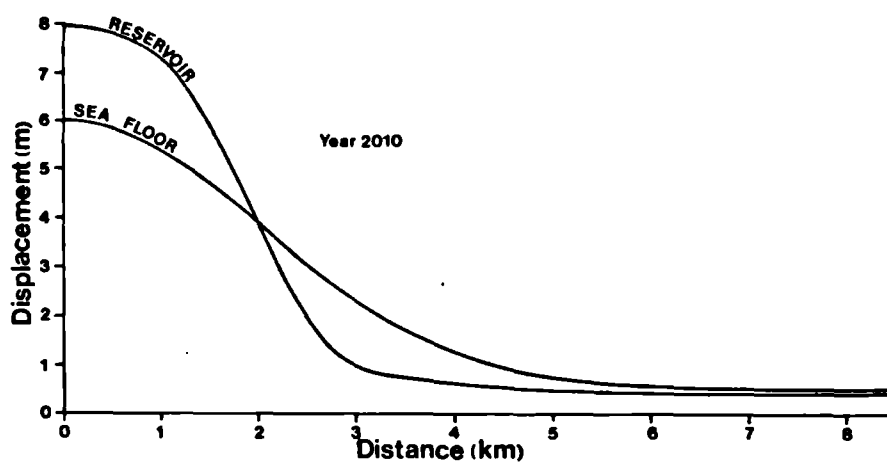


Figure. 7.10. Reservoir compaction and sea-floor subsidence predicted by a plane strain analysis of a short axis cross-section of the Ekofisk Oil Field.

7.3.4.2. *West Ekofisk Subsidence.*

Unlike Ekofisk, West Ekofisk offers a close approximation to an axi-symmetric system. The field is of smaller surface area but is at a comparable depth with comparable porosities, pore pressures and pore pressure changes, although exact equivalence between these parameters for the two fields does not occur. It follows, that because the West Ekofisk Reservoir is of smaller volume than Ekofisk, pore pressure reduction will occur more rapidly as the reservoir fluid is produced. Thus, although the onset of production of West Ekofisk post-dates Ekofisk, fluid pressure change in West Ekofisk has overtaken Ekofisk and pressures are now close to those predicted for the end of production.

Only one analysis of the West Ekofisk subsidence was undertaken which predicted that surface displacements would be small. The pattern of displacements (figure 7.11) show that the small surface settlements are due to a smaller transfer through the over burden. The determined subsidence/compaction ratio for West Ekofisk is 0.31 whilst at Ekofisk it is predicted to be 0.77. This is a consequence of the greater arching stress generated over the West Ekofisk reservoir, a product of its smaller surface area, and marginally steeper limb dips (figure 7.12).

7.3.4.3. *Eldfisk Subsidence.*

The Eldfisk Reservoir is an elongated structure, divided into two by an east/west trending structural feature. Because this reservoir is of unsuitable geometry for an axially symmetric analysis, a single plane strain analysis was conducted. This employed a cross-section, normal to the axis of the northern part of the field. An overestimation of the subsidence is therefore anticipated, but the alternative, a 3-D analysis, was not possible within the constraints of this study. The results of the plane strain analysis did not indicate that a serious subsidence problem would result from pressure decline in this reservoir.

The pattern of displacements that develop above the Eldfisk Reservoir, are illustrated in Figure 7.13. These show an asymmetry, which reflects an asymmetry in the porosity

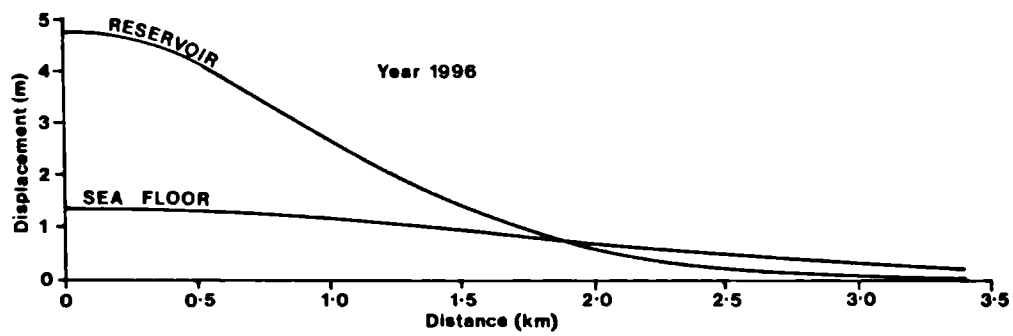


Figure. 7.11. Displacements that develop over the West Ekofisk Oil Field as a consequence of reservoir compaction.

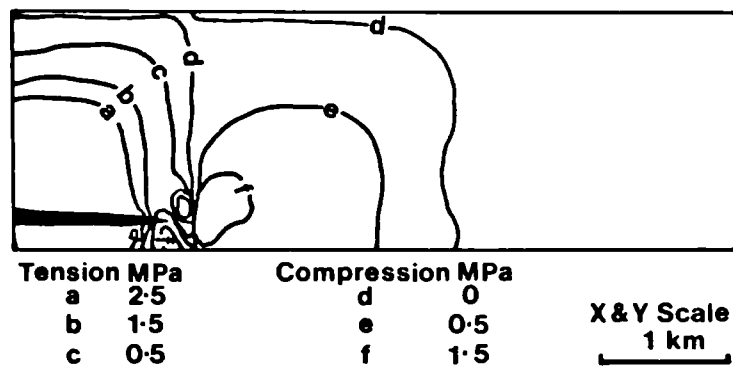


Figure. 7.12. Pattern of changes in total vertical stress that occur over the smaller West Ekofisk Oil Field as a consequence of reservoir compaction.

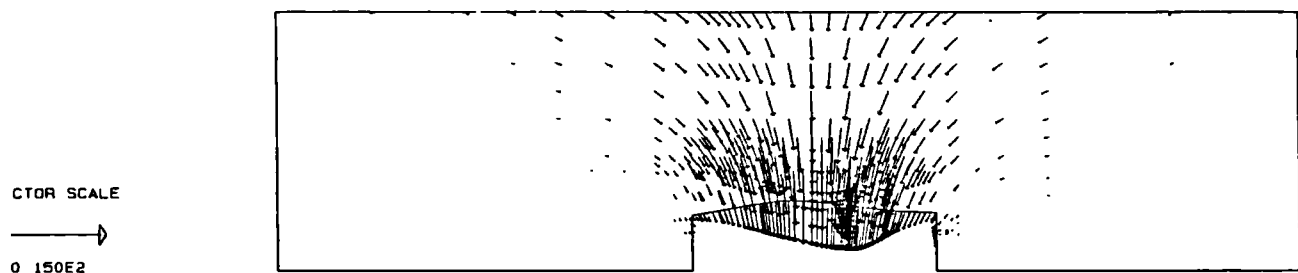


Figure. 7.13. The pattern of displacements that were modelled to develop over the Eldfisk Oil Field as a consequence of reservoir compaction.

distribution in the cross-section, and in the resulting compaction developed in the reservoir. The analysis gives a subsidence/compaction ratio of 0.4 which can be compared with the plane strain analysis of the East/West cross-section of Ekofisk where this ratio is 0.77. As with West Ekofisk, the small subsidence transfer ratio for Eldfisk is a consequence of the development of a larger stress arch over the shorter Eldfisk cross-section (figure 7.14), compared with the larger Ekofisk cross-section.

7.3.4.4. Valhall Subsidence.

The Valhall structure is also elongated in the North/South direction, but is internally more complex than Eldfisk. A single plane strain analysis was conducted for this field which indicated that subsidence did not constitute a risk to the surface installations.

The model used to investigate this field consisted of a half cross-section (chosen to reduce the number of elements in the model from over 2000 in the full cross-section to 850 in the half section). This model (figure 7.15) is interesting because it contains an abrupt increase in limb dip, which is associated with a decrease in the thickness of high porosity chalk. This geometry produces a stress arch which only develops over the crest of the structure. This is very intense (figure 7.15). The flanks of the reservoir are subject to increased loading from the arch. This is not necessarily happening at Valhall, as the geological model on which the analysis is based is specific to a single cross-section and not generalised. It cannot therefore be applied to other cross-sections. However, this is the only case studied, where the stress arch is seen to develop over only part of the reservoir, and demonstrates how sensitive the analysis is to the correct description of field geometry.

7.3.3 DISCUSSION OF CHALK OILFIELD COMPACTION AND SUBSIDENCE.

The major conclusion of this part of the study is that whilst compaction will occur in all high porosity chalk reservoirs produced through pressure depletion, only when necessary geometrical requirements are satisfied, will these displacements be transferred to the sea floor to produce a settlement of serious magnitude. Thus, reservoirs of large surface area, that are not excessively elongate, with a broad distribution of high porosity

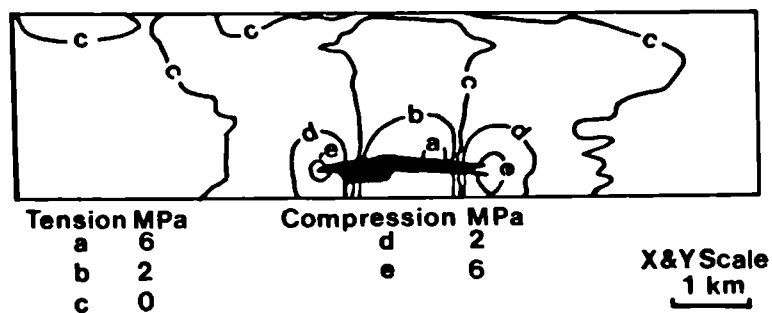


Figure. 7.14. The pattern of changes in the total vertical stress that were predicted to occur over the Eldfisk Field as a consequence of compaction.

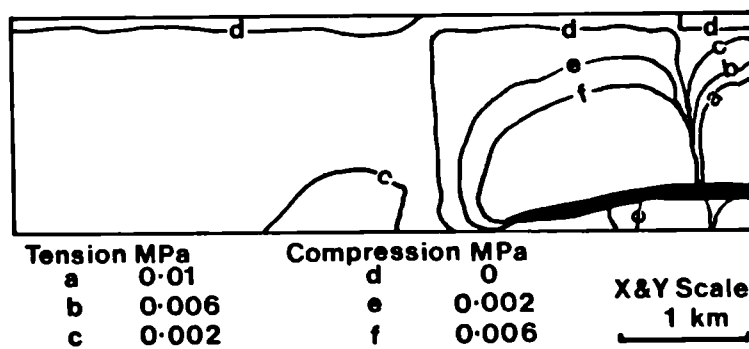


Figure. 7.15. The stress arch that develops due to compaction of the reservoir units in the Valhall model.

chalks (such as Ekofisk) will be prone to serious subsidence problems. Smaller reservoirs (such as West Ekofisk), and structures of more elongate geometry (Eldfisk and Valhall) will be protected from subsidence by the large arching stresses, generated as they compact. No other chalk hydrocarbon reservoirs of Ekofisk proportions have been discovered in the Norwegian sector of the North Sea. New subsidence problems in the Norwegian chalk fields are therefore unlikely.

The analyses reported for the Ekofisk subsidence are well constrained in terms of mechanical and geological variables. These analyses indicated a sea floor settlement of 4.4 metres for the end of 1986, although actual bathymetric measurements and satellite elevation data show that this was actually 3.8 metres at this time. However, the finite element analyses do not allow for any time dependence in the generation and transfer of the displacements. It has been observed that the subsidence process at Ekofisk is time dependent but the magnitude of this effect is uncertain.

The results of the analyses presented for the Ekofisk Field indicate that providing the analytical model is realistic, and the mechanical variables are well constrained, the finite element method can be used to assess the effect of different production strategies on the magnitudes of reservoir compaction and surface subsidence. In the above examples, sea floor subsidence over the Ekofisk Oil Field is significantly reduced if the pore pressure is maintained through the injection of considerable volumes of natural gas into the reservoir. However, this study does not address the economics of the situation. Since completion of this work for the Norwegian Petroleum Directorate, Phillips Petroleum Co. Norway have addressed the problem of surface subsidence directly by elevating the platforms of the Ekofisk Complex by 6 metres. Clearly, solutions to the subsidence problem that involve reinjection of valuable reservoir fluids, or major modifications to production complexes are expensive. It is therefore essential that the analytical models used to assess the need for, and applicability of, these solutions are well conceived and properly constrained.

7.4. FLOW OF CHALK IN THE NEAR WELLBORE REGION.

The experimental results presented in chapter six indicate that the response of the chalk to undrained shear is dependent on initial porosity and the state of compaction to which the chalk has been subject prior to shear. If undrained shear is initiated when the chalk is still essentially an elastic material it will sustain increases in shear stress up to its yield stress before collapsing by brittle failure. If the chalk has been compacted under a stress beyond yield, small changes in shear stress will result in collapse and flow. If, however, the chalk has been subject to large effective stresses and has started to strain harden, the onset of undrained shear will have little effect. It is apparent therefore, that reservoir chalks that are close to, or just beyond their yield stress, are particularly vulnerable to collapse and flow if subject to undrained shear.

It has been observed Ruddy (pers. comm., 1989) that under specific circumstances the chalk reservoir rock may become mobilised and flow through perforations, partially filling the production tubing in the well. This observations of low strength ductile behaviour in high porosity chalks, led to the experimental investigation, reported in chapter 6 where it was established that "flow" is a normal characteristic of chalk behaviour.

The invasion of producing oil wells by reservoir chalks occurs under specific conditions, nearly always occurring after a well has been shut-in for a period. During shut-in, fluid pressures in the well increase until the drawdown gradient between the well and the reservoir is equalised. When production is restarted, the fluid pressure in the well is rapidly reduced so that the draw-down gradient must then re-establish itself. This re-establishment will not be instantaneous in low permeability reservoir rocks such as the chalk (see chapter 5). When a shut-in well is brought back on-stream, a steep pressure gradient is created between the well and the adjacent formation. Large shear stresses are induced in the formation chalks (containing high pore fluid pressures) adjacent to the perforations (figure 6.2), due to the removal of pressure support from the well. Well

invasion there fore involves rapid, and effectively undrained, loading with development of large shear stresses that promote unrestrained flow.

The experimental investigation reported in chapter 6 has shown that under specific conditions of mean effective stress and shear stress, the chalk will become weak and will deform in a manner equivalent to a soil at the critical state condition. If the chalk has only experience of small consolidation pressures, it will strain soften and exhibit very weak behaviour, if on the other hand it has been subject to large consolidation stresses it will strain harden. At low consolidation pressures, elasticity permits the chalk to attain stress state beyond the critical state, but on yield, it returns to the critical state condition. The chalk exhibits a pronounced pore pressure response under undrained loading. This is most severe at low consolidation stresses where substantial increases in compressibility at the elastic limit lead to the transfer of stress from the mineral skeleton of the sediment to pore fluid, as cement bonds between grains are severed.

It is therefore the case, that if the chalk is stressed to a condition where intergranular cement bonds can break, destroying its elasticity, it will become a particulate material and exhibit critical state behaviour. Well invasion is an expression of chalk flow at the critical state. The chalk should not be subject to large shear stresses during hydrocarbon production if large strain deformations of the type reported above and in chapter 6 are to be avoided.

BIBLIOGRAPHY

- Aam, K., 1988, *Ekofisk subsidence: The problem, the solution and the future*, Proceedings of the International Conference on Behaviour of Offshore Structures, Trondheim, Volume 2, pp19-40.
- Addis, M. A., 1987, *Mechanisms of sediment compaction responsible for oil field subsidence*, PhD Thesis, University of London, Unpublished, p561.
- Addis, M. A., 1989, *The behaviour and modelling of weak rocks*, Rock at Great Depth Symposium, (eds. Maury, V. and Fourmaintraux, D.), Pau, France, Volume 2, A. A. Balkema, Rotterdam, pp899-905.
- Addis, M. A. and Jones, M. E., 1989, *Mechanical behaviour and strain rate dependence of high porosity chalk*, Proceedings of the International Chalk Symposium, Brighton, 4-7th September, 1989, pp111-116.
- Archer, J. S. and Wall, C. G., 1986, *Petroleum Engineering Principles and Practice*, Graham & Trotman, London, p362.
- Atkinson, J. H. and Bransby, P. L., 1978, *The Mechanics of Soils An Introduction to Critical State Soil Mechanics*, McGraw-Hill Book Company (UK) Limited, England, p175.
- Bakker, R. T., 1975, *Dinosaur renaissance*, In: The fossil record and Evolution, (ed. Laporte, L. F.), Scientific America, W. H. Freeman and Company, San Fransico, pp117-133.
- Barendes, F. B. J. and Spierenburg, S. E. J., 1989, *Peculiar aspects in man-induced land subsidence*, Proceedings of the 12th International Conference on Soil Mechanics and Foundation Engineering, Rio de Janerio, 14-17 August, 1989, Volume 3, A. A. Balkema, Rotterdam, pp1785-1790.
- Barr, F. T., 1962, *Upper Cretaceous planktonic foraminifera from the Isle of Wight, England*, Palaeontology, Volume 4, pp55-580.
- Barton, N., 1985, *An investigation of the Ekofisk subsidence using continuum and discontinuum computer modelling*, Confidential report to the Norwegian Petroleum Directorate.
- Barton, N., 1986, *An investigation of the Ekofisk subsidence using continuum and discontinuum computer modelling*, Confidential report to the Norwegian Petroleum Directorate.
- Belfiore, F., Colombo, P. F., Pezzetti, G. and Villani, B., 1989, *A contribution to the study of the subsidence of Bologna*, Proceedings of the 12th International Conference on Soil Mechanics and Foundation Engineering, Rio de Janerio, 14-17 August, 1989, Volume 3, A. A. Balkema, Rotterdam, pp1791-1795.
- Berget, O. P. and Tonstad, K., 1986, *Management of reservoirs under compaction*, presented at the Enhanced Oil and Gas Recovery Conference, London, March 1986.
- Berget, O. P., Dretvik, O., Tonstad, K. and Mathiesen, E., 1989, *Production of oil and gas from chalk reservoirs in the Norwegian part of the North Sea*, Proceedings of the International Chalk Symposium, Brighton, 4-7th September, 1989, pp315-320.
- Boade, R. R. and Chin, L. Y., 1986, *The Dynaflow procedure for simulating Ekofisk subsidence with results from two spring 1986 reservoir management scenarios*. Phillips Petroleum Co., Research and Development report 2975, (confidential).
- Boade, R. R., Chin, L. Y. and Seimers, W. T., 1988, *Forecasting of Ekofisk reservoir compaction and subsidence by numerical simulation*, Offshore Technology Conference, OTC 5622, pp51-62.
- Botter, B. J., 1985, *Pore collapse measurements on chalk cores*, Chalk Research Group Symposium, Stavanger, May 1986, Volume 2.
- Brewster, J. and Dangerfield, J., 1984, *Chalk Fields along the Lindesness Ridge*, Marine and Petroleum Geology, Volume 1, pp239- 278.

Brewster, J., Dangerfield, J. and Farrell, H., 1986, *The geology and geophysics of the Ekofisk Field waterflood*, Marine and Petroleum Geology, Volume 3, pp139-169.

Brighenti, G., 1967, *Influence of pore pressure decline on the behaviour of petroleum reservoir rocks*, Proceedings of the 7th World Petroleum Congress, Mexico City, Volume 2, pp97-105.

Brotzen, F., 1945, *De geologiska resultaten fran bormingarna vid Hollviken*, Sver. geol. UnderAfh., Series C, 456, pp1-64.

Brunsden, D., 1979, *Mass movements*, In: Process in geomorphology (eds. Embleton, C. and Thornes, J.), Edward Arnold (Publishers) Ltd, London. p436.

Brunsden, D. and Prior, D. B., 1984, *Slope instability*, John Wiley & Sons, Chichester, p620.

Buskinsky, G. I., 1954, *Litologija melovykh otlozhenij Dnieprovski-Donetskoj vpadiny*, Trudy GIN AN SSSR, p156, M.

Buxton, T. M. and Silbey, D. F., 1981, *Pressure solution features in a shallow buried limestone*, Journal of Sedimentary Petrology, Volume 51, pp19-26.

Carpenter, G. W. and Stephenson, R. W., 1986, *Permeability Testing in a Triaxial Cell*, Geotechnical Testing Journal, Volume 1., Number 1, March 1986, pp3-9.

Calder, N., 1974, *The weather machine*, BBC publication, Jolly and Barber Ltd, Rugby, p143.

Carter, J. P., Johnson, I. W., Chapman, G. A., Novello, E. A. and Kaggwa, W. S., 1988, *Triaxial testing of North Rankin calcarenite*, In: Engineering for calcareous sediments (eds. Jewell, R. J. and Andrews, D. C.), Proceedings of the International Conference on Calcareous Sediments, 15-18 March, Perth, A. A. Balkema, Rotterdam, Volume 2, pre-print 1/17-16/17.

Carter, P. G. and Mallard, D. J., 1974, *A study of the strength, compressibility, and density trends within the chalk of South East England*, Quarterly Journal of Engineering Geology, Volume 7, pp43-55.

Clayton, C. R. I., 1978, *Chalk as fill*, PhD thesis, University of Surrey. (Unpublished).

Clayton, C. R. I., 1989, *The mechanical properties of the chalk*, Keynote paper, Proceedings of the International Chalk Symposium, Brighton, 4-7th September, 1989, pre-print.

Colbert, E. H., 1965, *The age of Reptiles*, Weidenfeld and Nicolson, London, p227.

Crawford, C. B., 1963, *Cohesion in an undisturbed sensitive clay*, Geotechnique, Volume 13, Number 2, pp132-146.

Culec, L. E., 1975, *Restoration of the natural state of core samples*, Journal of the Society of Petroleum Engineers, SPE5634.

Deegan, C. E. and Scull, B. J., 1977, *A standard lithostratigraphic nomenclature for the central and northern North Sea*, Report for the Institute of Geological Sciences U.K., No.77/25, p33

De Loos, J. M., 1973, *In situ compaction measurements in Groningen observation wells*, Verhandelingen van het Koninklijk Nederlands Geologisch Mijnbouwkundig Genootschap, Volume 28, pp79-104.

D'Heur, M., 1984, *Porosity and Hydrocarbon distribution in North Sea Chalk Reservoirs*, Marine and Petroleum Geology, Volume 1, pp211-238.

D'Heur, M., 1986, *Characterisation of the Ekofisk Field overburden*. Confidential Report, Petrofina.

D'Heur, M., 1989, *Chalk and petroleum in North West Europe*, Keynote paper, Proceedings of the International Chalk Symposium, Brighton, 4-7th September, 1989, pre-print.

Dorby, R., Ladd, R. S., Reese, L. C. and Ng, T., 1988, *Modelling of pore pressures and shear moduli in calcareous soils by strain-controlled cyclic triaxial testing*, In: Engineering for calcareous sediments (eds. Jewell, R. J. and Andrews, D. C.), Proceedings of the International Conference on Calcareous Sediments, 15-18 March, Perth, A. A. Balkema, Rotterdam, Volume 2, pre-print 1/18-9/18.

Dunbaven, M., 1988, *Proposed constitutive model of calcarenite*, In: Engineering for calcareous sediments (eds. Jewell, R. J. and Andrews, D. C.), Proceedings of the International Conference on Calcareous Sediments, 15-18 March, Perth, A. A. Balkema, Rotterdam, Volume 2, pre-print 1/32-7/32.

Dunnington, H. V., 1967, *Aspects of diagenesis and shape change in stylolitic limestone reservoirs*: Proceedings of the 7th World Petroleum Congress, Mexico City, Volume 2, Number 3, pp339-352.

Ekdale, A. A. and Bromley, R. G., 1984, *Sedimentology and Ichnology of the Cretaceous-Tertiary Boundary in Denmark: Implications for the causes of the Terminal Cretaceous extinction*, Journal of Sedimentary Petrology, Volume 54, Number 3, pp681-703.

Elliott, G. M. and Brown, E. T., 1985, *Yield of a soft, high porosity rock*, Geotechnique, Volume 35, Number 4, pp413-423.

Fahey, M., 1988, *Self-boring pressure meter testing in calcareous soils*, In: Engineering for calcareous sediments (eds. Jewell, R. J. and Andrews, D. C.), Proceedings of the International Conference on Calcareous Sediments, 15-18 March, Perth, A. A. Balkema, Rotterdam, Volume 1, pp65-172.

Fatt, I. and Davis, D. M., 1952, *Reduction in permeability with overburden pressure*, Journal of Petroleum Technology, March 1952, pp64-66.

Gobran, B. D., Brigham, W. E. and Ramey, H. J., 1981, *Absolute permeability as a function of confining pressure, pore pressure and temperature*, Society of Petroleum Engineers, SPE10156.

Goldsmith, A. S., 1989, *Permeability decline and compressibility in sandstone reservoir rocks*, Rock at Great Depth Symposium, (eds. Maury, V. and Fourmaintraux, D.), Pau, France, Volume 2, A. A. Balkema, Rotterdam, pp923-928.

Goldsmith, A. S., Berget, O. P., Leddra, M. J. and Jones, M. E., 1989, *Application of specialist database for evaluation of the compaction behaviour of North Sea Chalk*, Proceedings of the International Chalk Symposium, Brighton, 4-7 September, 1988, pp335-339.

Golightly, C. R. and Hyde, A. F. L., 1988, *Some fundamental properties of carbonate sands*, In: Engineering for calcareous sediments (eds. Jewell, R. J. and Andrews, D. C.), Proceedings of the International Conference on Calcareous Sediments, 15-18 March, Perth, A. A. Balkema, Rotterdam, Volume 1, pp69-78.

Guy, D. G., 1989, *Classification and assessment of chalk on the M25 around the Gade Valley, Kings Langley, Hertfordshire*, Proceedings of the International Chalk Symposium, Brighton, 4-7th September, 1989, pp197-204.

Hailey, H. B. and Schmoker, J. S., 1983, *High-porosity Cenozoic carbonate rocks of South Florida: Progressive loss of porosity with depth*, American Association of Petroleum Geologists Bulletin, Volume 67, Number 2, pp191-200.

Hancock, J. M., 1975, *The Petrology of the Chalk*, Proceedings of the Geological Association, Volume 86, Number 4, pp499-535.

Hancock, J. M., 1983, *The setting of the Chalk and its initial Accumulation*, Joint Association for Petroleum Exploration Courses (U.K.), course notes Number 20, A1-A42.

Hancock, J. M., 1985, *Oil in chalk*, Geology Today, September- October, 1985, pp146-150.

Hancock, J. M., 1987, *The setting of the Chalk, its initial accumulation and its diagenesis*, Joint Association for Petroleum Exploration Courses (U.K.), course notes Number 54, A1-A40.

- Hancock, J. M. and Hubbard, J. A. E. B., 1980, *The stratigraphy and historical geology of Bahrain*, In: Geology, Geomorphology and Pedology of Bahrain (eds. Doorkamp, J. C., Brunsden, D. and Jones, D. K. C.), Geobooks, Norwich, pp21-86.
- Hancock, J. M. and Kauffman, E. G., 1979, *The great transgressions of the late Cretaceous*, Journal of the Geological Society of London, Volume 136, pp175-186.
- Hankansson, E., Bromley, R. and Perch-Nielsen, K., 1974, *Maastrichtian chalk of North-West Europe - a pelagic shelf sediment*, In: Pelagic sediments on land and under the sea (eds. Hsü, K. J. and Jenkyns, H. C.), International Association of Sedimentologists Special Publication, Volume 1, pp211-234.
- Hardman, R. F. P., 1982, *Chalk reservoirs of the North Sea*, Bulletin of the Geological Society of Denmark, Volume 30, pp119-137.
- Hardman, R. F. P., 1983, *Chalk hydrocarbon reservoirs of the North Sea - an introduction*, Joint Association for Petroleum Exploration Courses (U.K.), course notes No.20, D1-D33.
- Hardman, R. F. P. and Kennedy, W. J., 1980, *Chalks reservoirs of the Hod Fields, Norway*, In: The Sedimentation of the North Sea Reservoir rocks, Geilo, 11-14 May, 1980, Norwegian Petroleum Society, Oslo, pp1-31.
- Hattin, D. E., 1975, *Petrology and origin of faecal pellets in Upper Cretaceous strata of Kansas and Saskatchewan*, Journal of Sedimentary Petrology, Volume 45, pp686-696.
- Hatton, I. R., 1986, *Geometry of allochthonous Chalk Group members, Central Trough, North Sea*, Marine and Petroleum Geology, Volume 3, pp79-98.
- Highfield, R., 1988, *Microscopic algae changing the weather*, News paper report in the Daily Telegraph, from the International Geoscience and Remote Sensing Symposium, Edinburgh, 15th September, 1988, pp1.
- Hurst, C., 1983, *Petroleum geology of the Gorm Field, Danish North Sea*, Geologie en Mijnbouw, Volume 62, pp157-168.
- Hutchinson, J. N., 1980, *Various forms of cliff instability arising from coast-erosion in South-east England*, Fjellsprengningsteknikk Bergmekanikk Geoteknikk, Trondheim, pp1-32
- Hutchinson, J. N., 1983, *Engineering in a landscape*, Inaugural Lecture, 9th October, 1979, Imperial College of Science and Technology, University of London, p12.
- Hutchinson, J. N., 1988, *General report: Morphological and geotechnical parameters of landslides in relation to geology and hydrogeology*, In: Proceedings of the fifth International symposium on landslides (ed. Bonnard, C.), 10-15th July, 1988, Lausanne, A. A. Balkema, Rotterdam, pp3-35.
- Hutchinson, J. N., 1989, *Flow slides from chalk cliffs on the coasts of N. W. Europe*, Proceedings of the Geological Association, in preparation.
- Hvorslev, M. J., 1937, *On the physical properties of disturbed cohesive soils*, Ingeniørvidenskabelige Skrifter, A, Number 45, p159.
- Ingoldby, H. C., 1978, *The classification of chalk for embankment construction*, In: Clay Fills, Institute of Civil Engineers, London, pp137-142.
- Jewhurst, J. and Wiborg, R., 1986, *Ekofisk reservoir management in a compacting environment*. The Offshore Digest, Volume. 2, pp 54-67.
- Johnson, J. P. and Rhett, D. W., 1986, *Compaction behaviour of Ekofisk chalk as a function of stress*, Society of Petroleum Engineers, SPE 15872, pp221-225.

Johnson, J. P., Rhett, D. W. and Siemers, W. T., 1988, *Rock mechanics of the Ekofisk Reservoir in the evaluation of subsidence*, presented at the 20th Annual Offshore Technology Conference, Houston, 2-5 May, pp39-50.

Jones, M. E., 1988, *Determination of the mechanical properties of reservoir rocks using the triaxial test*, Norwegian Petroleum Directorate publication, YA-524, p78.

Jones, M. E., 1989, *Hydrocarbon production from the North Sea chalk: Geotechnical considerations*, Keynote paper, Proceedings of the International Chalk Symposium, Brighton, 4-7th September, 1989, pre-print.

Jones, M. E. and Addis, M. A., 1986, *Deformation mechanisms in the Chalk*. Paper 3, North Sea Chalk Symposium, Volume 2. Stavanger.

Jones, M. E., Addis, M. A., Preston, R. M. F., Goldsmith, A., Leddra, M. J., Yassir, N. A. and Rowbotham, J. D., 1985a, *Compaction analysis of the Ekofisk Field*; Confidential Report to the Norwegian Petroleum Directorate, August, 1985.

Jones, M. E., Addis, M. A., Preston, R. M. F., Leddra, M. J., Yassir, N. A., Goldsmith, A. S. and Rowbotham, J. D., 1985b, *Compactional analysis of the Ekofisk Field*, Final report; Confidential Report to the Norwegian Petroleum Directorate, November, 1985.

Jones, M. E., Bedford, J. and Clayton, C., 1984, *On natural deformation mechanisms in the chalk*, Journal of the Geological Society, London, Volume 141, pp675-683.

Jones, M. E. and Leddra, M. J., 1987, *Ground motions and seismicity due to fluid production from subsurface reservoirs*, Memoir of the Geological Society of China, Number 9, pp465-494.

Jones, M. E. and Leddra, M. J., 1989, *Compaction and flow of porous rocks at depth*; Rock at Great Depth Symposium, (eds. Maury, V. and Fourmaintraux, D.), Pau, France, 28-31 August, 1989, A. A. Balkema, Rotterdam, pp891-898.

Jones, M. E., Leddra, M. J. and Addis, M. A., 1987, *Reservoir Compaction and Surface Subsidence due to Hydrocarbon Extraction*, HMSO, OTH 87 276, p175.

Jones, M. E., Leddra, M. J. and Potts, D., 1989, *Ground motions due to hydrocarbon production from the chalk*, Proceedings of the International Chalk Symposium, Brighton, 4-7th September, 1989, pp341-347.

Jones, M. E., Leddra, M. J., Preston, F. M. F., Addis, M. A. and Yassir, N. A., 1986, *Ekofisk Project 3 Report: Analysis of the Ekofisk Oilfield Subsidence*; Confidential Report to the Norwegian Petroleum Directorate, April, 1986.

Kennedy, W. J., 1980, *Aspects of Chalk Sedimentation in the Southern Norwegian Offshore*, in: The Sedimentation of the North Sea Reservoir Rocks, Norwegian Petroleum Society, Geilo. 9, p29.

Kennedy, W. J., 1983, *A preliminary report on the sedimentology of the Chalk Group in the Southern Norwegian and Danish Sectors of the Central Graben*, for the Chalks Research Group.

Kennedy, W. J., 1985, *Sedimentology of the Late Cretaceous and Early Palaeocene Chalk Group, North Sea Central Graben*, Chalk Research Programme Symposium, Stavanger, May 1985. Book 1, pp1- 68.

Kennedy, W. J., 1986, *Sedimentology of Late Cretaceous - Palaeocene Chalk reservoirs, North Sea Central Graben*, In: Petroleum Geology of North West Europe (eds. Brooks, J. and Client, K. W.), Volume 1, pp469-483.

Kennedy, W. J., 1987a, *Late Cretaceous and early Palaeocene Chalk Group sedimentology in the Greater Ekofisk Area, North Sea Central Graben*, Bulletin Centres Research-Production Elf- Aquitaine, Volume 11, pp91-126.

Kennedy, W. J., 1987b, *Sedimentology of the late Cretaceous and early Palaeocene Chalk Group, in the North Sea basin and on its margins*, Joint Association for Petroleum Exploration Courses (U.K.), course notes No.54, B1-B97.

- Kennedy, W. J. and Garrison, R., 1975, *Morphology and genesis of nodular chalks and hardgrounds in the Upper Cretaceous of Southern England*, *Sedimentology*, Volume 22, pp311-386.
- Kennedy, W. J. and Juignet, P., 1974, *Carbonate banks and slump beds in the Upper Cretaceous (Upper Turonian - Santonian) of Haute Normandie, France*, *Sedimentology*, Volume 21, pp1-42.
- Lambe, T. W. and Whitman, R. V., 1979, *Soil Mechanics SI Version*, J. Wiley and Sons, New York, p553.
- Leddra M.J., 1987, *Analysis of the Valhall Oilfield subsidence*, confidential report to the Norwegian Petroleum Directorate, December 1987.
- Leddra M.J., 1988, *Analysis of the Eldfisk Oilfield subsidence*, confidential report to the Norwegian Petroleum Directorate, January 1988.
- Leddra, M. J., 1987, *Permeability analysis, Ekofisk chalks*, Confidential report for Norsk Hydro.
- Leddra, M. J., 1988, *Permeability analysis of Ekofisk reservoir chalks*, confidential report for Norsk Hydro.
- Leddra, M. J. and Jones, M. E., 1989, *Steady state flow during undrained loading of chalk*, Proceedings of the International Chalk Symposium, Brighton, 4-7th September, 1989, pp117-124.
- Leddra, M. J., Jones, M. E., Goldsmith, A. S. and Potts, D., 1989a, *Displacements of the sea floor due to hydrocarbon production*. Presented at the Brazil Offshore '89 Conference, Rio De Janeiro, Brazil, 21-25th August, 1989. in press.
- Leddra, M. J., Pederstad, K., Lønøy, A and Jones, M. E., 1989b, *The influence of increasing effective stress on the permeability of chalks under hydrocarbon reservoir conditions*, Proceedings of the International Chalk Symposium, Brighton, 4-7th September, 1989, pp125-132.
- Leonard, R. C. and Munns, J. W., 1987, *Valhall*, In: *Geology of the Norwegian Oil and Gas Fields* (eds. Spencer, A. M. et al.), Graham & Trotman, pp153-163.
- Leroueil, S., Kabbaj, M., Travenas, F. and Bouchard, R., 1985, *Stress-strain strain-rate relation for the compressibilities of sensitive natural clays*, *Geotechnique*, Number 2, Volume 35, pp159-180.
- Lewis, W. A. and Parsons, A. W., 1973, *The application of belt conveyors in road foundations and pavements*, Proceedings of the Institute of Civil Engineers, Part 1, Volume 56, pp425-450.
- Lloyd, R. M. and Hsu, K. J., 1972, *Stable-isotope investigations of sediments from the DSDP III cruise to South Atlantic*, *Sedimentology*, Volume 19, pp45-48.
- Marek, B. F., 1979, *Permeability loss in depletion of reservoirs*, Society of Petroleum Engineers, SPE 8433, pp23-26.
- Mapstone, N. B., 1975, *Diagenetic history of a North Sea Chalk*, *Sedimentology*, Volume 22, pp601-613.
- McClay, K. R., 1977, *Pressure solution and coble creep in rocks and minerals: a review*, *Journal of the Geological Society of London*, Volume 135, pp57-70.
- McLatchie, A. S., Hemstock, R. A. and Young, J. W., 1958, *The effective compressibility of reservoir rock and its effects on permeability*, *Journal of Petroleum Technology*, June 1958, pp49- 51.
- Michaud, F., 1987, *Eldfisk*, In: *Geology of the Norwegian Oil and Gas Fields* (eds. Spencer et al.), Graham & Trotman, pp89-105.
- Michelsen, O., 1982, *Geology of the Danish Central Graben*, *Danmarks Geologiske Undersøgelse*, series B, Number 8, pp1-333.
- Middleton, G. V. and Hampton, M. A., 1976, *Subaqueous sediment transport and deposition by sediment gravity flows*, In: *Marine Sediment Transport and Environmental Management* (eds. Stanley, D. J. and Swift, D. J. P.), John Wiley, New York.

Mimran, Y., 1975, *Fabric deformation induced in Cretaceous chalks by tectonic stresses*, Tectonophysics, Volume 26, pp309-316.

Mitchell, R. J., 1970, *On the yielding and mechanical strength of Leda clays*, Canadian Geotechnical Journal, Volume 7, pp297-312.

Morgan, J. T. and Gordon, D. T., 1970, *Influence of pore geometry on water-oil relative permeability*, Journal of Petroleum Technology, presented at the Society of Petroleum Engineers 44th Annual Fall meeting, Denver, September 28-October 1, 1969, pp1199-1208.

Moshanski, V. A. and Parabouchev, I. A., 1981, *The nature of strength and deformation of weak carbonaceous rocks*, Proceedings of the International Symposium on weak rock, Tokyo, 21-24 September, 1981, pp339-346.

Munns, J. W., 1985, *The Valhall Field: A geological overview*, Marine and Petroleum Geology, Volume 2, pp23-43.

Neugebauer, J., 1973, *The diagenetic problem of chalk - the role of pressure solution and pore fluid*, Neues Jahrbuch Fur Geologie und Palaontologie Abhandlungen, Volume 143, pp223-245.

Neugebauer, J., 1974, *Some aspects of cementation in Chalk*, In: Pelagic Sediments: on land and Under the Sea (Eds. Hsu, K. J. and Jenkyns, H. C.), International Association of Sedimentologists Special Publication, Volume 1, pp149-176.

Newell, D. N., 1963, *Crises in the history of life*, In: The fossil record and evolution, Scientific American, W. H. Freedman and Company, California, pp141-154.

Newman, G. H., 1981, *The effect of Water Chemistry on the Laboratory Compression and Permeability Characteristics of Some North Sea Chalks*, Society of Petroleum Engineers, SPE 10203.

Nygaard, E., Lieberkind, K. and Frykman, P., 1983, *Sedimentology and reservoir parameters of the Chalk Group in the Danish Central Graben*, Geologie en Mijnbouw, Volume 62, pp177-190.

Ofstad, K., 1981, *The Eldfisk Area*, Norwegian Petroleum Directorate Paper Number 30, p39.

Ofstad, K., 1983, *The Southermost part of the Norwegian section of the Central Trough*, Norwegian Petroleum Directorate Paper Number 32, p32.

Pederstad, K., Corrigan, T., Lonoy, A. and Fritsen, A., 1988, *Facies controls on reservoir quality, Ekofisk Field, North Sea*, Chalks Research Report, Norsk Hydro Research Centre, Bergen, pp1-21.

Pekot, L. J. and Gersib, G. A., 1987, *Ekofisk*, In: Geology of the Norwegian Oil and Gas Fields (eds. Spencer et al.), Graham & Trotman, pp73-87.

Perch-Nielsen, K., Ulleberg, K. and Evensen, J. E., 1979, *Comments on "The Terminal Cretaceous Event. A Geologic problem with an oceanographic solution"*, In: Proceedings Cretaceous- Tertiary Boundary Events Symposium (eds. Gartner and Keeney), Copenhagen, 1979, Volume 2, pp106-111.

Perry, S. H., 1978, *Behaviour of fill from soft chalk and soft chalk/clay mixtures*, In: Clay Fills, Institute of Civil Engineers, London, pp189-196.

Potts, D. M., Jones, M. E. and Berget, O. P., 1988, *Subsidence above the Ekofisk Oil Reservoir*, In: Proceedings of the International Conference on Behaviour of Offshore Structures, Trondheim, Norway, pp113-128.

Price, G. P., 1988a, *Fabrics of calcareous sediments at North Rankin 'A', North West Shelf*, In: Engineering for calcareous sediments (eds. Jewell R. J. and Andrews D. C.), Proceedings of the International Conference on Calcareous Sediments, 15-18 March, Perth, A. A. Balkema, Rotterdam, Volume 2, pre-print 1/4- 10/4.

Price, G. P., 1988b, *Effect of mechanical deformation on the fabrics of calcareous sediments from North Rankin 'A'*, In: Engineering for calcareous sediments (eds. Jewell R. J. and Andrews D. C.), Proceedings of the International Conference on Calcareous Sediments, 15-18 March, Perth, A. A. Balkema, Rotterdam, Volume 2, pre-print 1/21-11/21.

Privett, K. D., 1989, *Use of thick layers in earthworks at Port Solent marina, Portsmouth, Uk*, Proceedings of the International Chalk Symposium, Brighton, 4-7th September, 1989, pp181-188.

Puig, J., 1973, *Problemes de terrassement de la craie*, Bullitin Liaison Labo. P. et Ch., Special V 'la Craie', October, pp81-98.

Rat, M. and Schaeffner, M., 1989, *Classification of chalk and conditions of use in embankments*, Proceedings of the International Chalk Symposium, Brighton, 4-7th September, 1989, pp189-196.

Remy, J. P., 1973, *The measurement of small permeabilities*, Geotechnique, Volume 23, Number 3, pp454-458.

Rentsch, H. C. and Mes, M. J., 1988, *Measurement of Ekofisk subsidence*, Offshore Technology Conference, Houston, Texas, OTC5619, pp23-30.

Roscoe, K. H., 1953, *An apparatus for the application of simple shear to soil samples*, Proceedings of the 3rd International Conference on Soil Mechanics, Volume 1, pp186-191.

Roscoe, K. H., Schofield, A. N. and Wroth, C. P., 1958, *On the yielding of soils*, Geotechnique, Volume 8, Number 1, pp22-53.

Ruddy, I., Anderson, M. A., Pattillo, P. O., Bishlawi, M. and Foged, N., 1988, *Rock compressibility, compaction, and subsidence in a high porosity reservoir: A case study of Valhall Field*, Proceedings of Society of Petroleum Engineers 63rd Annual Technical Conference, Houston, USA, SPE 18278, pp179-186.

Rutter, E. H., 1976, *The kinetics of rock deformation by pressure solution*, Philosophical Transactions of the Royal Society, A283, pp203-219.

Sangrey, D. A., 1972, *Naturally cemented sensitive soils*, Geotechnique, Volume 22, Number 1, pp139-152.

Sarda, J. P., 1985, *Porosity and Permeability of Chalk Samples at Reservoir Temperature Under Isotropic Loading*, In: North Sea Chalks Symposium, Stavanger, Book 1, pp1-8.

Schatzinger, R. A., 1985, *Chalk pore systems: Qualitative evaluation and quantitative aspects of pore geometry at Ekofisk*, Chalk Research Group Symposium, Stavanger, Book 1, pp1-19.

Schlanger, S.O., Jenkyns, H. C. and Premoli-Silva, I., 1981, *Volcanism and vertical tectonics in the Pacific Basin related to global Cretaceous transgression*, Earth Planetary Sciences letters, Volume 52, pp435-449.

Schofield, A. N. and Wroth, C. P., 1968, *Critical State Soil Mechanics*, McGraw-Hill Book Co., London, 1968.

Schoonbeck, J. B., 1976, *Land subsidence as a result of gas extraction in Groningen, the Netherlands*, Proceedings Amaheim Symposium, 121, International Association of Scientific Hydrology, pp267-284.

Scholle, P. A., 1974, *Diagenesis of Upper Cretaceous Chalks from England Northern Ireland and the North Sea*, In: Pelagic Sediments: on land and Under the Sea (Eds. Hsu, K. J. and Jenkyns, H. C.), International Association of Sedimentologists Special Publication, Volume 1, pp177-210.

Scholle, P. A., 1977, *Chalk Diagenesis and its relation to Petroleum Exploration: Oil from Chalk, a modern miracle?*, American Association of Petroleum Geologists Bulletin, Volume 61, pp982-1009.

Scholle, P. A., Arthur, M. A. and Ekdale, A. A., 1983, *Pelagic environment*, In: Carbonate depositional environments (eds. Scholle, P. A., Bebout, D. G. and Moore, C. H.), American Association Of Petroleum Geologists Memoirs, Number 33, pp619- 691.

Seed, R. B., Anwar, H. A. and Nicholson, P. G., 1989, *Elimination of membrane compliance effects in undrained testing*, Proceedings of the 12th International Conference on Soil Mechanics and Foundation Engineering, Rio de Janerio, 14-17 August, 1989, Volume 1, A. A. Balkema, Rotterdam, pp111-114.

Selly, R. C., 1976, *The habitat of North Sea Oil*, Proceedings of the Geologists Association, Volume 87, Number 3, pp359-388.

Shinn, E. A. and Robbin, D. M., 1983, *Mechanical and chemical compaction in fine-grained shallow-water limestones*, Journal of Sedimentary Petrology, Volume 53, Number 2, pp595-618.

Skempton, A. W., 1954, *The pore pressure parameters A and B*, Geotechnique, Volume 4, Number 4, pp143-147.

Skovbro, B., 1983, *Depositional conditions during chalk sedimentation in the Ekofisk area Norwegian North Sea*, Geologie en Mijnbouw, Volume 62, pp169-175.

Sorensen, S., Jones. M. E., Hardman, R. F. P., Leutz, W. K. and Schwartz, P. H., 1986, *Reservoir characteristics of high- and low-productivity chalks from the Central North Sea*, In: Habitat of Hydrocarbons on the Norwegian Continental Shelf, Norwegian Petroleum Society, Graham & Trotman, pp91-110.

Steinich, G., 1967, *Sedimenstrukturen der Rugener Schreibkreide (Unter- Maastrich)*, Geologie, Volume 16, pp570-583.

Stroud, M. A. and Mitchell, J. M., 1989, *Collapse of old chalk fill at Brighton*, Keynote paper, Proceedings of the International Chalk Symposium, Brighton, 4-7th September, 1989, pre-print.

Sulak, R. and Danielsen, J., 1988, *Reservoir aspects of Ekofisk subsidence*, Offshore Technology Conference, Houston, Texas, OTC 5618, pp9-21.

Surlyk, F., 1979, *Guide to Stevns Klint*, In: Cretaceous-Tertiary Boundary Events, 1. The Maastrichtian and Danian of Denmark (eds. Birkelund, T. and Bromley, R. G.), University of Copenhagen, pp164-170.

Talwani, M. and Elmholt, O., 1977, *Evolution of the Norwegian- Greenland Sea*; Geological Society of America Bulletin, Volume 88, pp969-999.

Taylor, R. K., 1987, *Tailings Dams: The Liquefaction Hazard*, Memoir of the Geological Society of China, Number 9, December 1987, pp109-122.

Taylor, S. R. and Lapre, J. F., 1987, *North Sea chalk diagenesis: its effect on reservoir location and properties*, In: Petroleum Geology of North West Europe (Eds. Brooks, J. and Glennie, K.), Graham & Trotman, pp483-495.

Thomas, L. K., Dixon, T. N., Evans, C. E. and Vienot, M. E., 1987, *Ekofisk Waterflood Pilot*, Journal of Petroleum Technology, February 1987, pp221-232.

Thomson, G. H. and Buthee, N. R., 1989, *Treatment of chalk fill for light industrial development at West Thurrock*, Proceedings of the International Chalk Symposium, Brighton, 4-7th September, 1989, pp177-180.

Toll, D. G., 1988, *The behaviour of unsaturated compacted naturally occurring gravel*, PhD Thesis, University of London, Unpublished, p390.

Tsuchida, T., Kobayashi, M., Ifuku, S. and Fukuda, I., 1988, *Engineering properties of coral soils in Japanese South Western Islands*, In: Engineering for calcareous sediments (eds. Jewell, R. J. and Andrews, D. C.), Proceedings of the International Conference on Calcareous Sediments, 15-18 March, Perth, Balkema, Rotterdam, Volume 1, pp137-144.

Van Den Bark, E. and Thomas, O. D., 1980, In: *Ekofisk: First of the Giant Oil Fields on Western Europe* (ed. Halbouty, M.), Association of American Petroleum Geologists, Memoir 30, pp195- 224.

Van Den Bosch, W. J., 1983, *The Harlingen Filed, The only gas field in the Upper Cretaceous chalk of the Netherlands*, Geologie en Mijnbouw, Volume 62, pp145-156.

Van GolfRacht, T. D., 1982, *Fundamentals of fractured reservoir engineering*, Developments in Petroleum Science, 12, Elsevier Scientific Publications Company, Amsterdam, p710.

Van Kersternen, J., 1973a, *The analysis of surface subsidence resulting from gas production in Groningen field*, Verhandelingen van het Koninklijk Nederlands Geologisch Mijnbouwkundig Genootschap, Volume 28, pp11-18.

Van Kersternen, J., 1973b, *Estimate of compaction data representative of Groningen reservoir rock*, Verhandelingen van het Koninklijk Nederlands Geologisch Mijnbouwkundig Genootschap, Volume 28, pp33-42.

Watts, N. L., 1983, *Microfractures in Chalk of Albuskjell Field, Norwegian Sector, North Sea: Possible Origin and Distribution*, American Association of Petroleum Geologists Bulletin, Volume 67, Number 2, pp201-234.

Watts, N. L., Lapre, J. F., van Schijndel, F. S. and Ford, A. , 1980, *Upper Cretaceous and Lower Tertiary chalks of the Albuskjell area, North Sea: deposition in a slope and base-of-slope environment*, Geology, Volume 8, pp217-221.

Wiborg, R. and Jewhurst, J., 1986, *Ekofisk subsidence detailed and solutions assessed*, Technology, Oil and Gas Journal, February, 17, 1986, pp47-51.

Wilson, G. and Grace, H., 1942, *The settlement of London due to underdrainage of the London Clay*, Journal of the Institute of Civil Engineering, London, Volume 19, pp100-127.

Wise, S. W. and Hsu, K. J., 1971, *Genesis and lithification of a deep sea chalk*, Eclog. geol. Helv. 64. pp273-278.

Whitten, D. G. A. and Brooks, J. R. V., 1972, *The Penguin Dictionary of Geology*, Penguin Books Ltd., England.

Wolfe, M. J., 1986, *Lithification of a carbonate mud: Senonian Chalk in Northern Ireland*, Sedimentary Geology, Volume 2, pp263- 290.

Zeeveart, L., 1953, *Pore pressure measurement to investigate the main source of surface subsidence in Mexico City*, Proceedings of the International Conference on Soil Mechanics and Foundation Engineering, Zurich, pp299-304.

APPENDIX 1.

AP1.1. Introduction.

Thin sections and scanning electron micrographs were prepared from samples of two the outcrop chalks examined by this study. Chemical analysis and X-ray defraction determinations were also conducted to determine the clay content, silica content and calcite content of both types of material. The results are pre sented below.

AP1.2. Constituents of the Butser Hill and Stevn's Klint outcrop chalks.

Samples of both chalks were dissolved in 10% HCl to determine the acid insoluble component. The quartz content was also determined both by dissolution and by X-ray defraction. The results indicate the following average percentage components:

Table AP1.1

TYPE OF CHALK	ACID INSOLUBLE (%)	SILICA CONTENT (%)	CALCITE CONTENT (%)
Butser Hill	10.11	6.84	89.89
Stevn's Klint	0.58	0.32	99.42

X-ray defraction results indicate that only a small proportion of the silica content determined for the Butser Hill chalk repre sent free silica.

AP1.3. Thin section and scanning electron microscope analyses.

Six thin sections (three from both chalks) were prepared. These were useful in determining the low quantity of Foraminifera and large shell fragments. It was not possible, however, to undertake a detailed examination of the major constituents, namely the Coccolithophorids.

One of the primary aims of this investigation was to determine the presence of a calcite cement structure. It was impossible to identify contacts between the individual grains using the available thin sections due to the small size of the cement contacts.

Scanning electron micrographs were more useful for identifying both cementation and the types of Coccoliths present. Many of the complete and disaggregated Coccoliths show evidence of calcitic overgrowths (ie. plates AP1.1, 1.5-1.7). There is also clear evidence of the growth of secondary calcite (plates AP1.1, 1.4, 1.6, 1.7, 1.9-1.11). Even under the highest magnifications (35000x) (plate AP1.3) the presence of 'spot welding' at the grain contacts can not be seen. However, the structure of both chalks can be seen to consist of cemented aggregates of Coccoliths and Coccolith fragments surrounded by large voids (particularly in the Stevn's Klint samples (plates AP1.1-1.9).

Both the Butser Hill and Stevn's Klint chalks consist almost exclusively of Coccolith material. Several of the Coccoliths in the Stevn's Klint chalk were identifiable. These included *Ahmullerella Octoradiata* (plate AP1.1), *Prediscosphaera Cretacea* (plates AP1.2 and AP1.4), *Arkanselskiella Cymbiformis* (AP1.6) and *Cribrosphaerella Ehrenbergi* (plate AP1.9).

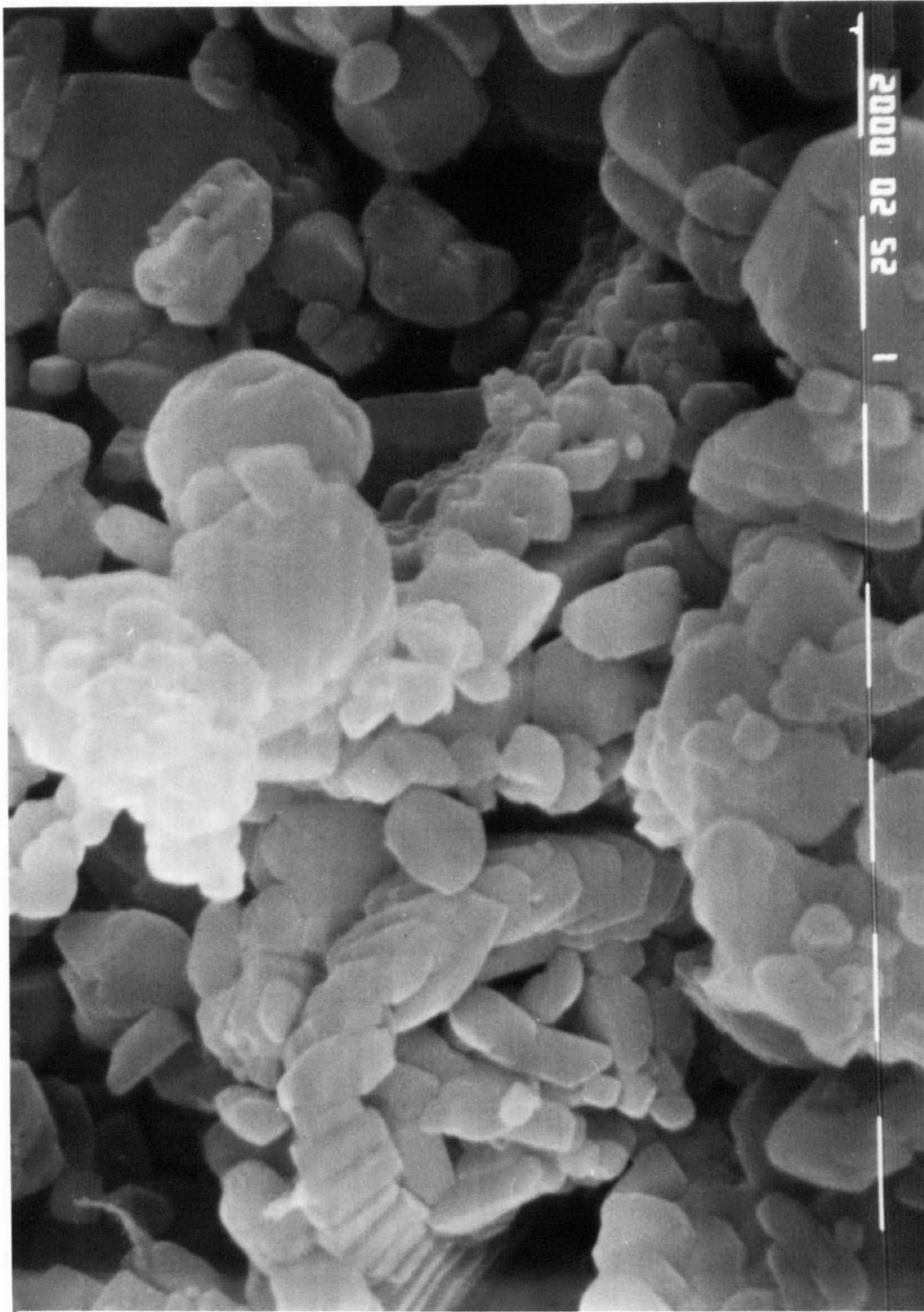


Plate AP1.1. Stevn's Klint chalk. Magnification 10000x. Contain ing an example of the Coccolith Ahmuellerella Octoradiata.

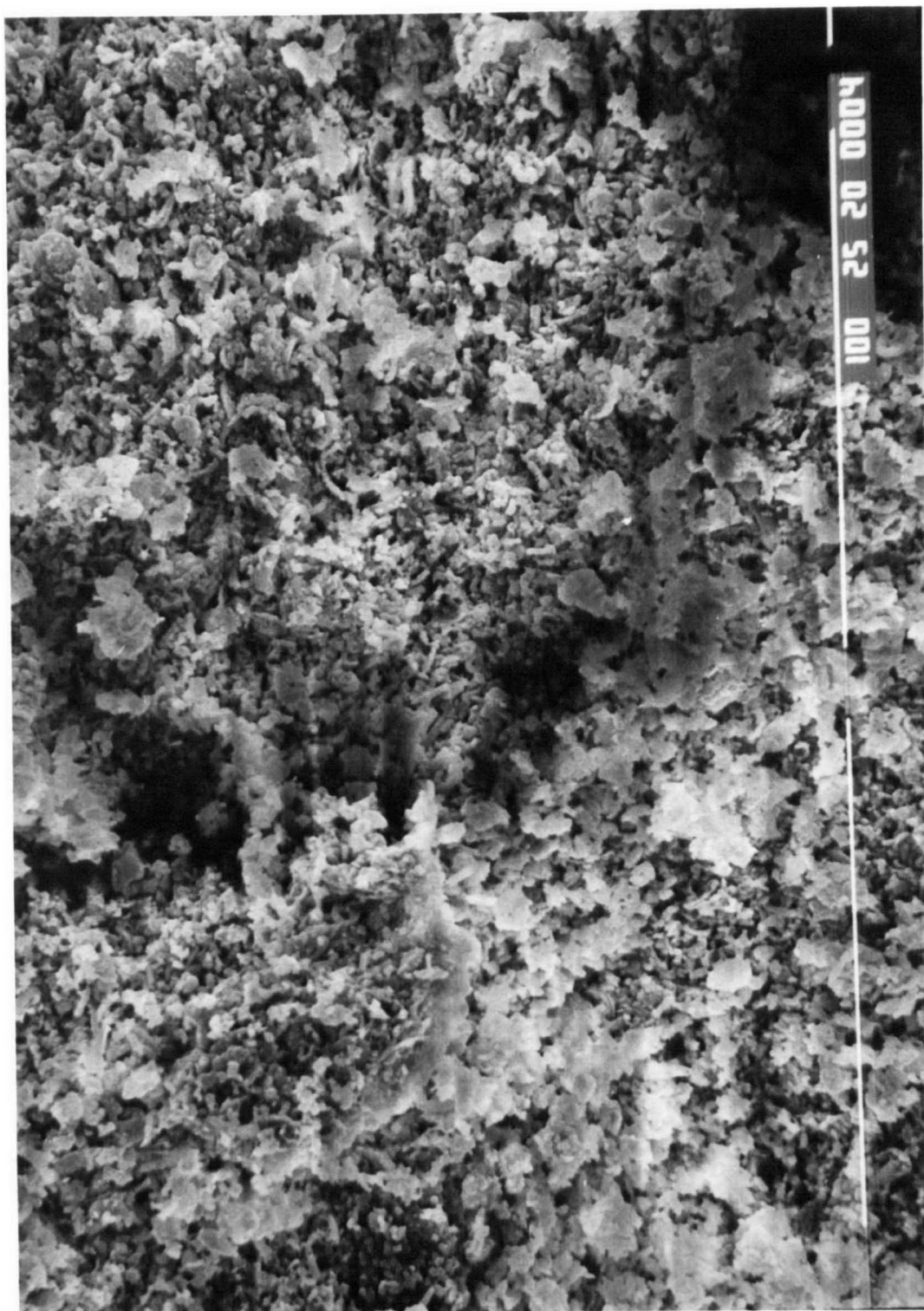


Plate AP1.2. Stevn's Klint chalk. Magnification 500x. Containing examples of the Coccoliths *Prediscosphaera* Cretacea. This micro graph clearly shows the zonation of cemented Coccolith debris and the resulting large voids.

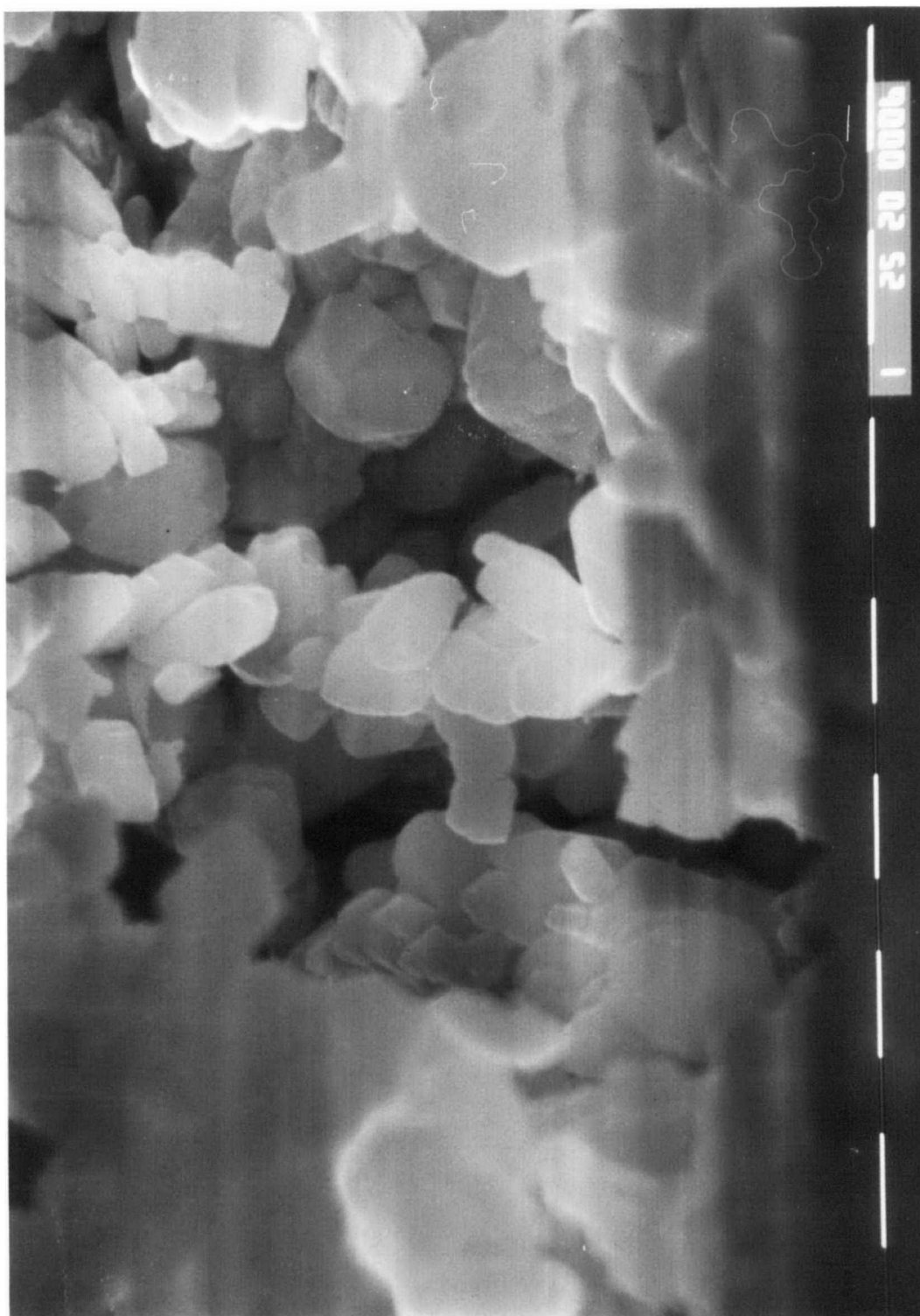


Plate AP1.3. Stevn's Klint chalk. Magnification 35000. A photo graph, taken at the highest magnification available showing several grain contacts. At this magnification the resolution of the photograph is not large enough to clearly determine the presence of 'spot welded' contacts.

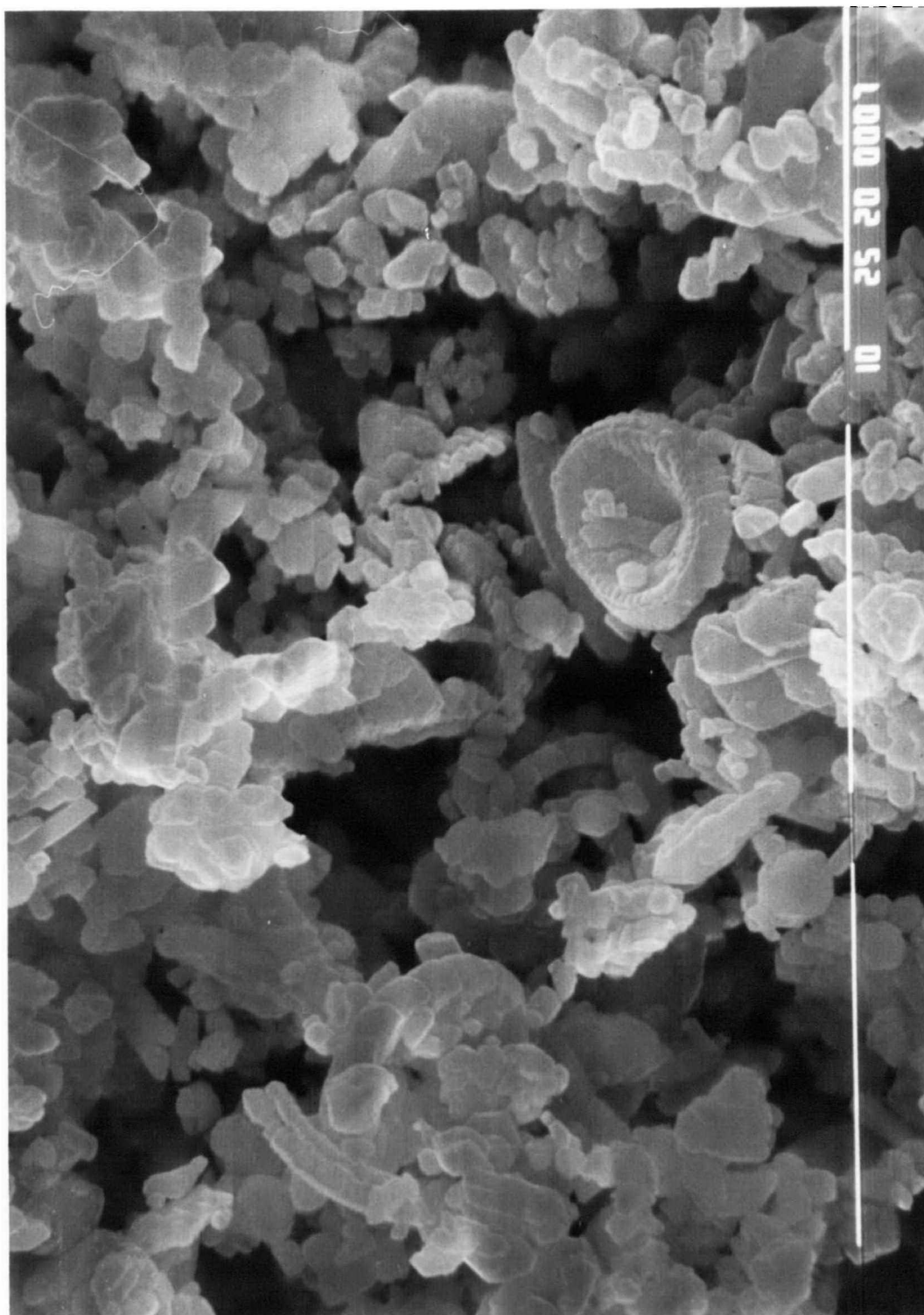


Plate AP1.4. Stevn's Klint chalk. Magnification 10000x. Contain ing an example of the Coccolith Prediscosphaera Cretacea.

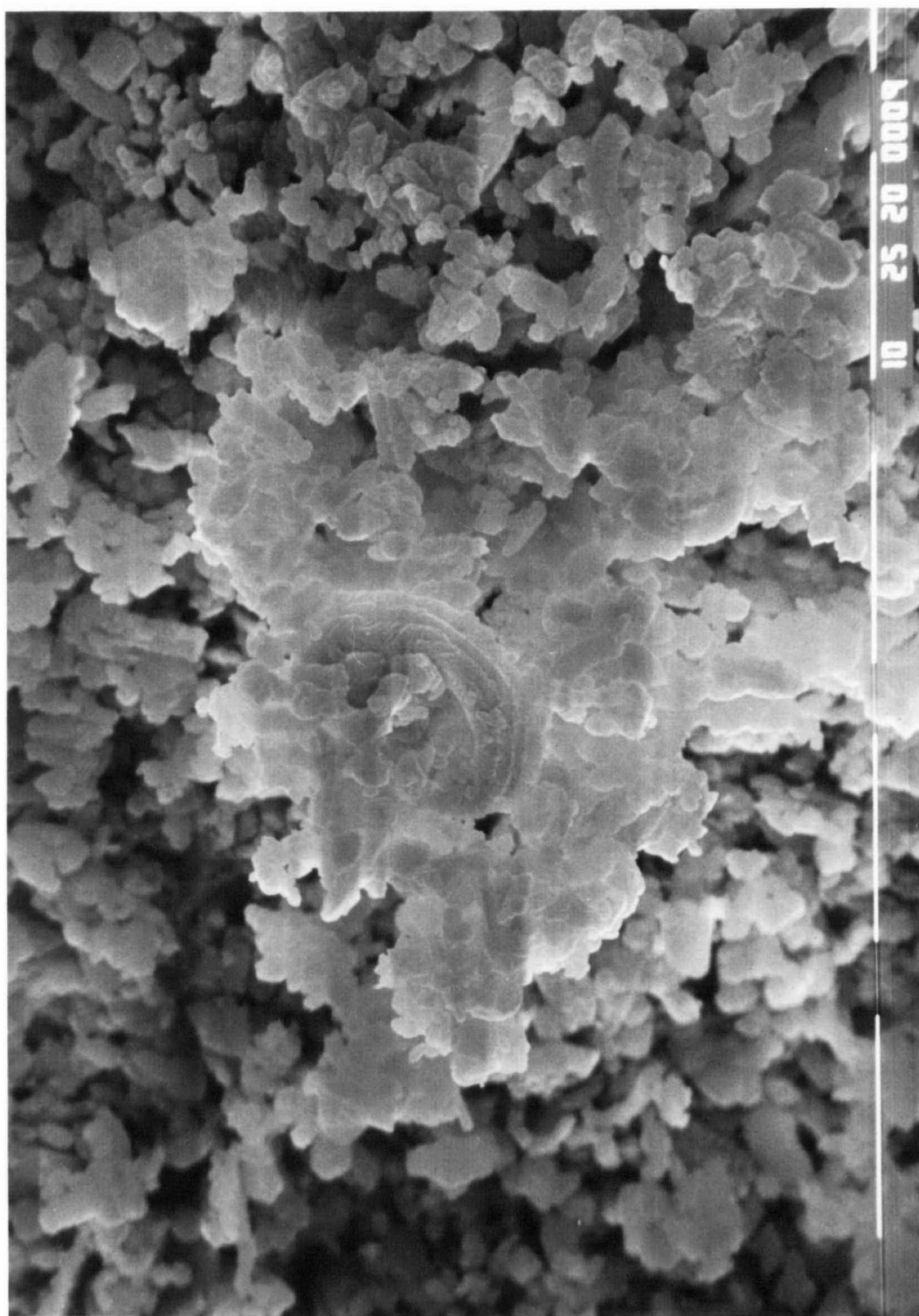


Plate AP1.5. Stevn's Klint chalk. Magnification 2000x.

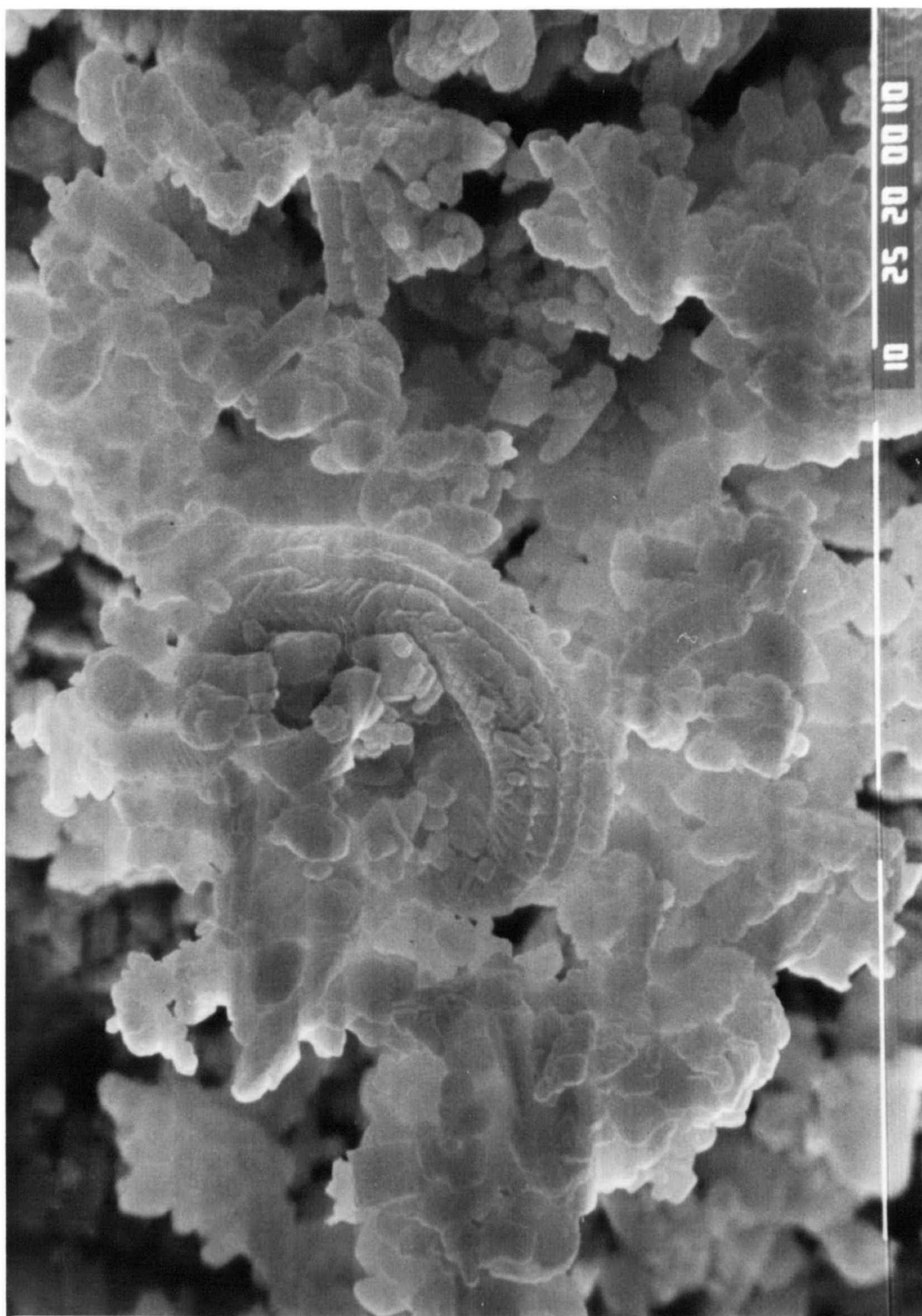


Plate AP1.6. Stevn's Klint chalk. Magnification 10000x. Contain ing an example of the Coccolith *Arkhanselskiella Cymbiformis*.

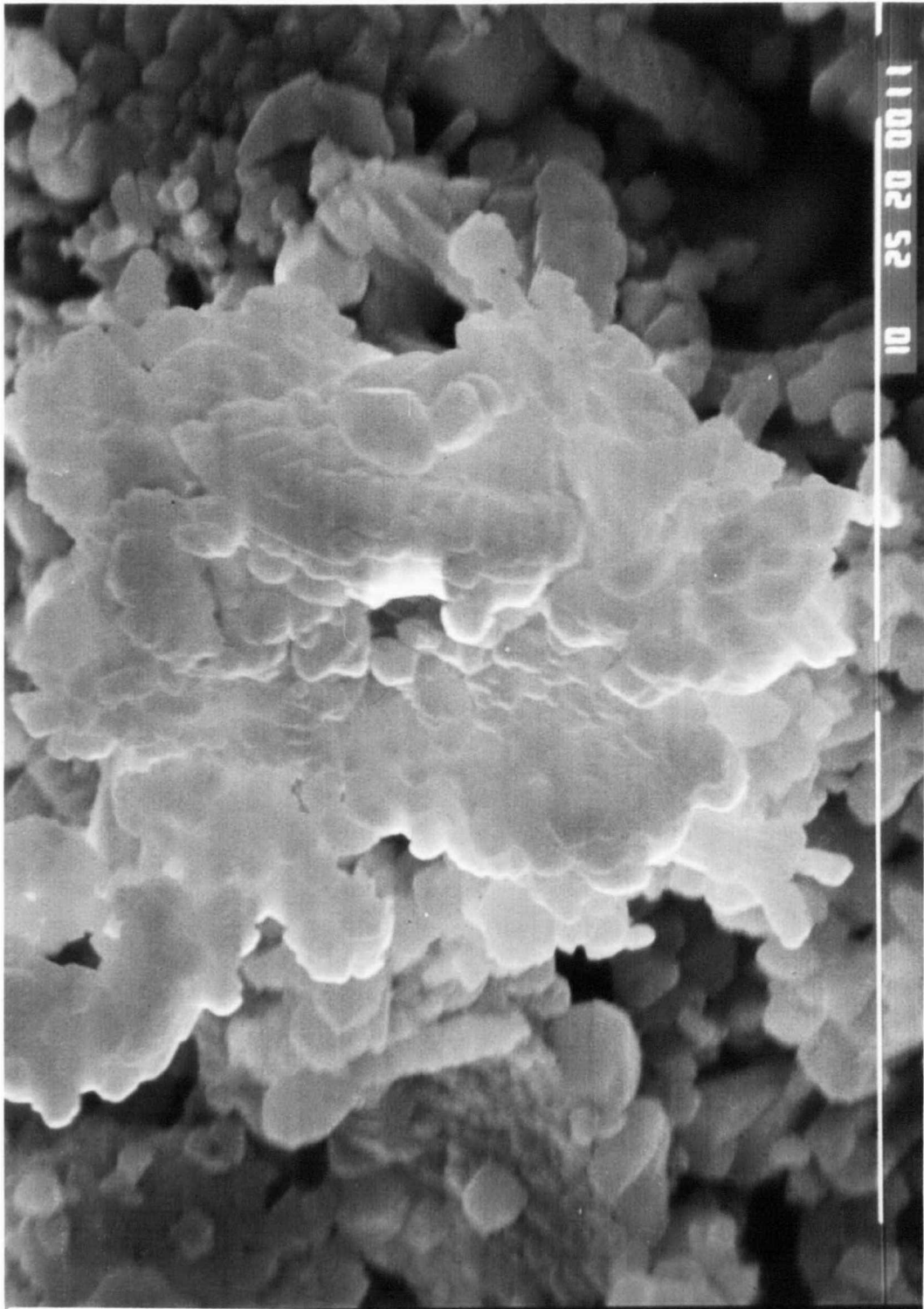


Plate AP1.7. Stevn's Klint chalk. Magnification 15000x.

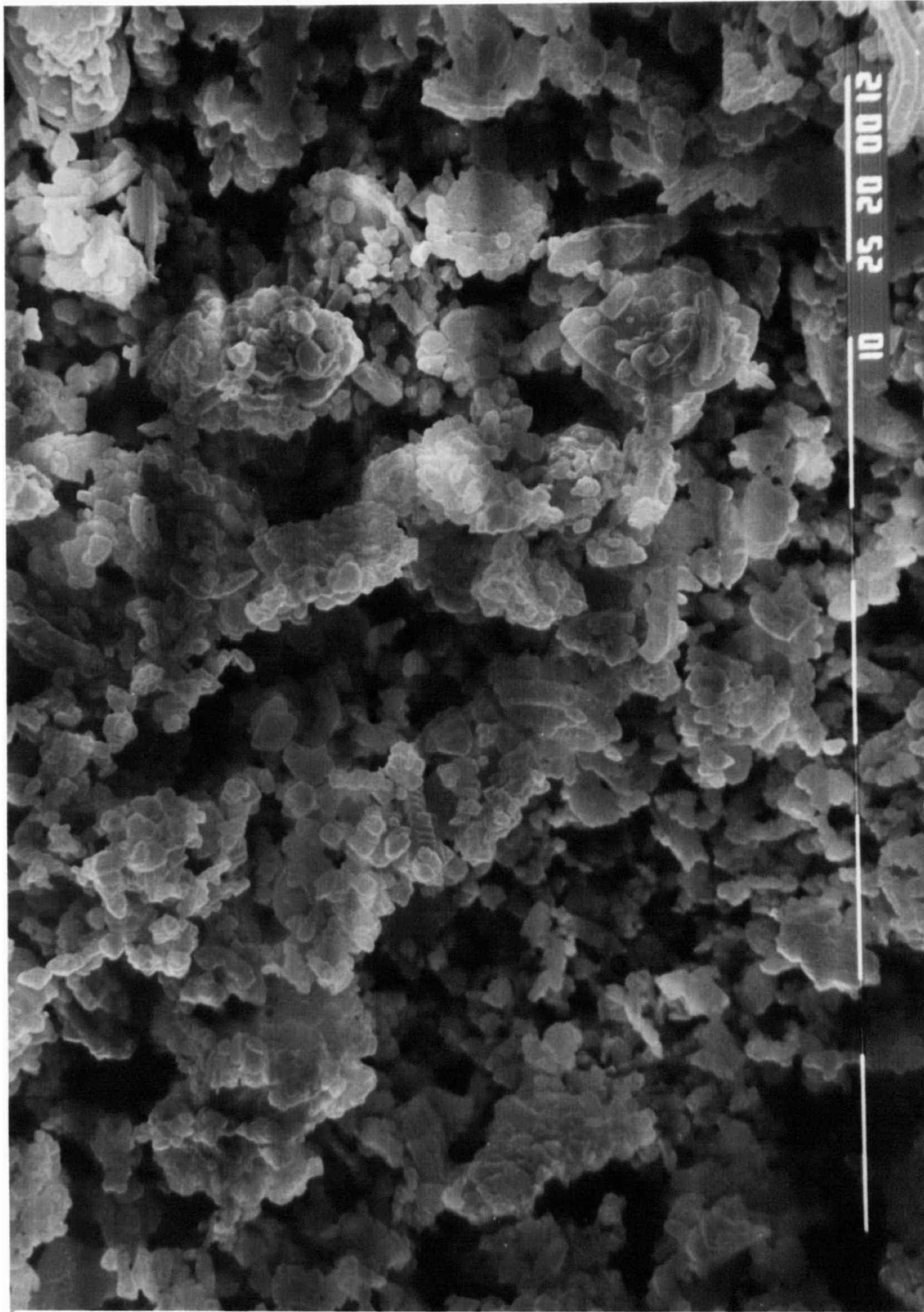


Plate AP1.8. Stevn's Klint chalk. Magnification 1500x. The micro graph shows that the chalk structure comprises of discretely cemented aggregates of Coccolith material.

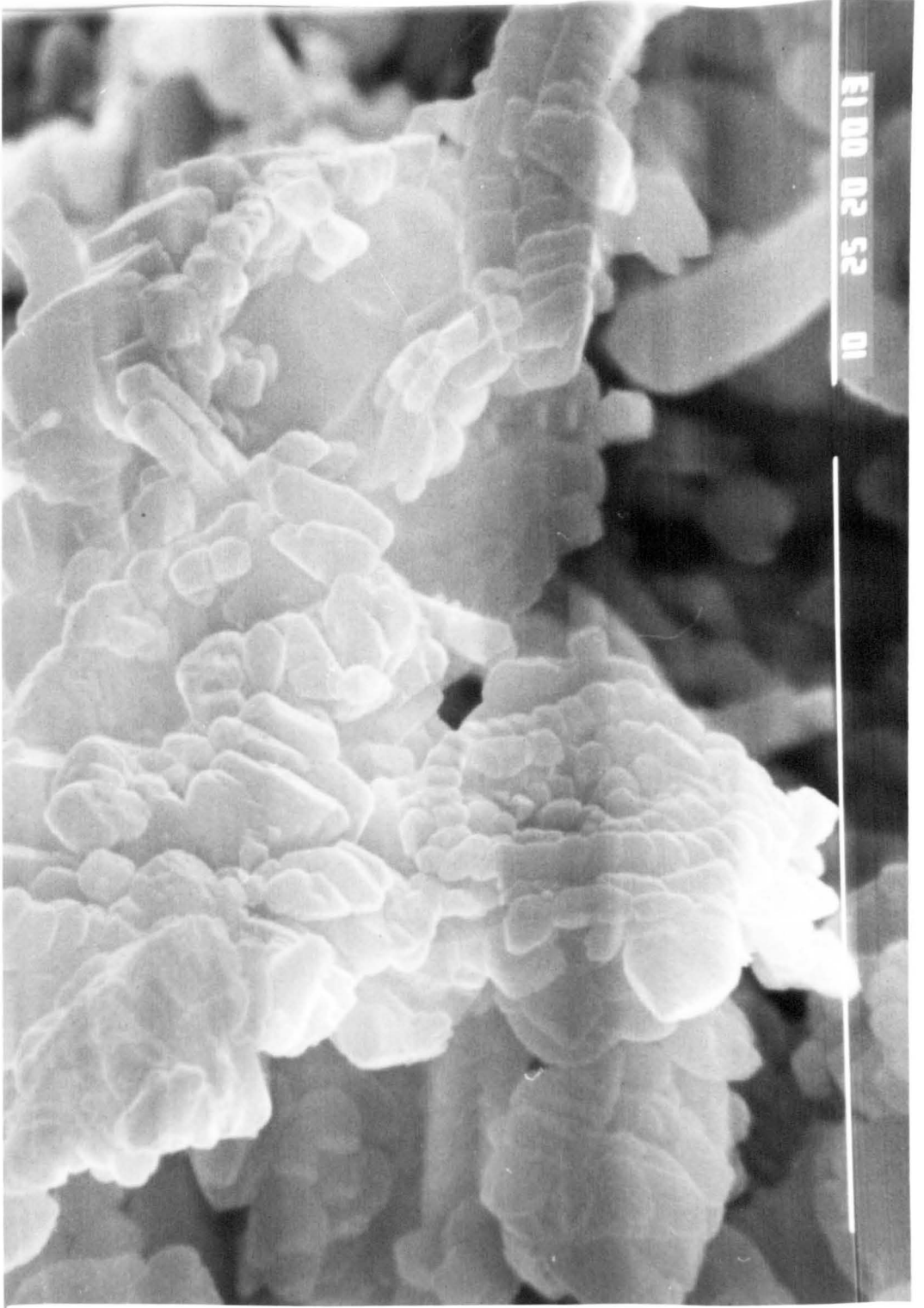


Plate AP1.9. Stevn's Klint chalk. Magnification 7500x. Containing an example of the Cocolith *Cribrosphaerella Ehrenbergi*.

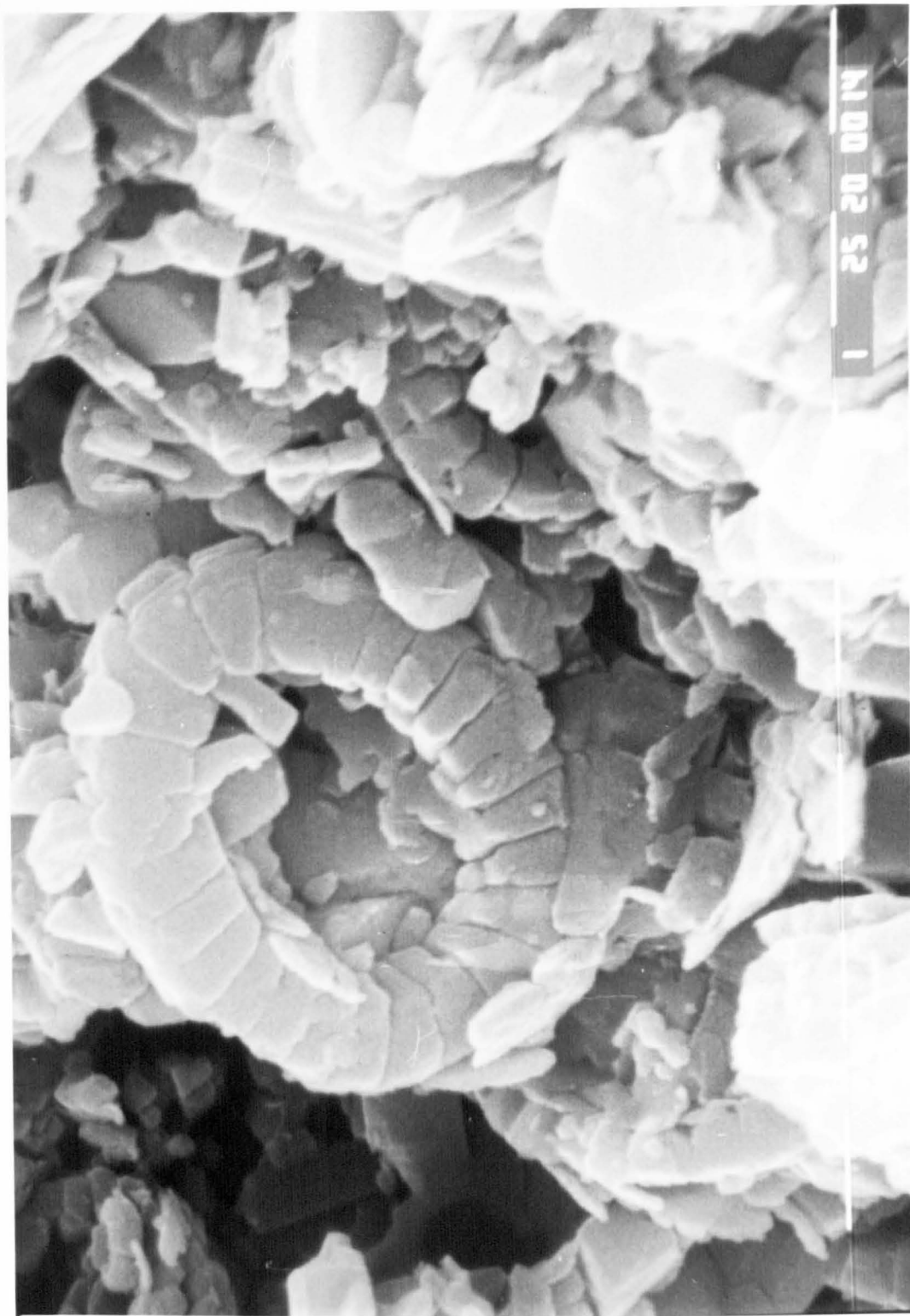


Plate AP1.10. Butser Hill chalk. Magnification 10000x.

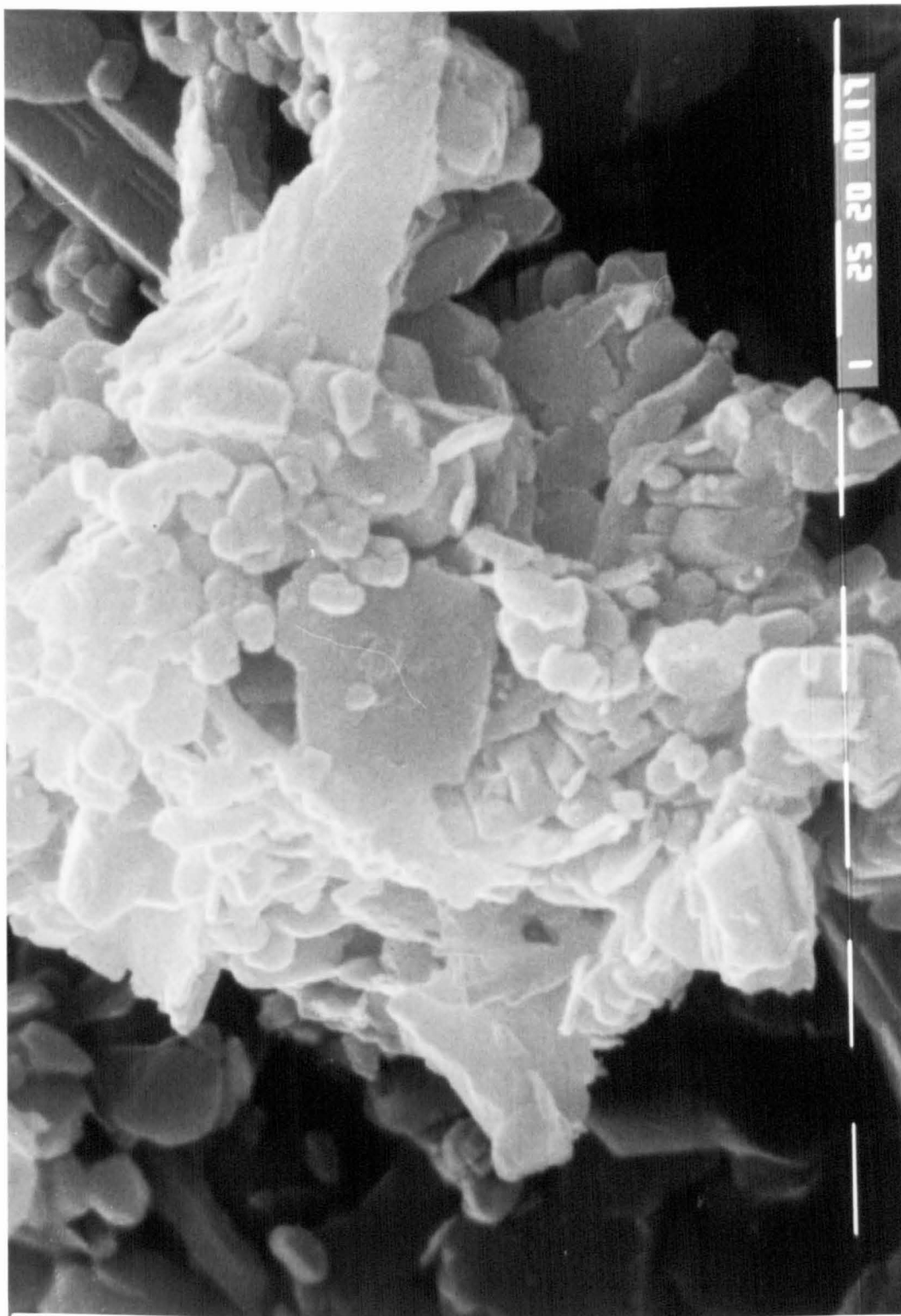


Plate AP1.11. Butser Hill chalk. Magnification 10000x.

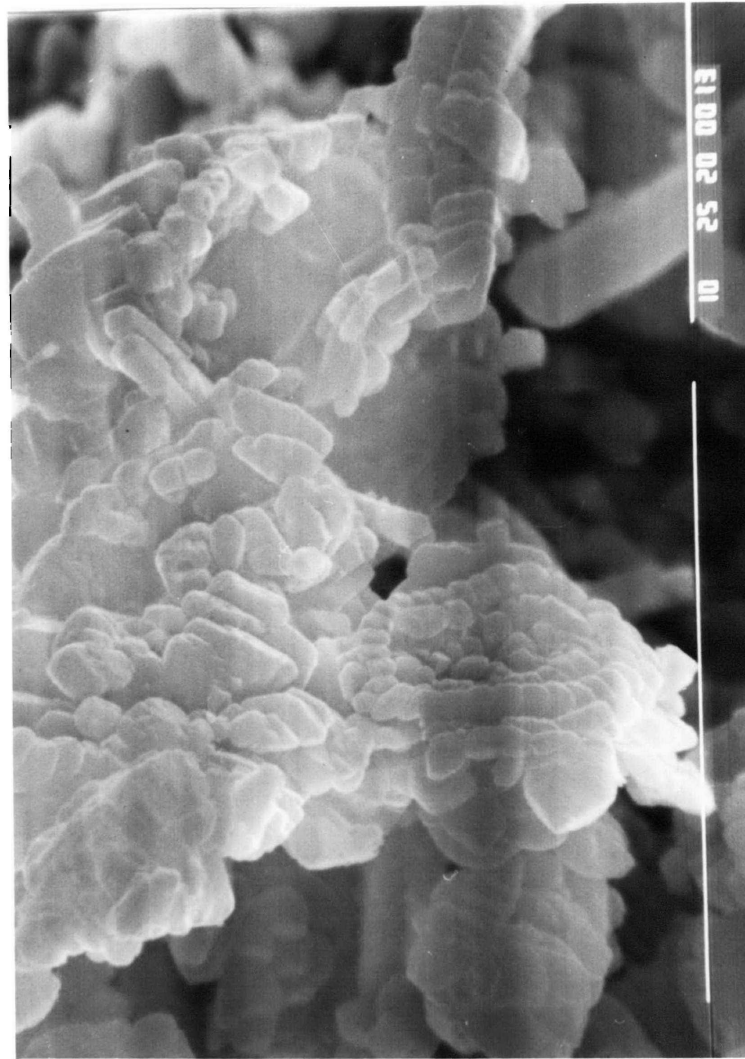


Plate AP1.9. Stevn's Klint chalk. Magnification 7500x. Containing an example of the Coccolith *Cribrosphaerella Ehrenbergi*.

Page 380

NHEC24	3124.5	U. EKO.	75.72	37.86	163.17	183.10
NEOC1	3093.3	U. EKO.	73.64	37.62	162.95	174.30
NEOC3	3126.6	U. EKO.	75.90	37.66	153.55	165.20
NEOC6	3201.3	L. EKO.	75.60	37.50	157.90	171.10
NEOC7	3231.0	U. TOR	75.64	37.66	157.95	174.50
NEOC8	2931.4	U. EKO.	73.38	37.70	143.45	158.10
NEOC9	2966.6	U. EKO.	73.54	37.76	155.93	168.30
NEOC11	3207.6	TOR	75.50	37.75	192.40	200.63
NEOC12	3146.3	U. EKO.	76.80	37.74	185.00	191.90
NEOC14	3197.4	L. EKO.	74.52	37.66	157.20	167.92
NEOC15	3215.2	L. EKO.	75.76	37.74	175.75	187.40
NEOC16	3275.7	U. TOR	76.04	37.86	191.40	202.65
NEOC17	3156.2	L. EKO.	76.64	37.70	178.10	187.15
NEOC18	3149.8	L. EKO.	72.64	37.75	172.38	180.45

Page 383

NEOC19	3121.5	U. EKO.	69.90	37.70	157.90	166.10
NEOC21	3216.6	TOR	68.20	37.64	152.65	162.20
NEOC22	3201.6	L. EKO.	75.70	37.70	185.20	176.60
WEC2	3124.2	U. EKO.	76.46	37.98	136.90	164.88
WEC3	3126.0	U. EKO.	76.06	37.82	140.06	167.80
WEC8	3277.2	U. TOR	76.46	37.98	136.90	164.88
EC18/26A	3040.0	L. EKO.	76.89	37.62	135.38	162.41
EC18/26B	3040.0	L. EKO.	76.30	37.70	138.80	166.31
EC29/25	3032.5	L. EKO.	75.47	37.54	132.00	160.90
EC2/24	3018.2	L. EKO.	74.40	37.60	123.52	157.90
VOHC1	3284.3	U. HOD	75.92	37.72	152.10	165.95
VOHC2	3303.6	U. HOD	76.10	37.90	163.55	182.05
VOHC3	3303.9	U. HOD	75.90	37.80	163.60	180.90
VOTC1	3268.2	L. TOR	76.08	37.70	143.00	163.00
ELOTC1	3146.0	L. TOR	76.78	37.78	156.30	171.05
ELOTC2	3150.0	L. TOR	76.22	37.70	163.68	177.90
ELOTC3	3090.5	L. TOR	76.80	37.70	150.60	165.05
ELOTC4	3166.9	L. TOR	74.62	37.74	155.08	165.76
ELOLEC1	3027.0	L. EKO.	76.64	37.70	165.70	175.05
ELOLEC2	3027.0	L. EKO.	70.10	37.70	144.55	154.00
ELOUEC1	3016.0	U. EKO.	73.26	37.60	138.65	153.40
ELONGC1	3175.7	L. EKO.	74.84	37.80	143.64	170.05
ELONGC2	3144.6	L. EKO.	75.48	37.54	134.98	164.80
ELONGC3	3169.0	L. EKO.	76.70	37.60	143.99	171.60
ELONGC4	3182.7	L. EKO.	76.89	37.62	140.91	167.58
BHWC1			76.68	37.66	144.90	176.78
BHWC2			74.78	37.64	138.85	169.90
BHWC3			75.06	37.64	139.90	172.70
BHWC4			75.50	37.66	142.80	174.10
BHWC5			71.98	37.66	135.00	165.50

BHWC6	75.50	37.64	140.85	174.35
BHWC7	76.68	37.66	143.12	176.90
BHWC8	74.26	37.66	138.70	171.40
BHWC9	72.74	37.64	136.65	168.20
SKWC1	75.68	37.58	118.50	159.10
SKWC3	75.50	37.60	115.60	151.28
SKWC4	74.58	37.80	113.50	155.40
SKWC5	76.00	37.74	113.90	157.15
SKWC6	76.08	37.56	118.40	160.00
SKWC7	76.10	37.52	115.00	157.75
SKWC8	76.00	37.62	116.50	159.00
SKWC9	75.68	37.56	116.40	158.00
SKWC10	74.98	37.52	114.50	156.30